GEOMAR REPORT

FS SONNE
FAHRTBERICHT SO146-1&2
CRUISE REPORT SO146-1&2
GEOPECO

GEOPHYSICAL EXPERIMENTS AT THE PERUVIAN CONTINENTAL MARGIN
INVESTIGATIONS OF TECTONICS, MECHANICS,
GASHYDRATES, AND FLUID TRANSPORT

ARICA - TALCAHUANO
MARCH 1 - MAY 4, 2000

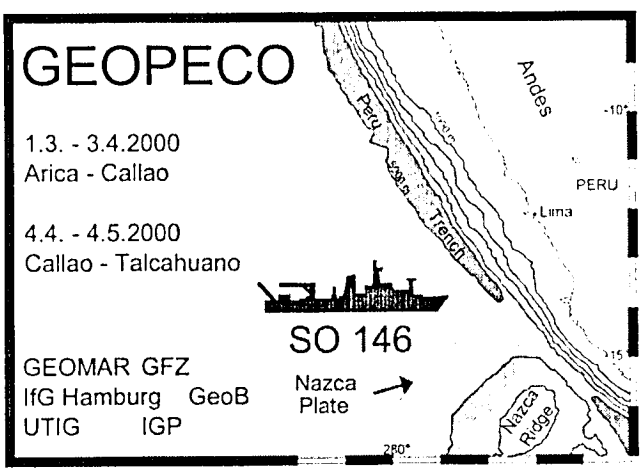

96

GEOMAR REPORT

doi: 10.3289 | geomar_rep_096_2000

FS SONNE
FAHRTBERICHT SO146-1&2
CRUISE REPORT SO146-1&2

GEOPECO

GEOPHYSICAL EXPERIMENTS AT THE PERUVIAN CONTINENTAL MARGIN
INVESTIGATIONS OF TECTONICS, MECHANICS,
GASHYDRATES, AND FLUID TRANSPORT

ARICA - TALCAHUANO
MARCH 1 - MAY 4, 2000

Edited by
Jörg Bialas and Nina Kukowski
with contributions of cruise participants

GEOMAR
Forschungszentrum
für marine Geowissenschaften
der Christian-Albrechts-Universität
zu Kiel

KIEL 2000

GEOMAR REPORT 96

GEOMAR
Research Center
for Marine Geosciences
Christian Albrechts University
in Kiel

Redaktion dieses Reports:
Jörg Bialas und Nina Kukowski

GEOMAR REPORT
ISSN 0936 - 5788

GEOMAR
Forschungszentrum
für marine Geowissenschaften
Wischhofstr. 1-3
D - 24148 Kiel
Tel. (0431) 600-2555, 600-2505

Editors of this issue:
Jörg Bialas and Nina Kukowski

GEOMAR REPORT
ISSN 0936 - 5788

GEOMAR
Research Center
for Marine Geosciences
Wischhofstr. 1-3
D - 24148 Kiel
Tel. (49) 431 / 600-2555, 600-2505

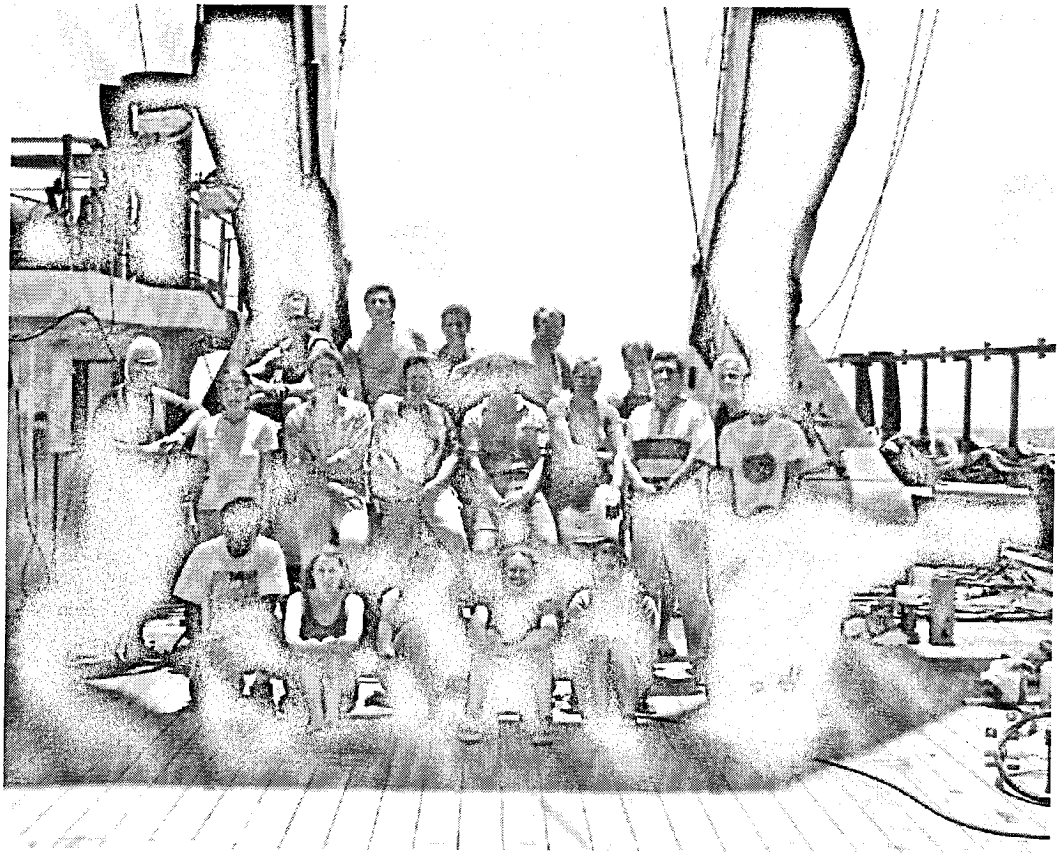

Cruise Participants SO146-1

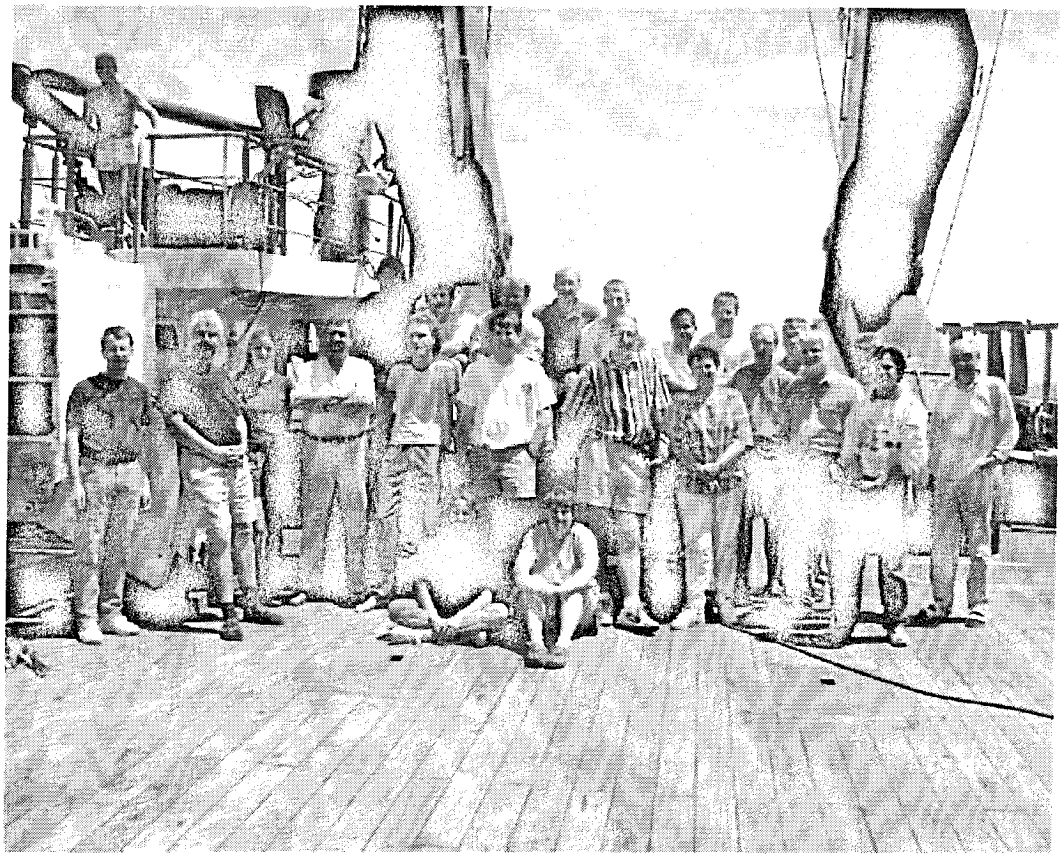

Cruise Participants SO146-2

Table of Contents – SO146-1 & 2

Zusammenfassung

Das Ziel der Forschungsfahrt SO146 GEOPECO (**GEO**physical experiments at the **PE**ruvian **CO**ntinental margin – investigations of tectonics, mechanics, gas hydrates, and fluid transport) war es, einen multidisziplinären geophysikalischen und geologischen Datensatz im Seegebiet vor Peru zwischen 15°S und 5°S aufzunehmen, um zum einen die Struktur und Geodynamik des peruanischen Abschnitts der andinen Subduktionszone sowie Gashydratsysteme in Bereichen mit unterschiedlicher tektonischer Entwicklung quantifizierend zu untersuchen.

Der durch das Abtauchen der ozeanischen, am Trench etwa 28 bis 38 Mill. Jahre alten Nazca Platte unter die südamerikanische Platte geprägte peruanische Kontinentalrand ist in den letzten etwa 8 Mill. Jahren durch die schiefe, von Nord nach Süd fortschreitende Subduktion des Nazca Rückens, eines lang gestreckten Basement-Hochs, gekennzeichnet. Dieser liegt rezent bei etwa 15°S und beeinflußt die Mechanik und den Massentransfer in entscheidender Weise. Die Anwesenheit von komplexen und wahrscheinlich transienten Gashydratsystemen ist durch die Identifizierung von BSRs in reflexionsseismischen Daten von verschiedenen Regionen des peruanischen Kontinentalhangs sowie Gashydratfunden in Bohrkernen von ODP Leg 112 belegt.

Auf dem ersten Fahrtabschnitt vom 01.03.2000 bis 03.04.2000 stand die Registrierung von sechs jeweils über 100 nm langen Weitwinkelprofilen, die mit neun bis 14 OBH/S belegt und mit drei 321 Bolt-Airguns überschossen wurden, im Mittelpunkt der durchgeführten Arbeiten. Weiterhin wurden umfangreiche reflexionsseismische, bathymetrische und gravimetrische Kartierungen durchgeführt. Im nördlichsten Arbeitsgebiet wurde bei Paita zusätzlich eine geologische Beprobung von cold-vent induzierten Baryt-Präzipitaten mit dem TV Greifer durchgeführt.

Der zweite Fahrtabschnitt vom 04.04.2000 bis 04.05.2000 war durch ein Wechselspiel von hochauflösenden seismischen Arbeiten mit einer kombinierten Datenregistrierung (OBH/S und Streamer), Wärmestrommessungen und der Beobachtung des Meeresbodens mit dem TV-Schlitten OFOS gekennzeichnet. Darüber hinaus wurde bei 8°S auf dem ersten Fahrtabschnitt begonnene bathymetrische und gravimetrische Kartierung auf der Nazca Platte direkt ozeanwärts des Trenchs erweitert und auch die auf dem ersten Fahrtabschnitt durchgeführte Kartierung im Bereich des Nazca Rückens ergänzt.

Auf beiden Fahrtabschnitten wurden 127 OBH/S erfolgreich zum Einsatz gebracht. Neben den großen Airguns für die Krustenseismik wurden GI-Guns für die hochauflösenden seismischen Arbeiten und am Meeresboden implodierende SEEBOSEIS Quellen für gezielte kleinräumige Experimente zur Ermittlung der Eigenschaften gashydratführender Sedimente eingesetzt. Wann immer möglich, wurde auf den seismischen Profilen und bei Kartierungen ein Gradiometer zum Einsatz gebracht. Eine Registrierung der natürlichen Seismizität mit einem im Lima Becken ausgebrachten, kleinen Netz aus OBH/S über einen Zeitraum von fast zwei Wochen zeigt, daß in diesem Gebiet eine Langzeitregistrierung mit einem onshore/offshore Netz sehr wünschenswert ist.

Zwei sich kreuzende Profile über den Nazca Rücken sowie entlang seines Kamms und über den Kontinentalhang zeigen, daß er eine asymmetrische Krustenwurzel aufweist und daß sein Abtauchen steiler verläuft als das der ungestörten Nazca Platte. Er weist eine deutliche positive gravimetrische Anomalie von etwa 200 mgal sowie eine meistens wenige hundert Meter mächtige Sedimentbedeckung auf. Auf dem Rücken befinden sich mehrere bis einige hundert Meter hohe submarine vulkanische Strukturen, z.T. mit ausgebildeten Calderen sowie kammartige Hochs. Zum Trench hin lassen sich etwa trenchparallel streichende Abschiebungen in den bathymetrischen Daten identifizien. Wo der Rücken subduziert wird, fehlt ein sedimentärer Akkretionskeil, dagegen finden sich am mittleren und oberen Hang relativ mächtige Sedimentlagen und Hinweise auf wiederkehrende Rutschungsereignisse.

Wie aus den weitwinkelseismischen Profilen bei 13.5°S 11.5°S und 8°S ersichtlich ist, ist die Mächtigkeit der Kruste der Nazca Platte variabel mit Mächtigkeiten zwischen 10 und 7 km. Auch die Sedimentbedeckung auf der ozeanischen Kruste weist eine sehr variable, jedoch immer geringe

Mächtigkeit auf. Im Bereich des nördlichsten Weitwinkelprofils zeigt die ozeanische Kruste bis etwa 80 km seewärts des Trenchs eine große Rauhigkeit. Diese prägt auch den Meeresboden mit kleinräumigen Reliefunterschieden von bis zu 800 m, wobei Sedimente nur in den Taschen zwischen den Hochs anwesend sind. Diese Strukturen streichen im nördlichen Bereich des kartierten Gebietes SSW-NNE, während im Bereich des Trenchs fast N-S streichende lineamentartige Strukturen zu erkennen sind. Etwas weiter südlich ist die Streichrichtung der morphologischen Lineamente jedoch verändert, so daß es schwierig ist zu entscheiden, ob ererbte Strukturen oder aus der Subduktion resultierende Deformationen die Ursache für diese ausgeprägten Lineamente sind. Der untere Hang ist jeweils sehr steil und durch eine variable Morphologie gekennzeichnet, während der mittlere und obere Hang relativ sanft ansteigen. Aufbauend auf diesen Daten und unterstützt durch simulierende Verfahren (Analogexperimente und numerische Modellrechnungen) läßt sich so ein verbessertes und quantitatives Verständnis der Mechanik des peruanischen Kontinentalrandes erlangen.

Daß Erdbeben auch in einem Zeitraum, der frei ist von Großereignissen und ihren Nachbeben, häufig vorkommen, zeigen die Ergebnisse einer fast zweiwöchigen Beobachtung der natürlichen Seismizität mit einem kleinen Netz aus mehreren, am Meeresboden ausgebrachten Seismometern, bei der etliche Ereignisse detektiert werden konnten. Daher wäre es sicher sehr lohnenswert, eine solche Beobachtung mit einem größeren Netz, daß sowohl den marinen als auch kontinentalen Bereich der seismogenen Zone umfaßt, über einen wesentlich längeren Zeitraum, mindestens mehrere Monate durchzuführen.

Bei der umfassenden reflexionsseismischen Kartierung des Yaquina Beckens wurden durch Anbinden an ODP Sites die Möglichkeit gegeben, die Stratigraphie und tektonische Entwicklung des gesamten Beckens abzuleiten. Weiterhin zeigten sich die Anwesenheit eines BSRs in einem komplexen Muster sowie Hinweise auf die Anwesenheit von Gas. Daher wurde eine dieser Linien für detaillierte Beobachtungen des Meeresbodens mit dem TV-Schlitten OFOS sowie mehrere Serien engabständiger Wärmestrommessungen ausgewählt. An mehreren Stellen wurden authigene Karbonate gesichtet, die als isolierte Blöcke oder ganze Karbonatkomplexe Chemoherme mit bis zu 15 m hohen und 500 m weite Plateaus bilden. Lebende Exemplare der auf H_2S- und methanhaltige Fluidaustritte hinweisende Muschel Calyptogena wurden hier gesichtet. Diese Karbonatbildungen sind sehr wahrscheinlich auf ein über längere Zeiträume erfolgtes ausströmen methanhaltiger Fluide zurückzuführen. Der typischerweise damit assoziierte Transport von H_2S ermöglicht es der beobachteten chemo-autotrophen Muschel Calyptogena oder den Röhrenwürmern der Gattung Vestimentifera, sich hier anzusiedeln. Höchstauflösende Sedimentecholotdaten zeigen, daß in vielen Fällen diese Populationen am Meeresboden dort, wo geneigte Sedimentschickten auskeilen, liegen. Diese Lokation wurde mit dem TV-Greifer erfolgreich beprobt. Die Wärmestromdaten zeigen ausgeprägte lokale Maxima an Stellen, wo Störungszonen am Meeresboden ausbeißen. Damit ist zum ersten Mal ein direkter Beweis für die Anwesenheit von Methansystemen und Triggerung des Transports und der Gashydratumsetzung an Störungszonen durch drei unabhängige Datensätze (Reflexionsseismik, Meeresbodenkartierung, Wärmestromdaten) gelungen. Dieser Datensatz wird im späteren die Durchführung mehrdimensionaler numerischer Modellrechnungen zum Wärme- und Fluidtransport zulassen. Weiterhin wurde entlang dieser Linie ein OBH/S Experiment mit einer seismischen Quelle im Hochfrequenzbereich durchgeführt, woraus sich die Geschwindigkeitsfeinstruktur ermitteln läßt. Entlang des refraktionsseimischen Profils wurden weitere Wärmestrommessungen durchgeführt, wobei die Meßwerte hier überraschenderweise entlang des Profil sehr homogen sind

Im Bereich des Lima Beckens und des benachbarten unteren Hangs wurden kombinierte Streamer und OBH/S Exeprimente mit den GI-Guns auf zahlreichen, sich kreuzenden Profilen durchgeführt, um das Anwesenheitsmuster des BSRs und die Stratigraphie vollständiger zu erfassen und damit die tektonisch gesteuerte BSR Unterdrückung in einem Gebiet mit sehr hohem C_{org}-Gehalt in den Sedimenten systematisch zu belegen. Im Rahmen der hochfrequenten Experimente ist es sowohl im Yaquina Becken als auch im Lima Becken gelungen, sehr starke konvertierte Scherwelleneinsätze aufzuzeichnen.

Auf zwei Profilen im Bereich des nördlichsten Lima Beckens, in Abschnitten mit einem deutlichen bzw. ohne BSR, wurden 10 bzw. 11 SEEBOSEIS Implosionsquellen gezündet. Die daraus resultierenden seismischen Signale konnten mit insgesamt 13, z.T. in der Linie, zum anderen Teil flächenhaft angeordneten OBH/S aufgezeichnet werden. Die OBH/S wurden dann auch mit einem engabständigen Profilnetz mit den GI-Guns bei gleichzeitiger Streamerregistrierung überschossen. Hieraus ergibt sich zusammen mit der Bathymetrie die Möglichkeit, mindestens 2.5D auszuwerten. In den OBH/S Daten konnten sowohl p- und s-Wellen als auch Scholtewellen identifiziert werden. Entlang der Linie 26 wurden diagenetische Karbonate am Meeresboden gefunden.

Am unteren Kontinentalhang wurden am Meeresboden auch vereinzelte Exemplare an Calyptogena in 3675 m Wassertiefe gefunden. Hier wurde ein weiteres Wärmestromprofil über die Termination eines BSR aufgenommen. Die gefundene homogene Verteilung der Wärmestromwerte geht einher mit einer ungestörten Sedimentdecke.

Bei der Beprobung im Arbeitsgebiet Paita konnten die dort vermuteten Baryte geborgen werden, ebenso wie Muscheln der Arten Calyptogena und Acharax sowie massive Karbonate.

Damit konnten die Ziele der Fahrt SO146 vollständig erreicht werden. Die ersten Auswertungen an Bord zeigen, daß die verschiedenen Datensätze überwiegend eine sehr gute Qualität aufweisen und somit weitergehende Aussagen erlauben werden.

Summary

The objectives of the research cruise SO146 GEOPECO (**GEO**physical experiments at the **PE**ruvian **CO**ntinental margin – investigations of tectonics, mechanics, gas hydrates, and fluid transport) was a multidisciplinary geophysical and geological investigation in the waters near Peru between 15° S and 5° S. This study focused on a quantitative characterization of the structures and geodynamics of the Peruvian section of the Andean subduction zone, and the associated gas hydrate systems in a region with differing tectonic development.

The Nazca oceanic plate, which is approximately 28 to 38 million years old at the trench, is subducting under the South American plate. The Peruvian continental margin has been influenced over the last 8 million years by the oblique subduction of the Nazca ridge, a long stretched-out basement high, which is progressing from north to south. It is presently in the area of 15° S and has influenced the mechanics and mass transfer in deciding ways. The presence of a complex and probably transient gas hydrate system is verified by the identification of BSRs from seismic reflection data in different regions on the Peruvian continental slope, and also from gas hydrate shows in core barrels from ODP Leg 112.

The first leg of the cruise from 01.03.2000 to 03.04.2000 focused upon the acquisition of 6 wide-angle profiles, each approximately 100+ nm long, shot with three 32 liter Bolt-airguns over 9 to 14 OBH/S instruments. In addition, extensive seismic reflection, bathymetric and gravimetric mapping was performed. In the northernmost working area near Paita, the TV-Grab carried out geological sampling of cold-vent induced Barite precipitates.

The second leg of the cruise from 04.04.2000 until 04.05.2000 was an interchange of high resolution seismic work with combined recording on OBH/Ss and a streamer, heat flow measurements, and observations of the ocean floor using the TV-sled OFOS. In addition, bathymetric and gravimetric mapping of the Nazca plate begun during the first leg of the cruise was expanded upon in the Nazca Ridge region and directly oceanwards of the trench at 8° S.

On both legs of the cruise a total of 127 OBH/S were successfully deployed. In addition to the large airguns for the crustal seismology work, we later used the GI-guns for high resolution seismics and, on the ocean floor, imploding SeeBoSeis sources for focused small-area experiments to study the properties of gas-hydrate-bearing sediments. Whenever possible, the gradiometer was deployed during seismic profiling and mapping. A survey of the natural seismicity within the Lima Basin was conducted using a small network of OBH/S over a time frame of nearly 2 weeks. It showed that a long term study in this area with an onshore/offshore network would be quite desirable.

Two cross-profiles over the Nazca Ridge, along it's crest, and over the continental shelf show that the ridge has an asymmetric crustal root which is subducting at a steeper angle than the undisturbed Nazca plate. The ridge has a clear positive gravity anomaly of about 200 mGal, and a sedimentary cover that is mostly a few hundred meters thick. On the ridge, submarine volcanic structures are found up to several hundred meters in height. Many of them have built up calderas and high crests. At the trench, there are displacements striking roughly parallel to trench which can be identified in the bathymetric data. Where the ridge is being subducted, there is no accretionary sediment wedge. A relatively thick sediment cover and evidence of recurring slide events are found on the middle and upper slope.

As seen on the wide angle seismic reflection profiles at 13.5° S, 11.5° S and 8° S , the crustal thickness of the Nazca plate ranges between 10 and 7 km. The sedimentary cover on the oceanic crust is also shown to be quite variable, however, it is always relatively thin. In the northernmost regions, wide angle profiles show the oceanic crust to have a very rough topography up to about 80 km seawards of the trench. This is expressed in the seafloor topography as small areas with relief differences up to 800 m. Sediments are present only in the pockets between the highs. In the northern part of the mapped area these structures are striking SSW-NNE, while in the area of

the trench, linear type structures striking nearly N-S are observed. Further to the south, however, the strike direction of the morphological lineaments is different. It is therefore difficult to determine, if these lineaments are original structures or the result of deformation from subduction. The lower slope is very steep and shows a variable morphology, while the middle and upper slope rises relatively gently. These data sets, supported by simulations (analog experiments and numerical modeling), should allow for an improved and quantitative understanding of the mechanics of the Peruvian continental margin.

Earthquakes are abundant in the Peruvian subduction zone and occur frequently also in a period which is characterized by the absence of major events. By deploying a small seismological array in Lima Basin for a time interval of close to two weeks, we could identify several events. Therefore, it is most desirable to observe natural seismicity for a much longer period, i.e. at least several months.

Extensive seismic reflection mapping of the Yaquina Basin, tied to ODP sites, gives the possibility of deriving the stratigraphy and tectonic development of the basin. Furthermore, the presence of a complex BSR patterns along with evidence for the presence of gas is observed. Therefore, we selected one of these lines for detailed study of the ocean floor with the TV-sled OFOS, and a series of narrowly spaced heat flow measurements. At several sites, authigenic carbonates were observed as isolated blocks and as entire carbonate complexes forming Chemoherm plateaus up to 15-m high and 500-m wide. We observed living Calyptogena muscles, indicating venting of H_2S and methane-bearing fluids. These carbonate structures are likely the results of venting of fluids containing methane over a long period of time. Such venting is usually accompanied by transport of H_2S, enabling the observed chemo-autotrophic muscle Calyptogena or the tubeworm species Vestimentifera to be colonized. High-resolution sediment sounding data indicate that in many cases, these populations occur on the ocean floor where tilted sedimentary layers pinch out against the surface. This locality was successfully examined with the OFOS. Heat flow data show distinct local maxima in places where fault zones are cropping out on the ocean floor. This is the first-ever direct evidence for the presence of methane systems, triggering transport and transformation of gas hydrate at fault zones through three independent data sets (seismic reflection, ocean floor mapping, heat flow data). These data sets enable us to constrain multidimensional numerical modeling of heat and fluid transport. Furthermore, along this line an OBH/S experiment was performed using a high frequency source for the investigation of the fine velocity structure. Additional heat flow measurements were made along the seismic refraction profiles and the measured values are surprisingly homogeneous.

In the area of the Lima Basin and the neighboring lower slope we completed several combined streamer and OBH/S experiments with the GI-guns and with crossing profiles in order to 1) better understand the pattern of the BSRs; 2) investigate stratigraphy, and 3) to systematically study the tectonically induced suppression of BSRs in a region where sediments have a very high C_{org}-content. We also succeeded in recording strong converted shear waves with the OBSs during these high-frequency experiments –both in the Yaquina and in the Lima Basin.

Along two profiles in the northernmost region of the Lima Basin, one of which is over an area with a clear BSR and the other over an area without a clear BSR, we detonated 10 and 11 SeeBoSeis implosive sources, respectively. The resulting seismic signal was recorded on 13 OBH/S, which were partly in inline, and partly in offline positions. A grid of densely spaced profiles was then shot over the OBH/S positions with a GI-gun while recording with the streamer. This data combined with the bathymetry gives the possibility of computing at least a 2.5-D model. In the OHB/S data both P and S waves and Scholte waves can be identified. Along line 26 diagenetic carbonates were found on the ocean floor.

On the lower continental slope occasional examples of Calyptogena were found at water depths of 3675 m on the ocean floor. Another heat flow profile was measured over the termination of a BSR at this location. The homogenous distribution of heat flow determinations is in agreement with an undistorted sediment cover and conductive heat flow.

During sampling of the work area in Paita, suspected Barites were recovered, as well as Calyptogena and Acharax type muscles and massive carbonates.

These accomplishments fully satisfied the objectives of cruise SO146. Initial evaluations show the different data sets to be of very high quality and will allow further interpretation and insight.

1. Introduction

(N. Kukowski, J. Bialas, I. Pecher)

Convergent continental margins, where oceanic plates are subducted beneath overriding continental plates, comprise the world's most dynamic regions and have large geo-hazard potentials. These plate boundaries are the loci of the Earth's most and strongest earthquakes. They are also the most important material pathways for crust and sediments returning to the mantle. Furthermore, at subduction zones, numerous accumulations of economic mineral and hydrocarbon deposits are present. In the submarine part of the continental slope, over large areas of the seafloor and the shallow subseafloor sediments, gas hydrates are stable.

The large dynamics of convergent margins is mirrored by complex deformation patterns and material transfer modes. Sediments arriving at the trench with the oceanic plate may be frontally or basally accreted (underplated) to the continent or subducted. Convergent margins are classified as accretive, intermediate, and erosive depending on the dominant mass transfer modes.

The Peruvian margin, part of the South American subduction zone, is characterized by the interaction of the subducting Nazca Ridge with the continental margin, by a variable and at some locations unusual thermal structure, fluid flow patterns related to strong dewatering and focused fluid flow in fault zones, fluid related mineralisation, and the presence of gas hydrates as indicated by a very complex pattern of BSR presence and solid hydrates as found in ODP Leg 112 drill cores. Seismicity of the Peruvian margin is high with several magnitude 8 events in the last century. While only minor amounts of sediment is brought to the trench by the oceanic Nazca Plate, thick sediment sequences at the slope is a result of high biological productivity through upwelling. These features make the Peruvian margin a top priority target for integrated geophysical surveys which apply multifold methods to yield a more systematic and quantitative understanding of interacting convergent margin processes.

1.1 Structure and tectonic evolution of the Peruvian margin

At the Peru margin, the oceanic Nazca Plate is subducted beneath the South American continent at a rate of about 78 mm/yr (Fig.1.1). The Nazca Plate is segmented by fracture zones, such that crust of different ages is subducted at different locations of the South American margin. Off southern Peru, the crustal age is about 38 Ma at the trench, while north of the Mendaña fracture zone, which enters the margin at about 10°S, the crustal age at the trench is ca. 28 Ma (Müller et al., 1995).

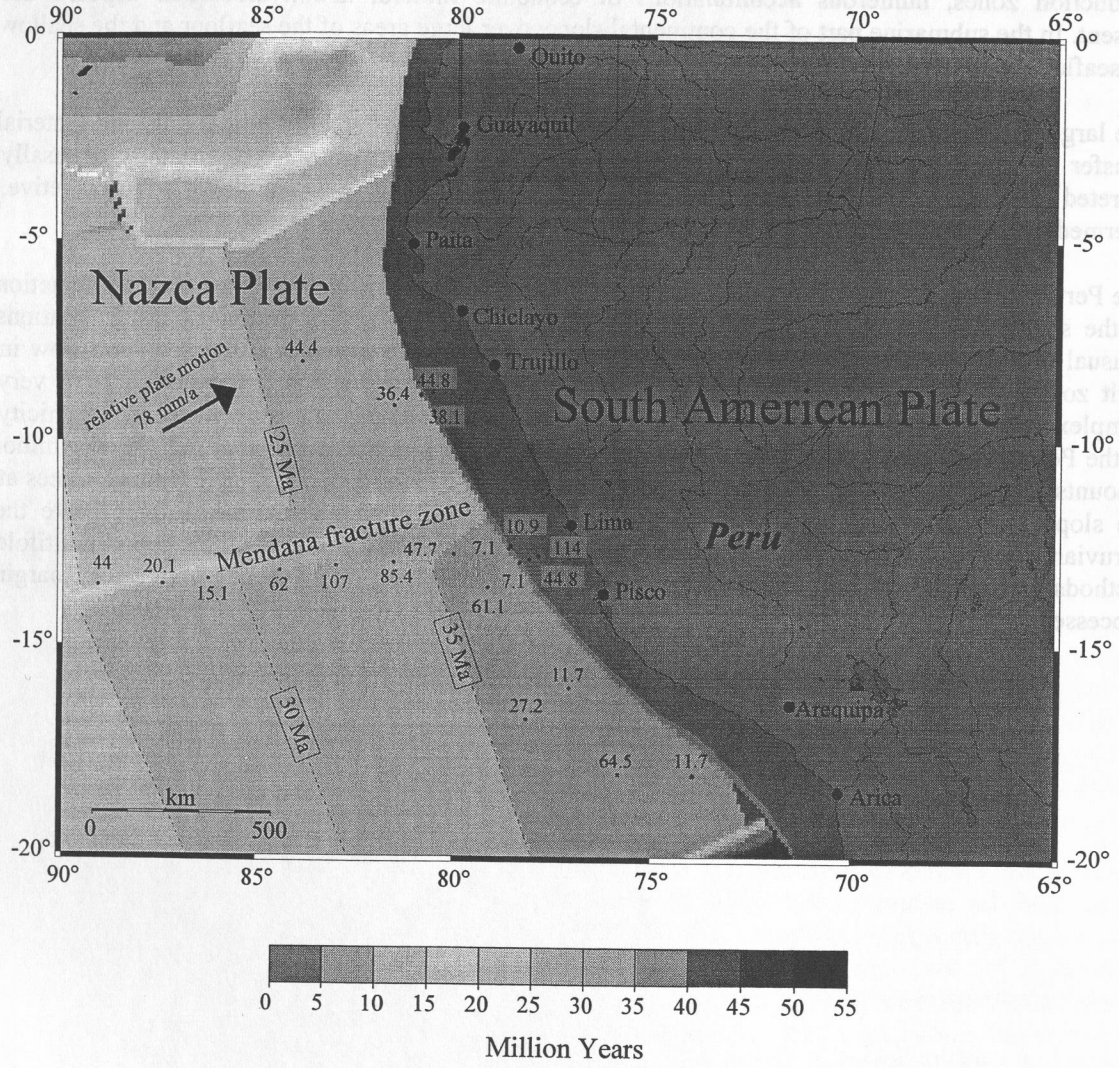

Fig.1.1: Location map showing the convergence between the Nazca Plate and South America. Gray tones indicate the crustal age of the oceanic plate, isochrons after Müller et al., 1995. Dots refer to conventional older heatflow measurements (numbers in mWm^{-2}) at locations relevant for the GEOPECO project (data from data bank at GGA, Hannover).

The post-Miocene tectonic history and mass transfer along the Peruvian margin between 8°S and 15° S is dominated by the oblique subduction of the Nazca Ridge (Fig.1.2). The Nazca Ridge is a basement high which originated at the Easter Island hot spot possibly simultaneously with Tuamotu Ridge at the other side of the spreading center (Pilger, 1984). The northeastern edge of the ridge entered the subduction zone at about 8° S some 8 Ma (Cande, 1985), passed the trench at 12°S about 4 Ma ago and currently enters it at about 15°S. Hence, the crest of the ridge sweeps north to south along the margin. Seismic profiles across the margin from 15° S to the north therefore display different stages of the margin's evolution after subduction of the Nazca Ridge.

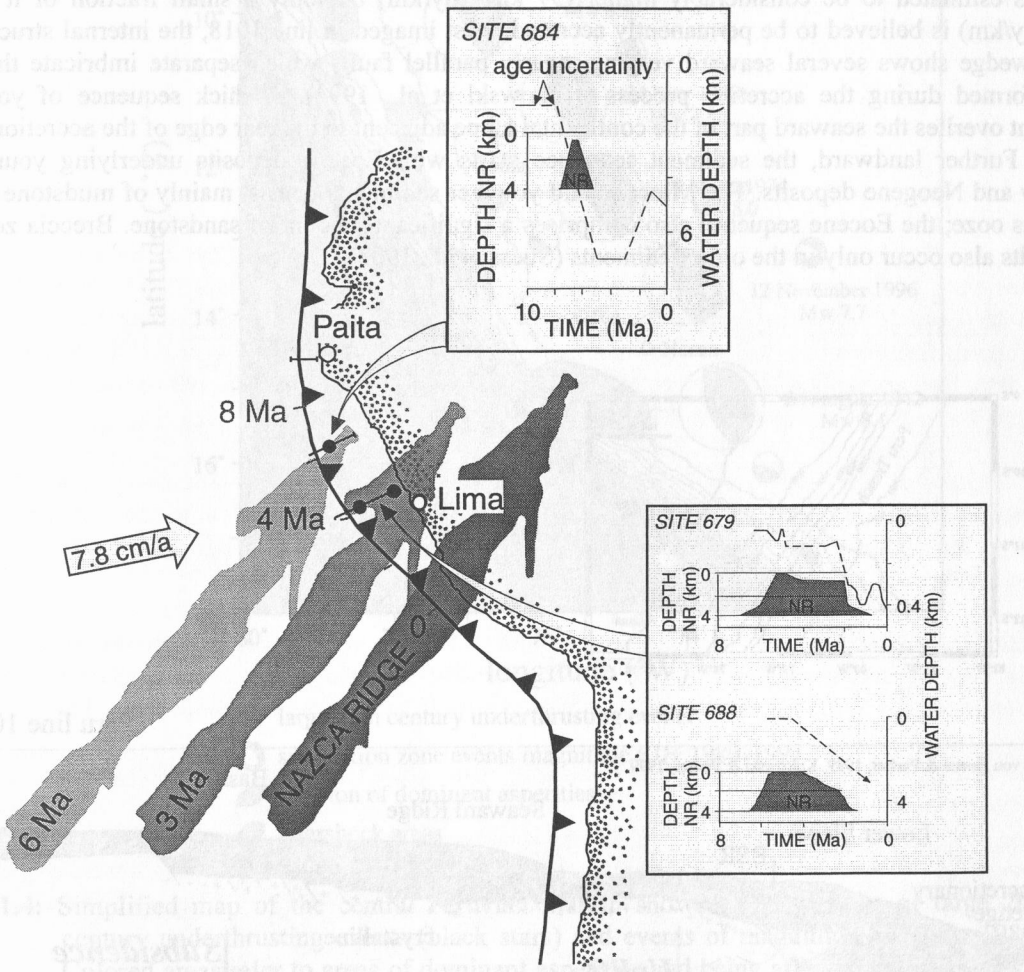

Fig.1.2: Sketch illustrating the southward migration of Nazca Ridge and its interaction with the Peruvian margin. The shape of the subducted part of the ridge is made visible by showing the outline of Tuamotu Ridge as a trajectory mirror image. Insets show paleo-bathymetry as a function of time as obtained from ODP Leg 112 drill cores (after von Huene et al., 1996).

Ridge subduction causes uplift of the margin and is thought to also erode a possibly older accretionary wedge (von Huene et al., 1996). Above the northern flank of the ridge, Quaternary coastal uplift is about 0.3 m/ky and 0.5 m/ky above its southern flank. This is the fastest rate of uplift reported from the coasts of Peru and Chile (Hsu, 1992). Currently it is hypothesized that after subduction of the ridge crest, the margin subsides and most of the incoming material is accreted to build a new accretionary wedge.

After the subduction of the Nazca Ridge crest, the growth of the recent accretionary wedge grew rapidly due to thicker sections of incoming sediments but has slowed because the influx of sediments is now less (300 m, von Huene et al., 1996), and because the proportion of subducting sediments has increased with time. At 12°S, where the ridge subducted about 4 Ma, over 30% of the incoming sediment of an estimated 11 km3/my/km (volume per time and distance along trench) of dry rock is being accreted, (60% of the sediments is frontally accreted, however part of it is later subducted) (von Huene et al., 1996). The crest of the ridge was subducted about 6.5 Ma at 9°S. Here, total sediment influx is estimated to be considerably higher (37 km3/my/km) but only a small fraction of it (~1 km/3/my/km) is believed to be permanently accreted. Best imaged in line 1018, the internal structure of the wedge shows several seaward verging, nearly parallel faults which separate imbricate thrust slices formed during the accretion process (Kukowski et al., 1994). A thick sequence of young sediment overlies the seaward part of the continental slope adjacent to the rear edge of the accretionary wedge. Further landward, the sediment sequence starts with Eocene deposits underlying younger Tertiary and Neogene deposits. The Miocene and younger sediments consist mainly of mudstone and siliceous ooze; the Eocene sequence also comprises a significant amount of sandstone. Breccia zones and faults also occur only in the older sediments (Suess et al., 1988).

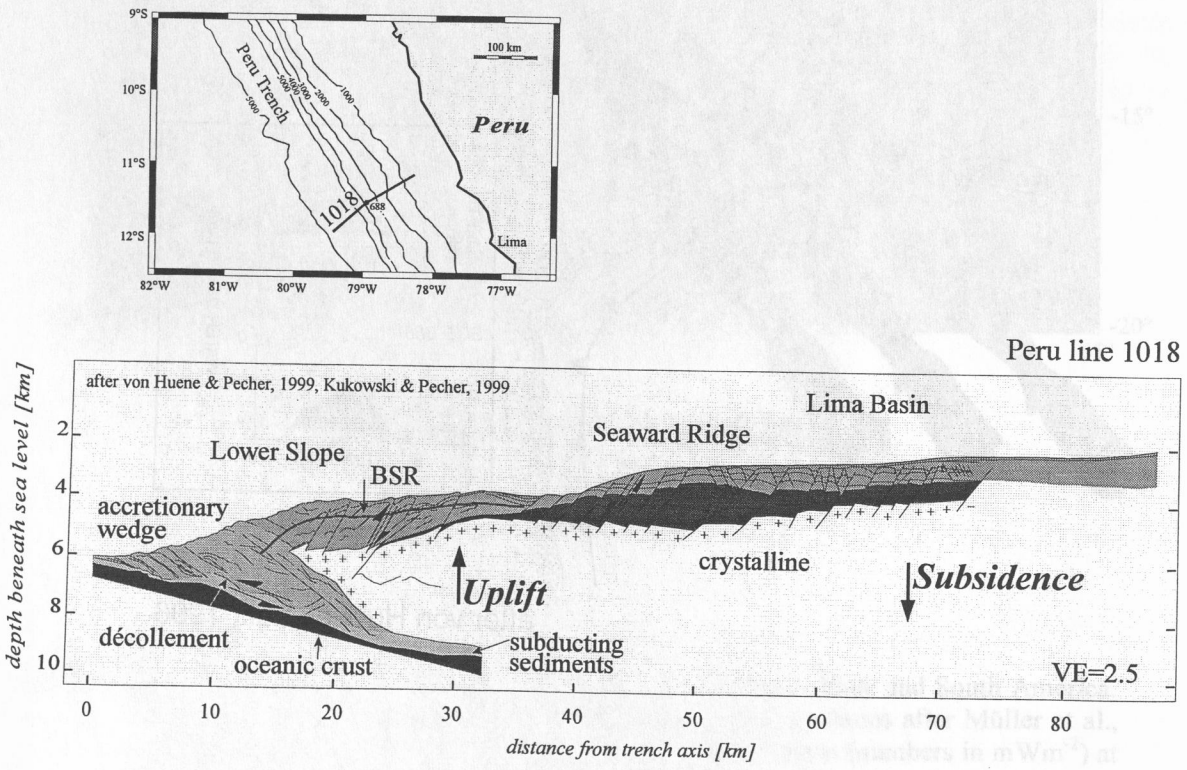

Fig.1.3: Tectonic interpretation of multichannel reflection seismic line Shell 1018 at 11.5°S. Note major fault zones in the uplifted part of the Lower Slope and significant extensional faulting in Lima Basin. Inset shows location of seismic line (After von Huene & Pecher, 1999, Kukowski & Pecher, 1999).

1.2 Seismicity at the Peruvian margin

The South American subduction zones has a naturally high rate of seismicity and has been the location of large plate boundary events for many centuries. In particular, The Peru segment of the Nazca Plate / South American Plate convergence has suffered from several large, i.e. about magnitude 8, events within the last 100 years (Beck & Ruff, 1989). With the exception of the 1942 and 1996 events, these events occurred north of Nazca Ridge (Fig.1.4). Many of theses Peruvian seismic events caused major tsunamis, e.g. the 1974 or 1996 events (Hartzell & Langer, 1993, Heinrich et al., 1998).

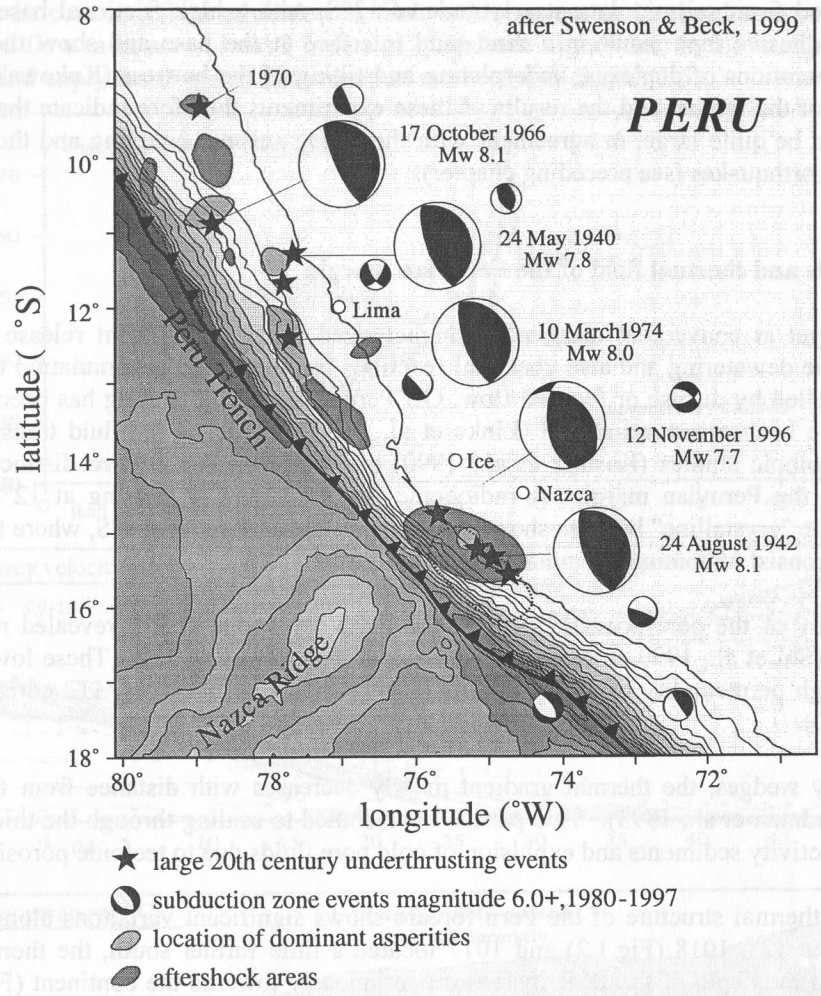

Fig.1.4: Simplified map of the central Peruvian margin showing the location of large 20th century underthrusting events (black stars) and events of magnitude >6 since 1980. Colored areas refer to areas of dominant asperities and being affected by aftershocks. Focal solutions are from the Harvard CMT catalog (after Swenson & Beck, 1999).

The pattern of seismicity in the Peruvian subduction zone is characterized by the occurrence of offshore events, the lack of events in depths between 150 km and 500 km as well as very deep events. Between the 1942 and 1974 rupture zones a seismic gap exists which probably has not failed within several hundred years (Swenson & Beck, 1999).

The 1942 and 1996 events occurred as a result of the subduction of the Nazca Ridge and indicate an important exception from the often cited hypothesis that basement ridges subduct aseismically (Spence et al., 1999). The 1996 event ruptured more than half of the shallow subduction interface of the Nazca Ridge and extended down to a depth of about 65 km.

1.3 Mechanics of the Peruvian margin

Mass transfer and deformation patterns at convergent margins are dominantly controlled by the nature of the plate interface. In case of a low basal friction, frontal accretion of imbricate thrust slices is the dominant mode of accretionary wedge growth while in case of high basal friction, a cyclic process alternating between frontal accretion and basal underplating is observed (Gutscher et al., 1998a,b). The Coulomb approach relates the geometry of the forearc (accretionary wedge) to its mechanical properties (Davis et al., 1983, Lallemand et al., 1994) and shows that large tapered wedges can only be built up and remain stable in case of high basal friction. The reflection seismic lines available for the Peruvian margin (cf also Fig.1.3) reveal a small wedge with a remarkably large taper. Analog sandbox modeling, scaled from seismic data at a latitude of 12°S, with a high frictional base made of sand sprinkled on adhesive tape result in a sand-sand interface at the base and show the formation of subsequent generations of duplexes, underplating and tilting of the buttress (Kukowski et al., 1994). The geometry of the forearc and the results of these experiments therefore indicate that basal friction off Peru should be quite large, in agreement with the strong seismic coupling and the occurrence of frequent large earthquakes (see preceding chapter).

1.4 Fluids and thermal field of the Peruvian margin

The fluid budget at convergent margins is characterized by the significant release of pore fluids through tectonic dewatering and also chemical reactions leading to the accumulation of excess fluids which are expelled by diffuse or focused flow. Off Peru, active fluid venting has been identified and flow rates have been measured at 9°S (Linke et al., 1994). Evidence for fluid transport at 12°S is revealed by isotopic studies (Kastner et al., 1990) and indicate at least two distinct fluid regimes existing along the Peruvian margin. A radiogenic isotope signal is missing at 12°S, although, in seismic data, the "crystalline" buttress shows the same characteristics as at 9°S, where the buttress was interpreted to consist of continental metamorphic basement.

An earlier study of the pore pressure field of the Peruvian wedge at 9°S revealed remarkably low overpressures (Shi et al., 1990 consistent with observations from Leg 112. These low overpressures may due to high permeability of sediments off Peru as indicated from Leg 112 cores (Marsters and Christian, 1990).

In accretionary wedges, the thermal gradient mostly decreases with distance from the deformation front (e.g. Hyndman et al., 1993). This pattern is attributed to sealing through the thickening of low-thermal-conductivity sediments and expulsion of cold pore fluids due to tectonic porosity loss.

However, the thermal structure of the Peru forearc shows significant variations along strike. In two MCS profiles at 12°, 1018 (Fig.1.2) and 1017 located a little further south, the thermal gradient as computed from the depth of the BSR increases continuously towards the continent (Fig.1.5). At 9°S, the thermal gradient decreases toward the continent indicating the more commonly observed thermal structure. Superimposed on the thermal field are strong small scale anomalies which can be correlated with major fault zones.

Conventional heat flow measurements (Yamano & Uyeda 1990) indicate an average heat flow density of about 40mWm^{-2} near the trench at 9°S; much lower than expected from the age of the downgoing Nazca plate. The relation between age of an oceanic plate and surface heat flow density, as given by Sclater et al (1980), predicts a heat flow of about 65.6 mWm^{-2}, for the Peruvian trench at 12°S and somewhat higher north of the Mendaña fracture zone. However, the lowest heat flow density was obtained close to the trench in the neighborhood of the Mendaña fracture zone. It has been suggested that these low values are caused by removal of heat by efficient fluid advection in fractured areas (Yamano & Uyeda, 1990). The observed increase of heat flow density towards the continent was suggested to be caused by frictional heating (Shi et al., 1990, Yamano & Uyeda, 1990).

By means of coupled hydrothermal modeling, we were able to match the thermal field (Fig. 1.5) with good accuracy using the constraints given from the BSR estimated thermal gradient and conventional heat flow measurements (Kukowski & Pecher, 1999). These constraints allow a quantitative estimate of the contribution of fluid advection, sediment advection, and frictional heating to the thermal budget. Fluid advection, most probably thermally, is not very relevant regionally, never contributing more than 10% to the thermal budget within the wedge and significantly less at the slope. Sediment advection contributes a few mWm^{-2} to the thermal field. Considerable frictional heating along the plate interface increasing with depth has to be invoked to explain the landward increase of the thermal gradient. Fluid advection rates in the wedge are in the range of several 10^{-11} ms^{-1} to several 10^{-10} ms^{-1} in the wedge and slightly lower on the slope indicating equivalently low rates of hydrate formation (Rempel & Buffett, 1997). In contrast, fluid advection at fault zones appear to be the dominant mode of heat transport. Fluid flow rates are at least 3 orders of magnitude higher than in the wedge (Kukowski & Pecher, 1999) and imply faster gas hydrate reaction rates (cf also chapter 1.5).

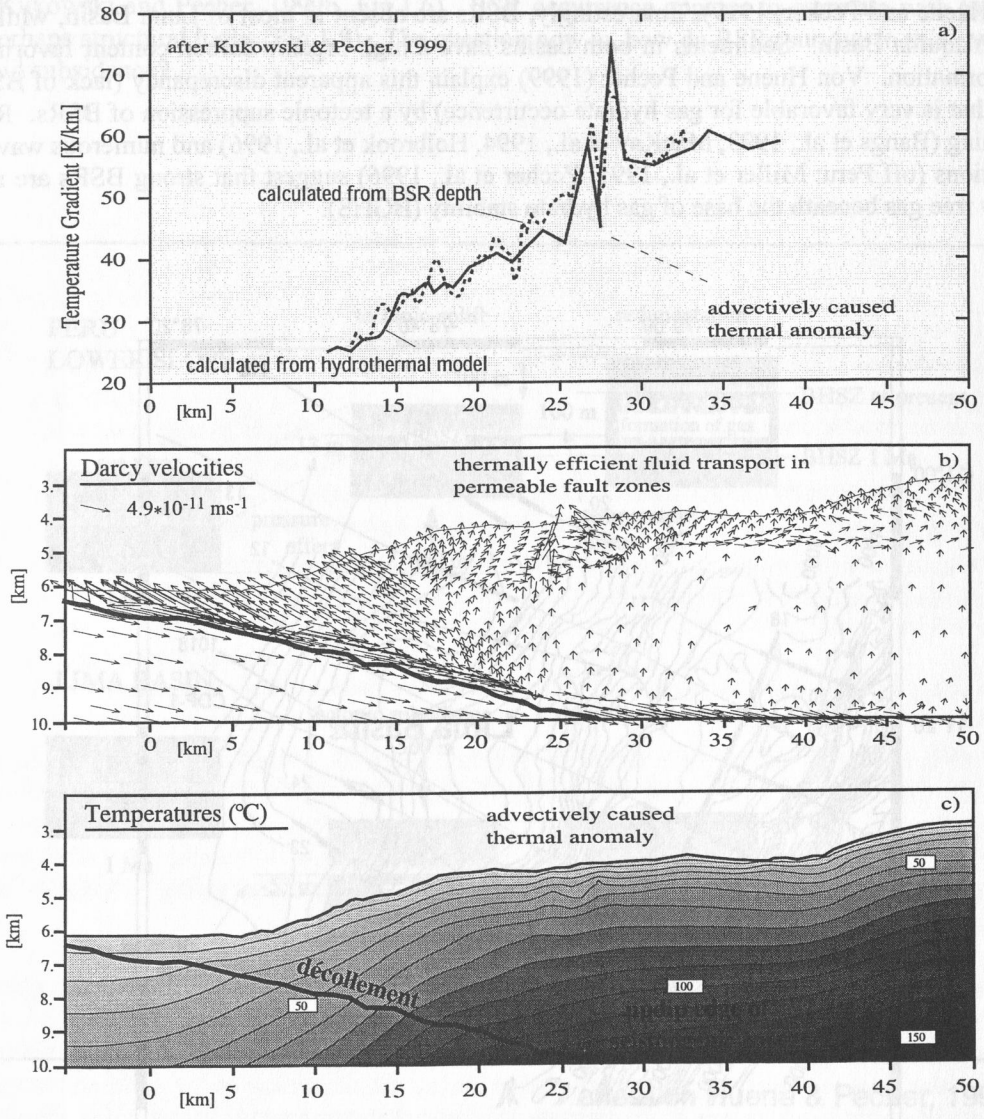

Fig.1.5: Thermal gradient, fluid flow magnitudes and directions, and thermal field obtained from the coupled hydrothermal model calculations of Kukowski & Pecher (1999). a) Comparison of thermal gradient computed from BSR depth, b) Darcy velocities obtained from model calculations, c) thermal field obtained from model calculations. Note local advective thermal anomalies. The updip edge of the seismogenic zone is located where the plate interface (décollement) meets the 125°C isotherm (Hyndman et al., 1993).

1.5 Gas hydrates at the Peruvian margin

The high organic carbon content over most of the Peru margin (up to 12% in ODP Leg 112 cores) indicates high organic activity which favors methane production and gas hydrate formation. During ODP Leg 112, solid gas hydrates were recovered at Sites 685 and 688. Low chlorinity indicated gas hydrate occurrence in most of the other deepwater Leg 112 sites. The ratio of methane to higher-order-hydrocarbons in both gas hydrate samples and pore water was generally over 99% suggesting a mainly microbial origin of methane. This conclusion is supported by low $\delta^{13}C$ values of –65.0 and –59.6 PDB in the gas hydrate samples.

Strong bottom simulating reflectors (BSRs) are present along much of the Peruvian lower slope (Fig. 1.6) and in the accretionary prism at 9°S. Absence of the BSR in the prism at 12°S is readily explained by the low predicted organic carbon content of the accreted hemi-pelagic and pelagic trench fill (von Huene and Pecher, 1999). Interestingly, BSRs are absent in most of Lima Basin, while they occur in Yaquina Basin. Sediments in both basins have a high organic carbon content favoring gas hydrate formation. Von Huene and Pecher (1999) explain this apparent discrepancy (lack of BSRs in a region that is very favorable for gas hydrate occurrence) by a tectonic suppression of BSRs. Results from drilling (Bangs et al., 1993, MacKay et al., 1994, Holbrook et al., 1996) and numerous waveform investigations (off Peru: Miller et al., 1991; Pecher et al., 1996) suggest that strong BSRs are mainly caused by free gas beneath the base of gas hydrate stability (BGHS).

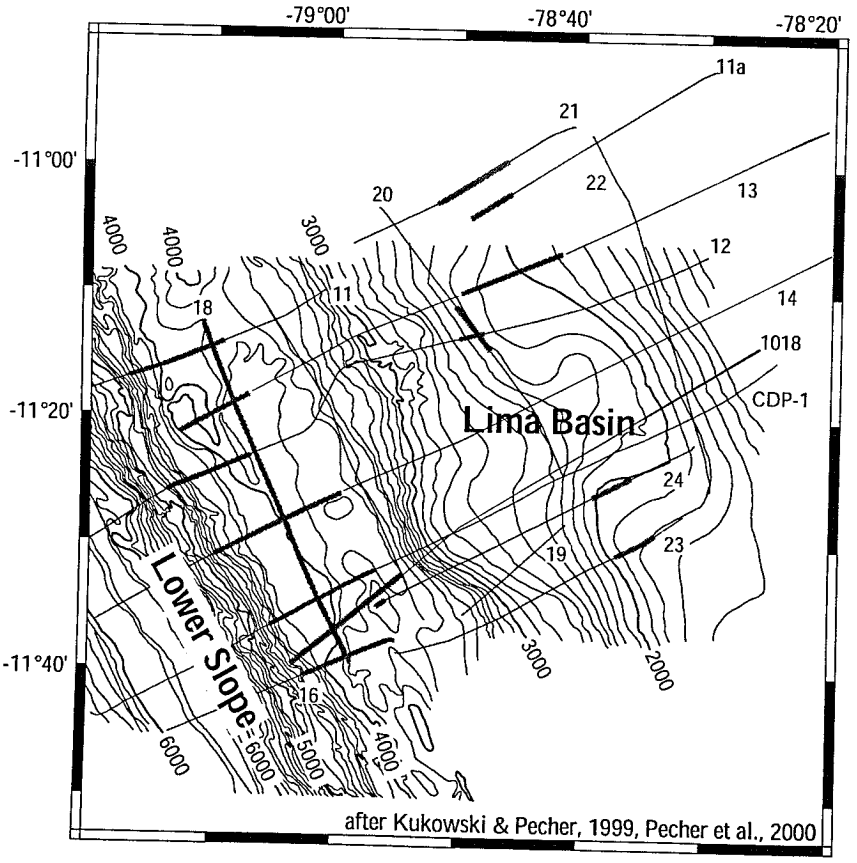

Fig.1.6: BSR distribution offshore central Peru as indicated from reflection seismic data (lines Shell 1018, CDP-1 of the Nazca Plate project acquired in the late 70ties and HIG lines acquired by the Hawaii Institute for Geophysics). Thick portions of seismic track lines indicate BSR identification (After Kukowski & Pecher, 1999b, Pecher et al., 2000).

Tectonic subsidence leads to an increase of pressure and hence, a movement of the BGHS towards higher temperatures, i.e., downward with respect to the sediment column. Based on information from ODP Site 679, von Huene and Pecher (1999) compared this effect to the vertical motion of the BGHS caused by an upward movement of isotherms due to sedimentation (Fig.1.7). The net-movement of the BGHS was indeed predicted to be downward. This may lead to an absorption of gas into the gas hydrate stability zone (GHSZ) and cause a suppression of BSRs. Yaquina Basin, on the other hand, is essentially stable which is in agreement with the presence of numerous BSRs. BSRs arguably are the most commonly used proxy for gas hydrates in marine sediments. An understanding of mechanisms that lead to a lack of BSRs beneath gas-hydrate-bearing sediments therefore are of significant importance for regional to global estimates of gas hydrate quantities.

BSRs have been observed, however, in small areas north and south of the Lima transect of ODP Leg 112 (Kukowski and Pecher, 1999b, Fig.1.6). BSR occurrence appears to correlate with topographic and perhaps structural highs (Fig.1.8). The question now is, how do BSRs survive in this environment of rapid subsidence?

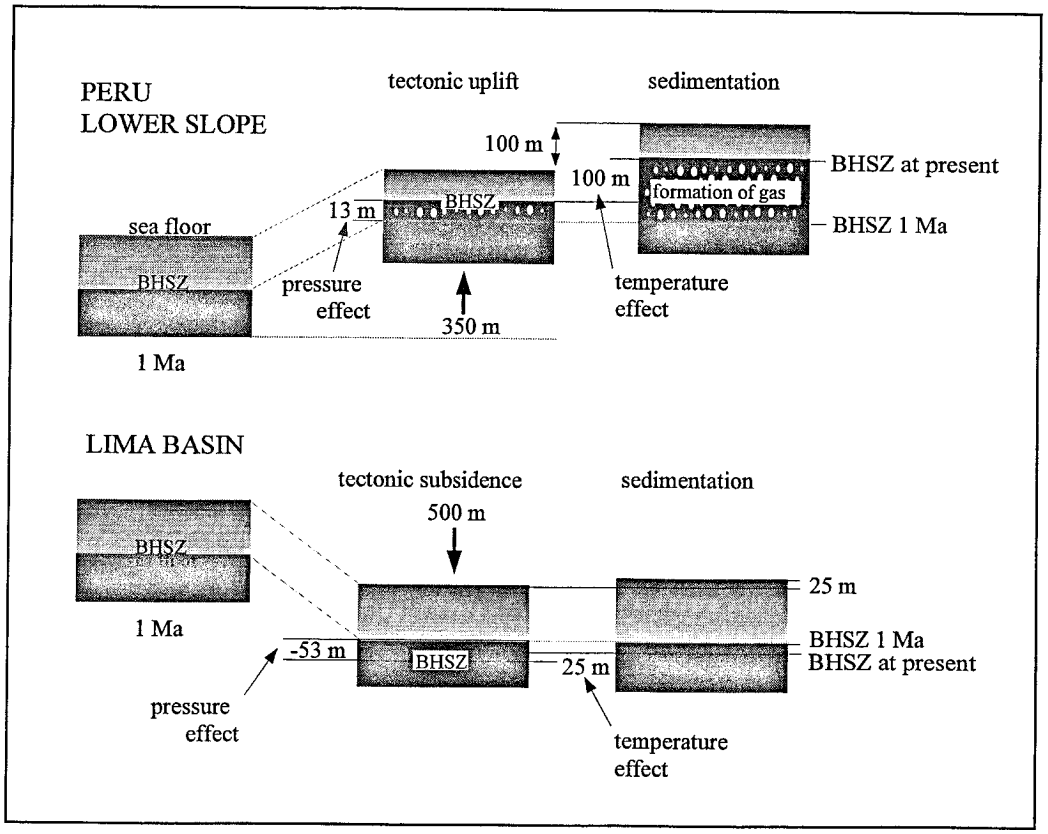

after von Huene & Pecher, 1999

Fig.1.7: Model concept of tectonic BSR suppression (after von Huene & Pecher, 1999).

A new approach to explain BSR formation is the concept of "critical methane flux" developed by Xu and Ruppel (1999) based on ODP Leg 164 on the Blake Ridge. Methane flux into the GHSZ has to exceed this flux rate before the top of free gas coincides with the base of gas hydrate occurrence at the BGHS. Assuming that this leads to BSRs in seismic reflection data, Xu and Ruppel (1999) were able to quantitatively explain BSR distribution over the Site 994/995/997 transect on the Blake Ridge. In light of this concept, the Lima Basin BSRs are perhaps maintained by elevated methane flux caused by focusing of fluid flow into the structural highs. The increased methane flux into the GHSZ may perhaps offset the absorption of gas at its base.

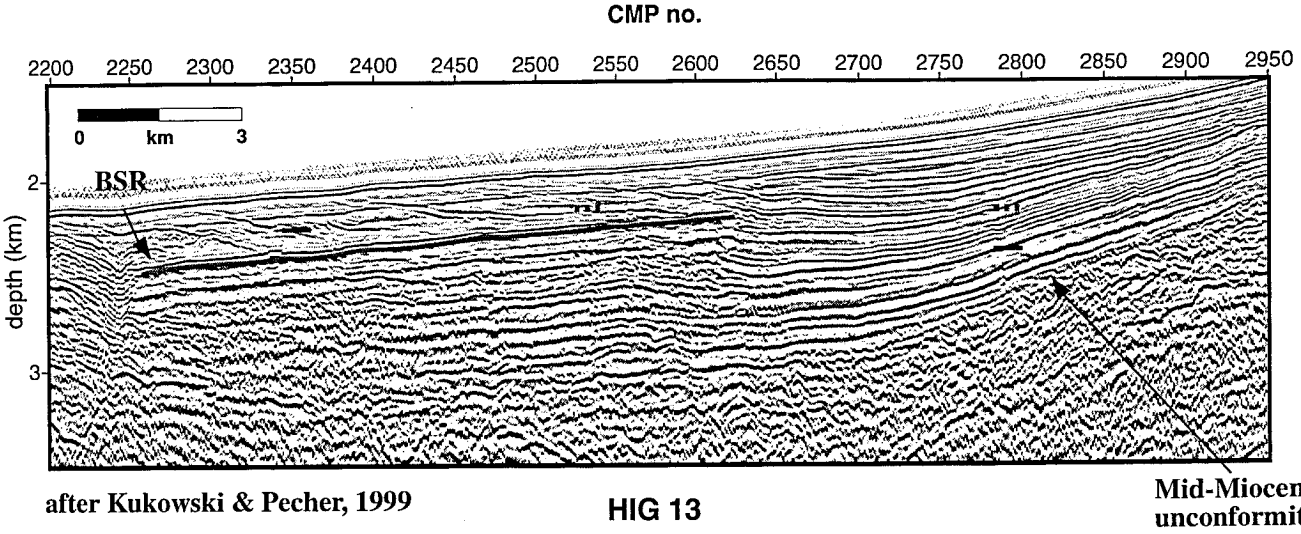

Fig.1.8: Depth migrated section of reflection seismic line HIG 13 displaying a portion with and without a BSR. Note that strata within the hydrate stability zone, where the BSR is present, are beneath the gas hydrate stability zone, where there is no BSR.

1.6 Major results of ODP Leg 112

Much of the current knowledge of the tectonics, geochemistry and stratigraphy of the Peruvian margin comes from ODP Leg 112 and related data acquisition. The objectives of Leg 112 included: 1) identifying the seaward edge of the continent, 2) deriving the tectonic history of the margin, 3) deriving the history of upwelling along the Peruvian margin, 4) obtaining the stratigraphy of sedimentary deposits and its relation to vertical tectonism, and 5) investigating diagenesis and pore fluids (Suess, von Huene et al., 1988).

Sediments down to the middle slope are of continental origin and made of Eocene to Quaternary sequences while the small accretionary wedge beneath the lower slope consists of Miocene to Quaternary hemi-pelagic sediments (von Huene, Suess et al., 1988). Several erosional phases took place since the Eocene: older deposits were eroded during the Oligocene at the shelf and upper slope and Paleogene deposits are missing. Stratigraphy of the major sedimentary basins along the slope, the Lima, Yaquina, and Trujillo Basins includes the whole sequence from the Eocene to Quaternary.

Penetration of the BSR was considered a drilling hazard for Leg 112, the boreholes were therefore located away from BSRs. Nevertheless, solid gas hydrates were recovered at Sites 685 and 688 and low chlorinity - indirect evidence for gas hydrate occurrences, was encountered at two other sites. Methane constitutes about 99% of the hydrocarbons in the pore water and gas hydrates, which together with low $\delta^{13}C$ values of –65.0 and –59.6‰ PDB in gas hydrate samples at Sites 685 and 688 indicates a mainly microbial origin of methane (Kvenvolden and Kastner, 1990)

1.7 Objectives of the project GEOPECO

The main goals of the project GEOPECO are to better understand the geodynamics and gas hydrate systems of this complex margin. To achieve this requires the application of several geophysical methods to specific key-areas along the margin and to supplement this data with direct observations of the sea-floor and geological sampling.

Therefore, specific aims during cruise SO146 were:

- To shoot several wide angle seismic lines to determine subduction characteristics and mechanics of the Peruvian margin. These lines were designed to cross the continental slope and extend out onto the oceanic crust approaching the trench. To image different stages of subduction after ridge subduction, these seismic lines were located at different latitudes, at locations not affected by the nearby fracture zones, and at different distances from Nazca Ridge.
- To observe natural seismicity by deploying several OBH/S in a network over a time interval of about two weeks. The results of this experiment should allow us to decide how worthwhile and to plan a larger offshore/onshore network deployed for a longer timespan, e.g. some months.
- To shoot wide-angle line across and along Nazca Ridge to image its structure and subduction geometry as well as to determine the thickness of its crustal root.
- To map specific areas with swath bathymetry to conduct morpho-tectonic studies and to extrapolate the findings of the seismic work to greater areal information.
- To map the sedimentary basins and their BSRs on the upper slope with high resolution seismic reflection for the purpose of investigating their evolution and subsidence history and bordering fault zones
- To acquire potential data (gravity and magnetics) to better constrain structures obtained from wider angle seismics and to investigate the nature of isostasy in the basins.
- To complete seismic experiments with imploding ocean bottom source (SEEBOSEIS) and to investigate in very high resolution the velocity structure of gas hydrate bearing sediments including shear waves and Scholte waves.
- To supplement the crustal scale seismics across the continental slope with high resolution seismic reflection in the neighborhood of major faults zones. These fault zones are assumed to play a major role for fluid transport.
- To complete narrowly spaced heat flow measurements across the sedimentary basins and continental slope where complex BSR structures have been image in the seismic data.
- To observe the seafloor with a TV camera and to search for vent sites and authigenic carbonates, features which are unequivocal characteristics of methane release at the sea floor.

To undertake these tasks, experiments applying the different methods were systematically related to each other as described in sections 5 to 10.

2. Participants

2.1 Scientists

2.1.1 Scientists – Leg SO146-1

Kukowski	Nina	GFZ,	Co-Chief Scientist
Bialas	Joerg	MGD,	Co-Chief Scientist
Letz	Horst	MGD	
Hampel	Andrea	MGD	
Bohnert	Jens	MGD	
Haase	Eric	MGD	
Harris	Abd	MGD	
Bollwerk	Sandra	MUG	
Eberle	Katja	MGD	
Petersen	Joerg	MGD	
Liersch	Petra	MGD	
Steffen	Klaus	KUM	
Huebscher	Christian	U-HH	
Wenz	Christian	U-HH	
Krueger	Maximilian	U-HH	
Kueck	Niel	U-HH	
Dehghani	Golem Ali	U-HH	
Heinbockel	Raphaela	U-HH	
Netzeband	Geza	U-HH	
Norabuena	Edmundo	GI Peru	

MGD	=	GEOMAR, Marine Geodynamik
MUG	=	GEOMAR, Umweltgeologie
GFZ	=	Geo Forschungszentrum Potsdam
GIP	=	Geophysical Institute of Peru
KUM	=	Umwelt und Meerestechnik Kiel GmbH
U-HH	=	Universität Hamburg, Institut für Geophysik

2.1.2 Scientists – Leg SO146-2

Bialas	Joerg	MGD,	Co-Cchief Scientist
Kukowski	Nina	GFZ,	Co-Cchief Scientist
Letz	Horst	MGD	
Hampel	Andrea	MGD	
Huhn	Katrin	GFZ	
Klaeschen	Dirk	MGD	
Leythaeuser	Thomas	MGD	
Harris	Abd	MGD	
Haase	Eric	MGD	
Greinert	Jens	MUG	
Nadler	Thomas	MUG	
Noeske	Karl	A-Z	
Huebscher	Christian	U-HH	
Herber	Rolf	U-HH	

Coman	Radu	U-HH
Herold	Christian	U-HH
Dehghani	Golem Ali	U-HH
Heinbockel	Raphaela	U-HH
Rechlin	Aissa	U-HH
Pecher	Ingo	UTIG
Kaul	Norbert	UHB
Harris	Robert	RSMAS
Heesemann	Bernd	UHB

A-Z	=	A bis Z Ingenieurs Dienstleistungen GmbH
MGD	=	GEOMAR, Marine Geodynamik
MUG	=	GEOMAR, Umweltgeologie
GFZ	=	Geo Forschungszentrum Potsdam
U-HH	=	Universität Hamburg, Institut für Geophysik
UHB	=	Universität Bremen, Sektion Geowissenschaften
UTIG	=	University of Texas, Institute for Geophysics
RSMAS	=	Rosenstiel School of Marine & Atmospheric Science, Miami

2.2 Crew

2.2.1 Crew – Leg SO146-1

Henning Papenhagen	Master
Roland Priebe	Chief Officer
Walter Baschek	1st Officer
Wolfgang Köthe	Radio Officer
Inga v. Sydow	Surgeon
Uwe Thaysen	Chief Engineer
Eberhard G. Bochnik	2nd Engineer
Werner Guzmán Navarrete	2nd Engineer
Thorsten Damman	Electrician
Kurt Stammer	Chief Electronic Engineer
Rainer Duthel	Electronic Engineer
Jens Grigel	System Operator
Andreas Klein	System Operator
Peter Schymatzek	Fitter
Heinrich Riedler	Motorman
Hans Bethge	Motorman
Herrmann Rademacher	Motorman
Frank Sebastian	Motorman
Klaus Hermann	Chief Cook
Volkhard Falk	2nd Cook
Johann Bronn	Chief Steward
Justine Hasler	2nd Steward
Werner Mueller	2nd Steward
Winfried Jahns	Boatswain
Karsten Bosselmann	A. B.
Norbert Kraeft	A. B.

Erhard Kähler	A. B.
Eugenius Dracopoulos	A. B.
Torsten Bierstedt	A. B.
Stefan Tamm	A. B.

2.2.2 Crew – Leg SO146-2

Henning Papenhagen	Master
Axel Bendien	Chief Officer
Walter Baschek	1st Officer
Wolfgang Köthe	Radio Officer
Inga v. Sydow	Surgeon
Uwe Thaysen	Chief Engineer
Eberhard G. Bochnik	2nd Engineer
Werner Guzmán Navarrete	2nd Engineer
Rolf Konrath	Electrician
Kurt Stammer	Chief Electronic Engineer
Rainer Duthel	Electronic Engineer
Jens Grigel	System Operator
Andreas Klein	System Operator
Peter Schymatzek	Fitter
Heinrich Riedler	Motorman
Hans Bethge	Motorman
Frank Sebastian	Motorman
Klaus Hermann	Chief Cook
Volkhard Falk	2nd Cook
Johann Bronn	Chief Steward
Andreas Wege	2nd Steward
Werner Mueller	2nd Steward
Joachim Mischker	Boatswain
Karsten Bosselmann	A. B.
Reiner Kaiser	A. B.
Erhard Kähler	A. B.
Eugenius Dracopoulos	A. B.
Torsten Bierstedt	A. B.
Stefan Tamm	A. B.

2.3 Addresses of Participating Institutions

GEOMAR: GEOMAR
Forschungszentrum für
marine Geowissenschaften der
Christian-Albrechts-Universität zu Kiel
Wischhofstraße 1-3
24148 Kiel
Germany
Tel.: 0049 - 431 - 600 - 2972
Fax: 0049 - 431 - 600 – 2922
e-mail: jbialas@geomar.de

A-Z: A bis Z Ingenieurs Dienstleistungen GmbH
Wischhofstr. 1-3
D-24148 Kiel
Germany
Tel.: 0049-431-721115
Fax: 0049-431-721256
e-mail: abisz@t-online.de

GFZ: Geo Forschungszentrum Potsdam
Telegrafenberg
D-14473 Potsdam
Germany
Tel.: 0049-331-288-1318
Fax: 0049-331-288-1370
e-mail: nina@gfz-potsdam.de

KUM: K.U.M.
Umwelt- und Meerestechnik Kiel Gmbh
Wischhofstr. 1-3, Geb. D5
24148 Kiel
Germany
Tel.: 0049 – 431 – 7209 – 220
Fax: 0049 – 431 – 7209 – 244
e-mail: KUM.Umweltmeerestechnik@t-online.de

UHB: Universitaet Bremen
Sektion Geowissenschaften
Klagenfurter Str.
D-28334 Bremen
Tel.: 0049-421-218-4511
Fax: 0049-421-218-7163
e-mail: vill@uni-bremen.de

U-HH: Universitaet Hamburg
Institut für Geophysik
Bundesstr. 55
D-20146 Hamburg
Germany
Tel.: 0049-40-42838-5184
Fax: 0049-40-42838-5441
e-mail: huebscher@dkrz.de

UTIG University of Texas
Institute for Geophysics
4412 Spicewood Spring Rd., Building 600
Austin, Texas 78759-8500
USA
Tel.: 001-512-471-0480
Fax: 001-512-471-8844
e-mail: ingo@ig.utexas.edu

RSMAS: University of Utah
Dept. of Geology & Geophysics
Rosenstiel School of Mines
Salt Lake City
Utah, 84102
USA
Tel.: 001-801-587-9366
Fax: 001-801-581-7065
e-mail: rmharris@mines.utah.edu

3. Agenda of the cruise SO146 GEOPECO

(N. Kukowski, J. Bialas)

Week March 01 to 07, 2000

After all scientific equipment which the participating groups brought with them was unpacked and installed, and land calibration for marine gravity measurements was finished, the R/V SONNE, with 20 scientists onboard, left the harbour of Arica on the evening of March 2, 2000 to transit to Peruvian waters to undertake multidisciplinary geophysical investigations of this complex subduction zone over the following two months. While heading towards the southernmost working area, the release systems for the OBH/S were tested on March 3, 2000. A measurement of the physical properties of the water column (CTD) was made down to depths of more than 5000m in the deep sea trench on March 4, 2000, to obtain a water sound-velocity profile for the bathymetry and a temperature profile. Afterwards, several profiles with Hydrosweep (swath bathymetry) and Parasound (3.5 kHz echo sounding) were acquired to map the morphology of Nazca Ridge and the internal structure of shallow sediments. Significant deformation was observed on the south-eastern flank of the ridge. This aseismic ridge, which is subducting at 15° S, has received little attention, however, it has a large influence on the geodynamic evolution of the Peruvian continental margin. We deployed 3 OBS and 6 OBH and shot a wide angle profile across Nazca Ridge with two 32l Bolt-Airguns between March 4 and 6, 2000. This line was also recorded with a 40m active length multichannel streamer, a gradiometer, as well as the gravimeter and Hydrosweep/Parasound, the latter three of which have been continuously recorded during the entire cruise. All OBH/S of the first profile were recovered successfully and recorded data. One instrument was left behind which marked the crosspoint for another profile along the crest of Nazca Ridge, and across the continental slope. All other instruments recorded data without any problems.

Between March 7 and 8, 2000, a profile with 10 OBH and 4 OBS was shot along the crest of the Nazca Ridge and across the continental slope with 3 32l Bolt-Airguns. When shooting began, the Peruvian coastguard observed us with interest and gave us their best wishes for our research.

Week March 08 to 14, 2000

On the afternoon of March 8th, after we finished shooting the wide angle profile along the crest of Nazca Ridge and across the continental slope with all three 32l Bolt-Airguns, the instruments that had been deployed on the ridge were successfully recovered while bathymetric mapping was performed. At the south-east flank of Nazca Ridge, a 46 nm x 27 nm large area was completely covered. Several elongated to nearly circular topographic highs were clearly identified, and are probably of volcanic origin. Thereafter, part of the profile across the continental slope was shot again with the GI-guns to image sediment structures at higher resolution. The remaining OBH/S were also successfully recovered.

From March 11th to March 14th we shot the third wide angle profile at about 13°S using all three Bolt-Airguns with 10 OBH and 4 OBS asymmetrically distributed over the slope. During this profile, we again also used one active segment of the streamer, now located at the rear of the guns, and the gradiometer.

Again with this profile, the GI-guns were used to shoot the landward section which crosses the southernmost part of Lima on the upper slope, and further on, another profile was shot oblique to the former profile for a better look at the structural evolution of the basin. Again, all deployed OBH/S were recovered without problems and the data obtained provided good coverage and constraints for modelling.

Week March 15 to 21, 2000

During our trip in the northern working area in the vicinity of the Lima Basin three OBS and 2 OBH were set out in a cross pattern with 20 nm axes to observe natural seismicity over an extended period of time. Thereafter, a TV-Grab station was conducted in our northernmost working area on the continental shelf in water depths greater than 3000 meters on the evening of March 17, 2000. Video observations, during the search for the most appropriate locality, showed numerous occurrences of living colonies of vent organisms. The successful grab-sampling deployment brought up three species of bivalves that included two species of Calyptogena, consolidated sediment with carbonate crusts, and also the sought-after fine structured barite crusts.

Another region, between 8° 10' S and 9° covering an area of 25 nm by 50 nm, was surveyed with Hydrosweep and Parasound. As suggested by a previous transit, this area proved to have a highly variable morphology, so very large overlap sections were chosen. The mapped region lies directly south and connects with another area which was bathymetrically surveyed by French scientists in 1986.

On the evening of March 19, 2000, we set out nine instruments at 8° 30' S in a 103 nm long OBH/S profile over the continental shelf and extends seaward to the undisturbed oceanic crust of the Nazca plate. This line was then shot with all three 321 Bolt-Airguns. The gradiometer and streamer were also deployed. Five of the instruments were later recovered during the landward trip. Four more were still recording on the ocean floor during the subsequent seismic reflection survey of the entire Yaquina Basin with the GI-Guns, which started on the evening of March 21, 2000.

As with the previous profiles, the retrieved OBH's placed on the oceanic plate show that the data quality is excellent and extends over the entire profile.

Week March 22 to 28, 2000

Shooting of this reflection seismic survey again with simultaneous recordings of Parasound, Hydrosweep, gravimeter and gradiometer continued until the evening of March, 25, 2000. Afterwards, the 4 OBH/S which had been left on the ocean floor from the previous wide angle seismic profile were recovered. On 26 March 2000 we traveled back to the Lima Basin utilizing the transit to perform bathymetric surveying.

In the late evening of the same day, we began to successfully recover the instruments set out to observe natural seismicity. The exploration of the structure of the continental margin and it's variability in strike should be followed-up in the Lima Basin area with two crossing wide-angle seismic reflection profiles, as was performed on the Nazca ridge. on the evening of March, 27, 2000, we started deploying all 14 instruments in a 120 nm long profile over the undisturbed oceanic plate, oceanic trench and the continental shelf. Shooting began in the morning of March, 28, 2000 .

Week March 29 to April 4, 2000

Shooting over the whole length of the profile with the three 321 Bolt-Airguns was finished March 29, 2000, at 11 hours UTC. The streamer and gradiometer were also deployed while shooting. During recovery of the instruments, one OBS failed to rise from the ocean floor. However, it answered multiple attempts to release and a good estimate of it's position was ascertained. Therefore, while setting out instruments for the sixth wide-angle profile which runs parallel to the strike of the continental margin, the TV-grab was deployed to search for the missing OBS. It was spotted three times, but was not grabbed. After shooting the next profiles, we decided to make another recovery effort.

On March 31st we completed the sixth wide-angle profile with three 32 l airguns and gradiometer. Due to wave impact from the side, the streamer needed to be cleared from the towing wires of the airguns. Despite all care, the streamer broke off in the morning hours of March 31st. After a short search the tail

buoy was found, the streamer recovered, and the profile successfully completed. After recovery of all OBH/S systems, the night hours of the 1st to the 2nd of April were used for a second recovery attempt of OBS59 while on the way to Callao. This time the TV grab was expanded with steel bars in order to at least touch the instrument and push it free of it's anchor, even if it didn't appear within the jaws of the grab. Again the OBS was found and, although it was touched, it could not be released from the anchor. Nevertheless, this raised hope for a successful third attempt to follow immediately after departure for the second leg.

The port call from the evening of April 2nd until the morning of April 4th was used to change members of the science crew. There are now 23 scientists representing 8 different working groups onboard R/V SONNE for the second leg. The 3rd of April was used to visit the Geophysical Institute of Peru where Ms. Kukowski gave a talk about the purpose and preliminary results of this cruise. And then in the afternoon, a group of 17 people visited the R/V SONNE. Unfortunately no Peruvian scientist volunteered to participate in the second leg.

After departure on the morning of April 4th, SONNE reached the position of OBS59 in the evening. Through careful maneuvering by the ship's officers and crew, it was possible to locate the OBS, which is less than 1 m in diameter, and in a water depth of 2400 m. This time the extended frame of the TV grab did release the instrument from it's anchor, and OBS59 was recovered without damage.

Week April 5 to 11, 2000

From the 5th to the 6th of April detailed profiling using the OBH/S and multichannel seismics was carried out in the Lima Basin to prepare for placement of the ocean bottom shots (SeeBoSeis). Thanks to the help of the WTD of R/V SONNE, the streamer was available again. 6 OBH and 3 OBS were deployed along a line with a spacing interval of 1 nm. Four profiles were run along the line and in a rectangular pattern using the GI-gun, streamer and gradiometer.

On April 7th R/V SONNE returned to the Yaquina basin area. Heat flow measurements and visual observations with the OFOS camera sled were undertaken along three selected profiles, each approximately 10 nm long. Locations were selected along MCS line 20 with variable BSR appearance. OFOS and heat flow measurement teams interchanged it intervals of about 10 to 12 hours.

For further mapping and detailed observation, a seismic experiment using both the streamer and OBH/S was completed along line 20 on the 10th of April, 2000. Crossing profiles allow for spatial mapping of horizons which included the previous lines from SO146-1. While profiling, two test shots of the SeeBoSeis source were performed successfully to gain experience for the upcoming experiments. Once again, an OBS failed to surface and was recovered using the TV-Grab. Precise maneuvering of the vessel and exact winch operation allowed us to grab the seismometer section of the instrument and haul it to the surface. The anchors were modified as much as possible utilizing the ship's available resources to make sure they will not sink into soft sediment as a consequence.

Week April 12 to 18,

On the 13th of April, we shot a reflection seismic line using the streamer and GI-guns over the oceanic plate to extend the wide angle line we had shot on the first leg. Until April, 16th, we acquired additional Hydrosweep and Parasound profiles to extend the mapping of the trench area and oceanic crust approaching the trench and to establish connection to the existing old French swath data sets.

On April 17th we returned to Lima basin and the first SeeBoSeis experiment was set in place. With anticipation of the expected high frequency signals, as well as in preparation for the slow 200 m/s surface waves, 9 OBH and 4 OBS were deployed in water depths of about 2000 m with offsets of only 300m. Closer offset distances would have been desirable, but could not be achieved for safely, due to the observed drifts of the instruments. However, to compensate for this, the offsets of the SeeBoSeis shots

were reduced to 100 m. After waiting for the time window of the preprogrammed shots to expire, the GI-gun and streamer were used to shoot crosswise above OBH/S positions, enabling more accurate relocation of the instrument's bottom positions.

For this purpose, 14 seismic profiles with connecting lines were shot within an area of 2 x 2 nm. All bottom sources which included glass spheres and metal tubes using either plunger or shotgun ammunition as firing mechanisms were successfully released.

After the first SeeBoSeis experiment, several tracks of observations of the sea floor with OFOS and heat flow measurements were undertaken on April, 18th again during alternating 10-12 hour intervals. Due to the hard sea floor conditions, the heat flow probe did not penetrate the bottom at all locations.

Week April 19 to 25, 2000

To complete the stratigraphic comparison with our profiles across the Lima basin, another 150 nm of reflection seismic lines were shot from April, 19th to 20th across the existing HIG lines.

Finally, on April, 21st, the second SeeBoSeis experiment was executed, south of the first one and along the same reflection seismic line at a location where a strong BSR is present This experiment was just as successful as the first one. Unfortunately, OBS119 did not return to the surface despite the fact that all commands were acknowledged. Although it should not become routine, the TV-grab was prepared again.

After finishing the SEEBOSEIS experiment, we did another reflection seismic experiment with 150 km profiling at the lower slope for which we also deployed four OBH for velocity information on April, 22th. After completion of the reflection seismic lines and successful recovery of the four OBHs, the TV-grab again was successfully used to recover OBS119.

On the 24th of April heatflow measurements along the seismics line 75 and TV observations were made. Before heading to Callao, we acquired some more Hydrosweep tracks to supplement our map.

Week April 26 to May 3, 2000

In the morning of April 26th, RV Sonne arrived at Callao to unload a container dedicated to another cruise. 2,5 hours later, the RV Sonne began the transit to Talcahuano with continuous registration of gravity and bathymetry. When we passed our first working area, the Nazca Ridge, some Hydrosweep profiles supplementing the survey begun on the first leg were acquired on April 27th. After 7 days of transit, Sonne arrived at Talcahuano on May 3rd, at 14:00.

4. Scientific equipment

4.1 Shipboard equipment

4.1.1 HYDROSWEEP

(J. Bohnert, K. Huhn)

Onboard the R/V SONNE, the swathmapping system HYDROSWEEP ("HYDROgraphic multi-beam SWEEPing survey echosounder", Atlas Elektronik GmbH, Bremen) was used for continuous recording of bathymetric data.

The input amplifier is situated perpendicular to the longitudinal axis of the ship. The swath produced by the HYDROSWEEP system has a look-angle of 90° and consists of 59 individual acoustic beams with a working frequency of 15.5 kHz. The resulting observation width is roughly equal to twice the water depth. Range of the central beam is up to 10,000 m with an error of 1% and for the outer beams up to 7,000 m. Precision is about 1% if roll is less than 10° and heave is less than about 5°. Corrections for roll, pitch, and heave are automatically applied. Due to the fixed angle between beams, resolution is dependent upon the water depth and varies from about 170 m to 200 m in water depths of 5,000 m to 6,000 m.

There are three methods to deal with water sound velocity and its variation with depth: i) it can be calculated during data acquisition by means of a mechanism of optimal self-calibration (Grant and Schreiber, 1990), or, ii), a constant average velocity may be assumed, or, iii), a water sound velocity depth profile obtained from a CTD (Conductivity-Depth-Temperature) instrument can be transferred to a step function with up to 20 discrete values and input to the system. Data (location, time, and water depth) are continuously written to magnetic tapes and can also be plotted as isoline charts during acquisition.

To calculate depths from echo time delays, the velocity of sound in the different waterlayers must be known. HYDROSWEEP uses a second set of transducers and a calibration scheme with soundings along track to determine an average water sound velocity profile (Schreiber & Schencke, 1990). As in certain areas, e.g. at steep slopes, this algorithm fails (c.f. Flueh and von Huene, 1994), direct measurement of sound velocity at different depths using a CTD is required.

4.1.2 PARASOUND

(C. Hübscher)

The PARASOUND system works both as a low-frequency sediment echosounder and as a high-frequency narrow beam sounder to determine the water depth. It utilizes the parametric effect, which produces additional frequencies through nonlinear acoustic interaction of finite amplitude waves. If two sound waves of similar frequencies (here 18 kHz and e.g. 22 kHz) are emitted simultaneously, a signal of the difference frequency (e.g. 4 kHz) is generated for sufficiently high primary amplitudes. The new component travels within the emission cone of the original high frequency waves, which are limited to an angle of only 4° for the equipment used. Therefore, the footprint size of 7% of the water depth is much smaller than for conventional systems and both vertical and lateral resolution are significantly improved.

The PARASOUND system is permanently installed on the ship. The hull-mounted transducer array has 128 elements within an area of ~ 1 m^2. It requires up to 70 kW of electric power due to the low degree of efficiency of the parametric effect. In 2 electronic cabinets, beam formation, signal

generation and the separation of the primary (18, 22 kHz) and secondary frequencies (4 kHz) is carried out. Using the third electronic cabinet located in the echosounder control room, the system is operated on a 24 hour watch schedule.

Since the two-way travel time in the deep sea is long compared to the length of the reception window of up to 266 ms, the PARASOUND System sends out a burst of pulses at 400 ms intervals, until the first echo returns. The coverage in this discontinuous mode is dependent on the water depth and also produces non-equidistant shot distances between bursts.

The main tasks of the operators are system and quality control and to adjust the start of the reception window. Because of the limited penetration of the echosounding signal into the sediment, only a short time window close to the sea floor is recorded.

In addition to the analog recording features with the b/w DESO 25 device, the PARASOUND System is equipped with the digital data acquisition system ParaDigMA, developed at the University of Bremen. The data is stored on removable hard disks using the standard, industry-compatible SEGY-format. The 486-processor based PC allows for buffering, transfer and storage of the digital seismograms at very high repetition rates. Of the emitted series of pulses, usually only every second pulse can be digitized and stored, resulting in recording intervals of 800 ms for a given pulse sequence. The seismograms were sampled at a frequency of 40 kHz, with a typical registration length of 266 ms for a depth window of ~200 m. The source signal was a band limited, 2-6 kHz sinusoidal wavelet with a dominant frequency of 4 kHz and duration of 1 period (~250 µs total length). Data was stored on DAT-tapes using Windows NT backup software.

During the entire cruise the combined PARASOUND/ParaDigMa system worked without significant problems. From time to time the tape drives had to be cleaned. Due to some problems with the ship's own data distribution network, no navigation data was written in the header of the PARASOUND data during certain time intervals.

4.1.3 Navigation

(J. Bialas)

A crucial prerequisite for all kinds of marine surveys is the precise knowledge of position information (latitude, longitude, altitude above/below a reference level). Since 1993 the global positioning system (GPS) is commercially available and widely used for marine surveys. It operates 24 satellites in synchronous orbits, thus at least 3 satellites are visible anywhere at any moment (Seeber, 1996). The full precision of this originally military service yields positioning accuracies of a few meters, yet this is restricted to military forces and usually unaccesible to commercial users (Blondel and Murton, 1997). For civilian purposes the precision is in the order of 100 meters.

The resolution of GPS can be enhanced with the Differential GPS (D-GPS) scheme (Blondel and Murton, 1997, Knickmeyer, 1996). Using several reference stations the determination of the ship's position can be corrected in real time and enhanced to a 1 m to 5 m accuracy. Since the cruise SO-109 (1996) D-GPS service is available onboard R/V SONNE. The ships ASHTEC system provides a validated accuracy better than 5 - 10 m in the area of the GEOPECO investigations.

D-GPS values were available from the ships navigation data base and could be extracted by a PC based end user interface program. Out of all ships sensor values the user could select the wanted variables and specify the output in various formats. The amount of data could be controled by the desired interval of extracted values which could be as short as one second. Stored on the "wiss-data" directory the extracted ASCII file was accessable from every workstation connected to the shipboard

network via ftp or volume access. Surprizingly the output data format writes decimal values separated by a colon instead of the standard american dot notation. According to information of the ships operator this is due to the choosen set up of the desktop program on the PC. Therefore a reformating program must be written prior to further computaional use of the values.

During preparing discussion it turned out that the coordinates stored within the data base were provided by the *Atlas ANP 2000* system which does not copy the exact GPS time values but adds time stamps of its internal uncontrolled clock to the high precision coordinates of the DGPS system. Accuracy of the time values is mainly dependend on the operators skills by manually setting the ANP clock to GPS time. A somewhat conservative method compared to the efforts of precise positioning. To enable the most accurate GPS related time stamps within the ANP system prior to each seismic survey the system operates were informed to reset the ANP.

This time the GEOMAR routines were applied to high resolution seismics with shot intervals of 8 to 10 s the first time. Due to the short interval coordinate interpolation with adjustment of source position with respect to antenna distance turned out to be sensitive to small variations of ships heading between two navigation samples taken every 5 seconds. In order to smooth navigation processing for this we decide to reduce the navigation sampling to every 20 seconds which provide an acceptable compromize this time. For future cruises the navigation routines need to be modified taking into account this small scale applications. Standard wide angle profiling will need a coordinate sample every 30 second and therefore not be sensible for short term heading variations due to balance ships course along the general azimuth of the line.

4.1.4 Geological sampling by TV-Grab (TVG)

(S. Bollwerk)

The TV-guided grab sampler (TVG; PREUSSAG) aboard RV SONNE is capable of sampling an area of 1,82 m^2 (1.06 x 1.72 m) by 40 cm deep and supplying a nearly undisturbed sediment profile in the center of the grab. The TVG is equipped with two video cameras (b/w SIMRAD CCD OE 1390/1391; color, DEEPSEA POWER LIGHT MicroSeacam 1001) and four lamps (REMOTE OCEAN SYSTEM, 4 x 150 W), allowing the surface operator to guide the instrument to a specific sample location along a track. Observations are recorded continuously on videotapes. It is possible to decide immediately after the grab was dropped whether or not the sampling attempt was successful by viewing the sample within the jaws. If unsuccessful, the TVG can be re-opened, discarding the contents of the jaw, and be repositioned for another attempt. The tool is lowered from the ship, deployed on the ocean bottom, and provides continuous visual observation by adjusting the winch to the appropriate height. The TVG is closed by hydraulic pressure (180 bar) with power supplied from batteries. This energy supply allows the TVG to be closed and re-opened up to 6 times. In addition the TVG is equipped with an SSBL system (SIMRAD HPR 507) to calculate the position of the grab at the bottom.

4.1.5. Ocean floor observations by OFOS

(J. Greinert, supported by R. Duthel, K. Stammer, Inga v. Sydow)

Equipment and general handling
The OFOS-sled (Ocean Floor Observation System) on board RV SONNE is equipped with two video cameras (b/w, SIMRAD CCD OE 1390/1391; color, DEEPSEA POWER LIGHT MicroSeacam 1001) and four lamps (DEEPSEA POWER LIGHT, 2 x 200 W, 2 x 150 W) for on-line observations. The video signals are recorded continuously on videotapes. Two still cameras to take images on slides (2 x KONGSBERG SIMRAD PhotoSea 5000) are mounted using two flashes (2 x BENTHOS 383 RH 600 W)

for additional light. Pictures can be taken manually on request from board or in fixed time intervals (here we used 30, 45 or 60 second intervals). The time intervals enable a statistical investigation of observed features. The still cameras were loaded with 30.5m slide films (KODAK Ektachrome, 200 ASA,), providing a capacity of 800 images. Three laser spots (DEEPSEA POWER LIGHT Micro SeaLaser) point downward in a distance of 20 cm as scale at the bottom. All videos and slides will be stored at GEOMAR and can be copied on request.

Depending on the distance to the bottom (between 1.5 and 4 m) a sector of about 12 square meter is visible; the distance is manually adjusted with the winch using a bottom-weight 1.7m below the sled as marker. In addition this weight is equipped with a thermometer (PT 100) measuring the temperature just above the bottom. Power is supplied from the ship via the cable which is also used for the video-transmission and on-line data transfer from a Seabird 19 memory CTD. The bottom position of the OFOS was calculated using the SSBL system (SIMRAD HPR 507) on board the RV SONNE. A compass (VECTOR 2X) gives the heading of the sled and the orientation of the top of the video image. The tow speed of the OFOS sled was between 0.4 and 1 knot (mean 0.7).

During two OFOS deployments an OBH was mounted on the sled to 'hear the sound of the deep sea', unfortunately, with little success.

Slide development and camera adjustment

To verify the quality of the slide exposures about 40 slides of each film were developed during the cruise (KODAK E6, HobbyPac) while the remainder will be developed in a professional laboratory on land. For the required constant temperature for the chemical solutions we used the water supply in the photo lab for a warm water bath of 30°C. Slides from OFOS 1 and 2 were developed as normal exposures, but they were much to dark due to the camera aperture (between 5.6 and 8) and the distance to the bottom (around 2.5m). To compensate, the test portions from OFOS 3-1 and 3-3 where developed by push-processing for 3 apertures pushed (longer first-developer times) giving slightly better results for the same camera adjustments but show to bright and unreadable 'red' time indices on the slides (only one filter was used). We obtained better results trying different apertures (5.6; 5.6-4; 4) as well as two and three filters for the time indices, but in general the two flashes used seem not to be powerful enough to illuminate the seafloor if the OFOS is not close enough to the bottom (< 1.7m = distance of the bottom-weight). Best results were obtained using a camera aperture between 5.6 and 4, 1.7 m distance to the bottom, tow filters for the time indices and a E6 development with 2 apertures pushed.

CTD data

CTD data from the SEABIRD 19 can be observed in real time during the track. Depth, temperature and conductivity are shown. We suggest the salinity would be more useful than the conductivity but this could not be changed during SO146. Because of problems with the pump for the conductivity sensor no correct conductivity data exists for the OFOS tracks before OFOS 4-1. Unfortunately, the hexadecimal raw data from the CTD can be not stored in the ship's database, thus making later calculations (e.g. the sound velocity or average calculations) more complicated than the use of the SEABIRD software. Therefore, we used a laptop which was directly connected to the CTD output at the OFOS decks-unit storing the raw date using the SEABIRD 'Seasave' software (OFOS 4-1; 4-2; 4-3; 5-1; 5-2). During OFOS 6-1 the memory-unit of the SEABIRD 19 was used to store the data. The data can be retrieved with the 'Term 19' application of the SEABIRD software.

OFOS protocols and Ships data

Seafloor observation protocols were written on-line in a VisualBasic modified EXCEL spreadsheet on a laptop. This computer also serves as a 'navigational' computer using WINGPS (shareware: http://ourworld.compuserve.com/hompages/wingps) for track planing and for on-line visualization of the ship's position above a bathymetric map. The VTG, GLL and GGA protocol were taken from the ship's GPS system. Data of the ship's movement as well as the SSBL OFOS-positions were selected and retrieved from the RV SONNE database.

4.1.6 Flare Imaging: Free gas emissions in the water column

(J. Greinert, supported by R. Duthel, K. Stammer)

Hydroacoustic observations at the Sakhalin Shelf (Sea of Okhotsk) and Hydrate Ridge (Oregon accretionary prism) have shown flare-like acoustic features in the water column which are rooted at the bottom. These backscattering features are induced by gas bubbles which are expulsed at the seafloor. Possible sources are free gas from below the BSR which migrate along faults through the sediment column or gas from decomposing gas hydrate closer to the sediment surface induced by upward migrating warmer fluids. To test the possibility of storing the 18 kHz pilot signal of the Parasound system in form of digital data the DESO 25 unit was manipulated during SO146-2, using the analog signal from the channel one interface (AZ 1027 G 430). Here, the contacts AC16 (signal) and AC2 (ground) can be used for signal output. Contact B13 from the AZ 1027 G 404 interface was used for the trigger signal. Both signals were amplified and the trigger signal was aditionally convertet to a RS232 seriel port in case it was needed (Fig. 4.1.6.1).

We used the amplifed signals as input for an ordinary soundcard. Preliminary results with the data acquisition tool from the MATLAB software show that the 18kHz signal can be recorded in general without disturbing the ParaDigMa system. Unfortunately, the development of usable software for on-line visualization of the signal and digital storage of the data could not be completed in time.

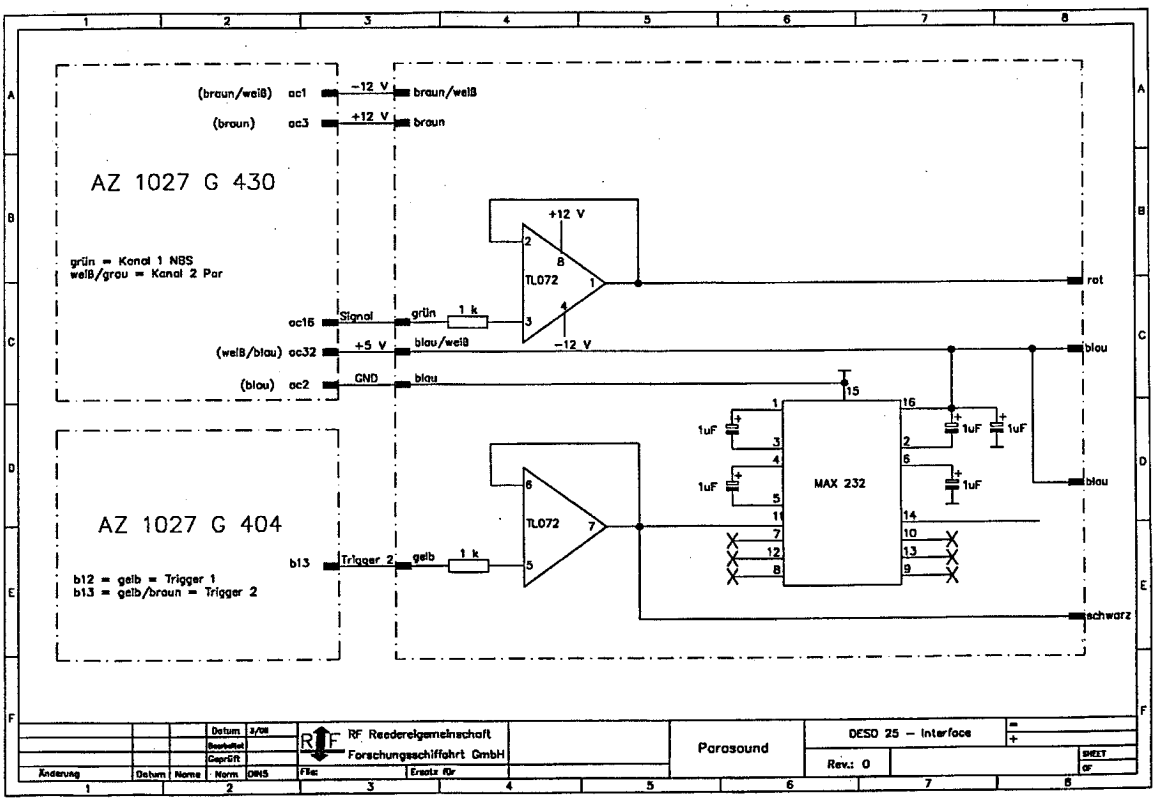

Fig. 4.1.6.1: Modification of the DESO 25 unit for the output of the 18 kHz analog signal from the Parasound system by K. Stammer.

4.1.7 CTDs

(J. Greinert)

To obtain accurate sound velocity profiles needed for the bathymetric mapping and for calibrating the Heat-Flow equipment we used the SEABIRD CTD 911 plus on board of RV SONNE which is additionally equipped with an oxygen sensor. Date collecting and post processing was done with the SEABIRD software. Down and up cast were stored separately. Winch speed was 0.8 m/s. All data will be stored as SEABIRD raw data file and ASCII file at GEOMAR.

4.2 Computer facilities

(J. Bialas)

The experiments and investigations during SO146 required special computing facilities in addition to the existing shipboard systems. For programming of ocean bottom stations, processing of seismic data and analysis of hydrosweep recordings several workstations were installed from the groups.

University of Texas, Austin installed a Sun Sparc-5 with 128 MB memory and 2 GB disk space. This unit was mainly used for high resolution processing and interpretation of OBH/S data. To enable data exchange with GEOMAR on short term basis this Sun was integrated into the GEOMAR workstation cluster.

University of Hamburg installed several PC based computing systems mainly dedicated to data recording purposes. These equipment is described within the chapters 4.5 and 4.6.

Due to the large amount of data transfer GEOMAR installed a workstation cluster onboard comprising the following systems:

1	"neolithikum"	SUN Sparc 20	2 CPU, 256 MB memory	14 GB disks, DAT, Exabyte, CD	Sun Solaris 2.5
2	"devonia"	SUN Ultra 60	2 CPU 1 GB memory	112 GB disks, 2.3 GB MO, 2x DAT, 2x Exabyte	Sun Solaris 2.6
3	"avalonia"	SUN Sparc 5	1 CPU, 64 MB memory	13 GB disks, DAT, CD, Methusalem	Sun Solaris 2.5
4	"galicia"	SUN Sparc 10	1 CPU, 96 MB memory	12 GB disks, DAT, Methusalem	SunOS 4.1.4
6	"MBS"	Pentium II 350 MHz	1 CPU, 128 MB memory	9 GB disks, 3x PCMCIA	Windows95

For seismic modelling two desktop Macintosh computers were installed:

1 PowerMacintosh G3/300 MHz

2 PowerMacintosh 7100/66

In addition to these computers, two X-Windows-Terminal NCD-15r and several laptops/powerbooks were used.

For plotting and printing two HP Postscript Laserprinters (papersize A3 and A4), one OYO-11"-thermoplotter, as well as the shipboard color plotters were available.

The workstation cluster was placed in the Reinlabor where it was set up according to a "client-server" model, with "neolithikum" being the server. The Macintosh computers were located in the Chemie-Naßlabor where they were connected to the ships network. All important file systems from the main server at GEOMAR were duplicated onto the "neolithikum"-disks. Using NFS-, NIS-, and automounter services the computing environment was identical to that at GEOMAR so every user found his/her familiar user interface. The convenience of network mounted file systems has to be paid for with a heavy network load, particularly during playback of OBH-data from tape to disk (c.f. SO123 cruise report, Flueh et al., 1997). This required a high-performance network, which was accomplished by a switched twisted-pair ethernet. A 12-port ethernet switching-hub (3COM-SuperstackII 1000) with an uplink connection of 100 Mbps to the server "neolithikum" and dedicated 10 Mbps ports for the client workstations maintained the necessary network performance. In order to keep the shipboard network undisturbed by the workstation cluster, but to allow for communication between them, the server "neolithikum" was equipped with two network interfaces and served as a router. This provided the additional benefit of a simplified network configuration. Considerable setup work was dedicated to "neolithikum", while the other workstations used the same IP-addresses and network configuration as at GEOMAR.

This network setup showed a reliable and stable performance, and no breakdowns were observed. The Macintosh computers could not access to the ships printers but with an additional network connection between ships hub and GEOMAR's switch neolithikum could be bypassed and access was possible to the GEOMAR network printers. Remote installation of the X-screens failed as they had problems loading their software across the ships network. Network perfomance tests of the ships system operators showed that all computers within the ships network could be contacted without package loss. Contacting the GEOMAR network causes severe loss of data packages and therefore reduces reply times severely. This was probably the reason for the boot failure of the X-screens. Therefore they were setup wihtin the Reinlabor and the neighbouring magnetic lab. For the unit in the magnetic lab a flying patch cable was installed as there are no cable canals available between Reinlabor and magnetic lab for safety reasons. Due to the heavy load of four workstations, one PC and a X-screen the air condition in the Reinlabor (which was not designed for such use) was not able to sufficently cool the room. Temperatures up to 27.8 °C were measured when the ships technician installed a mobile thermometer. As this set up of installation will be necessary on future cruises a mobile air condition system seems to be necessary as severe damage to the computer system caused by heating could no longer be excluded.

4.3 The GEOMAR Ocean Bottom Hydrophone / Seismometer (OBH/S)

(J. Bialas)

The Ocean Bottom Hydrophone

The first GEOMAR Ocean Bottom Hydrophone was built in 1991 and tested at sea in January 1992. A total of 10 OBH and 4 OBS instruments were available for SO146. This type of instrument has proved to have a high reliability; in fact during GEOPECO cruise the 1300th successful deployment was achived. Altogether 127 sites were occupied during the SO146 cruise.

The principle design of the instrument is shown in Figure 4.3.1, and a photograph showing the instrument upon deployment can be seen in Figure 4.3.2. The design is described in detail by Flueh and Bialas (1996).

The system components are mounted on a steel pipe which holds the buoyancy body on its top. The buoyancy is made of syntactic foam and is rated, as are all other components of the system, for a water depth of 6000 m, except for the pressure cylinders holding the recording electronics. Here, various models are available for variable depths (2500 m, 3000 m, and 6000 m). Attached to the buoyant body are a radio beacon, a flash light, a flag and a swimming line for retrieving from aboard the vessel. The hydrophone for the acoustic release is also mounted here. The release transponder is a model *RT661CE* made by *MORS Technology*. Communication with the instrument is possible through the ship's transducer system, and even at maximum speed and ranges of 4 to 5 miles release and range commands are successful. For anchors, we use pieces of railway tracks weighing about 40 kg each. The anchors are suspended 2 to 3 m below the instrument. The sensor is an *E-2PD* hydrophone from *OAS Inc.*, and the recording device is a *MBS recorder of SEND GmbH*, which is contained in its own pressure tube and mounted below the buoyant body opposite the release transponder (see Figures 4.3.1 and 4.3.2).

The Ocean Bottom Seismometer

The Ocean Bottom Seismometer (OBS) construction (Bialas and Flueh, 1999; Fig. 4.3.3) is based on the experiences with the GEOMAR OBH. For system compatibility the acoustic release, pressure tubes, and the hydrophone are identical to those used for the OBH. Syntactic foam was used as floatation again but of larger diameter due to the increased payload. In contrast to the OBH the OBS has three legs around a center post to which the anchor weight is attached (Fig. 4.3.4). While the OBH is floating about 1 m above the sea bottom, the OBS is positioned on the sea bottom to avoid collisions between the the seismometer cable and the anchor. The sensible seismometer is deployed about 1 m to the side of the system once the OBS lands on the sea floor. During descent to the ocean bottom, the footplate of the seismometer release lever is about one meter below the base of the anchor and therefore hits the seafloor first. At touch down the baseplate forces an upward movement of the lever which lays out the seismometer hook until the seismometer anchor is about 0.5 m above the seafloor. At about 45 degrees to the vertical the seismometer is released from its hook and falls to the sea floor from about 1 m height, ensuring coupling between the seismometer and the sea floor. At this time the only connection from the seismometer to the instrument is a cable and an attached wire which retracts the seismometer during ascent to the sea surface. All three channels are preamplified within the seismometer housing and recorded by the standard Methusalem recorder as used in the OBH units. Parallel to these three channels the standard hydrophone is recorded on the fourth channel. An oscillation or electrical current to the instrument is therefore not transmitted mechanically to the seismometer.

During this cruise three OBS instruments failed to rise to the surface after the release comand was given. This is the first occurrence of this type of OBS instrument not releasing. As all comands were replied to with a clear response and battery status as well as vertical orientation of the instrument were

fine, no technical error could be found. With continuous distance measurement the bottom position could be confirmed within a square of 100 * 100 m. Fortunately the TV-grab was availabe and could be used for recovery operations. For this purpose an additional frame of steel bars was mounted to the grab in order to be able to push the instruement from its anchor even if the OBS instrument does not appear directly under the grab. After several trials three chains were added at the corners of the frame with connecting ropes at their ends. Due to precise maneuvering and careful winch control the ships crew were able to recover lost instrument all three times. Recovery includes looking for an instrument less than 1 m in diameter using a 2 * 2 m wide view of the video camera mounted in the grab and lowered down to the 2500 m deep ocean floor. During the short video sequences when the system came into sight it was obvious, in the first two cases, that the anchor was stuck in the thick water saturated sequence of youngest sediment. Therfore the end plates of release and recording tube sunk into the mud as well. The release hook did not fall upon release command and the remaining buoyancy was not strong enough to pull the instrument out of the sea floor. For this purpose 20 * 20 cm wide wood plates were attached to the end of the tri-star shaped anchors to increase the dimension of the foot print while still avoiding the potential for system glide during descent in the water column. These small plates seemed to help on the next line. The third failure was caused by a misalignment of anchor and legs of the system carrier. When the OBS came into sight it was clearly seen that the legs of the OBS did not rest in the anchor frame but were twisted aside. Therefore the release did not open. The system was caught by the chains and rope and could be lifted with the TV grab. Finally, the release mechanism operated and the anchor fell off while rising to the surface.

Consequently the anchors need to be modified. Little plates at the end of the anchor legs will increase the size of the foot rest at the ground while their size and possible holes will avoide gliding during descent. Additional pads on top will increase the distance between foot plates of the tubes and sea floor to ensure that the release hook is always above ground. An asymetric shape of the legs will ensure better positioning of the achor's center of mass underneath the release hook. This will ensure that the legs of the OBS will keep in their position at the anchor legs.

Marine Broadband Seismic Recorder (MBS)

The so-called *Marine Broadband Seismic recorder (MBS;* Bialas and Flueh, 1999*)*, manufactured by *SEND GmbH*, was developed based upon experience with the DAT based recording unit Methusalem (Flueh and Bialas, 1996) over the last few years. This new recorder avoids a mechanically driven recording media, and the PCMCIA technology enables static flash memory cards to be used as unpowered storage media. Read/write errors due to failure in tape handling operations should not occur with this system. In addition, a data compression algorithm is implemented to increase data capacity. Redesign of the electronic layout enables a decreased power consumption (1.5 W) of about 25% compared to the *Methusalem* system. Depending on the sampling rate, data output could be in 16 to 18 bit signed data. Based on digital decimation filtering, the system was developed to serve a variety of seismic recording requirements. Therefore, the bandwidth reaches from 0.1 Hz for seismological observations to the 50 Hz range for refraction seismic experiments and up to 10 kHz for high resolution seismic surveys. The basic system is adapted to the required frequency range by setting up the appropriate analog front module. Alternatively, 1, 2, 3 or 4 analogue input channels may be processed. Operational handling of the recording unit is similar to the *Methusalem* system or by loading a file via command or automatically after power-on. The time base is based on a DTCXO with a 0.05 ppm accuracy over temperature. Setting and synchronizing the time as well as monitoring the drift is carried out automatically by synchronization signals (DCF77 format) from a GPS-based coded time signal generator. Clock synchronization and drift are checked after recovery and compared with the original GPS units. After software preamplification the signals are low-pass filtered using a 5-pole Bessel filter with a -3 dB corner frequency of 10 kHz. Then each channel is digitised using a sigma-delta A/D converter at a resolution of 22 bits producing 32-bit signed digital data. After delta modulation and Huffman coding the samples are saved on PCMCIA storage cards together with timing information. Up to 4 storage cards may be used. Currently, up to 440 MB per card are available. Data compression allows more than 2 GB data capacity. Recently technical

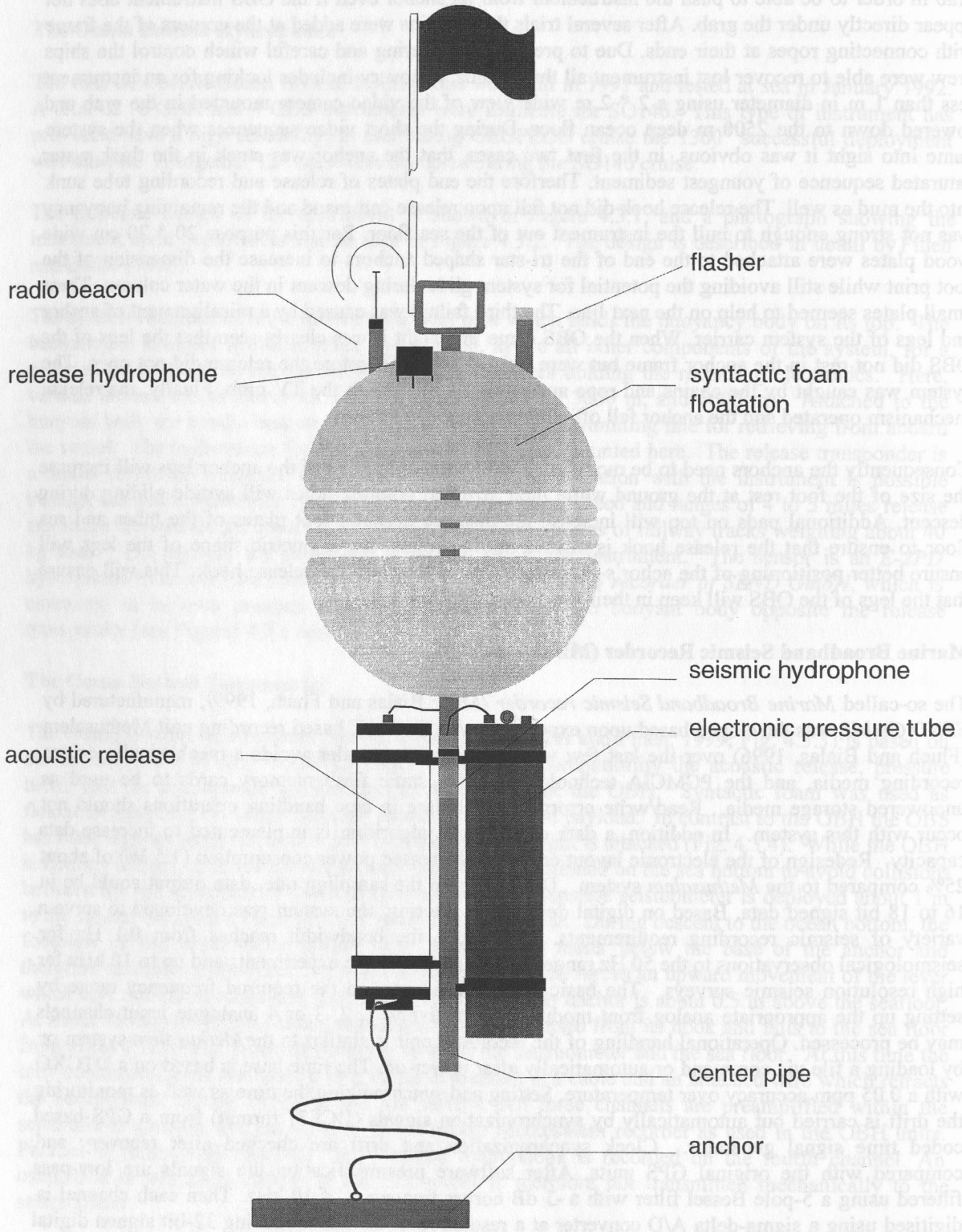

Figure 4.3.1: Principle design of the GEOMAR OBH (after Flueh and Bialas, 1996)

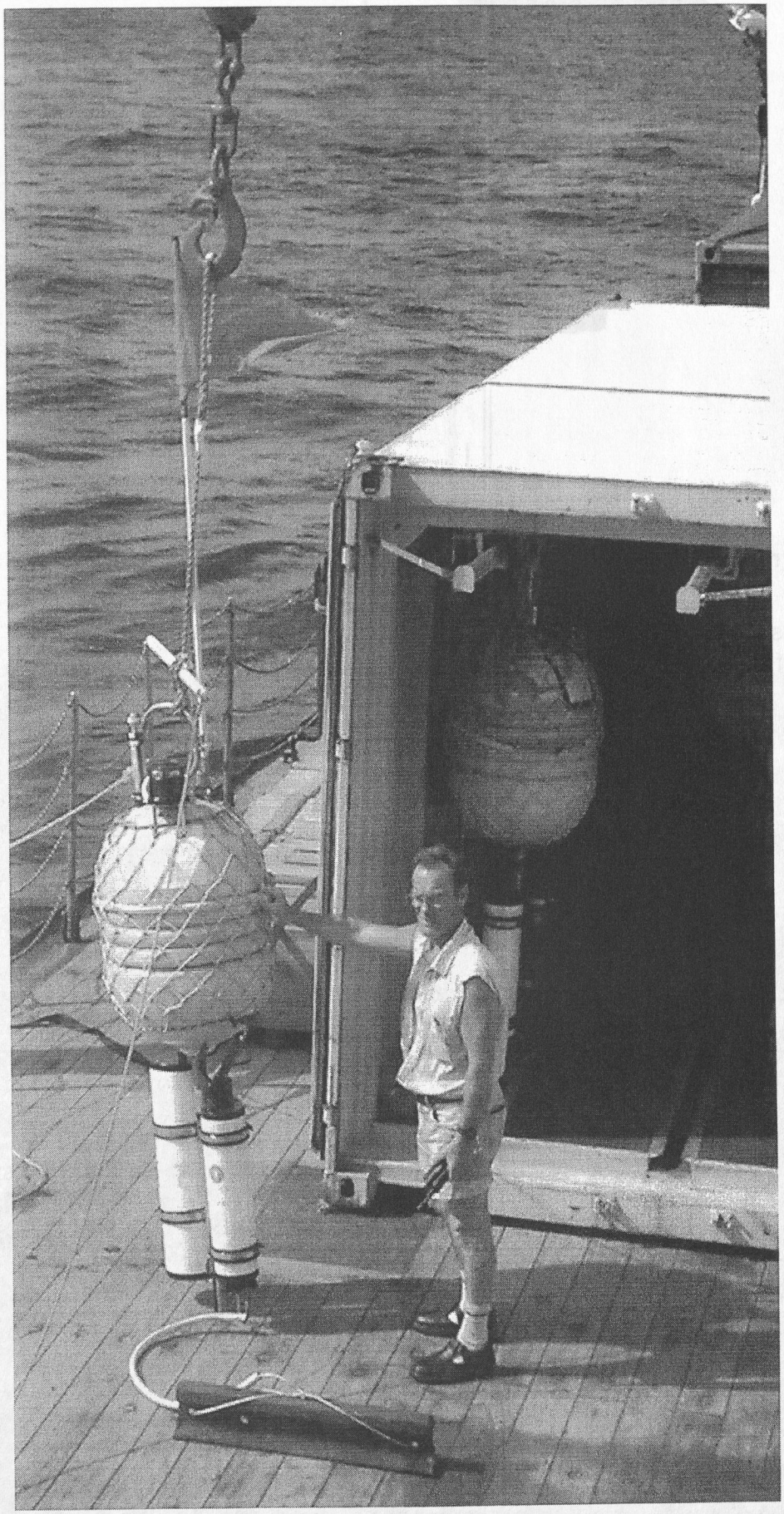

Figure 4.3.2: The GEOMAR OBH before deployment

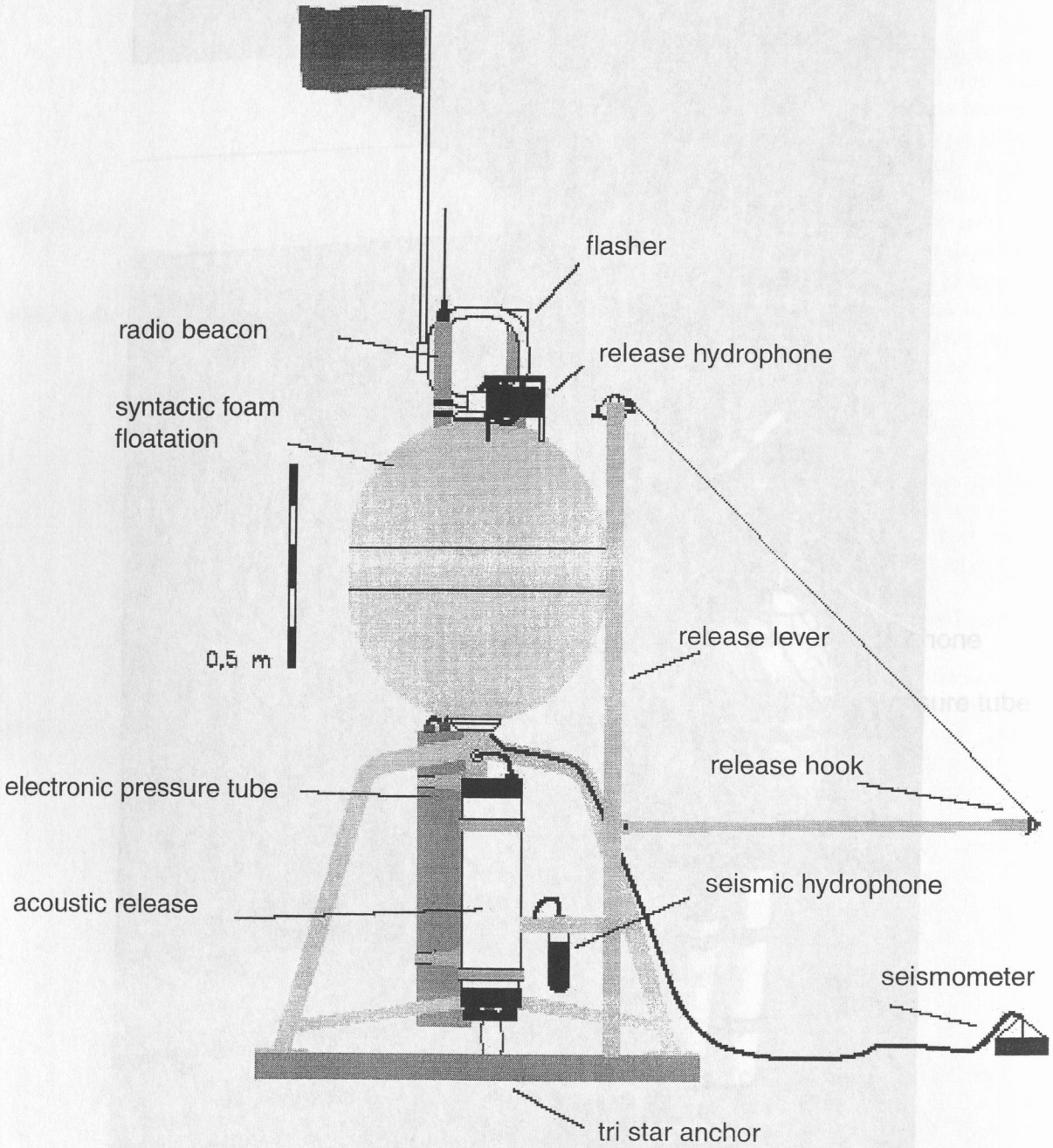

Figure 4.3.3: Priciple of the GEOMAR OBS (after Bialas and Flueh, 1999)

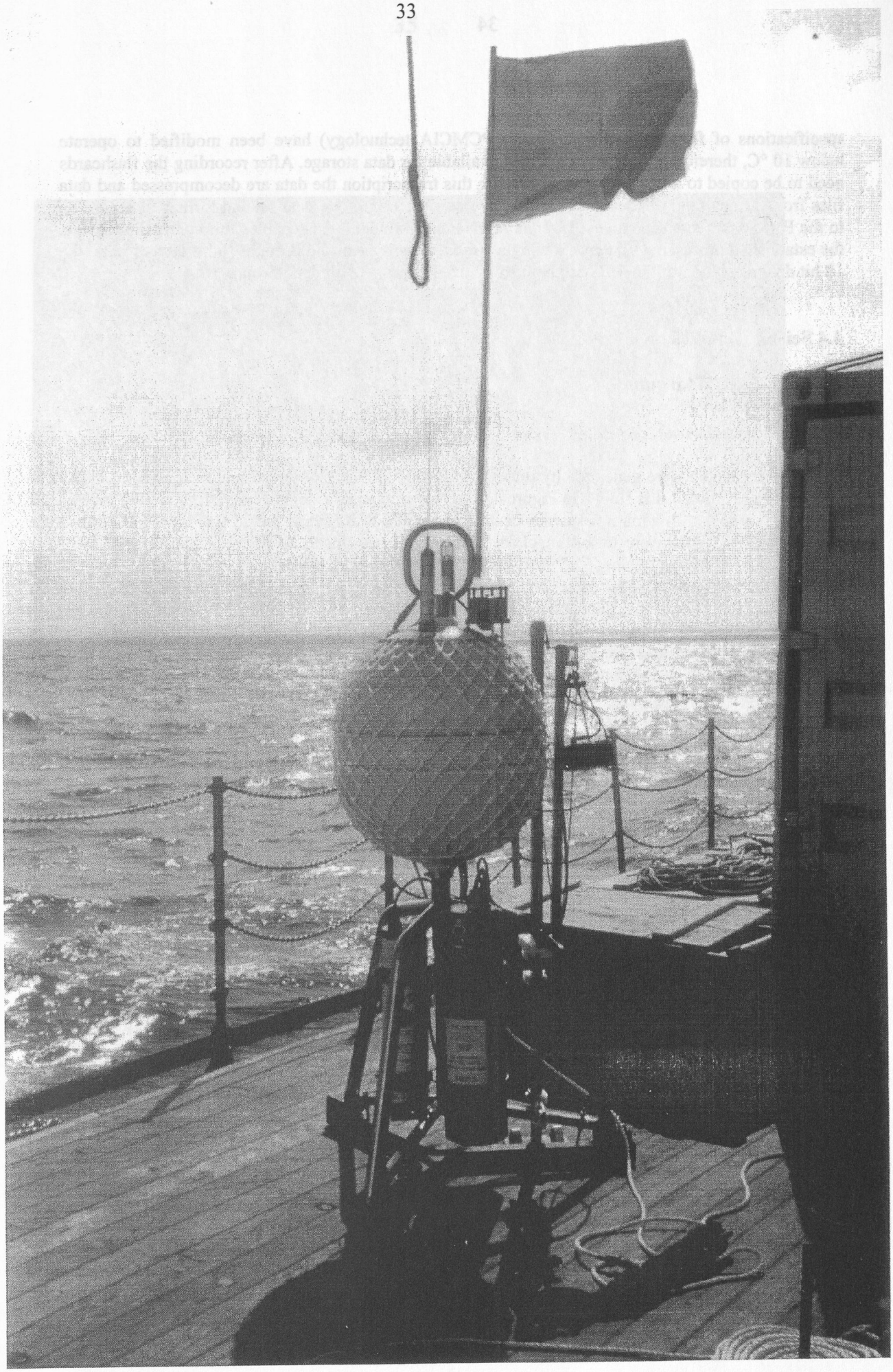

Figure 4.3.4: The GEOMAR OBS ready for deployment

specifications of flashdisks (disk drives of PCMCIA technology) have been modified to operate below 10 °C, therefore 1 GB drives are now available for data storage. After recording the flashcards need to be copied to a PC workstation. During this transcription the data are decompressed and data files from a maximum of four flash memory are combined into one data set and formatted according to the PASSCAL data scheme used by the *Methusalem* system. This enables full compatibility with the established processing system. While the *Methusalem* system did provide 16 bit integer data, the 18 bit data resolution of the *MBS* can be fully utilized using a 32 bit data format.

4.4 Seismic Sources

4.4.1 32 l BOLT Airguns

(K. P. Steffen, J. Bialas)

The seismic signals were generated by three Model 800 CT *BOLT* airguns (one on loan from UTIG); a photo of one of the guns is shown in Figure 4.4.1.1. Each gun has a volume of 32 liters (2000 inch^3), and generates a signal with a main frequency centered around 6 to 8 Hz and including higher harmonics (see also 4.9.1). Two guns were towed attached to blocks on the outer side of the A-frame, with two pier winches controlling the towing. The third gun was towed through the center block of the A-frame using the W6 deep sea cable. Trigger cables and airhoses were deployed manually. Each gun was suspended on two floats with an additional float attached to the supply lines to prevent contact between the gun and the towing wire. A sketch of the towing configuration is shown in Figure 4.4.1.2. The guns were towed 60 m behind the vessel and operated at 133 bar in 7 to 8 m depth. While onboard the guns were stored inside the A-frame from where the outside guns were launched without using an additional winch on the inside of the A-frame this time. Together with newly molded bold eyes on the guns to support crew handling with securing ropes handling of the guns was smooth at all times. The recent modifications on the deck (closing the slip) provided an easier launch and recovery operation compared to earlier cruises (e.g. SO103; Flueh, 1995). Due to the large distance needed for safety reasons between guns and the rear of the vessel the outer guns tend to drift to the center, leaving no space to have the third gun in between. Unfortunately no boom was available to take the force of the towing cable and provide a larger distance between port and starbord side gun. However the small boom used to lower the core carrier on starbord side and the magnetic boom on port side were used to hold pressure hoses and trigger cables farther to the side which helps prevent them from being damaged by the towing cable. The center gun was towed about 50 m behind the vessel to keep clear of the other two guns. This configuration is probably not appropriate during weather conditions with high sea state. Booms at the aft are necessary to further spread the guns away from each other.

During cruise SO146 GEOPECO, the guns were used along six seismic profiles. The first one with two guns while all others were shot with three guns. Along profile 3 the starboard gun was called on deck for service whereas all other lines were shot without interruptions. The total operation time was close to 155 hours, with more than 9300 shots being fired, always at a 60 s shot interval. This was well within the capability of the ship's compressor system, which worked smoothly and caused no delays or interruptions.

External Trigger

The trigger signal was supplied from the ships *Ashtech* GG24 GPS/Glonass receiver, and was available in the Geology Lab and the Seismic Lab. The receiver can provide a one millisecond long 5 V-TTL pulse at intervals between 0.2 and 999 s. The impulse should be stable to within the accuracy of the GPS Time, which is 70 nanoseconds. The impulse was delivered to the *BOLT* Par Airgun Firing Circuit FC300 and the *Real Time Systems* LongShot Seismic Source Controller. The shotbreaks, necessary for subsequent data processing and intstrument location, were stored on a MBS recorder and displayed in real time to

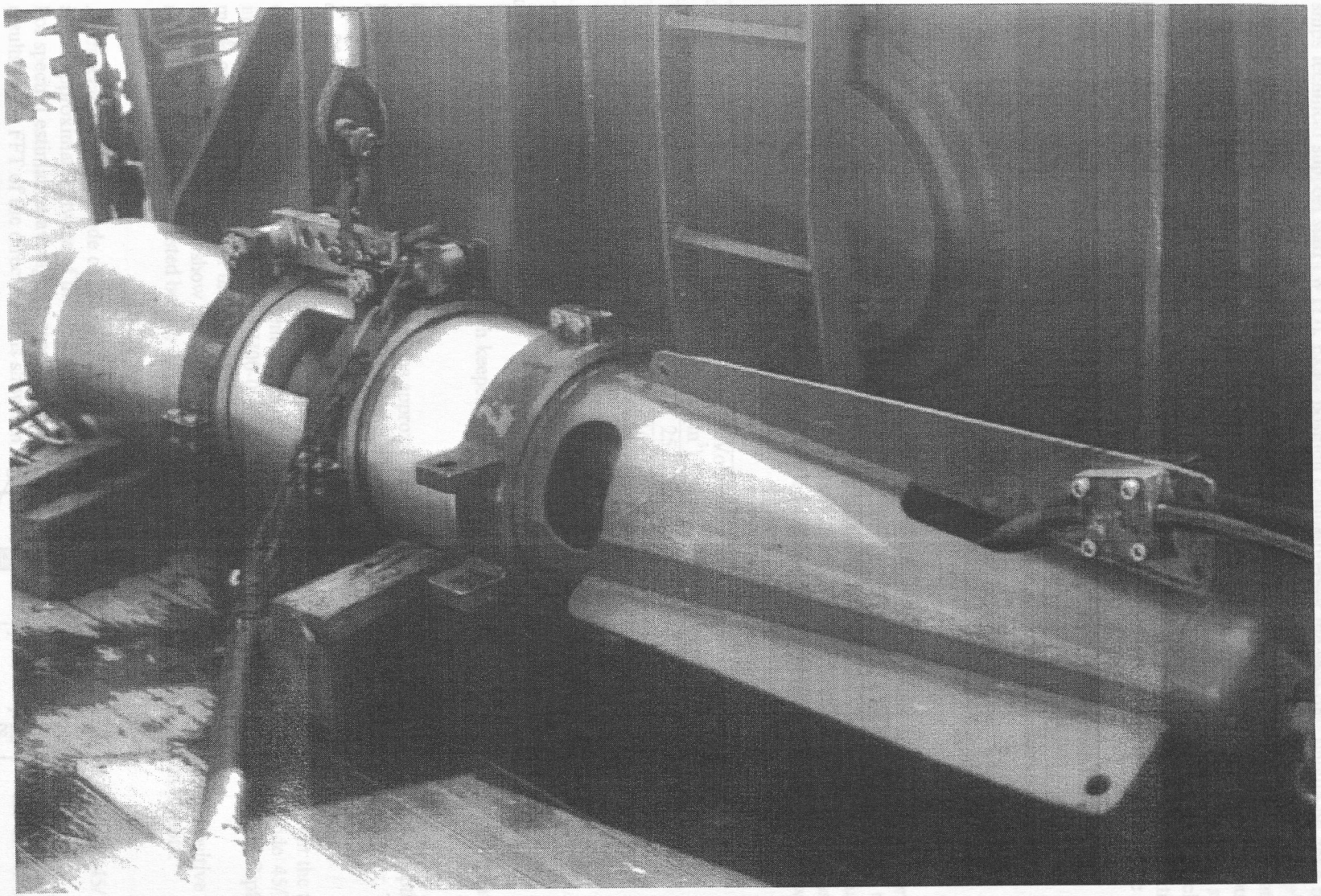

Figure 4.4.1.1: Photograph of a Bolt PAR 800 CT airgun with 32 l chamber

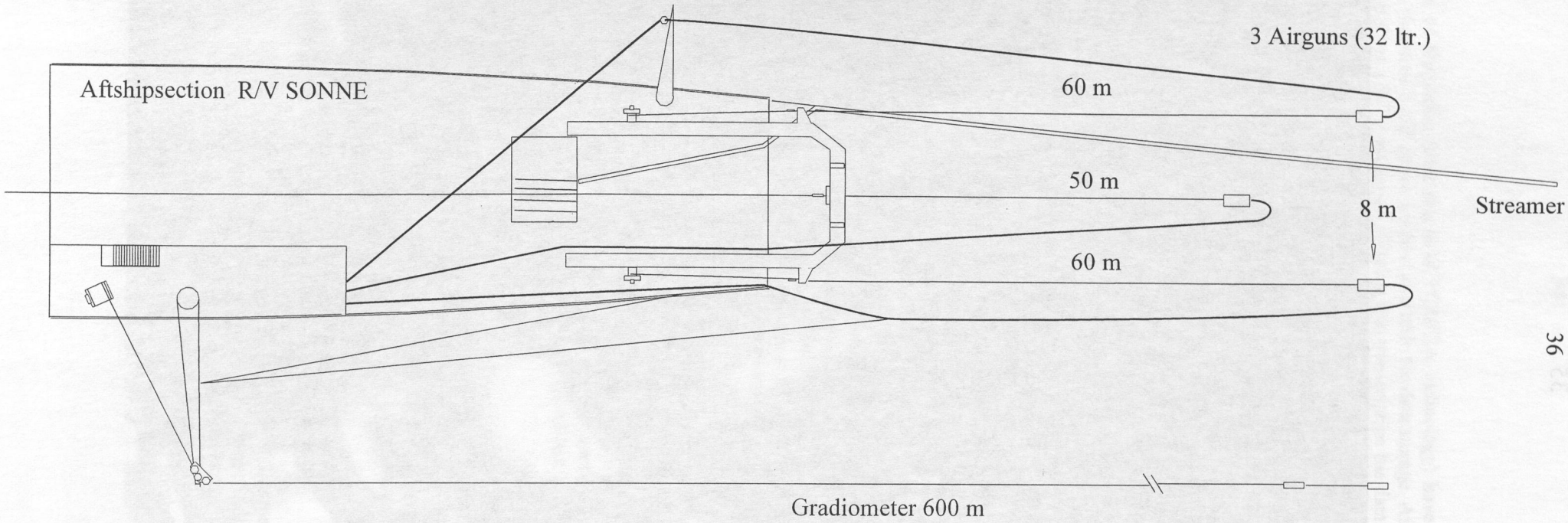

Figure 4.4.1.2: Scetch of tow configuration at the stern of R/V SONNE
3 * 32 l BOLT airgun, streamer and gradiometer

double check. For this process the same time basis was used that is used for the OBH (see chapter 4.4) and the trigger signal was converted into a 5 V TTL pulse of 250 ms length by a circuit provided from the ships technical support staff (WTD). Exact position calculation for the shot time should be done by later post-processing using shot time and UTC time values stored with DGPS coordinates in the ship's data base. During preliminary discussion, it was discovered that the coordinates stored within the data base were provided by the *Atlas ANP 2000* system, which does not copy the exact GPS time values but adds time stamps of its internal uncontrolled clock to the high precision coordinates of the DGPS system. Accuracy of the time values mainly depends on the operators skills by manually setting the ANP clock to GPS time. This is clearly a somewhat conservative method compared to the efforts of precise positioning. To enable the most accurate GPS related time stamps within the ANP system prior to each seismic survey the system operates were informed to reset the ANP.

4.4.2 GI-Gun

(C. Hübscher, C. Wenz)

Overview

Except for line HH00-064a two GI-Gun (Generator-Injector gun; Sodera) have been used to generate the seismic energy for high-resolution multichannel surveys. Basically a GI-Gun consists of two airguns in one. The first gun, the generator, produces the primary pulse. Depending on the used chamber volumes, which can be adjusted by volume reducers, the bubble can be significantly suppressed by triggering the second injector gun after a delay if the bubble collapses. The following configurations have been used:

Mode	Generator Volume (in^3)	Injector Volume (in^3)	Delay (ms)	Discharge Port
Harmonic	25	25	31	small
True GI	45	105	33	small
Harmonic	105	105	50	medium
Airgun	105	105	0	medium

Table 4.4.2.1: GI-Gun configurations

During operations the seismic watch keeper in the seismic lab checked the near field source signature of both guns with a digital scope.

A single gun hanger towed both GI-Guns approximately 25 m behind the ship stern in a water depth of 2.3 m. Towing depth remaind stable due to two buoys at the front and the end of the gun hanger. The guns worked without any significant problems.

In order to measure source signal characters in terms of signal strength and freuquency content the two GI-Guns were adjusted for different modes (Harmonic Mode (25/25 in^3) and true GI-mode 45/105 in^3)) during measurement of line HH00-003. Both sources were triggered in the alternating flipflop mode of the SureShot trigger unit. Water depth was 3250 m.
Figures 4.4.2.1 and 4.4.2.2 show the signals of the direct wave and the seafloor reflection. Positive and negative amplitudes are listed below. Average and amplitude ratio was computed from 6 shots.

As expected the amplitude of the source wavelet from the True GI-Mode configured GI-Gun (45/105 in^3) is approximately twice of the amplitude of the volume reduced (25/25 in^3) GI-Gun.
For spectral estimation averaged traces from the shots from the above tabels have been computed. The results of the FFT of the direct wave is shown in Fig. 4.4.2.3. The amplitude spectra of the direct wave

shows the maximum between 80 and 100 Hz. The local minimum at 330 Hz corresponds to a wavelength of 4.6 m. The destructive interference of the source ghost is at a wavelength of twice the waterdepth. Therefore we conclude that the spectral minimum corresponds to the towing depth of 2.3 m. The spectra shows that no significant increase in the frequency content can be obtained by using the 25 in^3 volume reducers. During this cruise the 25 in^3 volume reducers were not used again.

Direct Wave					
Harmonic Mode (25/25 in^3)			True GI-Mode (45/105 in^3)		
Shot	**Pos. Amplitude**	**Neg. Amplitude**	**Shot**	**Pos. Amplitude**	**Neg. Amplitude**
437	6702	-3130	**436**	11623	-5549
439	6071	-3190	**438**	13717	-6523
441	6279	-2788	**440**	13398	-6025
443	6878	-3061	**442**	14106	-6376
445	6035	-2602	**444**	14157	-5680
Av.	6393	-3154	**Av.**	13400	-6030

Table 4.4.2.2: Amplitudes of direct wave.

Seafloor reflection					
Harmonic Mode (25/25 in^3)			True GI-Mode (45/105 in^3)		
Shot	**Pos. Amplitude**	**Neg. Amplitude**	**Shot**	**Pos. Amplitude**	**Neg. Amplitude**
532	163	-104	**533**	269	-173
540	95	-141	**541**	159	-151
548	135	-115	**549**	169	-173
556	91	-72	**557**	145	-117
564	71	-55	**565**	130	-125
Av.	111	-97	**Av.**	174	-147

Table 4.4.2.3: Amplitude of seafloor reflections.

The comparation of the amplitudes yields:

	Direct Wave		Seafloor Reflection	
	Pos. Amplitude	**Neg. Amplitude**	**Pos. Amplitude**	**Neg. Amplitude**
True GI / Harmonic	2.1	1.9	1.6	1.53

Table 4.4.2.4: Amplitude ratios of Harmonic Mode and Tue GI-Mode

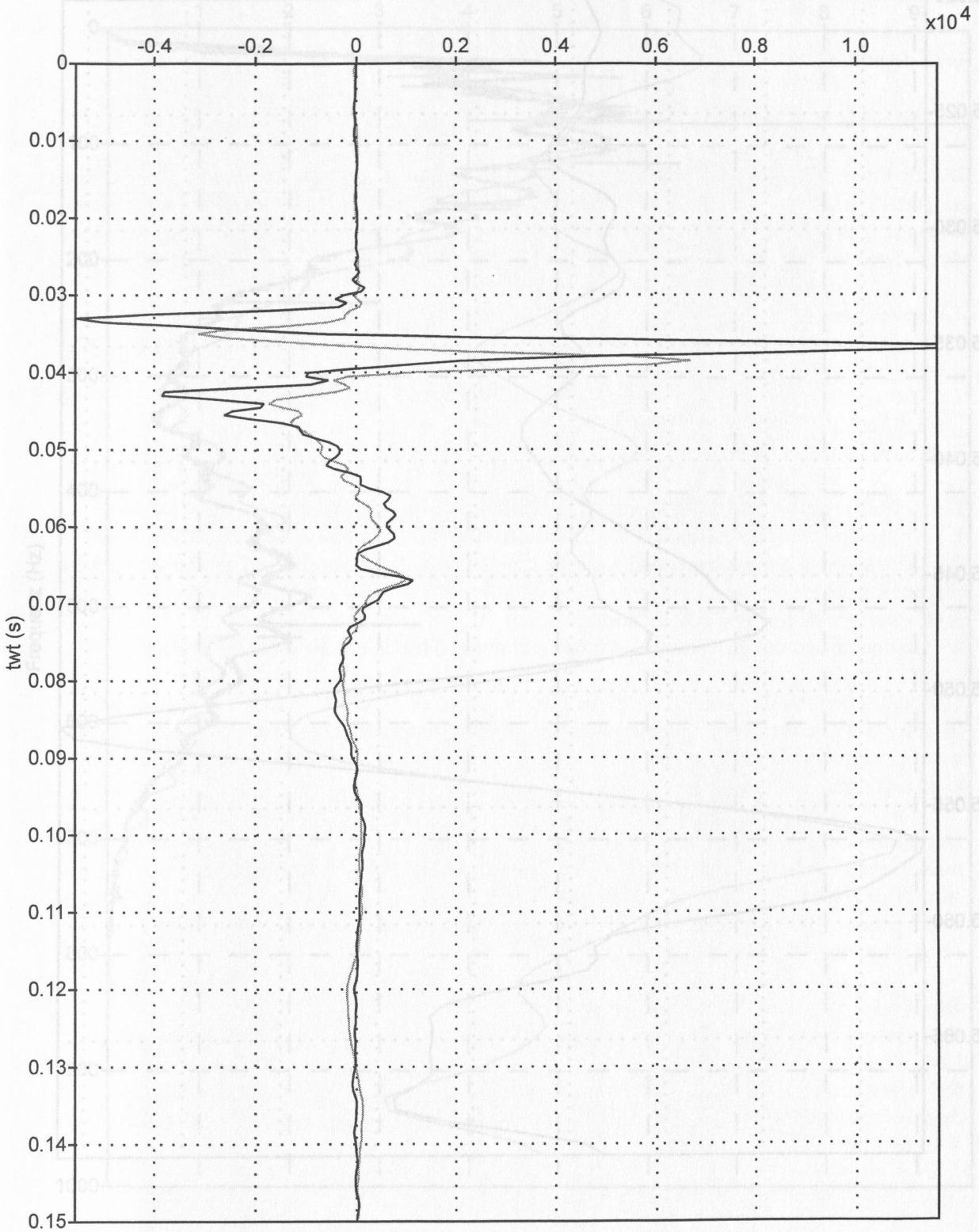

Fig. 4.4.2.1: Direct wave of True-GI-Gun (black) and Harmonic Gun (gray).

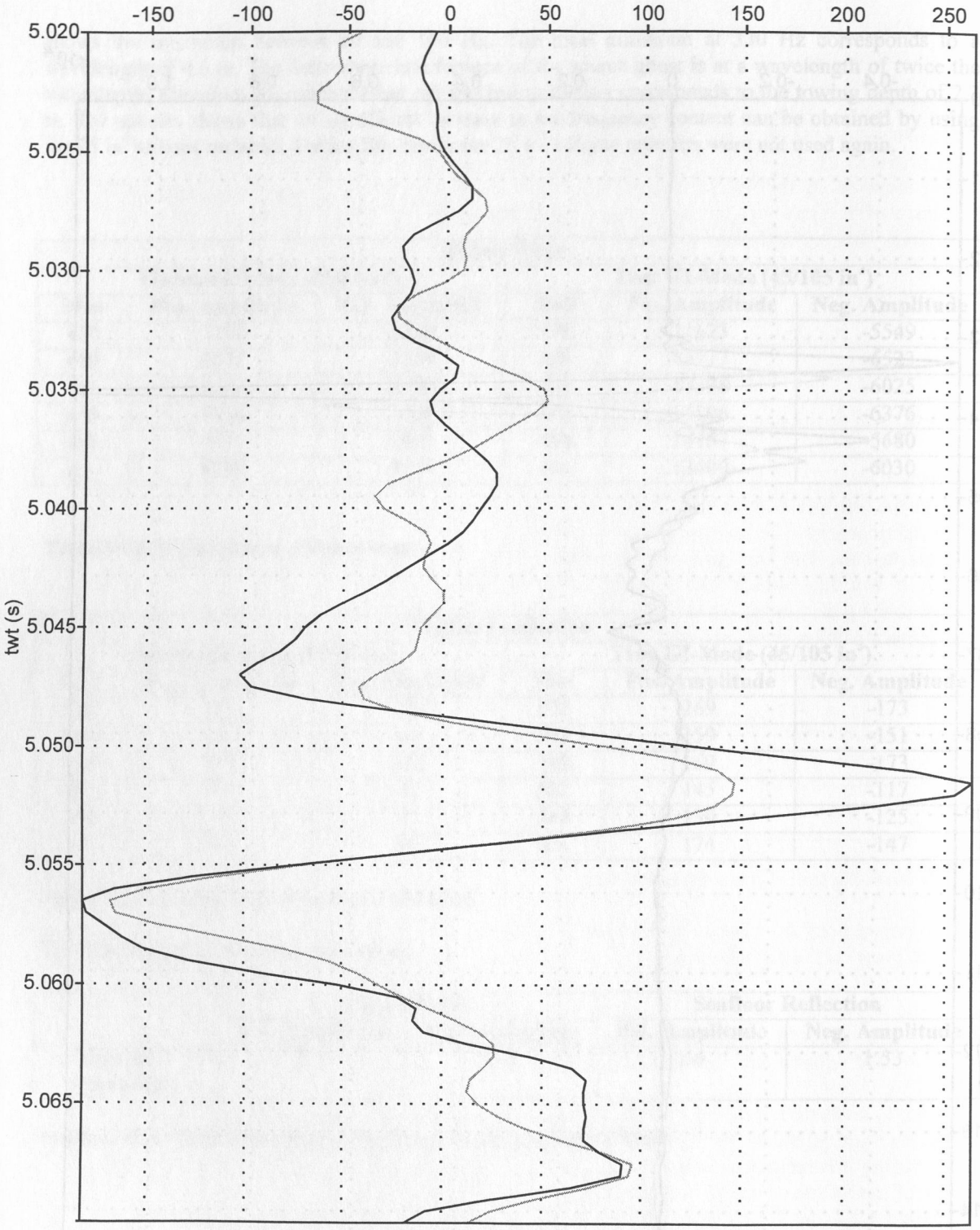

Fig. 4.4.2.2: Seafloor reflection of True-GI-Gun (black) and Harmonic Gun (gray).

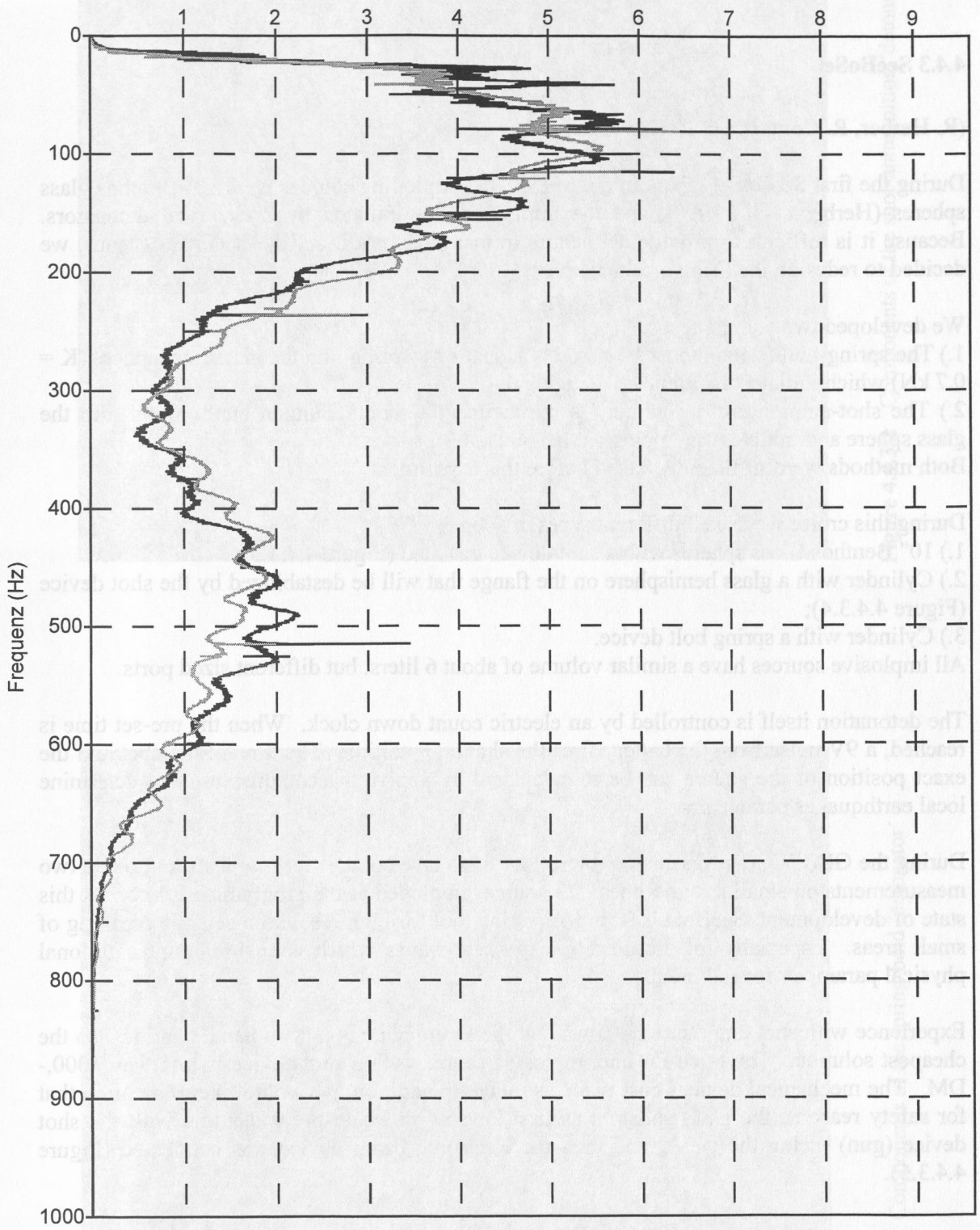

Fig. 4.4.2.3: Amplitude spectra of direct wave of True-GI-Gun (black) and Harmonic Gun (gray).

4.4.3 SeeBoSeis

(R. Herber, R. Coman, and C. Hübscher)

During the first SeeBoSeis Experiment in 1998 the imploding sources were 10" Benthos glass spheres (Herber et al., 1998), and the implosion was initiated by 2 electrical detonators. Because it is difficult to provide detonators in many countries, and for security reasons, we decided to redesign the firing mechanism.

We developed two techniques:
1.) The spring-bolt technique: a 1 kg iron bolt shot by a spring into the glass hemisphere (K = 0.7 kN) which initiates the implosion (Figure 4.4.3.1);
2.) The shot-ammunition technique: a miniature gun shoots shotgun ammunition into the glass sphere and initiates the implosion. (Figure 4.4.3.2)
Both methods were sufficiently tested before this experiment.

During this cruise we used 3 different types of sources:
1.) 10" Benthos Glass spheres with a shot device installed (Figure 4.4.3.3);
2.) Cylinder with a glass hemisphere on the flange that will be destabilized by the shot device (Figure 4.4.3.4);
3.) Cylinder with a spring bolt device.
All implosive sources have a similar volume of about 6 liters, but different sized ports.

The detonation itself is controlled by an electric count down clock. When the pre-set time is reached, a 9V pulse from the battery fires the shot ammunition. The time of the shot and the exact position of the source can be re-calculated by applying techniques used to determine local earthquakes parameters.

During the GEOPECO experiment we used 24 implosive sources for two tests and made two measurements on small seismic lines. 23 sources imploded at the programmed time. At this state of development, SeeBoSeis is an interesting tool for high resolution seismic profiling of small areas. Especially for the detection of shear-waves which is an important additional physical parameter for sediments.

Experience with shot ammunition shows that the shot device is easy to handle and is also the cheapest solution. The price for one implosive source with a shot device is less than 1000,- DM. The mechanical devices cost twice as much. In addition, we would like to mention that for safety reasons, the glass sphere was first lowered down to the water line with the shot device (gun) facing the water, and then the electronic firing device was connected (Figure 4.4.3.5).

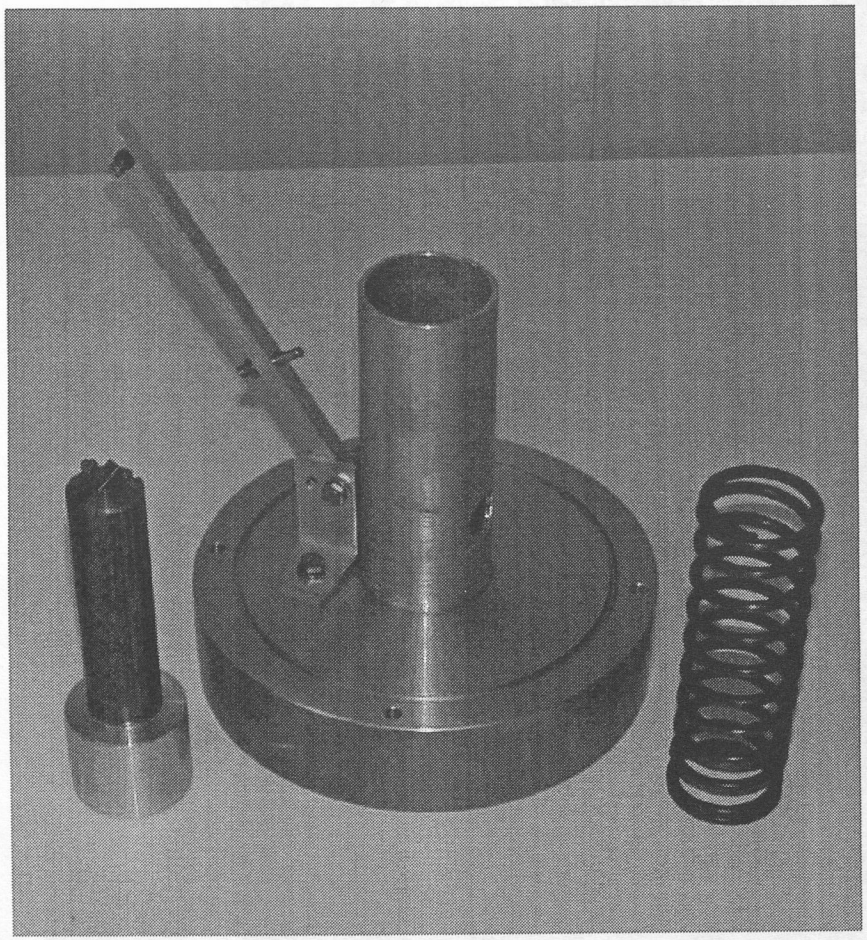

Figure 4.4.3.1 Components of the spring-bold ´detonator´

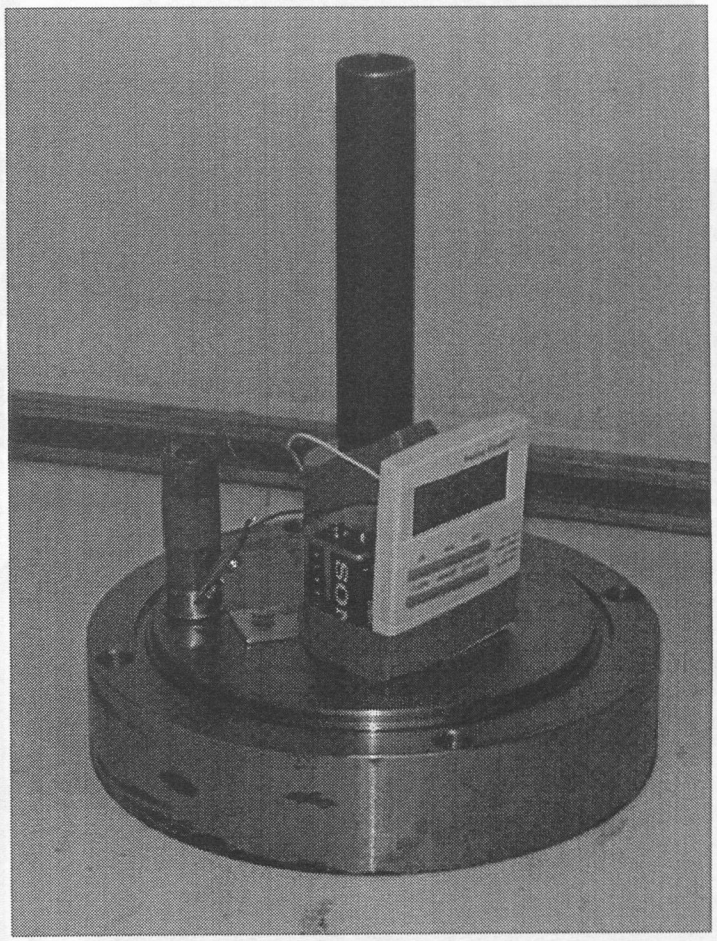

Figure 4.4.3.2 Components of the shot-ammunition ´detonator´

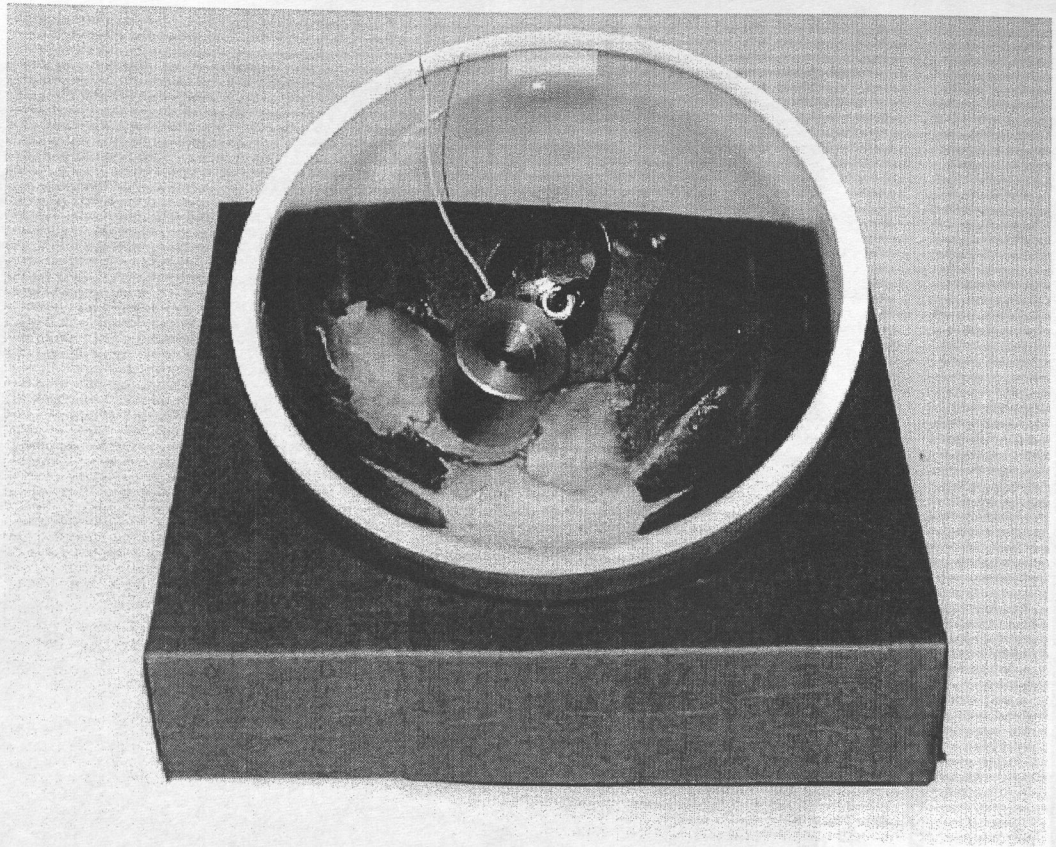

Figure 4.4.3.3 10´´ Benthos spherical source (here one hemisphere).

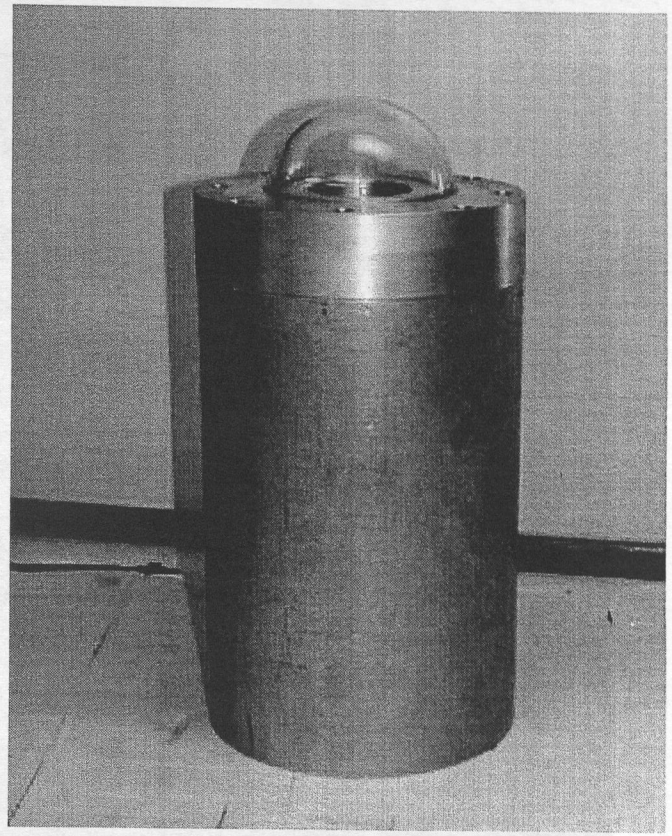

Figure 4.4.3.4 Cylindrical source

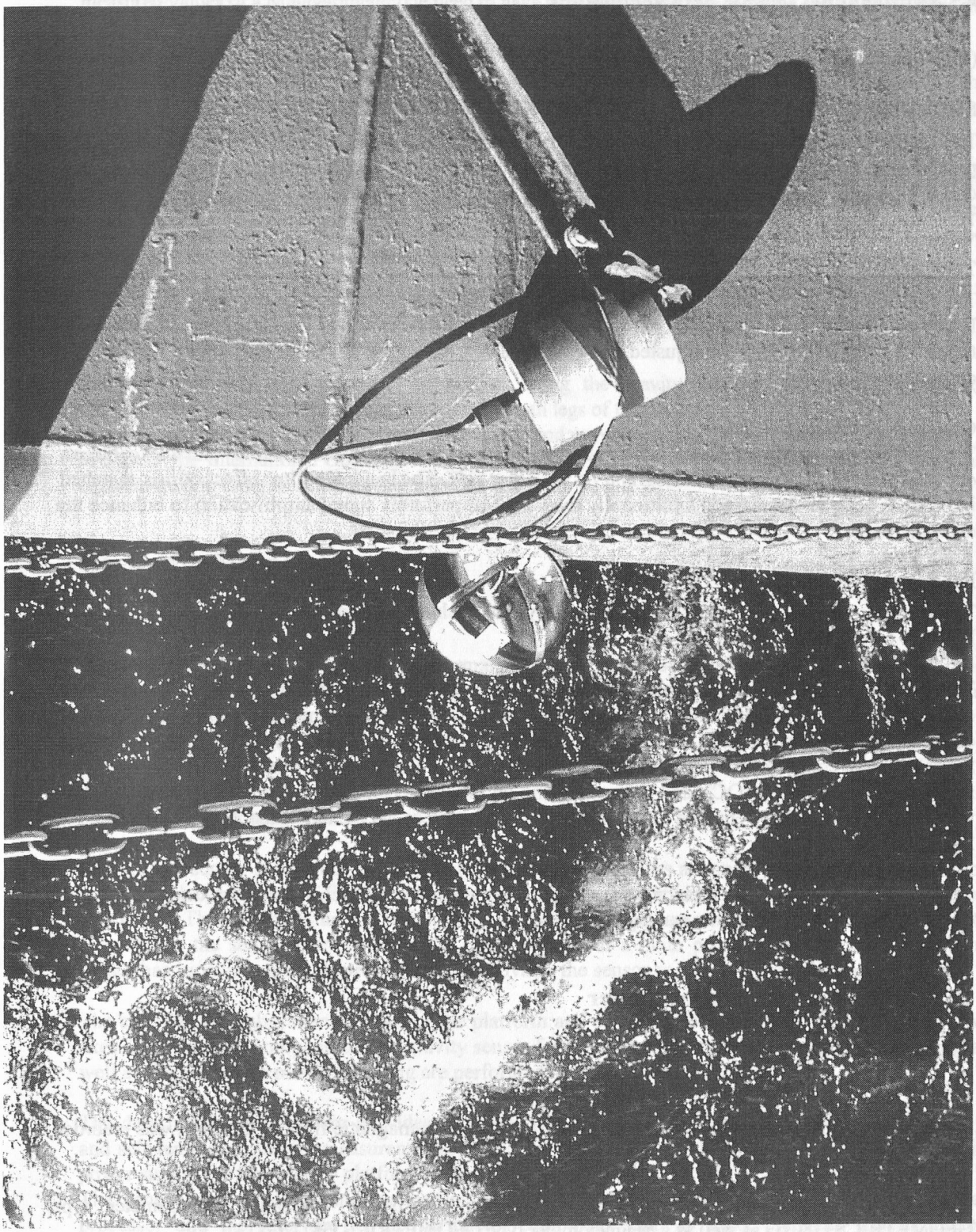

Figure 4.4.3.5 Deploying the glass sphere source

4.5 Multichannel seismic data acquisition

(C. Hübscher)

Streamer

The high resolution streamer of the University of Hamburg consists of a 120 m of tow-lead, two 10 m passive stretch sections, and three 50 active sections. Each active section houses 8 hydrophon groups of 4.9 m length. The distance between groups is 6.25 m, and the number of hydrophones per group is 16. During operation the 1st active group started 40 to 70 m behind the ship's stern.

Trigger Unit

The SureShot trigger system is a modular system of components that can be adapted to the need of 4 Prakla airguns or 2 GI-Guns. The PC based control unit includes a real time card for internal cycle times. One FourShot Unit is adjusted for Prakla valves, the other has standard output voltage and current for BOLT or GI-Guns.

Charge Amplifier (CHAMP)

This custom designed charge amplifier matches the impedance between streamer and deckcable on one side and the StrataView seismograph on the other side. The bandpass filter effect of mis-matched impedances can be decreased. Additionally the CHAMP performs signal amplification to enhance the dynamic range.

Recording System

The primary building blocks of the recording system include a seismograph with a controller unit. Both are connected via network.

The R36 StrataView is a PC based A/D converter with preamplification and anti-alias filtering options. During the SO146 cruise, 36 active channels were installed, giving a hot swap capacity of 12 channels. The dynamic range depends on sample rate, but is is always higher than 110 db. The StrataView is connected to the CHAMP (s.a.) and to the CNT-1 controller PC, which performs storing, qualtity controll (QC), and online plotting on the connected laser printer. Demultiplexed data were stored on two daisy chained DAT drives. For security reasons the tape capacity was decreased to 2 Gbyte.

Quality controll capabilities include several data display windows, which are shot window, gather plot, trigger window, noise window, and tape window.

4.6 Gradiometer and Magnetometer

(G. Ali Dehghani)

During the both legs of SO146 cruise the total intensity of the magnetic field of the earth was recorded along some gravity profiles.

The magnetic measurements were carried out using a proton precession Gradiometer type GEOMETRICS G801G as well as a Magnetometer type GEOMETRICS G811/G813.

The difference between these two instruments is that the magnetic measurements with a Gradiometer have no influence of the daily variations of the magnetic Field of the earth where as the measurements of magnetic with a one sensor magnetometer included these variations. In order to be able to reduce the

measured values of a Magnetometer one need to have a magnetic base station in the area or at least use the recorded magnetic field of an observatory near the research area.

The omnidirectional sensor of Magnetometer was towed 400 meter behind the ship. This distance of the sensor from the ship was long enough, so that the magnetic influence of the vessel could not produce any disturbances in the recorded magnetic field

The two sensors of Gradiometer were always towed 250 meters behind the ship with a distance of 10 meters between the two sensors. Although this distance of the sensors from the ship was under the given (regular?) distance (some 275 meters for the length of RV Sonne) the quality of data recorded was good enough, so that we decided to run the magnetic measurements using the Gradiometer most of time.

4.6.1 Magnetic Data

The magnetic data were recorded on profiles along the gravity lines. A total profile length of approximately 2500 km was measured during the both legs of this cruise.
The data were recorded digitally as well as analogue and were merged with the recorded navigation data .
We used the International Geomagnetic Reference Field (IGRF, 1995) for the epoch of 2000.3 as the regional field in order to calculate the magnetic rest field.

4.7 Gravity Meter System

(G.A. Dehghani)

During both legs of SO146, the high performance Gravity Meter System KSS30/31 was deployed. The system belongs to the Institute of Geophysics, University of Hamburg and is applied to prospecting and geophysical exploration of the Earth.
The system is organized into three major subsystems including:

- GSS 30 gravity sensor subsystem
- KT 30 stabilisation subsystem
- Data handling subsystem

The gravity sensor subsystem includes a non-astatized springmass assembly as basic gravity detector and control electronics, GE 30, with a voltage pulse rate converter output to the data handling subsystem. The sensor includes a sealed buffered battery unit as power-supply with sufficient capacity to maintain the sensor thermostat for 24 hours in case of a main power failure. Further more, the sensor has its own caging electronics, which activates the sensor caging mechanics in case of failure.

The stabilization subsystem consists of the platform and a vertical electrically erected gyro with two axes. The platform compensates the gravity sensor for roll and pitch. All logic functions of the gyro as well as the automatic platform caging are performed by the system controller ZE30.

The data handling subsystem provides all equipment necessary for filtering, logging, preprocessing and self-testing of gravity measurements. It also provides the control electronics of the platform, the power supply for the sensor, platform and monitor registration facilities.
The central part of data handling system is the system controller ZE 30 consisting of a central processor and the interface to the peripheral equipment such as gyro, platform, gravity meter, externally provided navigation data and the computer for the data logging and processing.

4.7.1 Principle of operation

The measuring system, based on a vertical sensor, consists of a tube-shaped mass (30 g) guided by 5 threads in a frictionless manner.
The sensor is non-astatized and the motion of the sensor mass is limited to one degree of freedom in the vertical direction. The constant gravitational acceleration is compensated by a mechanical spring and the gravity changes are detected by an electromagnetic system.
The measuring system is housed in the thermostatized, pressure-tight and magnetically shielded section.
An optimal tensioning is very important with respect to system sensitivity to external perturbing accelerations.
The sensor operates as a zero methode system. The mass is always fed back to zero position. The zero position detector is able to detect a mass displacement of less than 10 Å (less than 0.02 mGal).

4.7.2 Accuracy of the Gravity Meter Sensor

a- Accuracy on profile

Vertical Acceleration (mGal RMS)	**Sea State**	**Dynamic * (mGal RMS)**	**Effective** (mGal RMS)**
Less than 15000	Calm sea	0.5	0.2
15000 to 80000	Rough sea	1	0.4
80000 to 200000	Very rough sea	2	0.8

b- Accuracy during turn maneuver

Vertical Acceleration (mGal RMS)	**Sea State**	**Dynamic * (mGal RMS)**	**Effective** (mGal RMS)**
15000 to 80000	Turn maneuver	2.5***	1***

* Accuracy without applying data reduction.
** Accuracy applying data reduction procedures.
*** Depending on accuracy of navigation data.

4.7.3 Ball-Calibration Device

The sensor has a built-in scale factor and test facility which can be used in harbor before the cruise starts.
The principle consists of putting an additional weight (3 g) to the sensor mass. The additional mass is a ball approximately 2 mm diameter. It is located in the caging device. From a neutral position the ball is displaced by means of a lever and added to the measuring system.
The additional mass produces approximately 1000 mGal change in gravity. With this device one can check the measuring system in harbor before the cruise starts.

4.7.4 Navigation Computer Interface

The interface of ZE 30 to the navigation computer is performed with a standardized serial interface circuitry of RS 232c.
The ZE 30 expects the following unfiltered raw data from the navigation computer updated every second in the special format:
- Date and time
- Latitude and Longitude
- Heading and Course
- Speed and Velocity
-Depth

During both legs of SO146 cruise we were able to send all these information every second to the central proccesor of the gravity meter system, so that the system worked constantly without any problem.

4.7.5 Gravity Base Connections

(G. A. Dehghani and R. Heinbockel)

Dockside calibration of shipborn gravimeters are required to 1) tie values from local surveys to the World Gravity Net; and 2) provide a common base so that values measured by different instruments, organizations, and at different times can be combined. This calibration process ensures that measurements at sea become useful for global research. At the beginning and at the end of each leg of SO146 we preformed this calibration using the G260 LaCoste & Romberg land gravimeter so that values could be compared with the marine gravity data.

These dockside measurements were done in the harbours of Arica, Callao (two times) and Talcahuano. In order to determine the values of gravity at the docksides we used following International Gravity Base Stations (IGSN):

IGSN No.	Place	Absolute Value
IGSN 21639 B	Hamburg, Germany	981363.78 mGal
IGSN 36827 O	Lima, Peru	978292.37 mGal
IGSN 36880 M	Arica, Chile	978515.52 mGal

Using these stations we established a new base station in each harbour. The description of the new base stations are given in figures 4.7.5.1 - 4.7.5.3. and in the following table.

Place	Absolute Value	Reading Value
Arica	978515.50 mGal	-2328.50 mGal
Callao	978298.50 mGal	-2545.81 mGal
Talcahuano	979944.70 mGal	-899.60 mGal

For the whole period of cruise (63 days) a drift of 0.68 mGal was determined.

4.8 Heat Flow Survey and Instrumentation

(N.Kaul, R. Harris, and B. Heesemann)

4.8.1 Heat Probe and Shipboard Operation

On cruise SO146 the heat flow probe, a Lister type violin bow design (Figure 4.8.1), from the University of Bremen, Meerestechnik und Sensorik was used to obtain temperature gradients and in-situ thermal conductivity by a pulsed heat source method. The active length of the sensor string is 3 m, with 11 thermistors spaced every 0.3 m. Two 8-channel 16 bit A/D converters are used to record the digital data into solid state memory. This instrument is used in conjunction with an online data transmission and a short baseline navigation system (SSBL). Additionally, autonomous temperature data loggers were used in a field test to gain sediment temperatures.

On this cruise, following instruments were in service:

Parameters of Lister-type heat probe:

Probe #:	#6845
Pressure sensor:	#60779
Strings:	3/98, 5/96, 6/7/99, 4/96
Heating current:	8 Amp
Heat pulse:	600 J/m
Pulse duration:	20 sec
Sample rate:	10 sec
Online data transmission:	2400 Baud net via coax wire
Wire:	7760 m 18 mm deep sea cable (W1) with LWL and coax

The Lister type heat probe (figure 4.8.1) has the capability of autonomous operation for at least 48 hours due to memory and power capacity. During a single deployment a minimum of 20 heat pulses, equating to 20 sets of thermal conductivity measurements, can be made. Data security is guaranteed by twofold recording into solid state memory and on deck data logging.

Measurements are made in the so called 'pogo-style', performing many penetrations in a row at small distances. Each penetration consists of raising the probe some hundred meters above the sea floor from the previous penetration, slowly moving the ship to the next penetration site and letting the wire angle become nearly vertical before dropping the probe into the sediment for the next penetration. Once the probe is in the bottom it is left undisturbed for 7 minutes for the equilibrium temperature measurements and another 7 minutes if a thermal conductivity measurement is made. For the penetration spacing used in this survey, transit between penetration points lasts about 30 – 45 minutes, a recording cycle in the sea floor is either 7 or 14 minutes, yielding a rate of about one hour per penetration. Transit speed is governed by the tradeoff between keeping the wire angle small and minimizing the time between penetration points.

The relative position of the probe to the vessel is determined by SSBL. The position of subsurface unit is displayed in relation to the ship and in map co-ordinates. Geographical co-ordinates of the sub unit are available over shipboard data distribution.

Winch speed during layout and retrieval of wire is 1 m/s, so the initial penetration velocity is 1 m/s. Deployment of the instrument is amidships on the starboard side, employing a beam crane and one assistance crane. This procedure ensures safe operation even during medium sea state and minimum interference due to the ships vertical movement during station work. Three deckhands are necessary during deployment because the assistance crane can not be run simultaneously with the beam crane.

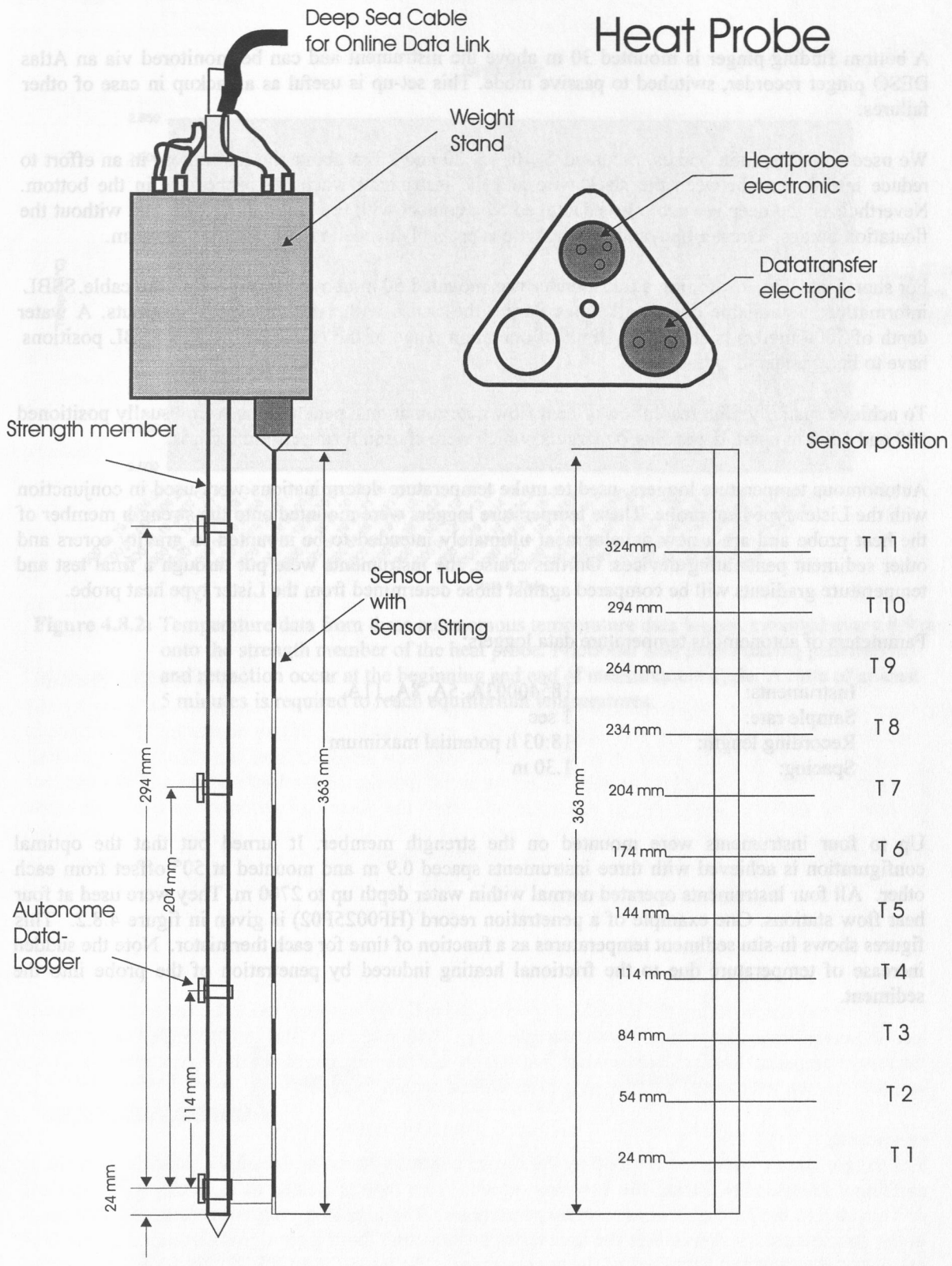

Figure 4.8.1: Lister type heat probe with mounted autonomous temperature data logger as used on cruise SO 146-2. Data recording unit is mounted in the weight stand within pressure proof containers, rated up to 4500 m water depth..

A bottom finding pinger is mounted 30 m above the instrument and can be monitored via an Atlas DESO pinger recorder, switched to passive mode. This set-up is useful as a backup in case of other failures.

We used five floatation bodies, mounted 5, 10, 15, 20 and 25 m above the instrument in an effort to reduce interference between the slack wire and the instrument when the probe was in the bottom. Nevertheless, the deep sea cable was damaged by a contact with the probe, both with and without the floatation bodies. Greater buoyancy on the wire is probably needed to alleviate this problem.

For short base line positioning a transponder was mounted 50 m above instrument on the cable. SSBL information is available during all times during the cruise with only temporary dropouts. A water depth of 3000 meters is at the very limit of operation range of the employed system. SSBL positions have to be considered with care.

To achieve spatially high resolution of heat flow determinations, penetrations were usually positioned 500 and 1000 m apart, depending on targets, which were chosen form seismic records.

Autonomous temperature loggers, used to make temperature determinations were used in conjunction with the Lister type heat probe. These temperature loggers were mounted onto the strength member of the heat probe and are a new development ultimately intended to be mounted to gravity corers and other sediment penetrating devices. On this cruise, the instruments were put through a final test and temperature gradients will be compared against those determined from the Lister type heat probe.

Parameters of autonomous temperature data loggers:

Instruments:	18540003A, 5A, 8A, 11A
Sample rate:	1 sec
Recording length:	18:03 h potential maximum
Spacing:	1.30 m

Up to four instruments were mounted on the strength member. It turned out that the optimal configuration is achieved with three instruments spaced 0.9 m and mounted at 50° offset from each other. All four instruments operated normal within water depth up to 2700 m. They were used at four heat flow stations. One example of a penetration record (HF0025P02) is given in figure 4.8.2. This figures shows in-situ sediment temperatures as a function of time for each thermistor. Note the sudden increase of temperature due to the frictional heating induced by penetration of the probe into the sediment.

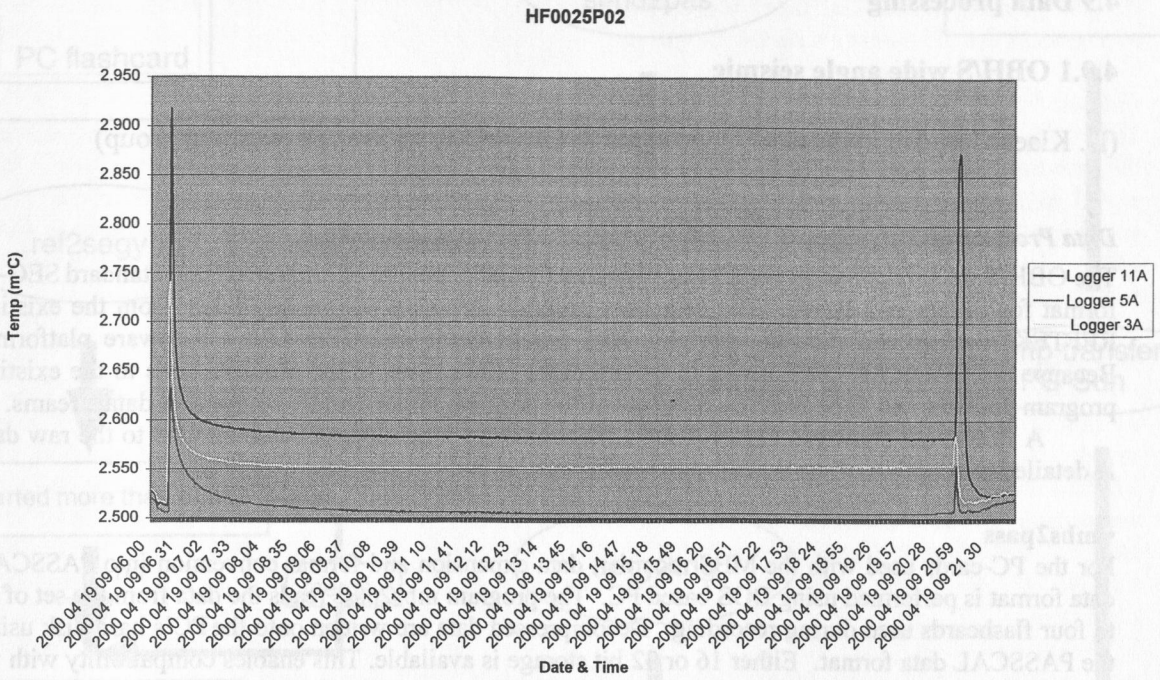

Figure 4.8.2: Temperature data from three autonomous temperature data logger, mounted every 0.9 m onto the strength member of the heat probe. Frictional heat pulses during penetration and retraction occur at the beginning and end of measurement cycle. A time of at least 5 minutes is required to reach equilibrium temperatures.

4.9 Data processing

4.9.1 OBH/S wide angle seismic

(D. Klaeschen, T. Leythaeuser, J. Petersen & GEOMAR wide-angle working group)

Data Processing

The OBH/S data recorded on the *Methusalem* and the *MBS* have to be converted into standard SEG-Y format for further processing. The necessary program structure was mainly taken from the existing REFTEK routines and modified for the OBH requirements and GEOMAR´s hardware platforms. Because the GEOMAR OBH works in a continuous mode, most of the modifications to the existing program package had to be done on the parts of the program which handle continuous data streams.

A flow chart shown in Figure 4.9.1.1 illustrates the processing scheme applied to the raw data. A detailed description of the main programs follows below:

• mbs2pass

For the PC-cards used with the MBS recorder, data expansion and format conversion into PASSCAL data format is performed using DOS based PC. The program mbs2pass reads the data from the set of up to four flashcards used during recording. Decompressed data are written onto the PC´s hard disk using the PASSCAL data format. Either 16 or 32 bit storage is available. This enables compatibility with the DAT recordings (s.b.). After ftp transmission to a SUN workstation, ref2segy and all other software can be used to handle and process the data files and store them as SEG-Y traces.

• ref2segy

Downloading the raw data from DAT tape to a hard disk of a SUN workstation is done by the program ref2segy. It will produce a pseudo SEG-Y trace consisting of one header and a continuous data trace containing all samples. For each channel (different amplifications) one file will be created. The name of this file contains the start time, the serial number of the *Methusalem* and the channel number. In addition, a log and an error file will track the download process. In a second mode PASSCAL disk files written by *mbs2pass* in either 16 or 32 bit format can be read in and included with the standard processing scheme. The file size of the data is directly related to the recording time. For example, a recording time of one hour sampled with 200 Hz will produce a file size of 1.44 MB per channel. A record with two channels and a recording time of two days will get a total data volume of 70 MB.

• merge

If a tape error occurs during the download process, the ref2segy program has to be restarted. This will lead to several data files with different starting times. Merging these files into a single file is done by the merge program. The gap between the last sample and the first sample of the consecutive data trace will be filled up with zeros. Overlapping parts will be cut out.

• segy2trig

The trigger signal, which is provided by the airgun control system, is recorded simultaneously on an additional *Methusalem* during the shooting period. This tape is treated as a regular data tape and downloaded to the hard disk via the ref2segy program. The segy2trig program detects the shot times in the data stream. It determines the shot times by detecting the trigger signal through a given slope steepness, duration and threshold of the trigger pulse. The output is an ASCII table consisting of the shot number and the shot time. The accuracy of the shot time is one of the most crucial matters in seismic wide-angle work. It has to be reproduced with a precision of 5 ms. Due to this demand the shot times have to be corrected with the shift of the internal recorder clock. As additional information, the trigger file contains the profile number and the start/end time of the profile and the

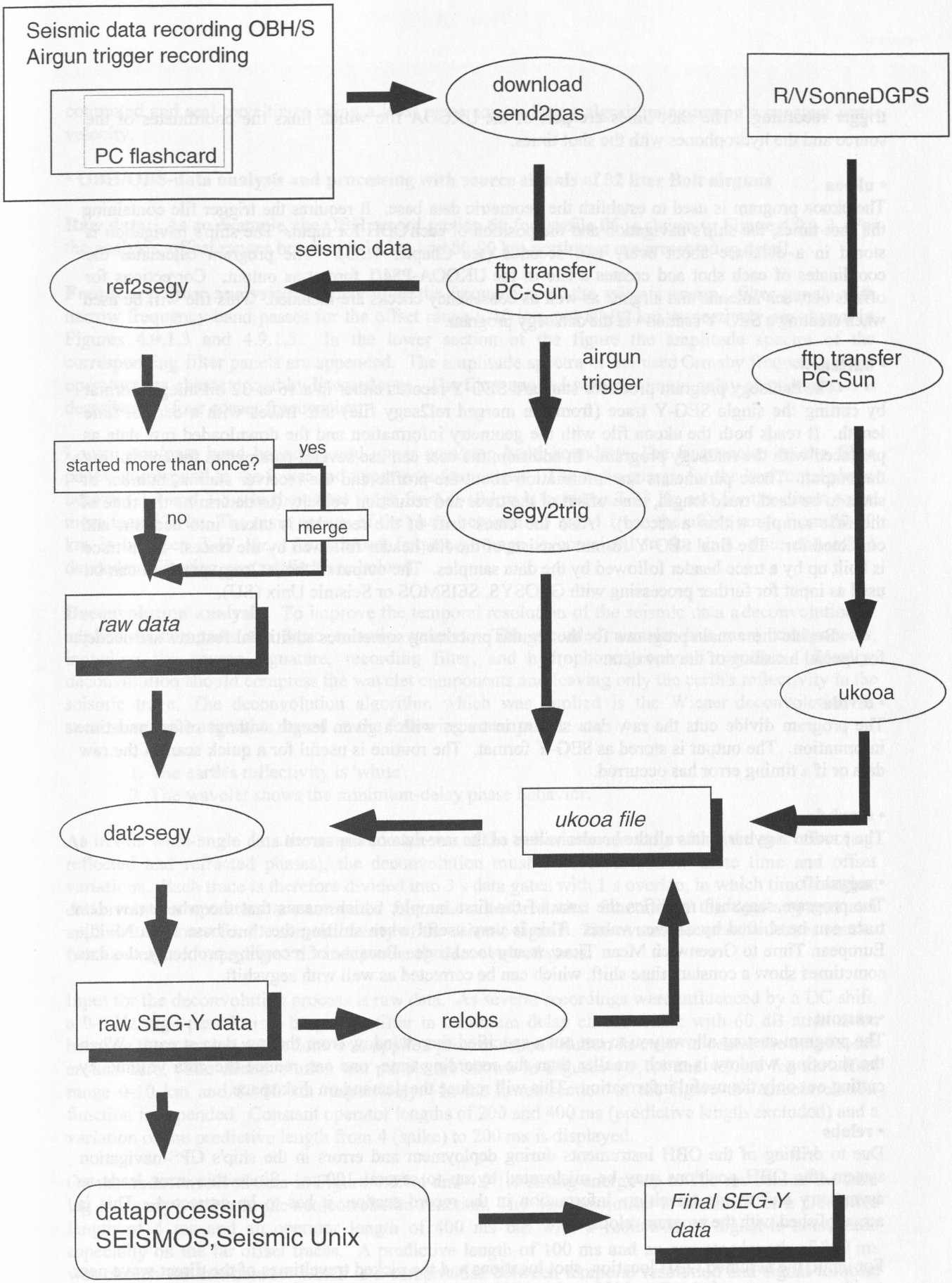

Figure 4.9.1.1: Processing flow of OBH/S data from raw data toSEG-Y records.

trigger recording. The shot times are part of the UKOOA file which links the coordinates of the source and the hydrophones with the shot times.

• ukooa

The ukooa program is used to establish the geometric data base. It requires the trigger file containing the shot times, the ship's navigation and the position of each OBH for input. The ship's navigation is stored in a database about every two seconds (see Chapter 4.1.3). The program calculates the coordinates of each shot and creates a file in the UKOOA-P84/1 format as output. Corrections for offsets between antenna and airguns as well as consistency checks are included. This file will be used when creating a SEG-Y section via the dat2segy program.

• dat2segy

The dat2segy program produces standard SEG-Y records either in a 16 or 32 bit integer format by cutting the single SEG-Y trace (from the merged ref2segy file) into traces with a certain time length. It reads both the ukooa file with the geometry information and the downloaded raw data as produced with the ref2segy program. In addition, the user can use several parameters for controlling the output. These parameters are information about the profile and the receiver station, number of shots to be used, trace length, time offset of the trace and reduction velocity (to determine the time of the first sample within a record). Also the clock drift of the recorder is taken into account and corrected for. The final SEG-Y format consists of the file header followed by the traces. Each trace is built up by a trace header followed by the data samples. The output of the dat2segy program can be used as input for further processing with GEOSYS, SEISMOS or Seismic Unix (SU).

Beside these main programs for the regular processing sometimes additional features are needed for special handling of the raw data:

• divide

The program divide cuts the raw data stream in traces with a given length without offset and time information. The output is stored as SEG-Y format. The routine is useful for a quick scan of the raw data or if a timing error has occurred.

• segyhdr

The routine segyhdr prints all the header values of the raw data on the screen.

• segyshift

The program segyshift modifies the time of the first sample, which means that the whole raw data trace can be shifted by a given value. This is very useful when shifting the time base from Middle European Time to Greenwich Mean Time or any local time. Because of recording problems, the data sometimes show a constant time shift, which can be corrected as well with segyshift.

• castout

The program castout allows you to cut out a specified time window from the raw data stream. When the shooting window is much smaller than the recording time, one can reduce the data volume by cutting out only the useful information. This will reduce the demand on disk space.

• relobs

Due to drifting of the OBH instruments during deployment and errors in the ship's GPS-navigation system, the OBH positions may be mislocated by up to several 100 m. Since this error leads to asymmetry and wrong traveltime information in the record section, it has to be corrected. This is accomplished with the program relobs.

For input, the assumed OBH location, shot locations and the picked traveltimes of the direct wave near to it's apex are needed. By shifting the OBH position, relobs minimizes the deviation between

computed and real traveltimes using a least mean square fitting algorithm assuming a constant water velocity.

• OBH/OBS-data analysis and processing with source signals of 32 liter Bolt airguns

Raw data: As an example, the OBH record section 65 for profile 06 is shown in Figure 4.9.1.2. For the analysis, offset ranges between 0-10 km and 80-90 km northwest are presented in detail.

Frequency filter analysis: To determine the frequencies of the seismic energy, filter panels with narrow frequency band passes for the offset range 0-10 km and 80-90 km respectively are shown in Figures 4.9.1.3 and 4.9.1.5. In the lower section of the figure the amplitude spectra of the corresponding filter panels are appended. The amplitude spectra of the used Ormsby frequency filter operators are characterized by linear slopes. The filter applied with minimum delay characteristics is described by four corner frequencies:

Lower stop/pass band boundary and upper pass/stop band boundary. The frequencies on the filter panels correspond to the lower and upper pass frequencies. The main energy for the horizontal phase between 3.4 and 3.8 s in the offset range from 0-10 km is between 3-23 Hz and for the direct wave more than 57 Hz. The main energy of the phase between 3.5 and 4.1 s in the offset range from 80-90 km is between 3-17 Hz. As a broad frequency range is contained in the data, time and offset dependent filtering was applied (see below).

Deconvolution analysis: To improve the temporal resolution of the seismic data a deconvolution is applied to compress the basic seismic wavelet. The recorded wavelet has many components, including the source signature, recording filter, and hydrophone/geophone response. Ideally, deconvolution should compress the wavelet components and leaving only the earth's reflectivity in the seismic trace. The deconvolution algorithm which was applied is the Wiener deconvolution in successive trace segments, based on the following assumptions:

1. The earth's reflectivity is 'white'.
2. The wavelet shows the minimum-delay phase behavior.

As in this wide-angle data the amplitude spectra of the seismic traces vary with time and offset (e.g. reflected and refracted phases), the deconvolution must be able to follow these time and offset variations. Each trace is therefore divided into 3 s data gates with 1 s overlap, in which time invariant deconvolution operators are computed from the autocorrelation function of the data segment and applied to account for the nonstationarity of the seismic signals. The overall deconvolved trace results from a weighted merging of the independently deconvolved gates.

Input for the deconvolution process is raw data. As several recordings were influenced by a DC shift, a 0-3 Hz high-pass Kaiser frequency filter in minimum delay characteristic with 60 dB attenuation between the pass and reject zone was applied prior to deconvolution in order to center the amplitudes around zero. The deconvolution test panels are shown in Figures 4.9.1.4 and 4.9.1.6 for the offset range 0-10 km and 80-90 km respectively. In the lower section of the figure the autocorrelation function is appended. Constant operator lengths of 200 and 400 ms (predictive length excluded) and a variation of the predictive length from 4 (spike) to 200 ms is displayed.

On the undeconvolved data in Figure 4.9.1.4 and 4.9.1.6 strong energy up to 500 ms behind the zero lag is clearly visible in the autocorrelation function. The best resolution is obtained for a predictive length of 4 ms and an operator length of 400 ms but with a reduction of signal-to-noise ratio especially on the far offset traces. A predictive length of 100 ms and an operator length of 200 ms was chosen for this data set which is a compromise between temporal resolution and signal-to-noise ratio.

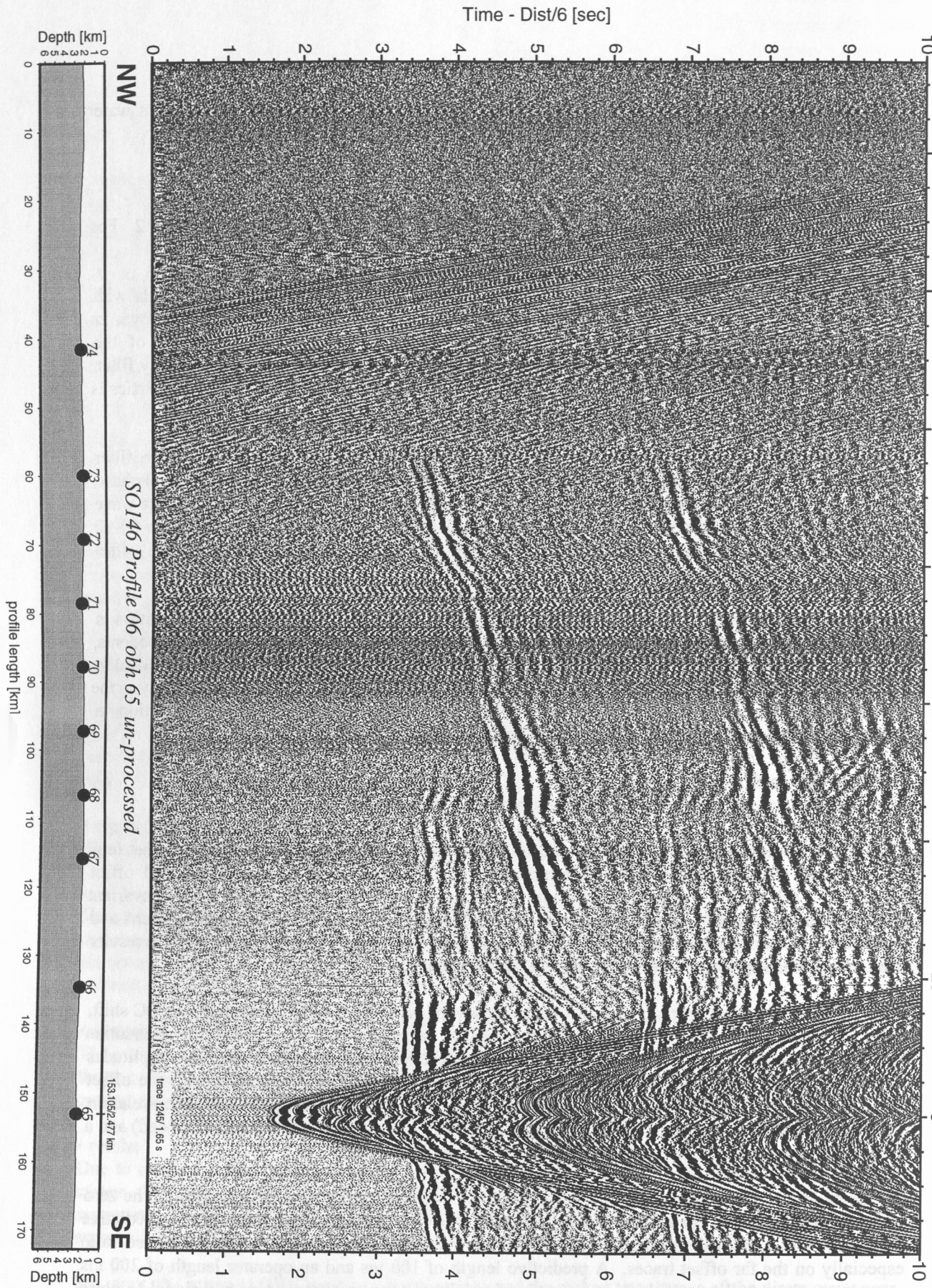

Figure 4.9.1.2: Un-processed record section from obh 65 , Profile 06.

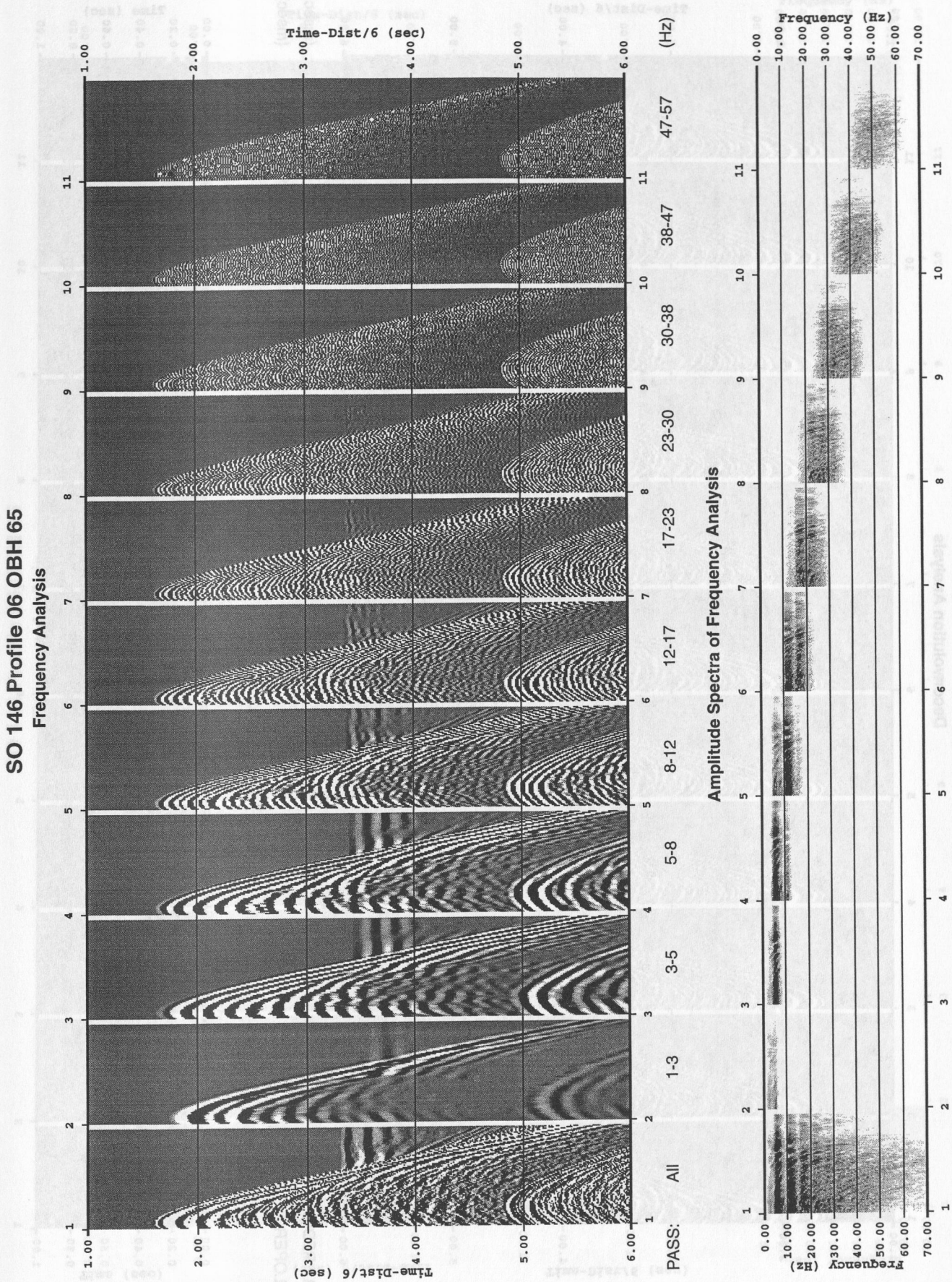

Figure 4.9.1.3: Frequency analysis in the offset range 0-10 km.

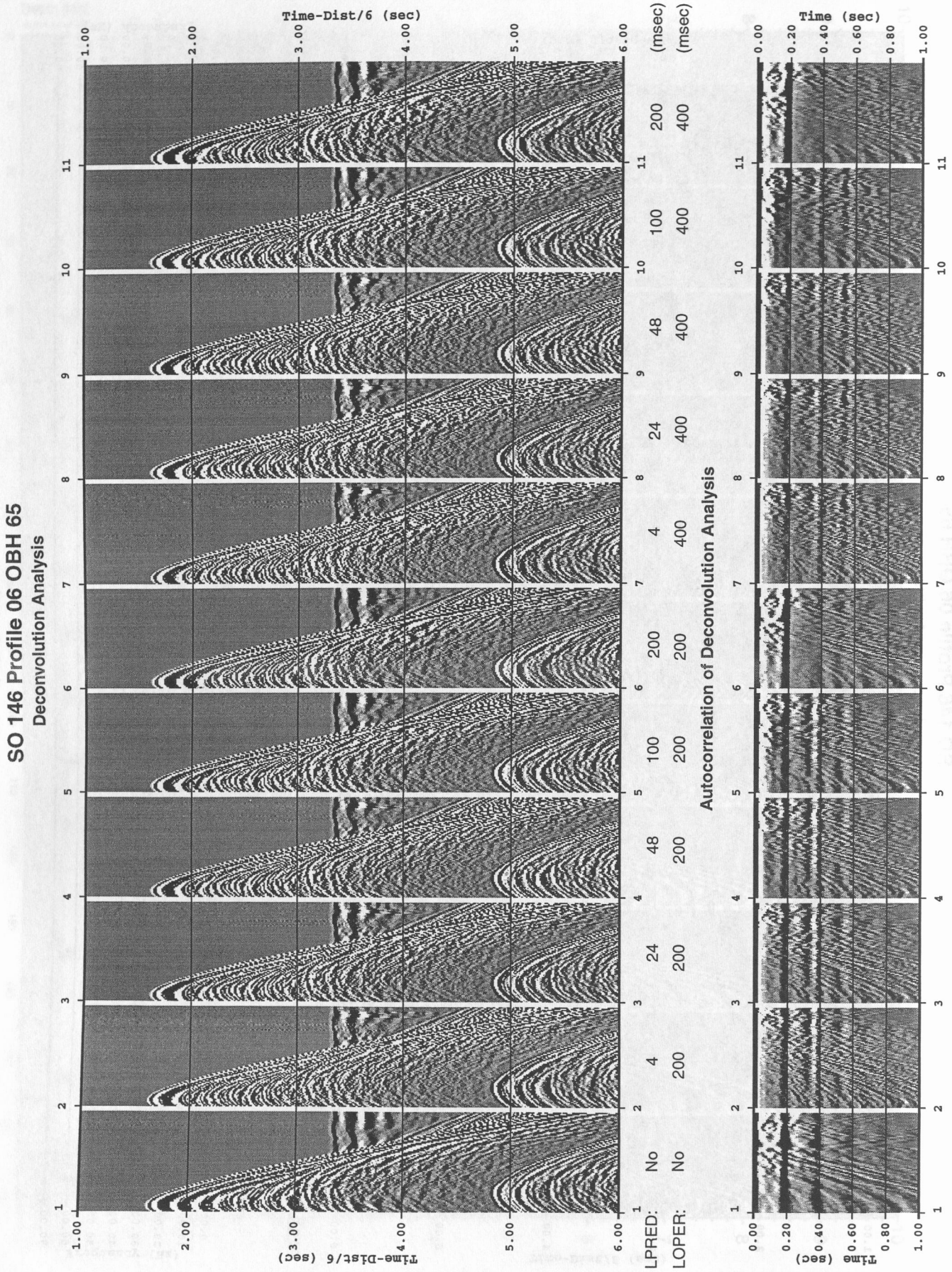

Figure 4.9.1.4: Deconvolution analysis in the offset range 0-10 km.

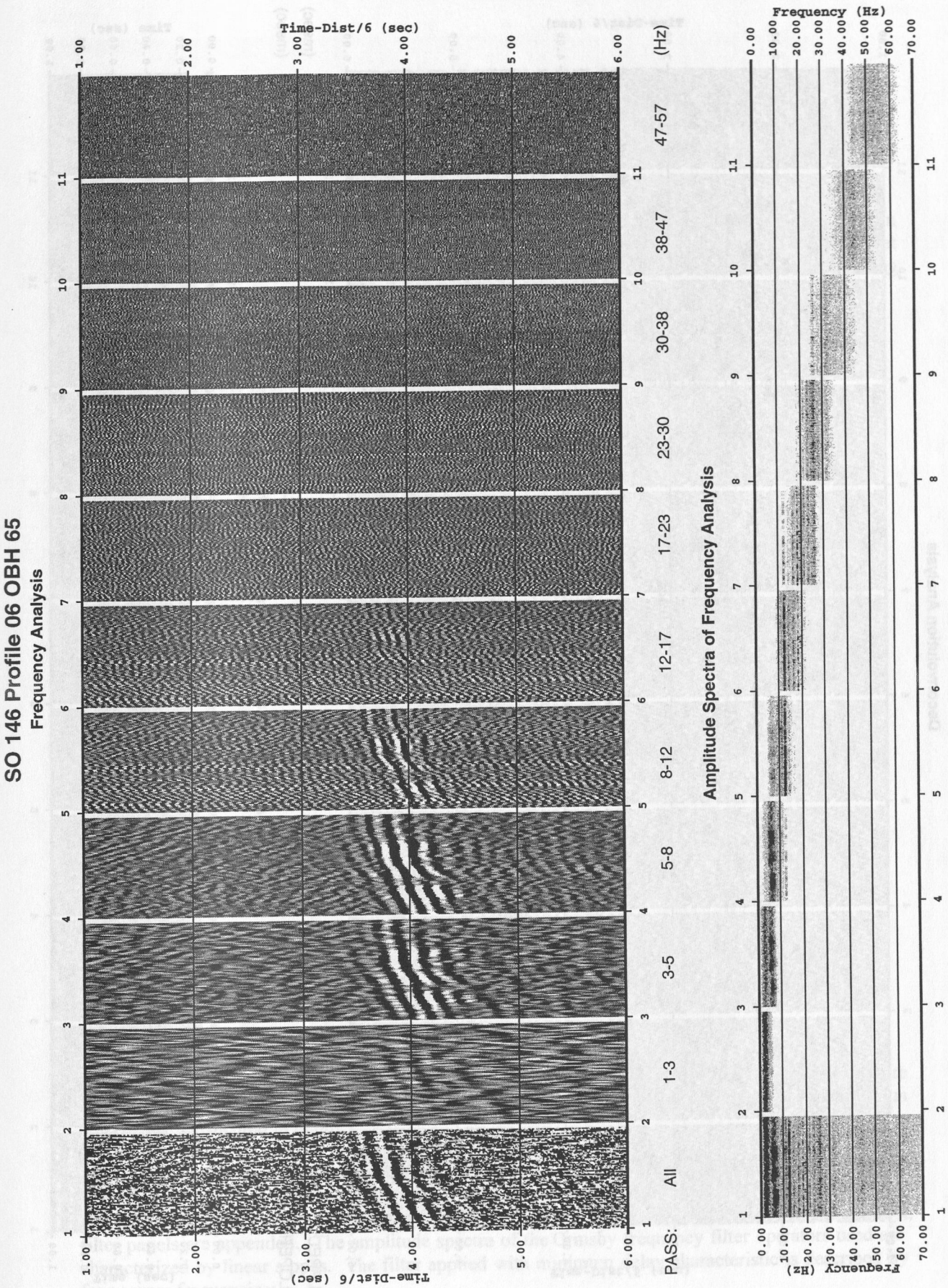

Figure 4.9.1.5: Frequency analysis in the offset range 80-90 km.

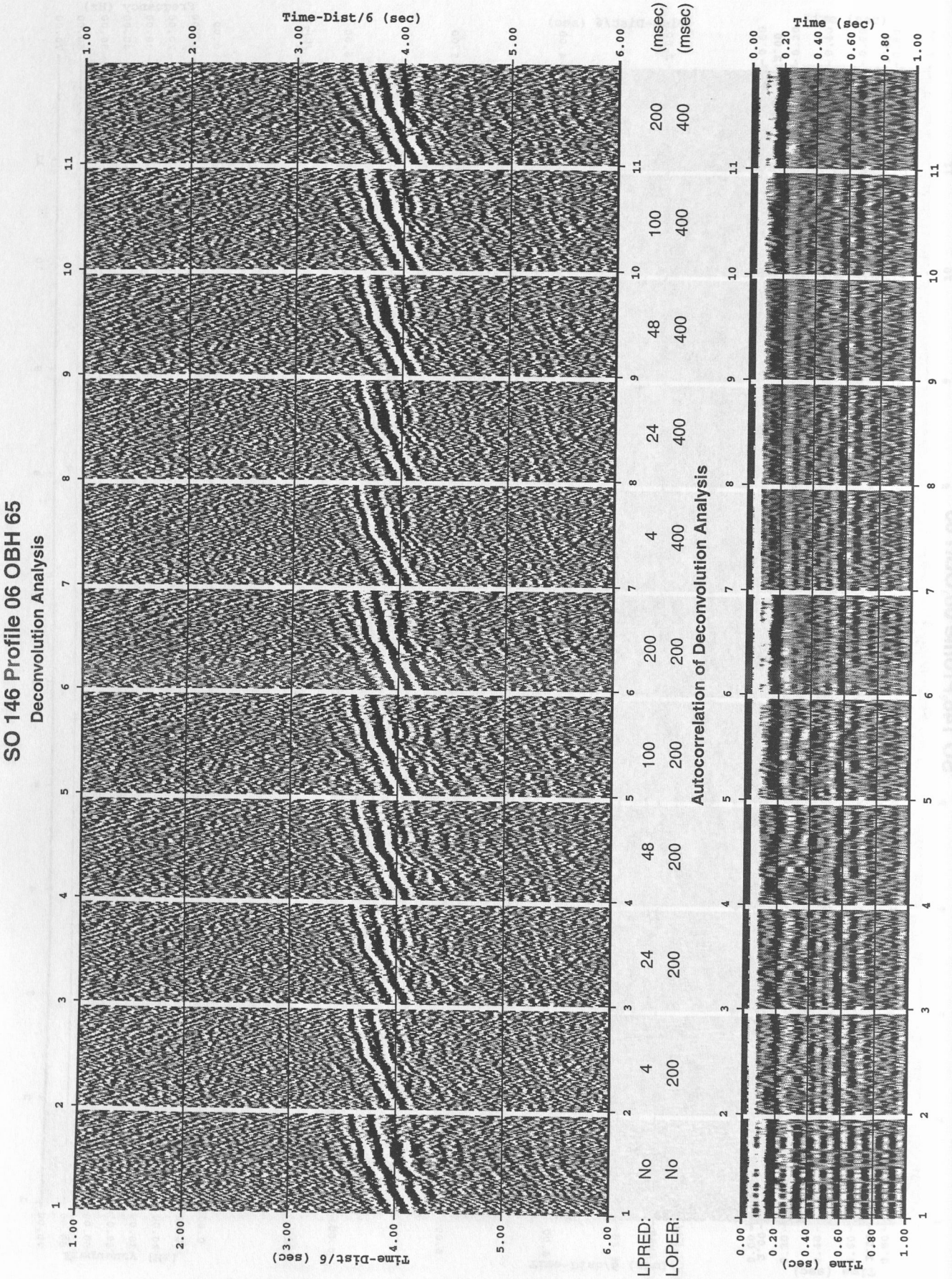

Figure 4.9.1.6: Deconvolution analysis in the offset range 80-90 km.

After deconvolution an offset- and time-variant Ormsby filter with minimum delay characteristic was applied. As the seafloor depth changes along the seismic lines, each trace was statically corrected to a fixed seafloor travel time of 11 s based on the water depth before filtering. This information is available in the trace headers. After this filter was applied, the data were shifted back to their original travel times.

Processed data: Comparison of the preprocessed data in Figure 4.9.1.7 to the unprocessed data in Figure 4.9.1.2 shows a clear reduction of the low and mono-frequency noise in the near and far offset traces and moderate compression of the wavelet signal. For the picking of events and model building by raytracing both sections were used to keep all available seismic information.

- **Final processing sequence**
  - Input: SEGY-data, 4 ms sampling rate with complete geometry information.
  - Tapering the first 0.5 s to zero to reduce the response of the debias filter operator.
  - Kaiser highpass (debias).
  - Gated Wiener deconvolution: gate length 3 s, overlap 1 s, length of merge region 1 s, operator length 200 ms (prediction interval excluded), prediction interval 100 ms.
  - Static correction to a fixed seafloor traveltime of 11 s.
  - Time and offset-dependent Ormsby frequency filter.

On time-shifted traces with a reduced time scale of 6 km/s the following filter parameters were used:

lower stop/pass	upper pass/stop (Hz)	offset(m)	beginfull(s)	endfull(s)
3/5	28/48	0	12.8	
		8000	0	12.6
		48000	0	0
3/5	23/38	0	13.7	14.3
		8800	13.5	14.4
		13200	13.0	13.9
		52000	1.0	2.0
		107000	0	0
3/5	18/28	0	15.3	16.8
		11700	15.1	16.6
		19200	14.8	16.3
		61700	7.0	10.1
		114000	2.0	3.0
		152000	0	0
3/5	13/18	0	19.0	trace length
		20000	18.4	trace length
		130000	3.5	trace length

- **OBH/OBS-data analysis and processing with source signals of 1.7 liter GI-guns**

Raw data: As an example, the hydrophone of OBS record section 76 of profile 07 is shown in Figure 4.9.1.8. For the analysis, the hydrophone and the vertical component in offset ranges between 0-4 km northeast are presented in detail.

Frequency analysis: To determine the frequencies of the seismic energy, filter panels with narrow frequency pass bands for the hydrophone and the vertical component are shown in Figures 4.9.1.9 and 4.9.1.10 respectively. In the lower section of the figure the amplitude spectra of the corresponding filter panels are appended. The amplitude spectra of the Ormsby frequency filter operators used are characterized by linear slopes. The filter applied with minimum delay characteristic is described by four corner frequencies:

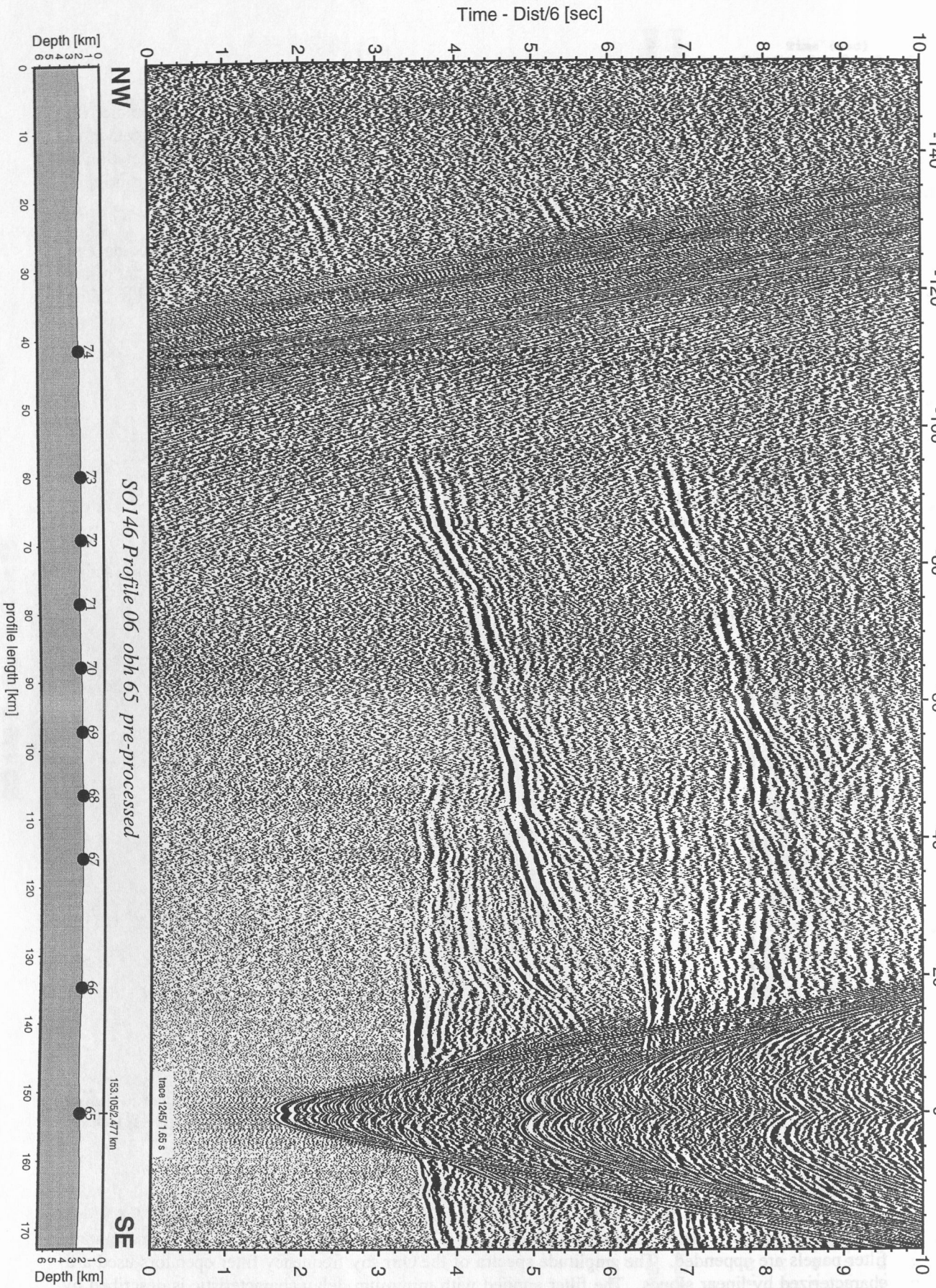

Figure 4.9.1.7: Pre-processed record section from obh 65 , Profile 06.

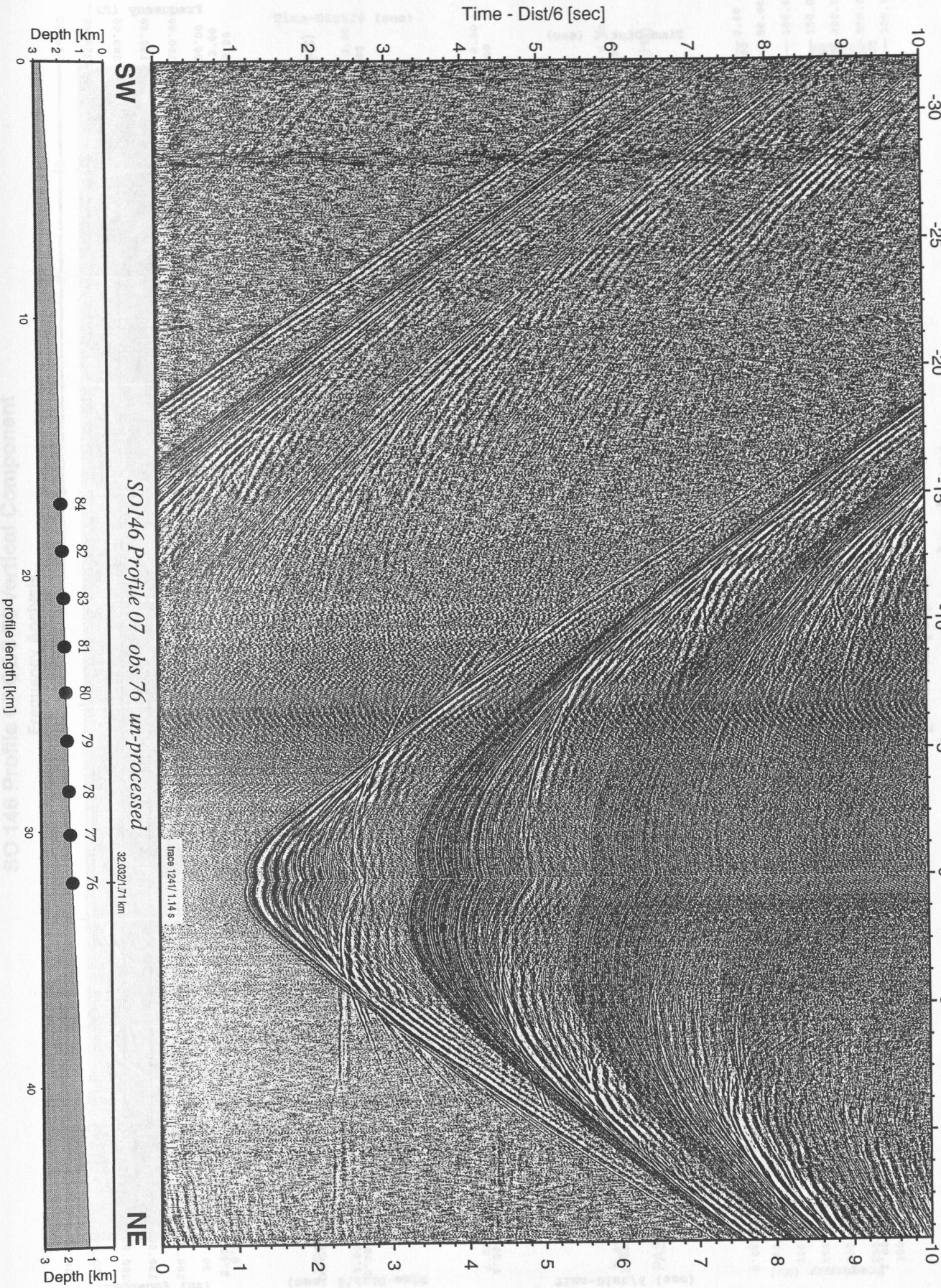

Figure 4.9.1.8: Un-processed record section from obs 76 hydrophone, Profile 07.

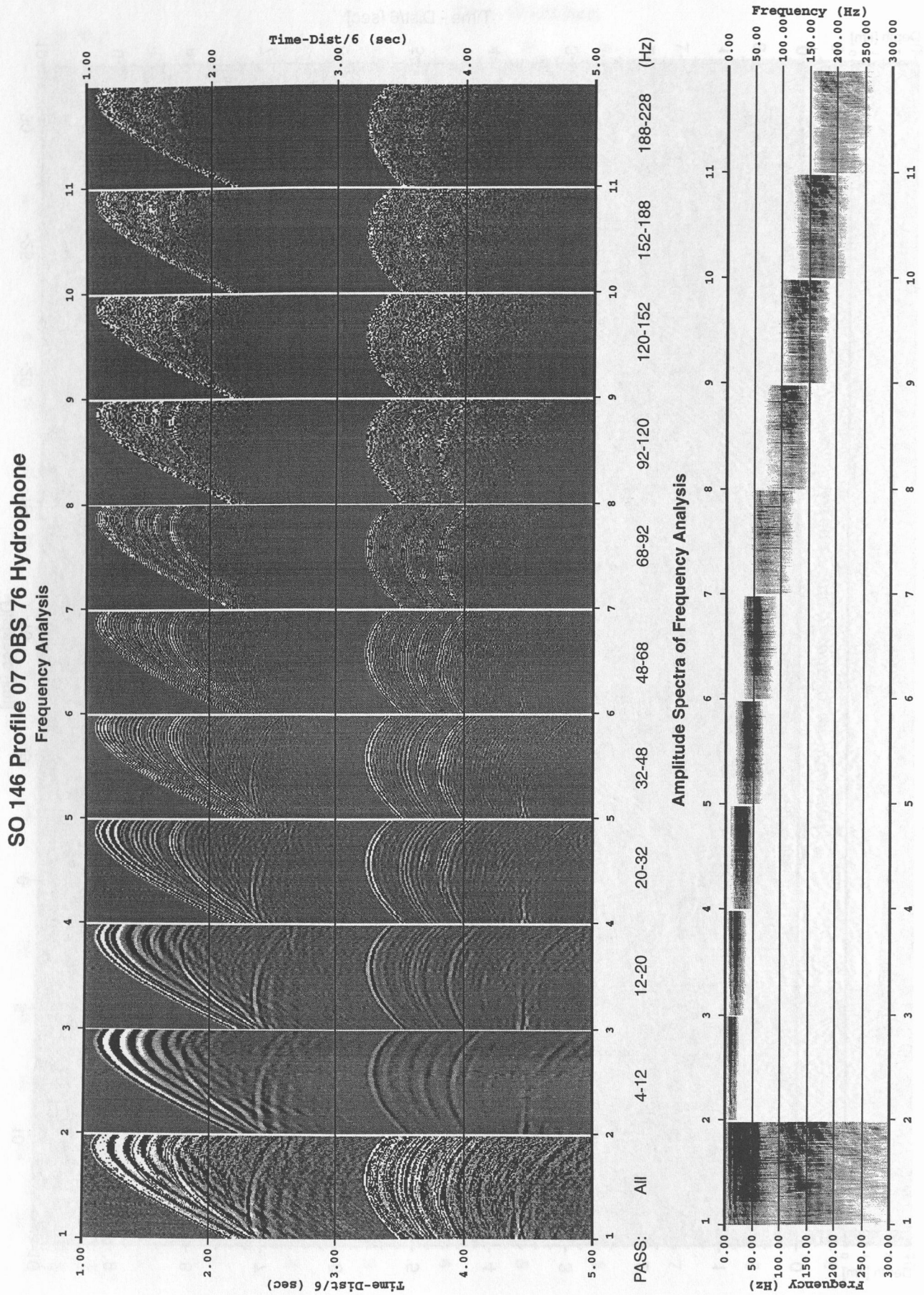

Figure 4.9.1.9: Frequency analysis in the offset range 0-4 km.

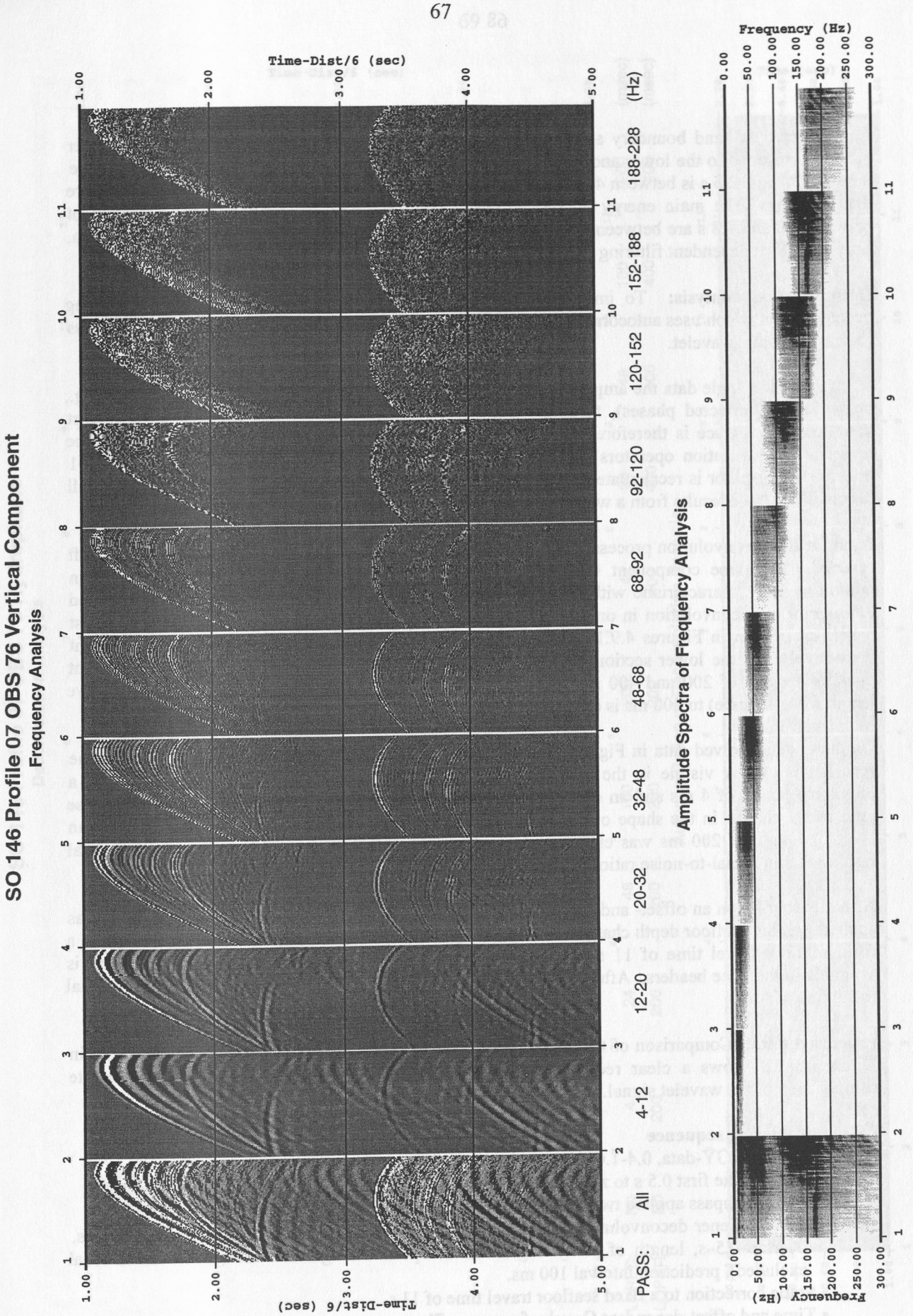

Figure 4.9.1.10: Frequency analysis in the offset range 0-4 km.

Lower stop/pass band boundary and upper pass/stop band boundary. The frequencies on the filter panels correspond to the lower and upper pass frequencies. The main energy for the reflected phase between 2.4 and 2.5 s is between 4-48 Hz and for the direct wave and shallow reflection phases more than 228 Hz. The main energy of the converted shear wave phases on the vertical component between 2.8 and 4.8 s are between 4-12 Hz. Since a broad frequency range is contained in the data, time and offset dependent filtering is applied (see below).

Deconvolution analysis: To improve the temporal resolution of the seismic data a roll-along deconvolution which uses autocorrelograms averaged over a number of traces is applied to compress the basic seismic wavelet.

As in this wide-angle data the amplitude spectra of the seismic traces vary with time and offset (e.g., pp, ps and ss-reflected phases), the deconvolution must be able to follow these time and offset variations. Each trace is therefore divided into 1.5 s data gates with 0.5 s overlap, in which time invariant deconvolution operators are computed from the average autocorrelation function of 101 traces. The operator is recalculated for every trace and each data segment and applied. The overall deconvolved trace results from a weighted merging of the independently deconvolved gates.

Input for the deconvolution process is raw data. As several recordings were influenced by a DC shift especially the three component OBS recordings, a 0-3 Hz high-pass Kaiser frequency filter in minimum delay characteristic with 60db attenuation between the pass and reject zone was applied twice prior to deconvolution in order to center the amplitudes around zero. The deconvolution test panels are shown in Figures 4.9.1.11 and 4.9.1.12 for the hydrophone and the vertical component respectively. In the lower section of the figure the autocorrelation function is appended. Constant operator lengths of 200 and 400 ms (predictive length excluded) and a variation of the predictive length from 4 (spike) to 200 ms is displayed.

On the undeconvolved data in Figures 4.9.1.11 and 4.9.1.12 strong energy up to 500 ms behind the zero lag is clearly visible in the autocorrelation function. The best resolution is obtained for a predictive length of 4 ms and an operator length of 400 ms, but with a reduction of signal-to-noise ratio and a change in the shape of the signal (phase error). A predictive length of 100 ms and an operator length of 200 ms was chosen for this data set which is a compromise between temporal resolution and signal-to-noise ratio.

After deconvolution an offset- and time-variant Ormsby filter with minimum delay characteristic was applied. As the seafloor depth changes along the seismic lines, each trace was statically corrected to a fixed seafloor travel time of 11 s based on the water depth before filtering. This information is available in the trace headers. After this filter was applied, the data were shifted back to their original travel times.

Processed data: Comparison of the preprocessed data in Figure 4.9.1.13 to the unprocessed data in Figure 4.9.1.8 shows a clear reduction of the low and mono-frequency noise and a moderate compression of the wavelet signal.

- **Final processing sequence**
  - Input: SEGY-data, 0.4-1.0 ms sampling rate with complete geometry information.
  - Tapering the first 0.5 s to zero to reduce the response of the debias filter operator.
  - Kaiser highpass applied twice (debias).
  - Gated Wiener deconvolution with autocorrelation average of 101 traces: gate length 1.5 s, overlap 0.5 s, length of merge region 0.5 s, operator length 200 ms (prediction interval excluded), prediction interval 100 ms.
  - Static correction to a fixed seafloor travel time of 11 s.
  - Time and offset-dependent Ormsby frequency filter.
  - Resampling to 2 ms sample rate.

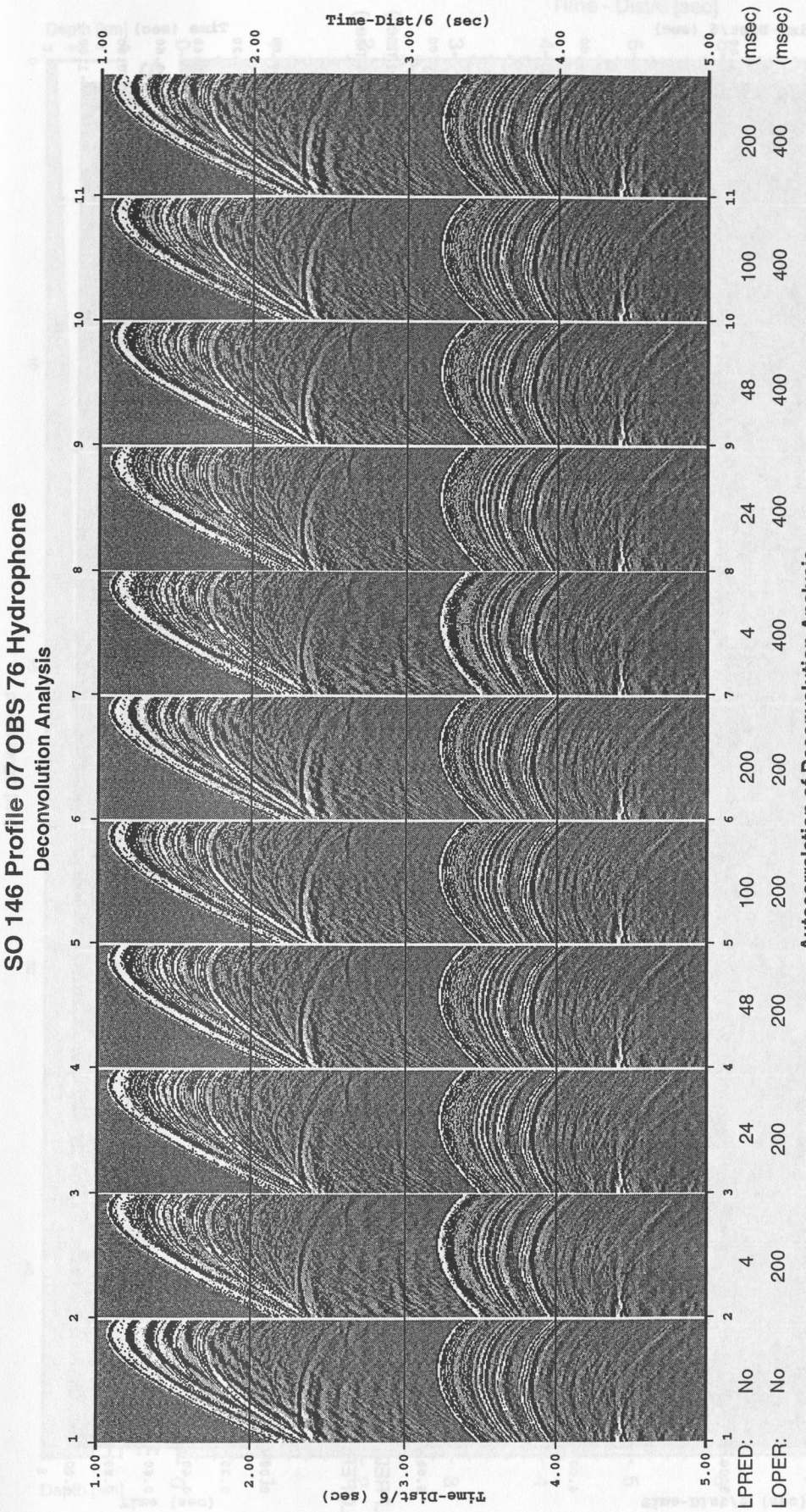

Figure 4.9.1.11: Deconvolution analysis in the offset range 0-4 km.

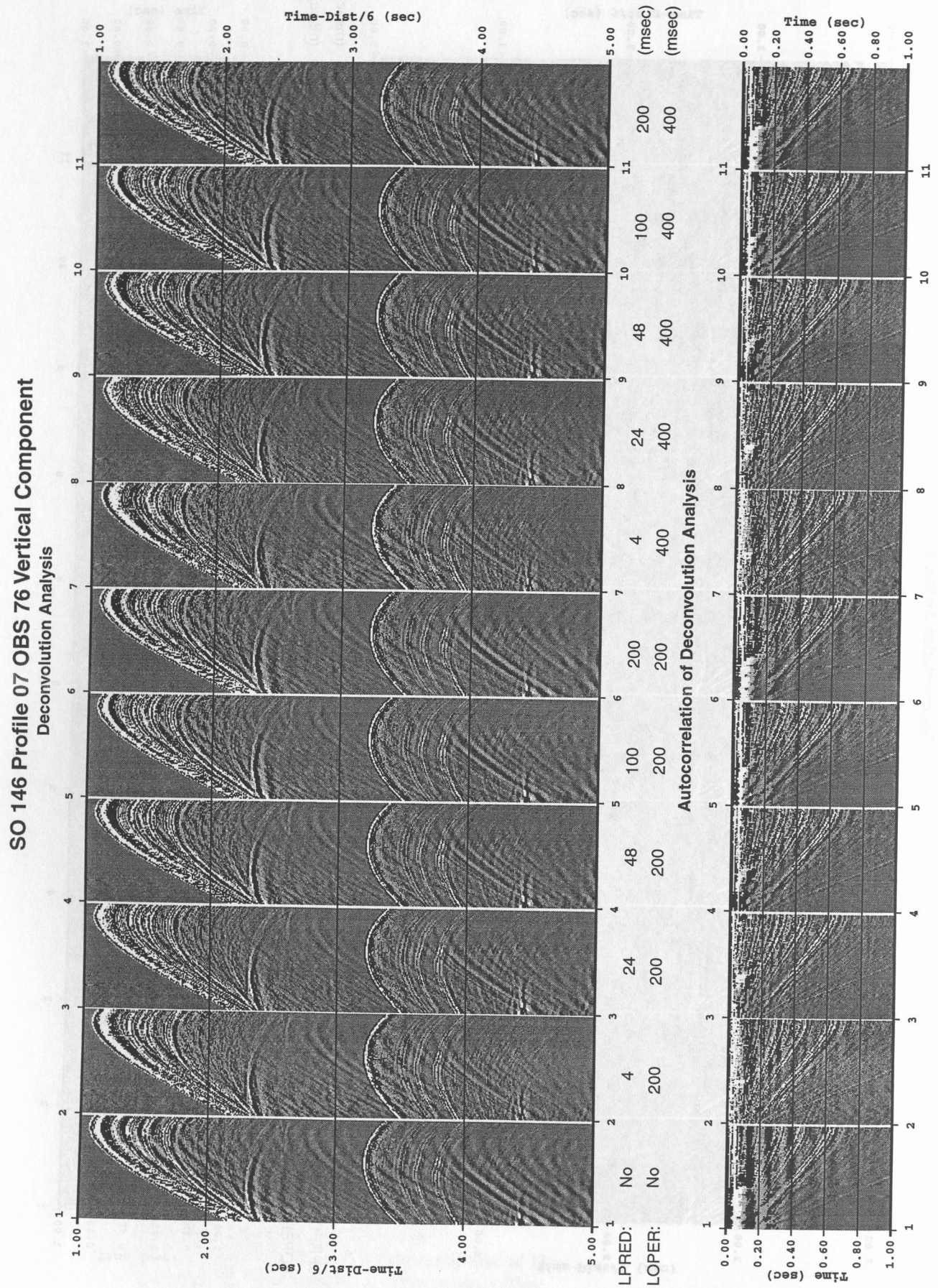

Figure 4.9.1.12: Deconvolution analysis in the offset range 0-4 km.

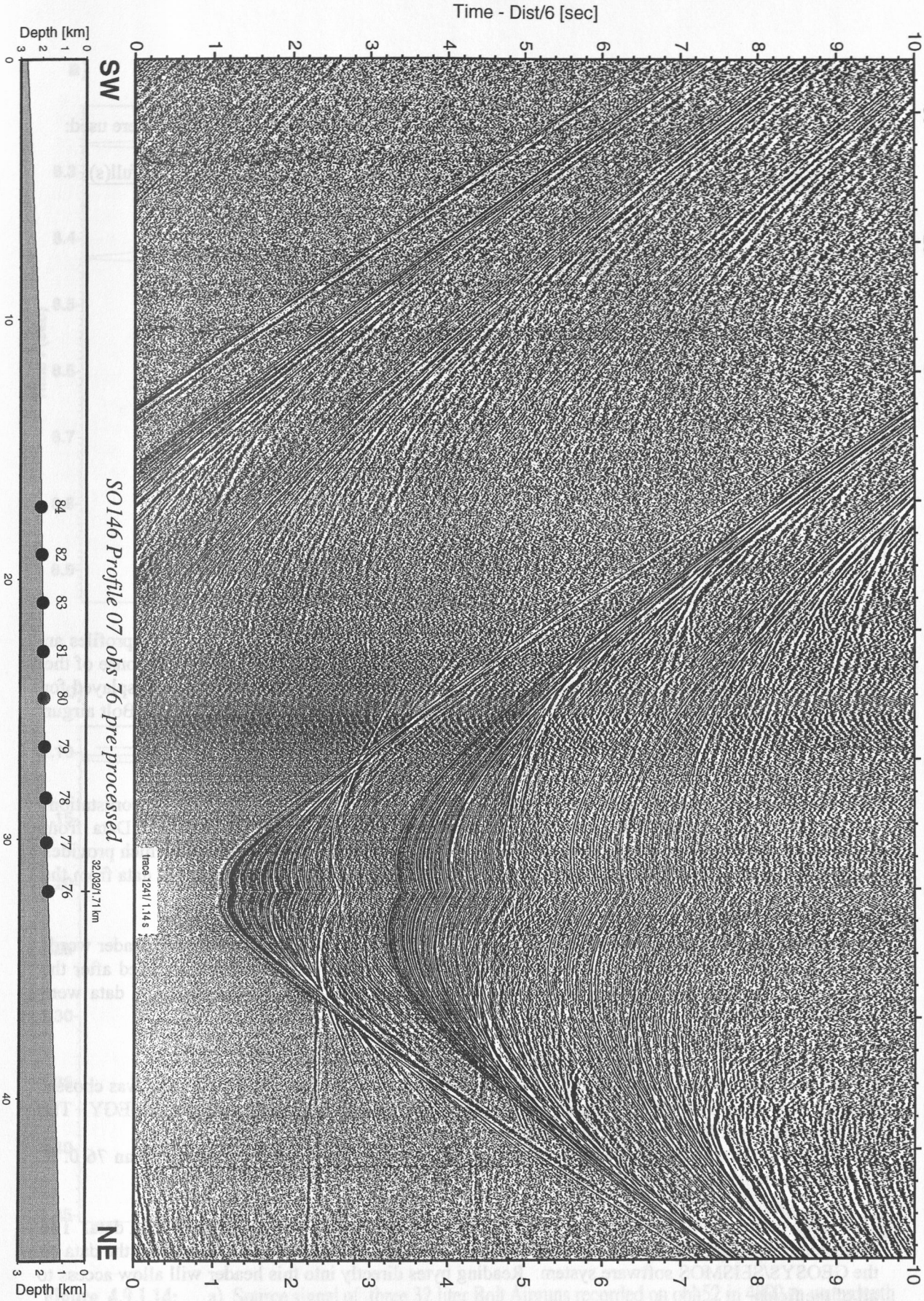

Figure 4.9.1.13: Pre-processed record section from obs 76 hydrophone, Profile 07.

On time-shifted traces with a reduced time scale of 6 km/s the following filter parameters were used:

lower stop/pass	upper pass/stop (Hz)	offset(m)	beginfull(s)	endfull(s)
3/5	200/250	0	0	12.8
	8000	0	12.6	
	48000	0	0	
3/5	50/100	0	13.7	14.3
	8800	13.5	14.4	
	13200	13.0	13.9	
	52000	1.0	2.0	
	107000	0	0	
3/5	25/50	0	15.3	16.8
	11700	15.1	16.6	
	19200	14.8	16.3	
	61700	7.0	10.1	
	114000	2.0	3.0	
	152000	0	0	
3/5	15/25	0	19.0	trace length
	20000	18.4	trace length	
	130000	3.5	trace length	

• Source signals

During the survey different seismic sources were used to image the subsurface. On some profiles an OBH was suspended several hundred meters above the seafloor to record the far-field response of the seismic source signal. In Figure 4.9.14 the source signal and the amplitude spectrum is displayed for three 32 liter Bolt airguns and two 1.7 liter GI-guns. Notice the strong reverberation of the Bolt airgun signal and the relative low frequency signals compared to the first pulse of the GI-guns.

• Data archiving

Data recorded with the MBS recorder on flash discs were transferred via a PC to a SUN workstation. On the workstation they were transformed into a so-called PSEUDO-SEGY format. Data from Methusalem DAT devices were played back using a SCSI compatible playback device which provides the data in the same PASSCAL data format as the MBS data on a Sun disk. Both the raw data from the flash discs and the PSEUDO-SEGY data were archived on DAT or Exabyte tapes.

After navigation data had been merged and SEGY formatted traces with the appropriate header words had been created, the data were also archived. Finally, a third set was stored and archived after the shipboard processing, as described above, had been applied. All final processed SEGY data were archived on tapes.

• Data exchange

For the exchange of the OBH/OBS data, the SEGY-format on disk with a Sun tar-format was chosen. The raw segy data is in Integer2 format with trailer bytes between the record structure of SEGY. The processed data is in IBM-floating point without trailer bytes between the records.
For UTM transformation into Cartesian coordinates use: WGS84 spheroid, central meridian 76 0. 0. W, southern hemisphere.

This is the definition of the segy trace header for the GEOMAR OBS wide-angle reflection data. The extension of the standard SEGY header from 181 to 240 byte is a layout in order to process the data on the GEOSYS/SEISMOS software system. Reading bytes directly into this header will allow access to all of the fields.

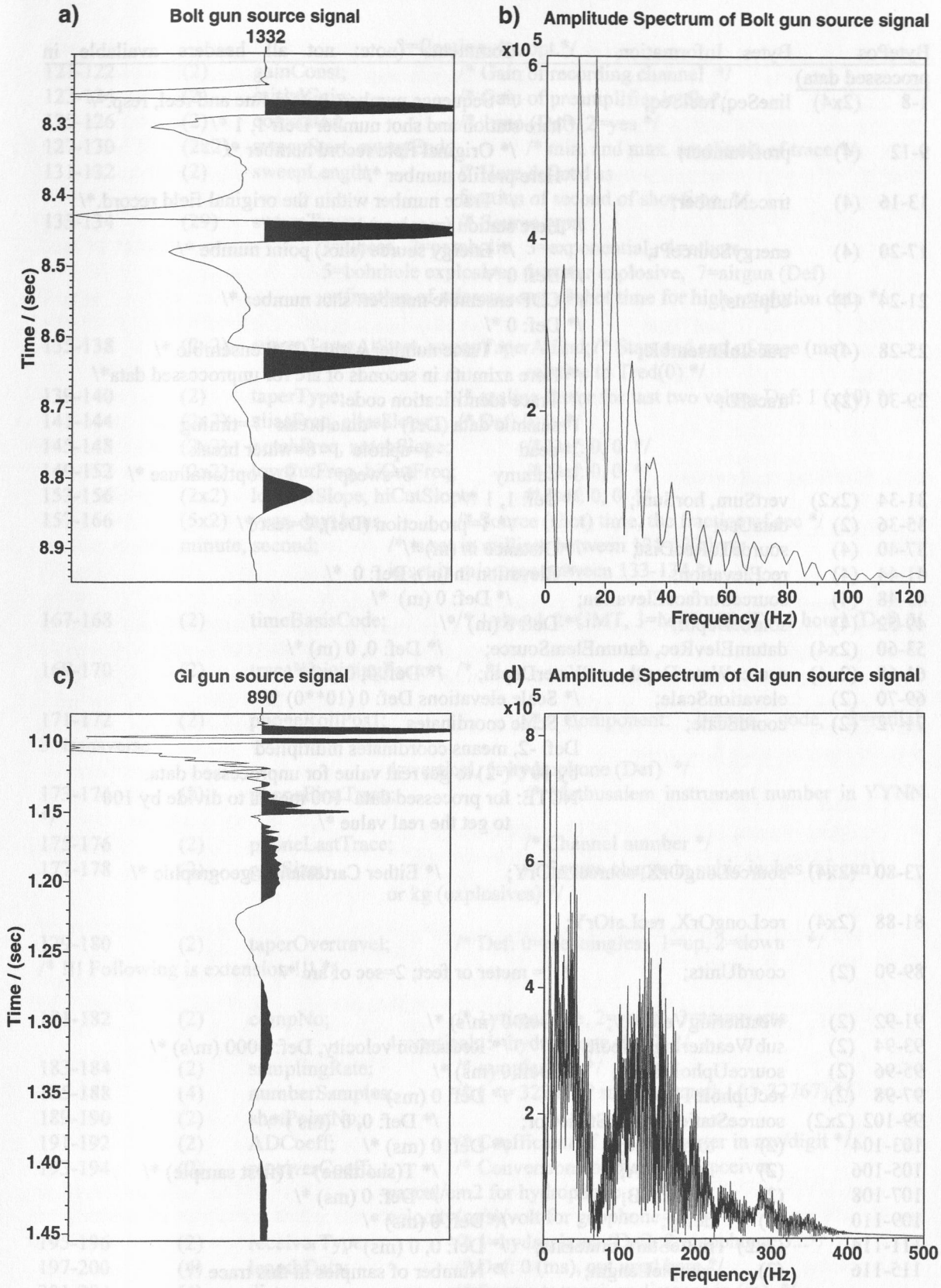

Figure 4.9.1.14: a) Source signal of three 32 liter Bolt Airguns recorded on obh52 in 4892 m waterdepth and its amplitude spectrum (b). c) Source signal of two 1.6 liter GI guns (true harmonic mode) recorded on obh81 in 1914 m waterdepth and its amplitude spectrum (d).

BytePos	Bytes	Information	Comments (note: not all headers available in processed data)
1-8	(2x4)	lineSeq, reelSeq;	/* Sequence numbers within line and reel, resp.*/
			/* here station and shot number Def: 1, 1 */
9-12	(4)	profNumber;	/* Original field record number */
			/* Here profile number */
13-16	(4)	traceNumber;	/* Trace number within the original field record.*/
			/* Here station (receiver) Number */
17-20	(4)	energySourcePt;	/* Energy source (shot) point numbe */
			/* Def: 0 */
21-24	(4)	cdpEns;	/* CDP ensemble number: shot number */
			/* Def: 0 */
25-28	(4)	traceInEnsemble;	/* Trace number within CDP ensemble */
			/* Here azimuth in seconds of arc for unprocessed data*/
29-30	(2)	traceID;	/* Trace identification code:
			1=seismic data (Def) 4=time break 7=timing
			2=dead 5=uphole 8=water break
			3=dummy 6=sweep 9..., optional use */
31-34	(2x2)	vertSum, horSum;	/* Def: 1, 1 */
35-36	(2)	dataUse;	/* 1=production (Def), 2=test */
37-40	(4)	sourceToRecDist;	/* Distance in (m) */
41-44	(4)	recElevation;	/* Elevation in (m), Def: 0 */
45-48	(4)	sourceSurfaceElevation;	/* Def: 0 (m) */
49-52	(4)	sourceDepth;	/* Def: 0 (m) */
53-60	(2x4)	datumElevRec, datumElemSource;	/* Def: 0, 0 (m) */
61-68	(2x4)	sourceWaterDepth, recWaterDepth;	/* Def: 0, 0 (m) */
69-70	(2)	elevationScale;	/* Scale elevations Def: 0 (10**0) */
71-72	(2)	coordScale;	/* Scale coordinates
			Def: -2, means coordinates multiplied
			by 10**(-2) to get real value for unprocessed data.
			NOTE: for processed data -100 means to divide by 100
			to get the real value */
73-80	(2x4)	sourceLongOrX, sourceLatOrY;	/* Either Cartesian or geographic */
81-88	(2x4)	recLongOrX, recLatOrY;	
89-90	(2)	coordUnits;	/* 1= meter or feet; 2=sec of arc */
91-92	(2)	weatheringVelocity;	/* Def: 0 (m/s) */
93-94	(2)	subWeatheringVelocity;	/* Reduction velocity, Def: 6000 (m/s) */
95-96	(2)	sourceUpholeTime;	/* Def: 0 (ms) */
97-98	(2)	recUpholeTime;	/* Def: 0 (ms) */
99-102	(2x2)	sourceStaticCor, recStaticCor;	/* Def: 0, 0 (ms) */
103-104	(2)	totalStatic;	/* Def: 0 (ms) */
105-106	(2)	lagTimeA;	/* T(shottime) - T(first sample) */
107-108	(2)	lagTimeB;	/* Def: 0 (ms) */
109-110	(2)	delay;	/* Def: 0 (ms) */
111-114	(2x2)	muteStart, muteEnd;	/* Def: 0, 0 (ms) */
115-116	(2)	sampleLength;	/* Number of samples in this trace */
			/* (> 32767)? = 32767
			set long samp_rate in 185-188 byte */
117-118	(2)	deltaSample;	/* Sampling interval in microseconds. */
119-120	(2)	gainType;	/* 1=fixed (Def), 2=binary,

```
                                3=floating, 4... opt.*/
121-122     (2)     gainConst;          /* Gain of recording channel  */
123-124     (2)     initialGain;        /* Gain of preamplifier in db */
125-126     (2)     correlated;         /* 1=no (Def), 2=yes */
127-130     (2x2)   sweepStart, sweepEnd;       /* min. and max. amplitude of trace */
131-132     (2)     sweepLength;        /* Here defined as
                                        fraction of second of shot time  */
133-134     (29)    sweepType;          /* Source type:
                        1=linear, 2=parabolic, 3=exponential, 4=others
                        5=bohrhole explosive, 6=water explosive, 7=airgun (Def)
                        or fraction of microsecond of shot time for high resolution data */

135-138     (2x2)   sweepTaperAtStart, sweepTaperAtEnd;/* Start and end of trace (ms)
                                                relative to Tred(0) */
139-140     (2)     taperType;          /* scaling factor for last two values Def: 1 (x10) */
141-144     (2x2)   aliasFreq, aliasSlope;  /* Def: 0, 0  */
145-148     (2x2)   notchFreq, notchSlope;      /* Def: 0, 0  */
149-152     (2x2)   lowCutFreq, hiCutFreq;      /* Def: 0, 0  */
153-156     (2x2)   lowCutSlope, hiCutSlope;    /* Def: 0, 0  */
157-166     (5x2)   year, day, hour,        /* Source (shot) time, the fraction of sec */
            minute, second;         /* is set in millisec between 131-132 byte
                                    is set in microsec between 133-134 */

167-168     (2)     timeBasisCode;      /* 1=local, 2=GMT, 3=MET (GMT + 1 hour) (Def) */

169-170     (2)     traceWeightingFactor;  /*  */

171-172     (2)     phoneRollPos1;              /*  Component:  1=time  code,  2=radial,
3=transverse
                                4=vertical, 5=hydrophone (Def)  */
173-174     (2)     phoneFirstTrace;            /* Methusalem instrument number in YYNN
*/
175-176     (2)     phoneLastTrace;             /* Channel number */
177-178     (2)     gapSize;                    /* Source charge in cubic inches (airgun)
                                or kg (explosives) */

179-180     (2)     taperOvertravel;    /* Def: 0=meaningless  1=up, 2=down    */
/* !!! Following is extension !!! */

181-182     (2)     compNo;             /* 1=time code, 2=radial, 3=transverse
                                4=vertical, 5=hydrophone (Def)  */
183-184     (2)     samplingRate;       /* samples/sec */
185-188     (4)     numberSamples;      /* ( <= 32767) ? sampleLength | ( > 32767) */
189-190     (2)     shotPointNo;
191-192     (2)     ADCoeff;            /* Coefficient of A/D converter in mv/digit */
193-194     (2)     receiverCoeff;      /* Conversion coefficient of receiver,
                                pascal/cm2 for hydrophone,
                                velocity(m/s)/volt for geophone */
195-196     (2)     receiverType;       /* 1=hydrophone (Def), 2=geophone, 3...*/
197-200     (4)     lengthData;         /* Def: 0 (ms), not used here */
201-204     (4)     distance;           /* Source to receiver distance in (m)  */
205-208     (4)     (float) scaleFactor;        /* Scale factor same as in <segy.h>
                                Here azimuth in second of arc for processed data */
209-210     (2)     azimuth;            /* Orientation of the component in min */
```

```
211-212   (2)   eigenperiod;      /* Eigenperiod of geo- or hydrophone in (ms) */
213-216   (4)   minAmpl;          /* Min. peak amplitude within trace    */
217-220   (4)   maxAmpl;          /* Max. peak amplitude within trace */
221-222   (2)   stationNo;        /* Station number */
223-224   (2)   channelNo;        /* Channel number (Default: 1) */
225-228   (4)   sourceCharge;     /* Charge in kg (explosive) or cc (airgun) */
229-230   (2)   redVelocity;      /* reduction velocity in (m/s);
                                  Def: 0 if no reduction velocity se */
231-232   (2)   timeOffset;              /* Time offset in (ms) of first sample
                                  relative to reduced source time:
                                  positive if earlier than reduced time  */
233-236   (4)   redTime;          /* Reduced time in (ms) = distance/redVel  */
237-238   (2)   unused2;
239-240   (2)   instNo;           /* Methusalem instrument number */
```

4.9.2 Multichannel seismic

(C. Hübscher, I. Pecher, M. Krüger)

The main purpose of on board processing of the multichannel seismic data was to produce brut stacks of shot gathers. For each line we selected a varying range of channels with optimized signal to noise ratio. For shallow water depth near offset traces were extracted to get almost vertical incidence angles. However, the ship noise is stronger on these channels. In areas with intricate BSRs or gas patterns just a few channels were taken to prevent signal distortion due to suboptimal stacking. In bigger water depth we stacked the entire set of active channels, just a few channels with low signal/noise ratios were rejected. NMO correction was carried out with an estimated source-receiver distance. The main steps of the processing flow were:

- Channel Selection, Editing
- Highpass Filtering (10 Hz Cut-Off Frequency)
- Trace Balancing
- NMO Correction
- Stacking
- 50 Hz Notch Filter (Lines HH00-026 to –033 only)
- Butterworth Bandpass Filtering
- Gain
- Plotting

4.9.3 HYDROSWEEP

(K. Huhn, J. Bohnert)

Onboard, HYDROSWEEP data can be processed with the ATLAS HYDROMAP software, based on the CARIS software package, (Atlas Elektronik GmbH, Bremen) which comprises of merging the navigation data, the calculation of depth and position of the footprints of the beams, removing artifacts and erroneous datapoints, and generation of a digital terrain model (DTM).

Another possibility is to process HYDROSWEEP using the free software MB-System developed at Lamont Doherty Earth Observatory by D. Caress and D. Chayes (1996), which is more suitable in areas like continental slopes as outlined in Flueh and von Huene (1994) and Weinrebe (1997). This

was done during cruise SO146 since the MS-System software was installed on the SUN workstations (cf chapter 4.2).

The raw echo time data were first converted to depth by complete ray tracing through the different water layers using the sound velocity profile measured in this area by the CTD probe at 16°S, 75° 36'W on March 4, 2000 (figure 4.9.3.1). A second CTD was run later on March 13, 2000, at 8° 21.71'S, 80° 44.09'W (cf Fig. 8.8.1). The results were rather similar. These depth converted sweep beams were then displayed on a screen and edited to eliminate erratic points. The edited data were then assembled, gridded and contoured with GMT software (Wessel & Smith, 1991). GMT allows different kinds of bathymetric imaging: i) as a 2D contour plot or as 3D perspective views both with/out illumination. No filters were used to smooth the data. Therefore, noise is still visible on the maps. However, this enables the viewer to decide if a small feature is a true tectonic structure or a map artifact.

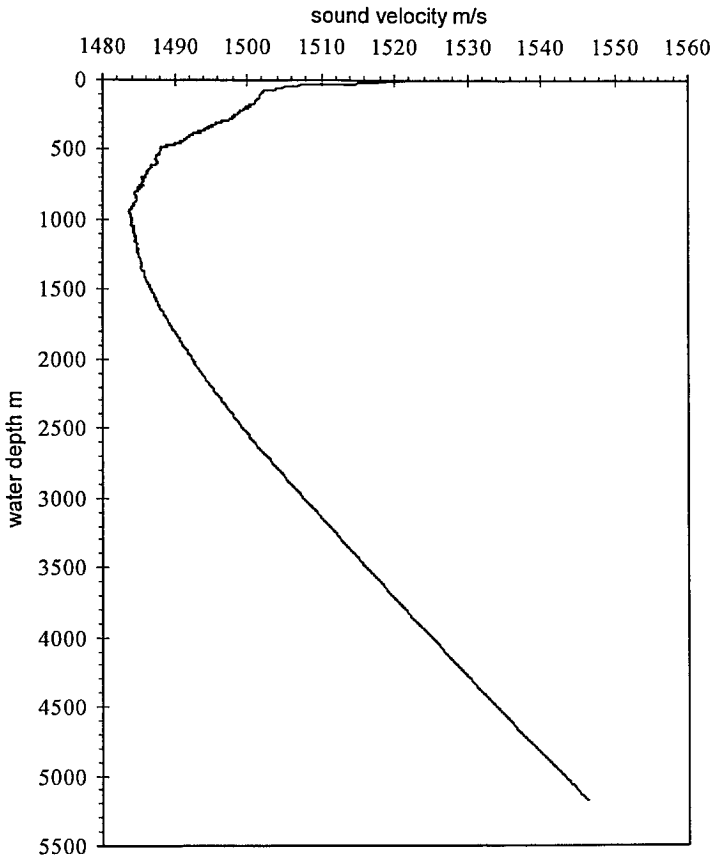

Figure 4.9.3.1: CTD – 1 The sound velocity profile measured in this area by the CTD probe at 16°S, 75° 36'W on March 4, 2000

HYDROSWEEP data were recorded during the entire SO146 cruise including the transits between the observation areas. Altogether 400,000 beams along 10,163 nm were collected. The ship's speed during mapping and transits was about 11-12 kn. The good weather conditions contributed to the collection of high data quality. During the acquisition of seismic data, OFOS, and heatflow measurements, the vessel speed was about 4 kn to 5 kn, and less than 1 kn respectively. This resulted in excellent bathymetry data quality, and shows only low amounts of noise resulting from minimal heave and pitch of the ship.

4.9.4 Gravity and magnetics

(G. Ali Dehghani)

The first step of data processing for gravity and magnetics data was performed on board the Sonne during the research work.
All recorded gravity and magnetics data (reading values) as well as the bathymetry data recorded with navigation data (central beam of Hydro Sweep) were plotted as a time series in order to be able to clean the data and remove large magnitude noise and spikes.

For the gravity data we calculated the Eoetvoes correction using the recorded navigation data as follow:

$$E = 7.507 \,.V.\sin(\alpha) \,.\, \cos(\varphi) + 0.06449 * V^2$$

With

E = Eoetvoes correction in mGal
V = vessel's speed in knots in direction of course
α = real course of the ship
φ = geographical latitude.

After calculating the Eoetvoes correction we applied following formula for estimating of Free-air anomaly:

$$F = (G-G_H) \,.\, K + G_{ABS} - G_N + E$$

Where

F = Free-air anomaly in mGal
G = measured (reading) gravity value in mGal
G_H = measured (reading) gravity value in the harbour in mGal
K = gravity constant of the sensor
G_N = normal gravity in mGal
G_{ABS} = absolute gravity value in the harbour in mGal
E = Eoetvoes correction in mGal.

The Bouguer anomaly was calculated the formula:

$$B = F + B_K$$

With

B = Bouguer anomaly in mGal
F = Free-air anomaly in mGal
B_K = Bouguer correction in mGal = $0.0419 \,.\, D \,.\, \delta\rho$

Where

D = water depth in meters
$\delta\rho$ = density difference between earth crust and sea water in g/cm^3 (normal 1.64 g/cm^3)

For the processing of magnetic data we applied the International Geomagnetic Reference Field (IGRF) for the epoch of 2000.3 as the regional field in order to determine the magnetic residual (rest) anomaly.

4.9.5 Parasound

(C. Hübscher)

For the processing of the Parasound data I used the SE processing software which was designed and kindly provided by Volkhard Spiess (University of Bremen). The first processing step is bandpass filtering (2-10 kHz) to suppress noise. This is similar to a standard seismic processing flows. The gain or amplitude processing is different for Parasound data. Spherical divergence is very low due to the small emitting angle of 4°. However, the reflection coefficient of the seafloor reflection is much higher than the coefficients from internal reflections. The goal of the amplitude scaling is to keep the ratios of the internal reflections constant. Therefore a simple clipping algorithm is used to decrease the amplitude differences between seafloor and internal reflections. A maximum value has to be carefully selected (in mV), which ranges from 200 to 400 mV. All higher amplitudes are clipped to this value. A small value enhances deeper and weaker reflections, but also enhances the noise level. Due to the small footprint of 7% of the water depth migration is not necessary for the suppression of diffraction hyperbolas. Since the number of samples per trace is mainly higher than the available dots per inch on the plotter, the gray or color value of each image pixel is computed from averaged samples which lie within this pixel.

Online processing was carried out in a similar manner during acquisition of the data. Parasound sections were plotted for all profiles with a vertical scale of several hundred meters. Most of the changes in window depth could thereby be eliminated. From these plots, an initial impression of the variations in sea floor morphology, sediment coverage and sedimentation patterns along the ships track could be gained.

A second dataset (PSI-files) is produced in a second processing step. All data are resampled by a factor of 5 to 0.125 ms and the dynamic range is reduced to 8 bit, which is good enough for pixel graphics (color or grey scale).

4.9.6 Heat flow data reduction

Processing temperature data includes calibration of thermistor sensors, calculation of sediment temperatures and temperature gradients, correction for probe tilt during penetration, and calculation of thermal conductivities. While the 7 minute wait is not long enough for the sediment temperatures to return to equilibrium after the frictional disturbance of penetration, it is long enough to extrapolate to an equilibrium temperature with a high degree of precision. Each temperature-time series, from each thermistor, is extrapolated to an equilibrium temperature by the program HFRD (Villinger and Davis, 1987) and alternatively in individual cases by the program T2C (Villinger and Hartmann, submitted). Because the calibration of each thermistor by the manufacturer is only good to 0.1°C, a secondary calibration is applied. This is usually done in deep marine environment (> 3000 m water depth) where negligible thermal gradients exist within the limits of observation. In other marine environments temperature gradients in the water column are surveyed with a CTD. For the secondary calibration purposes the heat flow probe is allowed to equilibrate at a certain depth (usually 200 m above seafloor). At this depth temperatures are calibrated to the CTD, including the local temperature gradient.

Fourier's law of heat conduction in one-dimension shows that heat flow (Q) is the product of the thermal gradient (dT/dz) and thermal conductivity (k). If these terms are constant over the depth of the measurements then the calculation of heat flow is trivial. However if these values are changing proportionately to each other, as is the case for a constant basal heat flux, then heat flow can be derived from Bullard's (1939) relation given by,

$$\Delta T = Q \, \Sigma \Delta z_i / k_i,$$

Where Δz_i is the thickness and k_i is the thermal conductvity over the ith interval. In this case heat flow can easily be calculated as the slope of the line given by the summation. To properly calculate the temperature gradient a correction for the penetration tilt angle is applied. In most cases the tilt angle is less than 10° (see Appendix) and the tilt correction is modest. Determination of thermal conductivity requires the knowledge of the amount of heat, dissipated into the sediment. Therefore a pulsed heat source is used (approximated by a 20 second pulse of 600 J/m), producing a set of 11 thermal conductivities. Because thermal conductivities are sensitive to the sediment porosity over the depth range of the measurements, these measurements can reflect the reduction of porosity within the upper three meters of sediment. Thermal conductivities are summarized as harmonic means (see Appendix VII).

5. Overview of the experiments undertaken

(N. Kukowski)

According to the multiple and interconnected goals of the project GEOPECO, we focused our data acquisition on a few key-transects across the margin: the Nazca Ridge area, a transect at 13.5°S, as well as transects through the Lima Basin at 11.5°S and the Yaquina Basin at 8°S. In the latter two working areas, more extended work included the gathering of areal information from multiple mapping methods, TV observations of the ocean floor and heat flow measurements. For all three transects we included the sites of ODP Leg 112 in the reflection seismic surveys so that the stratigraphy could be correlated. Finally, we planned transits between working areas in such a manner that we achieved areal bathymetric and gravity information and went north to 5° 39'S to sample barite crusts.

The Nazca Ridge experiment

At the Nazca Ridge we shot two cross profiles, one across the Nazca Ridge (WS#1) and th other along the crest of the ridge and continuing across the continental slope (WS#2). These profiles are designed to study the structure and internal geometry of the basement ridge and its subduction behavior. The leading edge of the ridge when entering the trench, i.e. its southeastern frontal flank, was also chosen for bathymetric mapping, as expect the highest degree of deformation here.

An initial analysis of the data indicates that the structure of Nazca Ridge is asymmetric, the south-eastern flank is offset by about 100m along a normal fault. Where the sea floor is quite flat, there is a sedimentary cover of a few hundreds of meters total thickness. The Parasound signal often penetrated more than 50 m to reveal the layered sediments. Close to the crest of the ridge, basement crops out. This basement may represent relicts of an ancient spreading center. The surface of the ridge comprises several cone shaped hills, linear structures, and seamounts of several hundreds of meters height. One major of these edifices is a caldera surface structure, another looks like an irregular oat cookie. These edifices are most probably of volcanic origin. The OBH/S data is of very good quality and show refractions up to 140 km away. Moho events can be clearly modeled. The crest of the ridge is also characterized by a strong negative magnetic anomaly.

The transect at 13.5°S

The main work done along this transect is at a location where the slope has significantly widened relative to the small width in the Nazca Ridge where wide angle profile (WS#3) was collected. This transect starts on the oceanic crust seaward of the trench, crosses the convergence zone, and continues across the continental slope to the shelf and is designed to image the subduction zone structure. The oceanic crust has a rough topography manifested as strong gravity anomalies. A wide accretionary prism, about 25 to 30 km in width, is imaged just adjacent to the trench. Additionally, reflection seismic data were acquired on the upper slope to better image a forearc basin. From the seismic lines of Lima Basin it is not clear if this forearc basin is the southern continuation of Lima Basin. Nevertheless, the acquired data allows a comparison with basin structures in the northern working areas. In the basin, a bottom simulating reflector (BSR) was identified. As one profile crosses over ODP Site 687, we will be able to correlate sediment structures. The slope itself seems to be characterized by slumping.

The Lima transect at 11.5°S

The continental slope at this latitude, the Lima Basin and parts of the lower slope were one of the main targets of the GEOPECO cruise. Here, we shot two wide angle profiles, one from the oceanic crust, over the trench and up to the shelf (WS#5). The second line (WS#6) crosses WS#5 in the Lima Basin. These lines are designed to image the structure of the downgoing and overriding plates and investigate

the along-strike variability of the forearc. Lima Basin is also the location for monitoring natural seismicity with a small cross shaped OBS/H network, and extensive reflection seismic profiling. The purpose of this data is to get more information on BSR patterns and calibrate stratigraphy with ODP Leg 112 sites. Additional data collected include a high resolution OBS/H experiment and two SeeBoSeis experiments, one shot along a portion of line 26 (coinciding with line HIG13 acquired in the 80's) where there is no BSR imaged, the other further south, just where a strong BSR is beginning. OFOS observations and heat flow measurements were completed on parts of the same line. On the lower slope, close to ODP site 688, reflection seismic profiling, OFOS observations, and heat flow measurements were undertaken to study the geophysical characteristics of this gas hydrate system.

As several seismic events could be detected in the data obtained from the mini-network, we suggest that this area is a good location for a long term observation of natural seismicity in a combined onshore/offshore experiment.

The wide angle profile across the slope shows a structure comparable with what has been obtained at the transect to the south. Along-strike, structures look quite homogeneous, however it seems as if Lima Basin has a more limited north-south extension than earlier thought. The high resolution OBS data show strong P-to-S-converted arrivals especially in areas where the seafloor is quite hard as confirmed with OFOS. Both SeeBoSeis experiments were successful; p-, S-, and also Scholte waves were detected in the recordings. Along line 26, carbonates are inferred from the TV seafloor observations. These carbonates are likely responsible for inhibiting the penetration of the heat flow probe along large sections of this profile. In contrast, heat flow measurements proceeded without problems at the lower slope and show only a slight variation in measured values. At the lower slope, a few individuals of Calyptogena were seen with the TV camera, however, only two of then were alive indicating that this part of the slope must have been a locus of active venting not long ago.

The Yaquina transect at 8°S

At this latitude, we shot our northernmost wide angle profile (WS#4) and did extensive reflection seismic profiling covering whole Yaquina Basin. Bathymetric and gravimetric mapping was completed on the lower slope and also on the oceanic crust seaward of the trench to study the morphology and lineament of the transition from the Nazca plate to the continental slope.

The oceanic crust of the Nazca plate is extremely rugged with differences in relief of up to 1000 meters. Sedimentary cover is found only in the pockets between topographic highs, otherwise the oceanic crust is not covered by sediments. This observation is of great importance to the mechanics of the continental margin as and suggests that at least the Chimbote part of the Peruvian margin might be erosive. To investigate the possible origins of the roughness of the oceanic crust, we shot an additional seismic reflection profile extending line WS#4 further westward on the Nazca plate. This revealed thin sediment coverage of a few hundreds of meters, however, this is significantly thicker than expected, given the infill of the grabens observed along profile 4. Here the roughness of the basement topography is still present but smoother with more elongated highs and lows.

During playback of the seismic reflection data, a complex pattern in the Bottom Simulating Reflector (BSR) was observed, particularly in the northern section of the Yaquina Basin. The BSR apparently pinches out by meeting the ocean floor in approximately 350 m water depth. At the same time, obvious blanking effects and the so called 'bright spots' due to the presence of gas are clearly evident over a wide area. During the survey, regions with and without a BSR were crossed, as well as areas with and without signs of gas. Therefore, we choose this region, especially reflection seismic line 20, for more detailed studies including high resolution OBH/S work, OFOS observations, and heat flow measurements on the second leg of the GEOPECO cruise.

The heat flow profiles exhibit clear positive anomalies at locations where seismic section interpretations show faults intersecting the sea floor. A zone containing gas was not completely

covered, but it's terminations were crossed and the heat flow values taken at these positions decreas below average. Ocean floor mapping and video reconnaissance using the OFOS was also successful. Along the lower slope, clear indications for fluid-venting, marked by fields of chemoautotroph muscles Calyptogena (only a few live specimens) were found. Farther up slope two 100 m wide by 20 m high carbonate complexes were located, one of them previously unknown. These so called Chemoherm complexes identify locations of cold methane rich fluids. These complexes are similar to those observed off Cascadia, which now can no longer be considered a unique phenomenon. In the area where the BSR pinches out at the sea floor, a field of diffuse venting was visually documented for the first time. White bacterial mats up to 1 m diameter were found above sandy sediment. Using the TV-Grab, samples of the observed localities were collected, and after multiple tries we were able to get a sample of the very hard Chemoherms as well.

The Paita area

This area was suggested to be one of the few among continental margins where barite crusts is found. Therefore, we searched for a suitable position and could sample barite crusts together with massive carbonates and three different sorts of mussels with the TV grab.

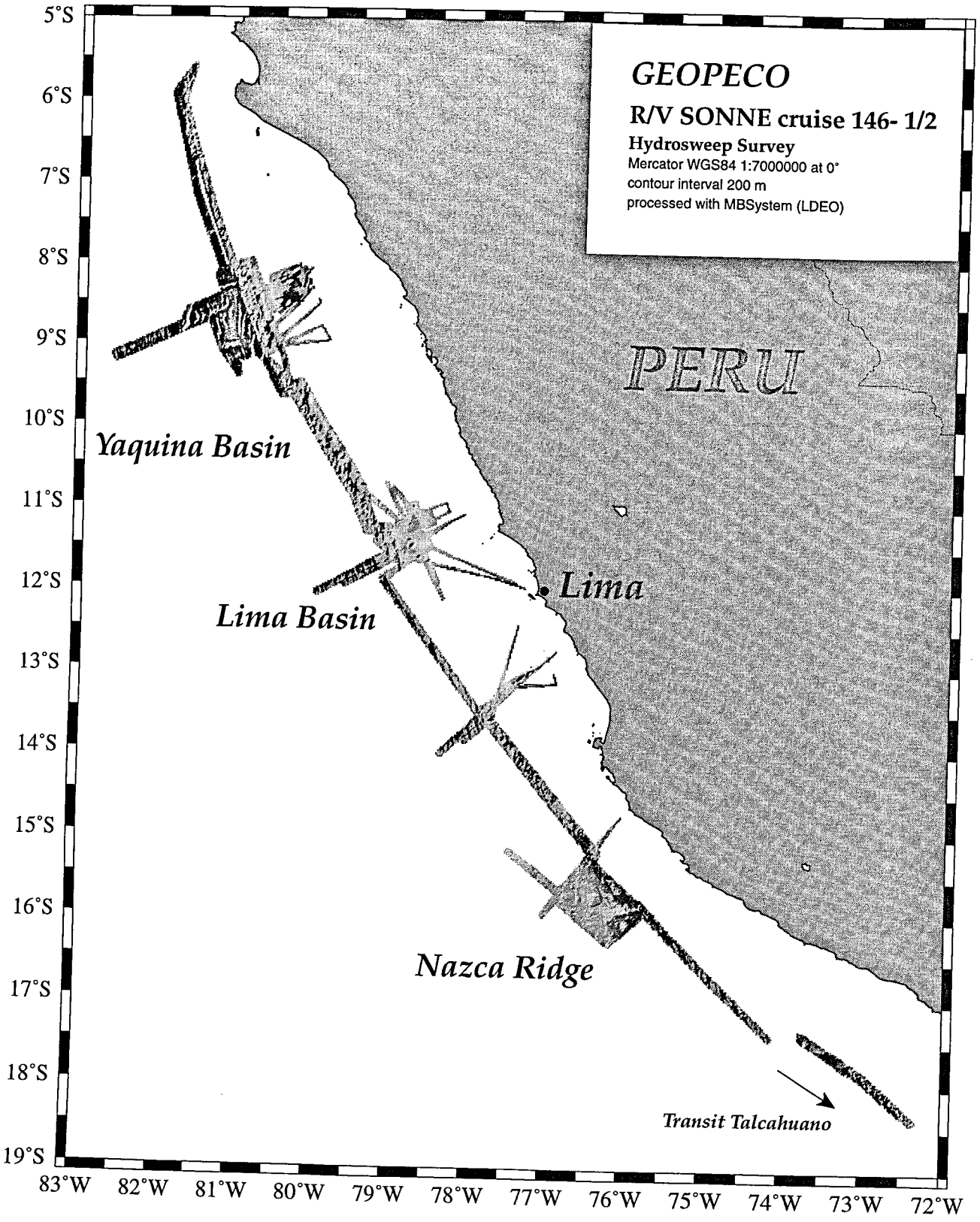

Figure 5.1: Bathymetric data aquired during SONNE cruise SO146 - 1/2.

6 The Nazca Ridge Experiment

6.1 Ocean floor morphology of Nazca Ridge

(J. Bohnert, N. Kukowski, K. Huhn)

At the southeastern flank of Nazca Ridge, which marks the leading edge entering the trench, a 120 nm by 90 nm large area was completely covered with swath mapping. The southwest edge of the area is bounded by wide angle profile WS#1, the northwestern by wide angle profile WS#2 and the northeastern edge by the trench such that the mapped area extends from the crest of Nazca Ridge down its southeastern flank towards its toe.

Generally, this area gently dips to the northeast and southeast and in large portions comprises a quite homogeneous surface (Figs. 6.1.1, 6.1.2). However, several seamounts and linear structures of up to several hundreds of meters of height are observed in this area. Most all these features are likely of volcanic origin

A remarkable seamount is located close to the center of the mapped area. It shows a typical effusive volcanic structure with a diameter of about 20 km and a height of approximately 600 - 700 m. Its surface shows small scale roughness, perhaps the result of surficial erosion. Another seamount, imaged to the west, has a caldera like top structure. Both seamounts show a smooth topography and no rugged structures are observed. The roundness of seamount together with the caldera is being much greater than that of the central seamount resembles a 5 edge polygon.

Close to the caldera-seamount, numerous small cone shaped peaks, of about 200 m height, are identified. These flanks do not show much roughness perhaps indicating that they have not undegone much erosion. Several ridge-shaped linear structures trend approximately north. It looks as if at least the most southern seamounts is made of a sequence of individual peeks. All of these structures are compatible with very late stages of active volcanism.

In contrast to these seamounts, the mountains to the southeast show a much rougher structure. They appear much more massive but are much higher than the individual seamounts. Steep single peaks and rugged walls are observed. These features suggests that they are made of material quite indurated and do have considerable sediment cover. The observation that the topography is more gentle to the south may indicate the presence of a sediment cover or erosional debris fill.

Where Nazca Ridge approaches the trench, several trench parallel striking lineament are identified. These might be the result of extension tectonics due to the bending of the plate before being subducted.

Figure 6.1.1: Perspective image of the Nazca Ridge. View from the southwest with illumination from northwest.

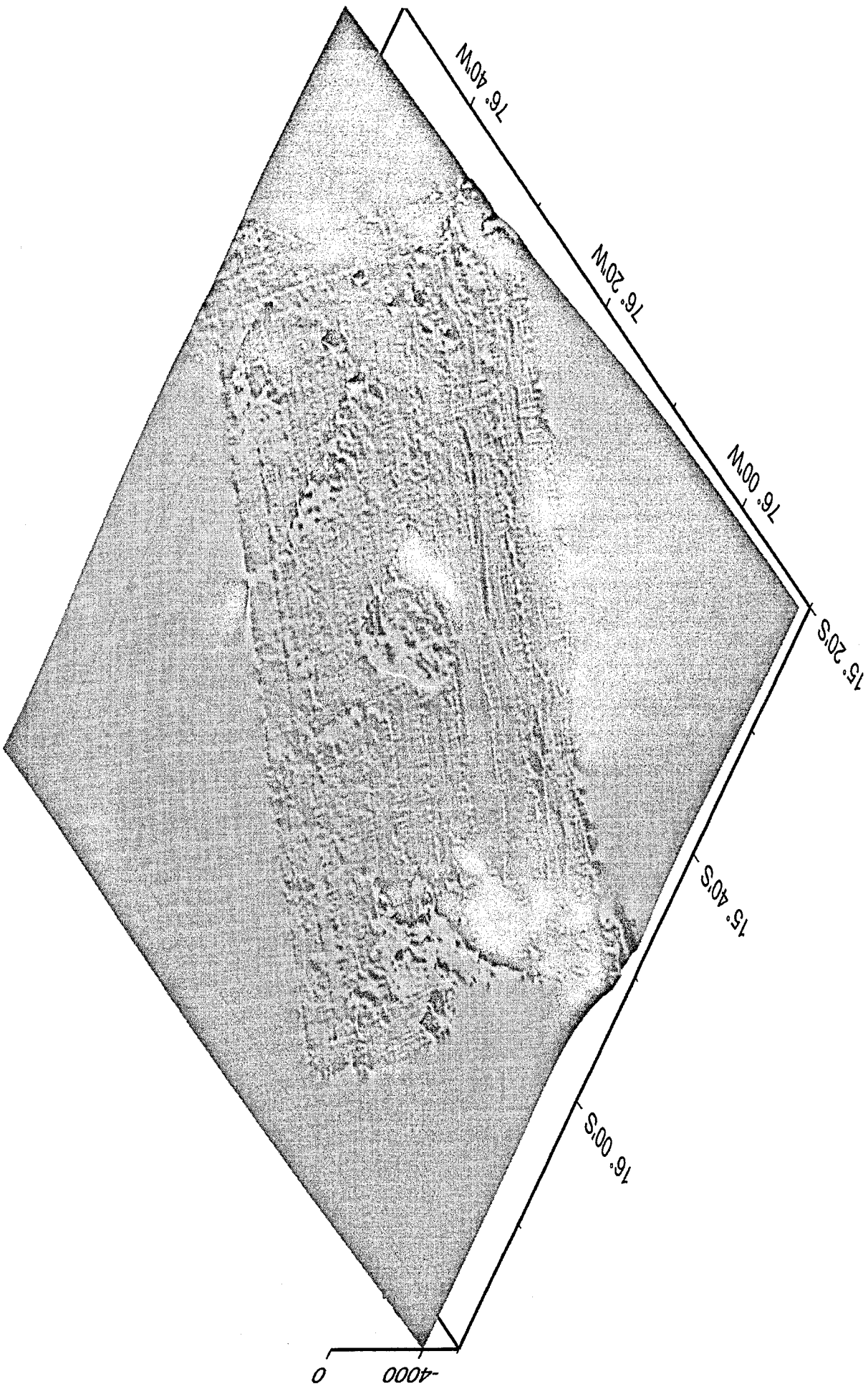

Figure 6.1.2: Perspective image of the Nazca Ridge. View from the northwest.

6.2 Wide angle seismics

6.2.1 Profile SO 146-01

(A. Hampel, P. Liersch)

The first refraction and wide-angle reflection seismic profile of this cruise was situated across the Nazca Ridge, just before it's intersection with the Peru Trench (figure 6.2.1.1). Nine instruments were deployed, among them were three OBS, which were symmetrically distributed along a 98 nm long profile perpendicular to the ridge axis. OBS 5 was positioned in the middle of profile SO 146-01, and was also used as the most seaward instrument for profile SO1 46-02, in order to correlate the recorded refractions and reflections of the two profiles. All instruments registered well except for the seismometer on OBS 5, so only its hydrophone recorded data.

The data quality is very good. Most instruments including the hydrophone of OBS 5 show clear signals over the entire profile length, but at least to a distance of about 100 km and occasionally up to 140 km. The recorded refractions and reflections have an approximately symmetrical shape. The clear refraction signals indicate only little sediment and a rapid increase in the apparent velocity of up to about 8.2 km/s at the crust-mantle boundary. Moreover, on all instruments, precritical reflections from the upper layers could be identified. Wide angle reflections from the Moho were registered by most stations, but were especially clear on OBH 4.

Modeling

To characterize the structure and the velocity field of the Nazca Ridge, the refraction and reflection signals from the hydrophones were picked and modeled by raytracing. The coincident reflection seismic profile was used to constrain the structure and thickness of the upper layers.

First, the 1-dimensional modeling program R1D (Luetgert, 1992) was used to get an idea of the velocity function at station 5. The results confirmed the notion of a rapid increase of the seismic velocity from 2.4 km/s for the sediment layer to 7.9 km/s at about 20 km depth. For modeling of the whole profile, the raytracing program MacRay (Luetgert, 1992) was used. The construction of the model was based on stations 1, 4, 5 and 9 and cross-checked with other stations during modeling. Figure 6.2.1.17 shows the picked traveltimes above the corresponding stations and the preliminary model, which consists of 4 layers above the Moho and already fits well with the observed and calculated traveltimes.

The preliminary model shows that the Nazca Ridge is only covered by several hundred meters of sediment (layer A), as is also indicated by the reflection seismic profile, which has velocities of 2.0 – 2.3 km/s. Beneath the axis of the ridge, layer B is thickened and characterized by velocities of about 3.6 km/s. This could correspond to the outcrop of rocks which differ from the surrounding sediments, as can be seen on the reflection seismic profile. The boundary between layer B and C is located at a depth of 4 – 5 km. Layer C shows a velocity increase from 5.1 – 5.4 km/s. The top of the basement (layer D) at 7 km depth seems to have no marked undulations. In opposition to that, the Moho depth increases from 16 km in the north to 19 km at the root of the ridge. At the southern end of the profile, the Moho is located at a depth of 15 km.

According to this preliminary model, the upper part of the Nazca Ridge is nearly symmetrical, with a topographic high at the ridge axis. In contrast to the upper layers, the Nazca Ridge shows an asymmetrical root, where the crust reaches a thickness of 16.5 km. The southeastern flank of the root is steeper than the northwestern side, therefore the corresponding thickness of the crust is about 12.5 km in the north, and 11.5 km in the south. The layers of the model can be correlated with the standard model of the oceanic crust. Layer 1, the sediments, is thin for the case of the Nazca Ridge. Layers B (~ 3.6 km/s) and C (~5.2 km/s) of the model may correspond to Layer 2 of the standard model, which is subdivided into Layers 2a and 2b. They represent pillow lava flows and sheeted dikes, respectively. Layer D of the Nazca Ridge model has a velocity of about 6.9 km/s and is comparable to Layer 3 in the standard model of the oceanic crust, which consists of Gabbro and has velocities of about 7.2 km.

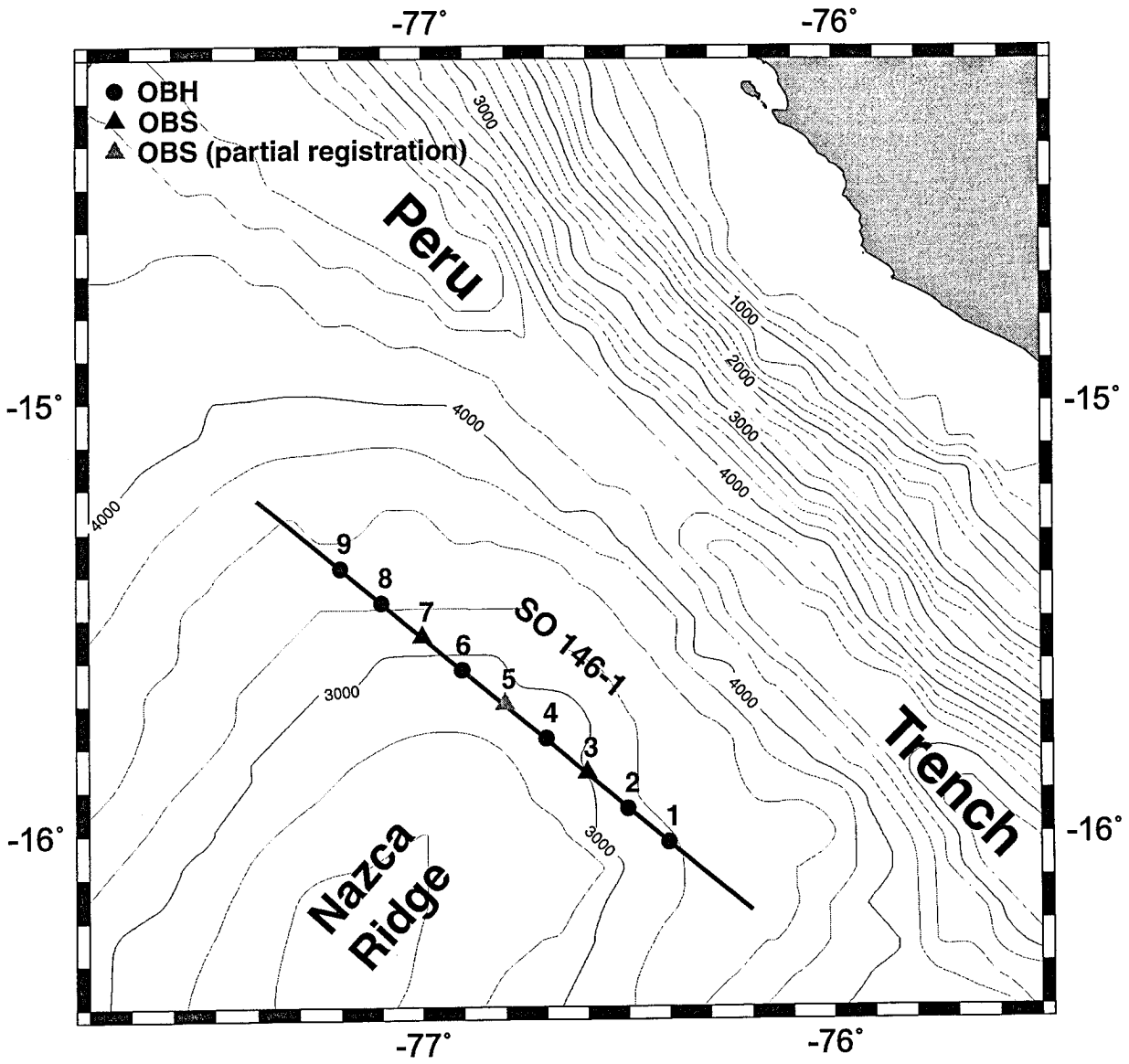

Figure 6.2.1.1: Location map of profile SO 146-01.

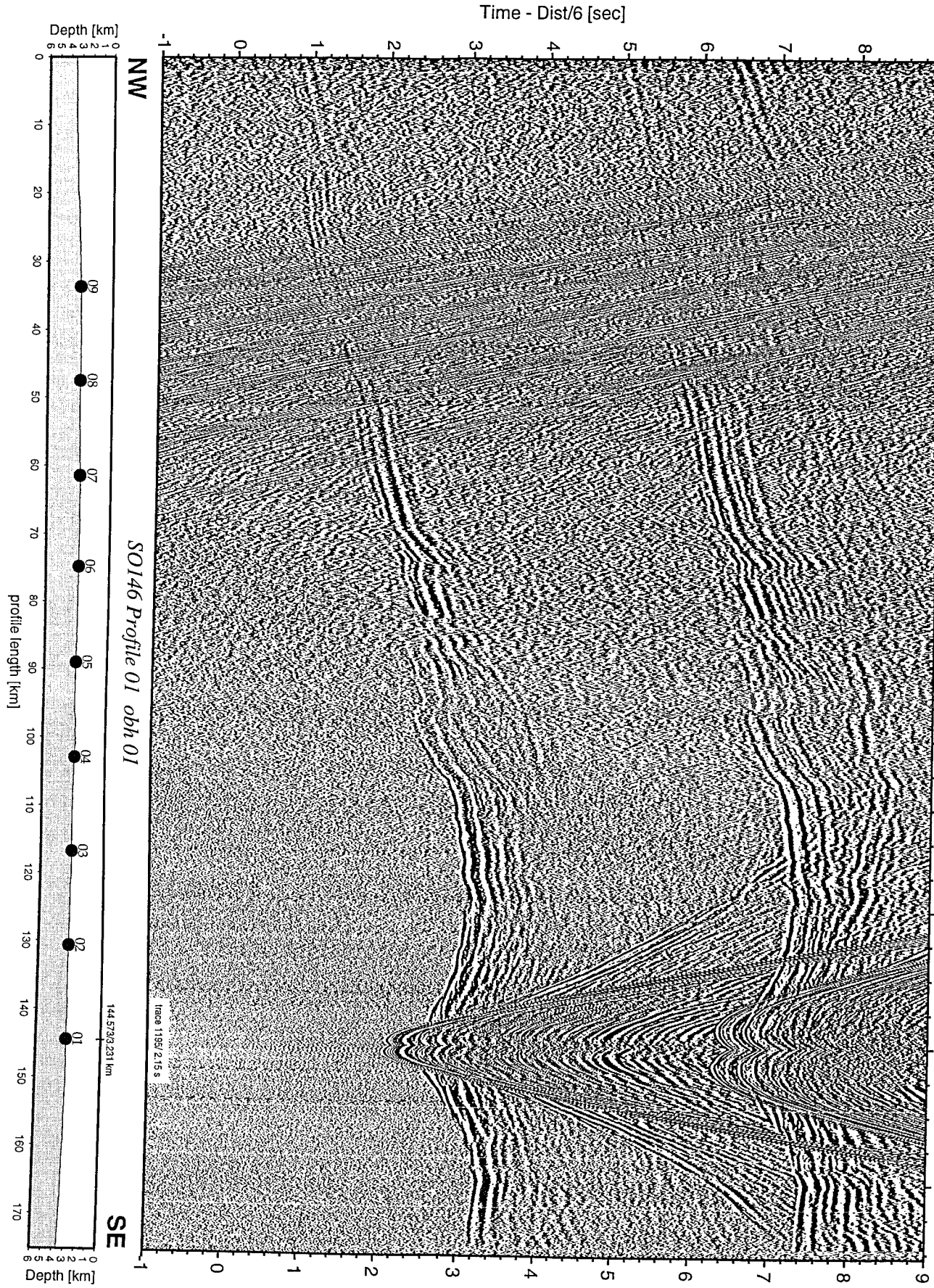

Figure 6.2.1.2: Record section from obh 01 , Profile 01.

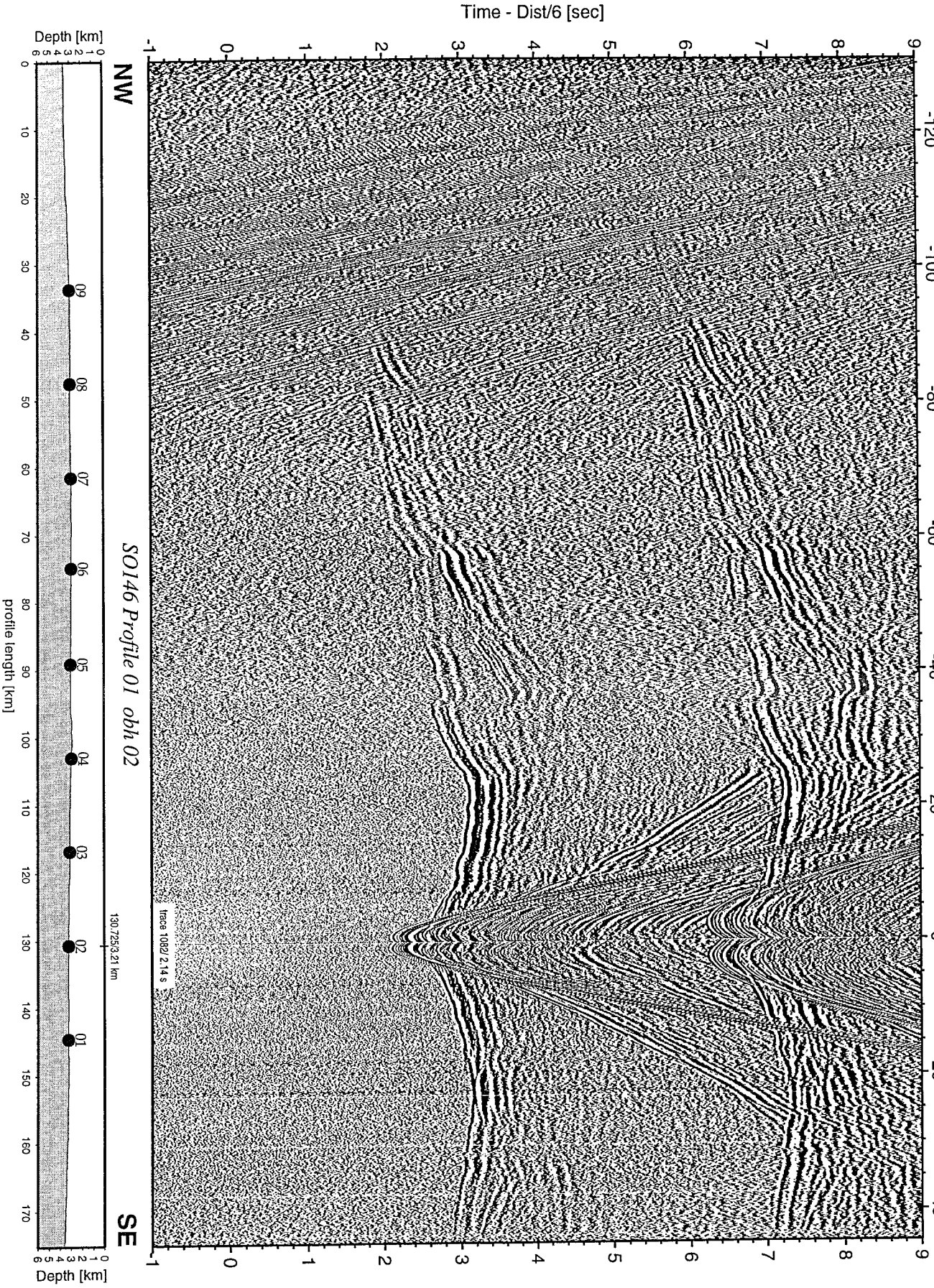

Figure 6.2.1.3: Record section from obh 02 , Profile 01.

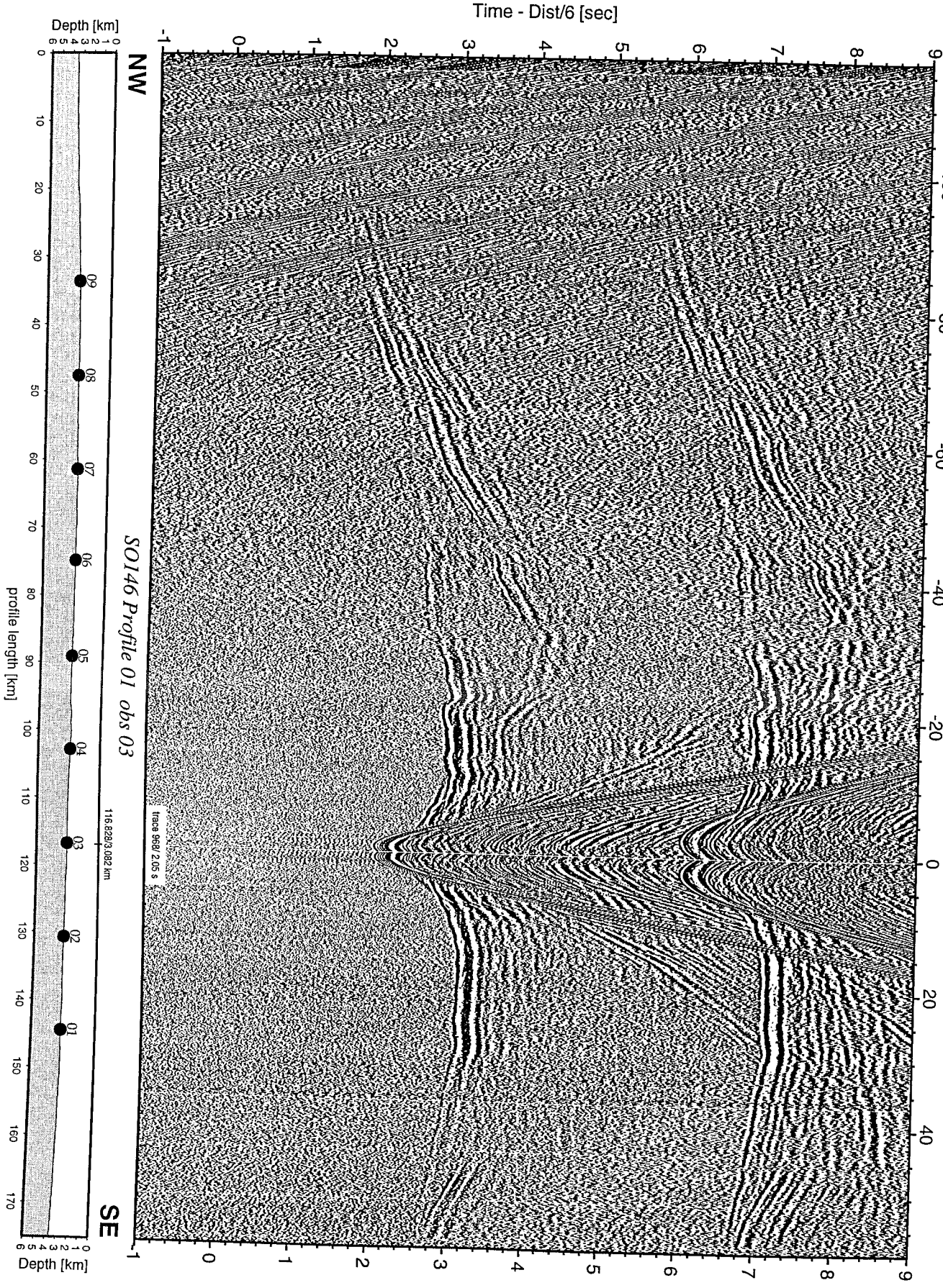

Figure 6.2.1.4: Record section from obs 03 hydrophone, Profile 01.

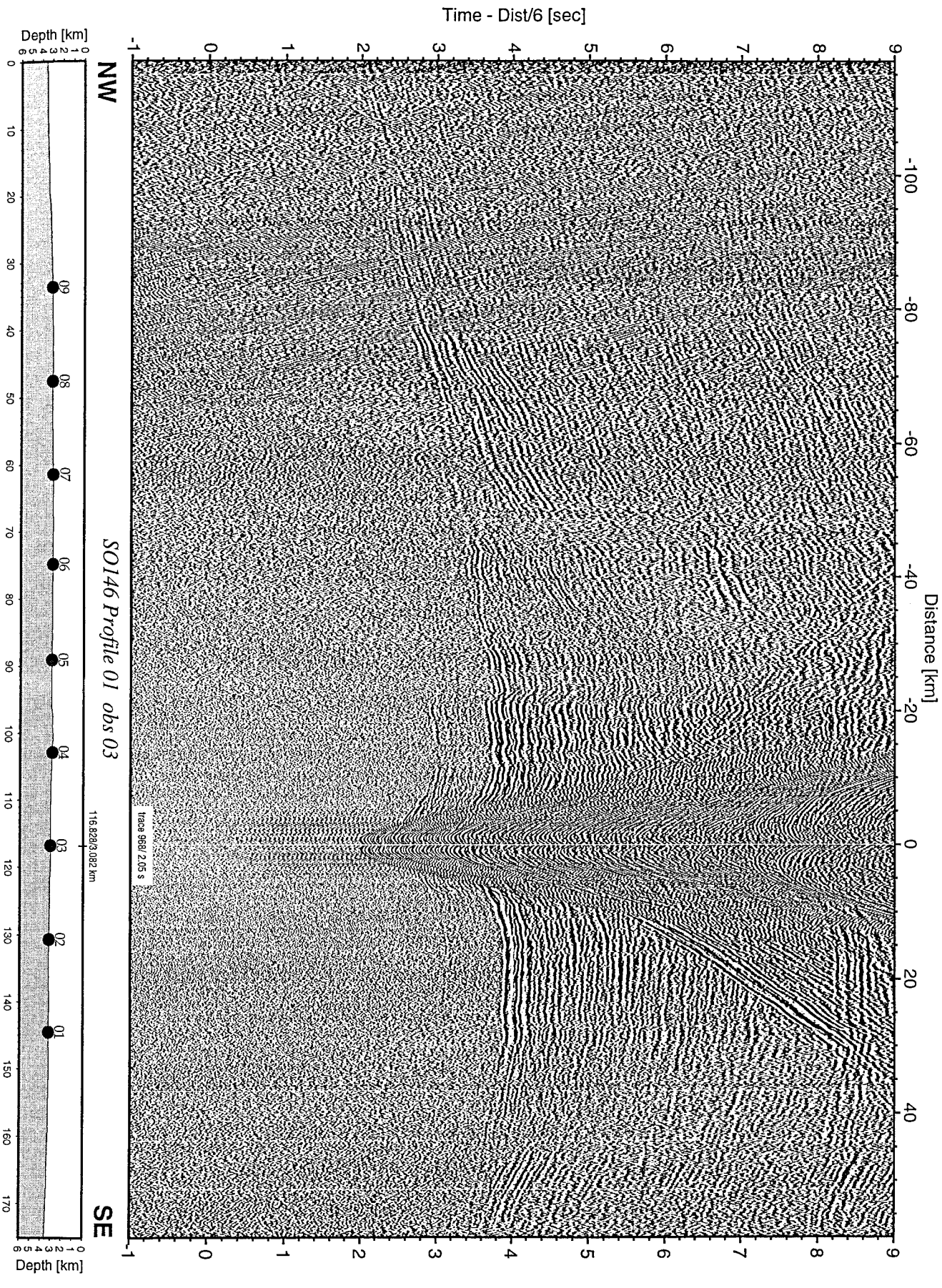

Figure 6.2.1.5: Record section from obs 03 horizontal component 1, Profile 01.

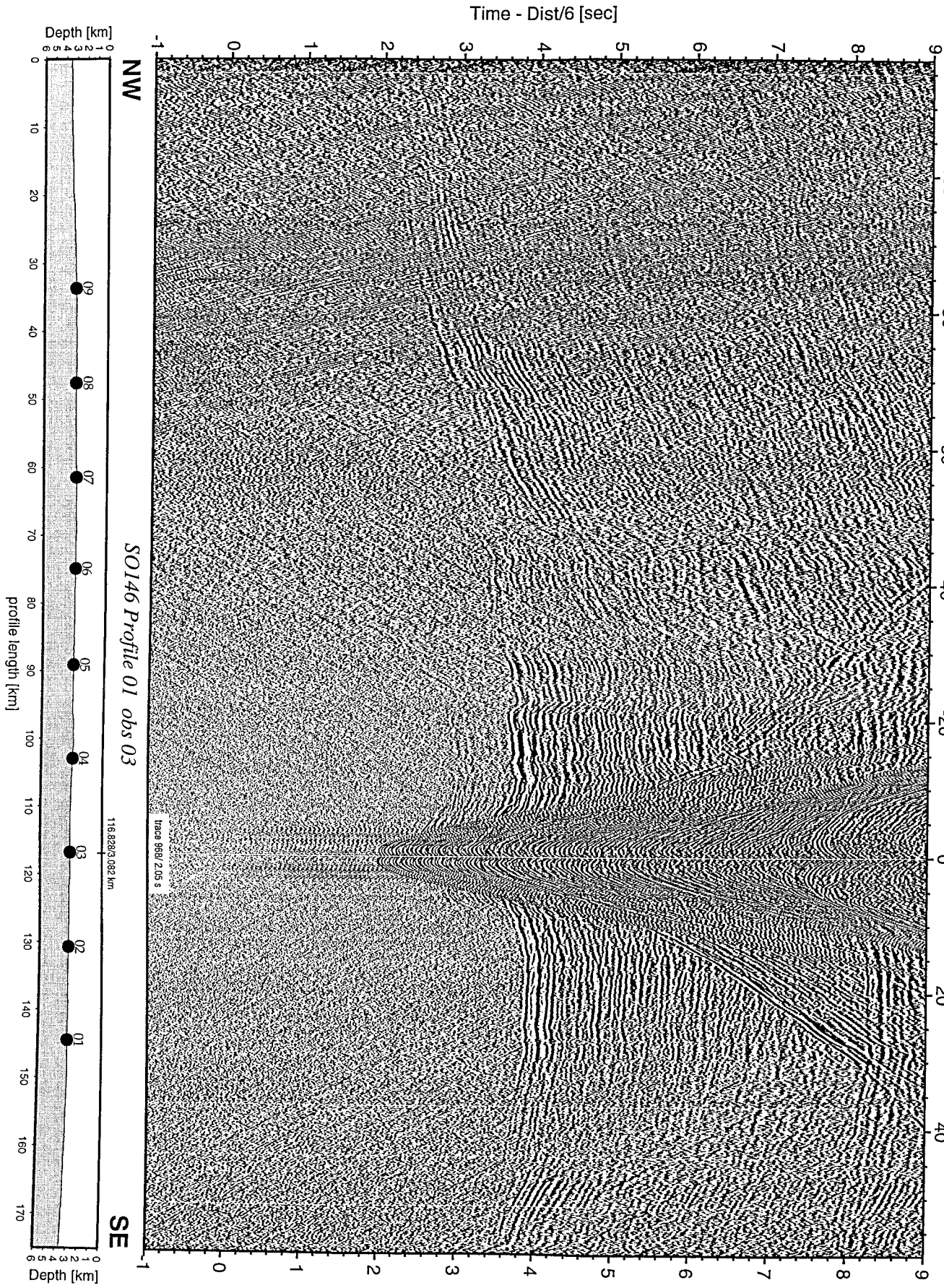

Figure 6.2.1.6: Record section from obs 03 horizontal component 2, Profile 01.

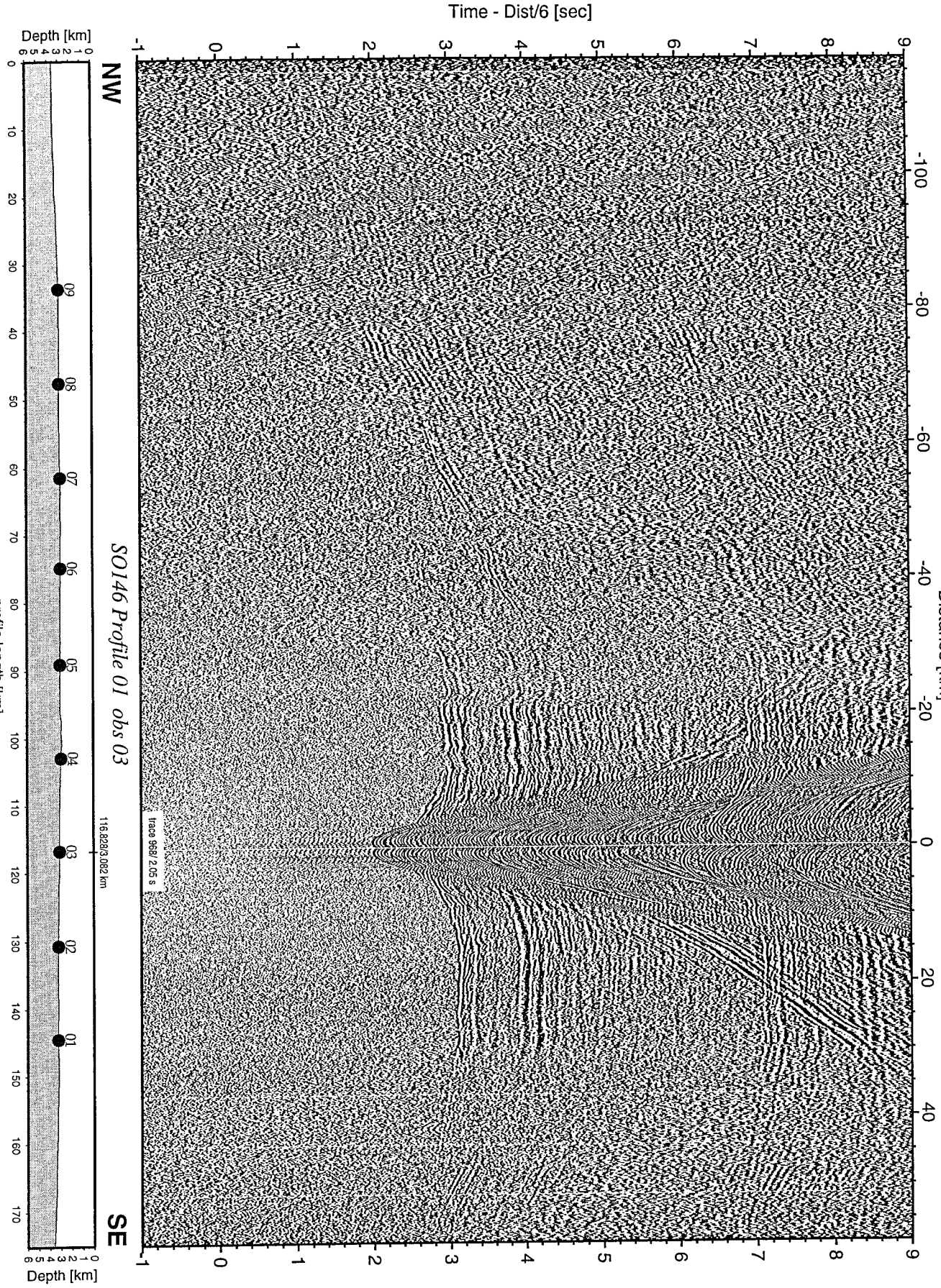

Figure 6.2.1.7: Record section from obs 03 vertical component, Profile 01.

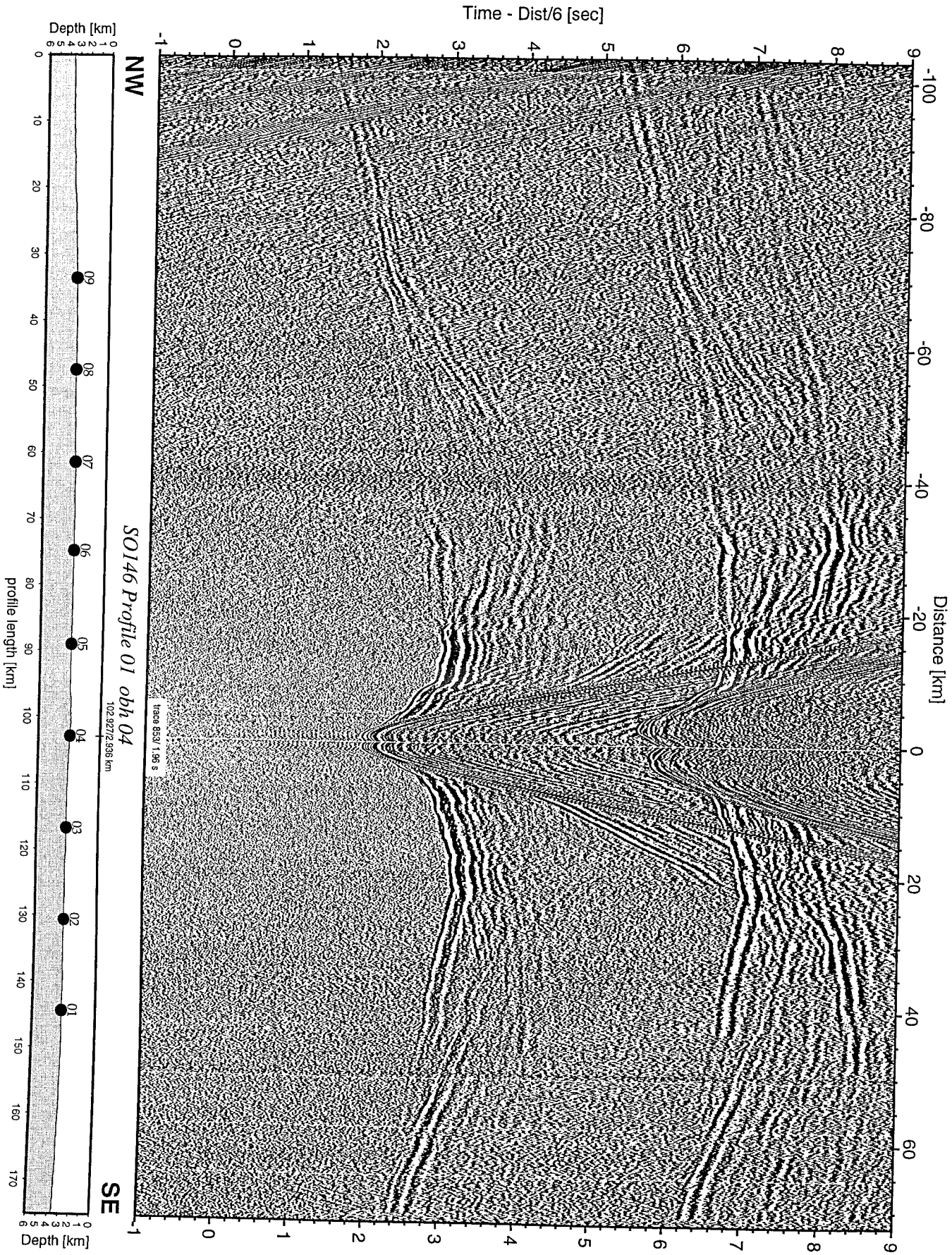

Figure 6.2.1.8: Record section from obh 04 , Profile 01.

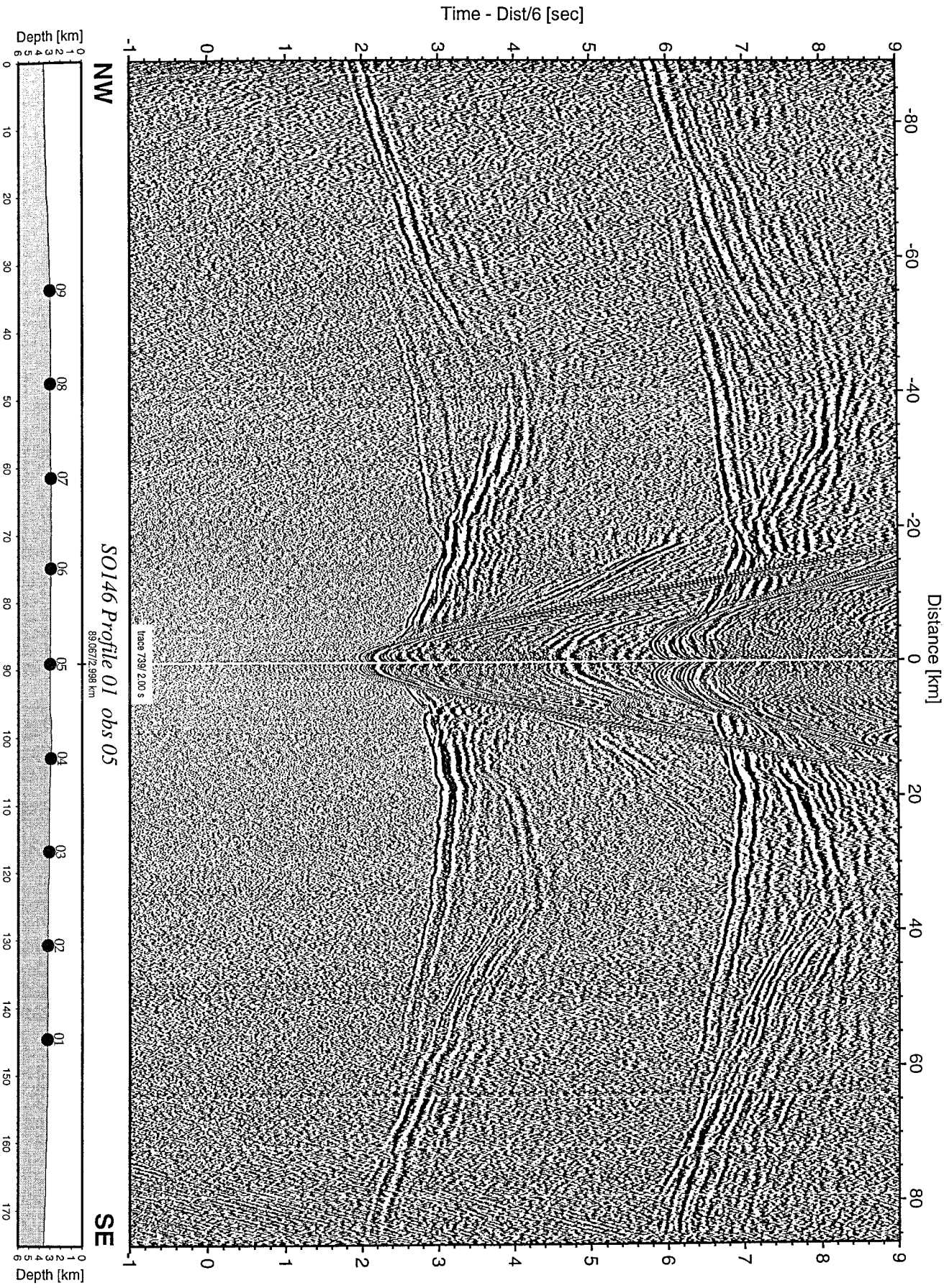

Figure 6.2.1.9: Record section from obs 05 hydrophone, Profile 01.

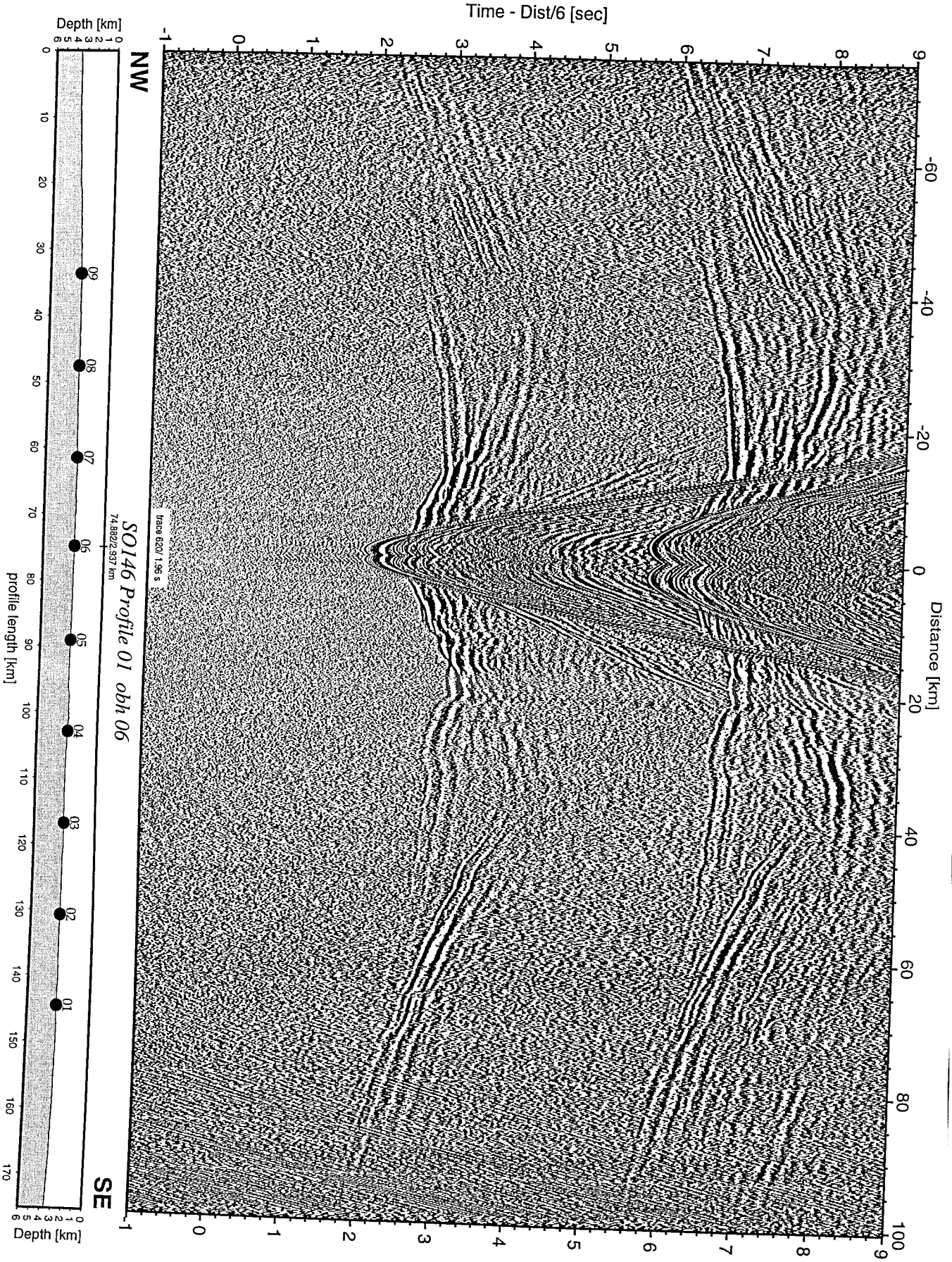

Figure 6.2.1.10: Record section from obh 06 , Profile 01.

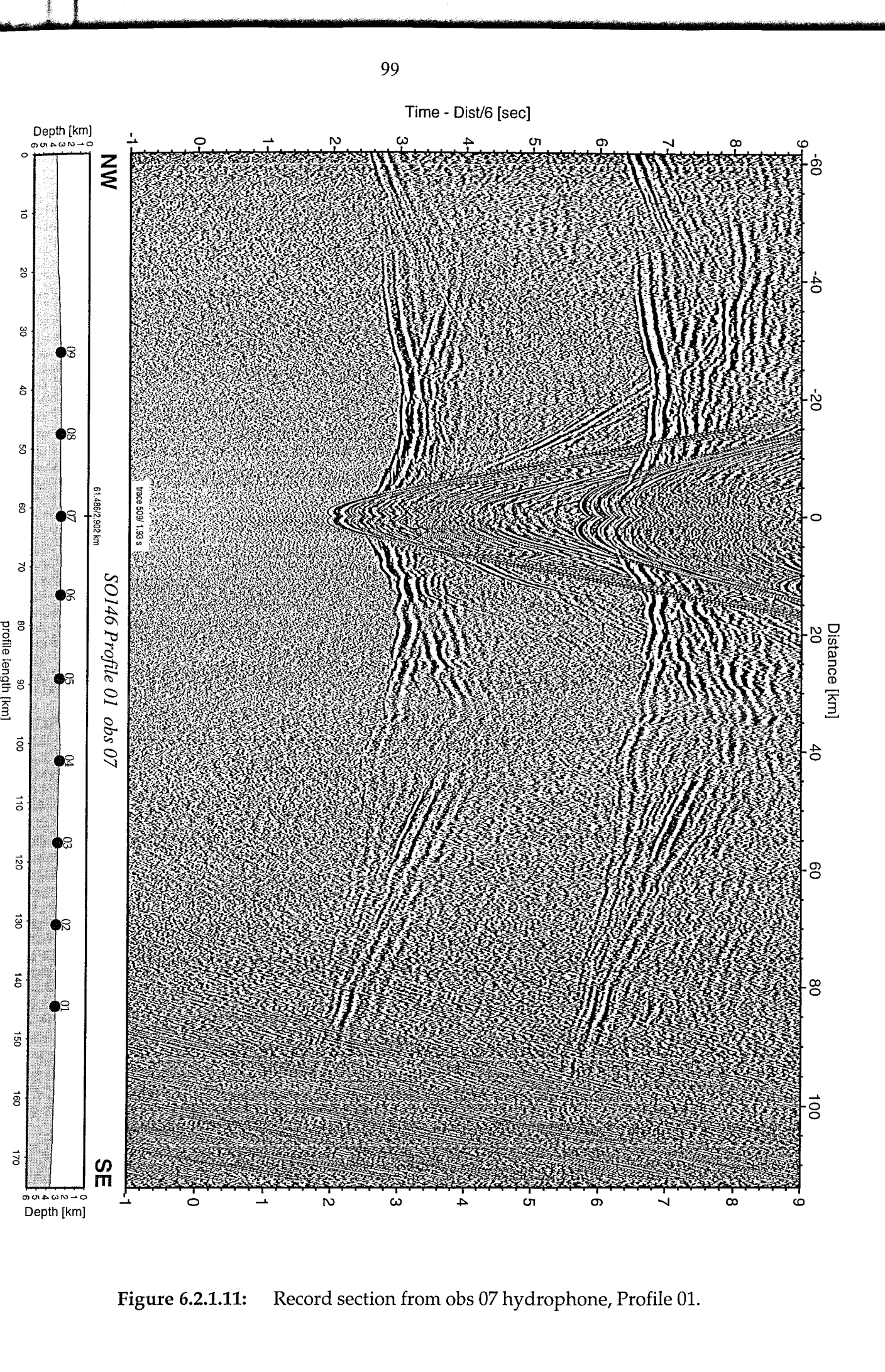

Figure 6.2.1.11: Record section from obs 07 hydrophone, Profile 01.

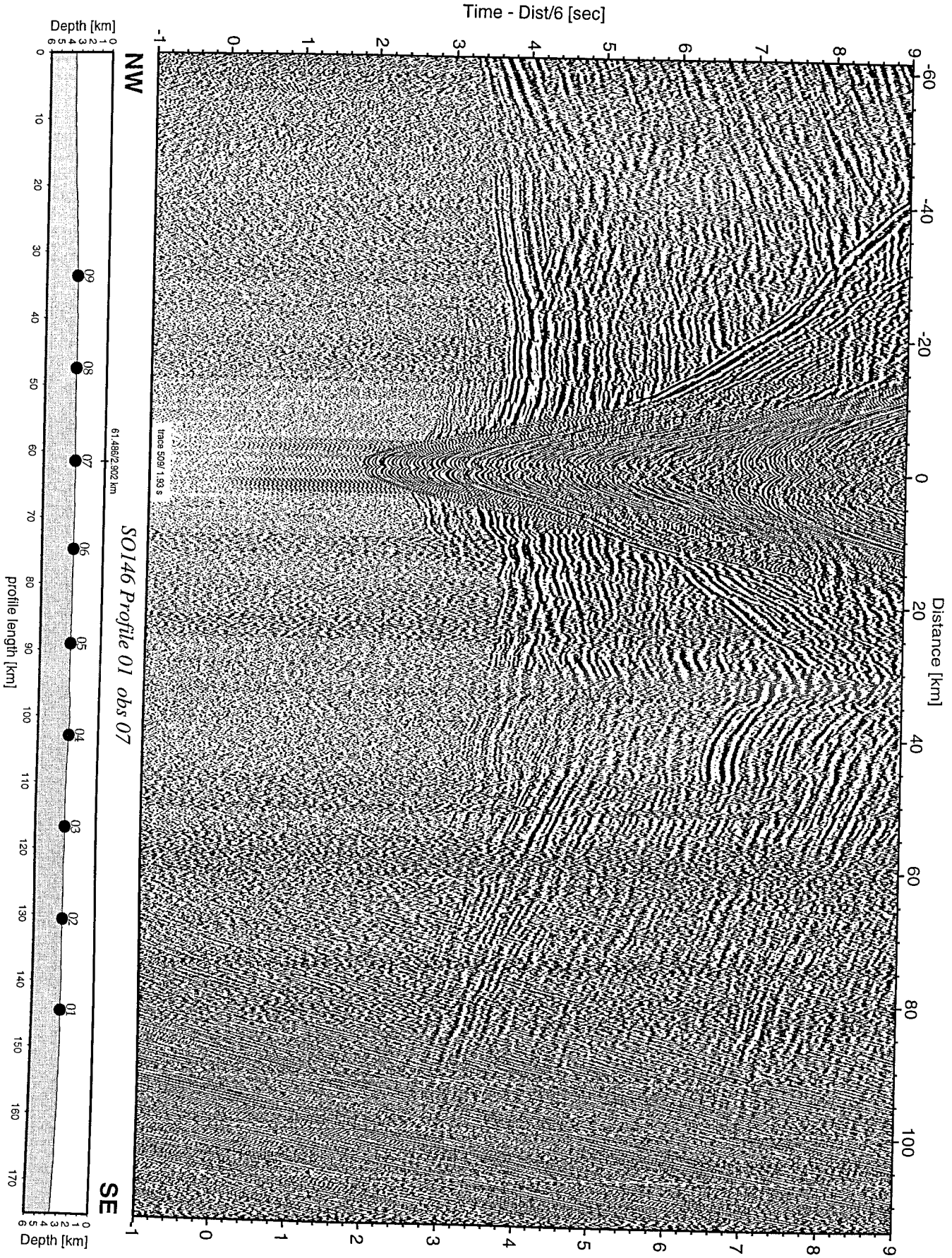

Figure 6.2.1.12: Record section from obs 07 horizontal component 1, Profile 01.

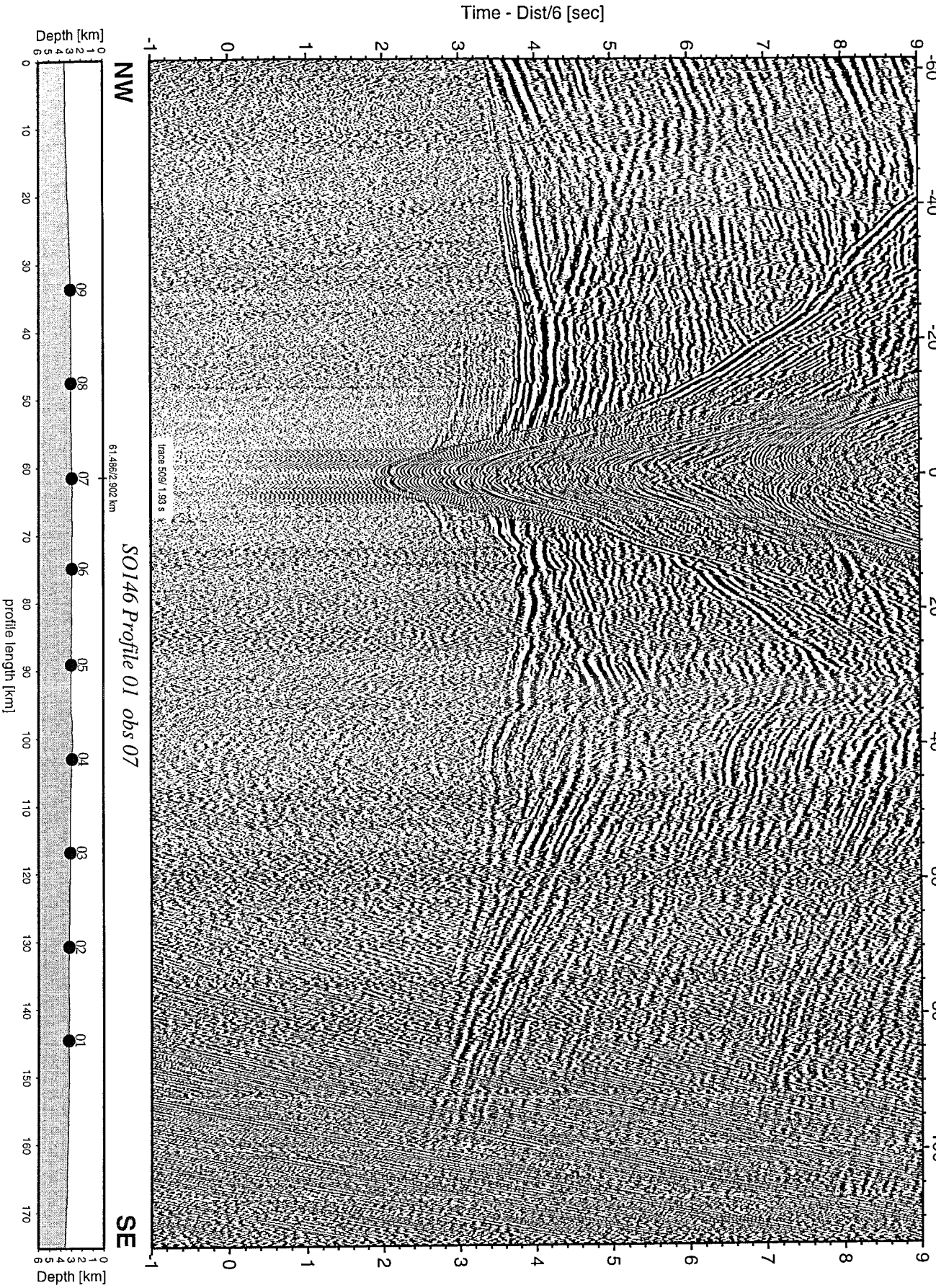

Figure 6.2.1.13: Record section from obs 07 horizontal component 2, Profile 01.

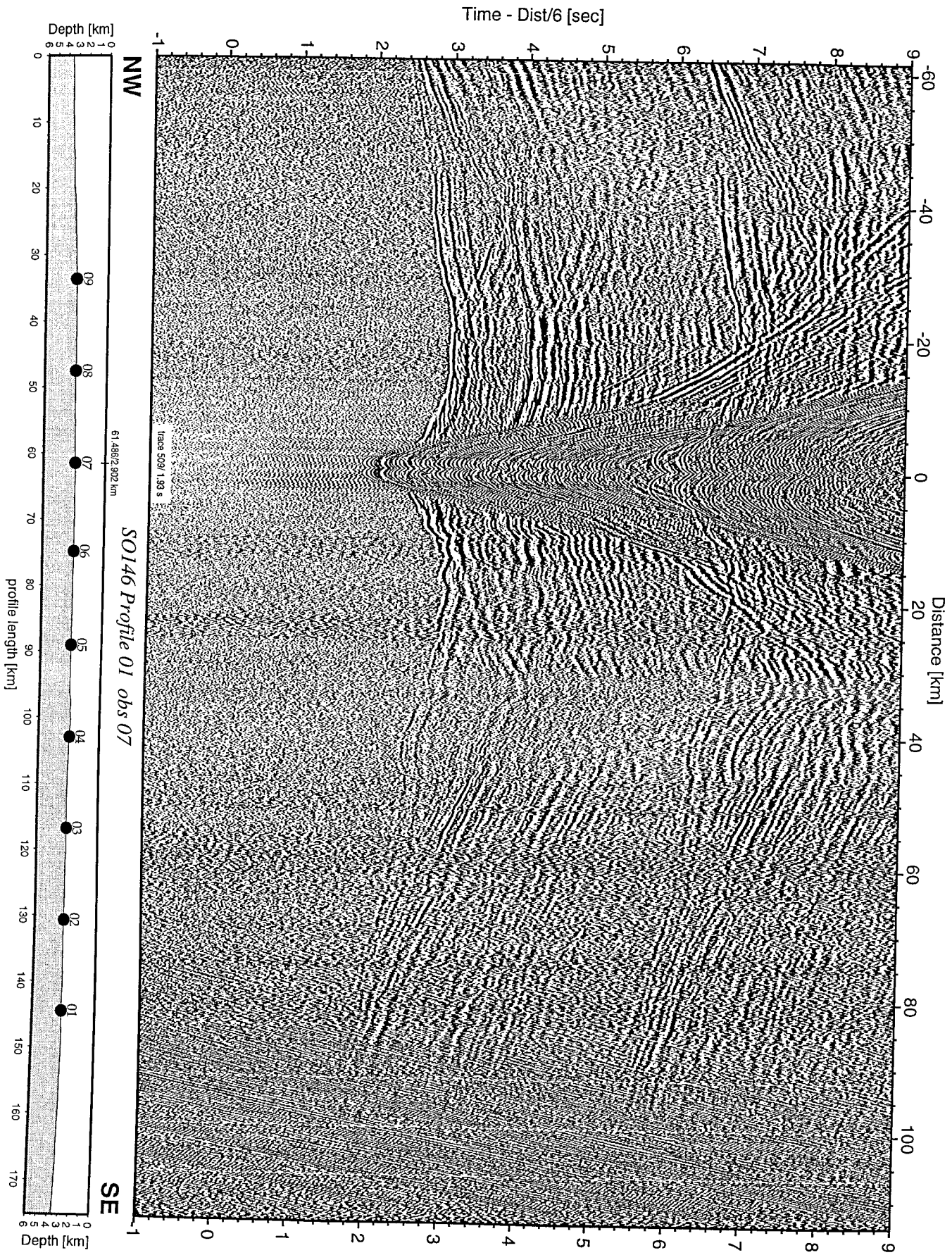

Figure 6.2.1.14: Record section from obs 07 vertical component, Profile 01.

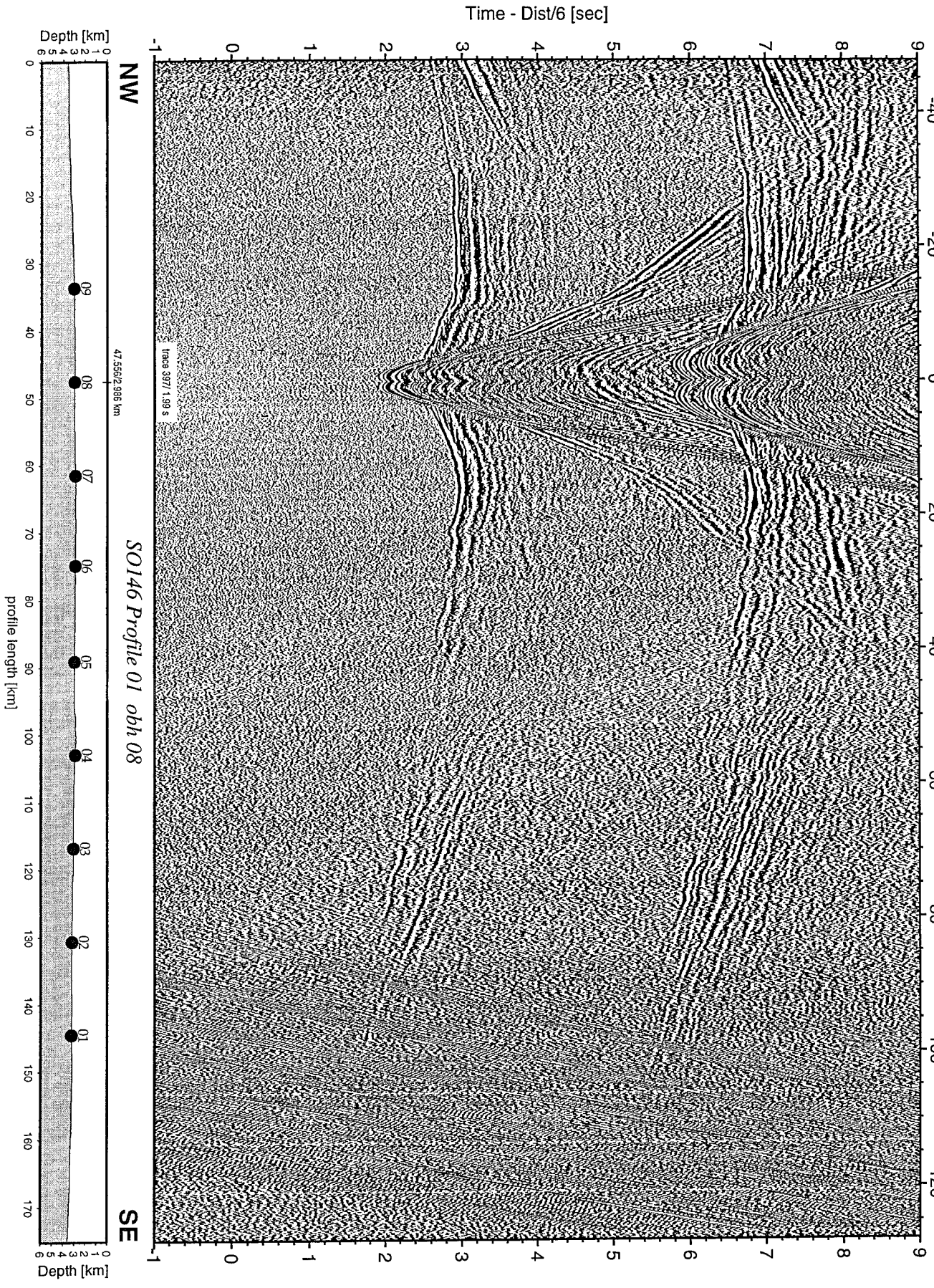

Figure 6.2.1.15: Record section from obh 08 , Profile 01.

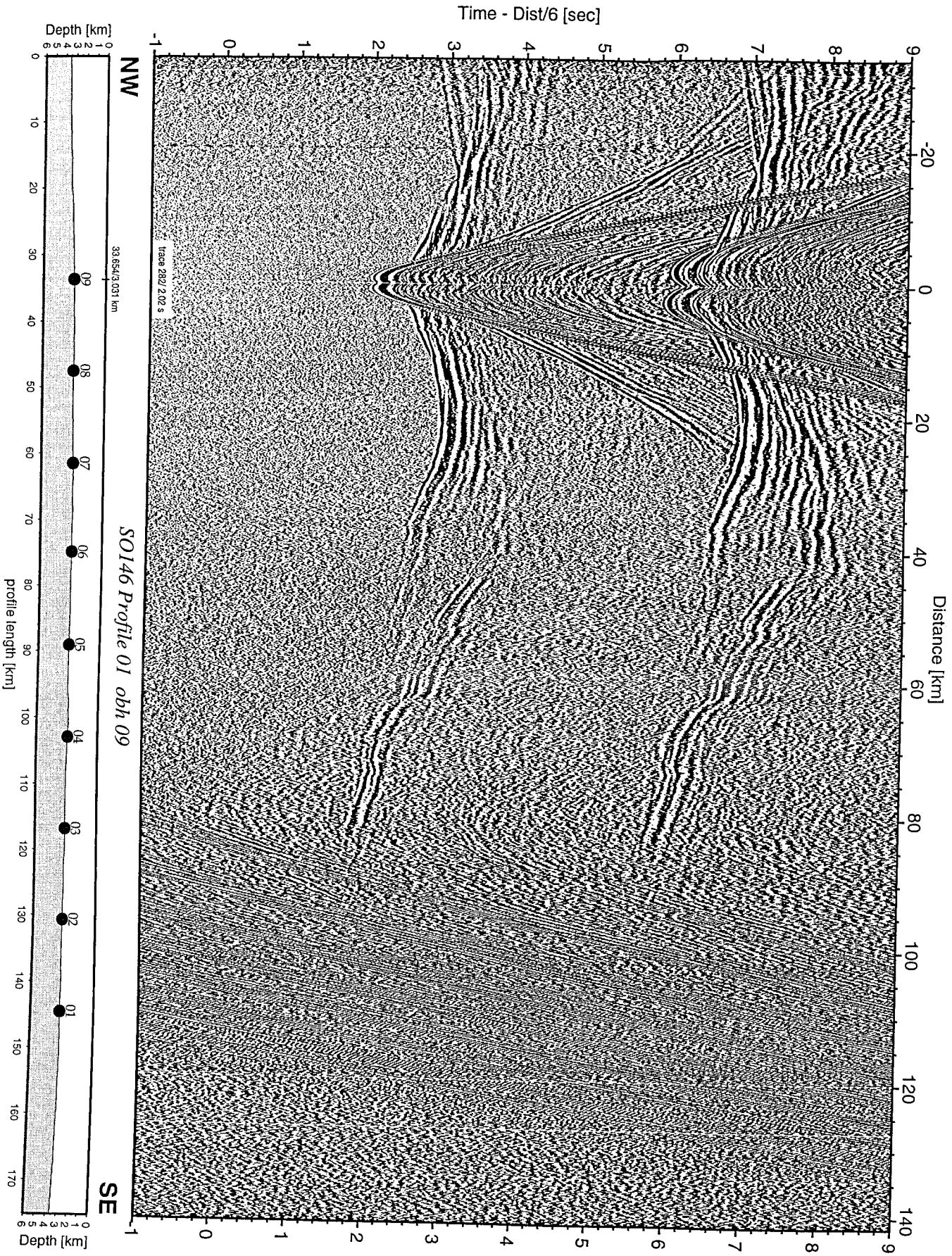

Figure 6.2.1.16: Record section from obh 09 , Profile 01.

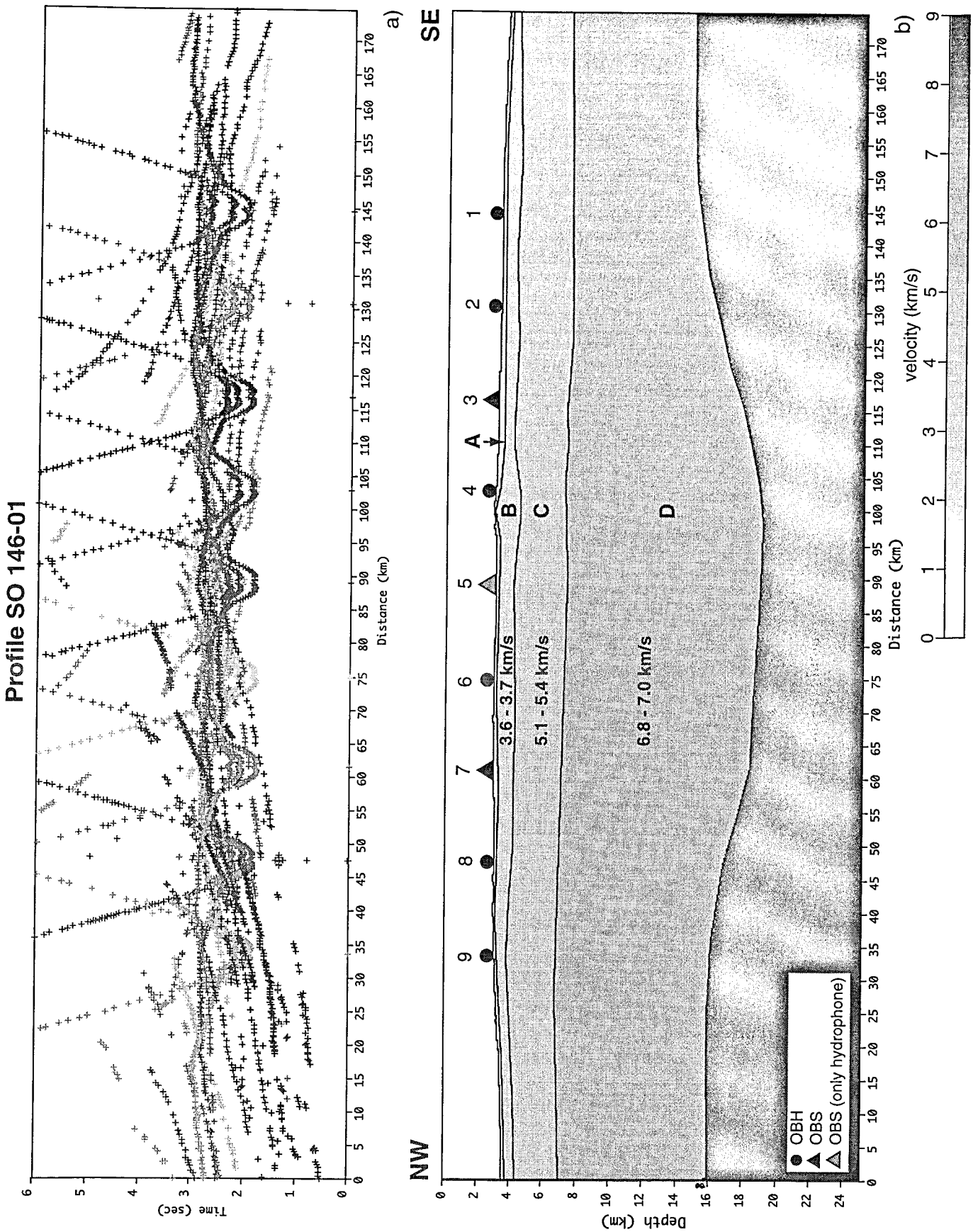

Figure 6.2.1.17: a) Picks extracted from the record sections of profile SO 146-01, b) crustal cross section for profile 01 derived from preliminary analysis of wide angle data.

6.2.2 Profile SO146-02 at 15° South

(H. Letz, A. Haris and E. Norabuena)

Profile SO146-02 is centered along the crest of the Nazca Ridge at the south-western end of the profile, extending towards the NW across the Peru Trench and onto the continental shelf. The aim of the experiment was to investigate the velocity – depth distribution following the strike of the Nazca Ridge and the lateral extension of the crust – mantle boundary in the subduction zone formed by the Nazca Plate and the South American Plate. The main topographic feature is the Peru Trench with a maximum depth of about 5000 meters on this section.

Profile SO146-02 intersects with Profile SO146-01 at a right angle over OBS05 (15° 41.59'S, 76° 47.59"W) which recorded shots of both profiles while at the same position. A total of 10 OBHs and 4 OBSs were deployed between 7th March 2000 and 8th March 2000. The spacing between the stations OBH05 and OBH10 was 10 nm and then continued at about 7.5 nm to OBH14 and for the remaining stations at intervals of about 3.5 – 4.5 nm. The distance between OBS05 and OBH22 (14° 48.00'S, 76° 04.05'W) is 126 km (68 nm). The total coverage of the profile is 177 km at a strike of 38° NW. Station coordinates are listed within appendix II. A location map of the profile including bathymetry is given in Figure 6.2.2.1.

Shooting of the profile started on 7th March at 17:57 UTC at about 25 km NE of OBH22 and was carried out by an array of three 32 l Bolt airguns (2000 cu. inch each) firing every 60 seconds, for a total of 1449 shots. While shooting, the speed of the vessel remained at a constant 5 kn. Shooting was completed on 8th March at 18:06 UTC. While part of the equipment was retrieved (OBS05 to OBH15), the remaining stations (OBH16 to OBH22) were left in position to record the shots of the GI guns. This short profile SO146-02a was shot to test the performance of GI guns for wide angle profiling. Initial evaluation of the data indicated, that shots were only recorded at a very short distance. Profile SO146-02a was finished on 8th March and all remaining OBS/OBH were recovered. Along with the seismic profiling a gradiometer were deployed.

The OBS/OBH data was processed as described in Chapter 4.9.1. Nearly all equipment worked without a glitch, with exception of OBS05, where only the hydrophone channel recorded data as the seismometer was flooded by water. Unfortunately, OBH10, OBH13 and OBH15 failed to record any data at all thus leaving a 37 km observational gap between OBS05 and OBH11. Generally the quality of the data is very good. The record sections from the hydrophone channels of each OBS/OBH are shown in Figure 6.2.2.2 to 6.2.2.21. The reduction velocity of all seismic sections is V_{red} 6 km/s.

Modeling and Interpretation

For evaluation of data recorded on profile SO146-02 only the hydrophone channels were used. Most prominent phases, first arrivals, plus the reflected and refracted phases were picked for every record section using Xzplot software (Zelt and Smith, 1992). V (z) plots were prepared for most of the stations using R1D software to establish the initial model. This also included the morphology and some information on sediment layers from seismic reflection profiling. Modeling was done using H. Luetgert's MacRay 2D (Luetgert, 1992) modeling software.

First arrivals were easily fit to the uppermost sedimentary layer with velocities of 1.8 km/s to 2.2 km/s. The thickness of this layer as shown in Figure 6.2.2.22 is relatively thin. There are variations between 0.4 km to 0.6 km in the trench area with slight increases to 1.2 – 1.5 km in small sedimentary basins towards the continental shelf. The thickness of sediment cover SW of the Peru Trench compares directly to the reflection seismic cross-section of this profile (chapter 6.3.).

The lower sedimentary unit consists of three layers with velocities ranging between 2.5 km/s – 4.5 km/s followed by the upper crust with velocities of 5.5 km/s – 6.5 km/s. Velocities between 6.6 km/s to 7.0 km/s are associated with the crust and can be correlated on most record sections. Reflections of the lower crust have been correlated on sections obtained from OBS05, OBH11, OBH12, OBS16,

OBS18 (Figures 6.2.2.2, 6.2.2.3, 6.2.2.4, 6.2.2.9, 6.2.2.14) with velocities between 7.2 – 7.3 km/s. Another discontinuity is seen at 16 km depth with velocities of 7.6 – 7.8 km/s. The velocity of the upper mantle is >8.0 km/s.

As a preliminary result, the model of the subduction zone between the Nazca Plate and the South American Plate indicates that the ridge crust with a thickness of 17 km is gently dipping NE at about β=11.7° beneath the continental plate, where the confirmed depth on this cross-section reaches 27 km. Due to the lack of clear PmP and Pn phases recorded at the stations placed on the continental shelf (i.e. OBH17, OBH19, OBH20, OBH21, OBH22), there is very little constraint over the NE extension of the crust – mantle boundary at greater depth.

It appears that the Nazca ridge subducts completely beneath the continental margin, which is modeled with velocities between 4.8 – 6.0 km/s. The lower slope angle measures α_1=5.9°, the mid slope angle is α_2=4.4° and α_3=2.4° respectively. Depths and velocities of the ray-tracing model were converted to density contrasts and compared with the measured Free-Air Anomaly recorded along the profile. The measured gravity is in good agreement with the structural model. A more detailed description of the gravity model is given in Chapter 6.5.

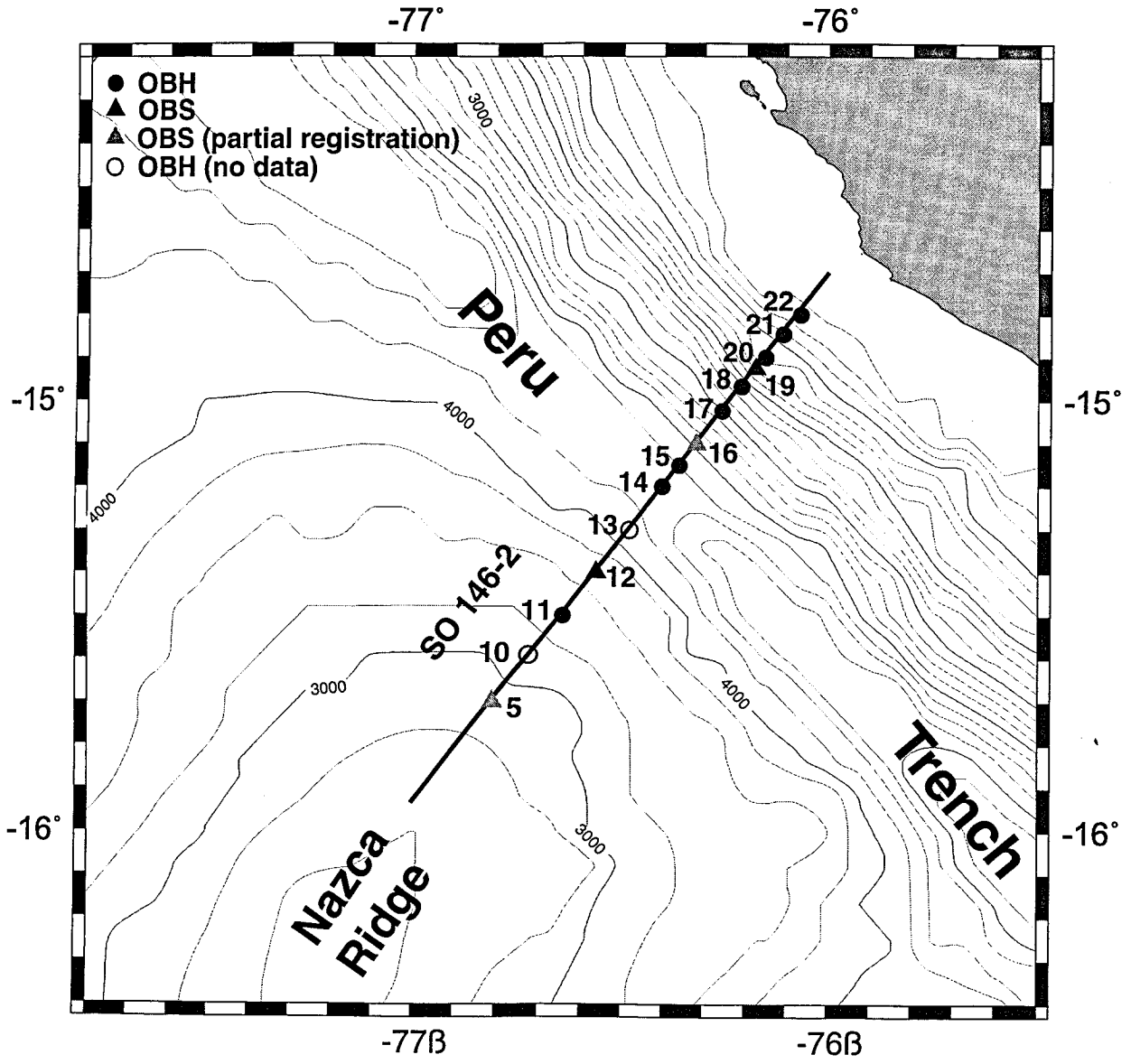

Figure 6.2.2.1: Location map of profile SO 146-02.

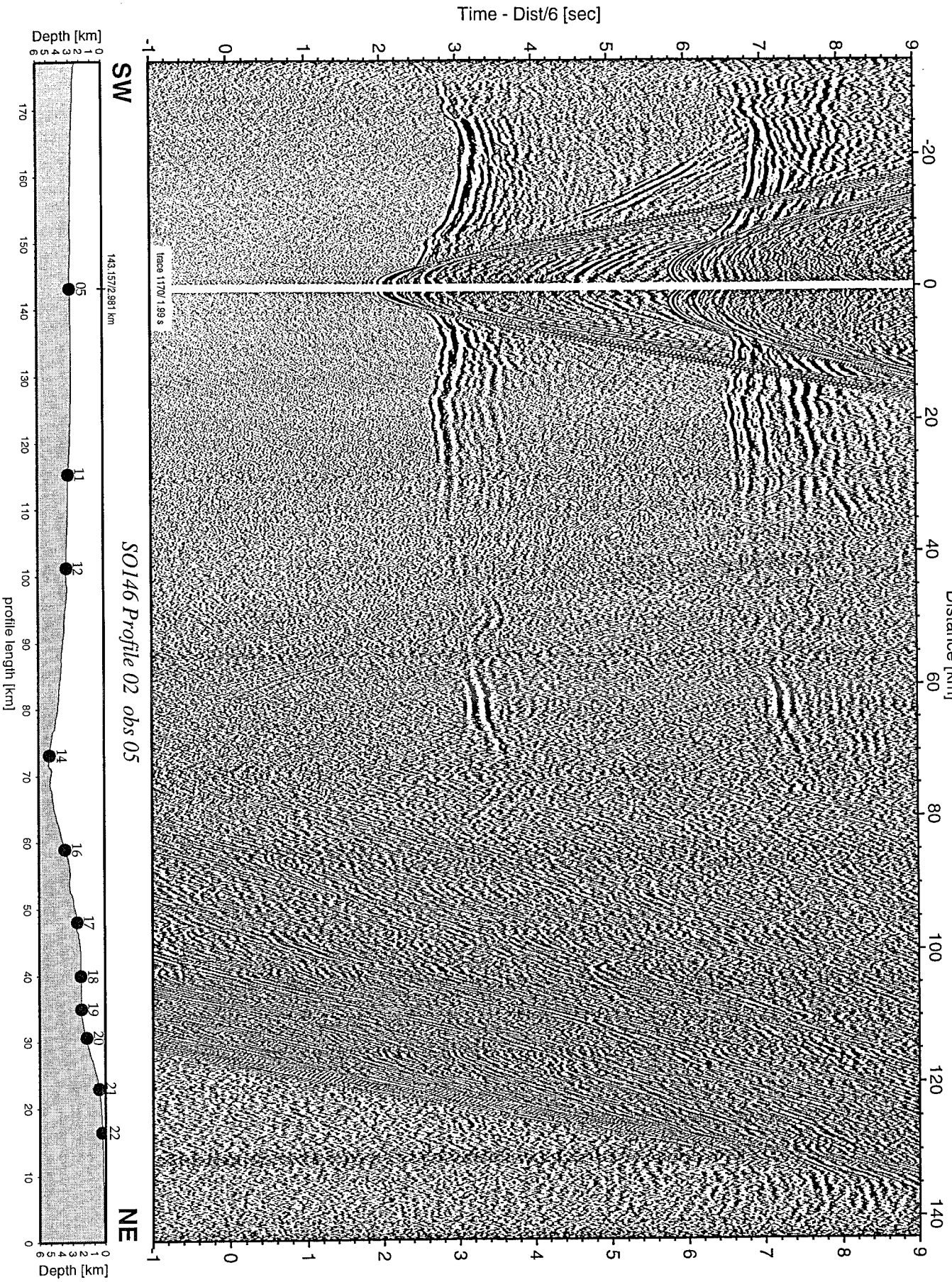

Figure 6.2.2.2: Record section from obs 05 hydrophone, Profile 02.

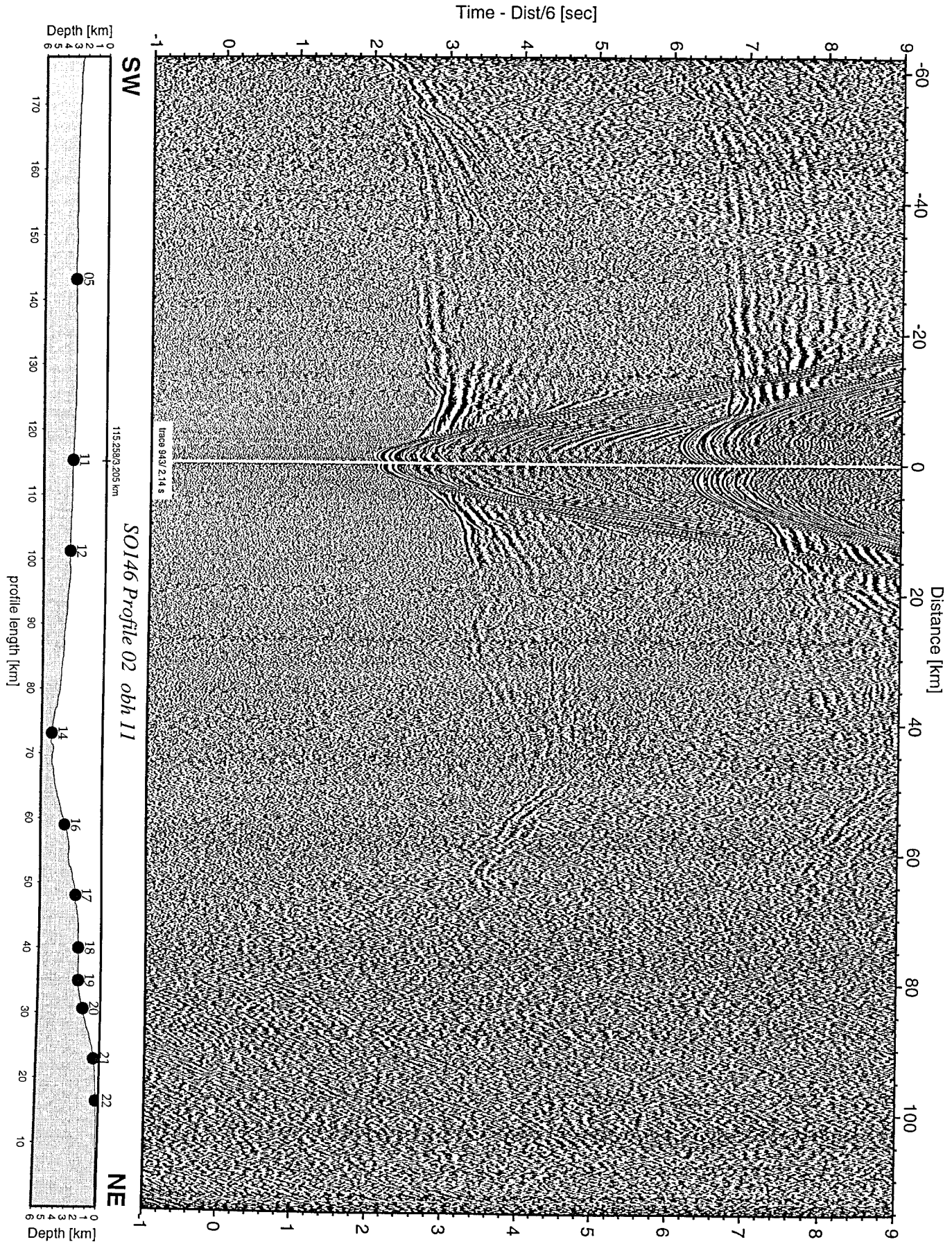

Figure 6.2.2.3: Record section from obh 11 , Profile 02.

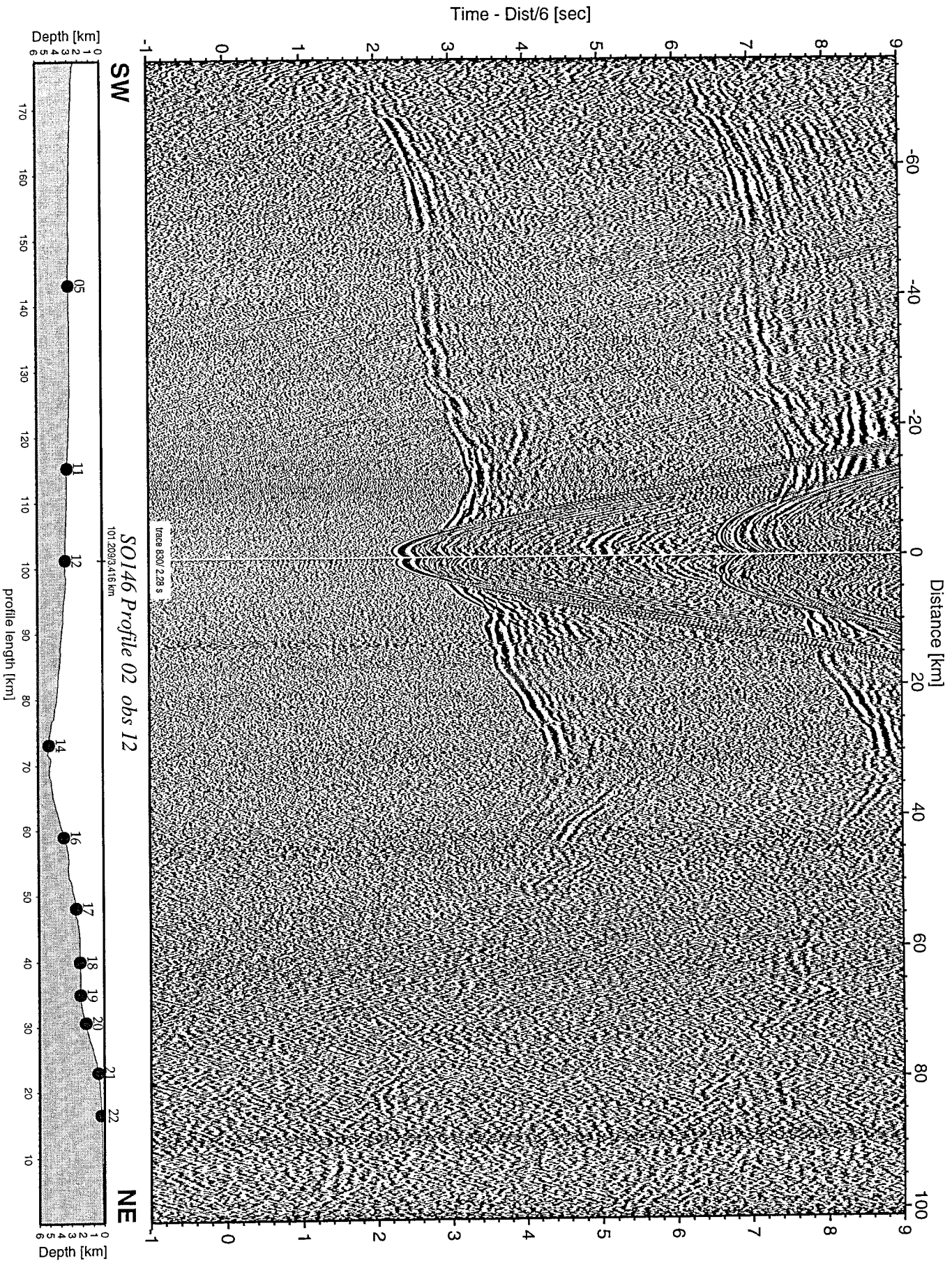

Figure 6.2.2.4: Record section from obs 12 hydrophone, Profile 02.

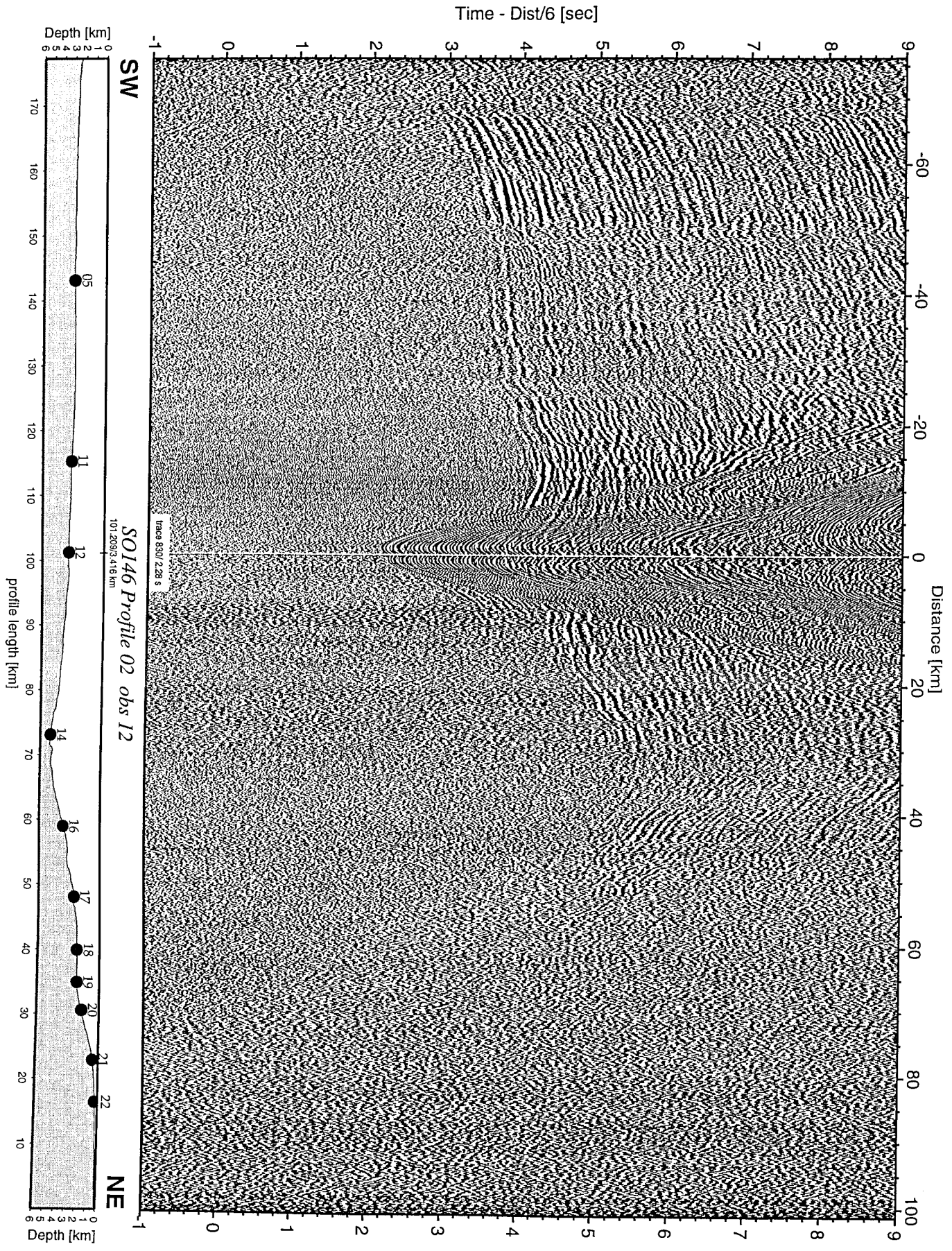

Figure 6.2.2.5: Record section from obs 12 horizontal component 1, Profile 02.

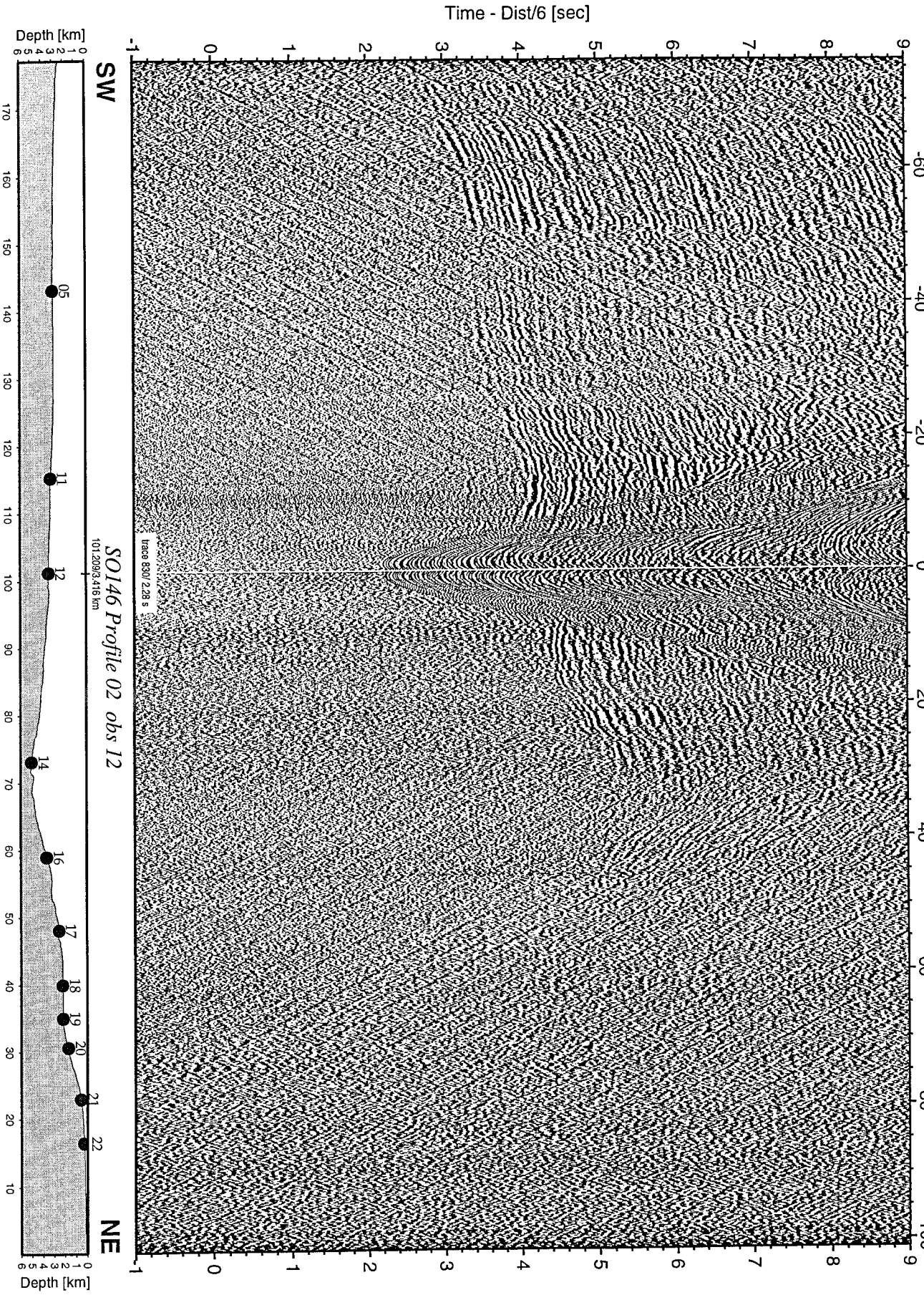

Figure 6.2.2.6: Record section from obs 12 horizontal component 2, Profile 02.

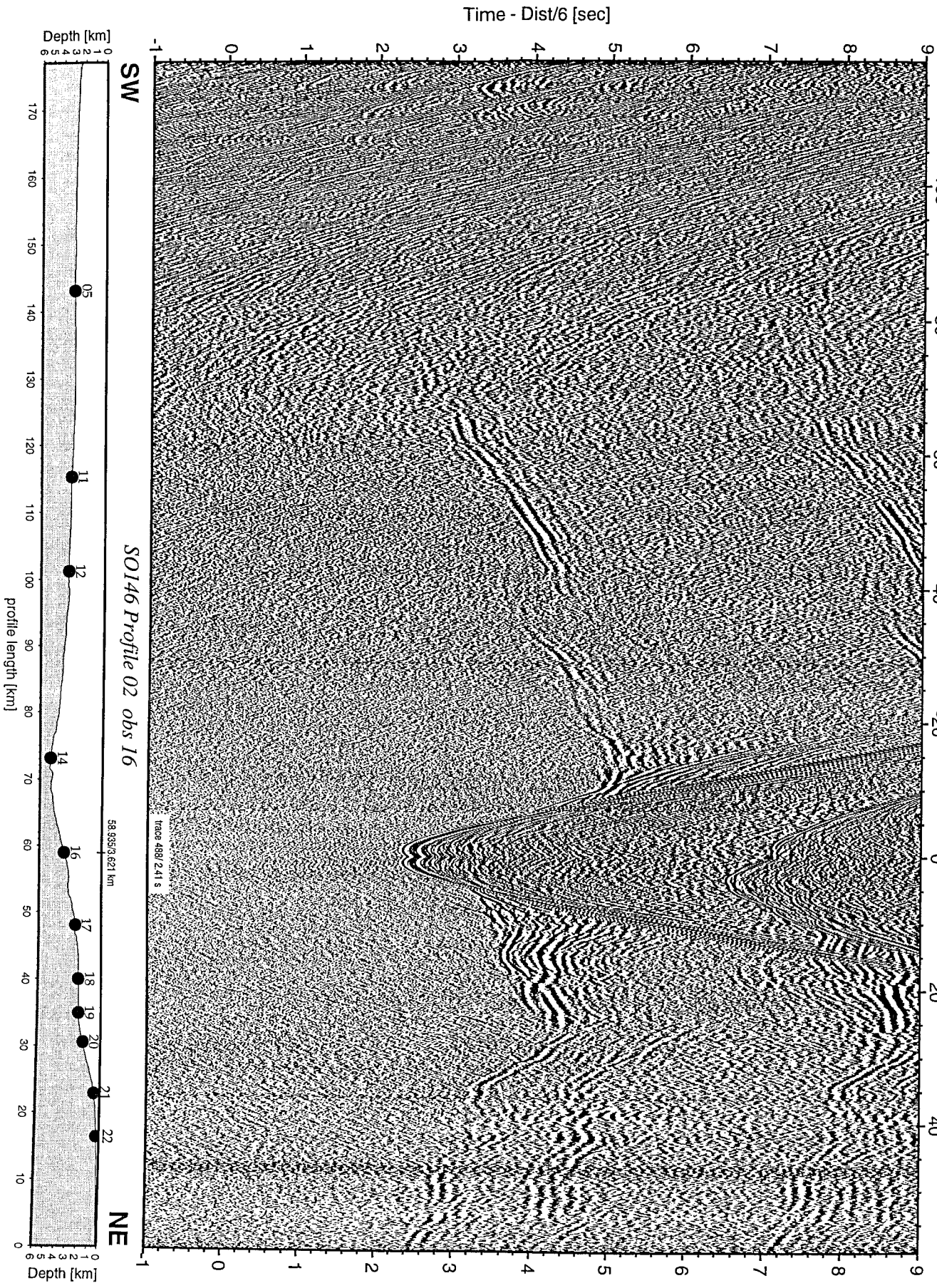

Figure 6.2.2.9: Record section from obs 16 hydrophone, Profile 02.

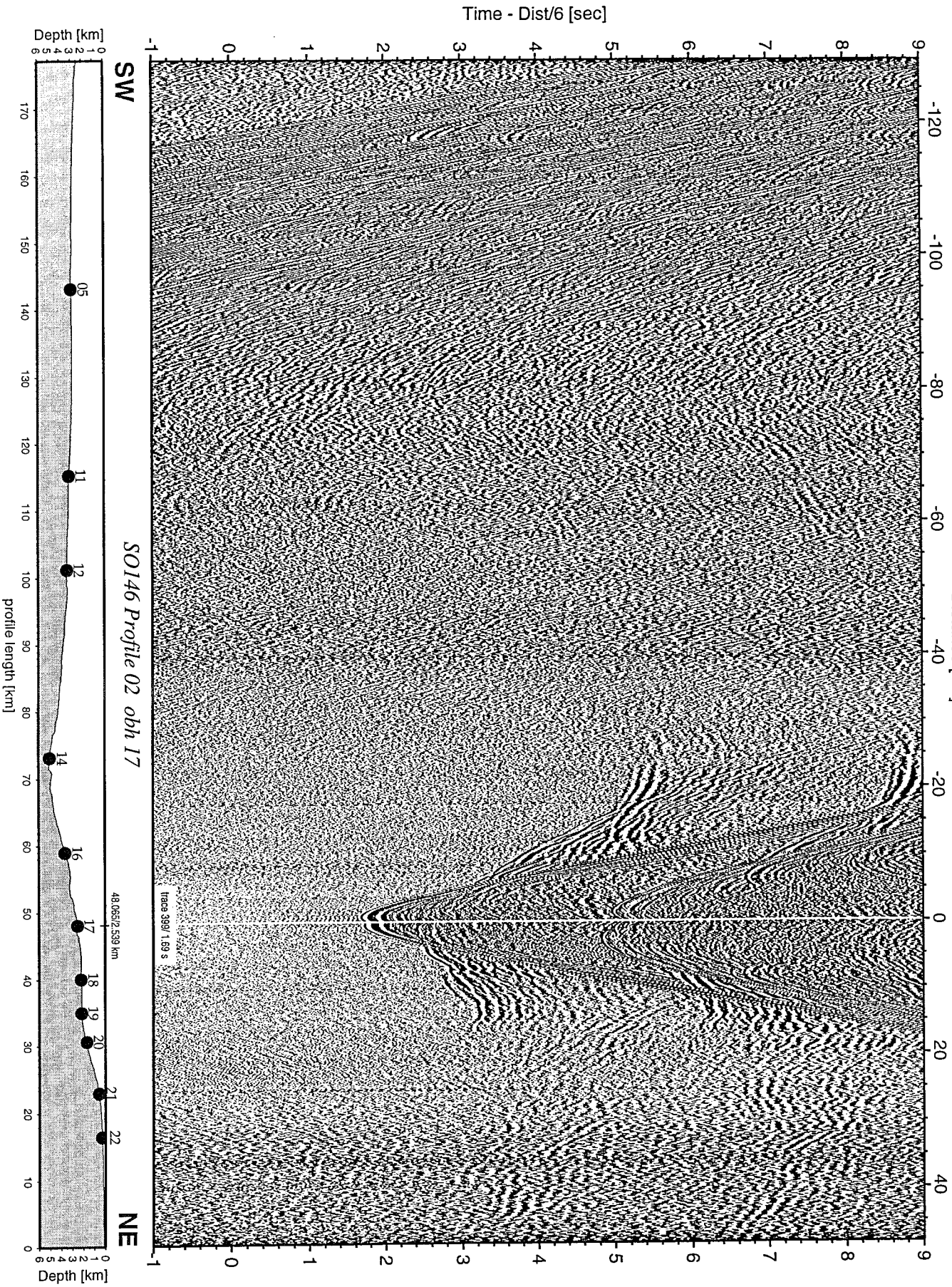

Figure 6.2.2.10: Record section from obh 17 , Profile 02.

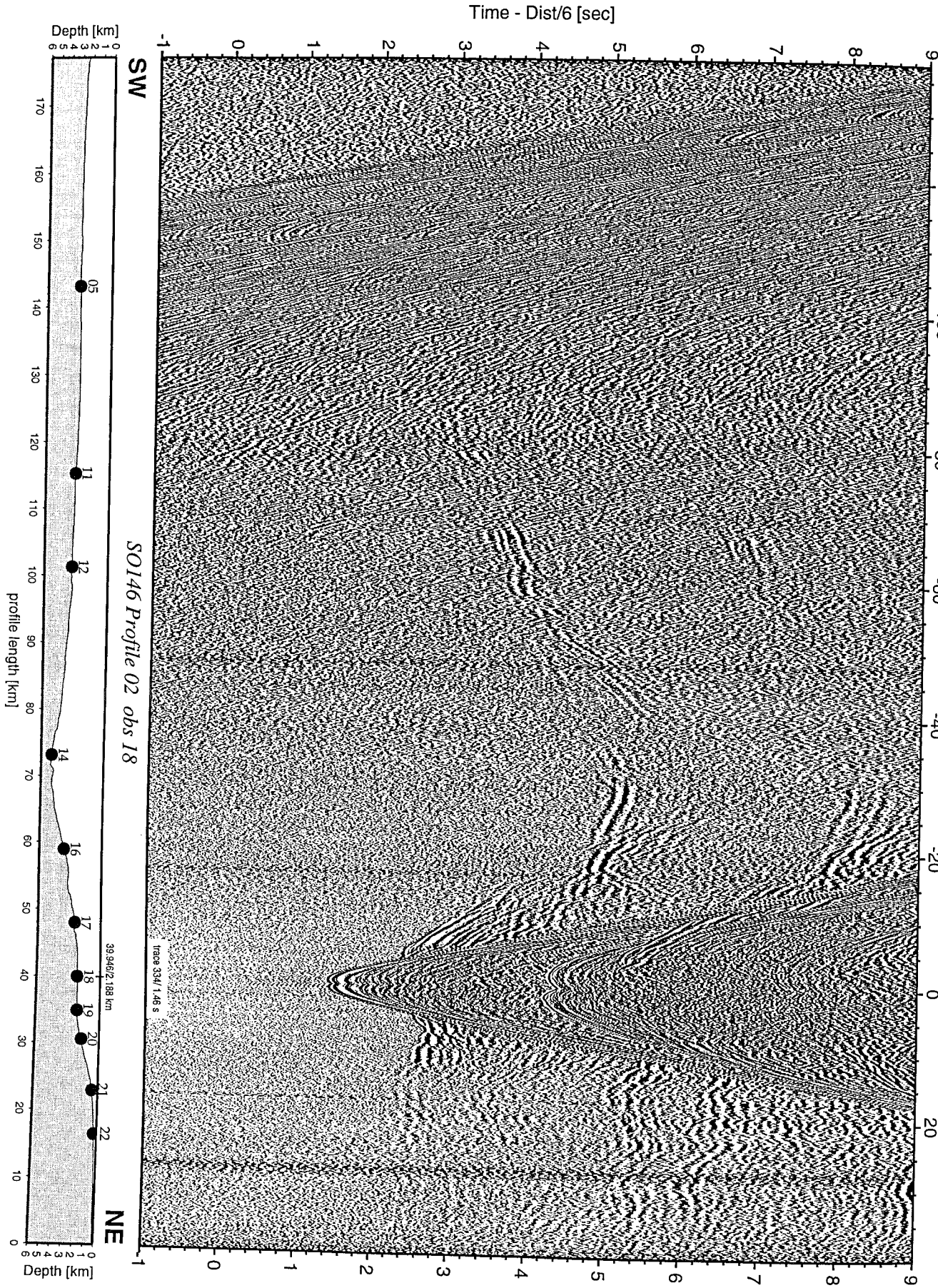

Figure 6.2.2.11: Record section from obs 18 hydrophone, Profile 02.

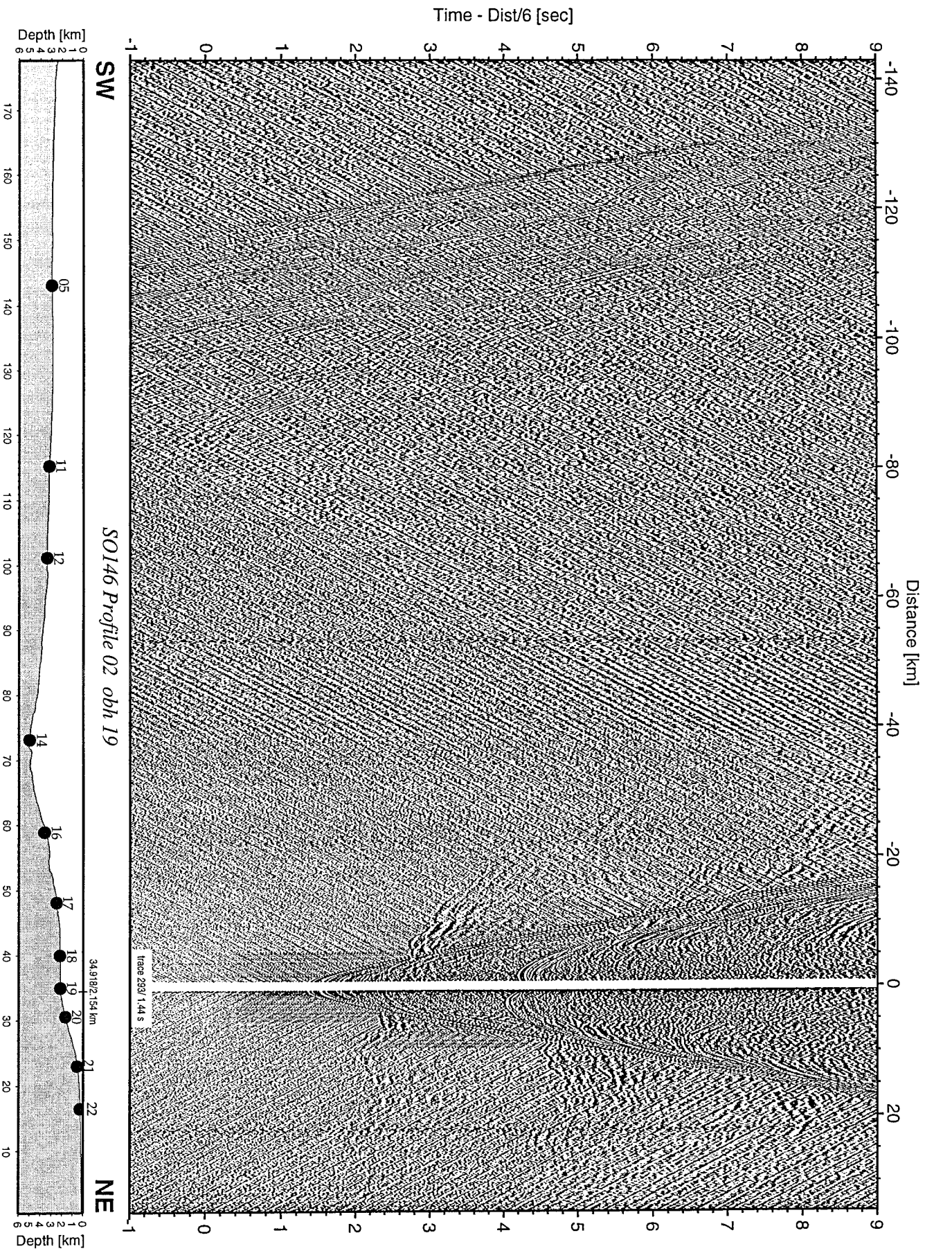

Figure 6.2.2.12: Record section from obh 19 , Profile 02.

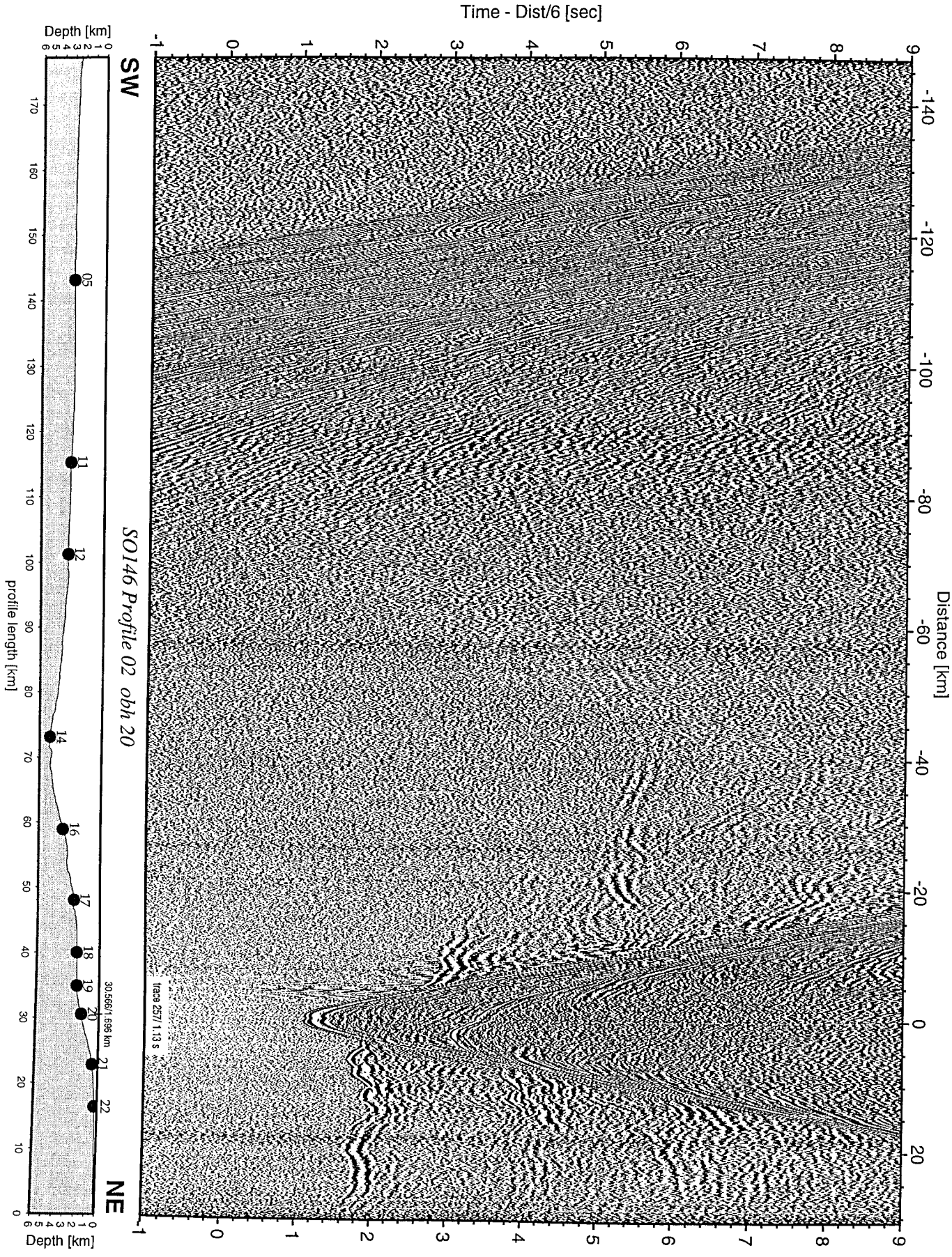

Figure 6.2.2.13: Record section from obh 20 , Profile 02.

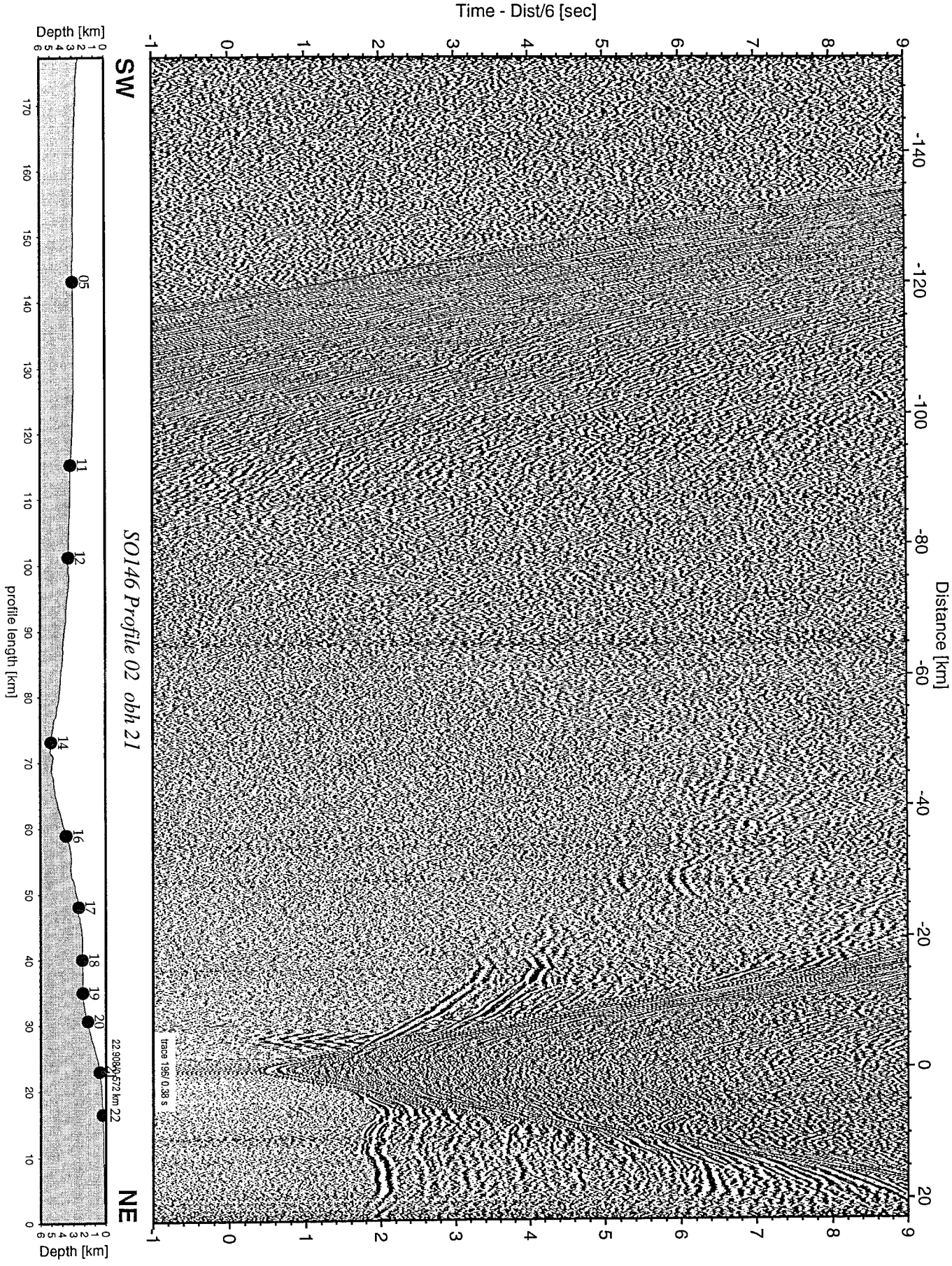

Figure 6.2.2.14: Record section from obh 21 , Profile 02.

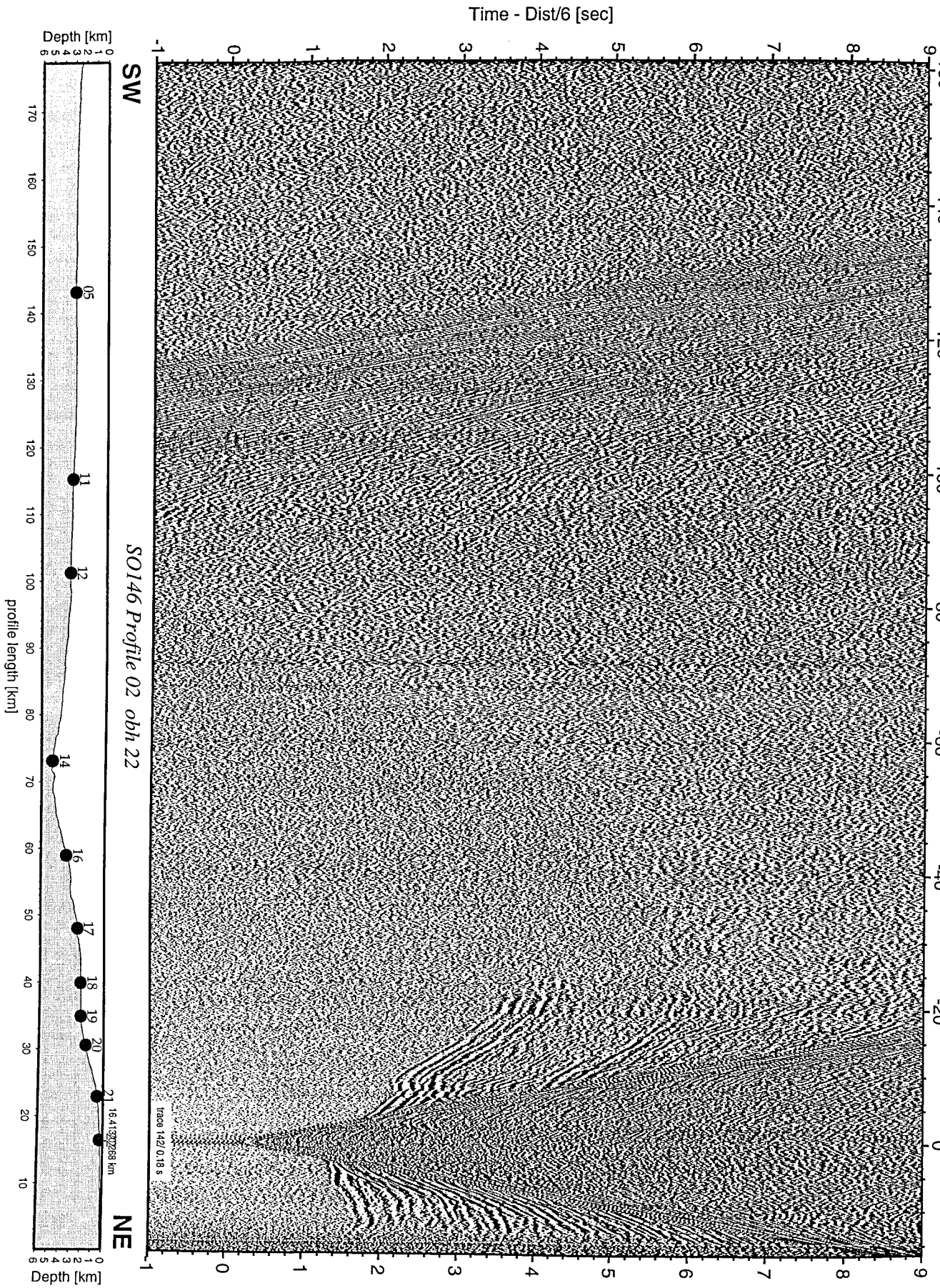

Figure 6.2.2.15: Record section from obh 22 , Profile 02.

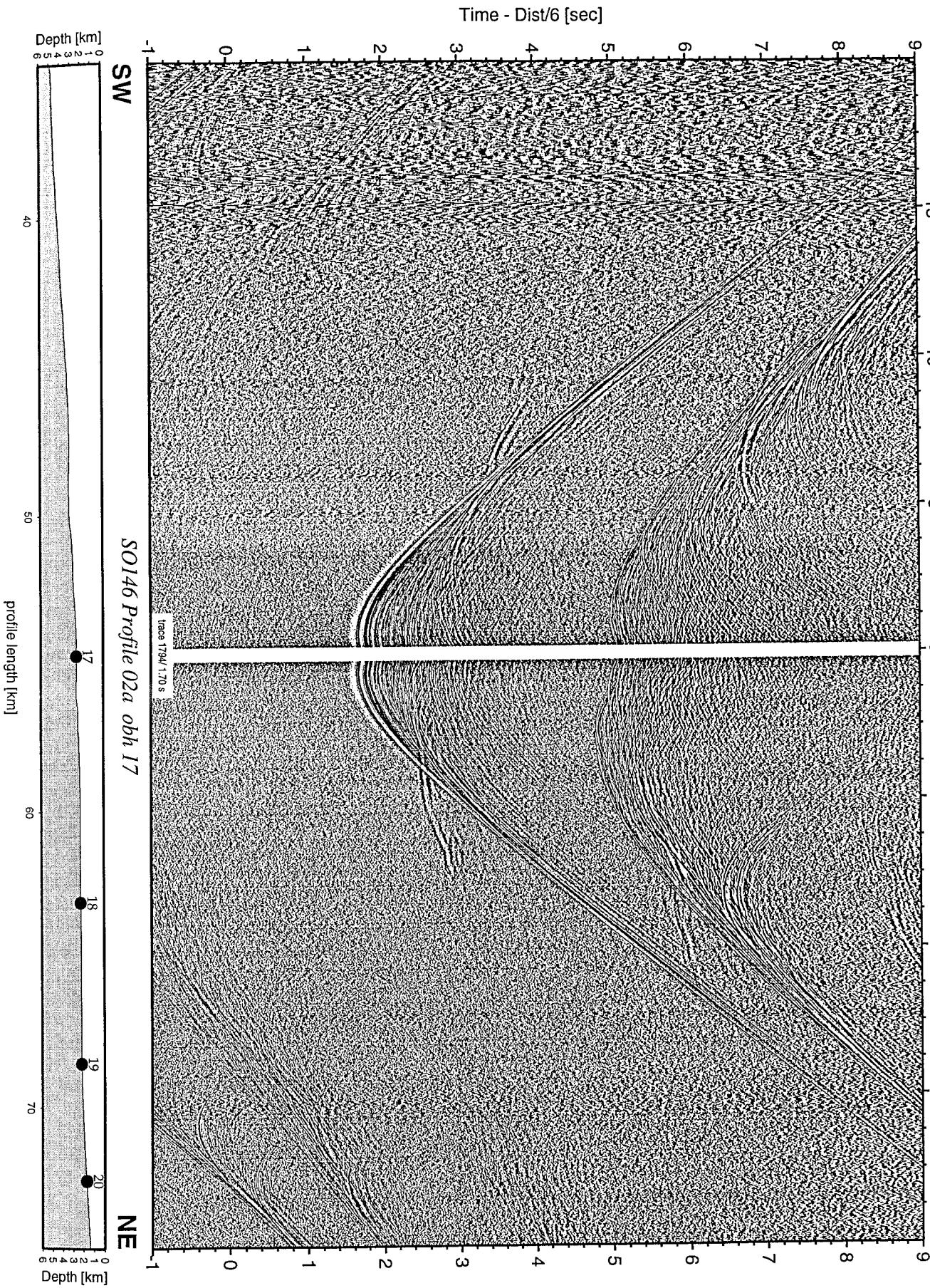

Figure 6.2.2.16: Record section from obh 17 , Profile 02a.

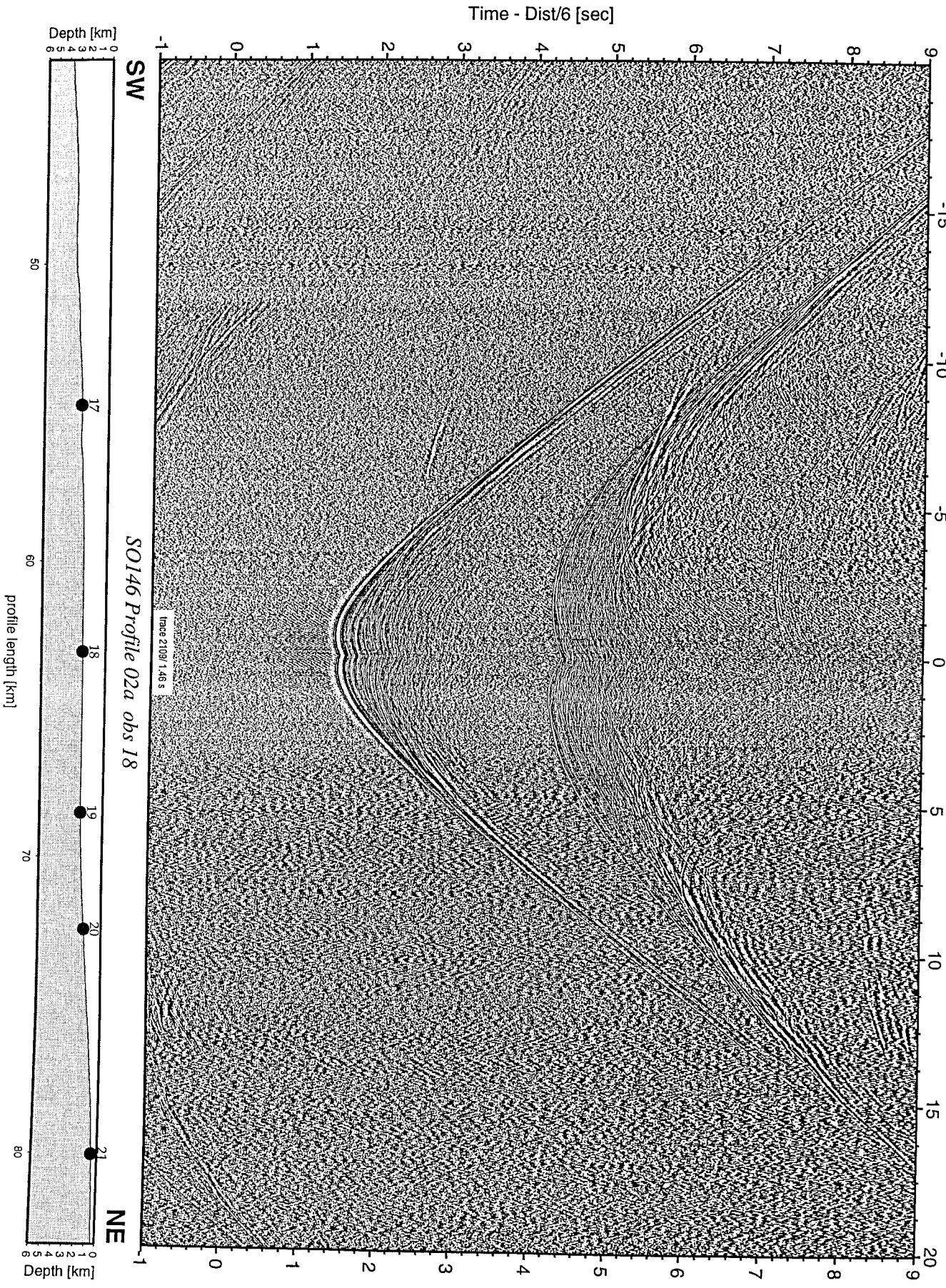

Figure 6.2.2.17: Record section from obs 18 hydrophone, Profile 02a.

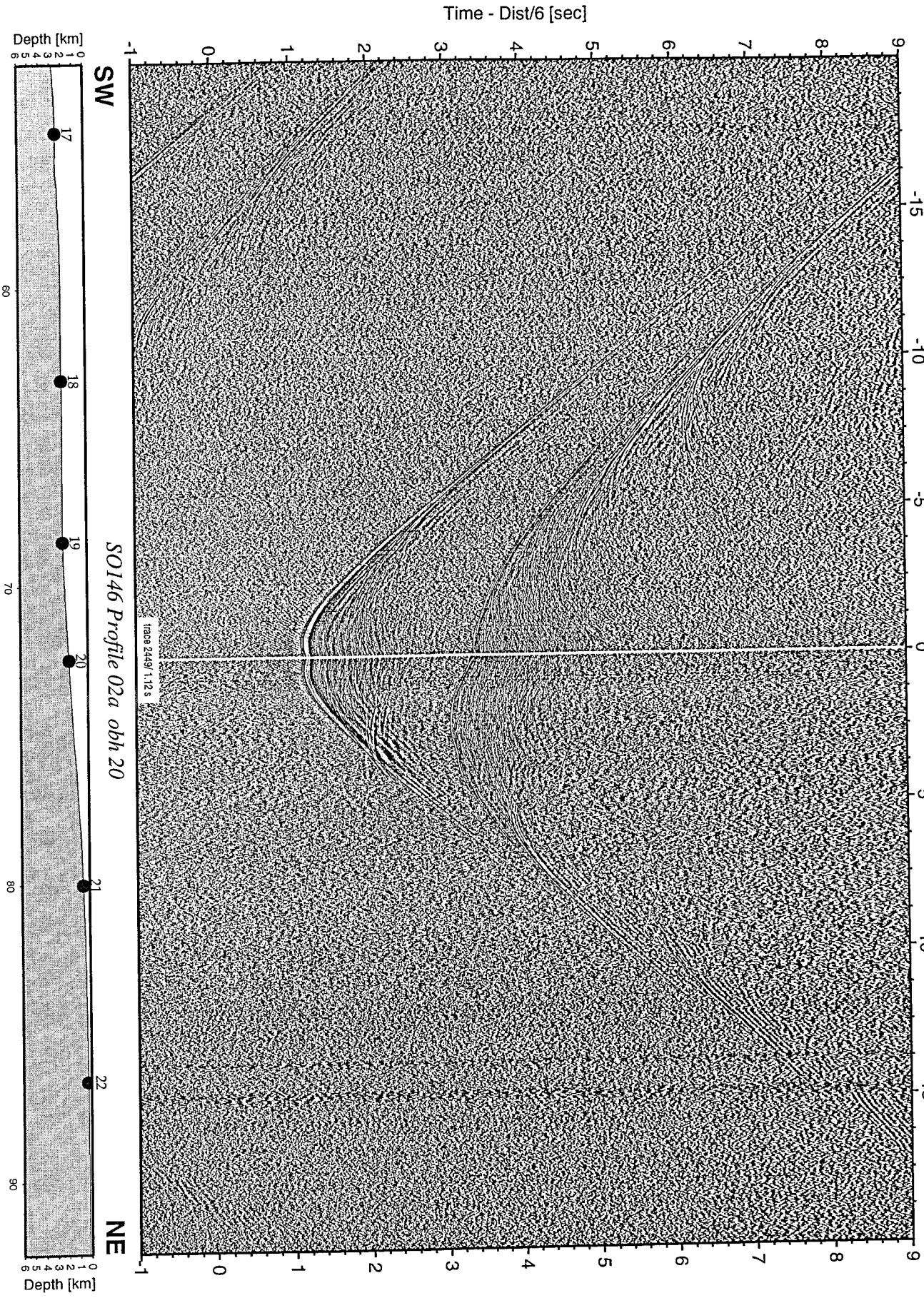

Figure 6.2.2.18: Record section from obh 20 , Profile 02a.

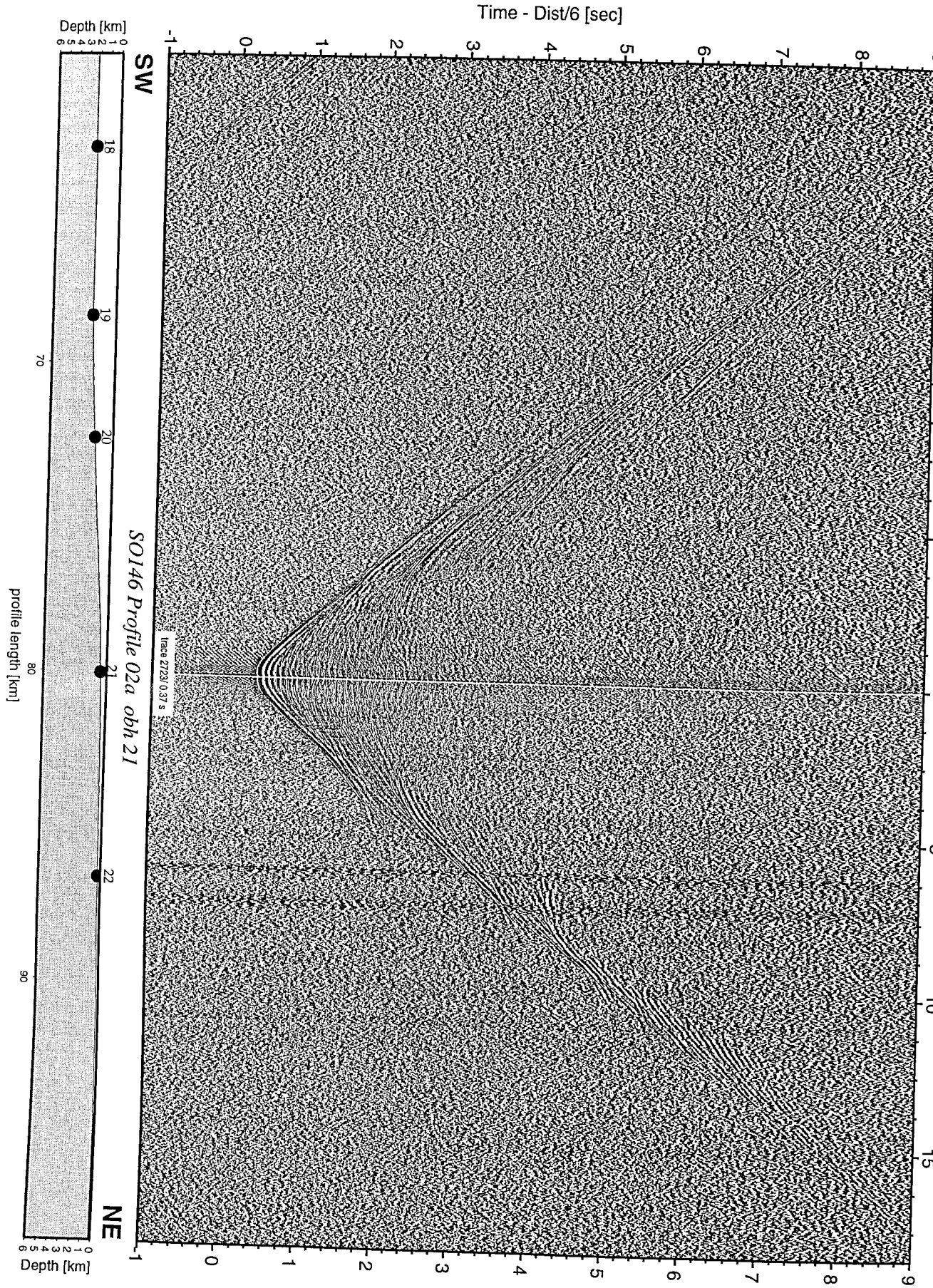

Figure 6.2.2.19: Record section from obh 21 , Profile 02a.

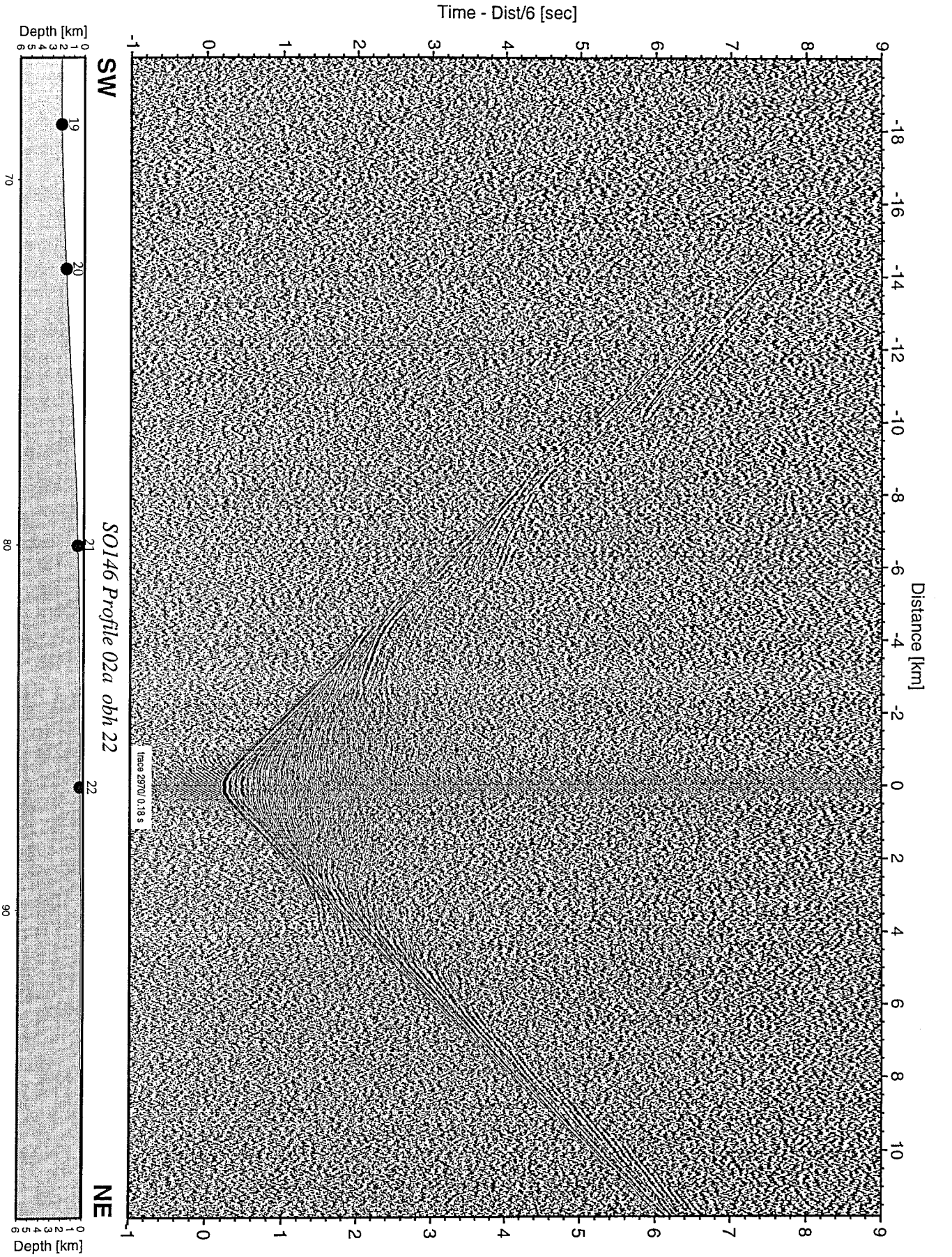

Figure 6.2.2.20: Record section from obh 22 , Profile 02a.

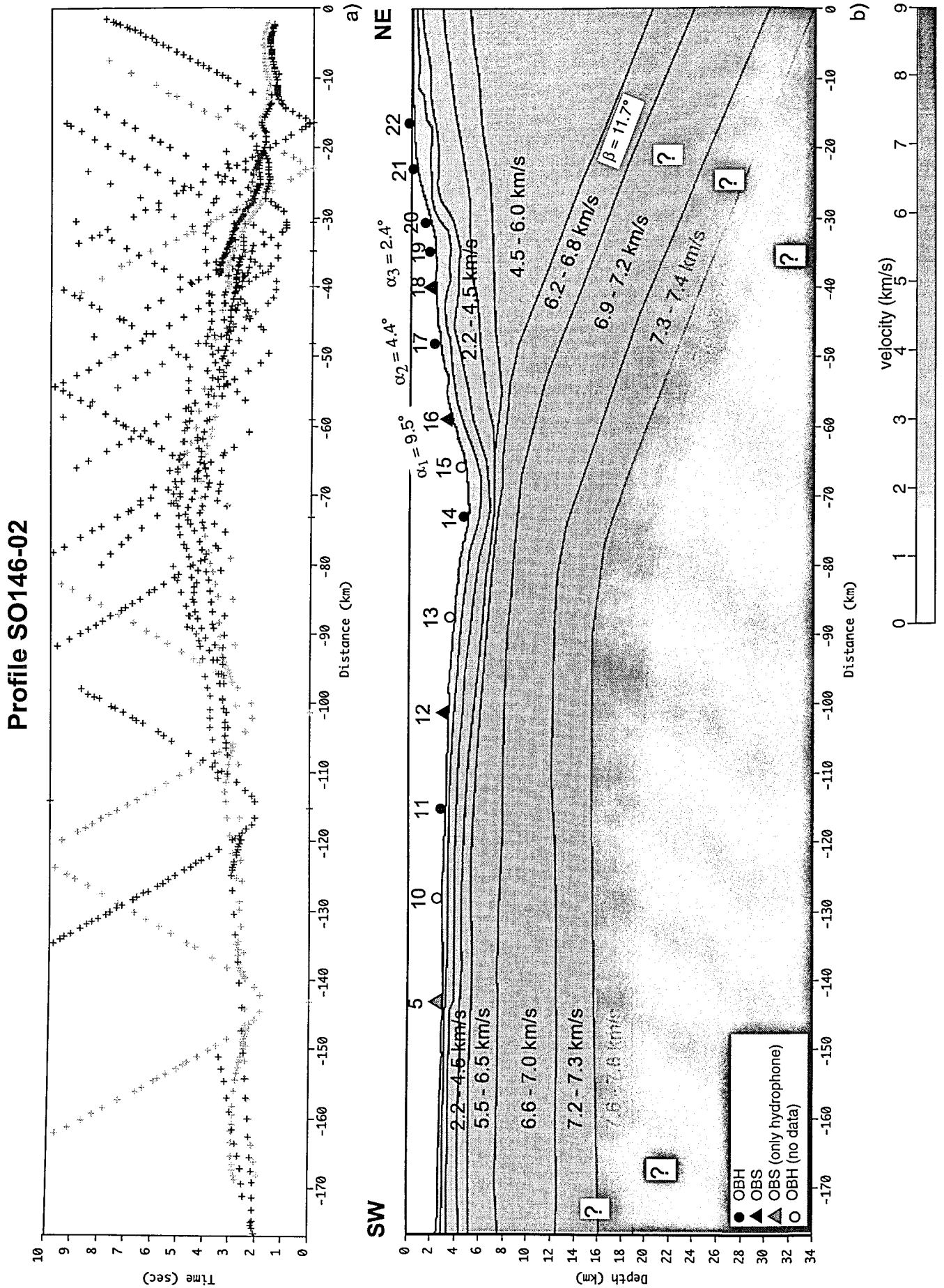

Figure 6.2.2.21: a) Picks extracted from the record sections of profile SO 146-02, b) crustal cross section for profile 02 derived from preliminary analysis of wide angle data.

6.3 Reflection Seismic

(C. Hübscher, N. Kück, M. Krüger, C. Wenz)

We contributed to the Nazca experiment streamer recordings of the BOLT-Gun used along wide angle / refraction lines #1 and #2, lines HH00-001 and HH00-002, and a high-resolution multichannel profile HH00-003, also along line HH00-002 (Fig. 6.3.1).

HH00-001 runs perpendicular to the ridge axis (Fig. 6.3.2). The shot distance is 120 m. Here the sediment thickness remains nearly constant at 400 ms TWT (app. 300m). Close to the center of the line basement crops out through the sedimentary cover at shot number 750. The height of the edifice is 800 ms TWT on the right side of the section. At a depth of 4.25s TWT strong reflections are intercalated with the pelagic cover on both sides of the outcrop; this is interpreted as sill layers. A caldera or abandoned spreading axis is centered around shot number 640 (TWT 4.4 s). The basement depression at shot number 1130 might also be interpreted as a caldera. It seems that the Nazca Ridge is underlain by a magma chamber which has partly collapsed.

Line HH00-002 which covers the slope, trench and oceanic crust is shown in Fig. 6.3.3. Four single basement highs are observed with a height of up to 700 ms TWT. To both sides of the basement high at shot number 1200 the strong reflection amplitudes also indicate sill layers intercalated into the sedimentary cover. A triangular basin is present at a depth of 2200m. Only a small accretionary wedge has been produced.

MCS line HH00-003 covers the oceanic crust, the entire continental slope and the shelf (Fig. 6.3.4). The shelf is characterized by several normal faults, overlain by a unit with parallel reflections.

Nazca-Ridge

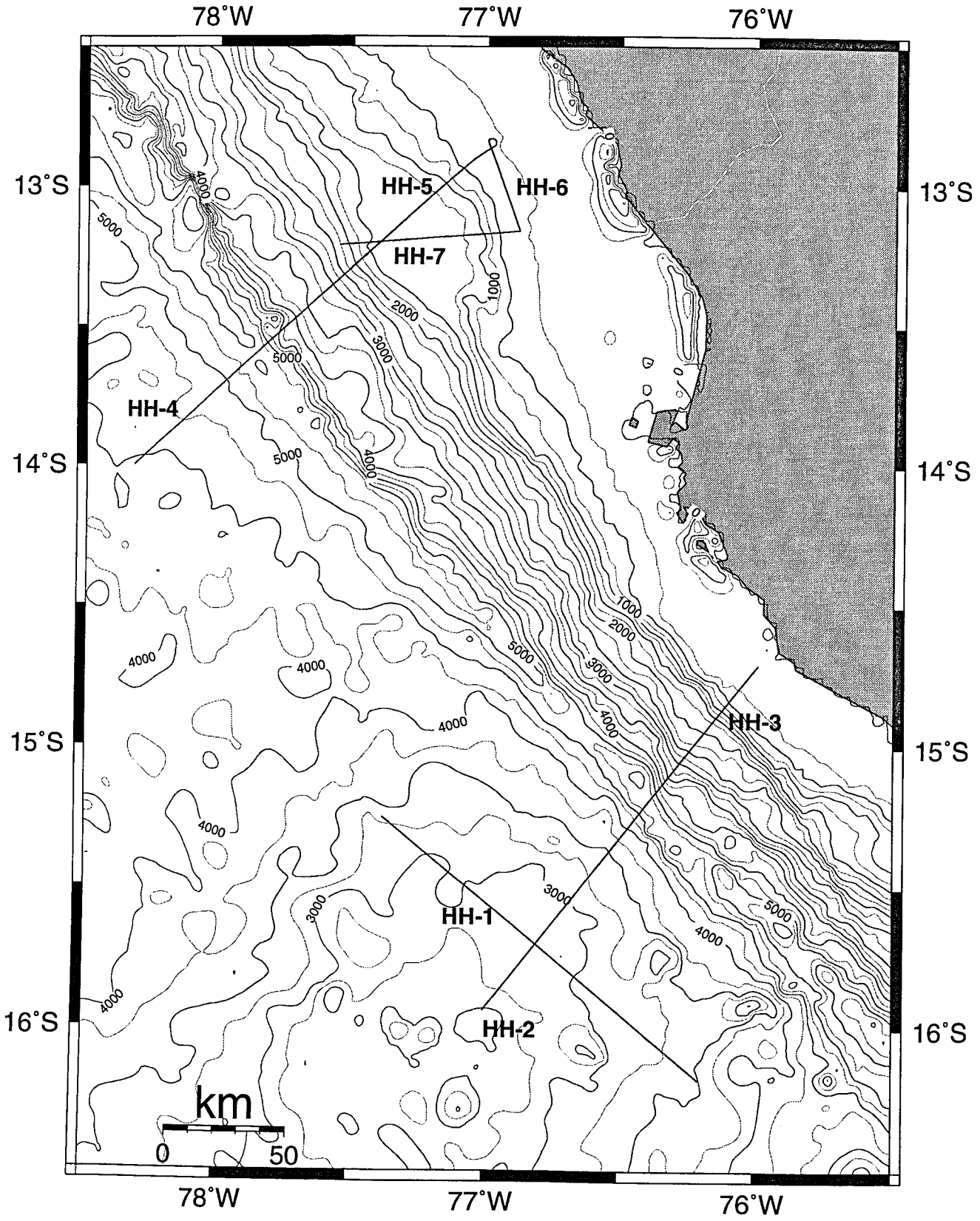

Figure 6.3.1: Seismic lines Nazca Ridge

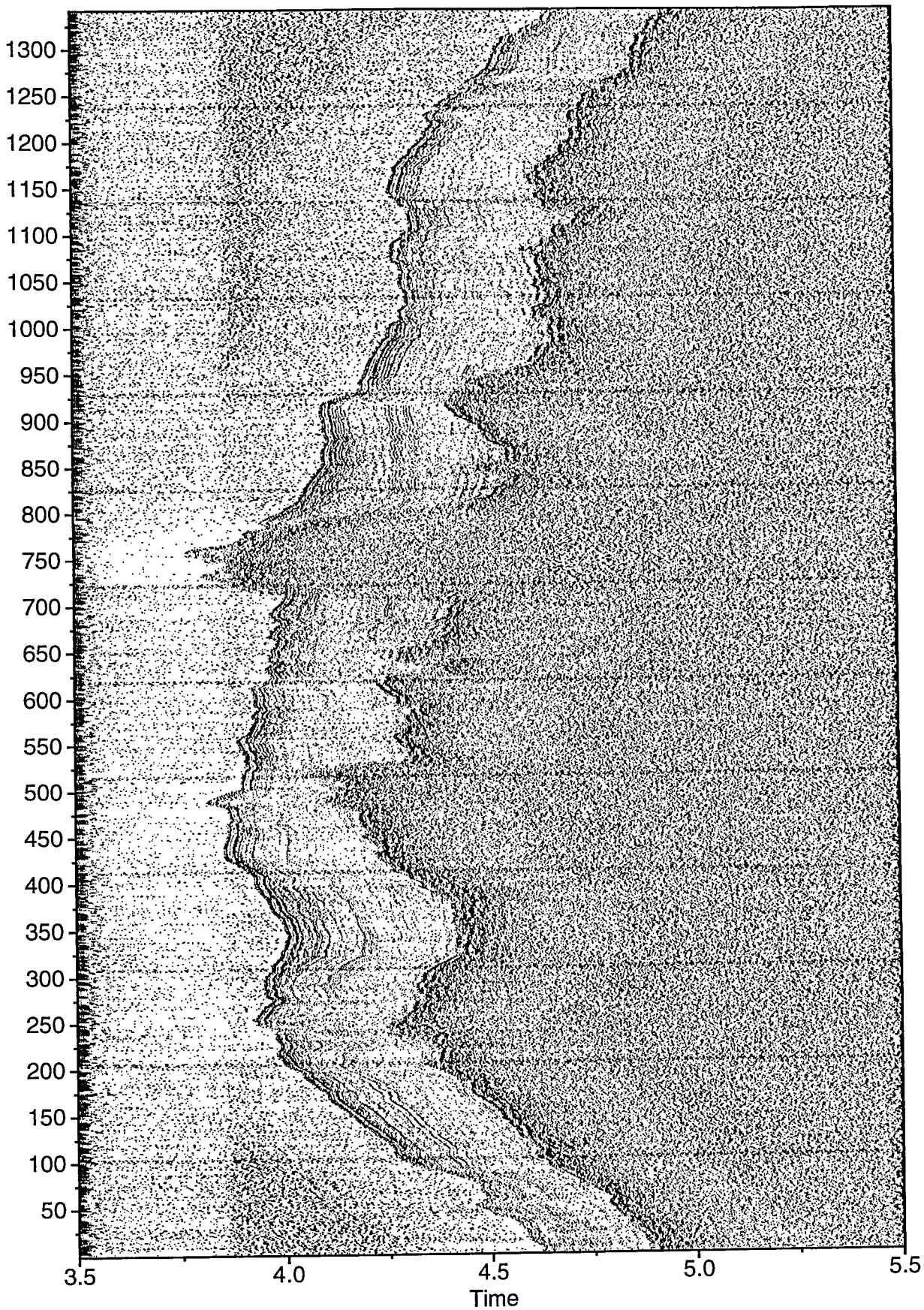

Fig. 6.3.2: Line HH00-001. Shotdistance 120m

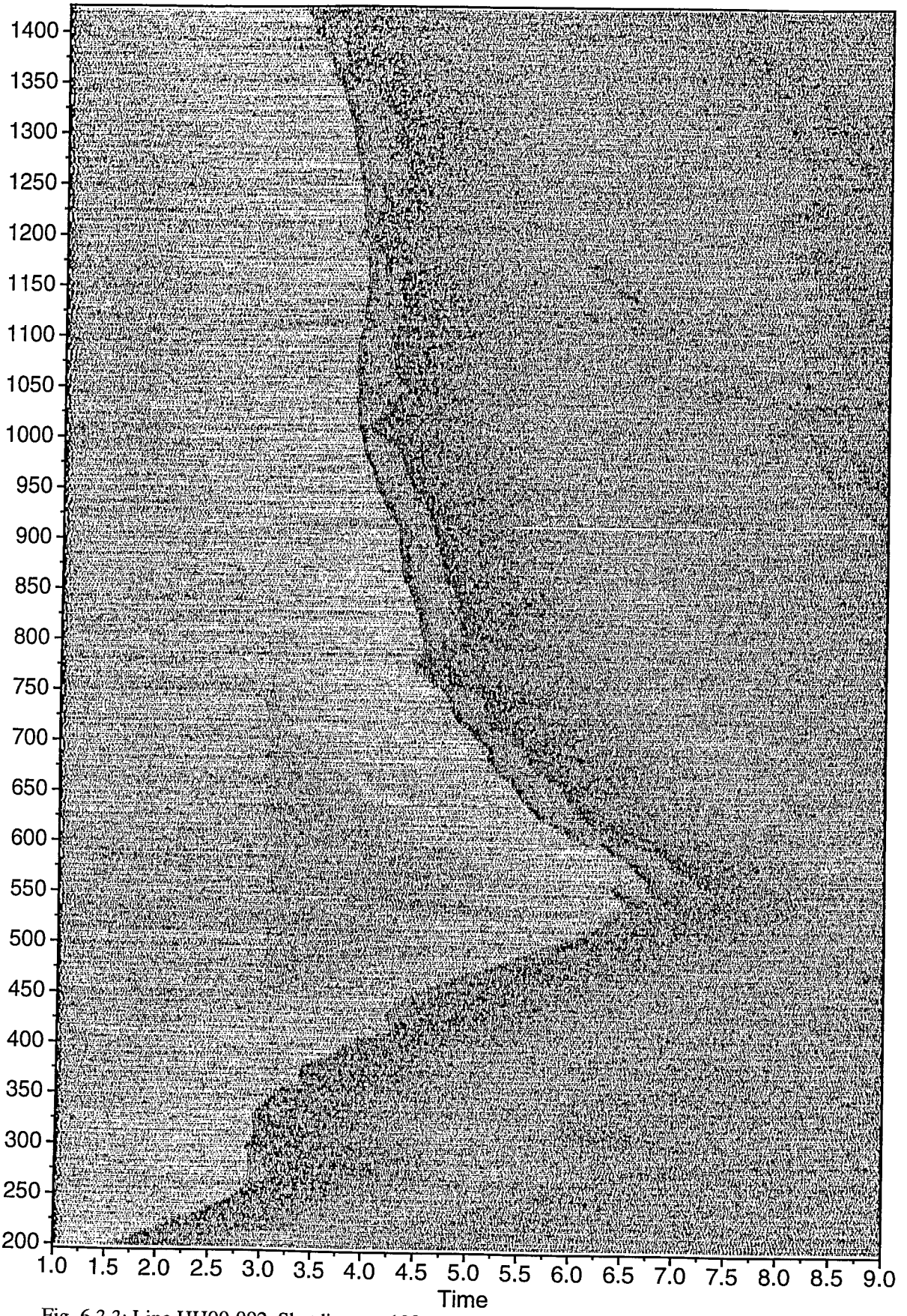

Fig. 6.3.3: Line HH00-002. Shotdistance 120m

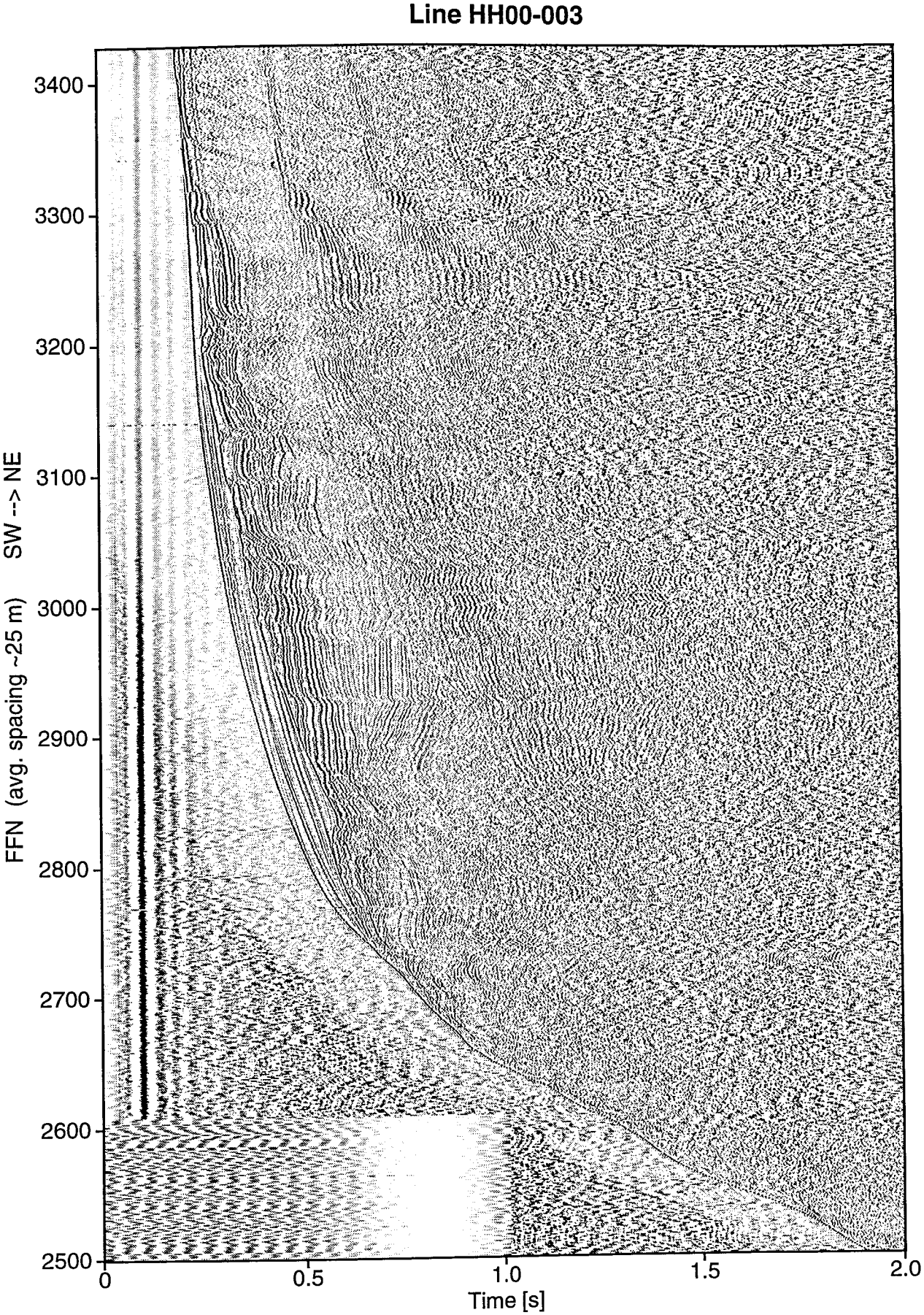

Fig. 6.3.4: MCS line 03. BP 10/20-150/200 Hz; Trace bal.; AGC 0.5 s.

6.4 Parasound

(C. Hübscher)

The reflection characteristics of Parasound data from the Nazca Ridge is well known from pelagic regions of the world oceans (Fig. 6.4.1). The hemi-pelagic deposits drape the basement and reflect basement topography except for areas with high slope angles. Therefore bathymetry maps can be used for morphotectonic investigations. They can be supported by mapping of Parasound data along the dense grid of track lines in this realm, because small seafloor undulations are better resolved with Parasound than with Hydrosweep. The undisturbed areas represent an ideal record of carbonatic sediments, which could be sampled e.g. for paleoceanographic studies.
In the center of the section we presumably observed an ancient spreading center or a caldera. The structures observed indicate several blocks which tilted away from the depression axis.

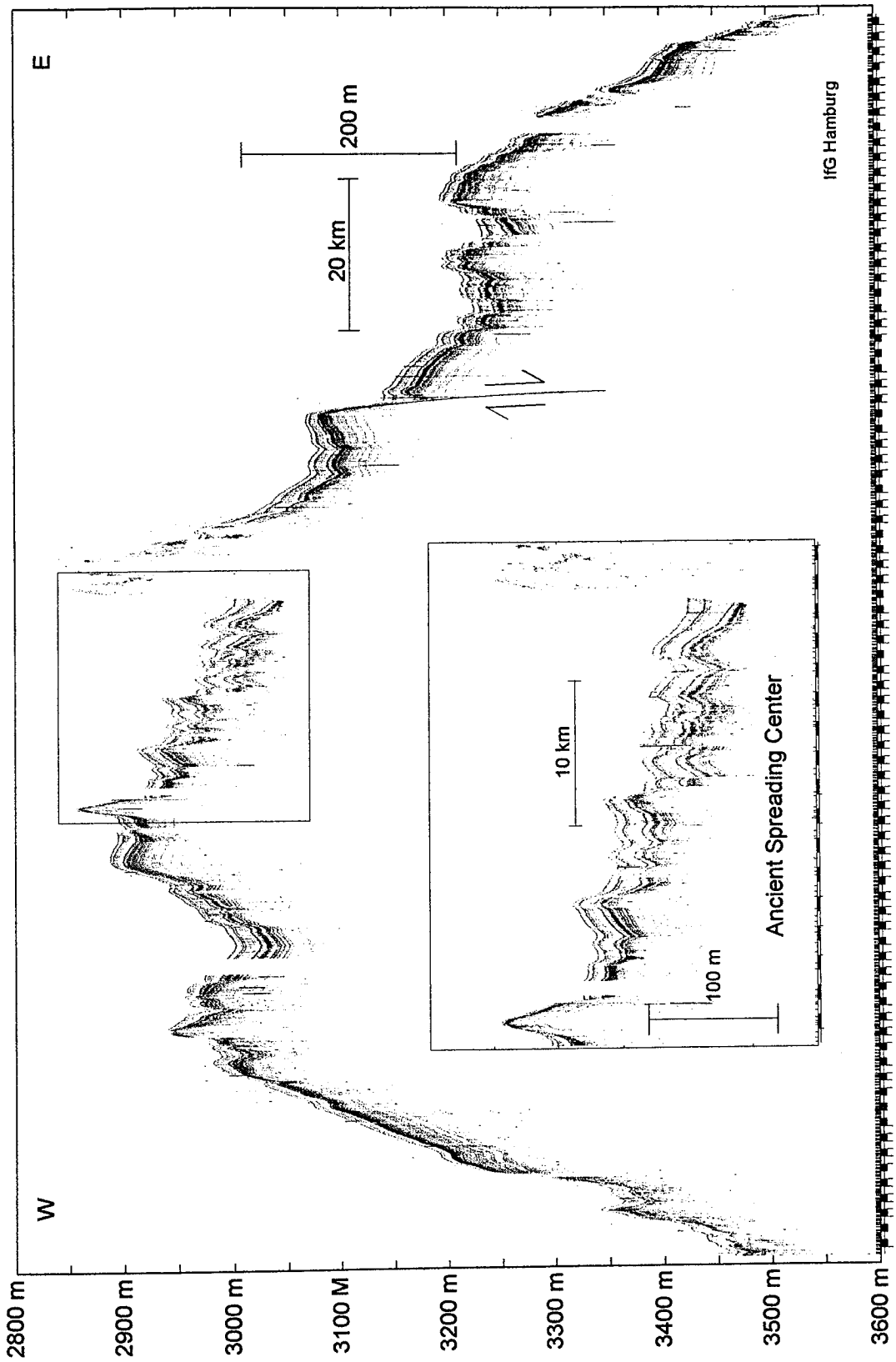

Fig. 6.4.1: Parasound crossection of the Nazca Ridge along line HH00-001 and WS/RS1, respectively.

6.5. Gravity and Magnetics

(R. Heinbockel and G. A. Dehghani)

In figures 6.5.1 and 6.5.2 the preliminary gravity (Free-Air) and magnetic anomaly (residual field) of profiles 1 and 2 are presented. The Free-Air anomaly, bathymetry, and magnetic anomaly are shown in the upper, middle, and bottom portion of the figure, respectively. All anomalies are presented as a time series (Julian day).

The Free-Air anomaly along profile 1 shows three positive anomalies with amplitudes of 15, 10 and 8 mGal. Each anomaly is well correlated with bathymetric features. On top of the Nazca ridge a relatively strong magnetic anomaly is observed. This anomaly has an amplitude of -500 nT, a clear sign of magmatic material in this area. The positive anomaly to the NW of this anomaly could be a typical sea floor spreading anomaly.

Although the gravity anomaly is a little noisy along this profile, with simple filtering of the data, the three positive anomalies are well suited for 2-D modelling.

Gravity anomalies along profile 2 are less noisy. The Free-Air gravity has values of 0 mGal near the coast but reach values of less than -150 mGal over the bathymetrically deepest part of the profile (water depth of 5000 meters). Over the oceanic part of the profile the gravity anomaly increases again to values of more than 20 mGal. The most interesting features on this profile are the typical sea floor spreading anomalies in the oceanic part of the profiles in the magnetic data.

Gravity and Magnetic Anomaly of Profile 1

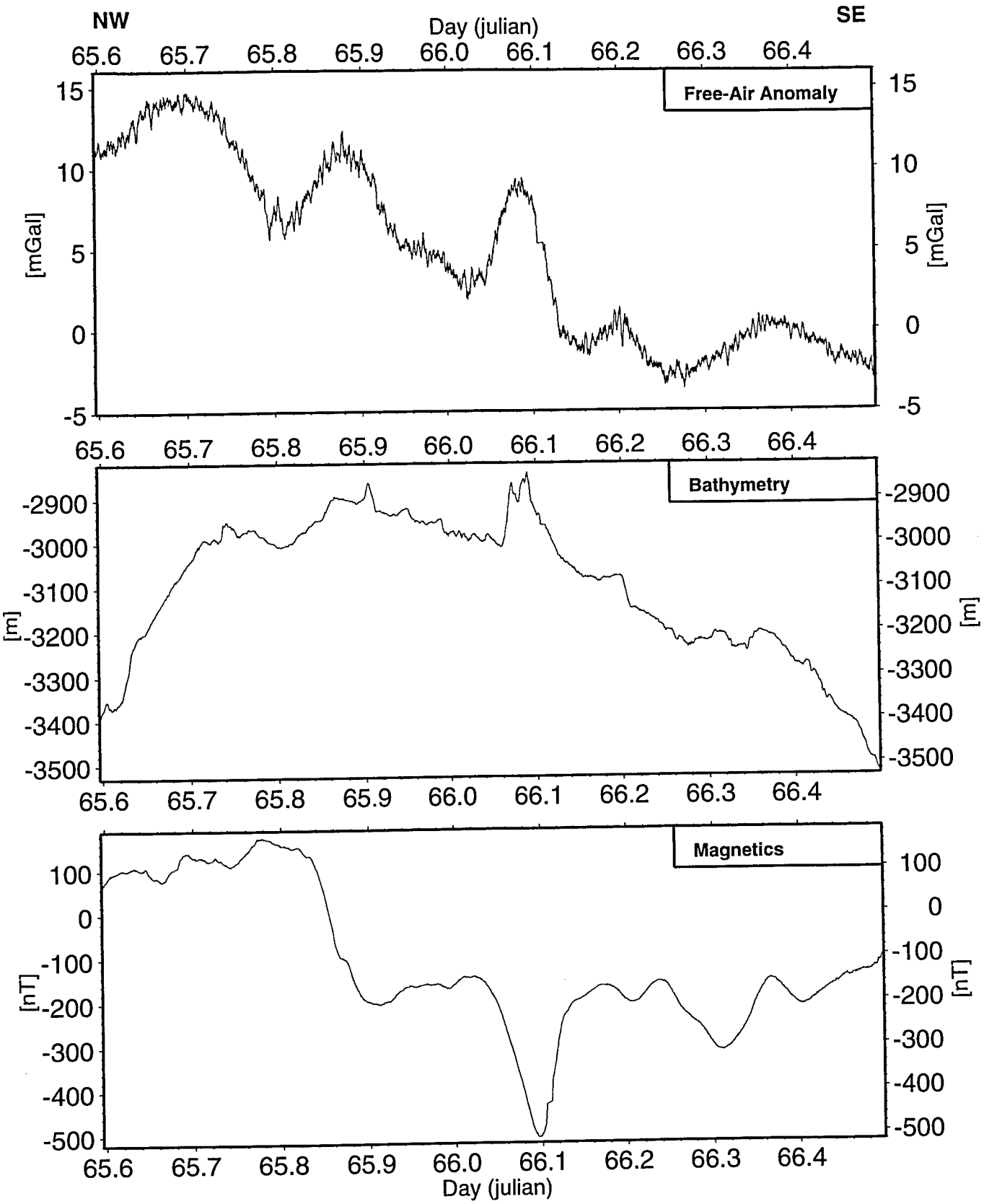

Figure 6.5.1

Gravity and Magnetic Anomaly of Profile 2

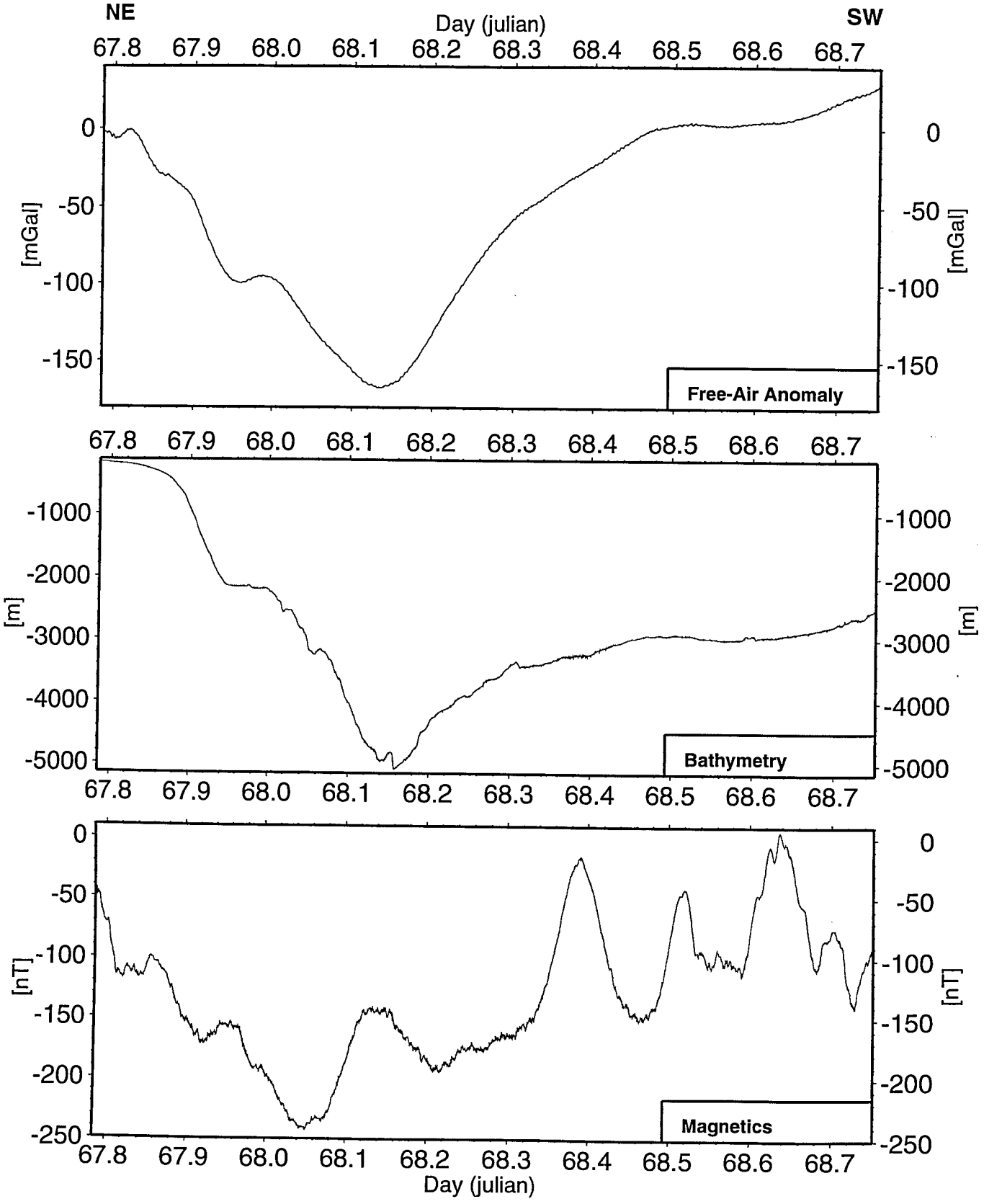

Figure 6.5.2

7. Imaging the structure of the Peruvian Forearc

7.1 Profile SO146 - 02 at 15° south

(H. Letz, A. Haris, E. Norabuena)

Profile SO146-02 is centered along the crest of the Nazca Ridge at the south-western end of the profile, extending towards the NW across the Peru Trench and onto the continental shelf. Station coordinates are listed within appendix II. A location map of the profile including bathymetry is given in Figure 6.2.2.1 and the seismic sections are displayed in figures 6.2.2.2 to 6.2.2.22.

Inferred from the reflection seismic data and very short refraction events with slow apparent velocities within the wide angle sections sediment coverage on the oceanic part is thin. A thickening of this sequence is modeled toward the trench, which is consistent with an increasing of the topography observed within the bathymetric map. The sediment thickness increases to about 500 m within the trench and continuous constant along the lower slope. The ridge crust, with a thickness of 17 km, is dipping NE at about 11.7° beneath the continental plate, where the confirmed depth on this cross-section reaches 27 km. With a lower slope angle $\alpha_l = 9.5°$ the taper of the slope is about 21° which confirms the observed lack of an accretionary prism as these value indicates strong basal friction. It appears that the Nazca ridge subducts completely beneath the continental margin, which is modeled with velocities between 4.8 – 6.0 km/s.

7.2 Profile SO146 – 03 at 13.5° south

(J. Petersen, E. Haase)

Profile SO146-03 was shot in the Lima, Peru area following the dip direction across the continental margin. The line started on the upper continental shelf and extended about 70 km seawards beyond the oceanic trench, ensuring full coverage of the subducting oceanic plate. A map showing the location of the line is given in Figure 7.2.1.

Between 18:30 on 11th March 2000 and 04:00 on 12th March 2000, a total of 10 OBHs and 4 OBSs were deployed using a spacing interval of 4.5 nm to 7 nm, except for the two outermost stations on each end of the line which were separated by 9 nm. A list containing the exact positions of the instruments is given in the Appendix II.

Shooting of the line with the array of three 32l Bolt Air Guns started at 05:25 on 12th March 2000 and ended at 09:10 on 13th March 2000 extending over a total distance of 204 km. Recovery of the OBH and OBS instruments was then completed in two stages. First, immediately after shooting with the Bolt Air Gun array, OBH station numbers 23 through 30 were intermittently retrieved during swathmapping with Hydrosweep and Parasound. Shooting was then performed again across the remaining station numbers 31 through 36 using the GI-Air Gun array in order to acquire higher resolution data of the potential gas hydrate bearing sediments on the upper continental slope. This was started at 22:00 on 13th March and lasted until 18:40 on 14th March 2000. Afterwards, all remaining instruments were recovered and work was completed by 04:25 on 15th March 2000.

The OBH data obtained with the Bolt Air Gun source were processed using methods described in section 4.4. The record sections of the processed data are shown in figures 7.2.2 to 7.2.15.

Modeling and interpretation

Preliminary modeling was performed for the data acquired with the Bolt Air Guns using MacRay software (Luetgert, 1992). Due to the limited time onboard, only the arrivals recorded by the hydrophones were picked for modeling (picks are shown in figure 7.2.16 a). All fourteen instruments recorded useful phases for modeling including: reflection and refraction phases from the sedimentary layers, clear arrivals from the basement and, except for OBH35 and OBH36, distinct reflection and refraction phases of an intracrustal interface, plus the Moho.

In addition, OBH24 and OBS25 yielded phases which were faster than Moho velocities, indicating a layered mantle structure which can be observed up to an offset of 140 km along the line, but have not yet been taken into account for the modeling process. Additionally, at offsets greater than 50 km, the record sections of OBS30 and OBH31 show clear reflections arriving about one second after the first arrivals which cannot be explained by the applied P-wave model, but will hopefully be resolved by consideration of the S-waves.

Data quality is excellent at all stations so it should be possible to develop a well constrained model of the subsurface geometries. The preliminary model is given in figure 7.2.16 b) and is shown with a vertical exaggeration of 2.36. The model suggests a total oceanic crust thickness of about 8 km seawards of the trench. The oceanic basement is overlain by a thin sedimentary layer with an average thickness of 500 m, and velocities ranging from 1.6 to 4.1 km/s. An intracrustal layer with velocities from 7.0 to 7.9 km/s has also been imaged at a depth of ~ 10 km, and produces the high velocity phases seen at stations south of the trench. At OBS 30 the Moho appears at a depth of 14 km in the southwest region of the profile and can be followed down to a depth of 25 km, to the offset of –50 km. The continental Moho cannot be resolved with the data, which leaves the continental structure below 20 km undefined.

Stations 25 through 31 reveal the accretionary prism to have a lateral extent of about 24 km, a vertical thickness of 3.5 km, with velocities ranging from 1.6 to 4.4 km/s. An approximate slope inclination angle of 5.6° indicates that the material has high basal friction (Kukowski, Pecher 1998). The underthrusting slab has velocities that range from 4.8 to 7.9 km/s. The initial velocity of 4.8 is clearly not basement, but can be attributed to sediments that are being compacted and dehydrated during subduction, and are not being accreted. This notion is reinforced by the low volume of sediment presently contained in the accretionary prism (von Huene et al. 1996).

Landwards of the accretionary complex, the continental shelf rises with a slope of about 2.8°. In the offset range from –110 km to –70 km, the sediment cover has an average thickness of about 2 km. At an offset of –70 km, there is a sedimentary basin which is shown to have a lateral extent of roughly 13 km and thickness of 3.2 km, which is also well constrained by the overlying stations (31 to 35). This structure is believed to be the southern elongation of Lima basin. Further to the northeast the sediment layer thins down to a thickness of about 500 m.

The continental basement begins with velocities of 5.3 km/s below the sediment strata and is modeled by two layers. The first layer has an average thickness of about 4 km and is underlain by the second layer, which is characterized by an increase in velocity from 5.9 km/s to 6.3 km/s.

In conclusion, the subducting plate can be followed to an offset of –50 km, and the angle of subduction obtained from the model is about 7.1°. The data analysis begun onboard the F.S. Sonne will continue and incorporate the 3-component OBS data to produce a more thorough model.

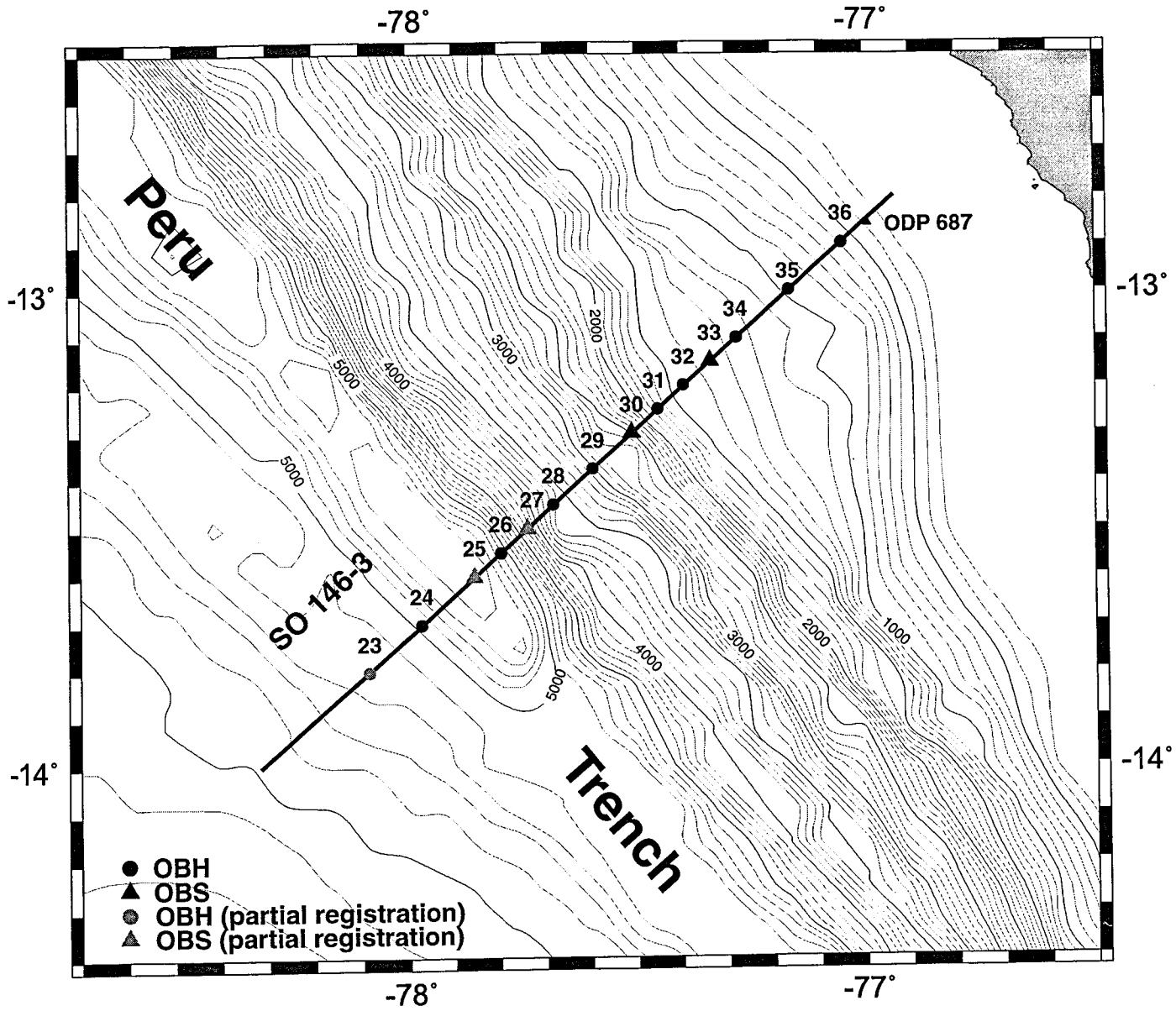

Figure 7.2.1: Location map of profile SO 146-03.

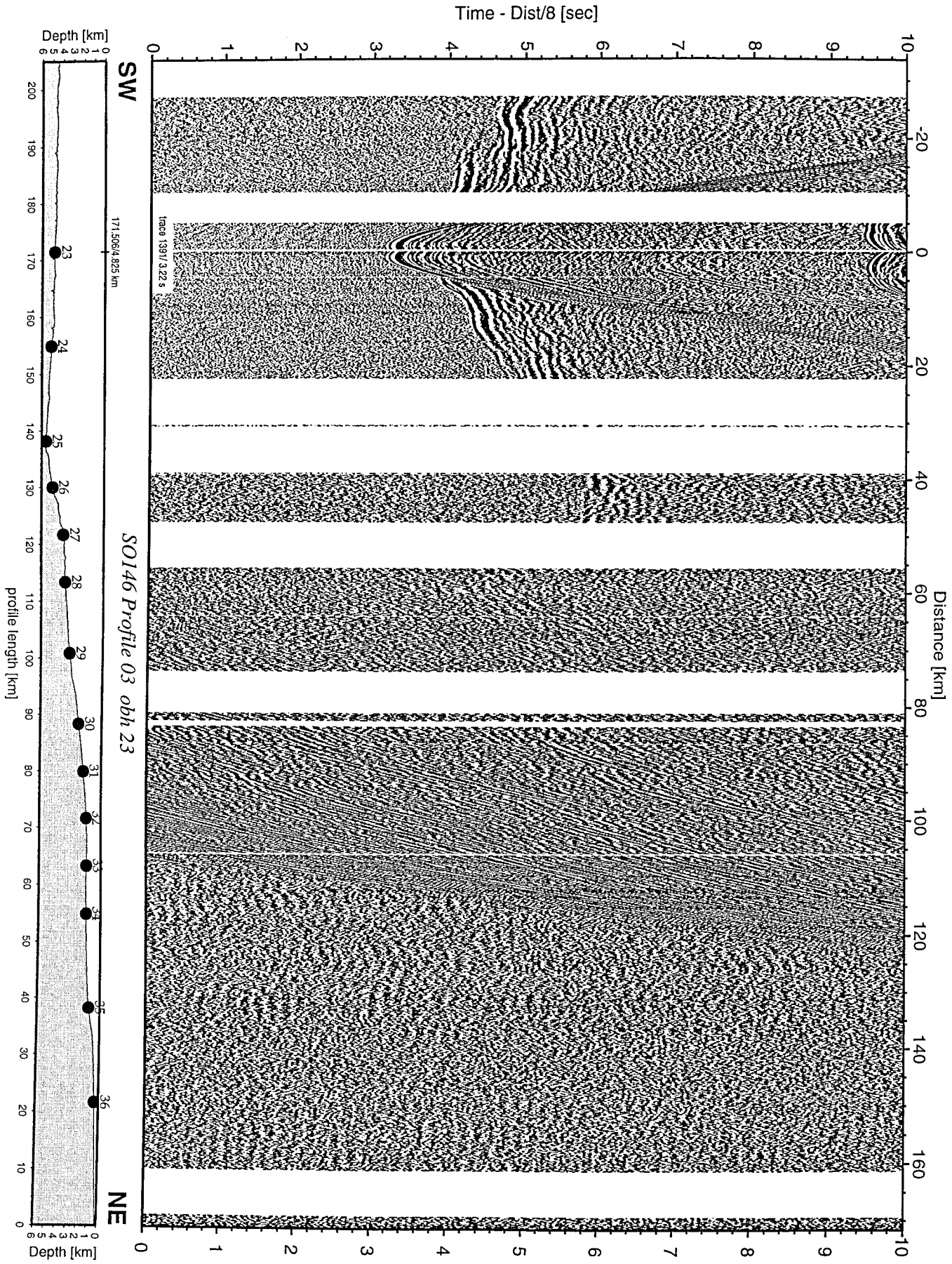

Figure 7.2.2: Record section from obh 23 , Profile 03.

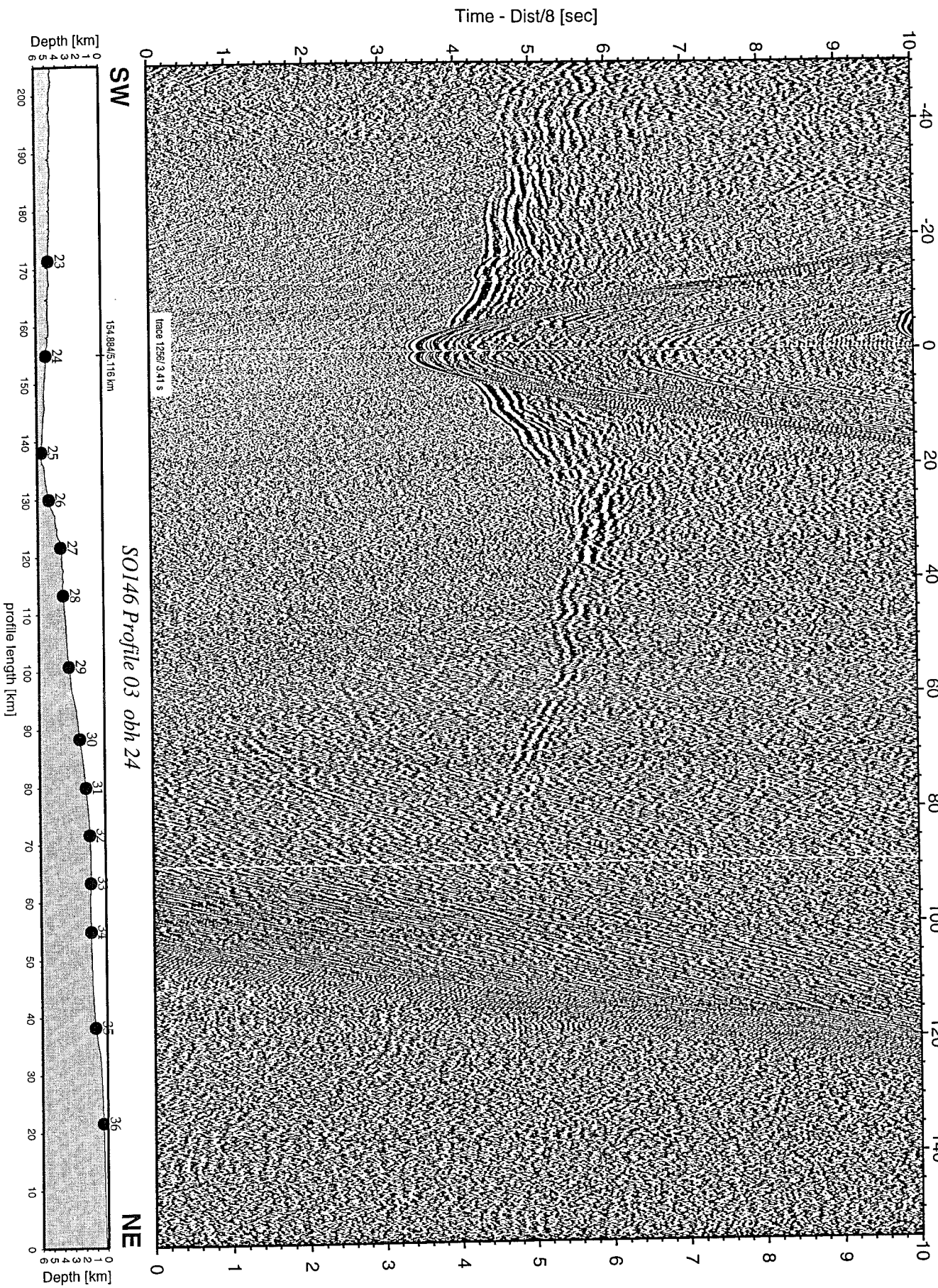

Figure 7.2.3: Record section from obh 24 , Profile 03.

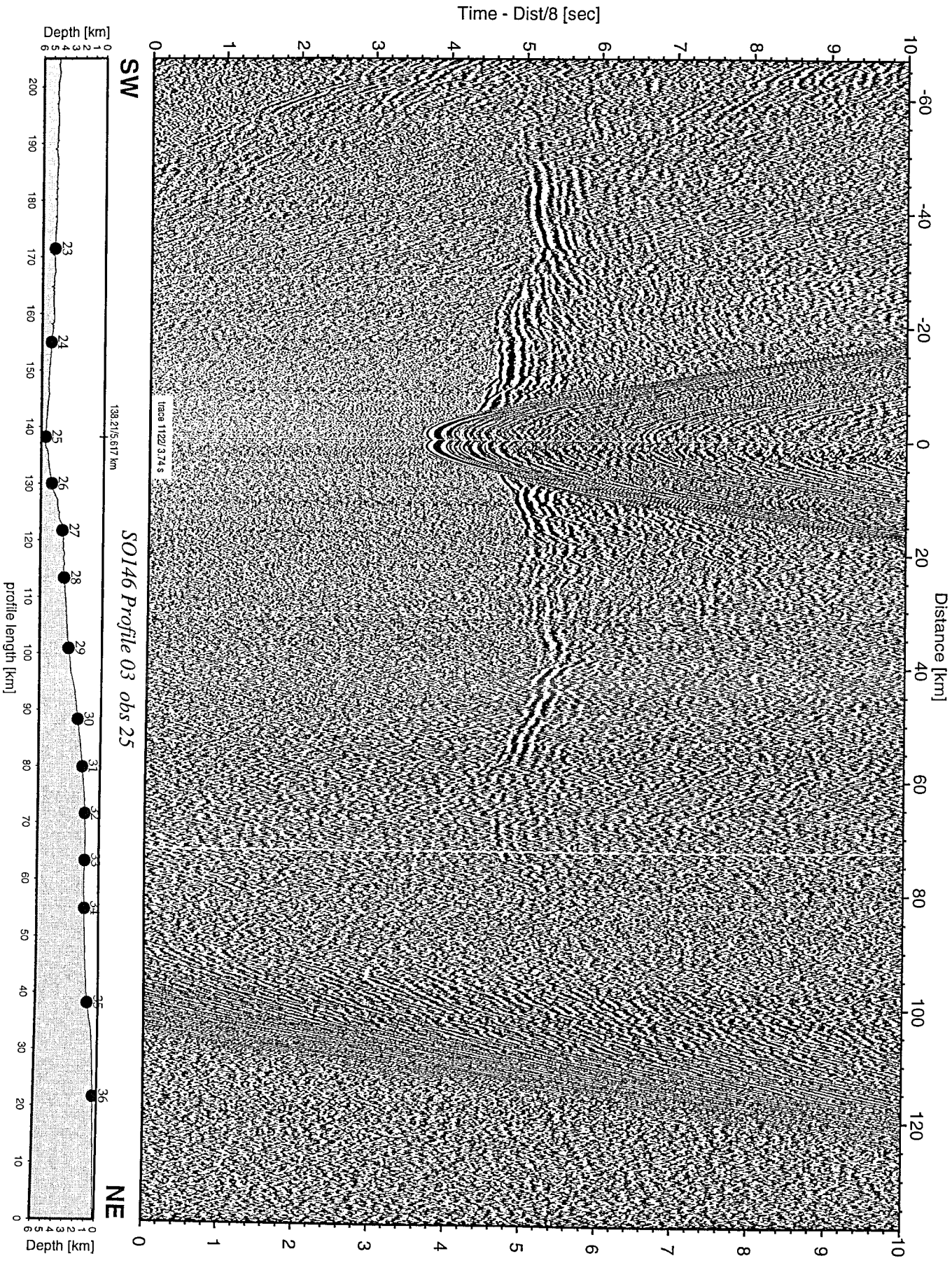

Figure 7.2.4: Record section from obs 25 hydrophone, Profile 03.

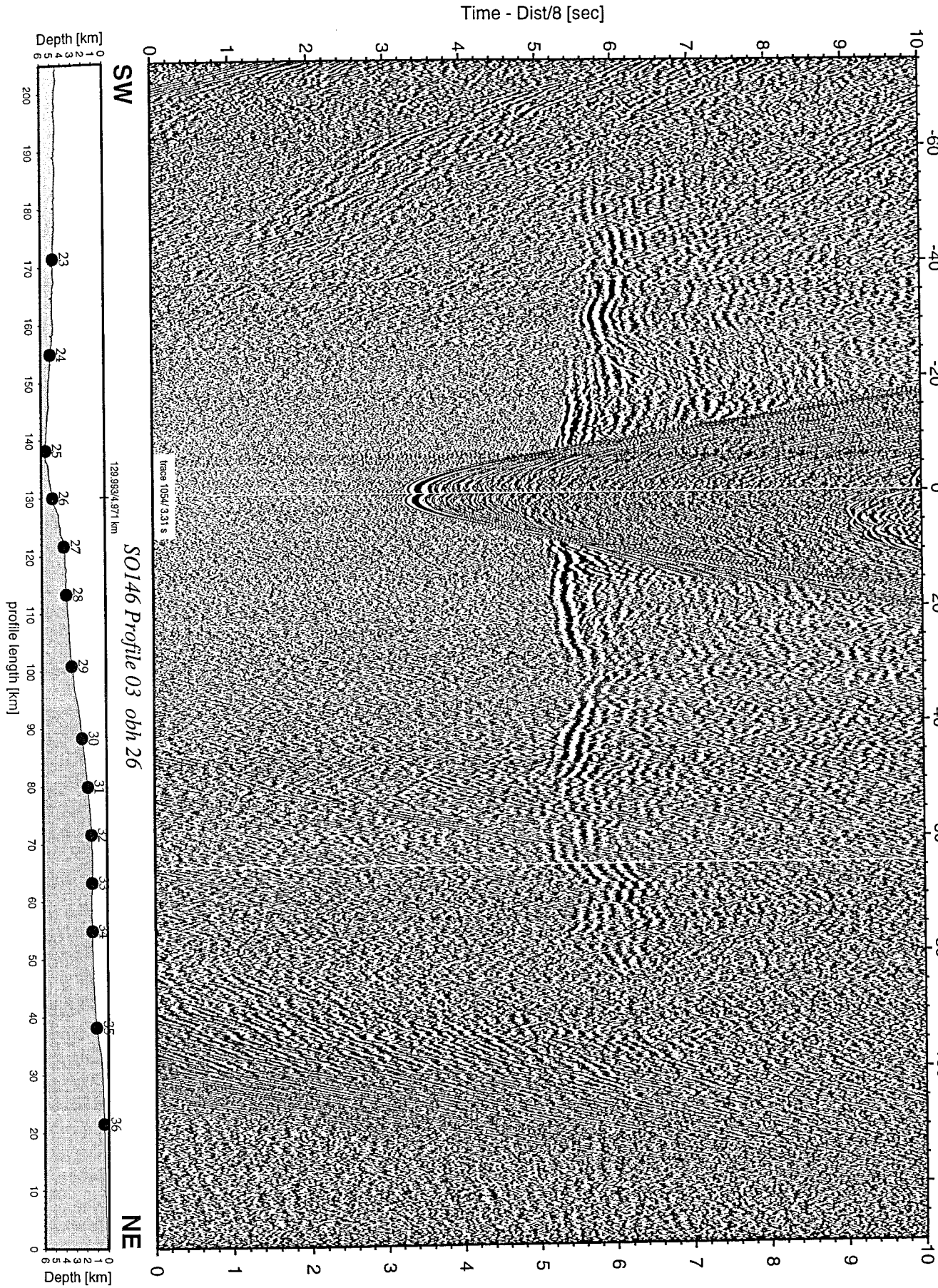

Figure 7.2.5: Record section from obh 26 , Profile 03.

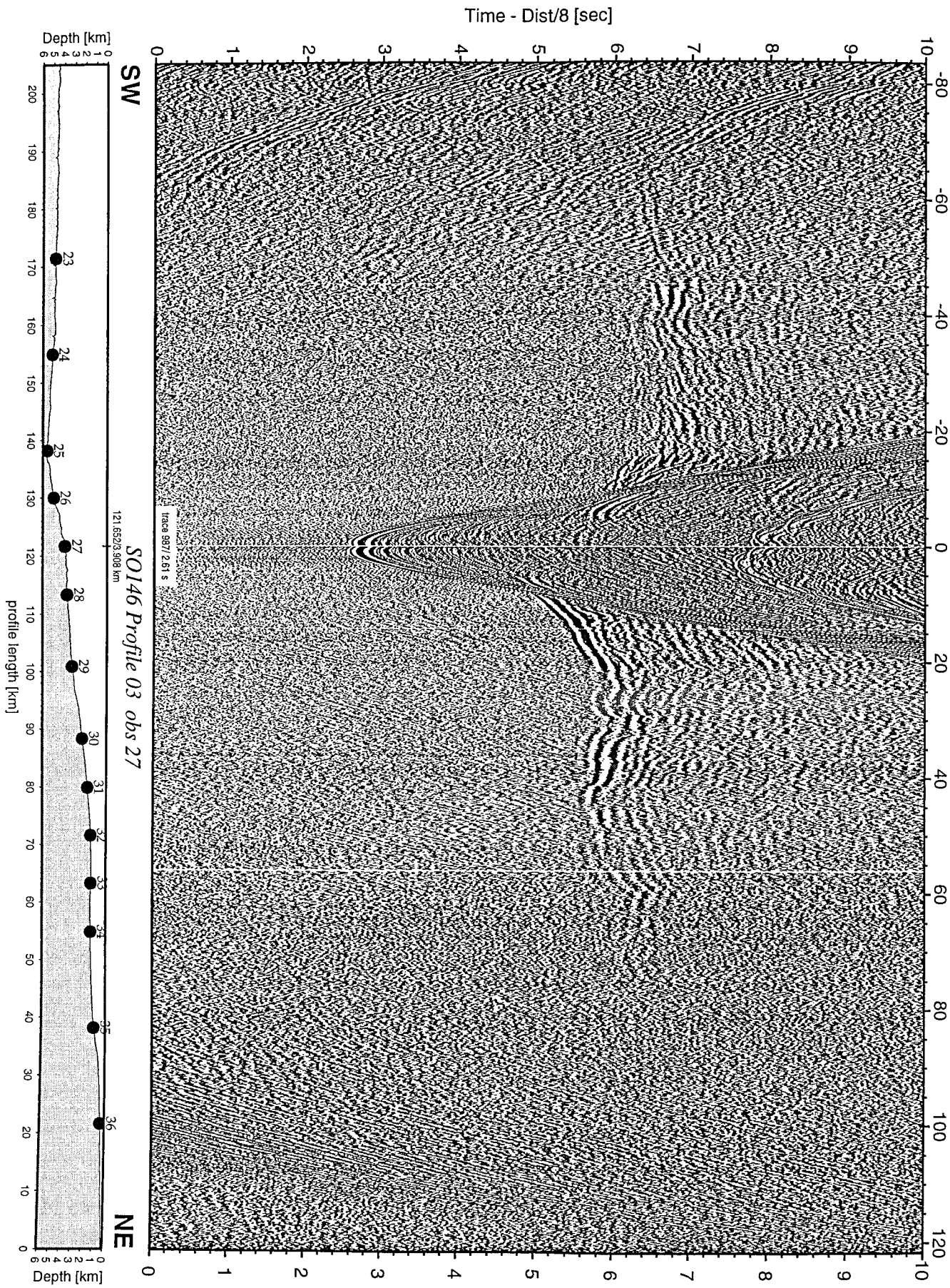

Figure 7.2.6: Record section from obs 27 hydrophone, Profile 03.

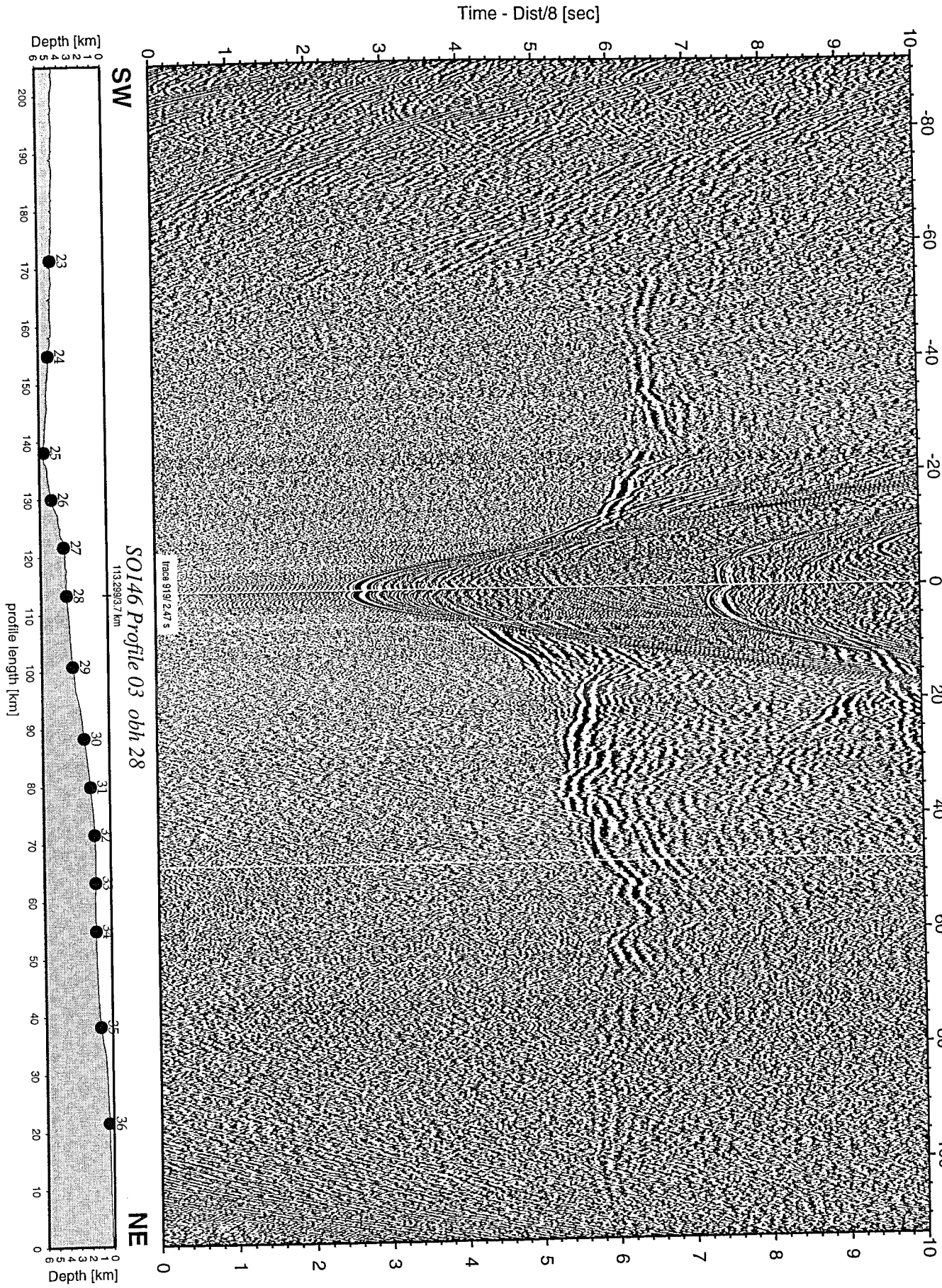

Figure 7.2.7: Record section from obh 28 , Profile 03.

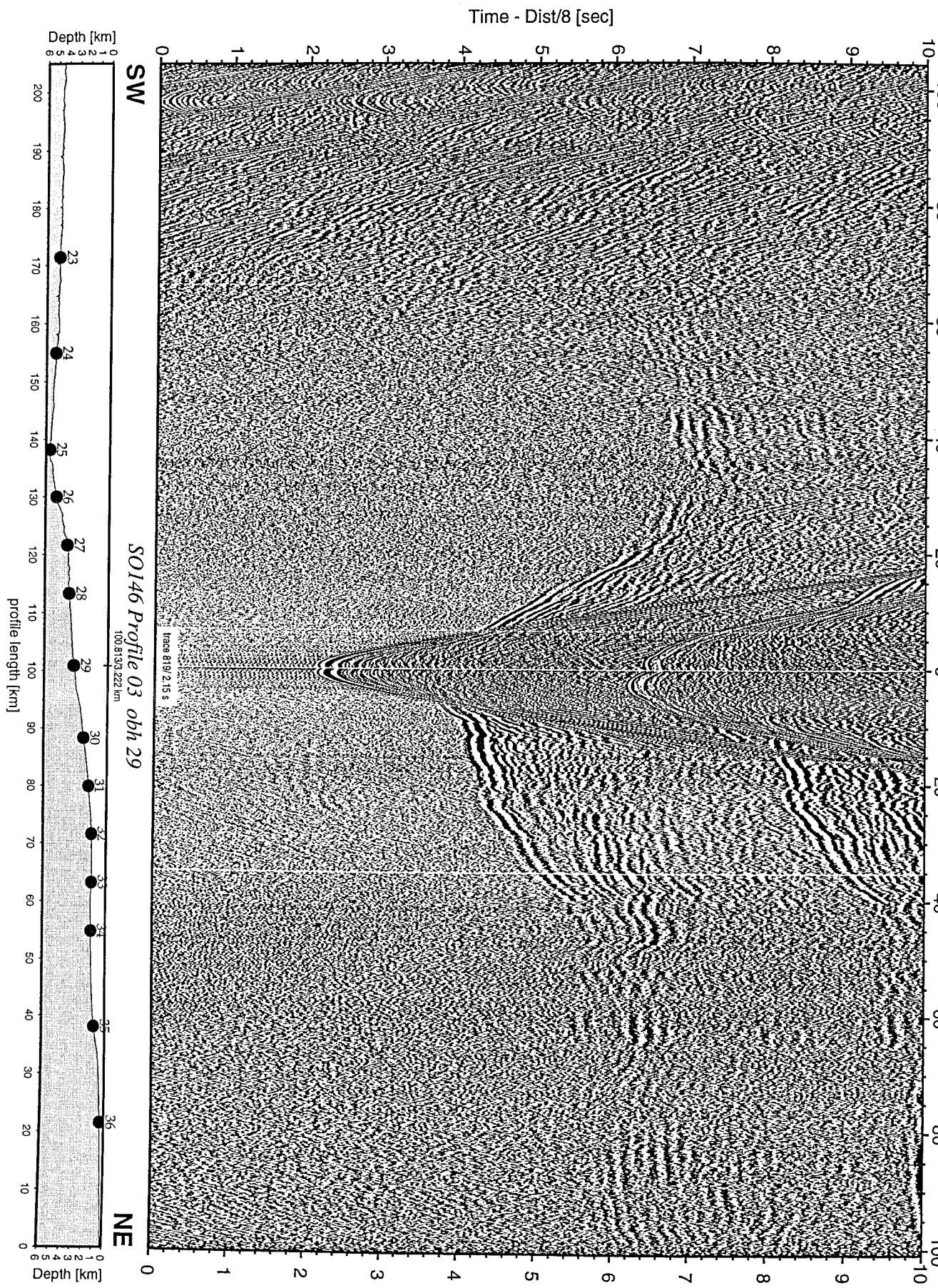

Figure 7.2.8: Record section from obh 29 , Profile 03.

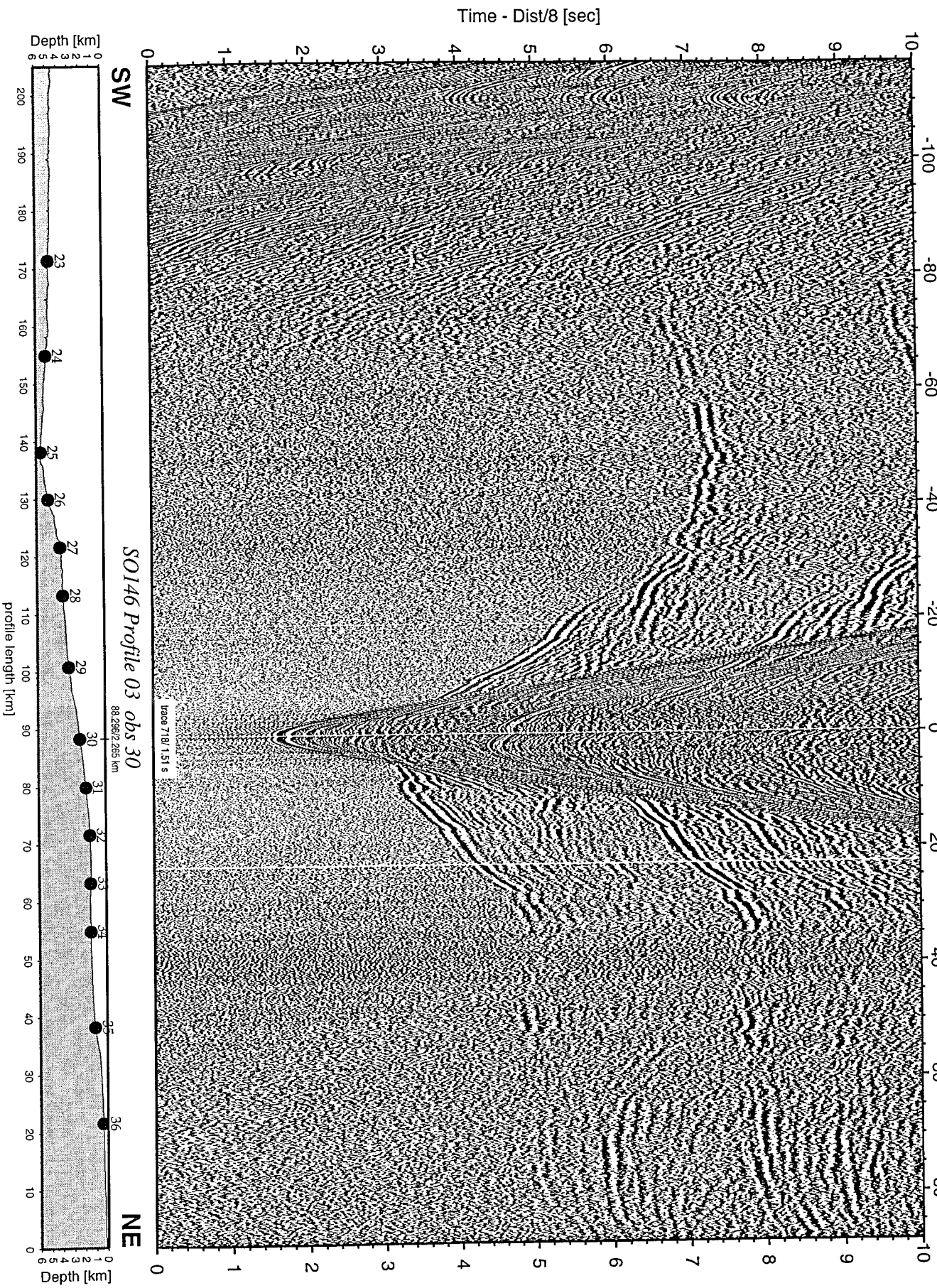

Figure 7.2.9: Record section from obs 30 hydrophone, Profile 03.

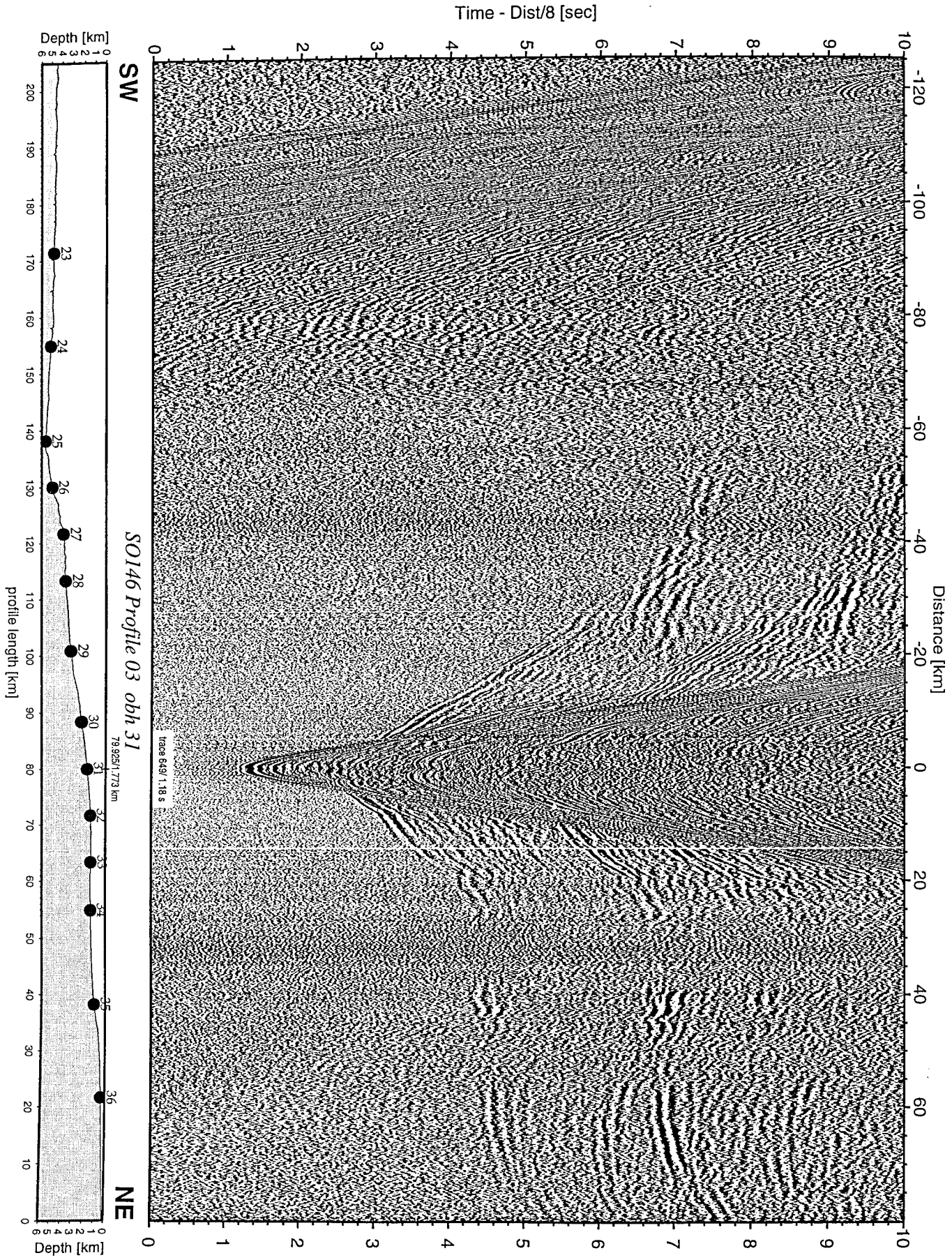

Figure 7.2.10: Record section from obh 31 , Profile 03.

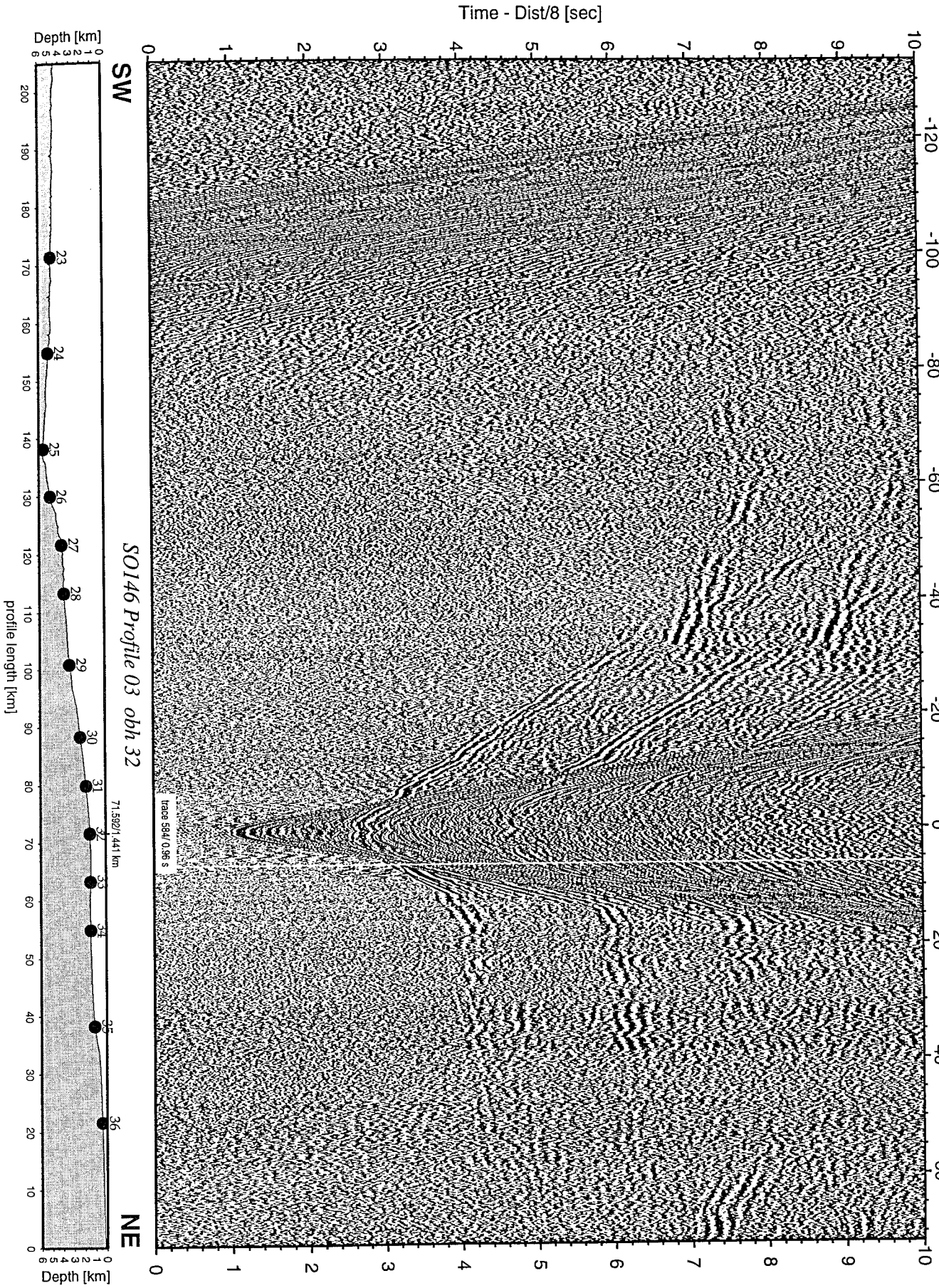

Figure 7.2.11: Record section from obh 32 , Profile 03.

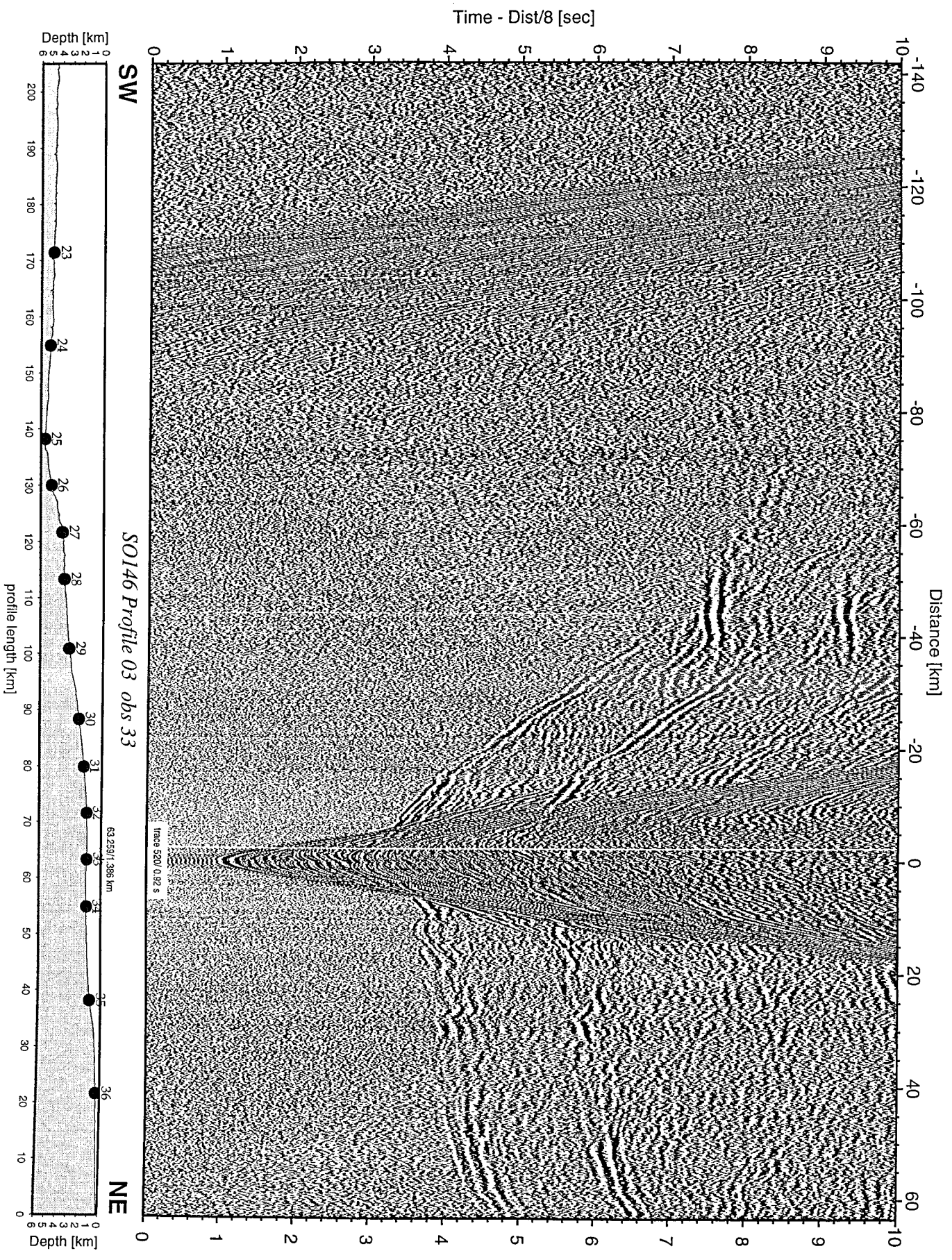

Figure 7.2.12: Record section from obs 33 hydrophone, Profile 03.

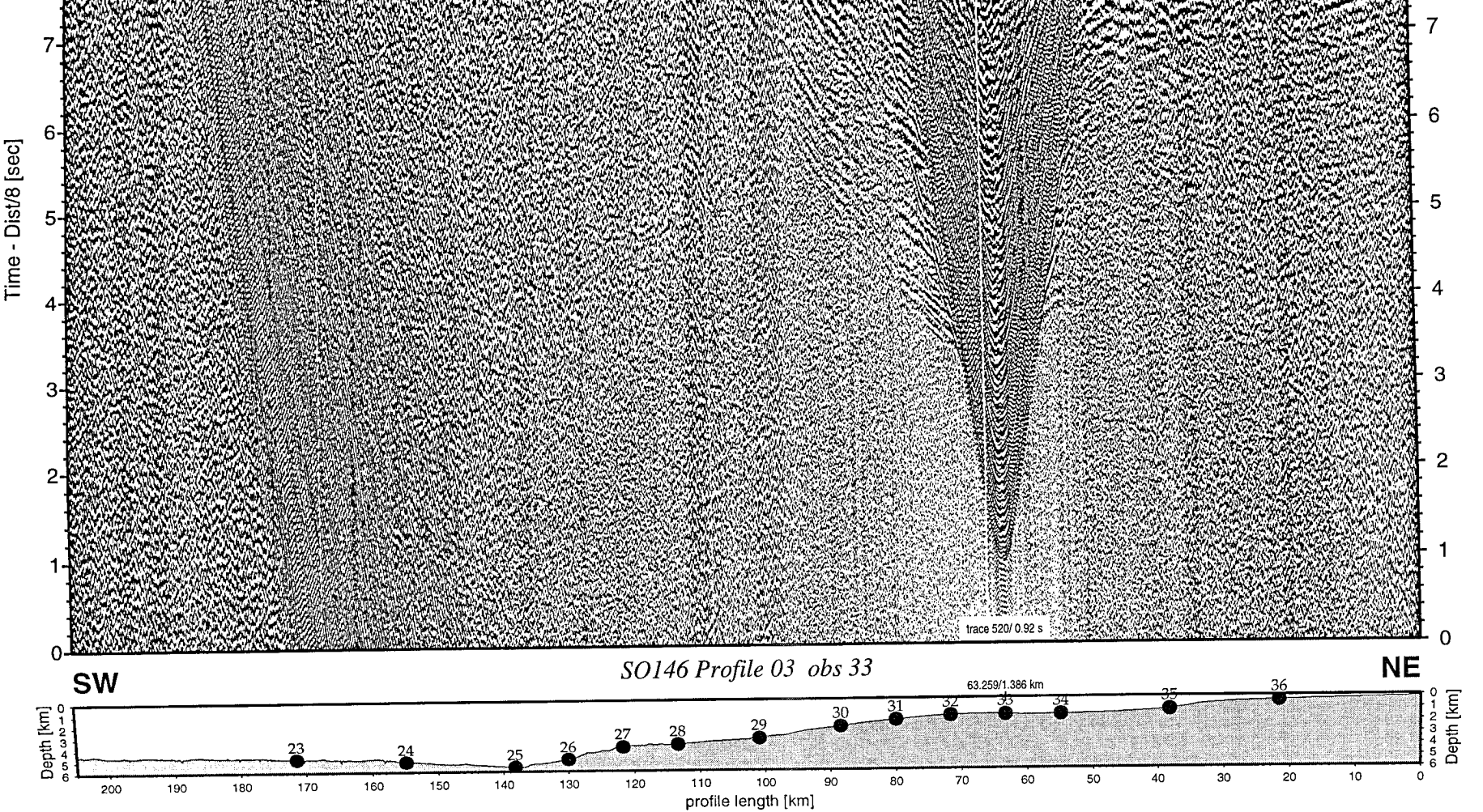

Figure 7.2.13: Record section from obs 33 horizontal co

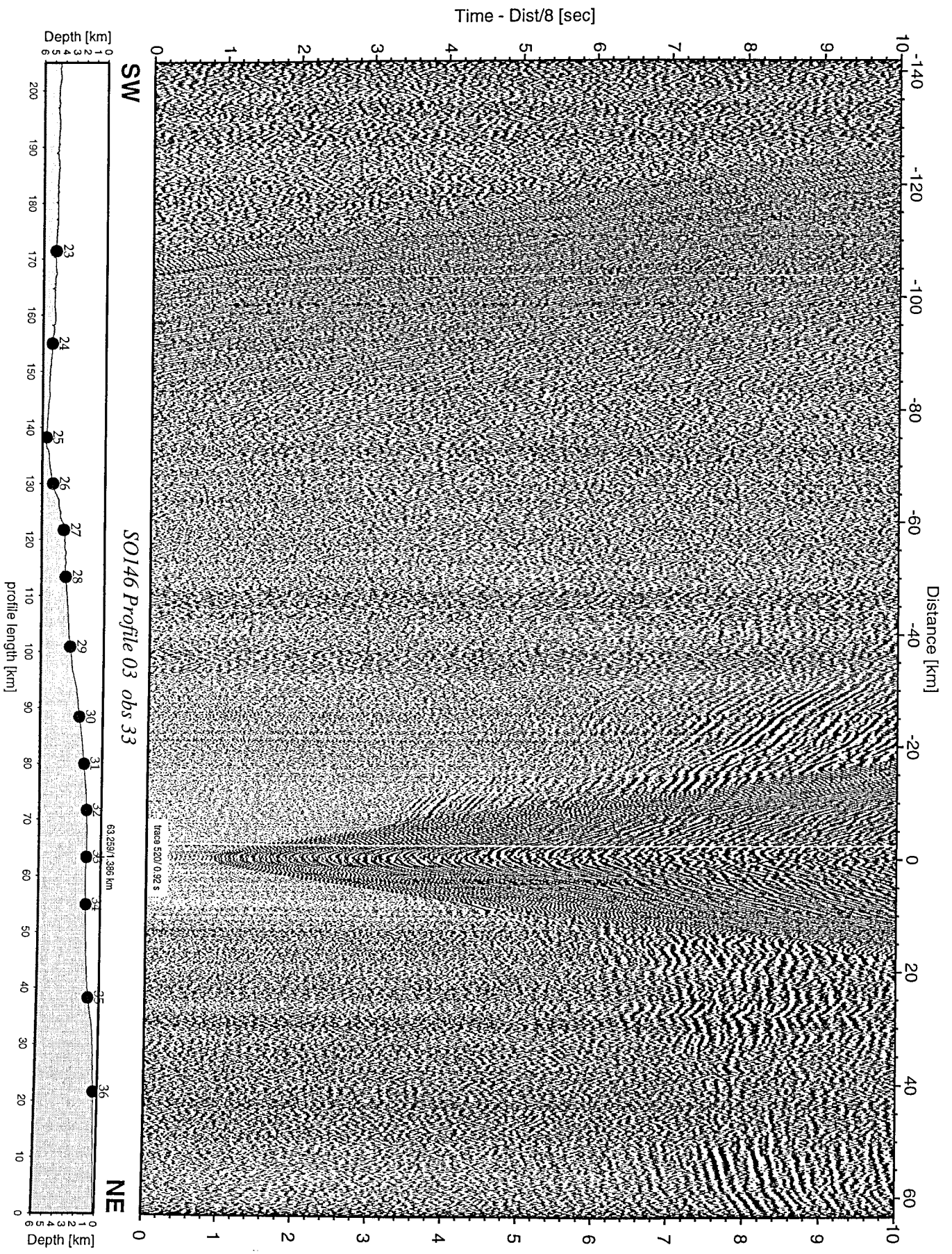

Figure 7.2.14: Record section from obs 33 horizontal component 2, Profile 03.

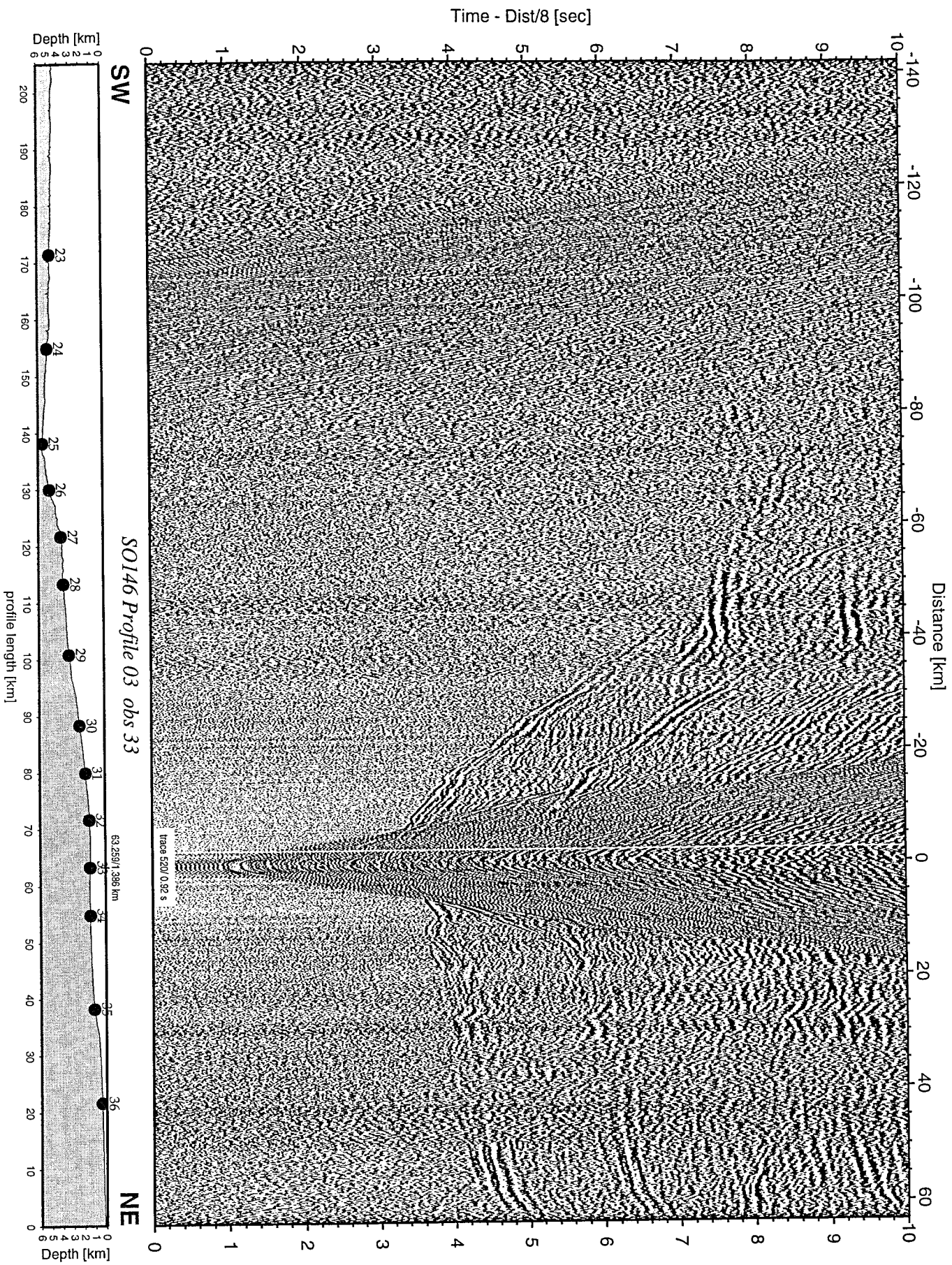

Figure 7.2.15: Record section from obs 33 vertical component, Profile 03.

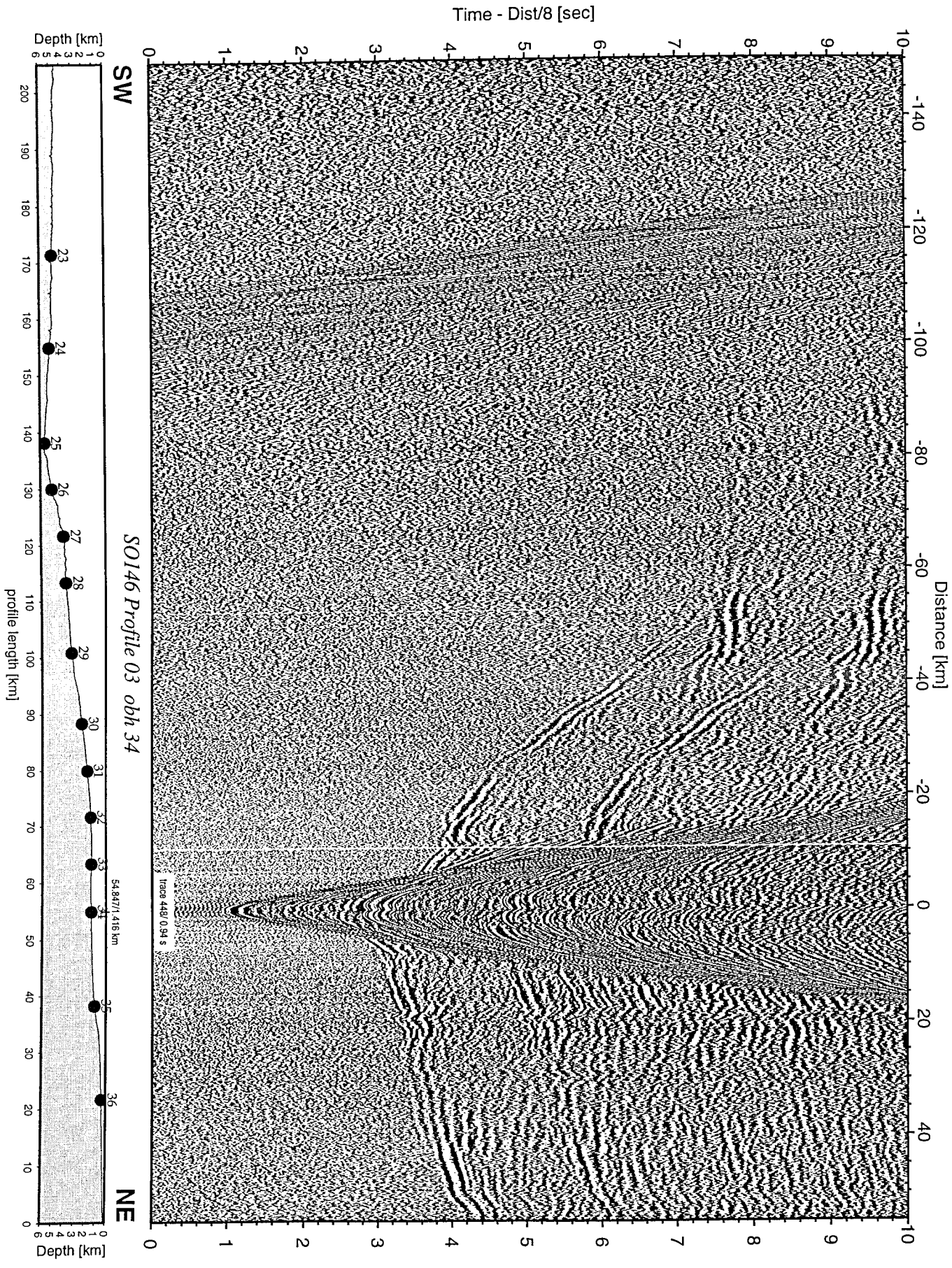

Figure 7.2.16: Record section from obh 34 , Profile 03.

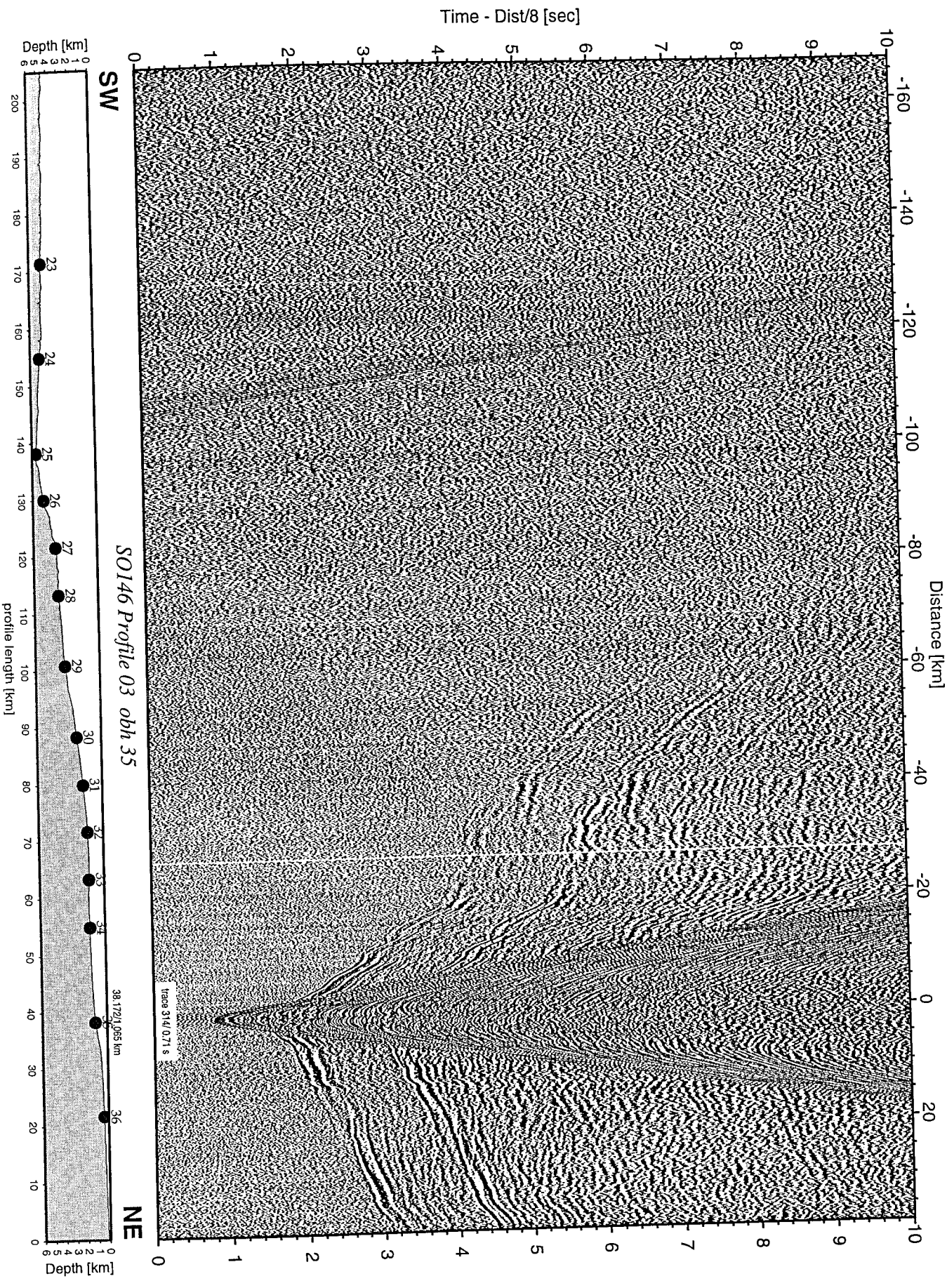

Figure 7.2.17: Record section from obh 35 , Profile 03.

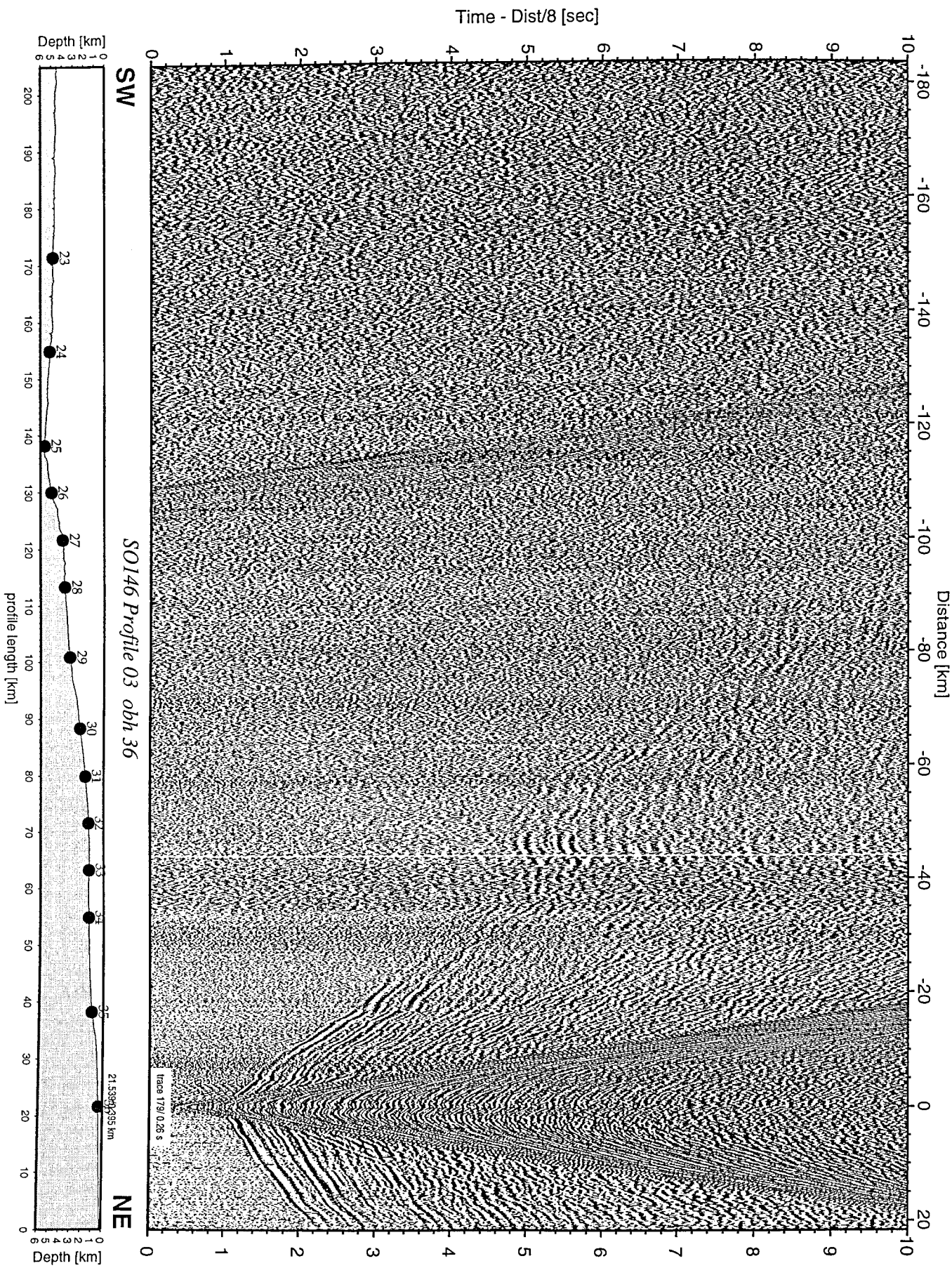

Figure 7.2.18: Record section from obh 36 , Profile 03.

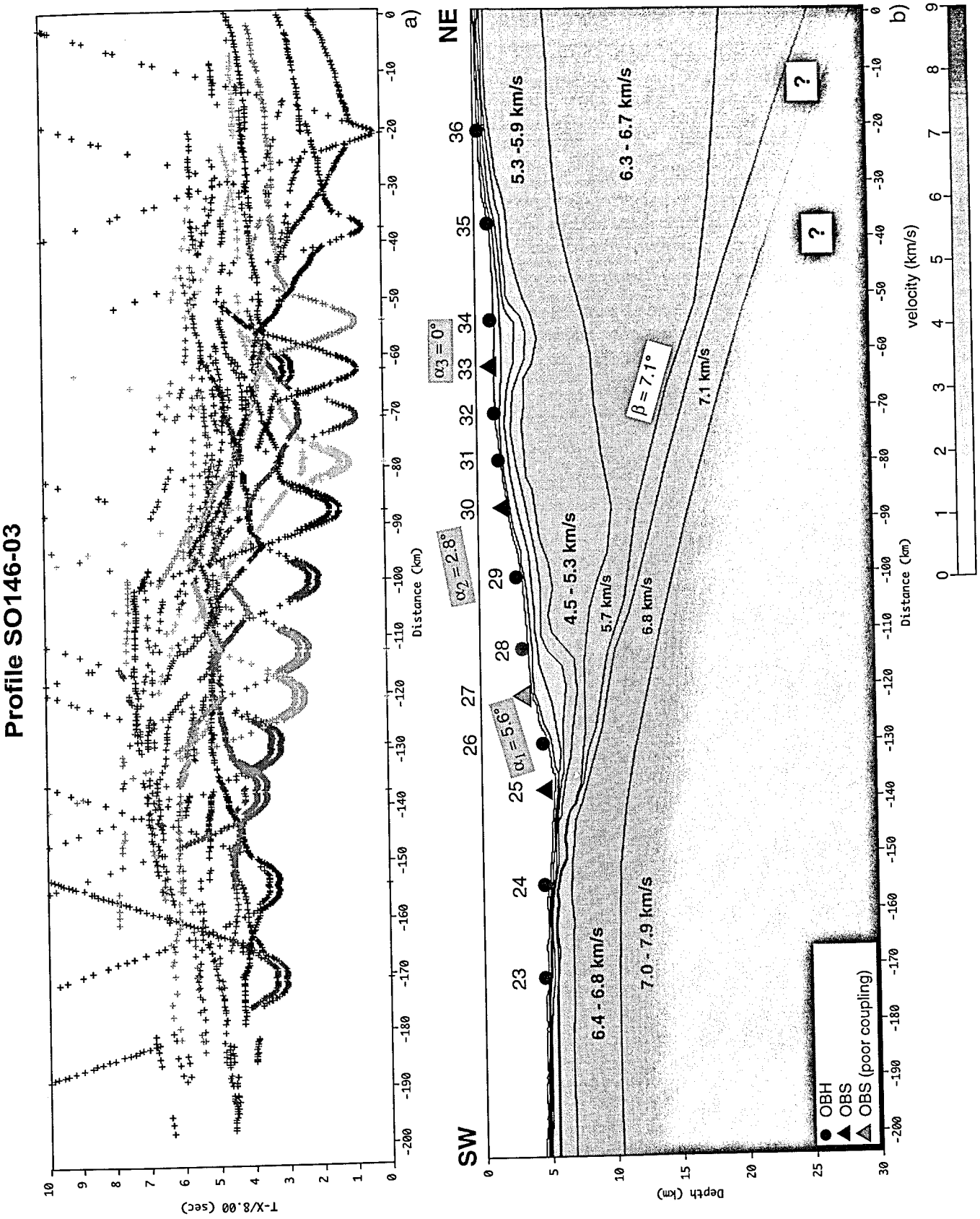

Figure 7.2.19: a) Picks extracted from the record sections of profile SO 146-03, b) crustal cross section for profile 03 derived from preliminary analysis of wide angle data.

7.3. Wide angle profiles at 12° S

Profile SO146 - 05

(A. Haris)

Profile SO146-05 is located over the Lima basin at about 11.5° S with northeastern direction of about 30°. The main purpose of this profile is to determine the velocity structure of tectonic plate and identify the structure of the Lima basin and velocity variations along strike.

This profile crosses the profile SO146-06 at the center of Lima basin. OBS 59 is the closest station to their intersection point. A detailed location map is shown in figure 7.3.1. All 14 instruments (4 OBS and 10 OBH with station numbers 51 to 64) were deployed with variable spacing starting at 16.00 PM, March 28, 2000. The total length of this profile is 220 km.

The 321 Bolt airguns were used to shoot this profile. Shooting was performed at constant vessel speed (5 kn.) and the airgun were fired every 60 seconds. Magnetic, gravity and hydroacoustic measurements were also recorded while shooting. Immediately after shooting all instruments were safely recovered, with the exception OBS 59. After three attempts, and using the TV grab, this OBS was recovered on April 5. Detailed information about instruments and shots are given in Appendices II.

Modeling and interpretation

All OBS and OBH data were processed using standard processing onboard. A detailed flow charts of data processing is given in chapter 4.9.1. Unfortunately, not all instruments worked and recorded data properly. The data from OBS 62 and OBH 63 could not be processed due to problems of the data logger. This leads to a data gap of 45 km between OBS 61 and OBH 64. Record sections along the profile are shown in figures 7.3.2 through 7.3.13. In general the data quality is good. The recorded data of the hydrophone show better quality than from the geophone channels, so that it is reliable to use these data for interpretation. A detectable phase in all record sections can be clearly seen to the maximum extension of 150 km. The first arrival in near offset indicate low velocities and remarkable phase changes appear at short offset distances (4 – 6 km), where velocities increase from 2.6 to 4 km/s.

OBH51 is located at seaward part near the SW end of the profile. The record shows prominent phases to a maximum offset of 60 km (see figure 7.3.2). The traveltime information from this station gave control to a maximum depth of 11 km. OBH52 gave better coverage than OBH51. A detectable phase can be seen to a maximum offset of 100 km. Subsurface features in the subduction zone are displayed very clearly. The travel time information from this station indicates the point where the oceanic plate began to bend down beneath the continental plate.

Four stations (OBH53, OBH54, OBS55 and OBH56) are located close to the oceanic trench. These stations have full coverage (220 km) along the profile (see figure 7.3.4 –7.3.8). The data were helpful in determining the structure and velocity variation along strike and also to determine the dip angle of the oceanic plate subducting beneath the continental plate. In addition, the extension of dip direction could be modeled using the information from station 57 – 64.

One-dimensional velocity-depth model of OBH59 were constructed and compared to a one-dimensional velocity-depth model of OBS69 from profile SO146-06. Stations OBS59 and OBS69 are the closest to the intersection point of the two profiles. The comparison between one-dimensional velocity-depth models indicate a good agreement for the depth range covered by raypathes on both sections (4 and 10 km) and are characterized by velocities between 4 to 6 km/s.

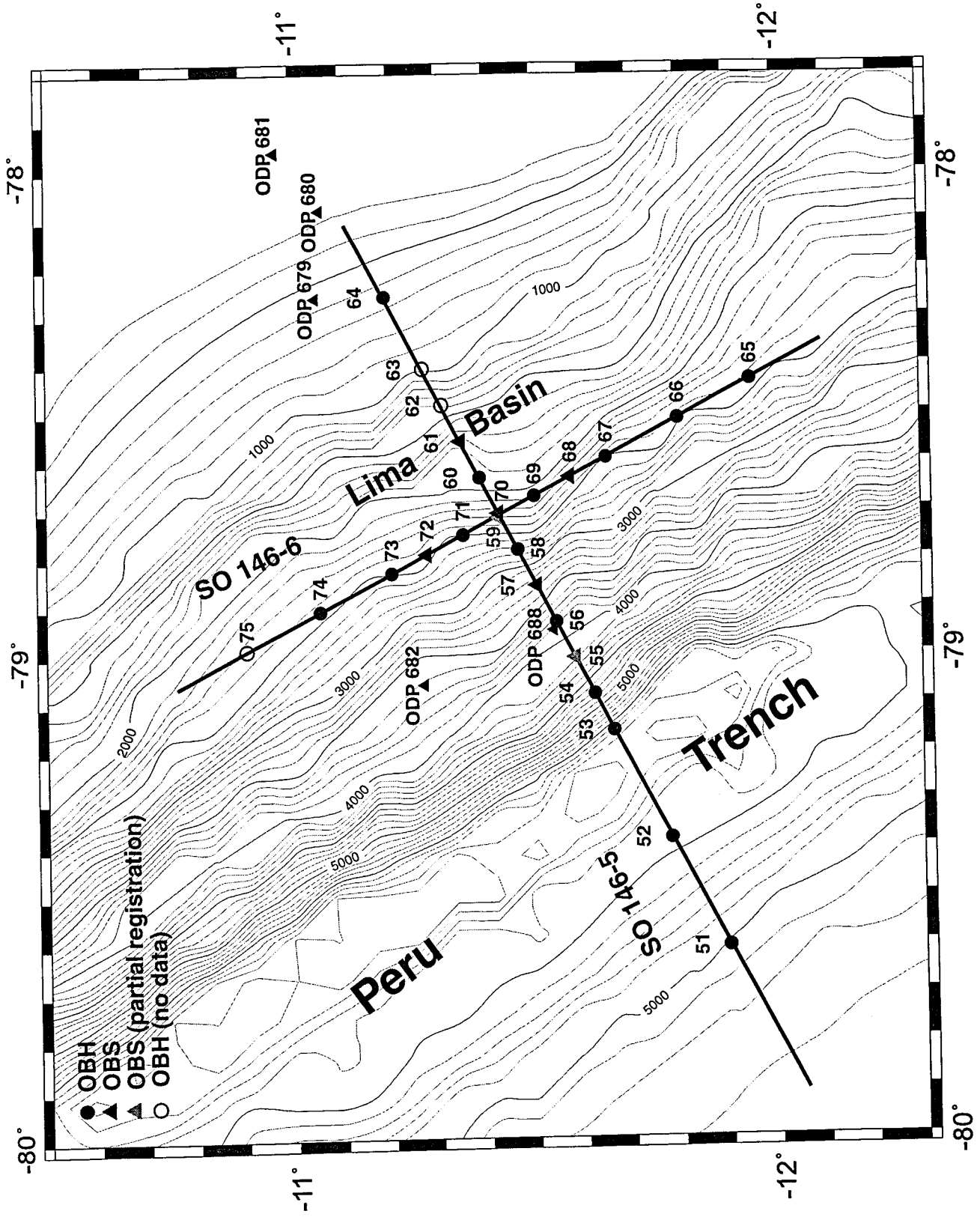

Figure 7.3.1: Location map of profiles SO 146-05 and SO 146-06.

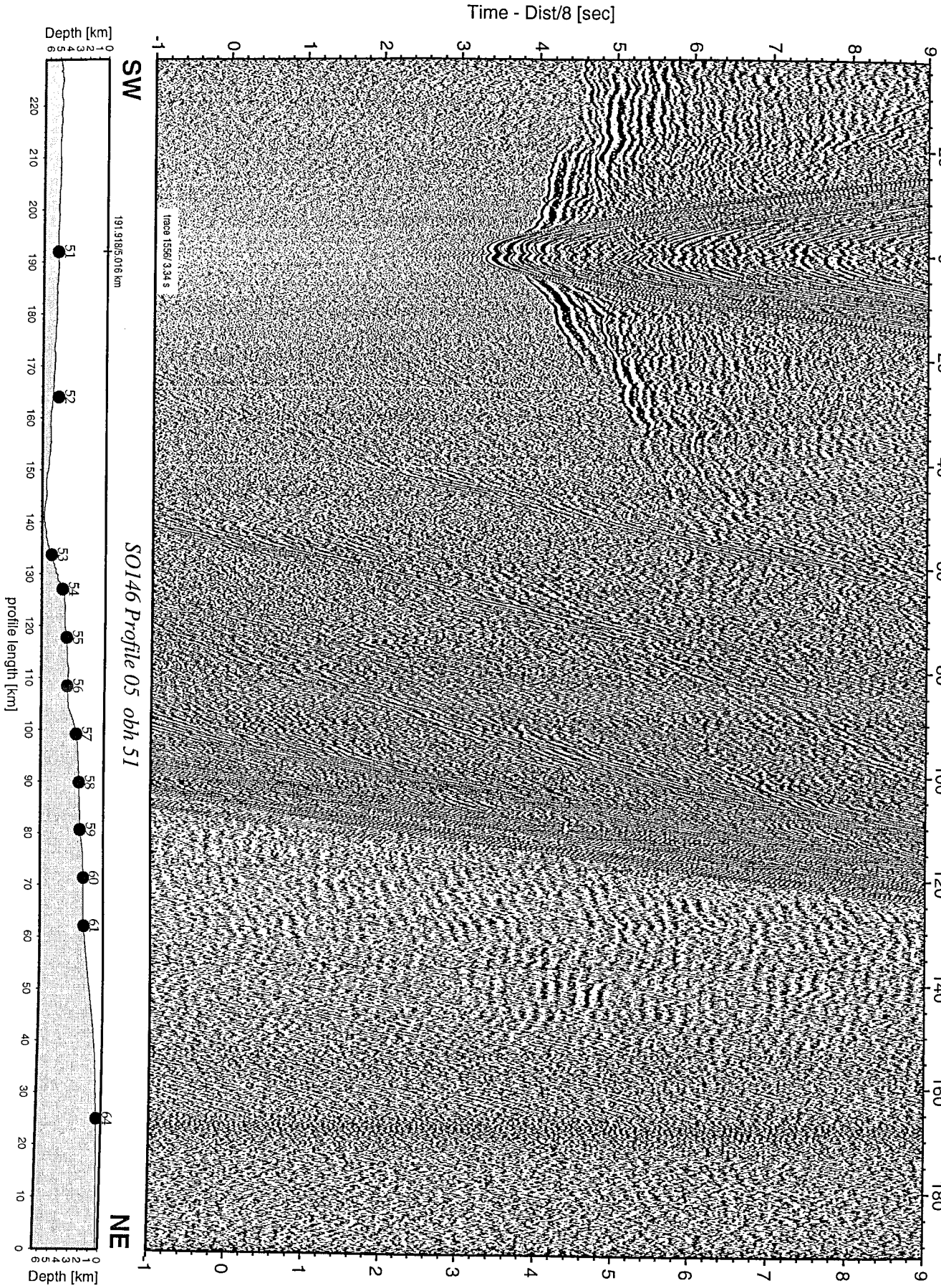

Figure 7.3.2: Record section from obh 51 , Profile 05.

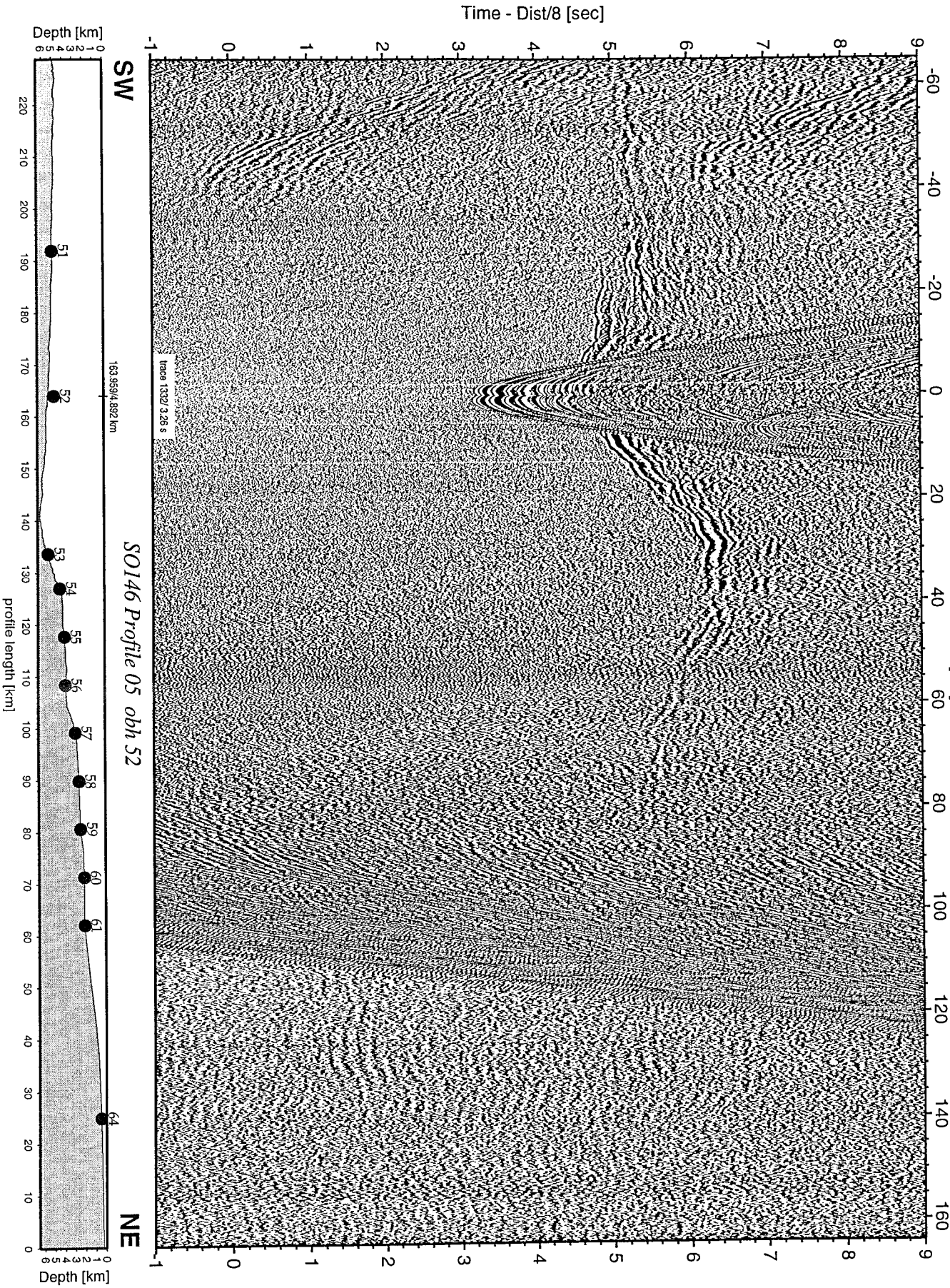

Figure 7.3.3: Record section from obh 52 , Profile 05.

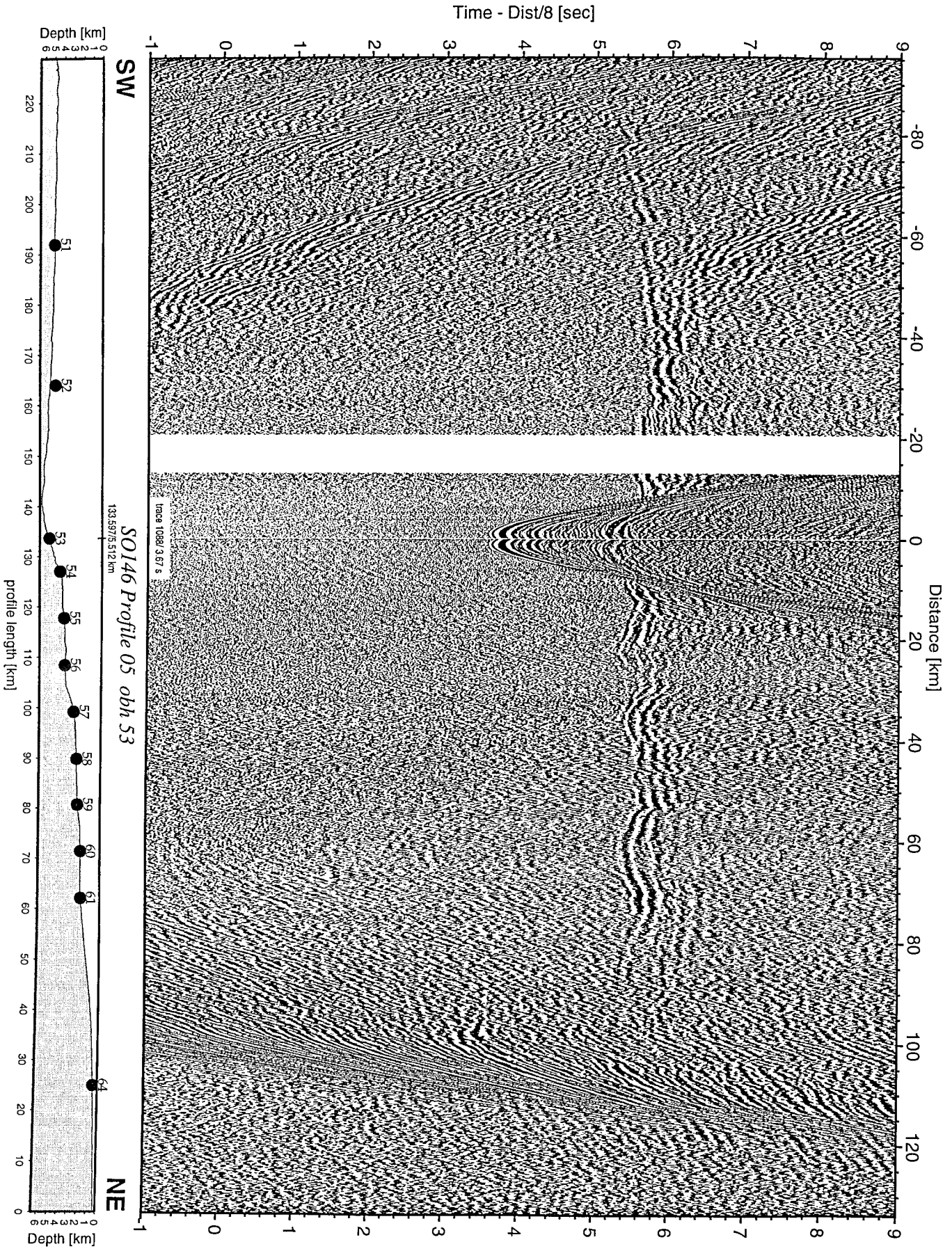

Figure 7.3.4: Record section from obh 53 , Profile 05.

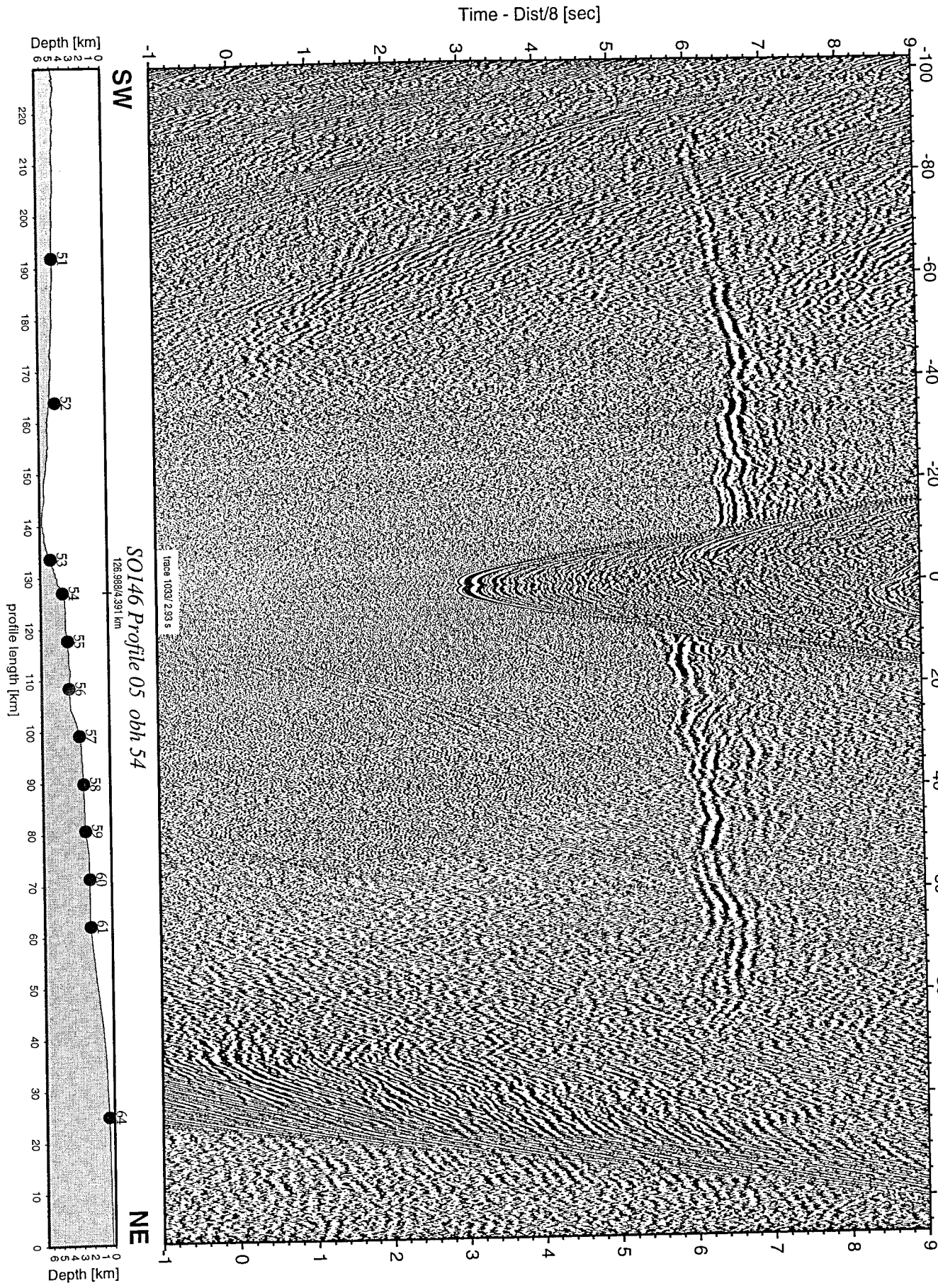

Figure 7.3.5: Record section from obh 54 , Profile 05.

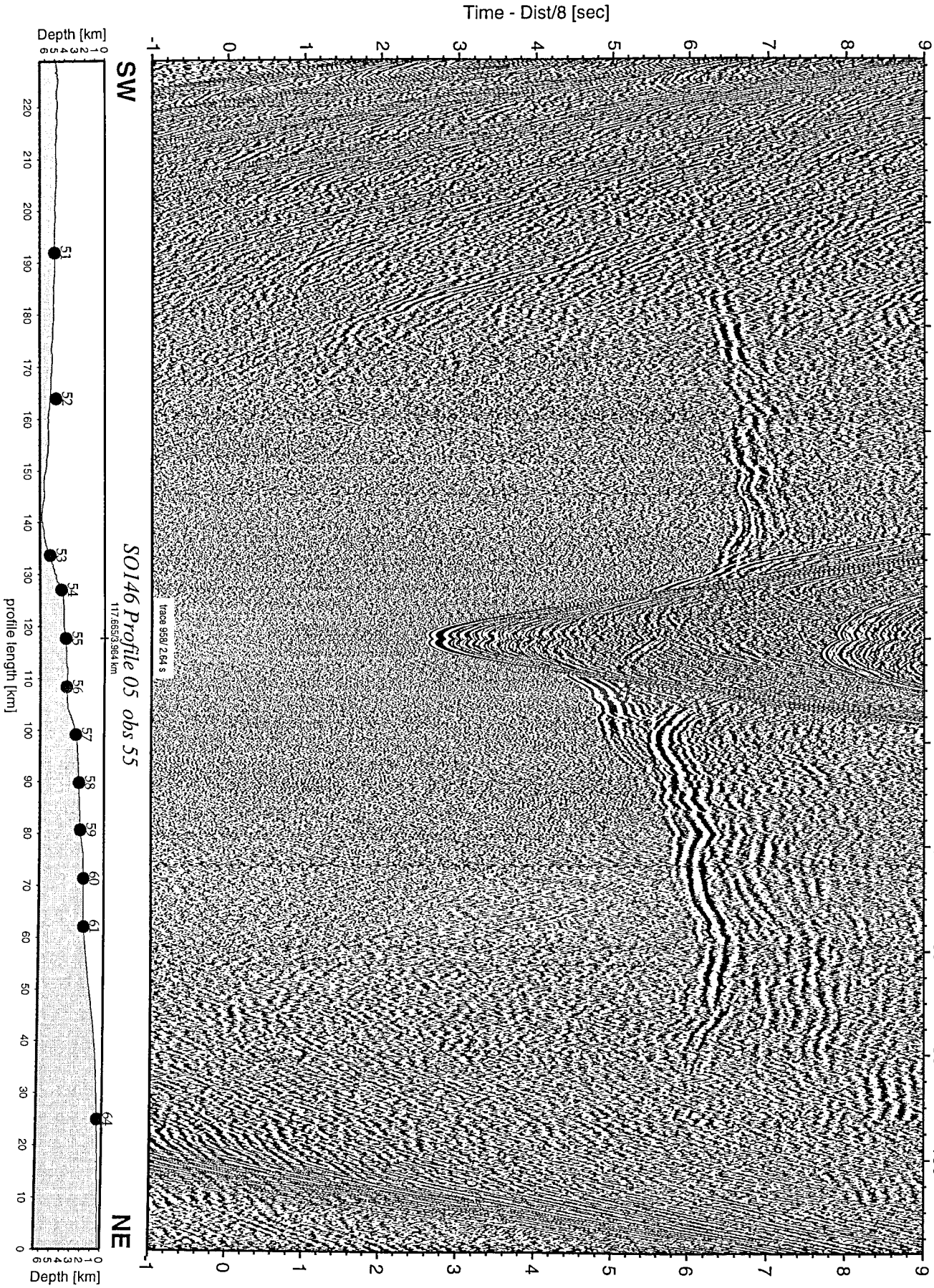

Figure 7.3.6: Record section from obs 55 hydrophone, Profile 05.

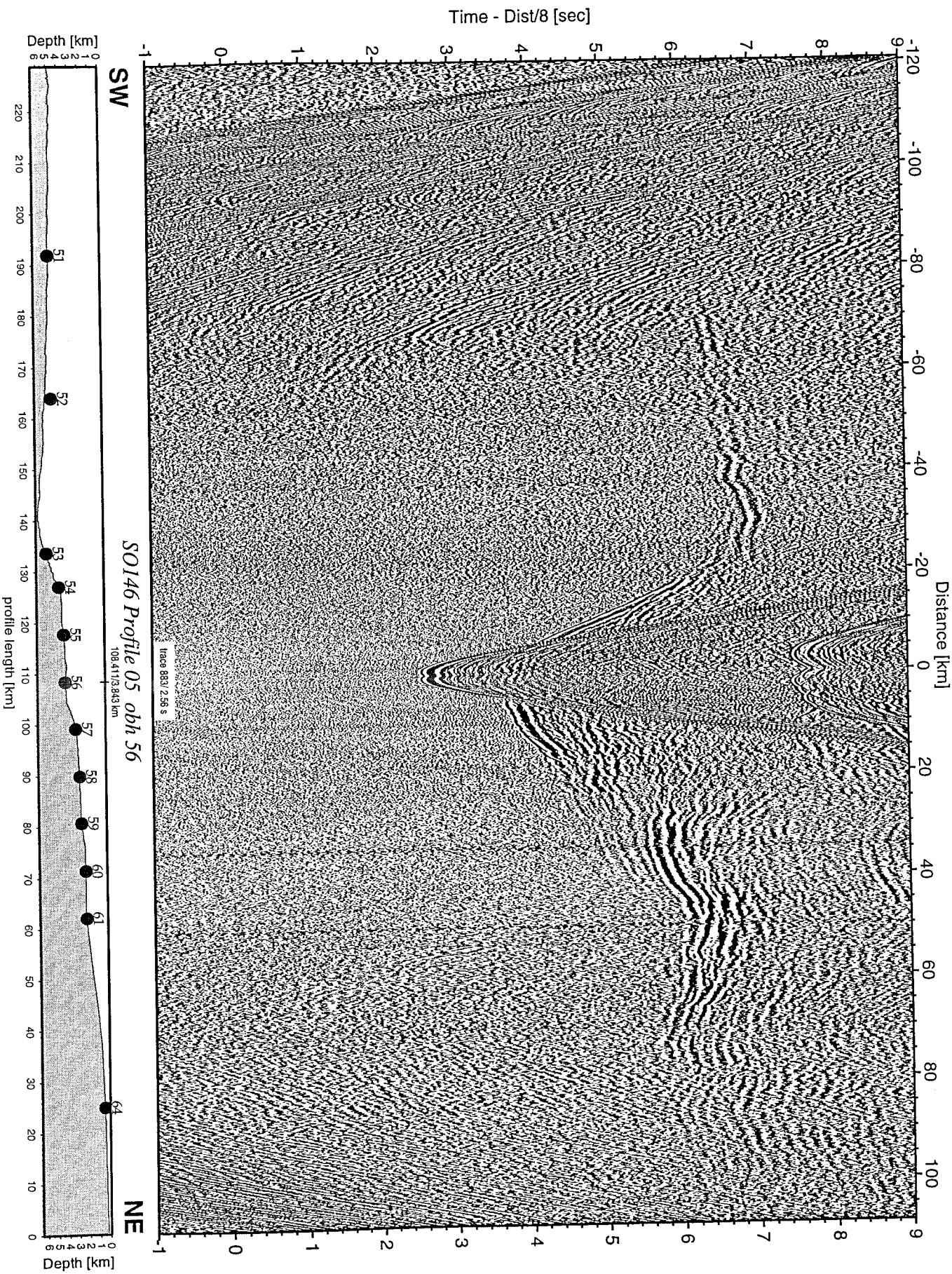

Figure 7.3.7: Record section from obh 56 , Profile 05.

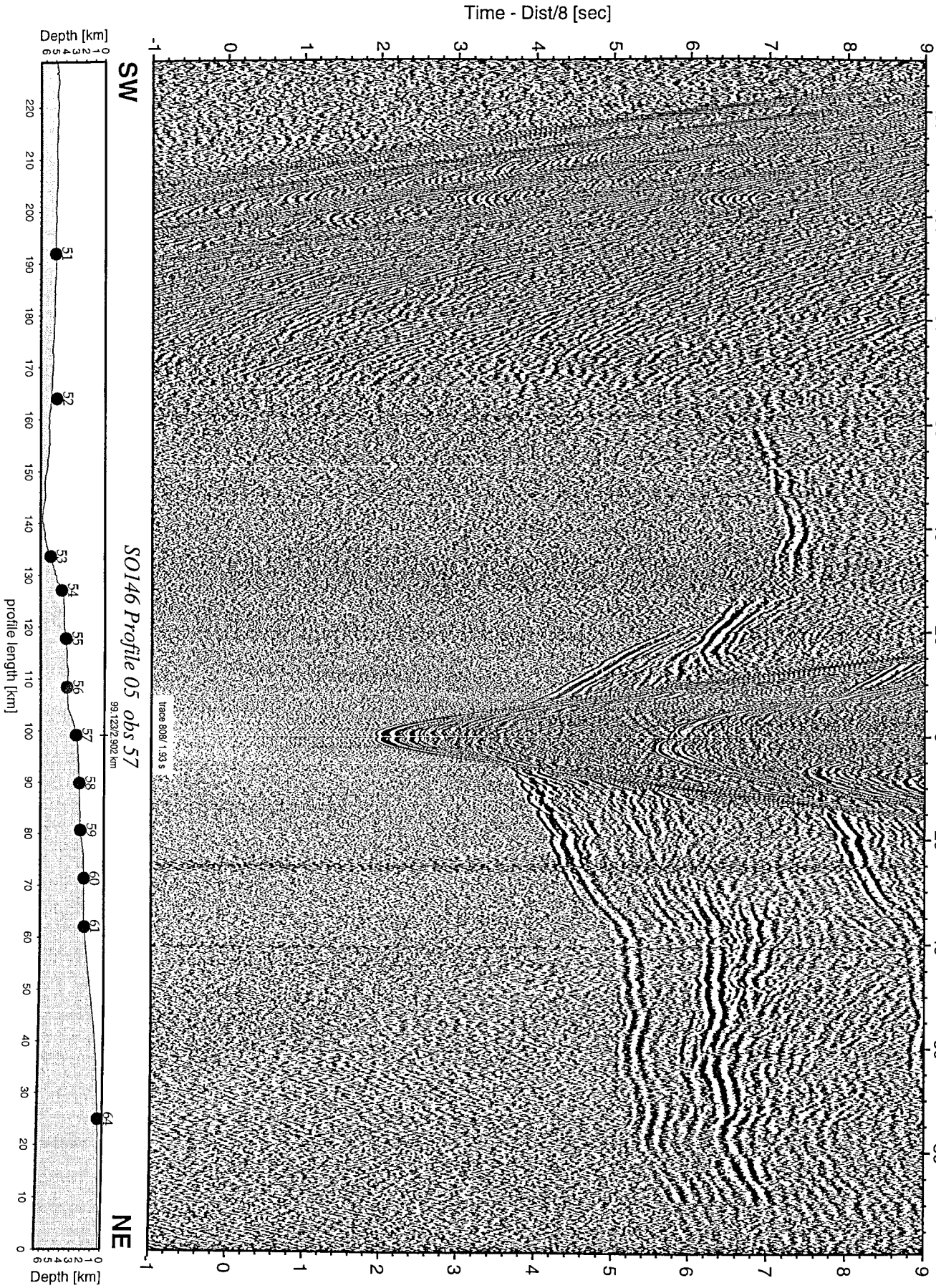

Figure 7.3.8: Record section from obs 57 hydrophone, Profile 05.

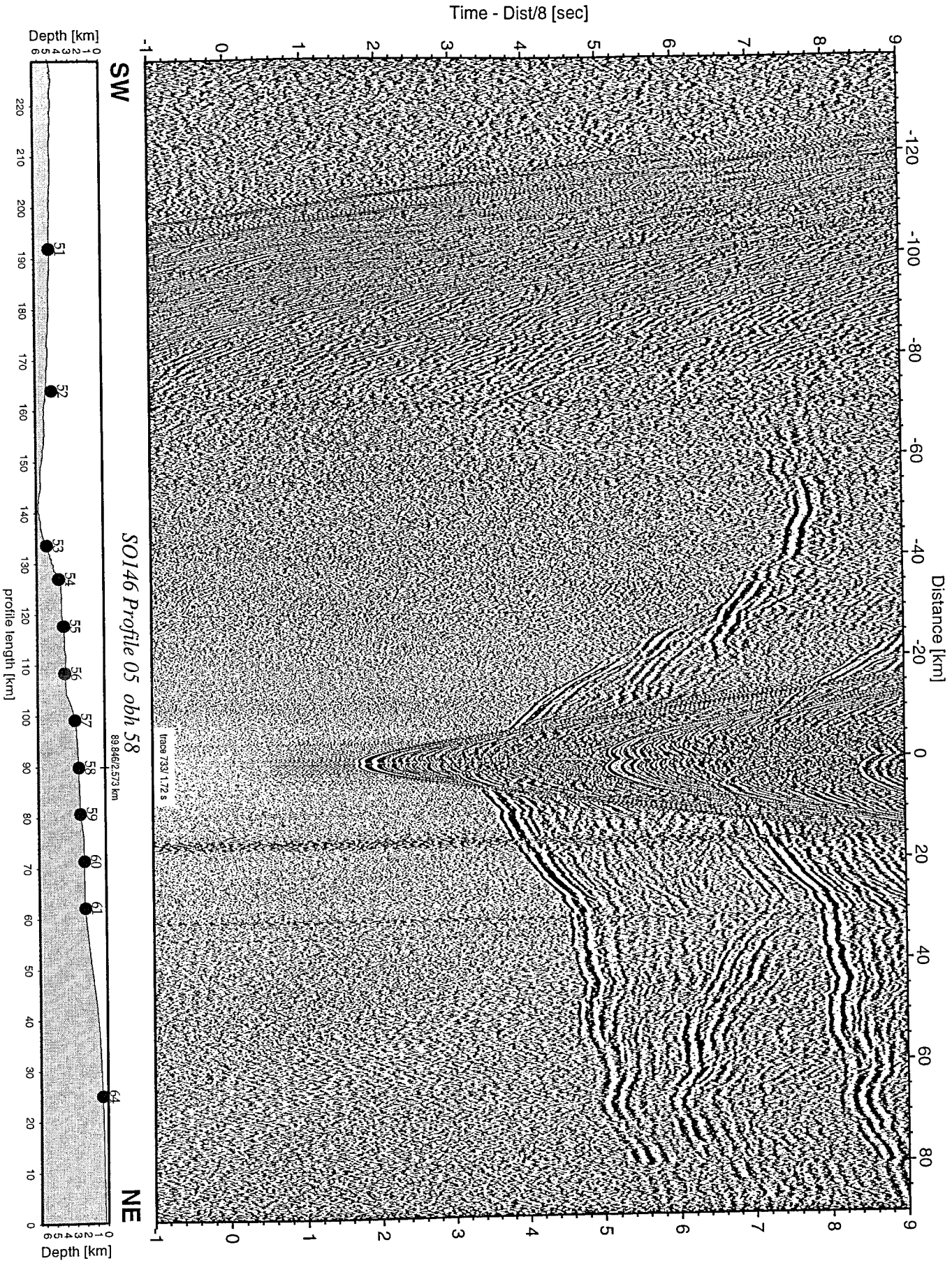

Figure 7.3.9: Record section from obh 58 , Profile 05.

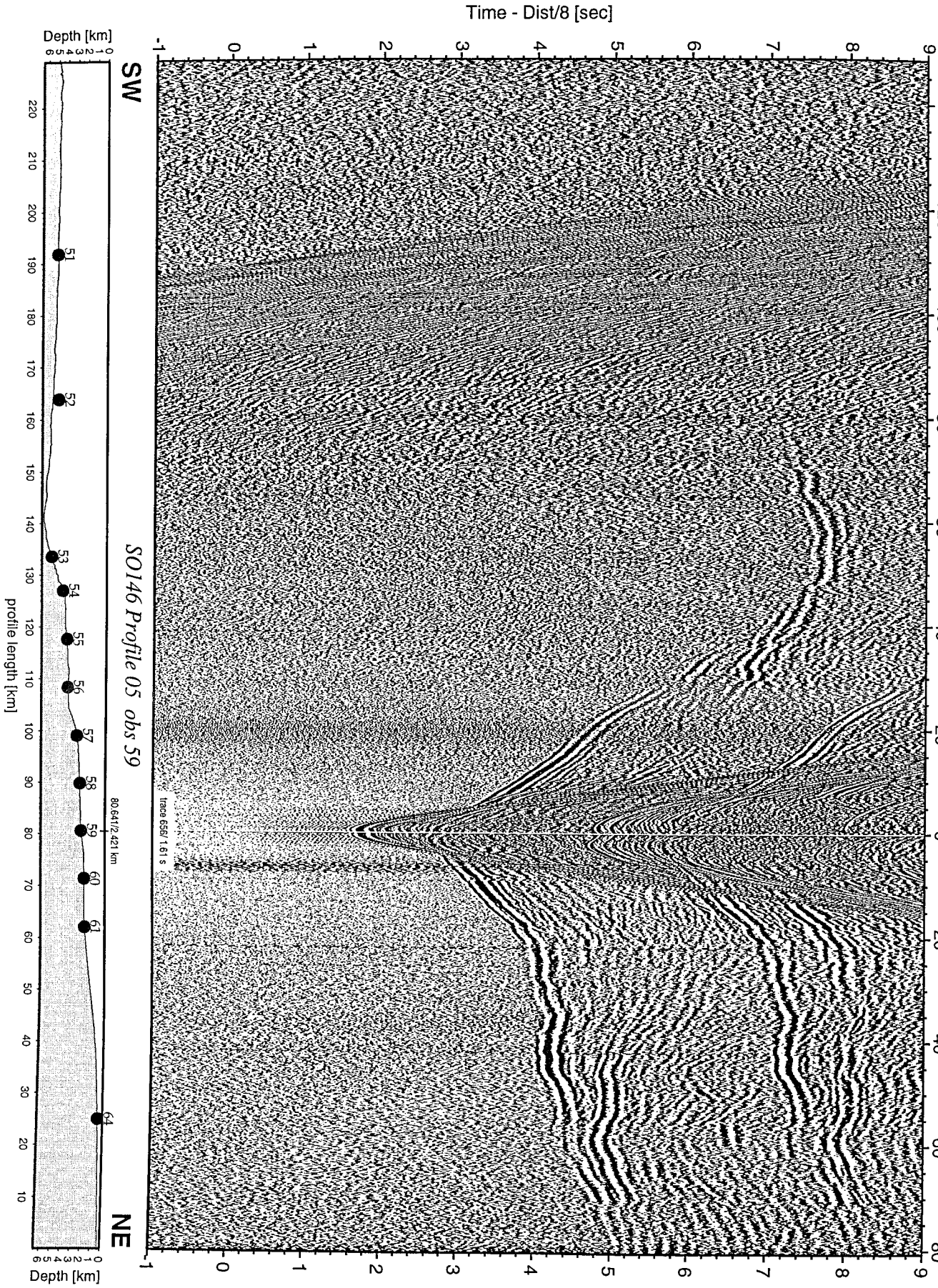

Figure 7.3.10: Record section from obs 59 hydrophone, Profile 05.

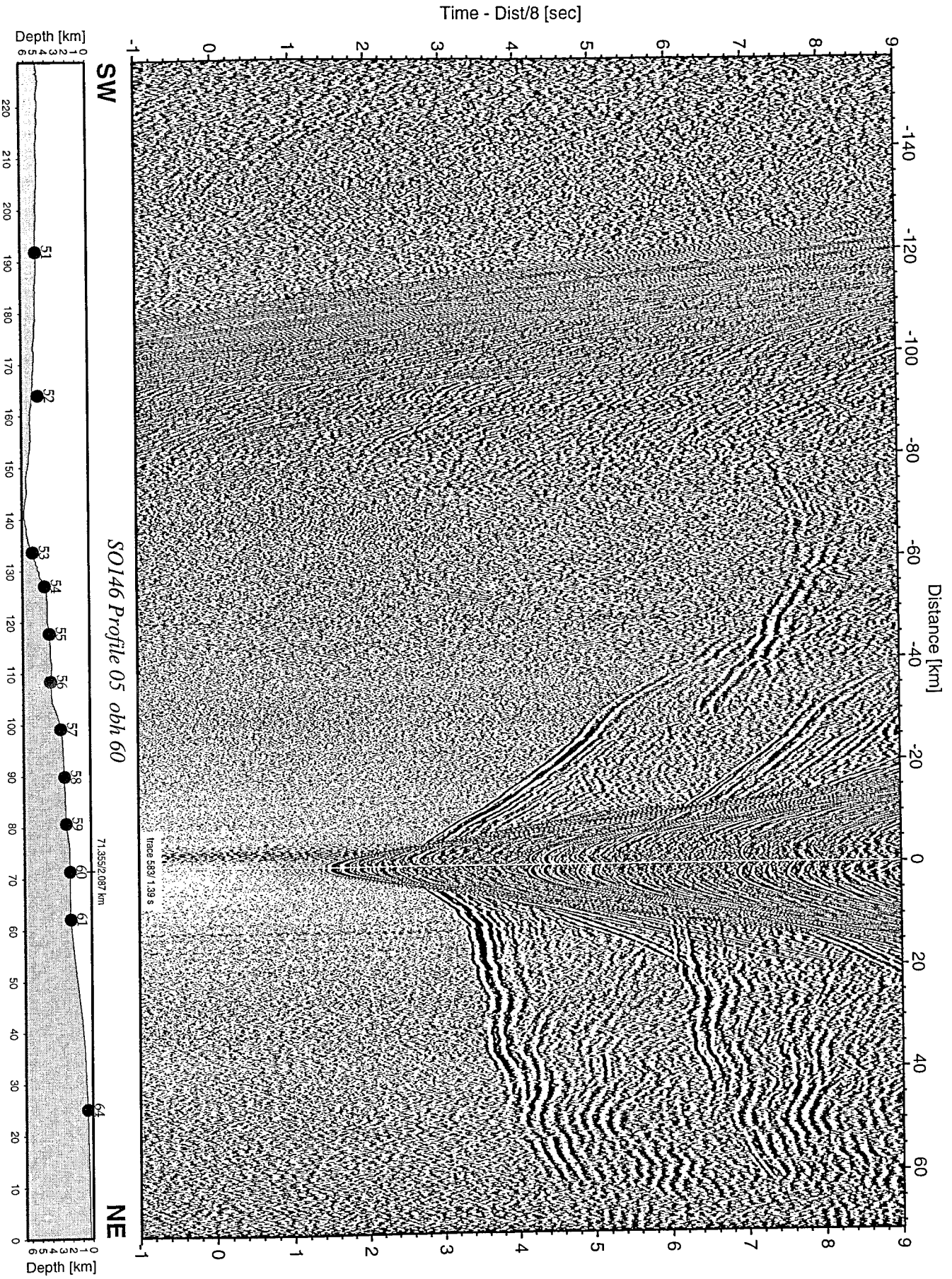

Figure 7.3.11: Record section from obh 60 , Profile 05.

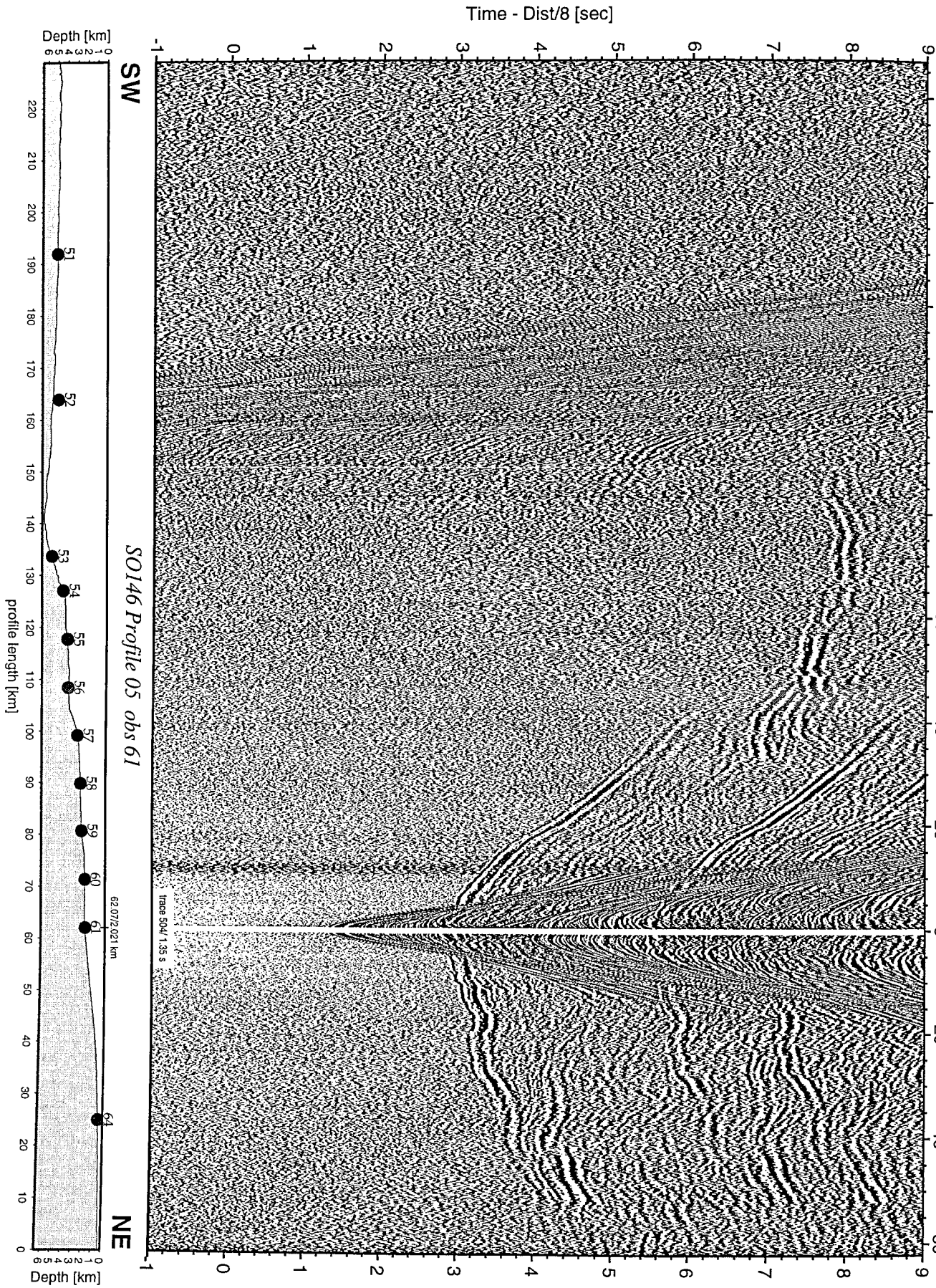

Figure 7.3.12: Record section from obs 61 hydrophone, Profile 05.

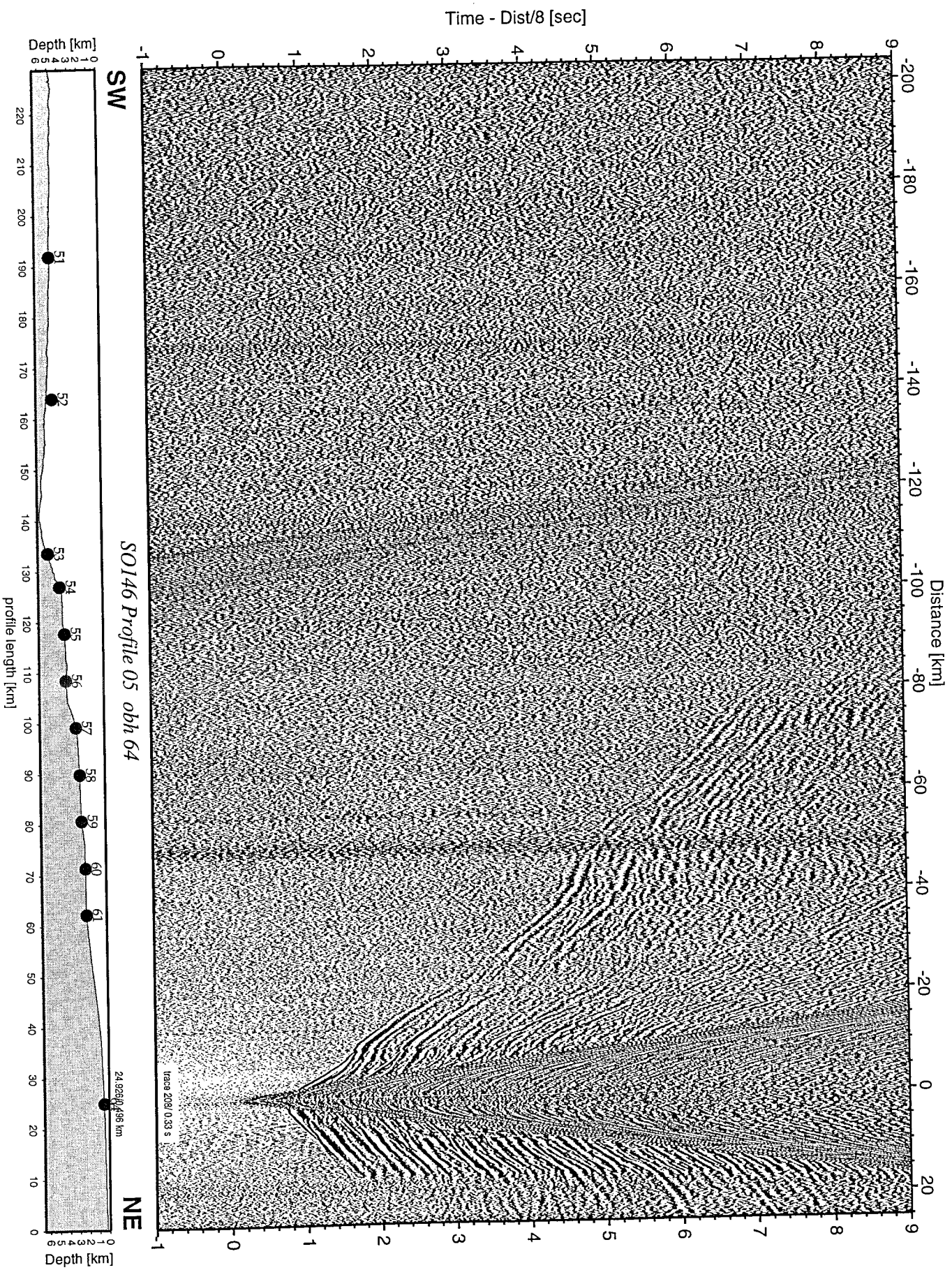

Figure 7.3.13: Record section from obh 64 , Profile 05.

A preliminary two-dimensional model for profile SO146-05 has been constructed (figure 7.3.30), using MacRay 2D modeling software, on board the RV SONNE. The sedimentary section was modeled using multichannel seismic data and refractions. Modeling was performed from the top to the bottom layer. The preliminary model shows that the upper sedimentary unit has a velocity structure increasing from 1.55 km/s at the top to 4.6 km/s at the bottom and a high velocity gradient (3.6 s^{-1}) . This unit was modeled using three thin layers with various thicknesses ranging between 0.5 and 2 km. The underlying basement shows an almost constant velocity of 6.2 – 6.7 km/s. This velocity is interpreted as an upper part of the oceanic crust. This layer is at relatively shallow depth (7 km) to the SW, but extends to deeper depths (~15 km) to the NE. Immediately landward, continental basement, with average velocities between 5.6 km/s and 6.4 km/s below the sedimentary section is modeled using two layers. The upper layer has an average thickness of about 4 km and is underlain by a second layer with an average thickness of 5 km. The continental crust is characterized by velocities between 6.4 and 6.6 km/s and has an average thickness of about 10 km. At the depth of 14 km the Moho discontinuity is modeled with a velocities greater than 8 km/s. The model indicates that the subducting geometry of oceanic crust varies from nearly horizontal to a subducting dip of β=7.6°. The angle of the accretionary prism is measured with α_1=9.5°, resulting into a taper of 17.1°. These values indicate high basal friction during subduction and therefore support the interpretation of complete subduction derived from the velocity distribution within the model.

Profile SO146-06

(A. Haris)

Profile SO146-06 intersects profile SO146-05 near station OBS 69, and is parallel to the thrench axis with a northwest trend. This profile is intended to supplement the information acquired from profile SO146-p05 along the trench strike. Further profile SO-146-06 will aid in determining the velocity structure of the continental margin and velocity variations along strike in the collision zone between the Nazca and South American plates.

Between 11:24 on 31st March 2000 and 06:00 on 1st April 2000, 10 instruments (3 OBS and 8 OBH; station numbers 65 to 75) were deployed using an interval of 5 to 9 nm. The two outermost stations on each end of the line have an interval of 10 nm. A detail location map is shown in figure 7.3.1 and a table containing the exact positions of each instrument is given in the Appendix II. Using an array of three 32 ltr. Bolt Air Guns, shooting started at 06:11 on 1st April 2000 and ended at 09:20 on 2nd April 2000. The total profile length is over 170 km. Recovery of the OBH and OBS instruments was then completed on 2 April, 2000. All instruments were safely recovered.

The recorded OBH and OBS were processed using methods described in 4.9.1. The data along this profile were processed using SEISMOS package software from GECO-Prakla. The results indicate good quality. Record sections of the processed data are shown in figures 7.3.14 through 7.3.29.

Modeling and interpretation

In general the data quality is very good. Most instruments recorded data and show clear signals over the entire profile length with exception OBH 75. The recorded refractions and reflections have an approximately symmetrical shape. The clear refraction signals indicate only thin sediment coverage and a rapid increase in the apparent velocity of up to about >7.6 km/s. Moreover, on all instruments, precritical reflections from the upper layers are clearly identified. Wide angle reflections from the Moho are registered by most stations, but are especially clear on OBH65 and OBH74. They were used to estimate the Moho discontinuity.

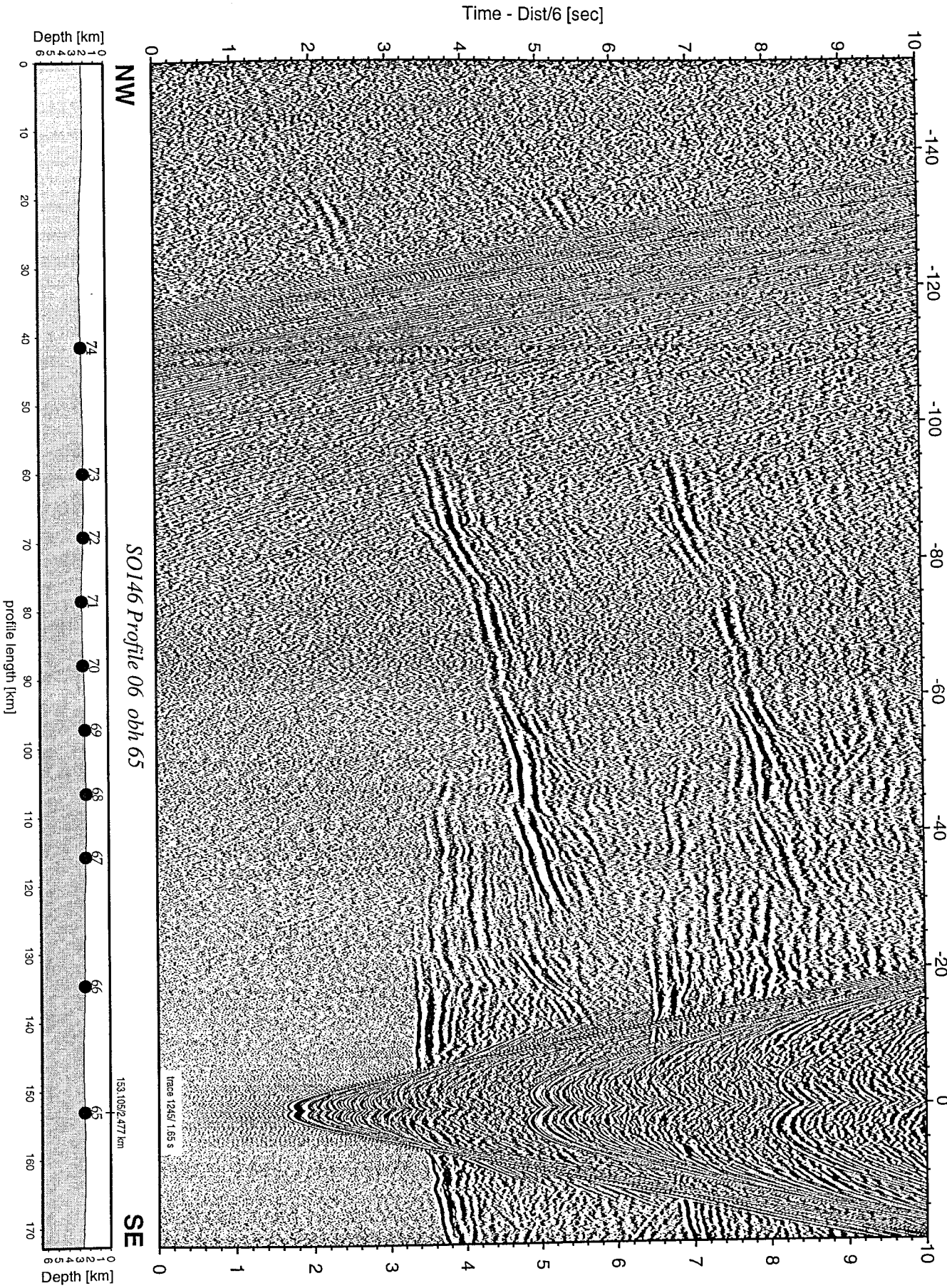

Figure 7.3.14: Record section from obh 65 , Profile 06.

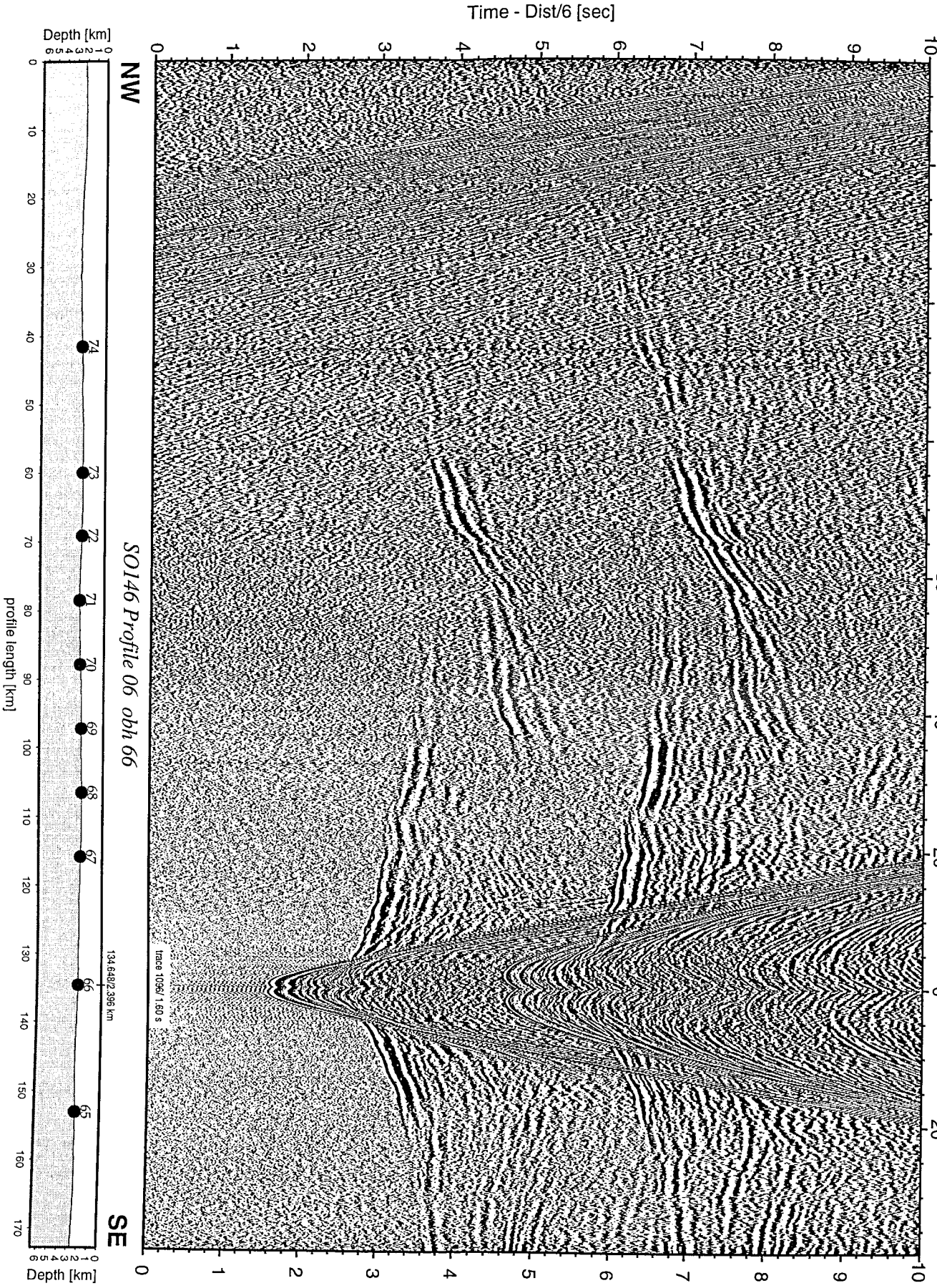

Figure 7.3.15: Record section from obh 66 , Profile 06.

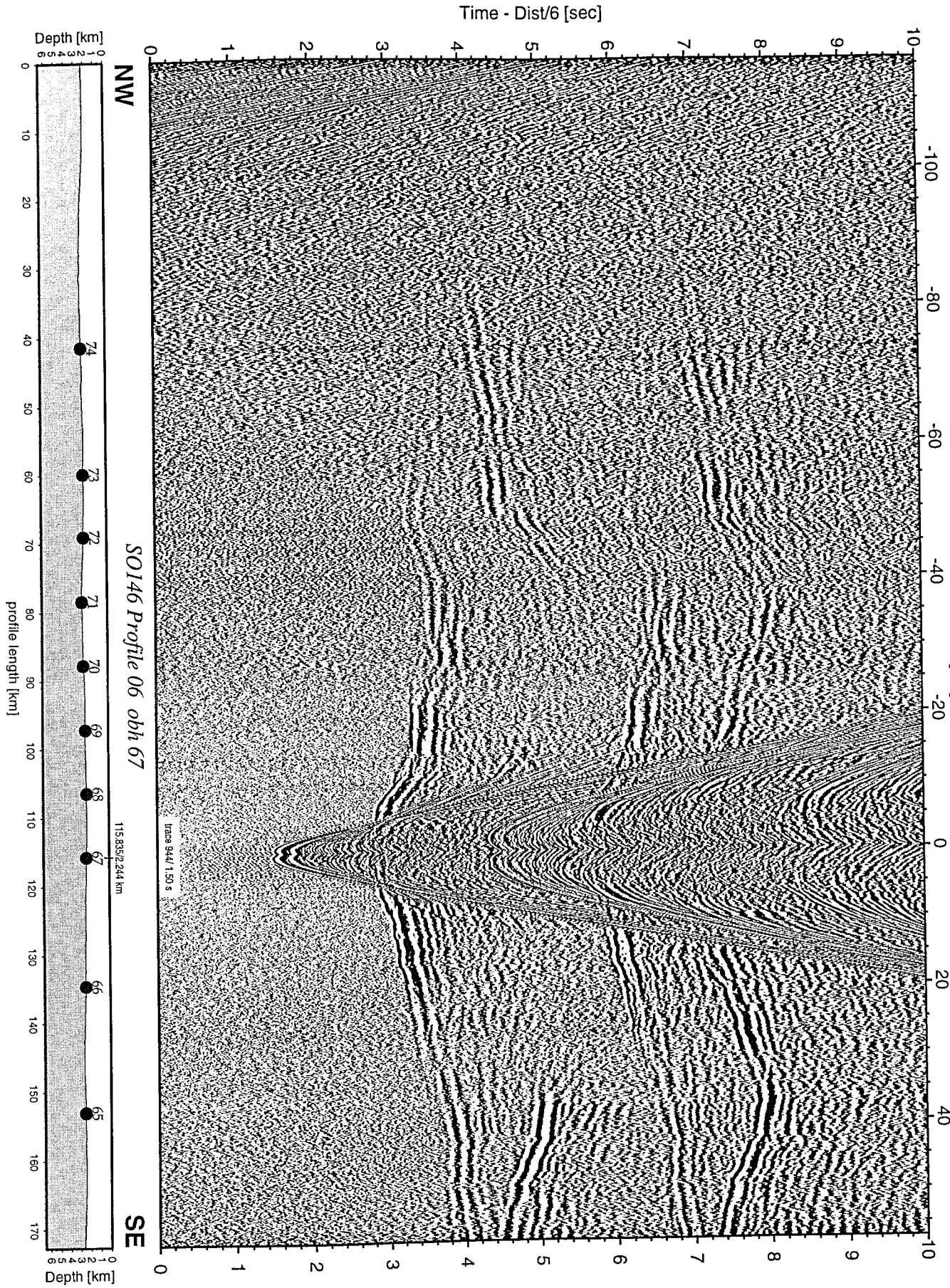

Figure 7.3.16: Record section from obh 67 , Profile 06.

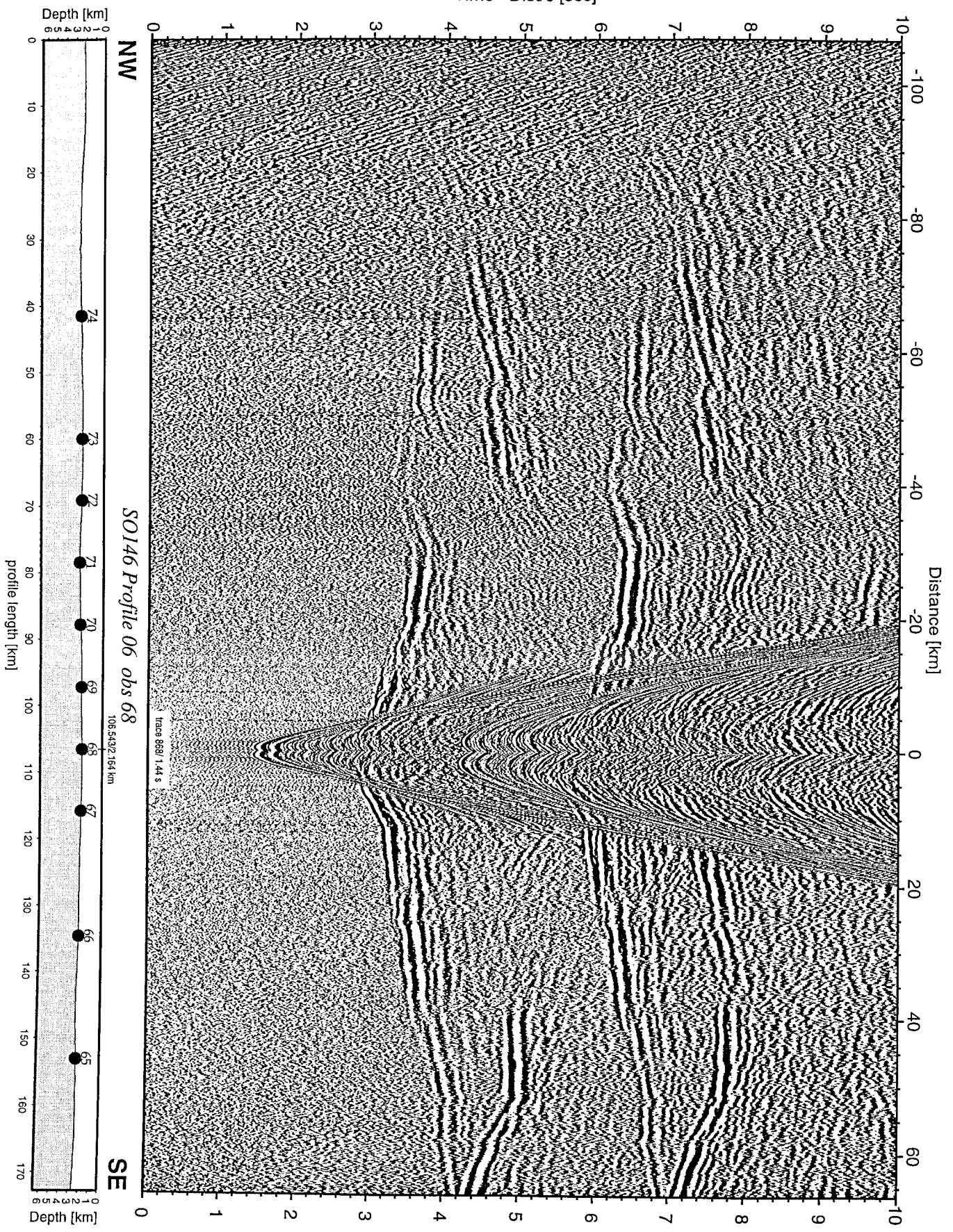

Figure 7.3.17: Record section from obs 68 hydrophone, Profile 06.

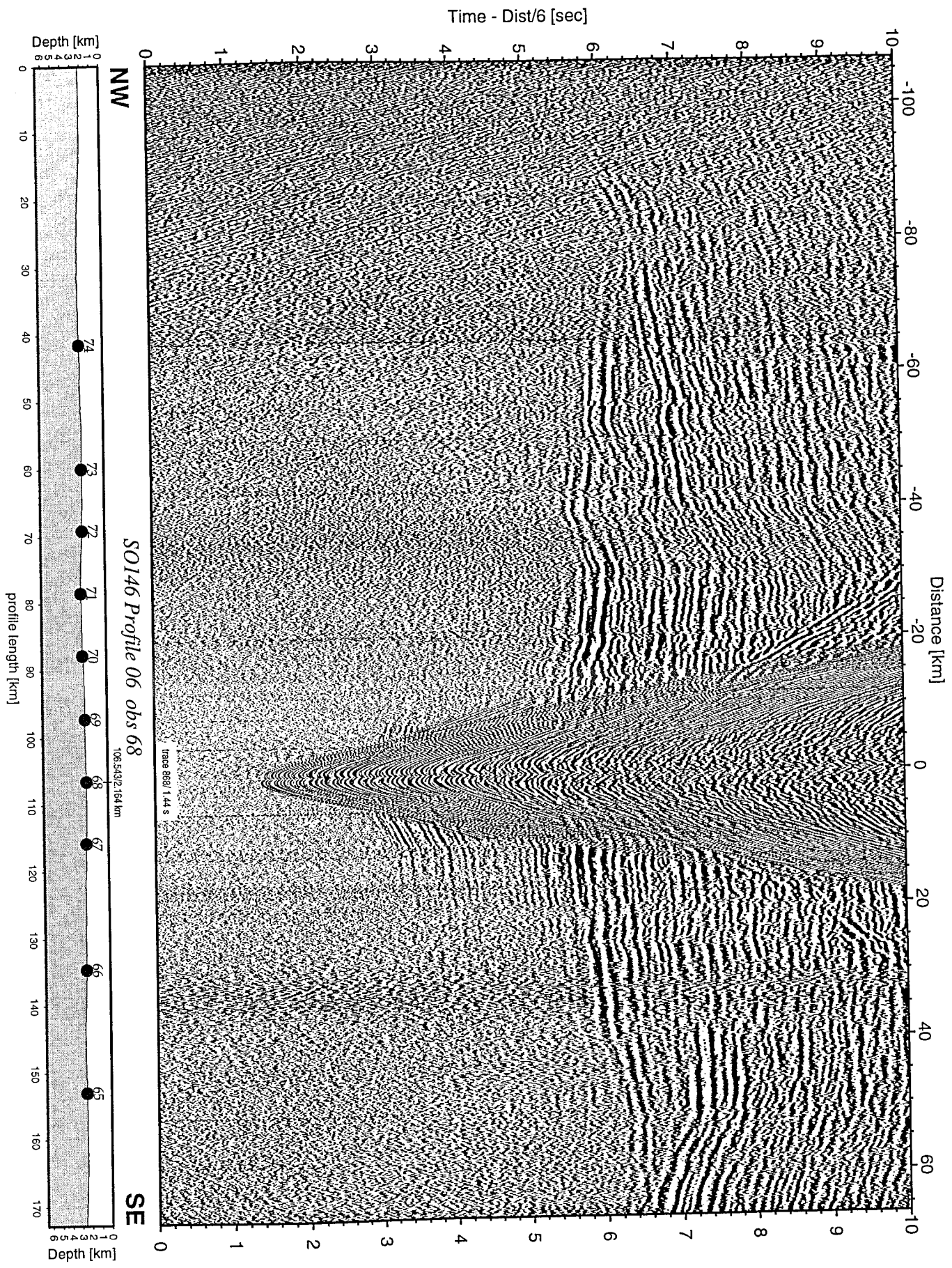

Figure 7.3.18: Record section from obs 68 horizontal component 1, Profile 06.

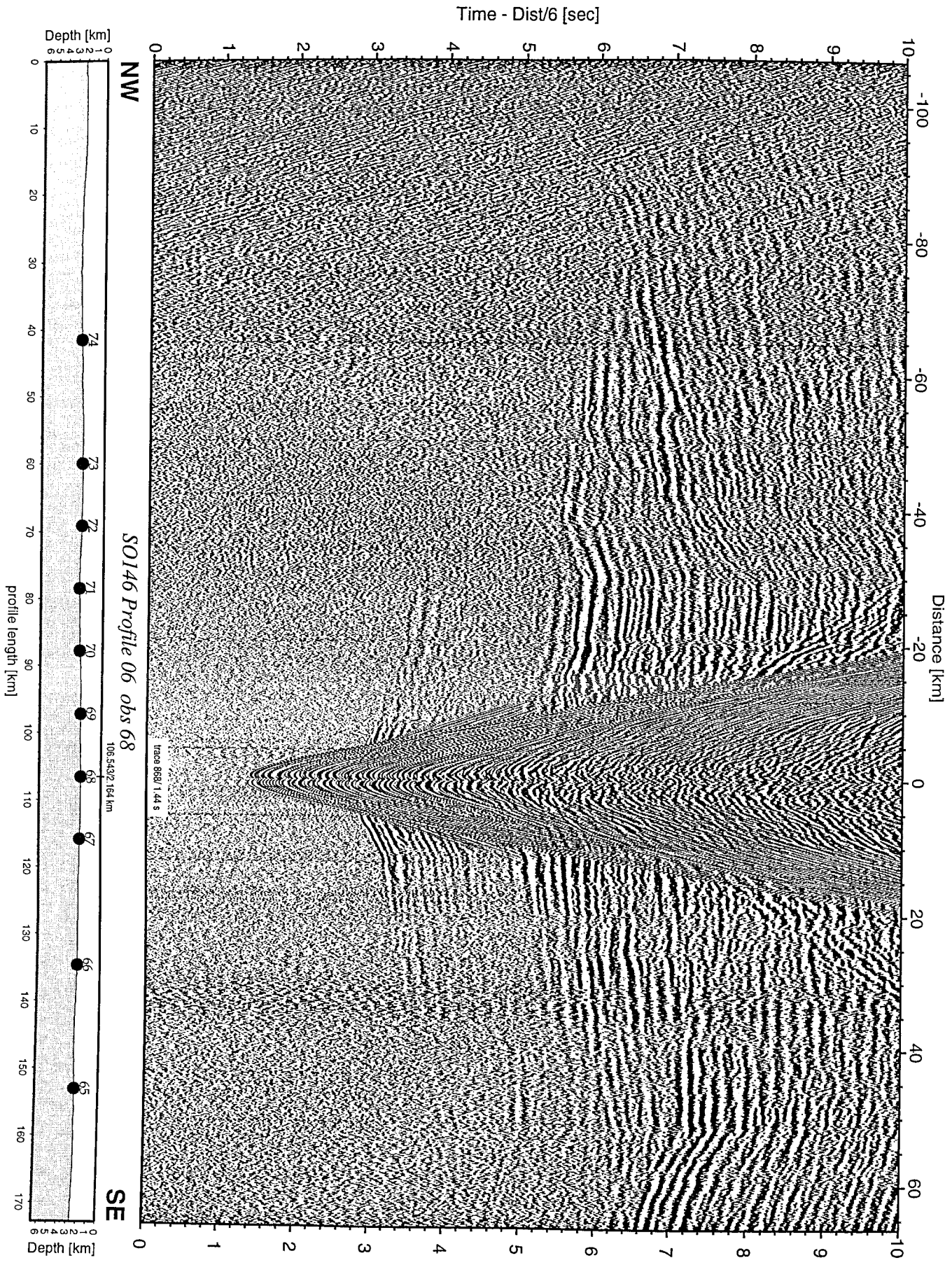

Figure 7.3.19: Record section from obs 68 horizontal component 2, Profile 06.

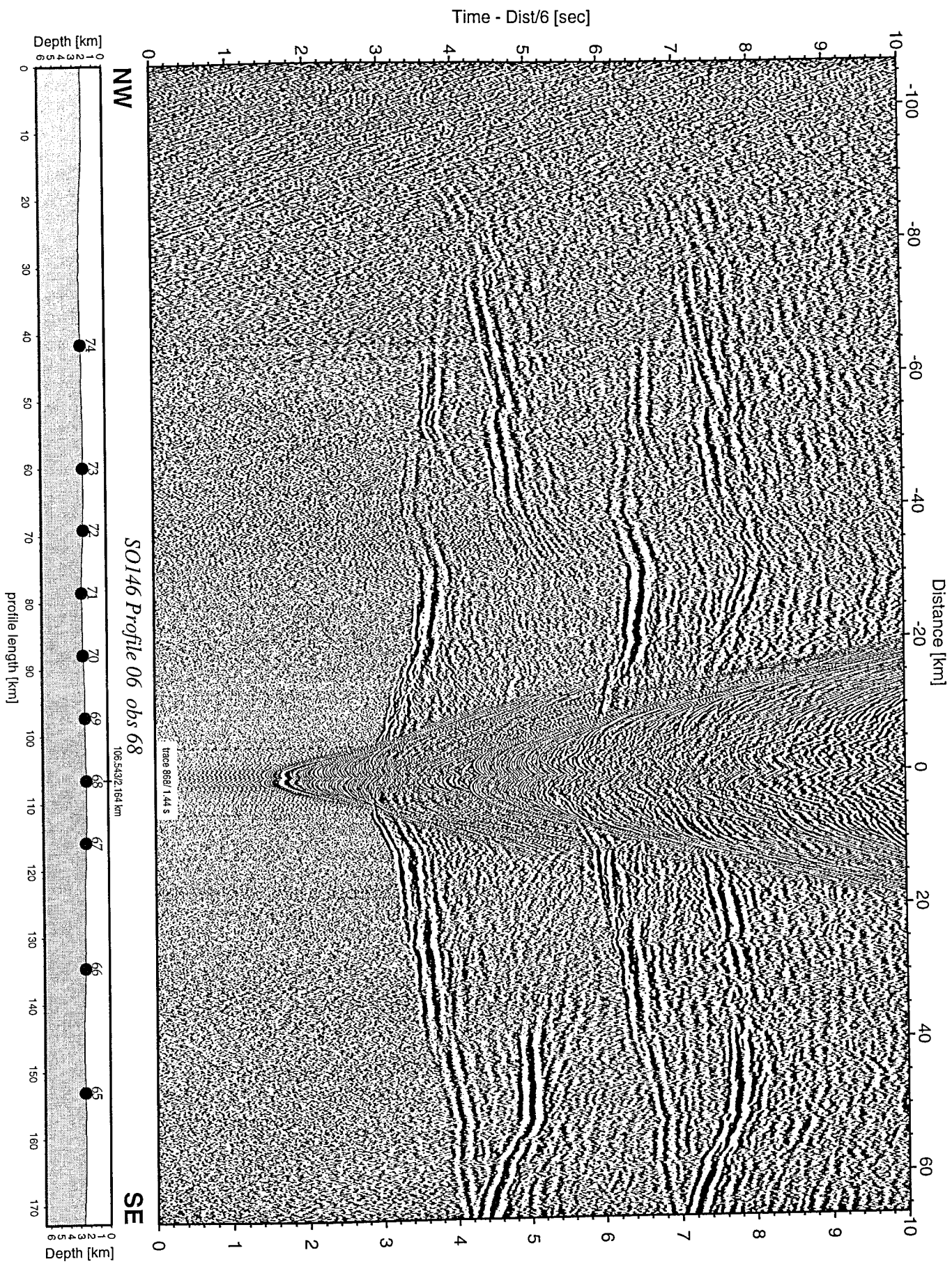

Figure 7.3.20: Record section from obs 68 vertical component, Profile 06.

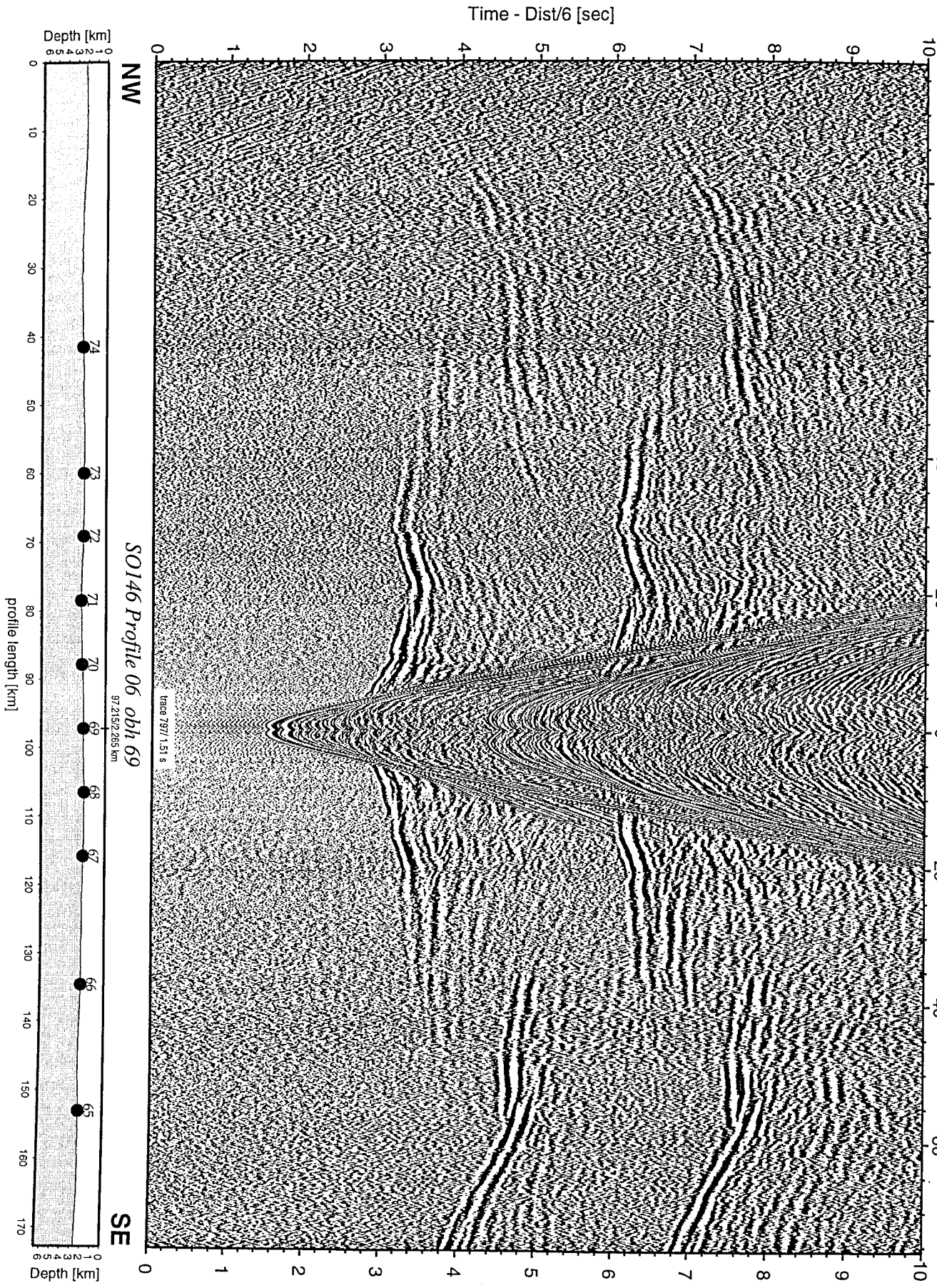

Figure 7.3.21: Record section from obh 69 , Profile 06.

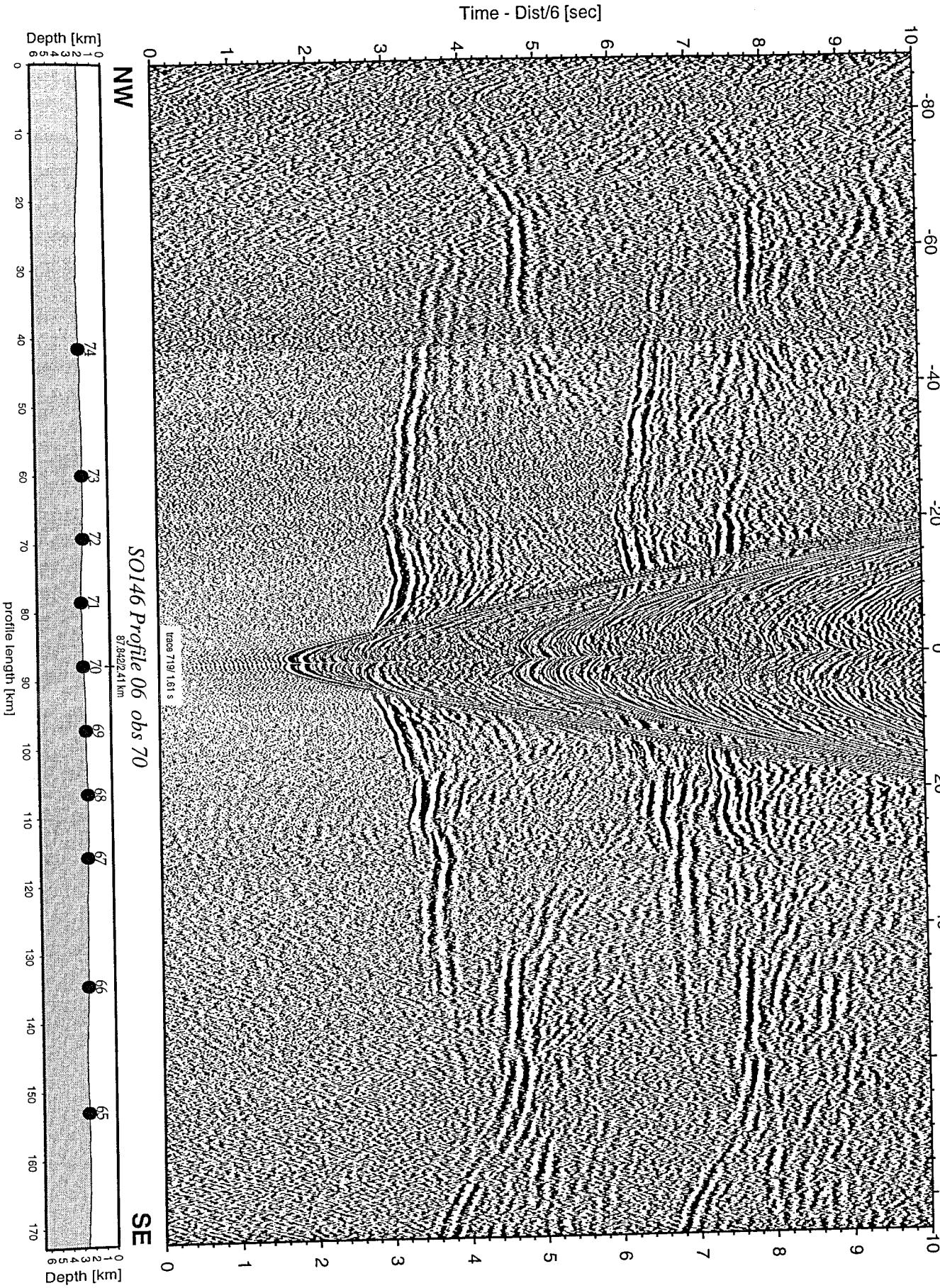

Figure 7.3.22: Record section from obs 70 hydrophone, Profile 06.

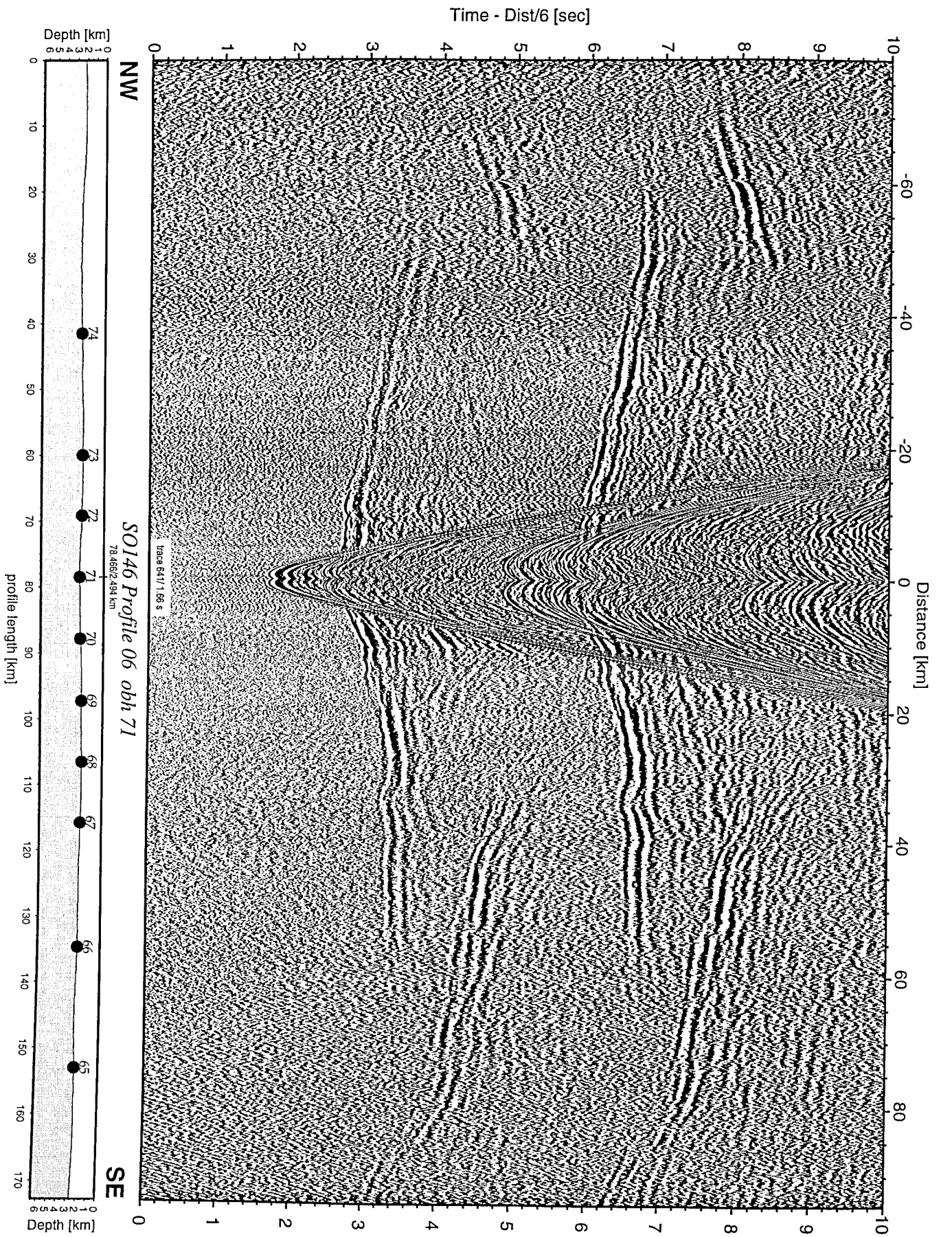

Figure 7.3.23: Record section from obh 71 , Profile 06.

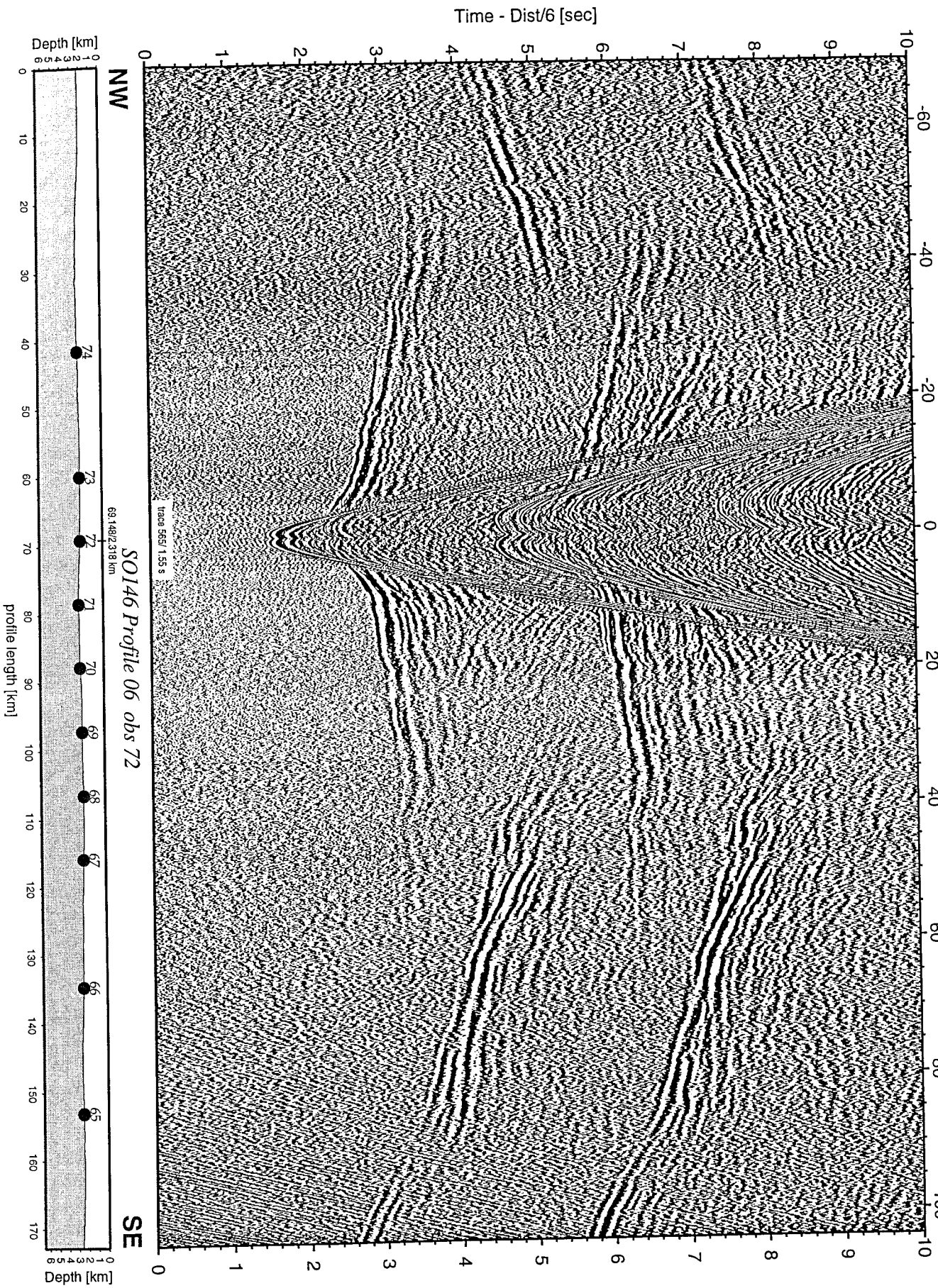

Figure 7.3.24: Record section from obs 72 hydrophone, Profile 06.

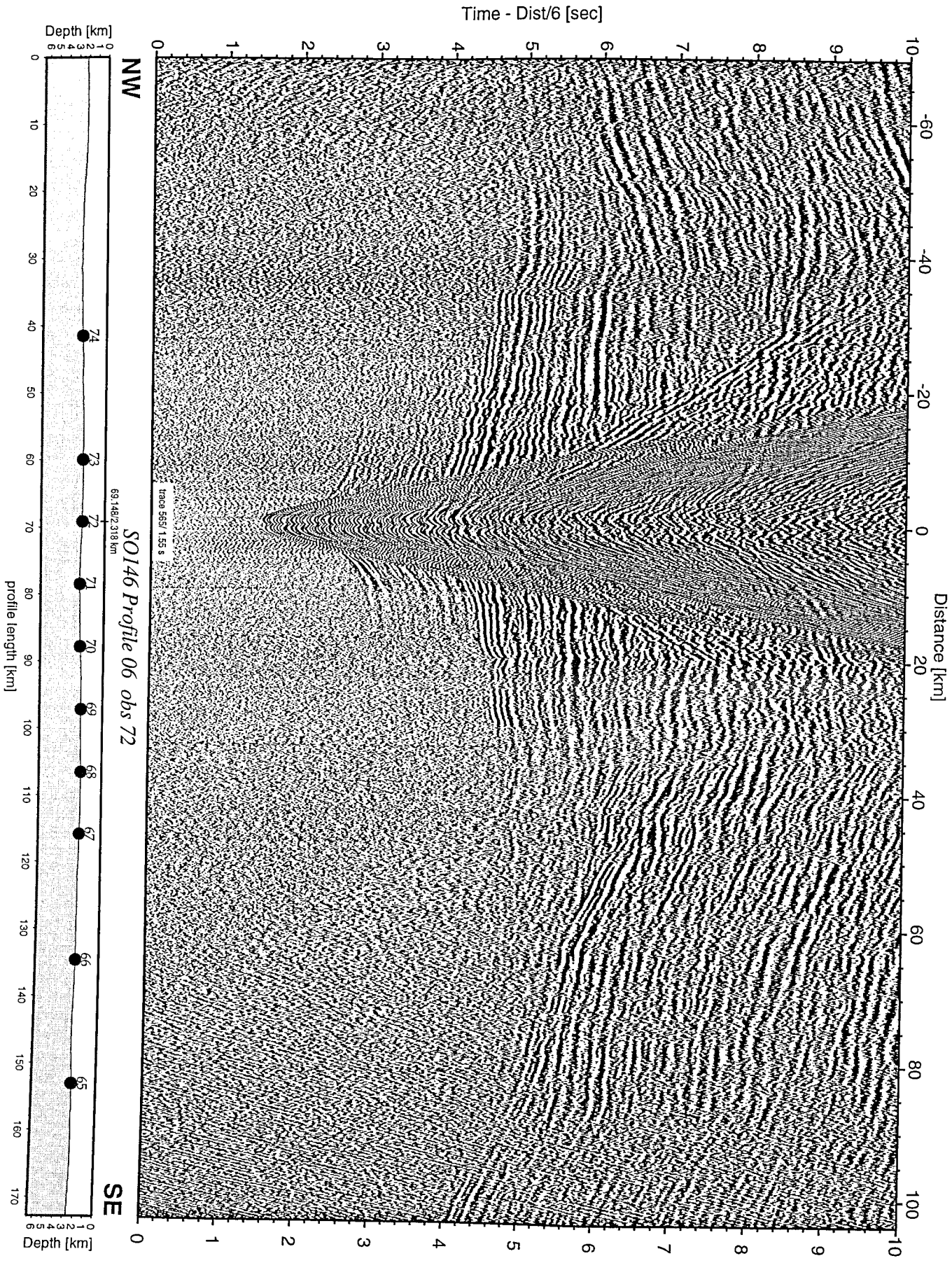

Figure 7.3.25: Record section from obs 72 horizontal component 1, Profile 06.

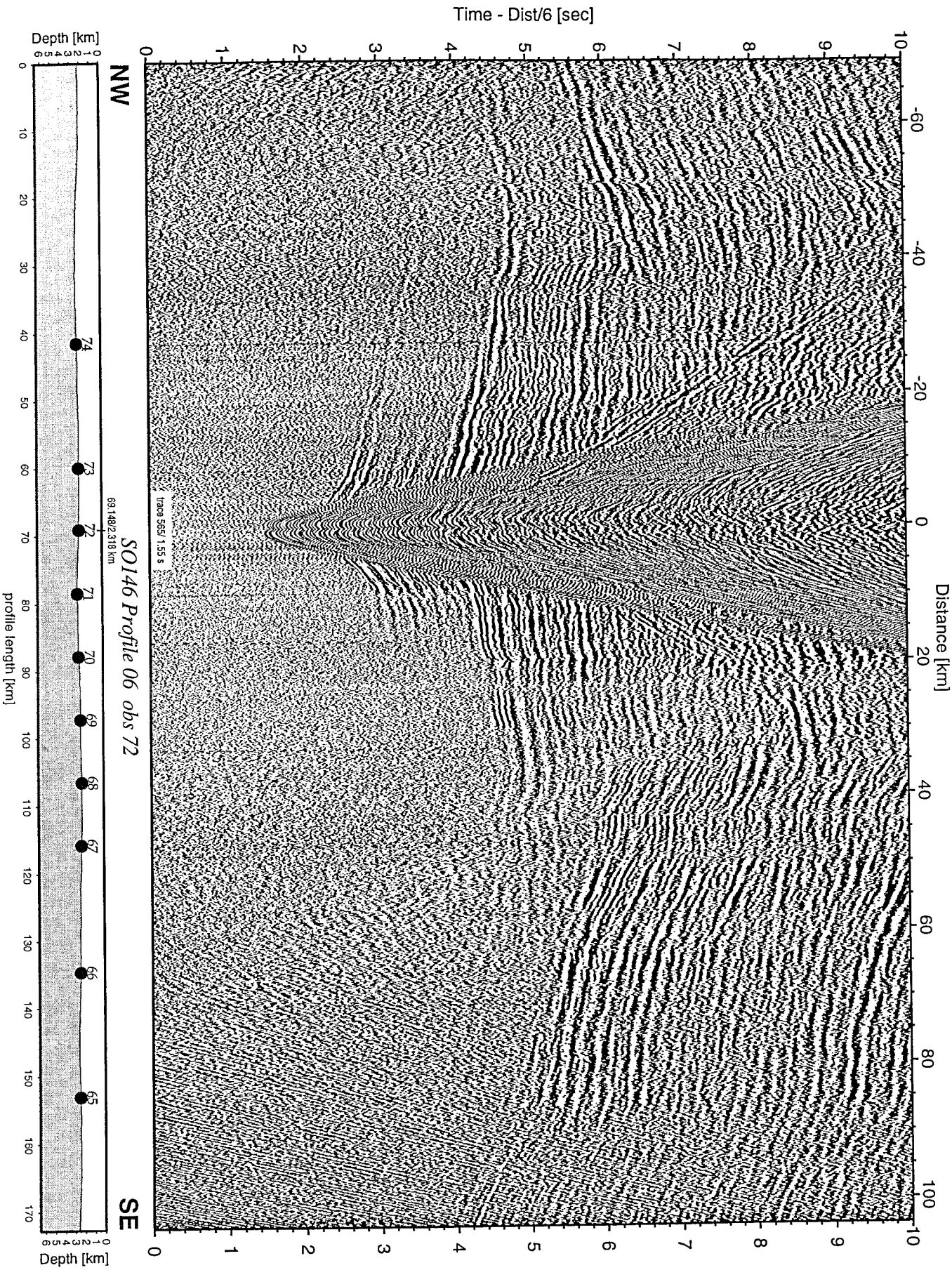

Figure 7.3.26: Record section from obs 72 horizontal component 2, Profile 06.

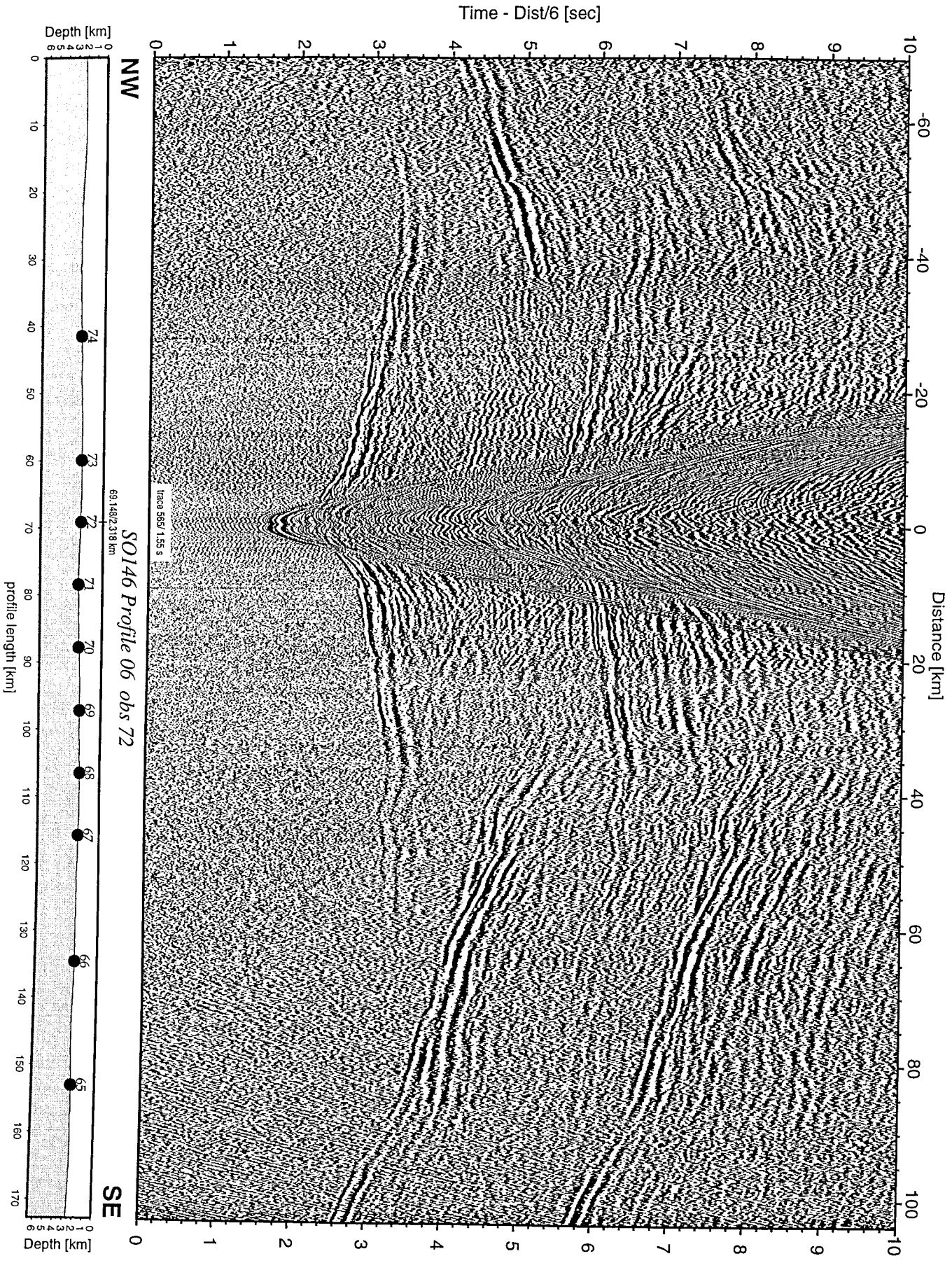

Figure 7.3.27: Record section from obs 72 vertical component, Profile 06.

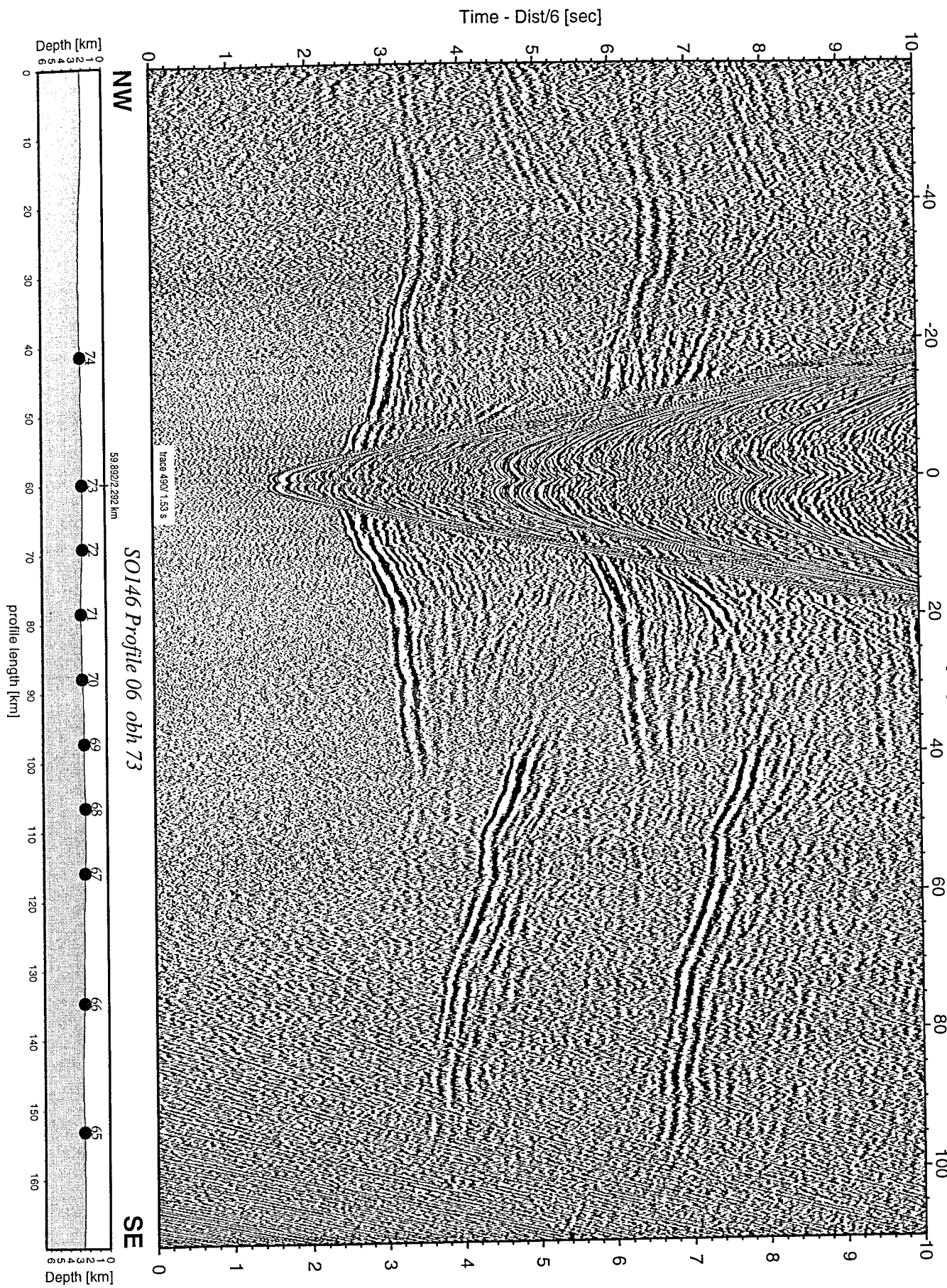

Figure 7.3.28: Record section from obh 73 , Profile 06.

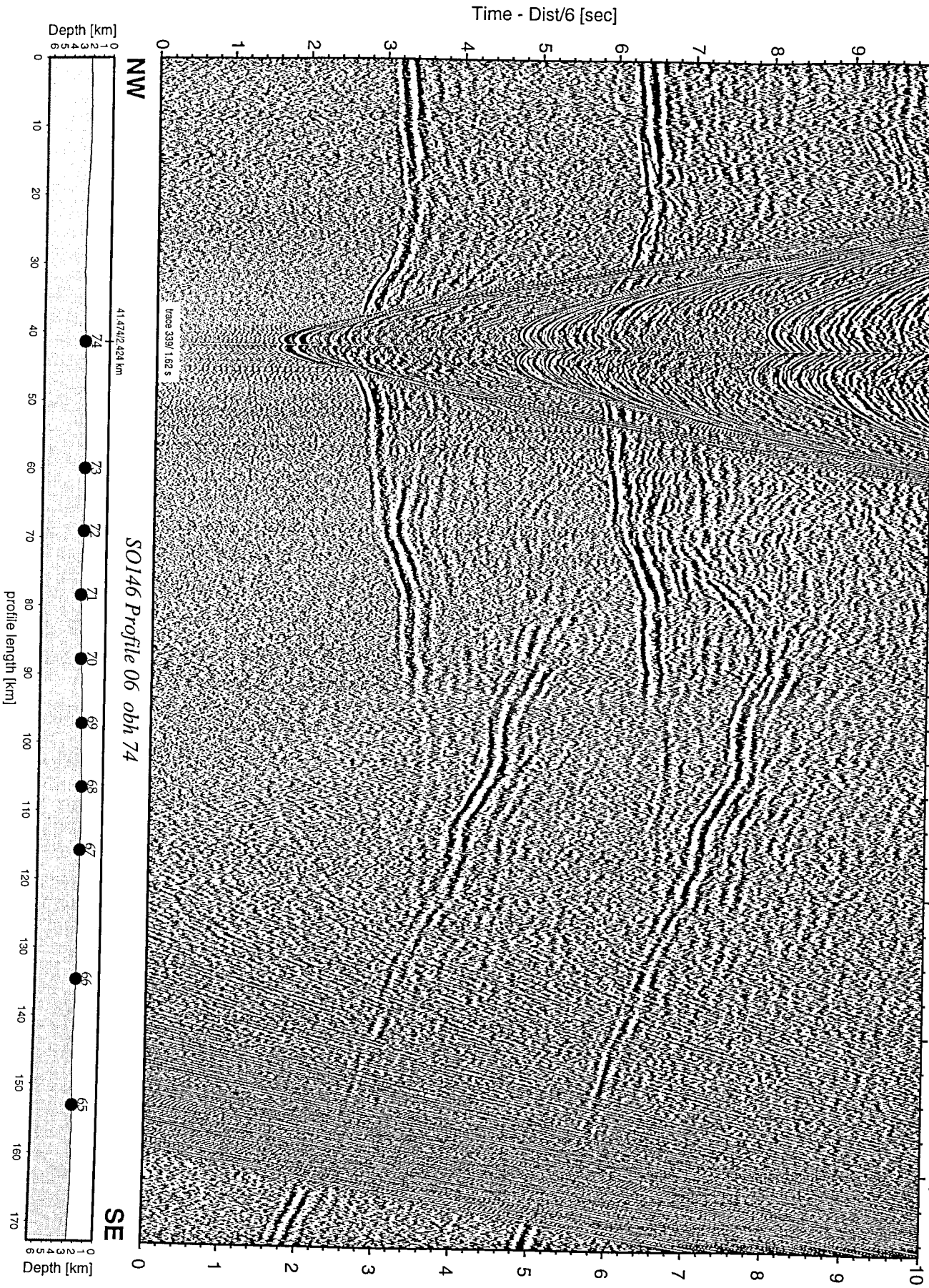

Figure 7.3.29: Record section from obh 74 , Profile 06.

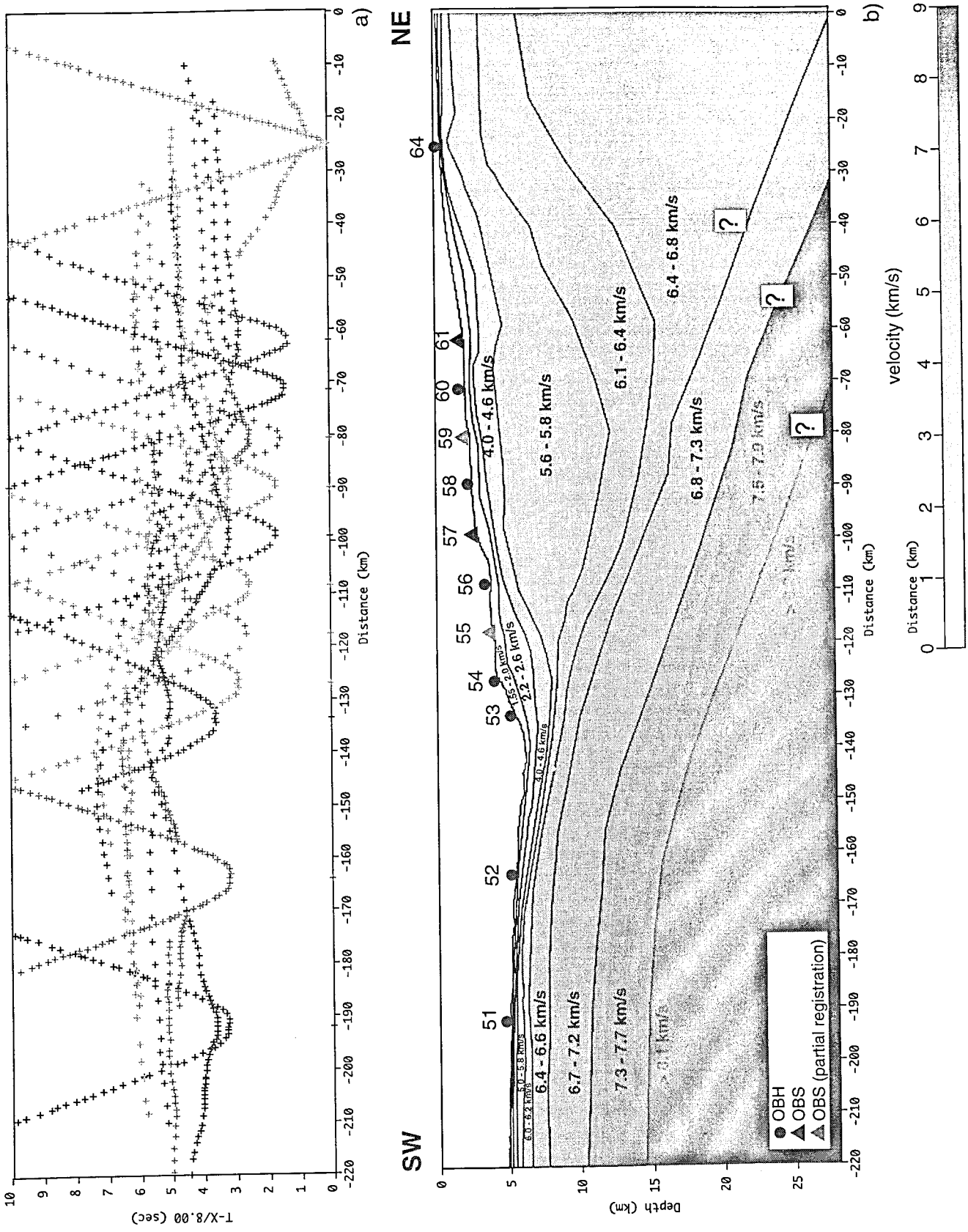

Figure 7.3.30: a) Picks extracted from the record sections of profile SO 146-05, b) crustal cross section for profile 05 derived from preliminary analysis of wide angle data.

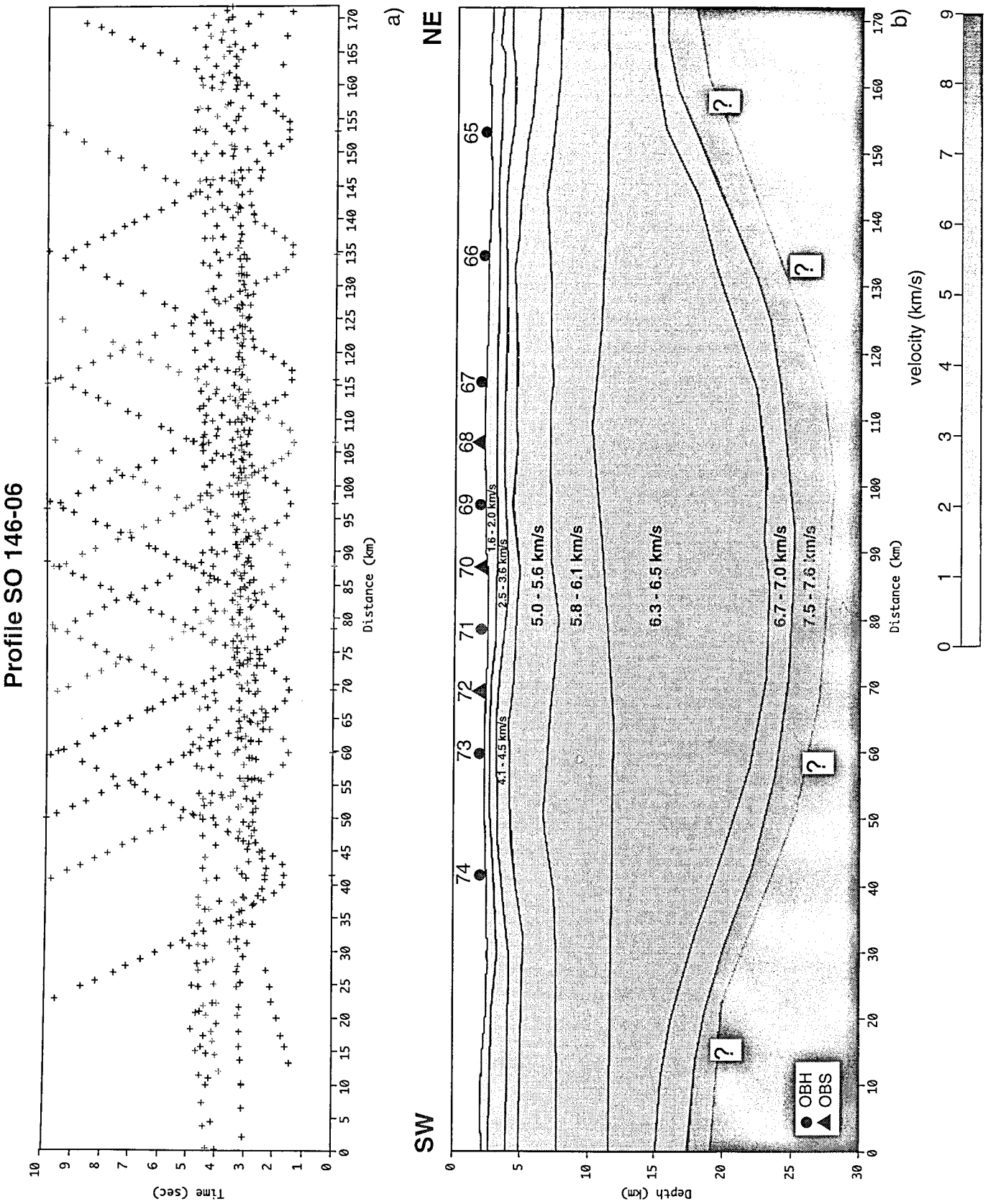

Figure 7.3.31: a) Picks extracted from the record sections of profile SO 146-06, b) crustal cross section for profile 06 derived from preliminary analysis of wide angle data.

A one-dimensional velocity-depth model of OBS69 was constructed, using the 2D MacRay tracing algorithm, to get a reference velocity-depth profile. This model was correlated to OBS59 on profile SO146-05, and as mentioned in chapter 7.3.1, the comparison of the velocity-depth variation between OBS69 and OBS59 shows good agreement. All stations were used to constrain the geometry of the model, from the sedimentary section up to upper layers of the continental crust. The deeper layer, characterized with velocities greater than 7.5 km/s, is constrained by station OBH65 and OBH74 and according to profile 5 related to the subducted oceanic plate.

The preliminary model indicates that the sedimentary layers are characterized by velocity values between 1.6 km/s and 4.5 km/s. This section is parameterized in terms of three layers and can be identified to a depth of about 5 km.. The uppermost layer is characterized by velocity values between 1.6 km/s and 2.5 km/s and an average thickness of about 1.5 km. The middle layer has velocity values between 2.9 km/s and 4.1 km/s while the lower layer has a velocity values between 4.2 km/s and 4.5 km/s. The thickness of the middle and lower layer are about 1.5 km and 2 km, respectively. The underlying basement has an almost constant velocity of 5.1 – 6.1 km/s. This velocity is interpreted as upper part of continent crust. This layer is relatively flat along the line and reaches from depths of 5 km to depths of 12 km. It is parameterized by two layers. The upper one has an average thickness of about 2.5 km and is underlain by a second layer with an average thickness of 4 km. Two layers at a depths of about 15 km with a geometry resembling a syncline are charactrized by velocities between 6.7 km/s and 7.6 km/s. Based on the prelimenary model of profile SO146-05, this layer is interpreted as downgoing subducting oceanic crust. This layer has an average thickness of about 2 km – 2.5 km.

7.4 Profile SO 146-04

(A. Hampel)

The refraction and wide-angle reflection seismic profile SO 146-04 is located perpendicular to the continental slope in the working area off Lima at 12° S (see figure 7.4.1), where the Nazca Plate subducts under the South American continent. A total of 5 OBH and 4 OBS were deployed on the 195 km long profile. All instruments were successfully recovered and recorded well except for stations 46 and 47. OBH 46 shows only signals from the northeastern end of the profile, and OBH 47 did not record at all.

The data quality is good in general. Especially OBH 42 and 43 which were positioned in the trench recorded very clear signals over the entire profile length. Stations 48 to 50 which were located on the shelf show signals that reach as far as 50 km. The recorded refractions and reflections have an asymmetrical shape due to the strongly variable topography. The clear refraction signals on OBH 42 and 43 indicate only little sediment on the subducting oceanic Nazca Plate and a rapid increase of the apparent velocity up to about 8 km/s at the crust-mantle boundary. On these seaward stations, the Moho can be clearly followed to a depth of about 28 km beneath the continental slope.

Modeling and interpretation

To characterize the structure and the velocity field of the Peruvian margin at 12° S, the refraction and reflection signals from the hydrophones were picked and modeled using raytracing. For the first step, the 1-dimensional modeling program R1D (Luetgert, 1992) was used to approximate the velocity functions at stations 43 and 48, which were located in the trench and on the shelf, respectively. According to the 1D-modelling of OBH 43, there is a rapid increase of the seismic velocity from 2.0 km/s for the thin sediment layer to over 8 km/s at 11 to 12 km depth in the trench. The continental slope (OBS 48) shows velocities about 2.0 to 2.3 km/s to a depth of about 2 km and then a slower increase up to mantle velocity.

For modeling the whole profile, the raytracing program MacRay (Luetgert, 1992) was used. The construction of the model was based on OBH 42 and 43 for the trench area, the refractions of the down going plate and the Moho, whereas stations 48 to 50 were used to model the upper slope and shelf. From OBHs 44 and 45 located at the foot of the slope, informations about both the trench area and the continental slope are available. In addition to that, they recorded also refractions from the subducting plate. Figure 7.4.9 shows the picked traveltimes above the according stations and the preliminary model. The calculated traveltimes based on this model already match the observed quite well except those refraction signals of OBH 44 which are related to the continental slope.

The preliminary model shows that the subducting Nazca Plate has a rough surface with only little sediment cover. At the southwestern end of the profile, a bathymetric high of about several hundred meters approaches the trench area. The subducting plate can be subdivided into 5 layers. The first layer represents the sediments with velocities of about 2.0 km/s. The thickness of the layer A beneath the sediments varies, but is on the average about 500 m, its velocity is about 4.6 km/s. This indicates the top of the oceanic basement. In comparison to the structure of typical oceanic crust, layer A corresponds to the basaltic Layer 2a. Layers B and C show velocities of 5.3 - 5.6 km/s and 6.2 - 6.5 km/s, which can be correlated to Layers 2b and 2c of the standard model, consisting of pillow lava and sheeted dikes. Layer D with velocities of 7.4 - 7.7 km/s can be related to the gabbroic Layer 3. Refractions from the mantle indicate a depth of the Moho of about 11 km and velocities of over 8.3 km/s for the mantle.

Records of OBH 44 and 45 show that the sediment layer on the lower slope can be subdivided into a layer of 1.9 - 2.0 km/s above sediments with 2.1 - 2.3 km/s. The accretionary wedge seems to consist only of a small thrust slice. Its angle is $\alpha_1 = 8.4°$, which flattens to $\alpha_2 = 4.7°$ at profile kilometer 90. The upper slope has an angle of about $\alpha_3 = 2°$. For OBH 44, the refractions especially of the upper layers could be matched only roughly. There are indications that there could be local variations in velocity which do not have a strong influence on the neighbor stations. The structure of the lower slope in this preliminary model is therefore mainly based on OBH 45.

The northeastern part of the profile landward of the trench is characterized by a sediment layer of 2 -3 km thickness. A sediment basin (Yaquina Basin) is located on the upper slope. Beneath the sediments, a layer with velocities of 4.6 - 4.8 km/s can be found. Between this layer and the top of the subducting plate lies the crystalline part of the upper plate, which shows velocities of 5.4 - 5.7 km/s. The subducting plate itself is marked by higher velocities for layers A to D than in the trench area. According to the preliminary model, the thickness of the crust remains, so that the whole plate seems to be subducted. The dip of the plate of about $\beta = 7.1°$ is constrained by refractions recorded on stations 42 and 43 to a depth of about 28 km.

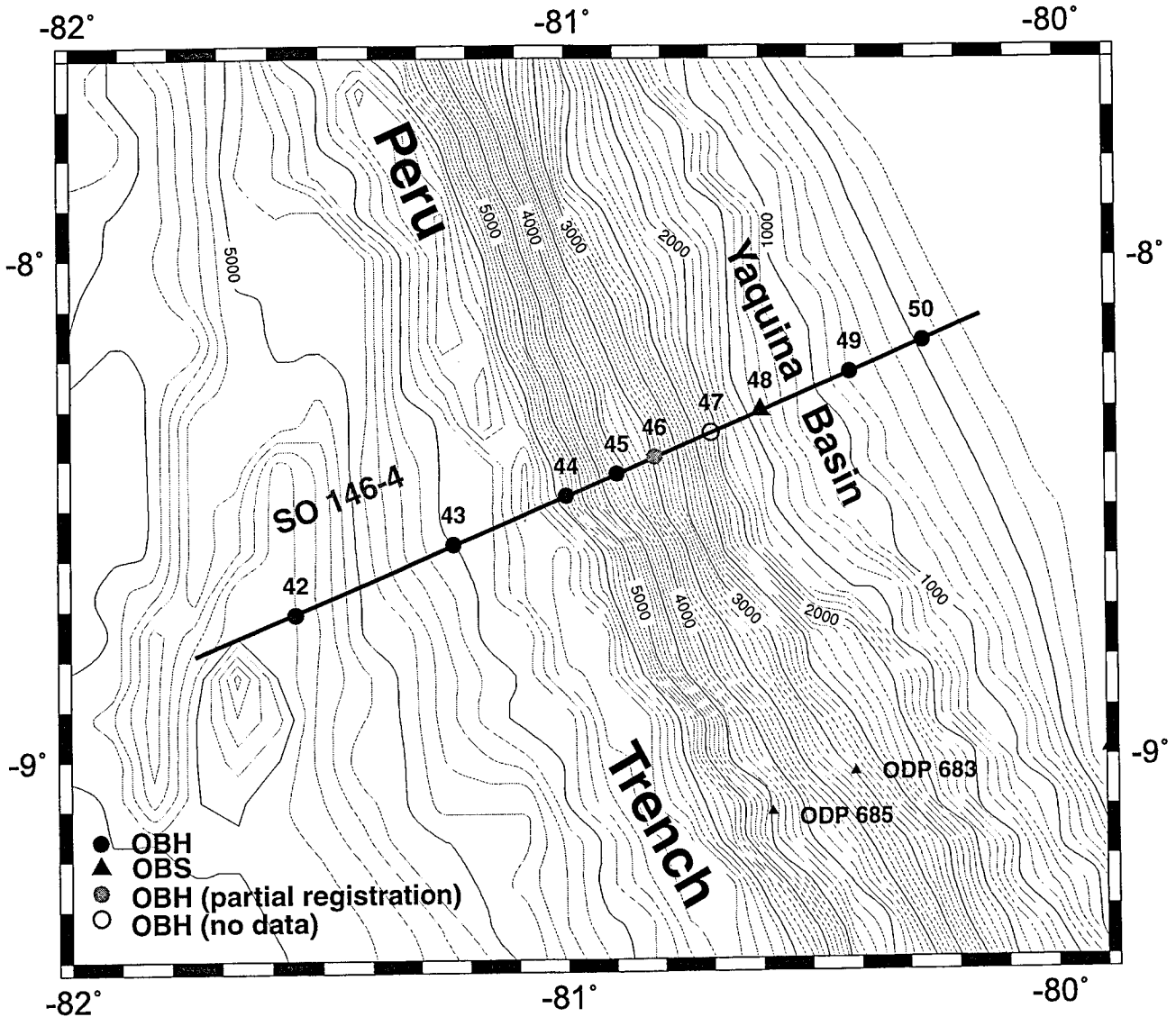

Figure 7.4.1: Location map of profile SO 146-04.

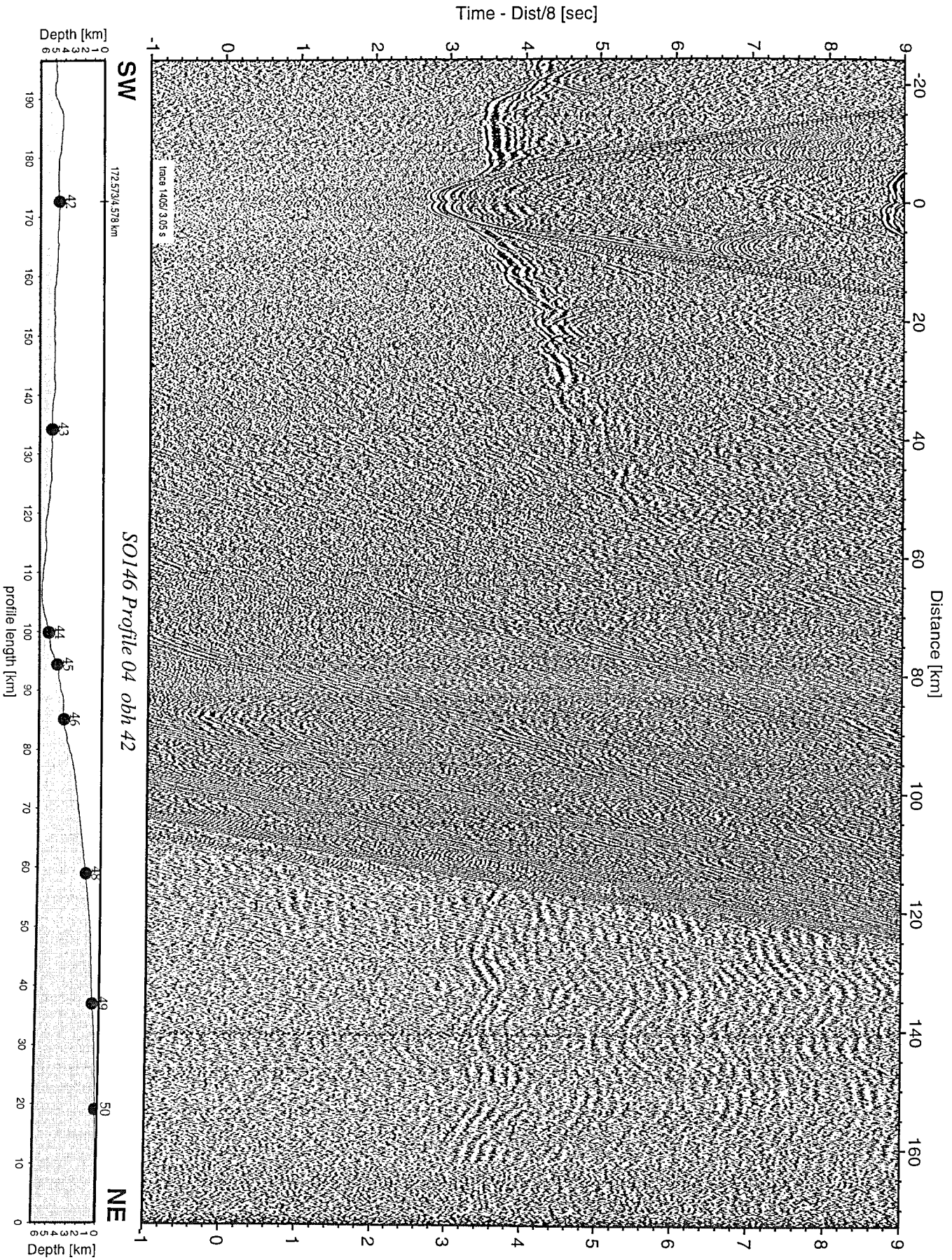

Figure 7.4.2: Record section from obh 42 , Profile 04.

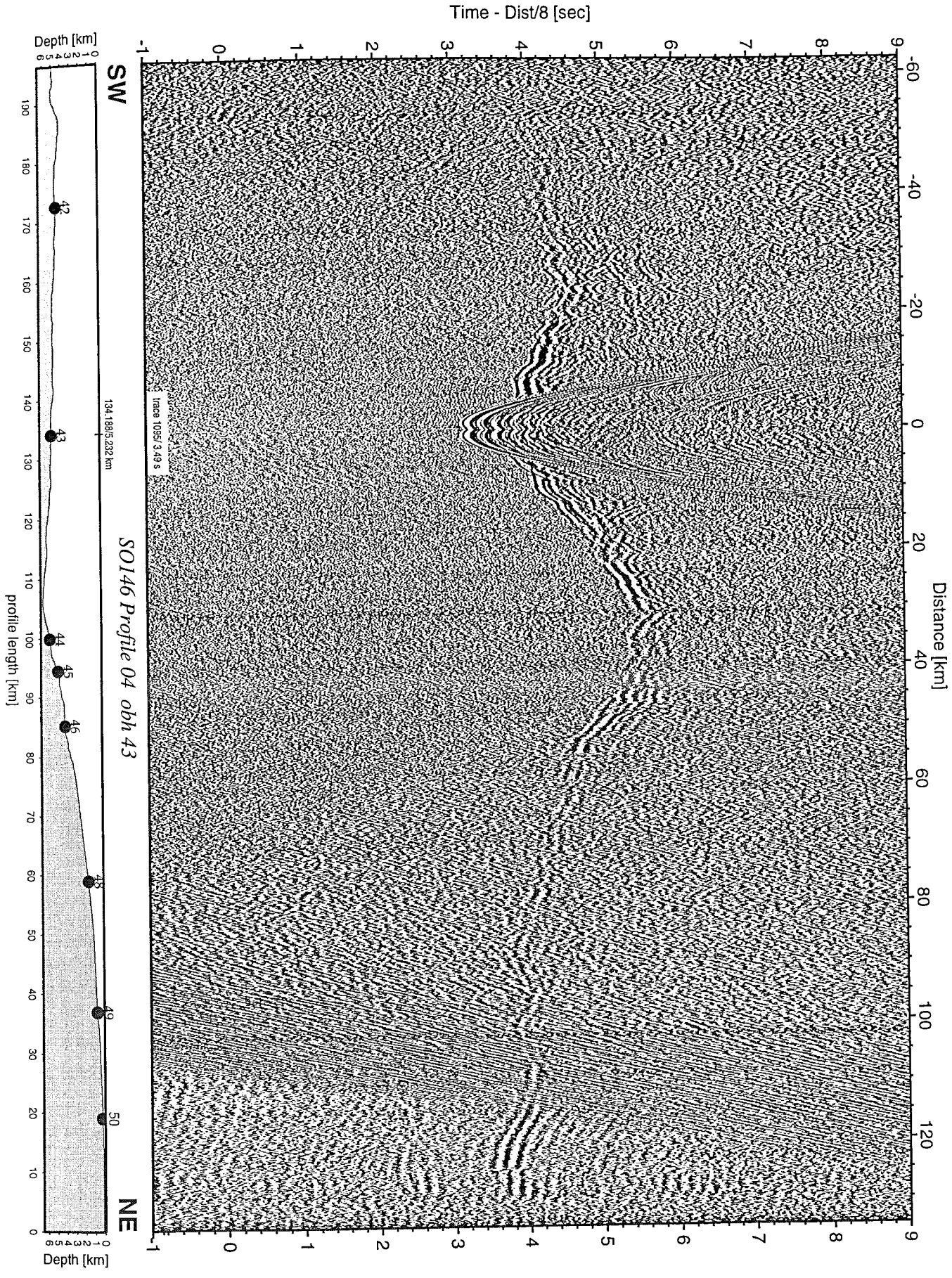

Figure 7.4.3: Record section from obh 43 , Profile 04.

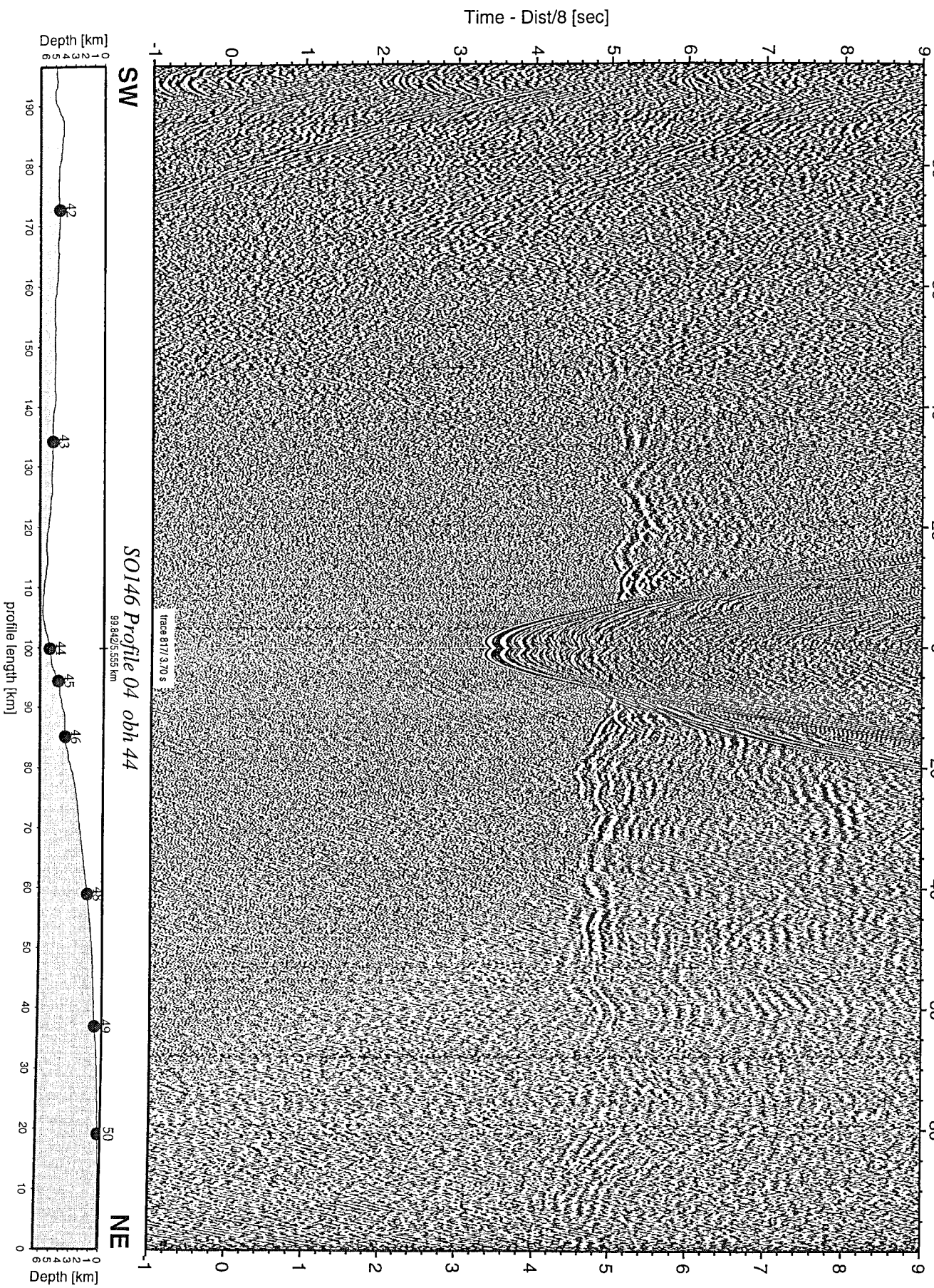

Figure 7.4.4: Record section from obh 44 , Profile 04.

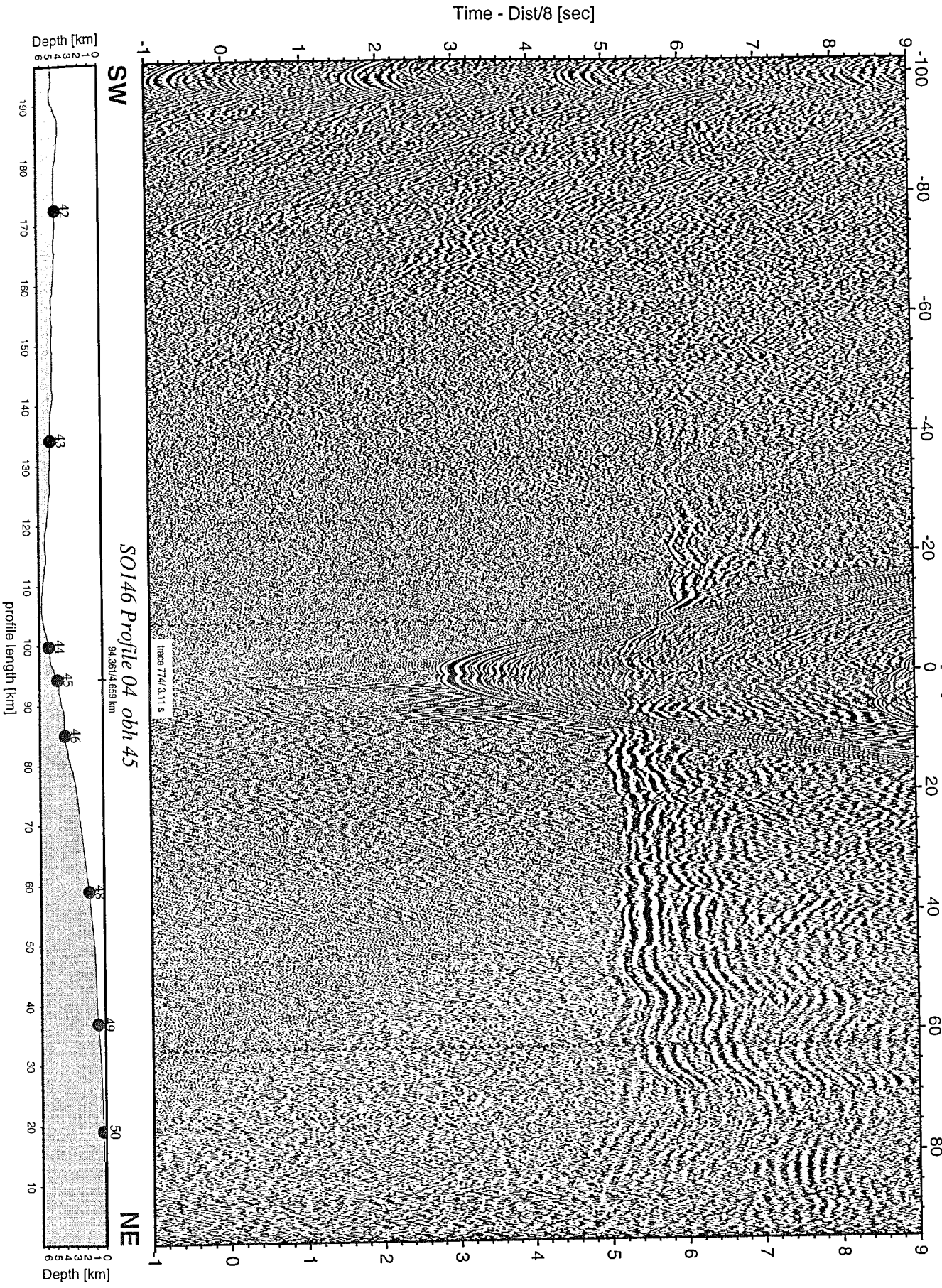

Figure 7.4.5: Record section from obh 45 , Profile 04.

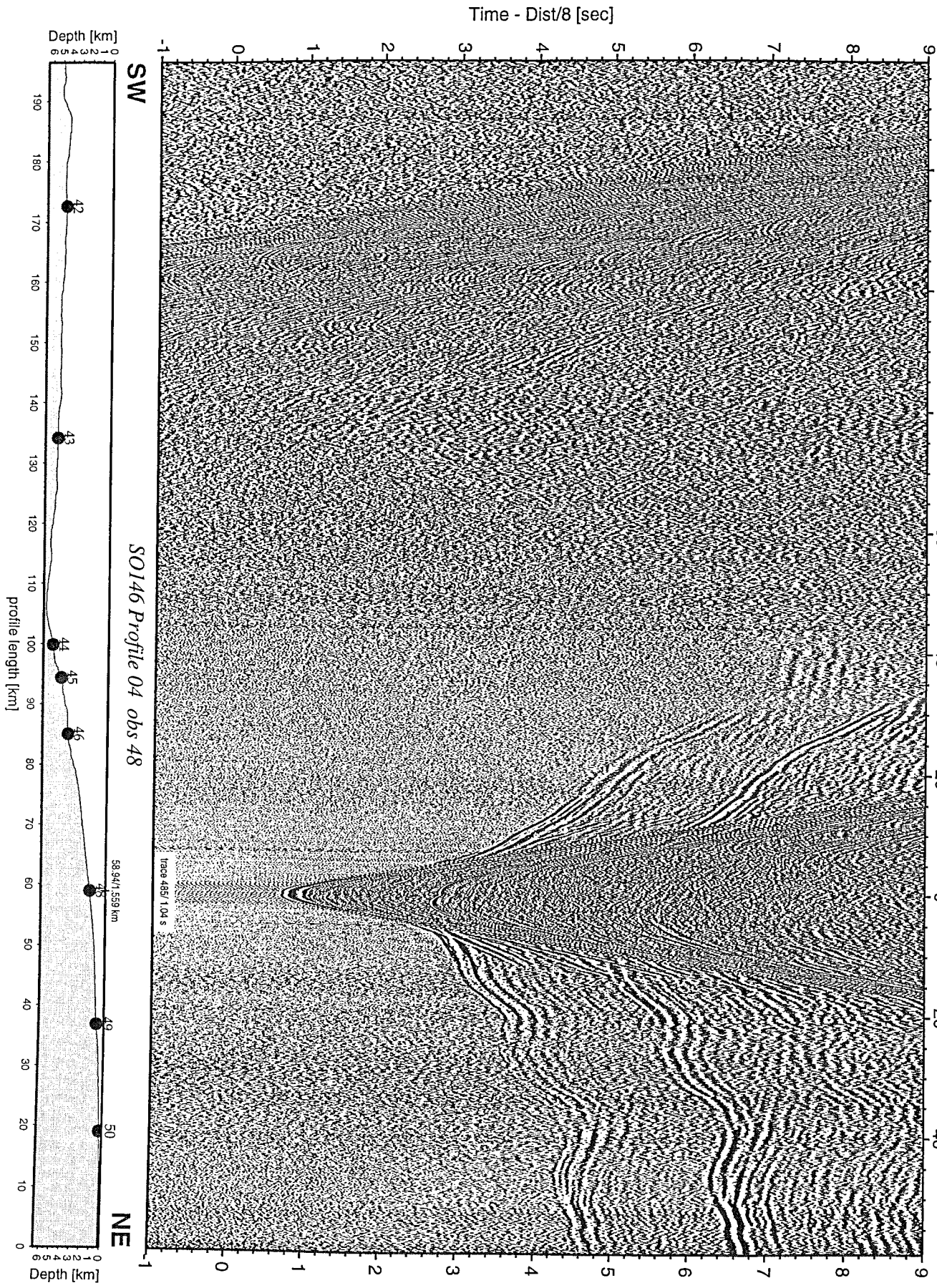

Figure 7.4.6: Record section from obs 48 hydrophone, Profile 04.

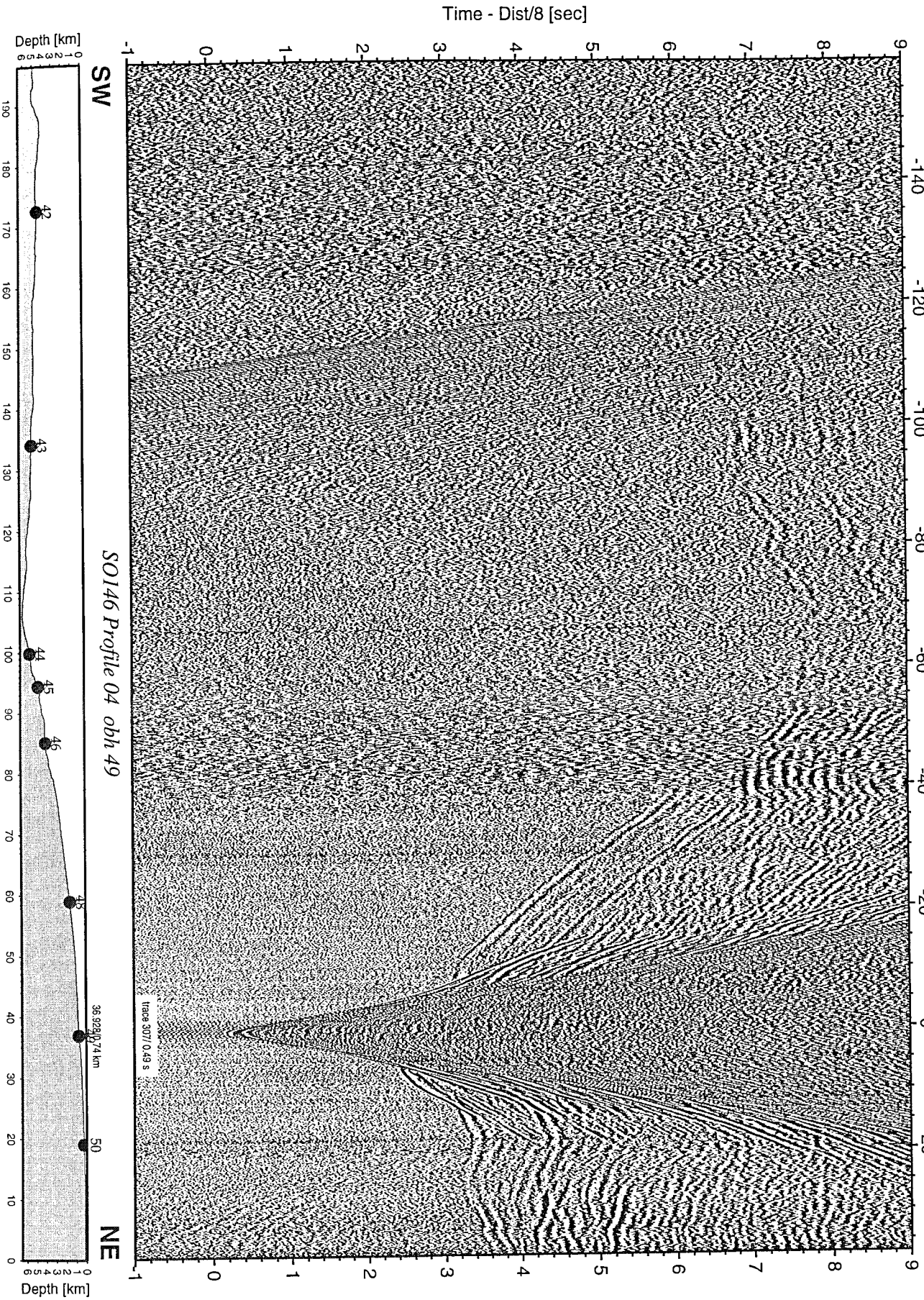

Figure 7.4.7: Record section from obh 49 , Profile 04.

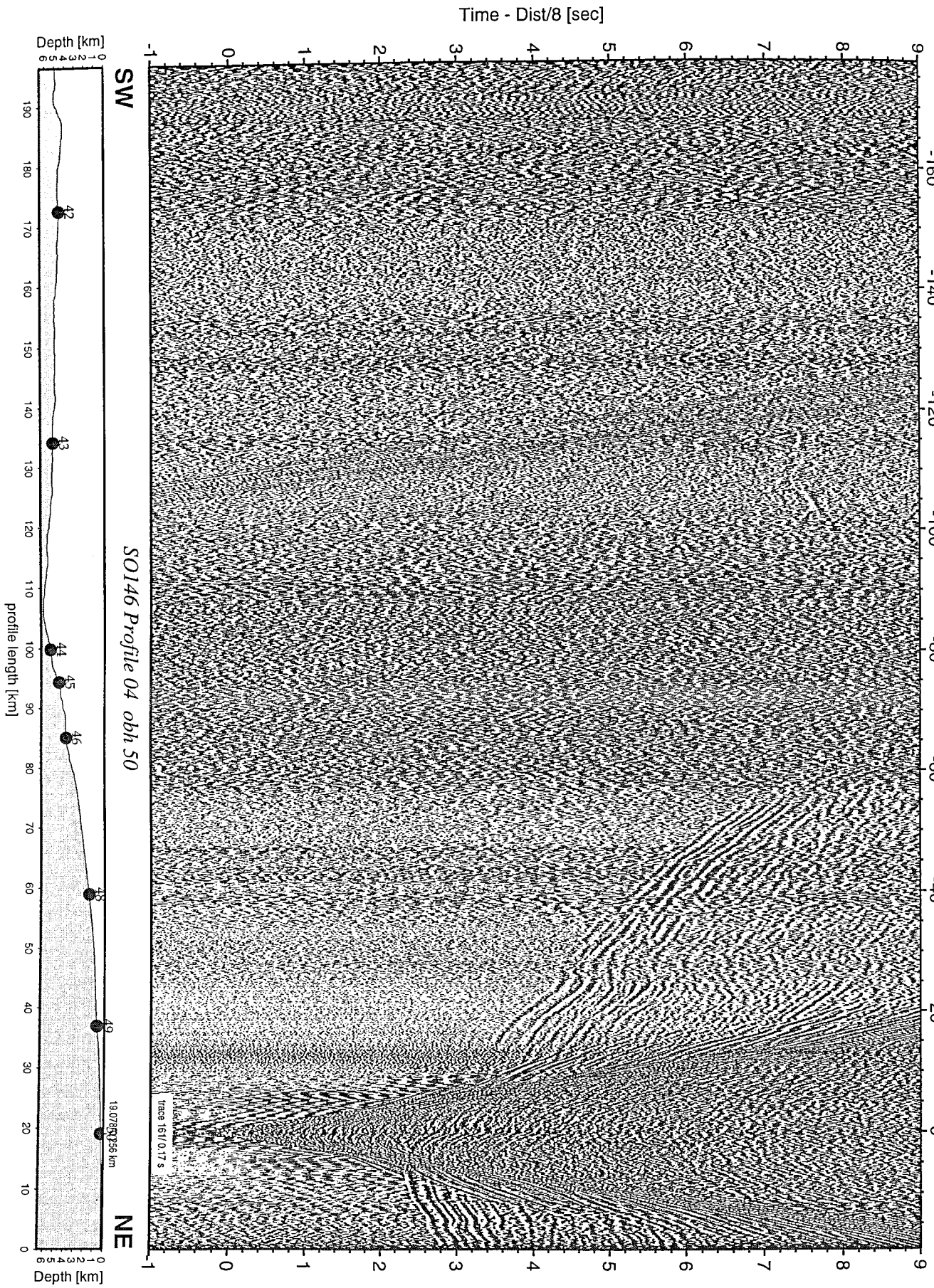

Figure 7.4.8: Record section from obh 50 , Profile 04.

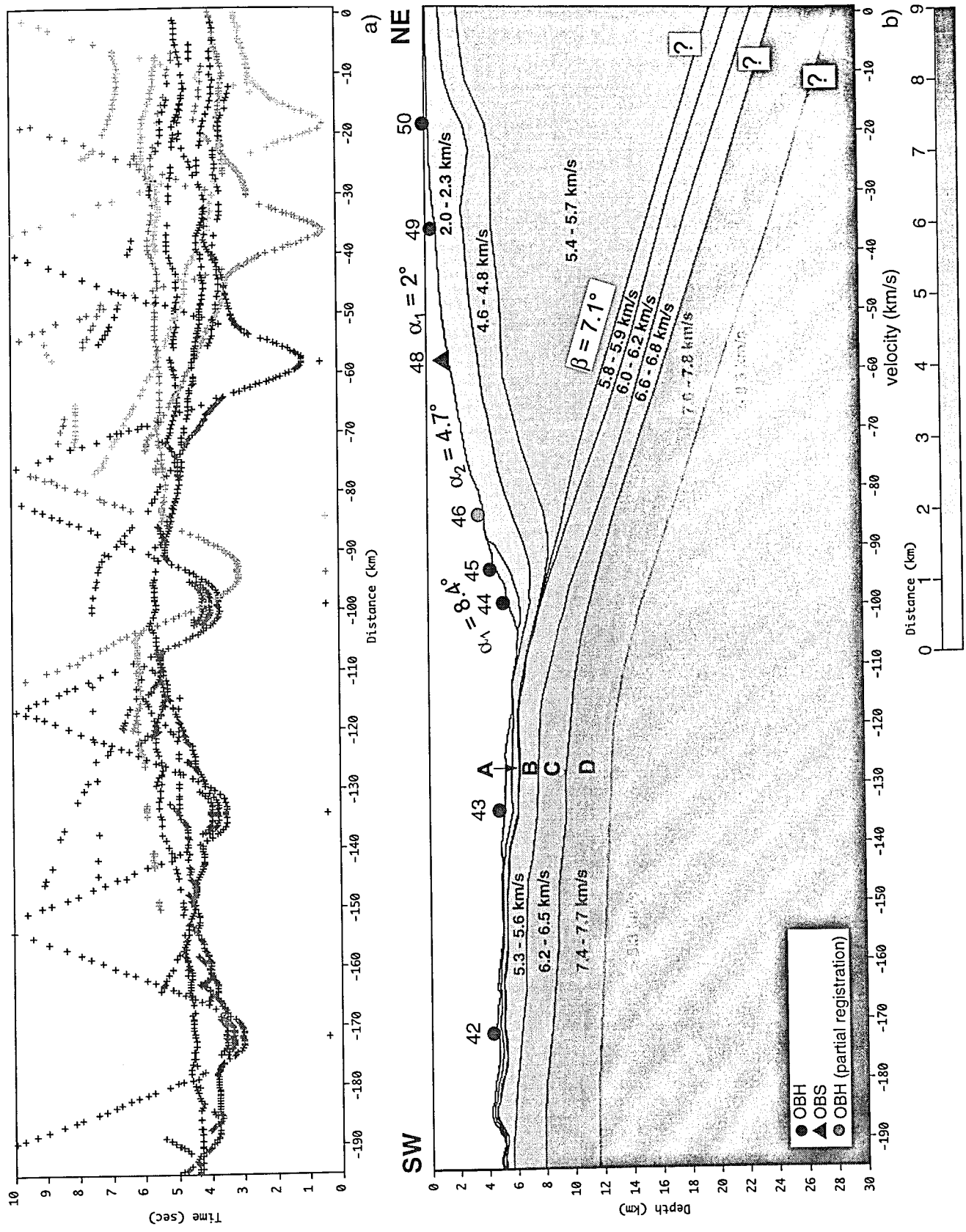

Figure 7.4.9: a) Picks extracted from the record sections of profile SO 146-04, b) crustal cross section for profile 04 derived from preliminary analysis of wide angle data.

7.5 Gravity and magnetics along profiles 2 and 3

(G. A. Dehghani, R. Heinbockel)

As described in chapter 6.5 (Figure 6.5.2) the gravity anomaly along profile 2 has a higher signal to noise ratio and shows a strong minimum of less than minus –150 mGal coinciding with the trench axis.

This minimum is not as well developed on profile 3 (Figure 7.5.1). The Free-air anomaly along profile 3 starts in the north eastern part with values of about 0 mGal, reaches a minimum of –90 mGal at kilometre 55 and a second minimum at approximately kilometre 130 with values of –115 mGal.
In the oceanic part of the profile the Free-air anomaly increases to values of about 0 mGal.
A relative positive anomaly with an amplitude of –50 mGal is observed at kilometre 70 along profile 3. This strong local anomaly is considerably smaller along profile 2.

Using the preliminary 2-dimensional seismic model we constructed a preliminary 2-dimensional gravity model along profile 2. We obtained the densities from modelled seismic velocities. The result is presented in figure 7.5.2. In the oceanic part of the model there is a very good agreement between the measured and the calculated values, whereas in the continental part calculated gravity values are higher than the measured anomaly, although both anomaly curves show the same general trend. The difference between the observed and modelled values could be caused by too shallow of an angle of subduction in the seismic model. Another possibility is a lateral change of densities between the continental and oceanic part of the profile.

The magnetic data of profile 3 also shows dipole anomalies but which are less developed than those observed in profile 2. The interesting feature of sea floor spreading anomalies observed on profile 2 are subdued along this profile. The strong positive residual magnetic anomaly with values of about 50 nT coincide with the relative maximum of Free-air anomaly at kilometre 70. The source of this anomaly could be intruded magmatic material.

Gravity and Magnetic Anomaly of Profile 3

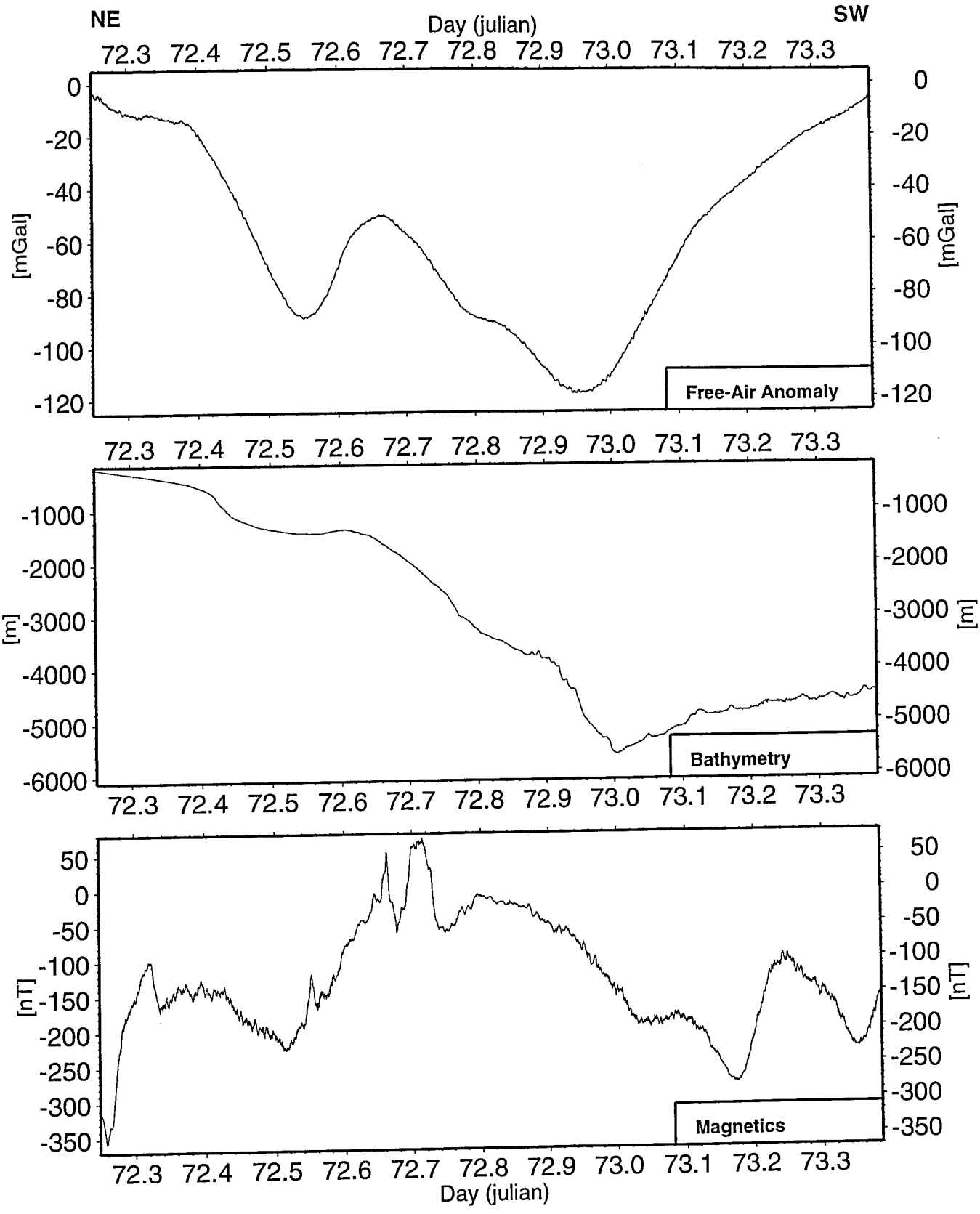

Figure 7.5.1

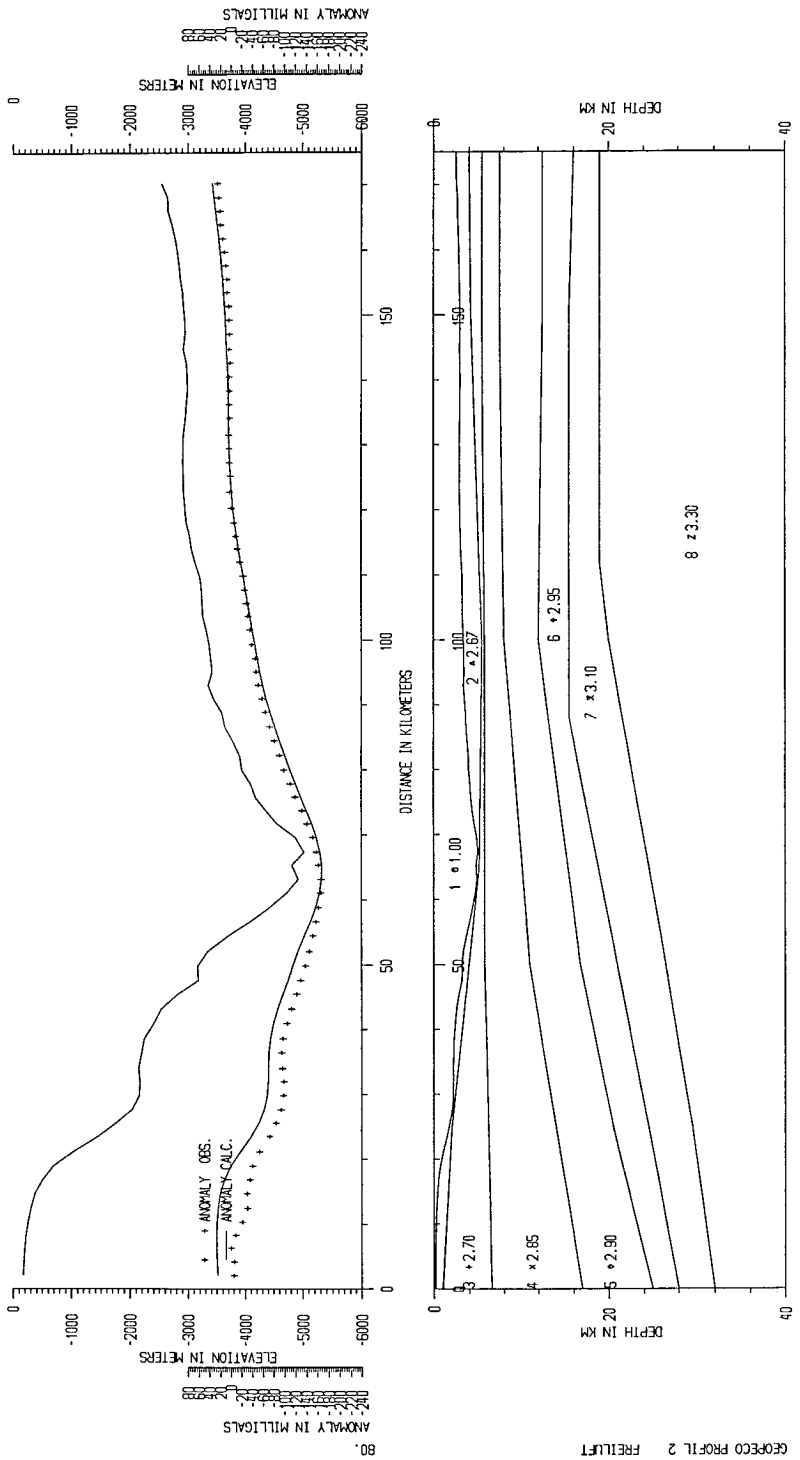
ANOMALY IN MILLIGALS
ELEVATION IN METERS
ANOMALY OBS.
ANOMALY CALC.
DISTANCE IN KILOMETERS
DEPTH IN KM
1 ρ1.00
2 ρ2.67
3 ρ2.70
4 ρ2.85
5 ρ2.90
6 ρ2.95
7 ρ3.10
8 ρ3.30
GEOFECO PROFIL 2 FREILUFT

Figure 7.5.2

7.6 Multichannel seismic

(C. Hübscher, M. Krüger, N. Kück, C. Wenz)

Overview

The seismic group of the University of Hamburg supported the Peruvian Forearc experiments in two different ways. First, we recorded the nearly vertical incident reflections during the wide angle / refraction measurements with our multichannel streamer. These data resolve the sedimentary layers of the oceanic crust and basin fill deposits of the continental slope. Due to the shot distance of 120 m and the short streamer we stacked shot gathers for interpretation. The large Fresnel zones and steep slope angles prevent detailed resolution of other slope features such as the accretionary prism. The mapping of sediment thickness, mainly on the oceanic crust helps to generate a starting model for ray tracing. The mapped basement topography gives useful constraints for modeling the subduction process in terms of frictional resistance.

Secondly, we acquired high-resolution multichannel seismic data in selected areas to support or supplement the deep seismic sounding lines and to learn about sedimentary and erosional processes acting on the slope. Line tracks are shown in Fig. 7.6.1.

13.5°S (southern Lima Basin)

The streamer recording of the BOLT-gun shots show the hummocky basement surface of the oceanic crust (HH00-004, Fig. 7.6.2). Flat structural highs are draped by pelagic sediments while steeper outcrops without deposits on the top are present. The high-resolution multichannel seismic lines HH00-005 and -007 cover the southern Lima Basin. The upper basin shoulder is an approximately 600 m high slump scar where diverging reflections are truncated (Fig. 7.6.3). This erosional horizon prolongs under the basin deposits, where it represents the upper boundary of an acoustic blanking unit. A disrupted BSR is present within the gassy sediments. The basin deposits onlap against a tilted block that represents the lower basin shoulder.

12°S (Lima Basin)

The simultaneously acquired streamer data (line HH00-024) from wide-angle / refraction line 4 illuminates the morphology of the oceanic crust and its tectonic faults at the early stages of subduction beneath the trench (Fig. 7.6.4). The basement undulates on a smaller scale than in the southern Lima Basin and is fully covered by sediments. Some large scale sedimentary structures are visible on the shelf, the Lima Basin and the lower slope basin. Since the basement is well exposed in this part of the line, sediment thicknesses can be estimated by using velocities from OBS/H data. MCS data from this area are described in chapter 9 (this volume). No data are available along WS/RS line 5.

8°S (Yaquina Basin)

Basement highs up to 1s TWT high with sediment pockets in between them characterize the oceanic crust in the Yaquina Basin (HH00-008, Fig. 7.6.5). This line exhibits the smallest sediment cover, indicating that the accretionary wedge is poorly developed. We extended this line seawards with high-resolution MCS line HH00-043 to map the transition from almost sediment free basement to the developing (hemi-)pelagic cover (Fig. 7.6.6). Significant sediments are present directly seaward of the basement depression at the end of HH00-008, basement undulations become smaller in height and width.

Peruvian Forearc Experiment

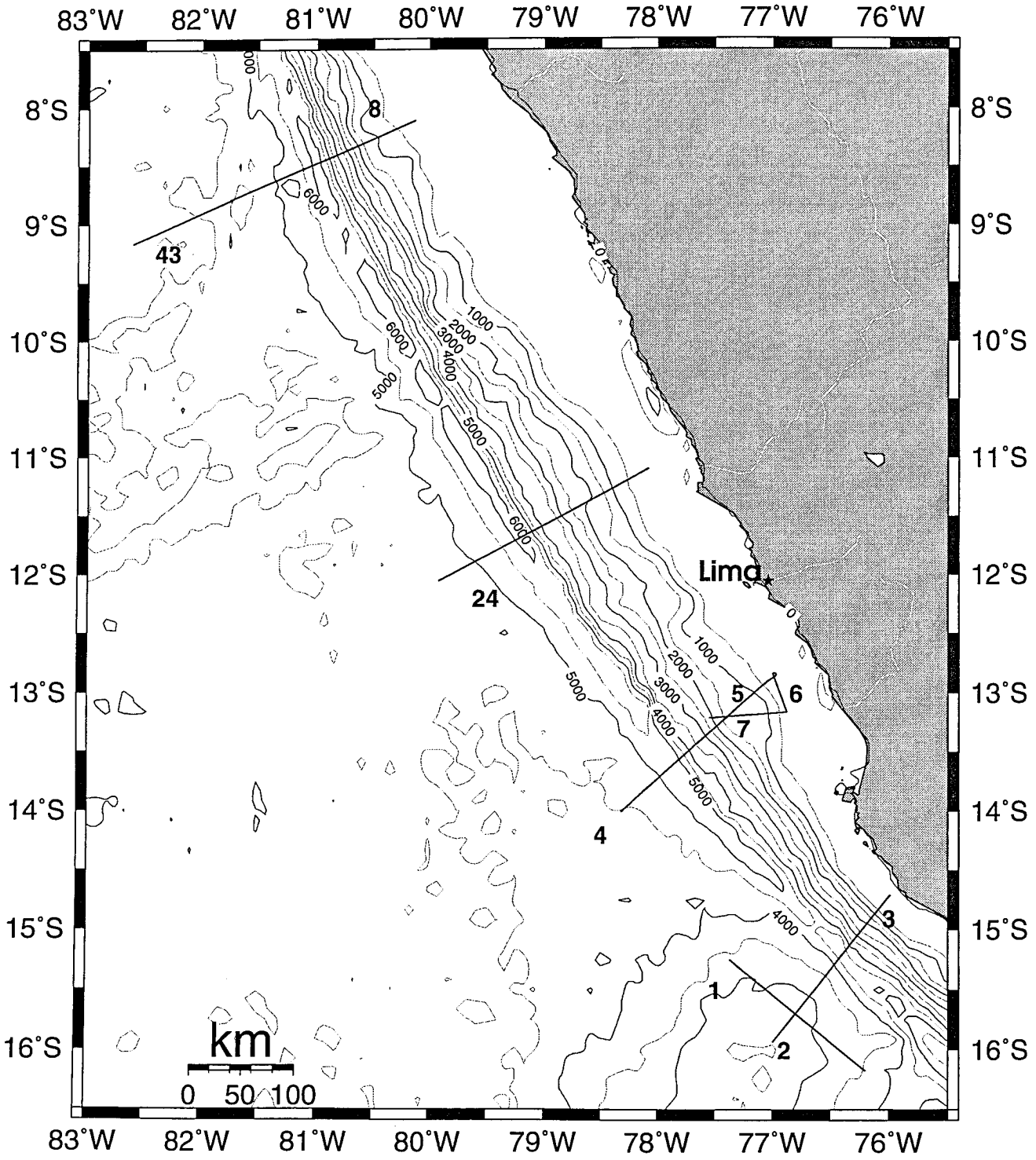

Figure 7.6.1: MCS lines from peruvian forearc experiment, bathymetry: gtopo30

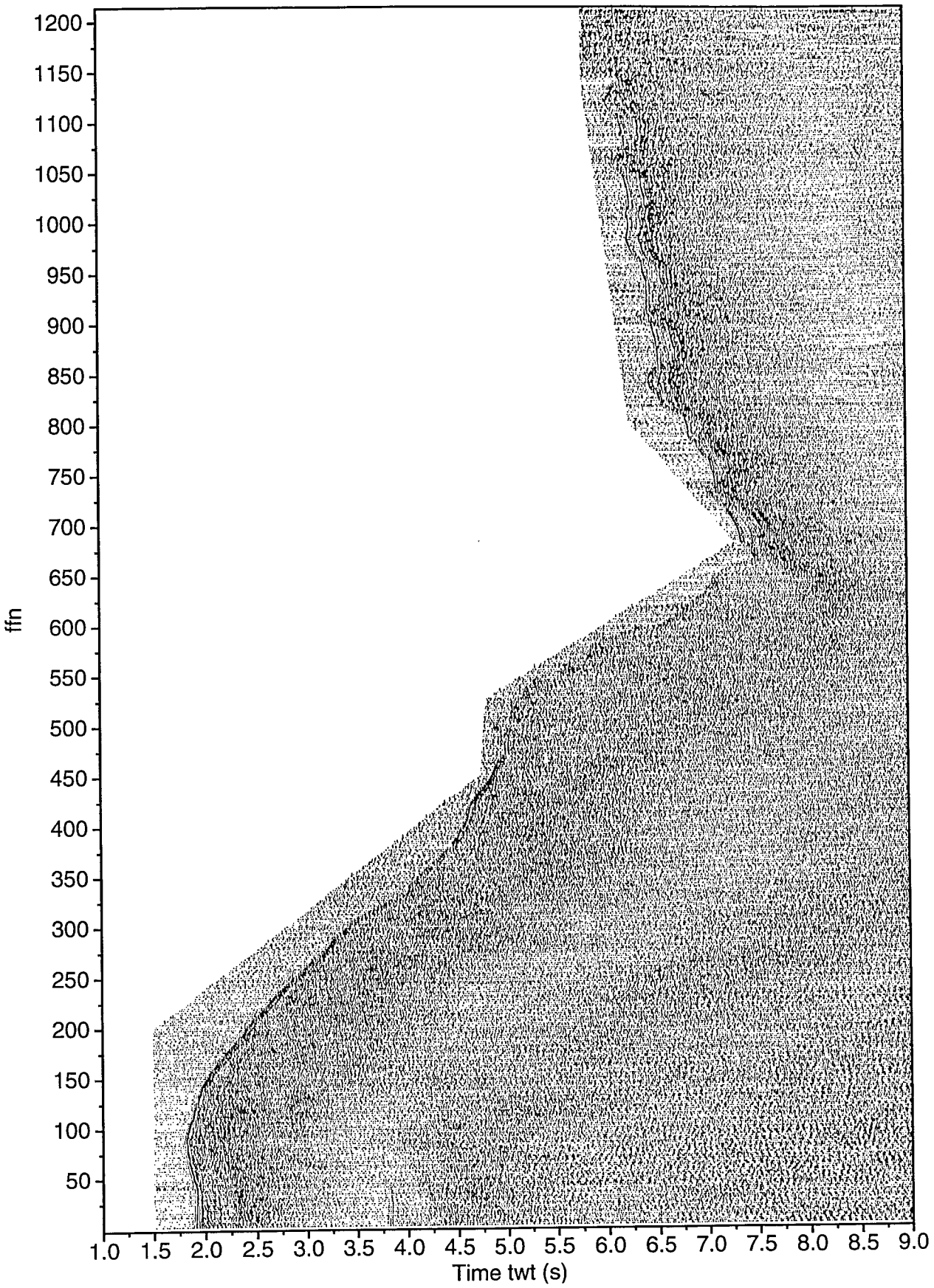

Fig. 7.6.2: Line HH00-004. Shotdistance 120m

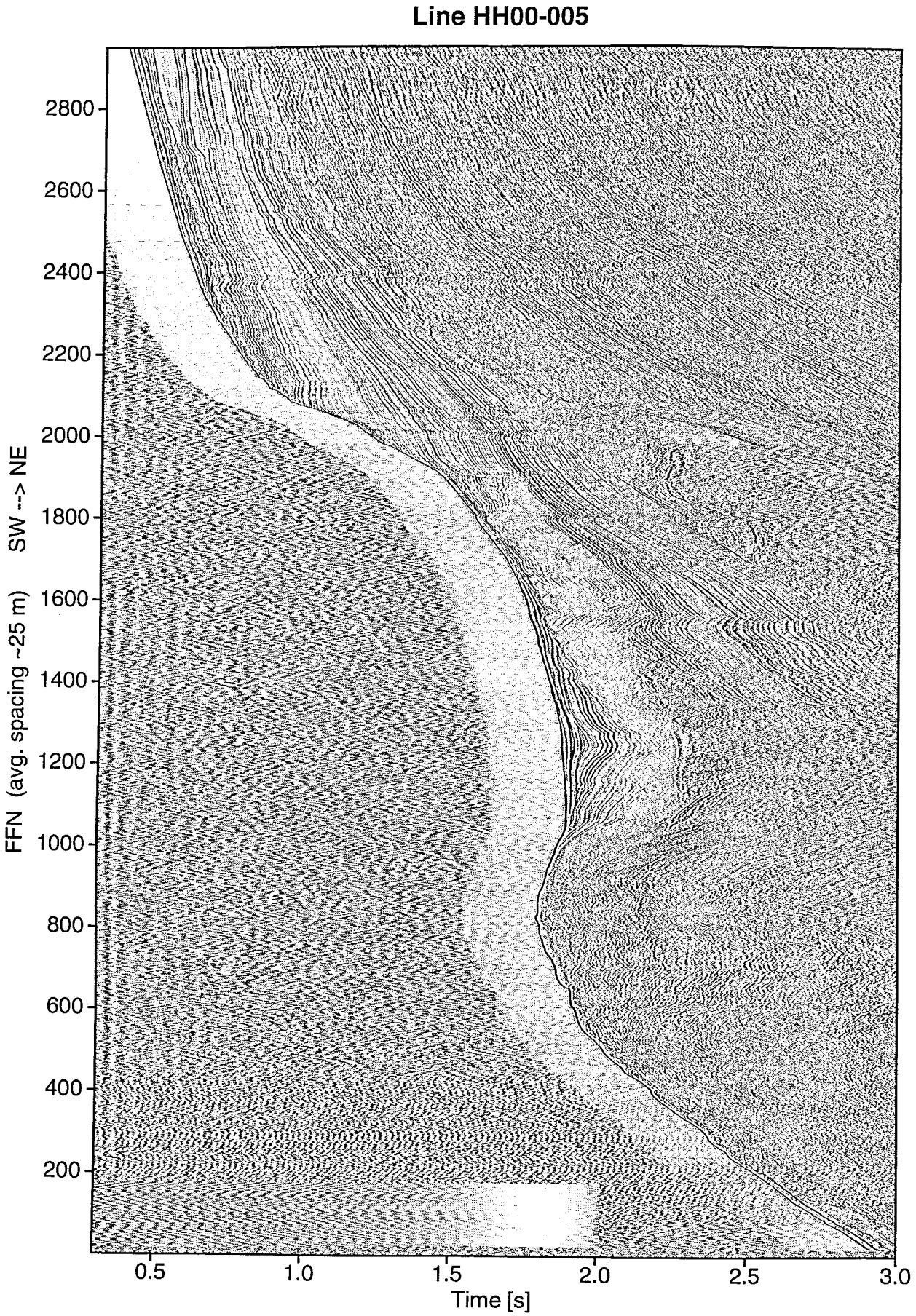

Fig. 7.6.3: MCS line 05. BP 10/20-150/200 Hz; Trace bal.; AGC 0.5 s.

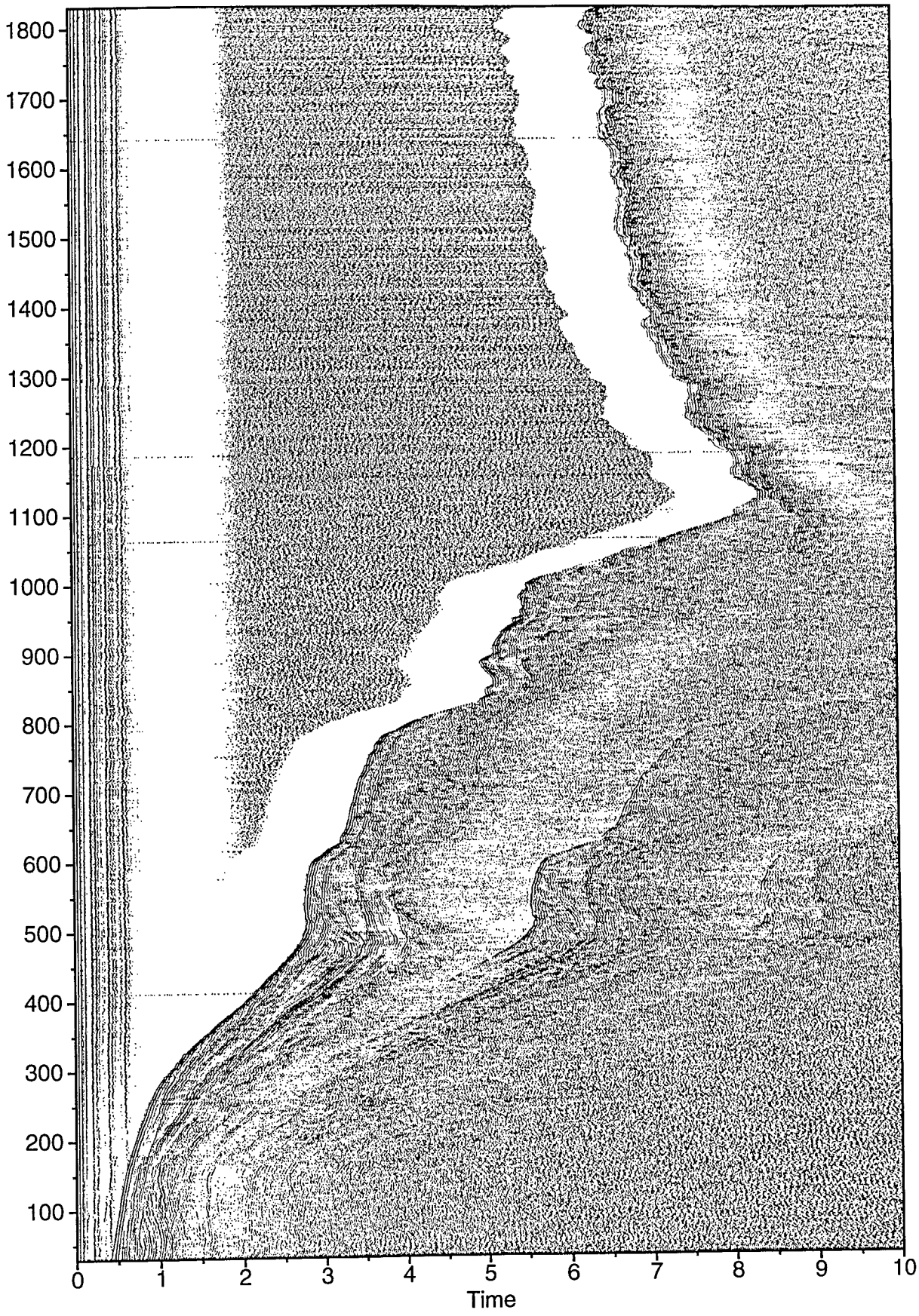

Fig. 7.6.4: Line HH00-024. Shotdistance 120m

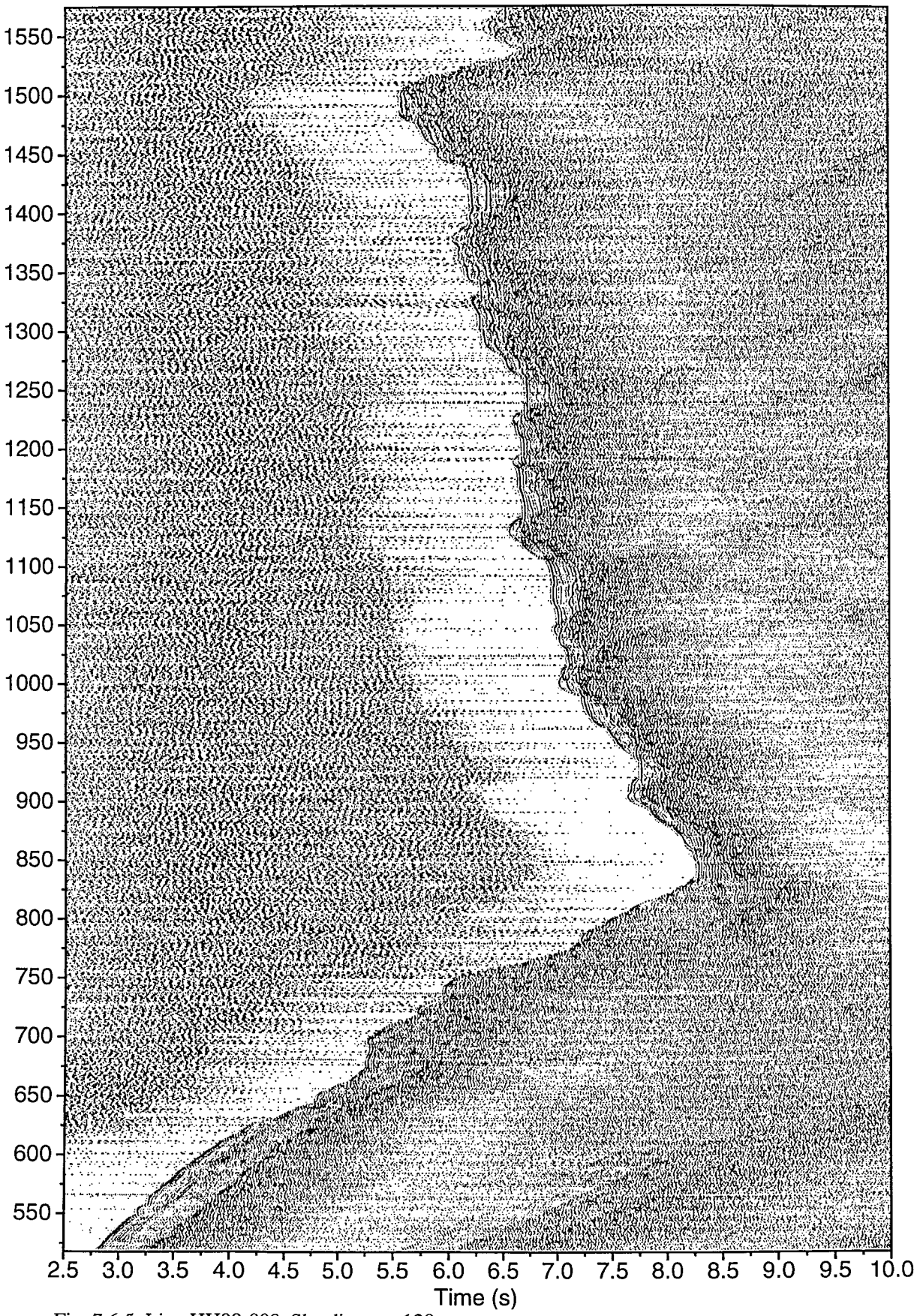

Fig. 7.6.5: Line HH00-008. Shotdistance 120m

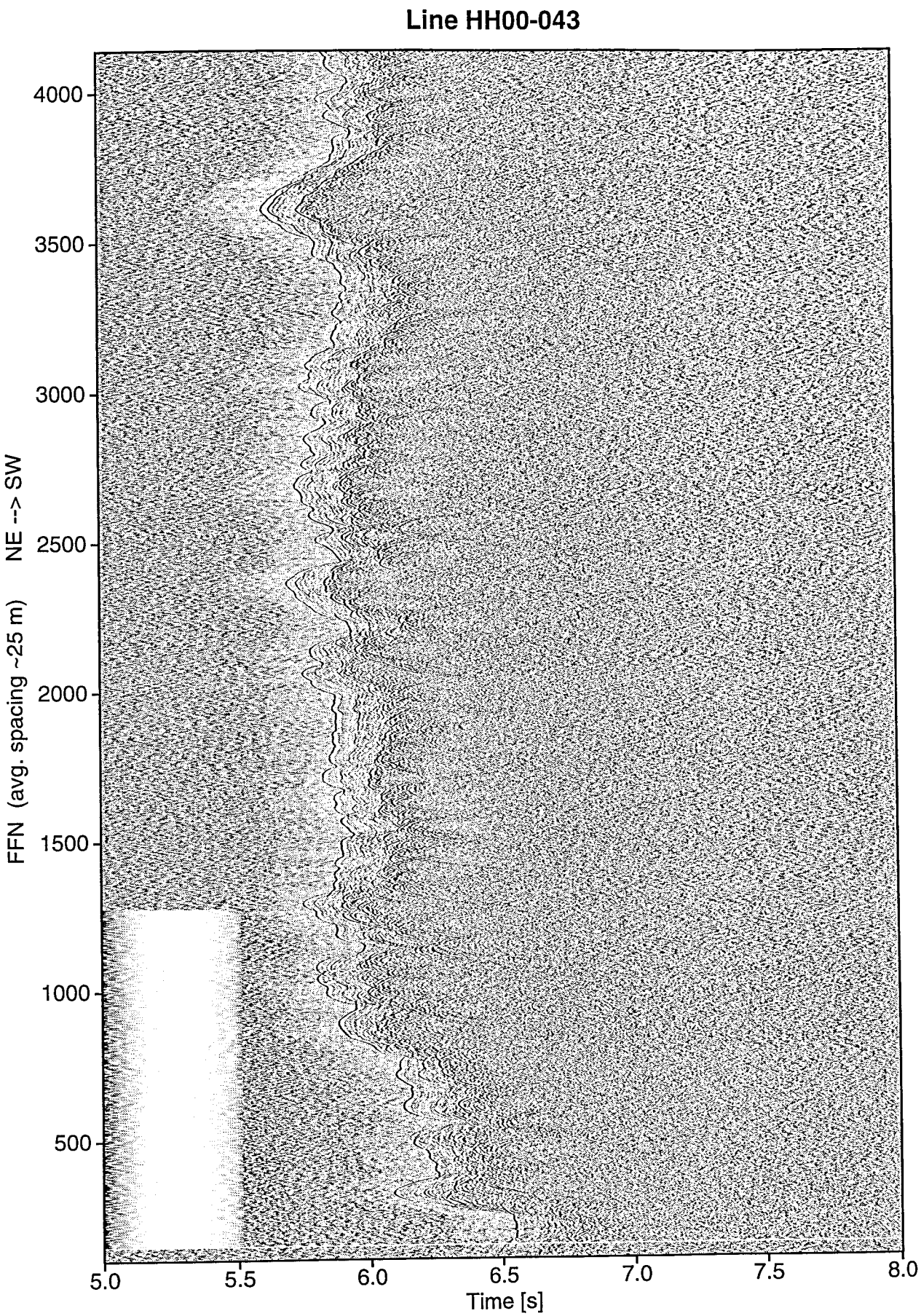

Fig. 7.6.6: MCS line 43. BP 10/20-150/200 Hz; Trace bal.; AGC 0.5 s.

7.7. Subduction along the Peruvian Margin

(J. Bialas, N. Kukowski)

Four wide angle seismic lines were shot across the Peruvian continental margin and span portions of the oceanic Nazca plate, the subduction trench, and shelf area. Two of these seismic lines have crosslines, one over the Nazca ridge the other across the Lima basin. The southernmost profile, line 2, is located along strike of the subducting Nazca ridge. Line 3 terminates at ODP location 687 and cuts the margin within the seismic gap area. Line 5 was shot some 250 km to the northwest and crosses the Lima basin. Line 6 was shot along strike of the Lima basin. North of the Mendana Fracture Zone, Line 4 crosses the lower and middle slope and terminates landwards of Yaquina basin. This set of seismic lines covers a range of 0 to 6 Ma after trespassing of the subducting Nazca ridge (v.Huene et al., 1996) and therefore allows the study of different stages of the accreationary development along this convergent margin.

Some remarkable features were revealed from preliminary ray tracing modelling of these wide angle refraction seismic lines. The four profiles crossing the Peruvian trench do not show a prominent accreationary wedge. Sediment coverage on the oceanic plate of all lines is thin and with respect to the multichannel seismic lines modelled with some 300 m thickness. Different from the other lines profile 2 along the subducting Nazca ridge does show a thickening of sediment towards the trench. This increase in sediment thickness corresponds with topographic highs identified on the bathymetry map. Their locations correlate well with rough seafloor topography found on cross profile no. 1 of the wide angle modelling and multichannel seismics. These features are interpreted as remnents of an earlier active and productive ridge. The homogeneous thickness of the sediment coverage on the lower slope indicates that there is no active accreation but sedimentation at high rates or due to young slumping.

Modeling of the of the subducted ridge to a depth of 27 km, indicates a subduction dip angle of 11.7°. These values are in good agreement with the dip angles 10° - 12° postulated by Spence et al. (1999) from the 1996-97 earthquake series. Obvoiusly, the thickended and more ridgid crust of the ridge is stronger bended beneath the trench with a still increasing dip at greater depth than the subducted Nazca plate further north (see below). The size and structure of the topographic highs are not resolved by wide angle modelling and do not indicate increased velocities. Due to the thin sediment coverage high apparent velocity events cover possible short range observations caused by these strucutres. Future detailed modelling of these features might yield more information about their nature. Nevertheless the constant sediment coverage across the trench continuing some 30 km landwards on the lower slope is still striking. Sediment coverage of the oceanic plate is not accreated and according to the velocity distribution of the raytracing model, complete subduction of sediments is assumed. The lower slope angle of 9.5° is very steep and slumping is possible. This might be one source for smoothly distributed sediments even accross the trench.

A different set of models is developed for the subduction of oceanic crust of Nazca plate to the north. Again thin sediment cover is found on the oceanic plate and does not increase until reaching the trench. In contrast to the Nazca ridge, a small accreationary wedge is observed on all three profiles. The size of the wedge, about 30 km wide and 2.5 km thick, is very similar on line 3 and 5, located south of Mendana fracture zone. Because only 2 Ma passed since ridge subduction took place at 13° S (Profile 3) the small wedge has been developed within a short time. The size of the wedge on profile 5 is similar to profile 3, although the ridge subduction took place some 4 Ma. The steepness of the wedge angle, or lower slope angle α_1, also differs along these three lines. Along line 2 and 5 the angle is measured with 9.5° whereas it is only 5.6° on line 3. One interpretation is that during ridge subduction and erosion of a possible earlier wedge, the lower slope is modulated by it's maximum steepness. After trespassing of the ridge, sediment accreation establishes a small wedge with small wedge angles during the early stages. With increasing thickness the angle again becomes steeper. After time has passed, the angle has reached it's maximum again and forces needed to continuously accreate become larger than the friction needed to subduct the sediment. This stage is tentatively

identified along line 5. On both profiles (3 & 5) the continental crust landwards of the wedge area is modeled with an upstep of the 4.0 – 4.5 km/s isoline. Wide angle modeling suggests that this step may form the back stop for sediment accreation. Comparison of the tapers along these three lines indicate high basal friction along the Peruvian margin. The highest taper value of 21° is found with the subducting Nazca ridge, from which a non aseismic subduction scheme is expected. The taper values of lines 3, 5 and 4, with 13°, 16°, 15°, respectively, all in the range indicating high basal friction (e.g. Davis et al., 1983; Kukowski et al., 1994; Gutscher et al., 1998). This non accreationary margin is consistent with the idea that sediments can more easily be subducted than accreated.

Models indicate that the crustal thickness for the oceanic plate along line 3 is 10 km. The velocity distribution along the line indicates that the oceanic Nazca plate is completely subducted or at most only small amounts of sediment might be accreated. To the north, along line 5 in front of Lima basin, the Moho could not be modeled from events identified during shipboard processing. Nevertheless, the crustal part again is interpreted to be completely subducted. Velocities used to fit the observed traveltimes with 2-D raytracing are remarkably low compared to velocities at the same depth on the other lines.

Farther to the north, line 4 was shot north of the Mendana fracture zone where a younger part of Nazca plate subducts under the continent. Nazca ridge passed this area some 6 Ma ago. With the exceptions of lines 3 and 5, sediment and basement do not show large undulations accross the slope area. Again, no sediment wedge accumulation along the continental slope close to the trench is observed. The oceanic Moho is modelled at a depth of 12 km, shallower than on the southern lines, but expected due to the 10 Ma younger age (28 Ma) of the oceanic crust compared to 35 Ma south of Mendana fracture zone. The subduction angle is only 6.7°. The lower slope angle is 8° compared to the 9.5° modeled at line 5. Differences were also found within the oceanic crust. Large scale horst and graben structures were found north of Mendana fracture zone where grabens are thinly infilled with sediments, relative to the other lines. These structures are modeled with the OBH/S data at the SW termination of line 4. The multichannel line (see chapter 8.1) shot out into the pacific ocean reveal a basement with rough topography but less pronounced than at the trench. Therefore the enhancement of these features is thought to be related to the bending of the plate when entering the trench area of subduction. These structures were not observed on the lines south of Mandana fracture zone. Nevertheless, on line 3, the top of oceanic basement is modeled with undulations of several hundret meters amplitude some 40 km seawards of the trench where the isovelocity lines indicate increased dip towards the subduction slab.

Remarkable differences are also found within the continetal slope area. The three lines south of Mendana fracture zone show some relief along the top of continetal basement. The shortest wavelength is modeled with the subduction of Nazca ridge which might be related to recent uplift of the margin (Hsu et al., 1992). Along line 3, the undulations are mainly reduced to the onstep landwards of the margin and a depression where the elongation of Lima basin is located. At this site, the basement has a depth anomaly of approximately 1 km. Water depth here is about 2000 m.

In contrast to the southern extension of Lima basin (line 3, 10 km width) the topography is less pronounced on line 5. The main part of Lima basin is 5 km wide and is 500 m deep. Water depth at this site is 2500 m and might therefore refer to increased subsidence of the margin within this area. Profile 6 was shot along strike of Lima basin to reveal it's structure in more detail. Wide angle modelling reveals an undulating sedimentary cover which might be related to varying water depth along the line. More remarkable though is the trough like shape at the top of basement, possibly indicating that Lima basin and it's southern elongation at 13° S are not directly related with each other.

To the North line 4 was modeled with a smooth basement top showing only one major depression with Yaquina basin.The structure is about 20 km wide and 2 km deep. Water depth is 500 to 1000 m. The differences found in the margin structure and crustal shape of the oceanic plate need further investigation. Nevertheless they imply, at first sight, that there are differences in the convergent margin to the North and South of Mendana fracture zone.

8 Yaquina Transect

8.1 Yaquina Basin

(C. Hübscher, R. Coman, C. Herold, N. Kück, M. Krüger, I. Pecher, C. Wenz)

Overview

In order to study the stratigraphy and distribution of gas and gas hydrate related seismic facies we surveyed the Yaquina basin between 8°00'S and 9°10'S. The survey was also designed to compare features observed here with the Lima Basin survey to the south. The main target was to investigate the interaction of tectonism, subsidence, and the presence of gas hydrates and BSRs. For a detailed discussion of the scientific objectives see chapter 9 (this volume).

The present knowledge about the stratigraphy of the Yaquina Basin is based mainly on seismic lines acquired in 1985 by the Hawaii Institute of Geophysics (HIG) (Ballesteros et al., 1988). These data cover the area between 8°50'S and 9°10'S. Five stratigraphic sequences have been defined ranging presumably from the middle Eocene to the late Pliocene-Quaternary.

Due to the high-frequency sources we used during both SO146 legs, the layers deposited since the late Miocene-Pliocene are best resolved. Our seismic lines extend the stratigraphy from ODP sites 683/684 (Leg 112) to the north and document the northward increasing abundance of gas and gas hydrate related facies. A narrowly spaced OBH/S survey was undertaken to unravel the nature of the severe cross stratigraphy reflections and to distinguish between lithological and non-lithological reflectors (see chapter 8.2). A map with seismic lines is shown in (Fig. 8.1.1).

Observations

The first MCS line we acquired in the Yaquina Basin was along WS/RS4 line (HH00-009). Sediment waves are present at the lower slope just above an erosional escarpment (Fig.8.1.2). At about 600ms TWT below seafloor a disrupted BSR coincides with a hummocky reflection unit. This BSR vanishes further upslope at shot number 1100. Internal reflections are sparsely resolved due to acoustic blanking. Between shots 1600 and 1800 a small depression with parallel fill deposits is observed. No clear BSR is seen in line HH00-011, however the hummocky reflection package from line HH00-009 extends beneath the depression. The same observation was made along line HH00-013, which covers line CDP-2 (Ballesteros et al., 1985) and ODP Site 683 (Fig. 8.1.3). The entire slope downslope of the depression gives clear evidence for seafloor erosion and slump scars. Line HH00-015 crosses the most shallow ODP Site 684 in the Yaquina Basin (Fig. 8.1.4). The data give similar information than HH00-013.

Our preliminary conclusion was that the development of gas and gashydrate related seismic facies occurrs between line HH00-009 and line HH00-013. As a result, we changed the planned track lines during the survey and condensed the seismic line network between these lines.

Seismic line HH00-016 fills the gap between HH00-013 and HH00-011. Most seismic features in this line have lithological origin, no BSRs are present. The shelf parallel line, HH00-017, covers a paleo-canyon with parallel to subparallel infill deposits. The canyon shoulders are faulted, and a parallel layered sediment cover creates the smooth seafloor topography (Fig. 8.1.5). The first BSRs appear in line HH00-019, they coincide with the hummocky reflections as observed previously (Fig. 8.1.6).

A wide variety of BSRs and other gas caused seismic features such as blanking, acoustic turbulences, velocity pulldowns and structural highs (the chemoherms, see chapter 8.3, this volume) are observed in line HH00-020 (Fig. 8.1.7). In order to unravel the origin of these seismic features and facies a detailed survey was planed (see below). During Leg 2 this line was the target of OFOS and heat flow experiments to increase our understanding of the nature and surface expression of gas and BSRs in this unique environment. We choose this line because the abundance of different seismic features decreases further north, where acoustic blanking dominates the data in water depth greater than 600 m (Fig. 8.1.8).

In order to unravel the origin of the structures observed in line HH00-020 we designed an OBS/H and MCS survey in this vicinity. We deployed OBS instruments in the crucial areas and decreased the recorder distance with OBH instruments (see chapter 8.2, this volume). Four MCS lines cross the OBS sites parallel to the slope (HH00-034, -036, -038, -040), line HH00-042, on which the OBH are placed, runs along HH00-020. Several disrupted high-amplitude reflections with a phase shift of Pi can be seen in line HH00-036 at different depths (Fig. 8.1.9). The negative reflection coefficients is not fully understood because acoustic blanking, the main indication for gassy sediments, is present above and below these reflections. Basically line HH00-038 exhibits similar structures. Some peculiar reflections cross the stratigraphy in line HH00-040 (Fig. 8.1.10).

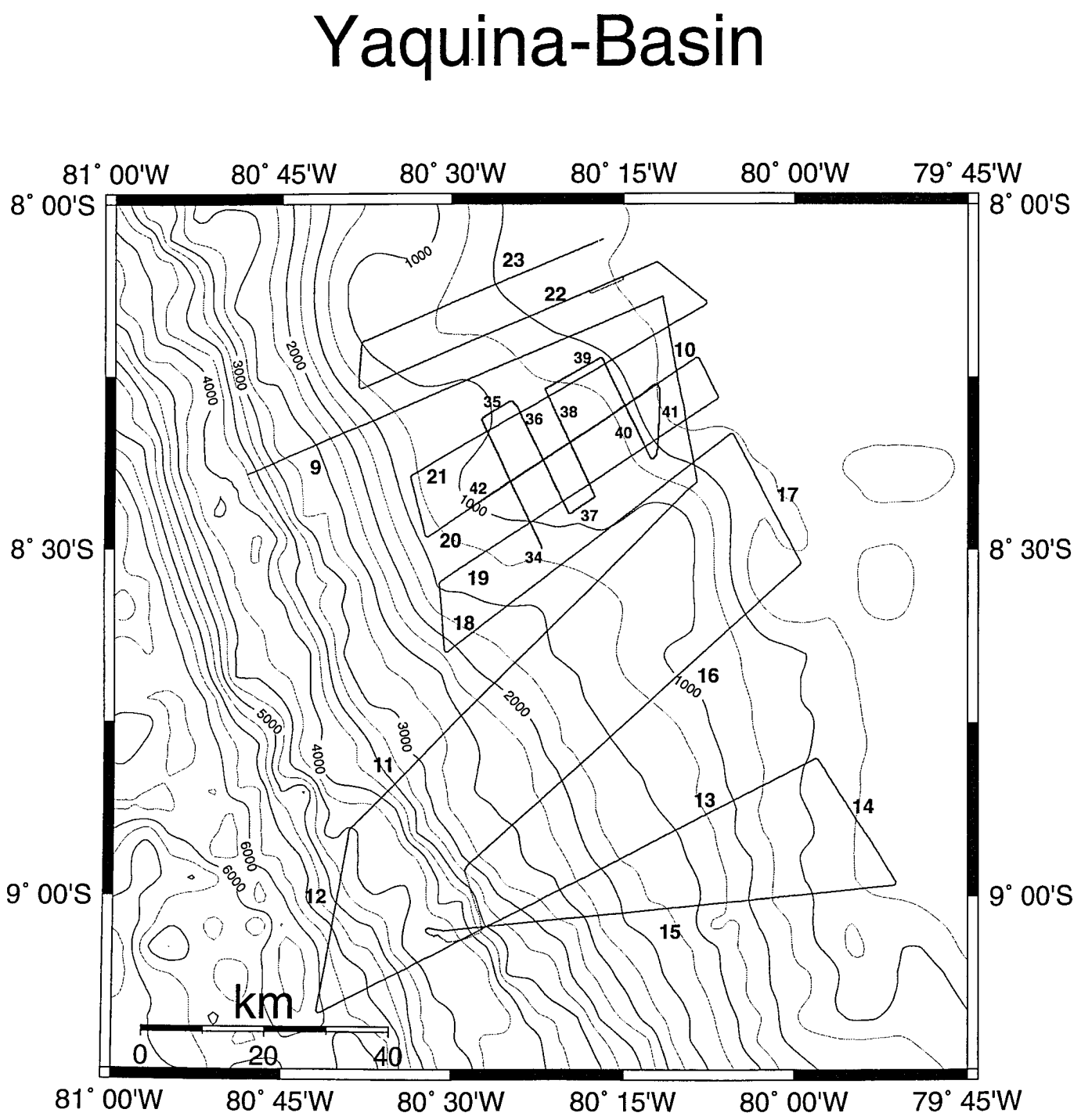

Figure 8.1.1a: Seismic lines Yaquina Basin, bathymetry from gtopo30

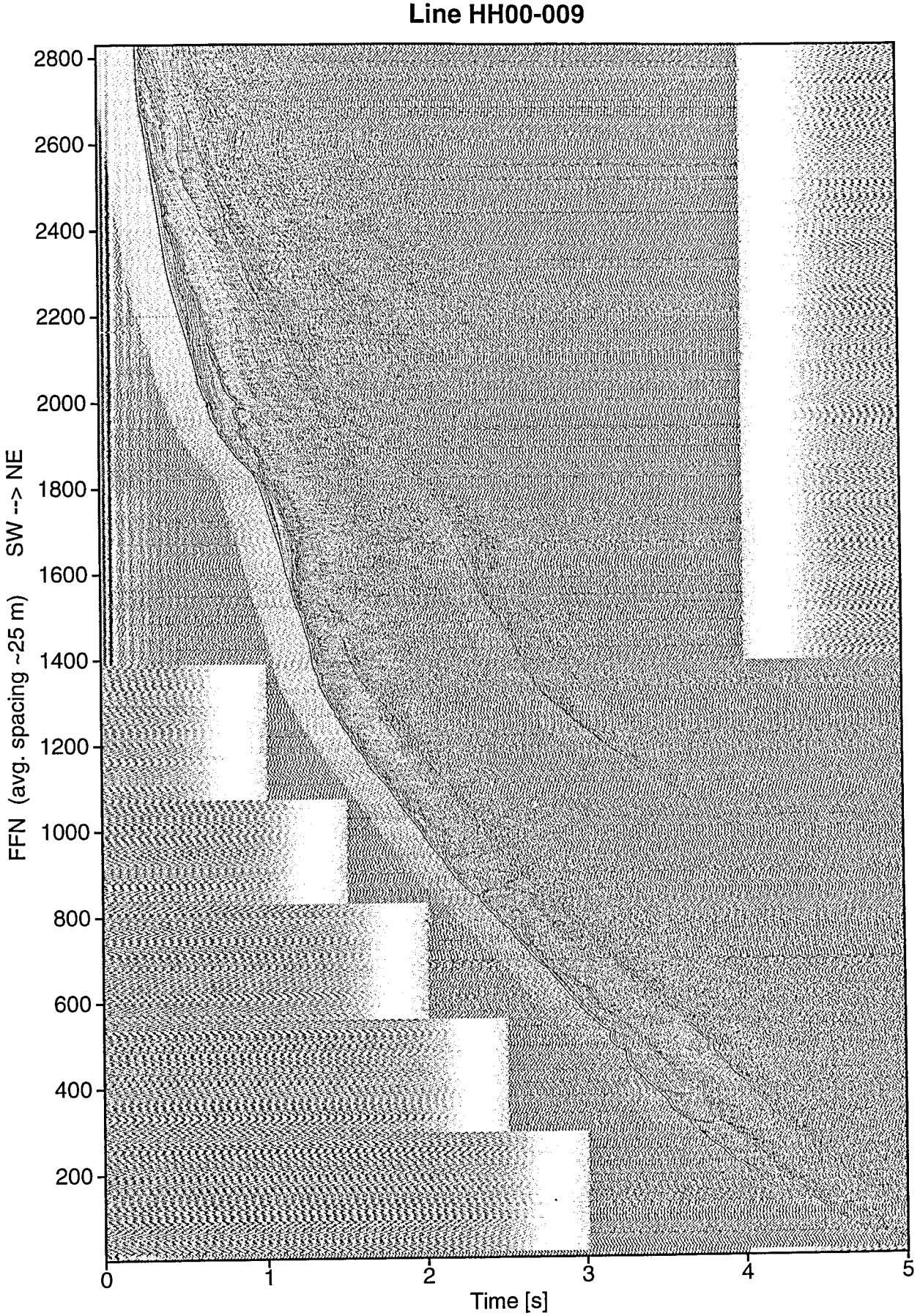

Fig. 8.1.2: MCS line 09. BP 10/20-150/200 Hz; Trace bal.; AGC 0.5 s.

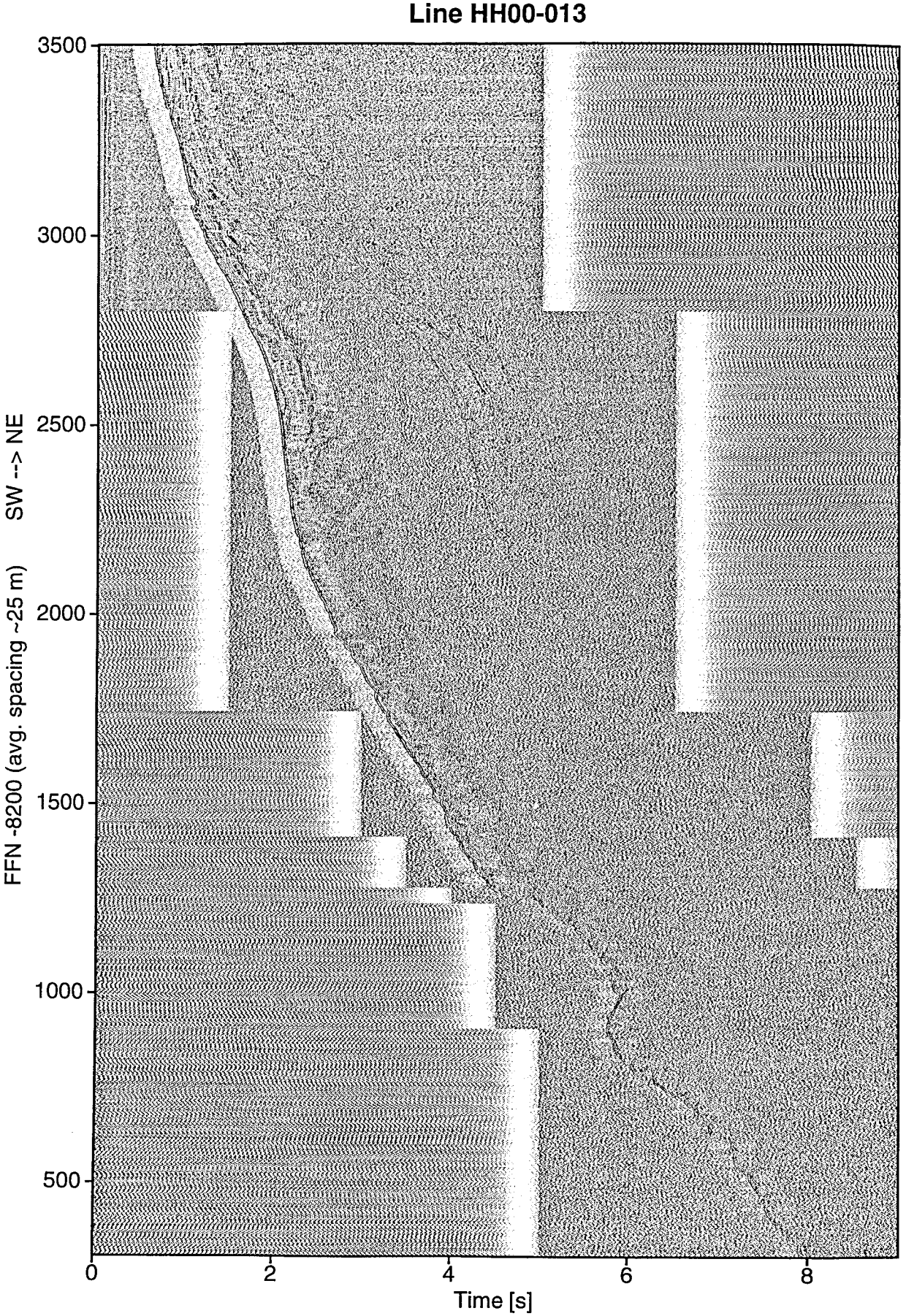

Fig. 8.1.3: MCS line 13. BP 10/20-150/200 Hz; Trace bal.; AGC 0.5 s.

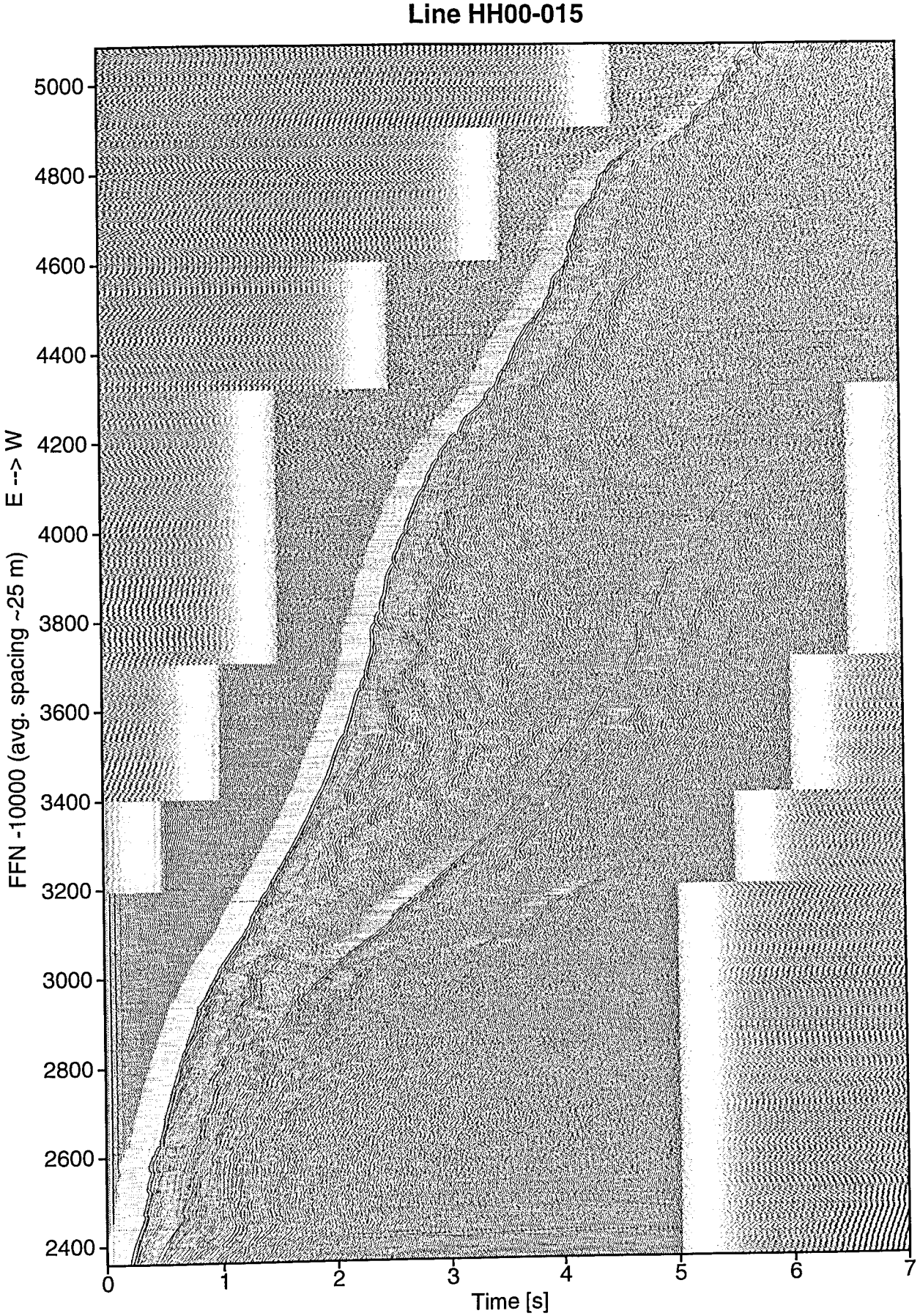

Fig. 8.1.4: MCS line 15. BP 10/20-150/200 Hz; Trace bal.; AGC 0.5 s.

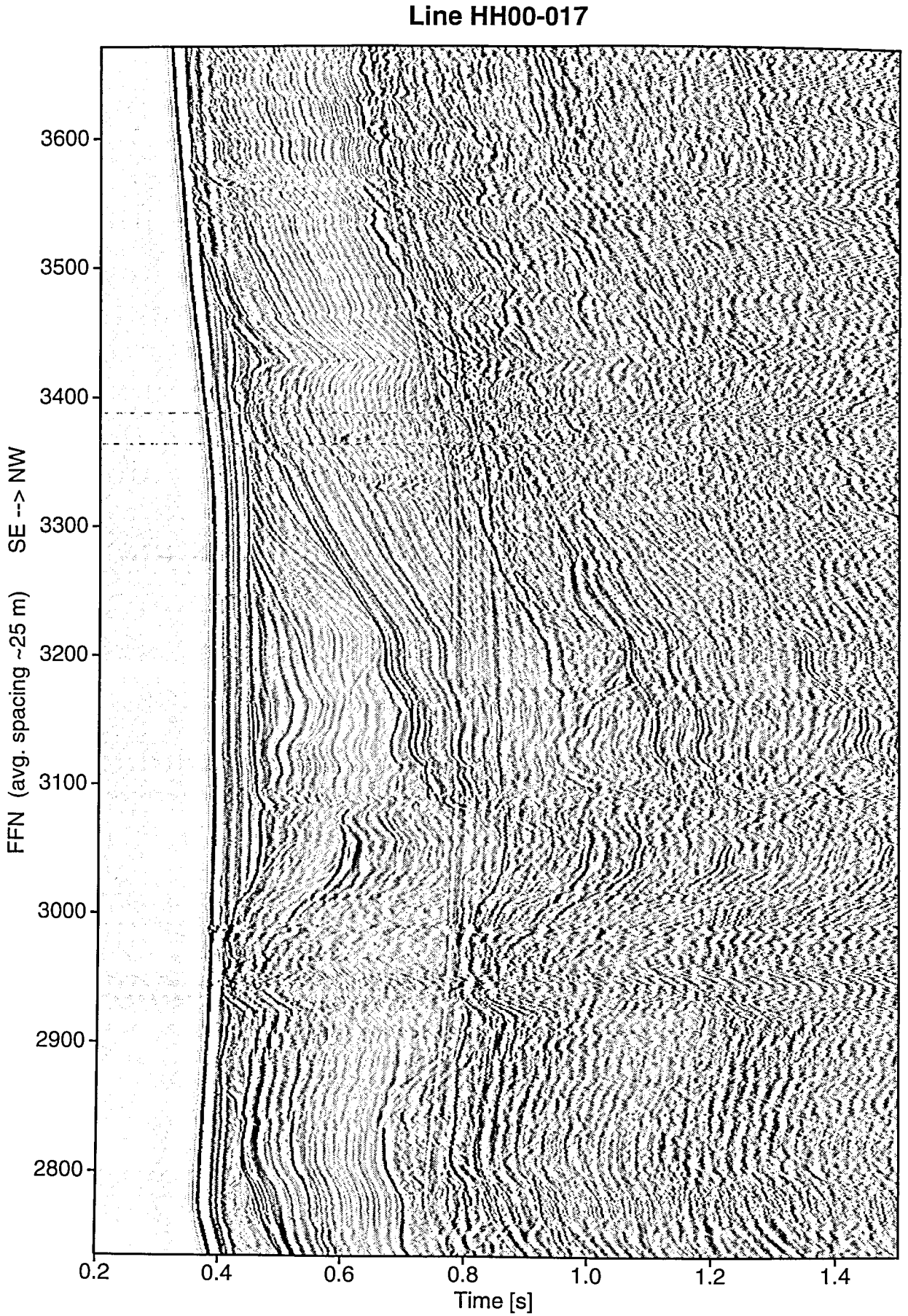

Fig. 8.1.5: MCS line 17. BP 10/20-150/200 Hz; Trace bal.; AGC 0.5 s.

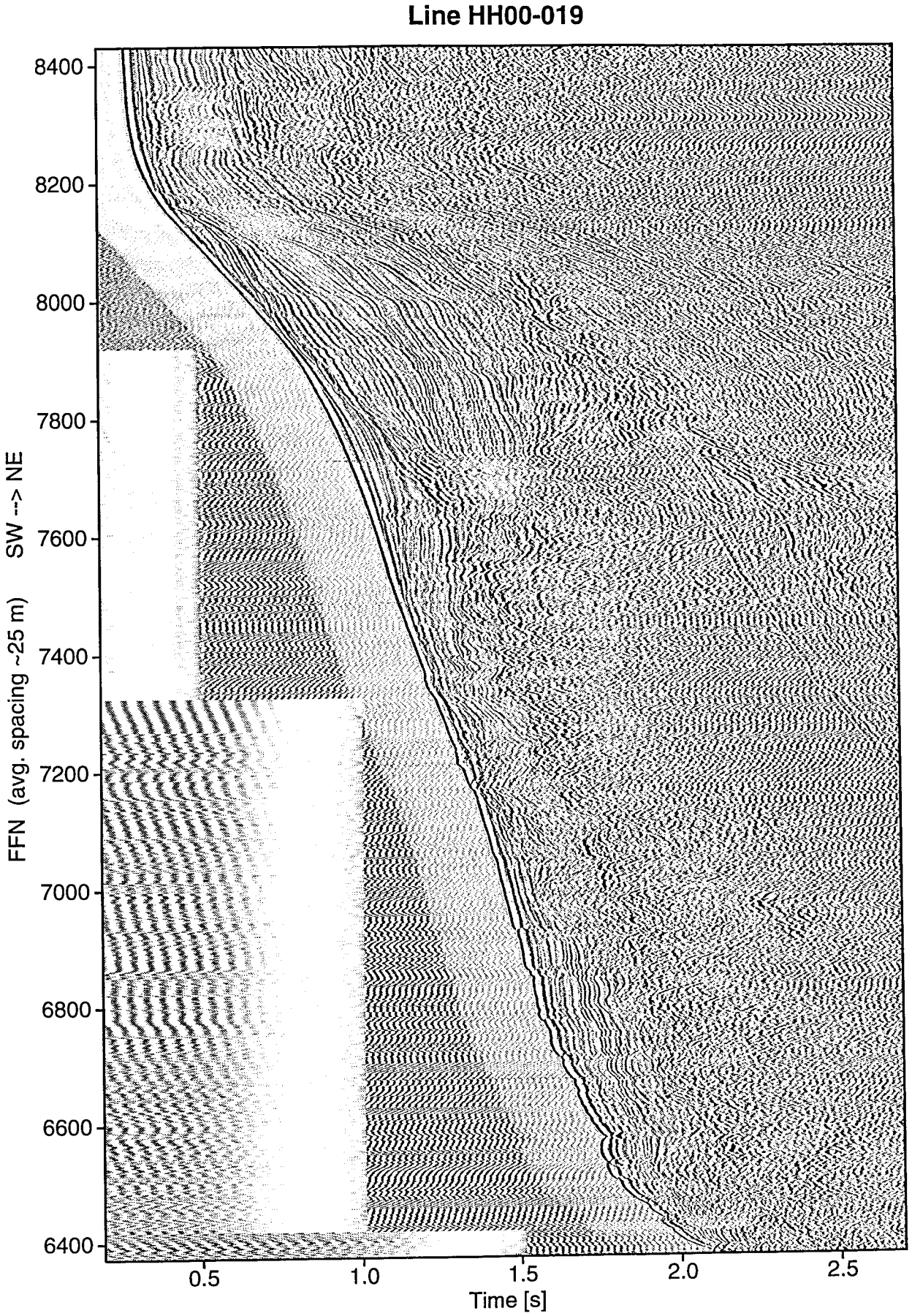

Fig. 8.1.6: MCS line 19. BP 10/20-150/200 Hz; Trace bal.; AGC 0.5 s.

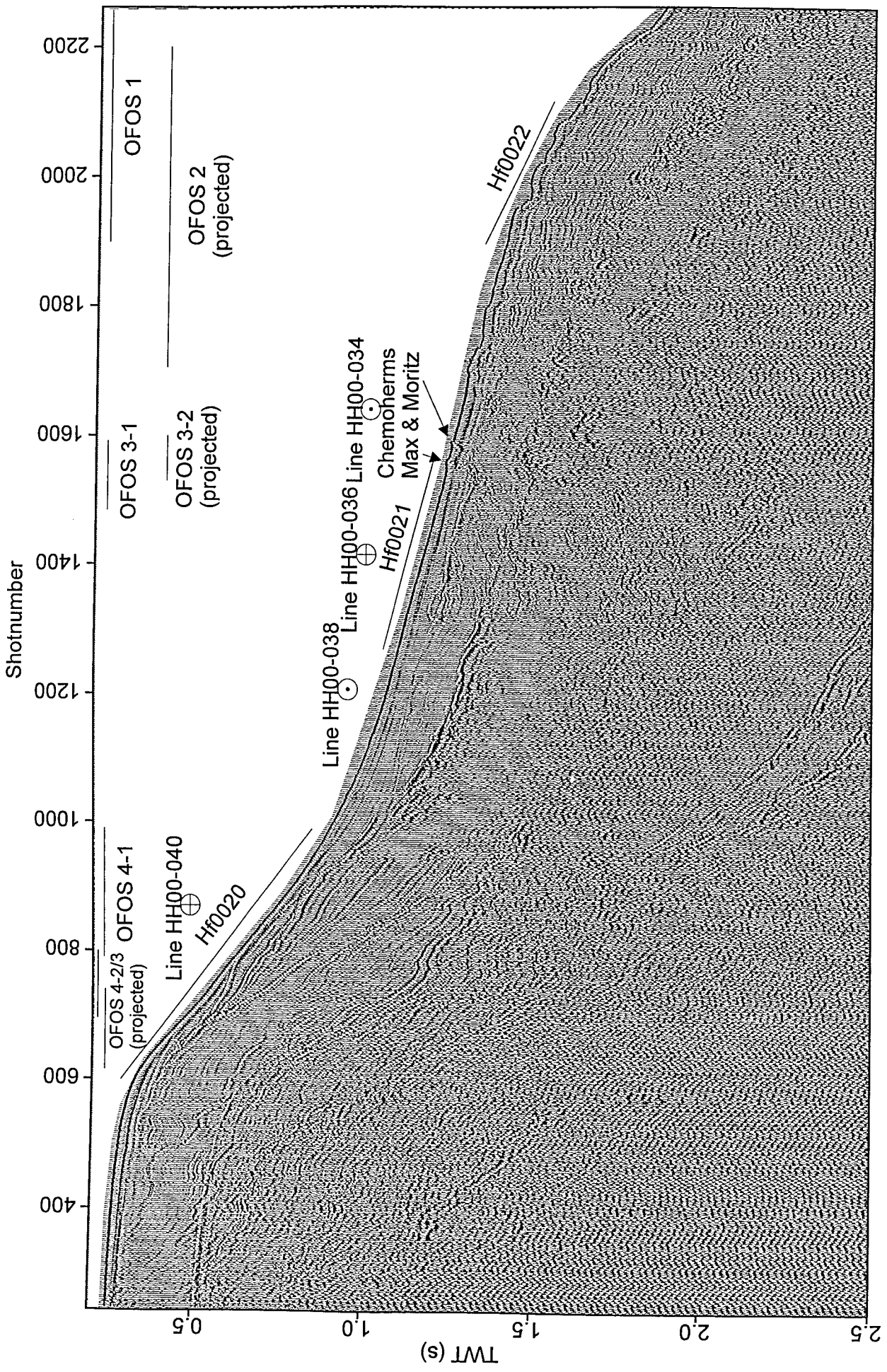

Fig. 8.1.7: Line HH00-020 with OFOS and heat flow locations. The cross points of line HH00-034, -036, -038, -040 are marked.

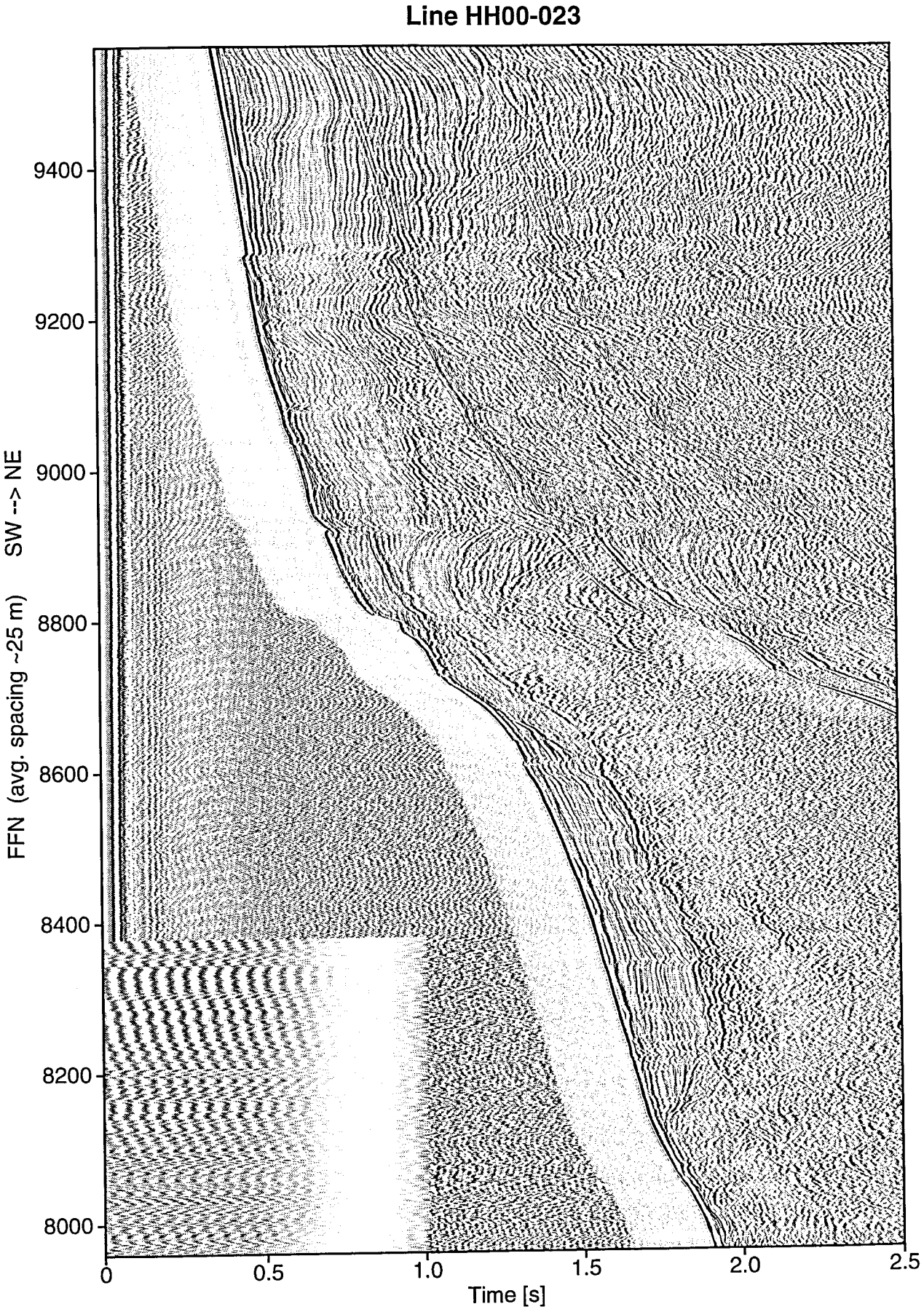

Fig. 8.1.8: MCS line 23. BP 10/20-150/200 Hz; Trace bal.; AGC 0.5 s.

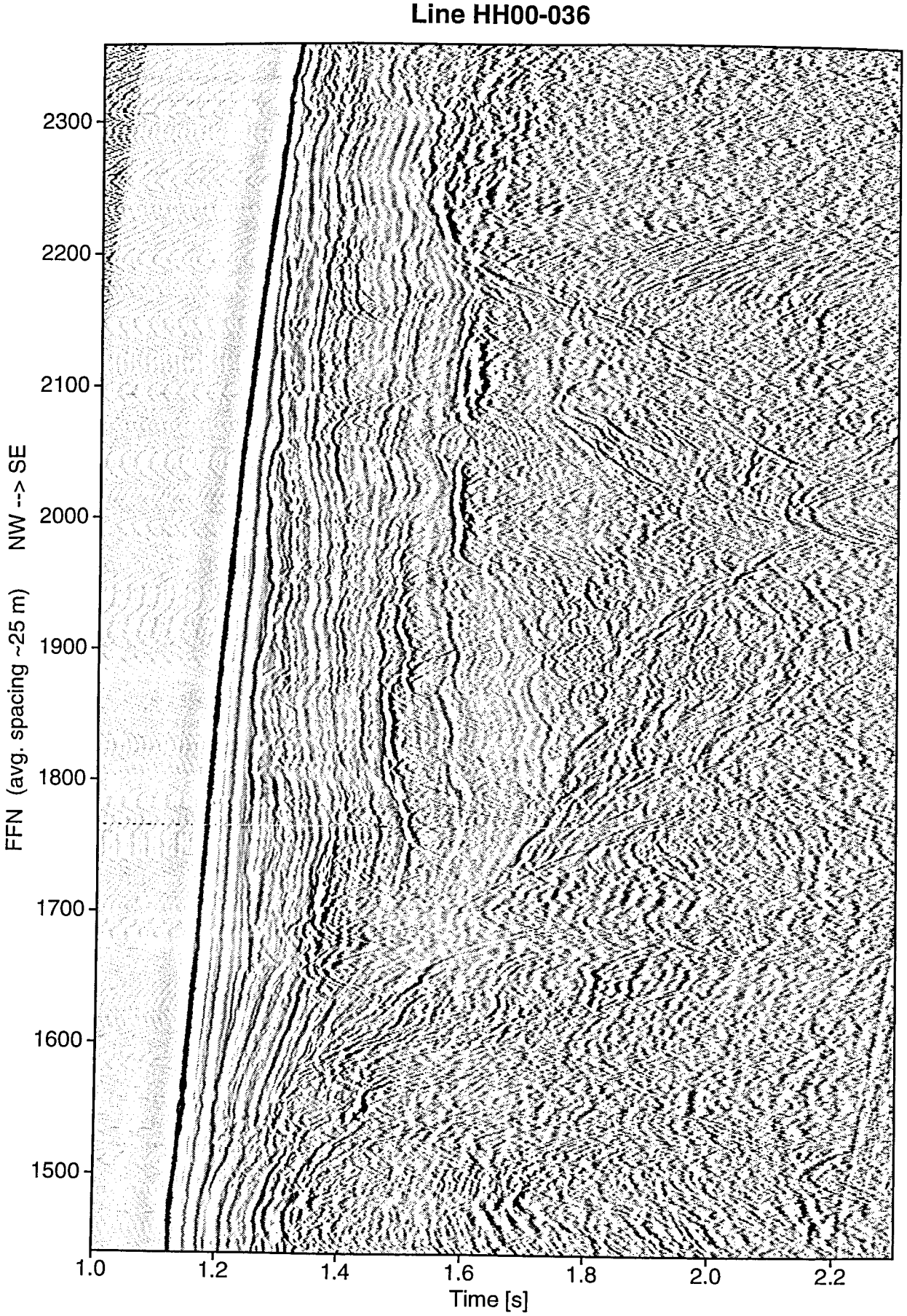

Fig. 8.1.9: MCS line 36. BP 10/20-150/200 Hz; Trace bal.; AGC 0.5 s.

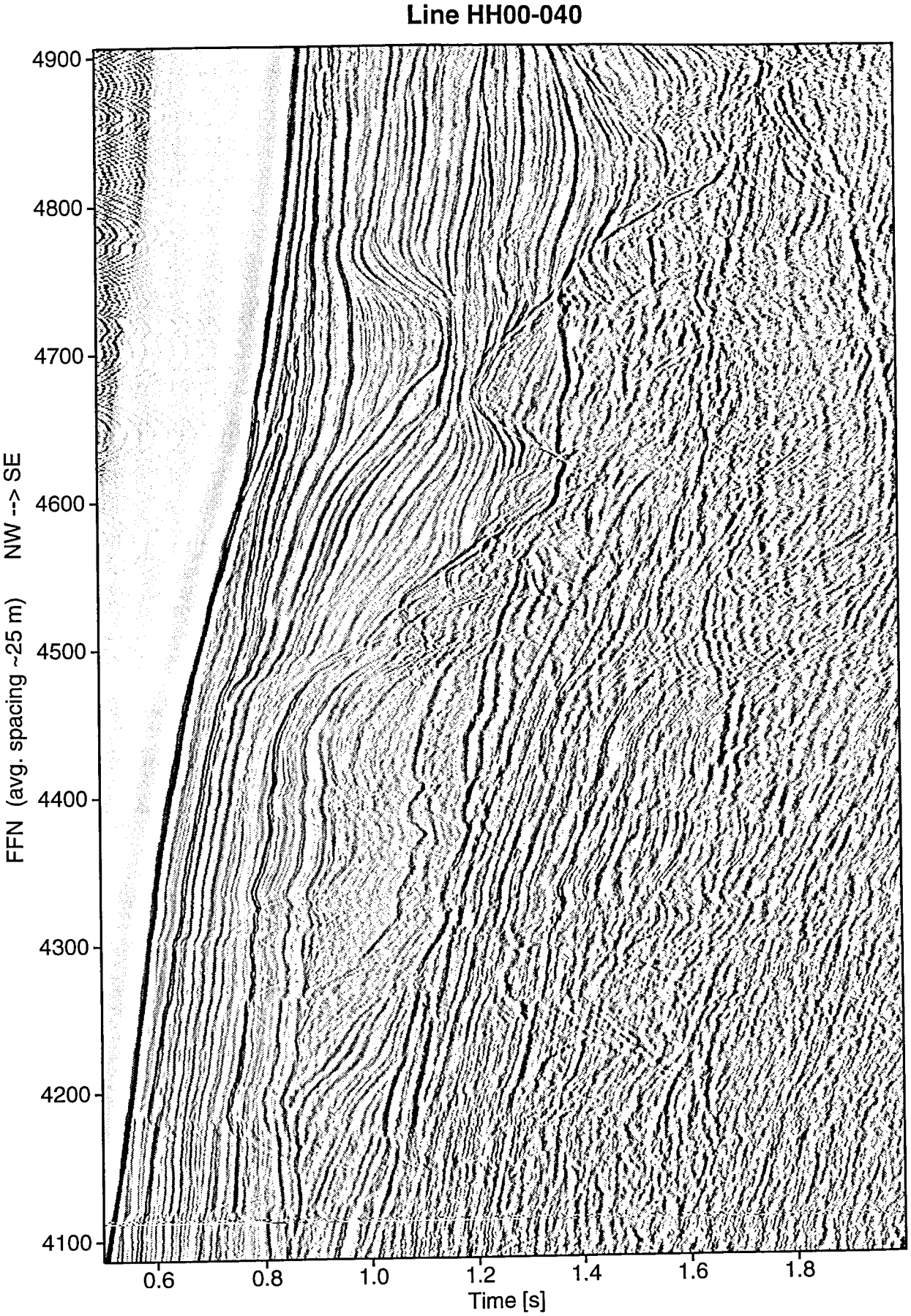

Fig. 8.1.10: MCS line 40. BP 10/20-150/200 Hz; Trace bal.; AGC 0.5 s.

8.2 OBH/S seismics along profile 08 Yaquina basin

Profile08 was shot on top of seismic reflection line 20 where strong variations within BSR occurance were observed (chapter 8.1). 9 OBH and 4 OBS were deployed (fig. 8.2.1), this time at distances between 0.7 nm up to 2 nm. The short offsets between the instruments should enable dense data coverage with high resolution in space and time as two GI-guns were shot for signal generation.

Data quality of the seismic sections derived is very good. Besides clear near vertical reflections refracted events were observed out to distances of about 18 kilometers offset. On most sections wide angle reflections from basement are identified. Reflected events from BSR were also present.

Although the data set provides a high quality base to retrieve high resolution velocity-depth information our efforts for preliminary interpretations and thematic data handling were concentrated on the data of profile 7.

To provide an impression of the high data quality we display a selection of data sections at this place.

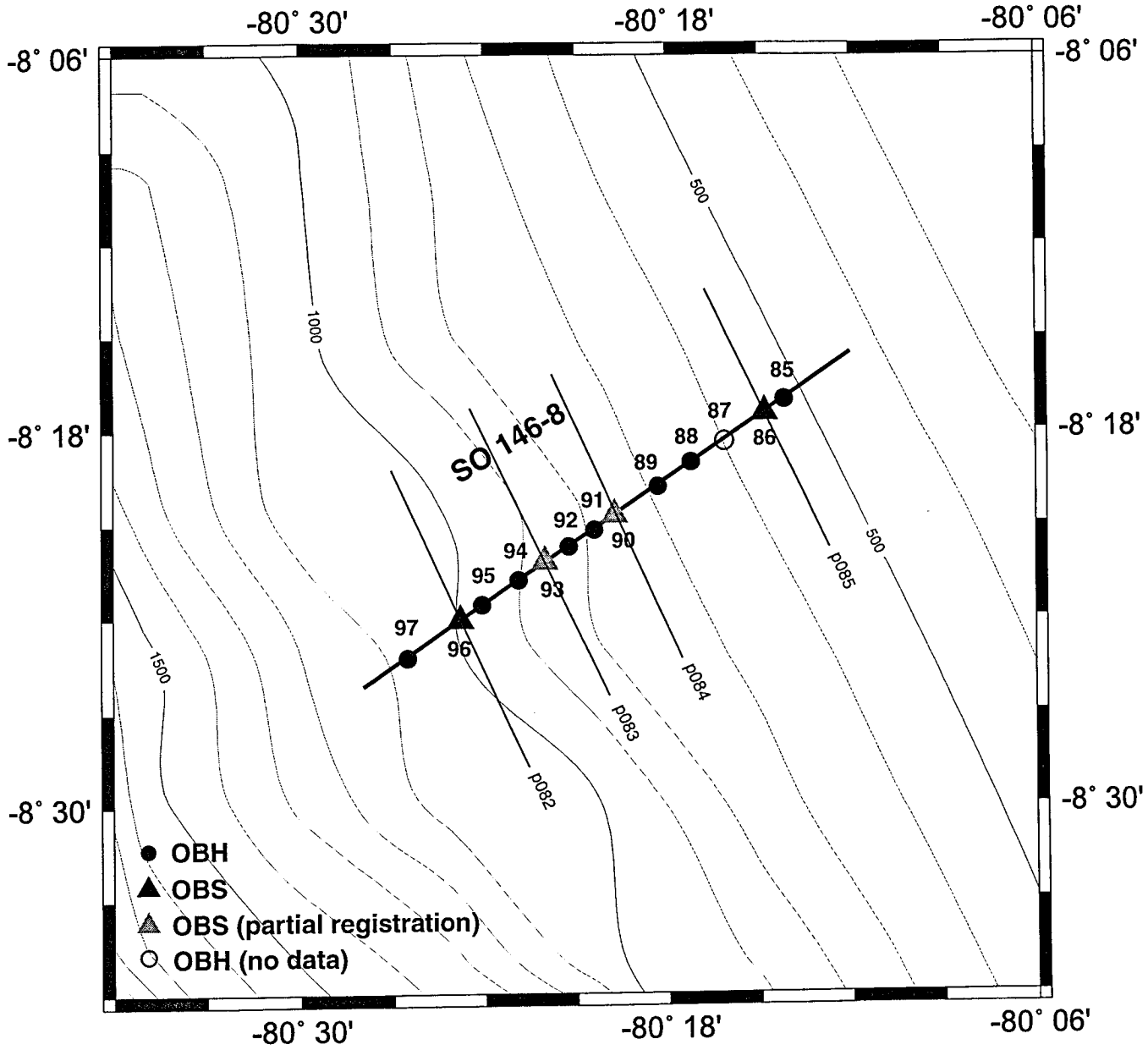

Figure 8.2.1: Location map of profile SO 146-08.

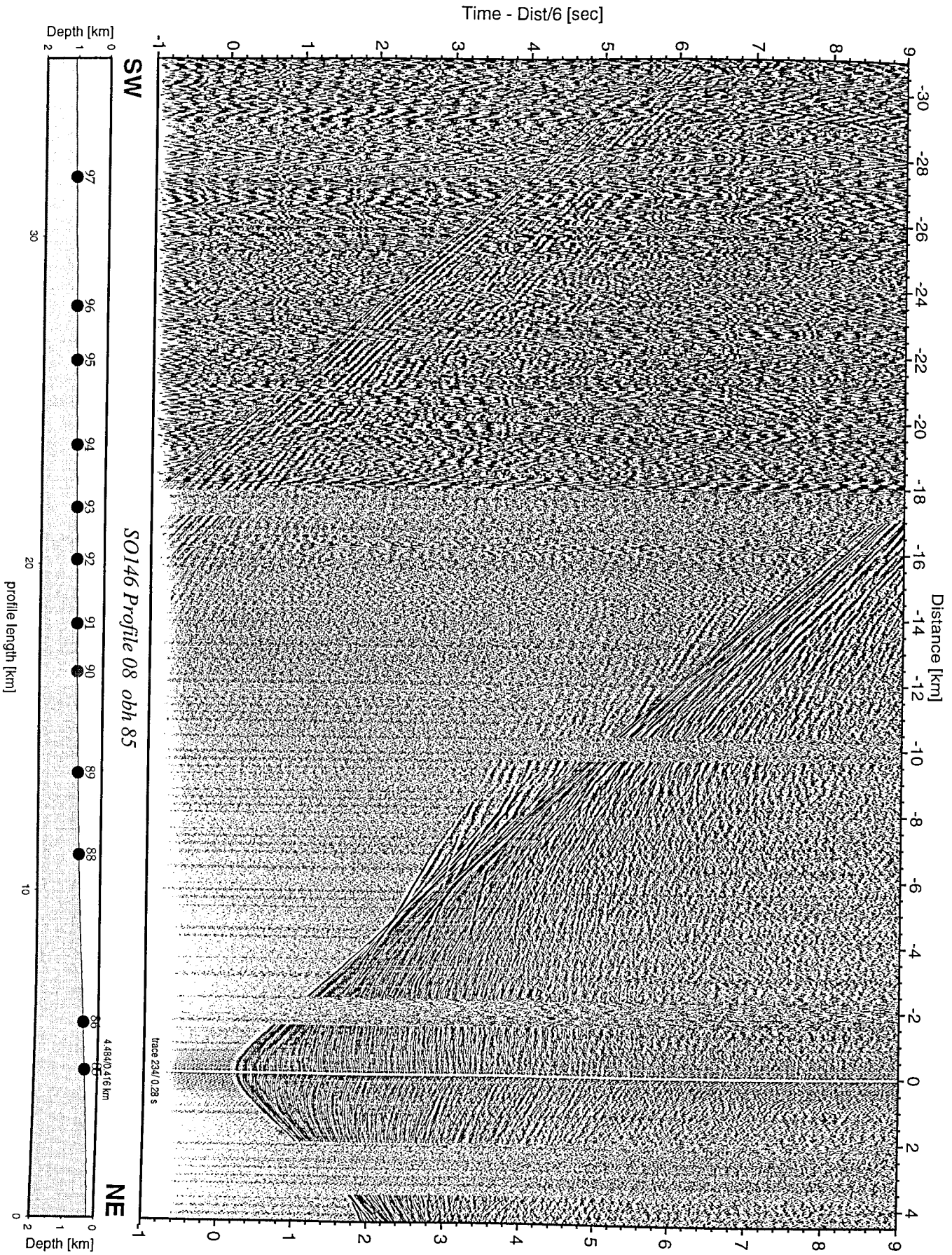

Figure 8.2.2: Record section from obh 85 , Profile 08.

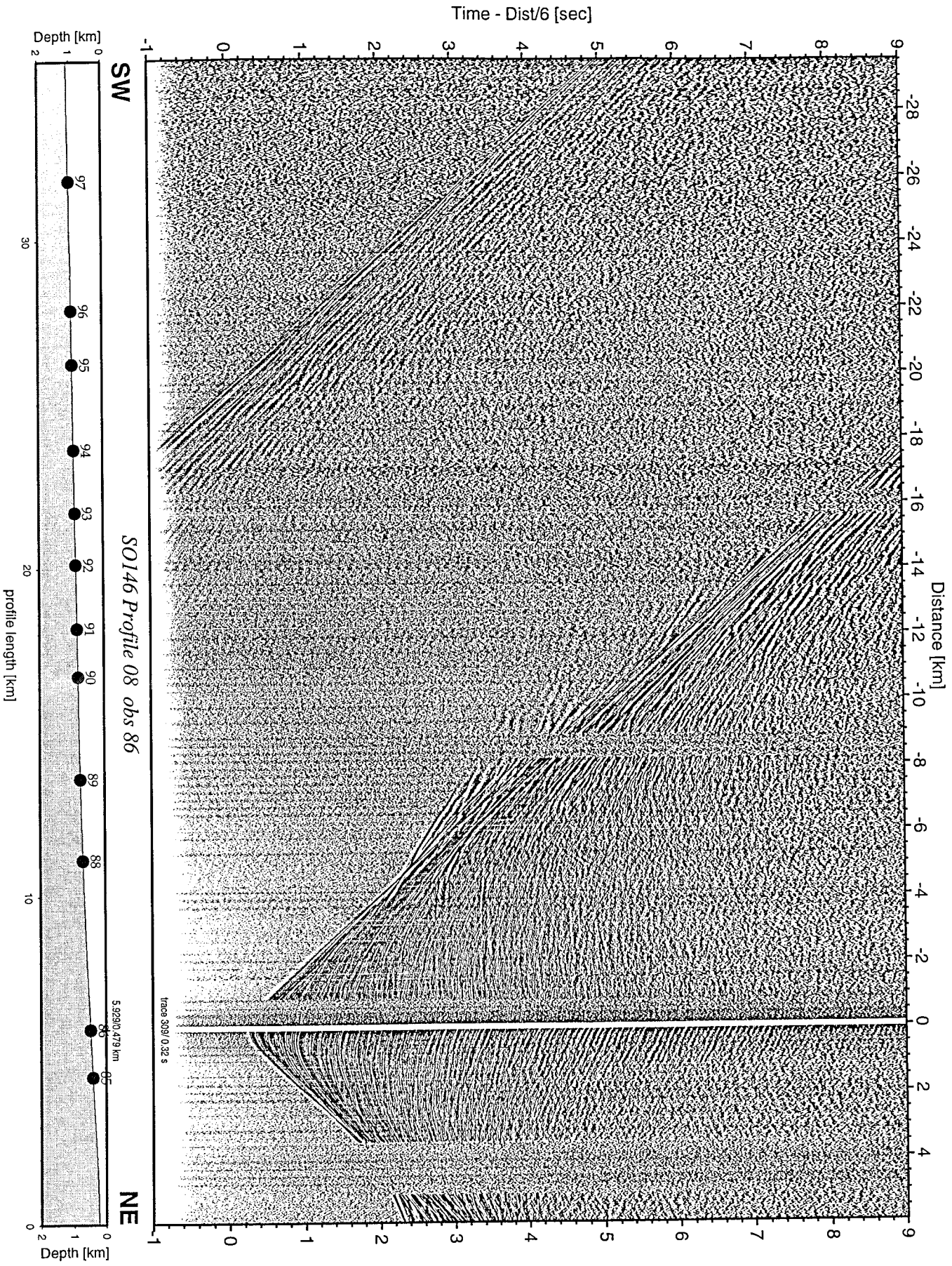

Figure 8.2.3: Record section from obs 86 hydrophone, Profile 08.

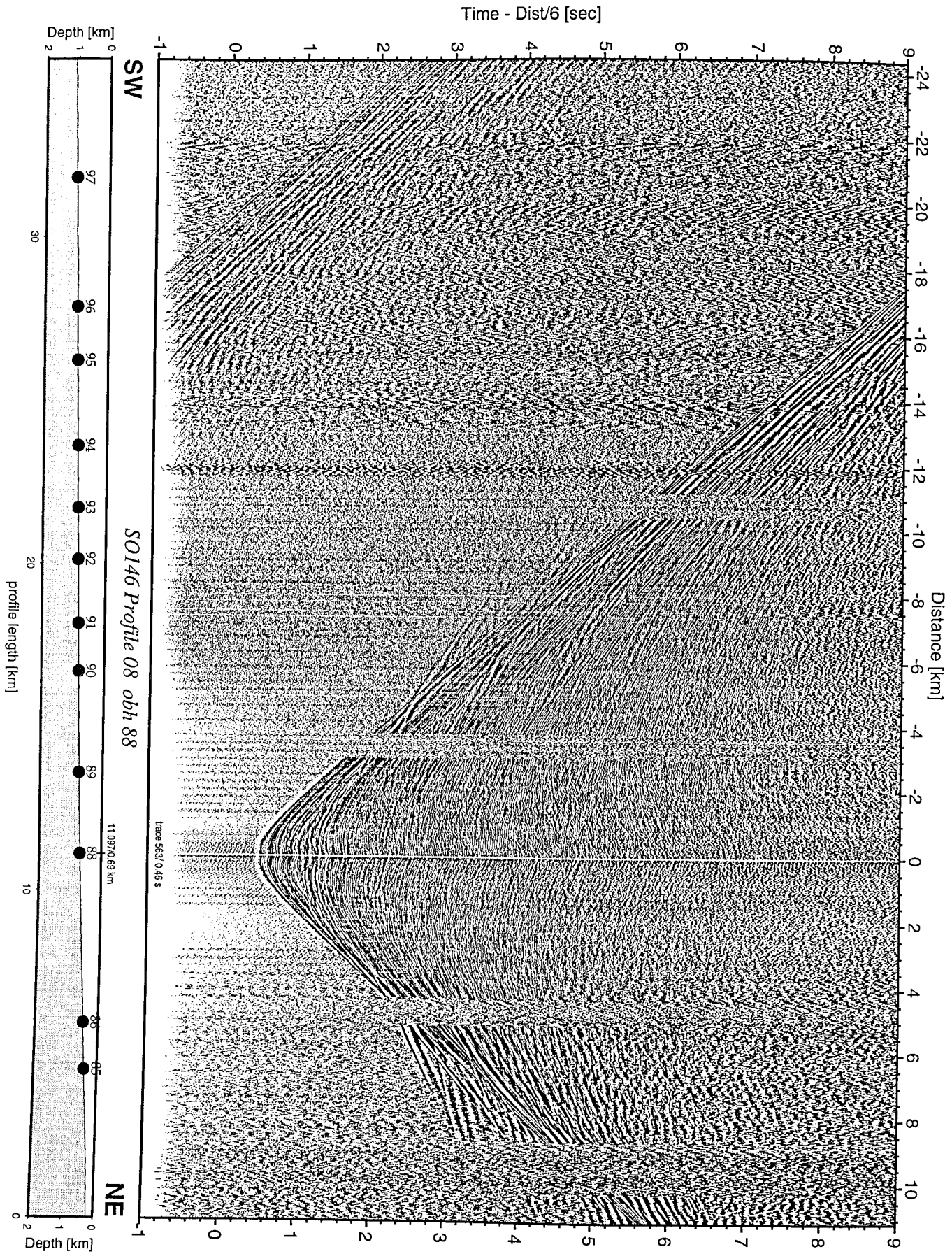

Figure 8.2.4: Record section from obh 88 , Profile 08.

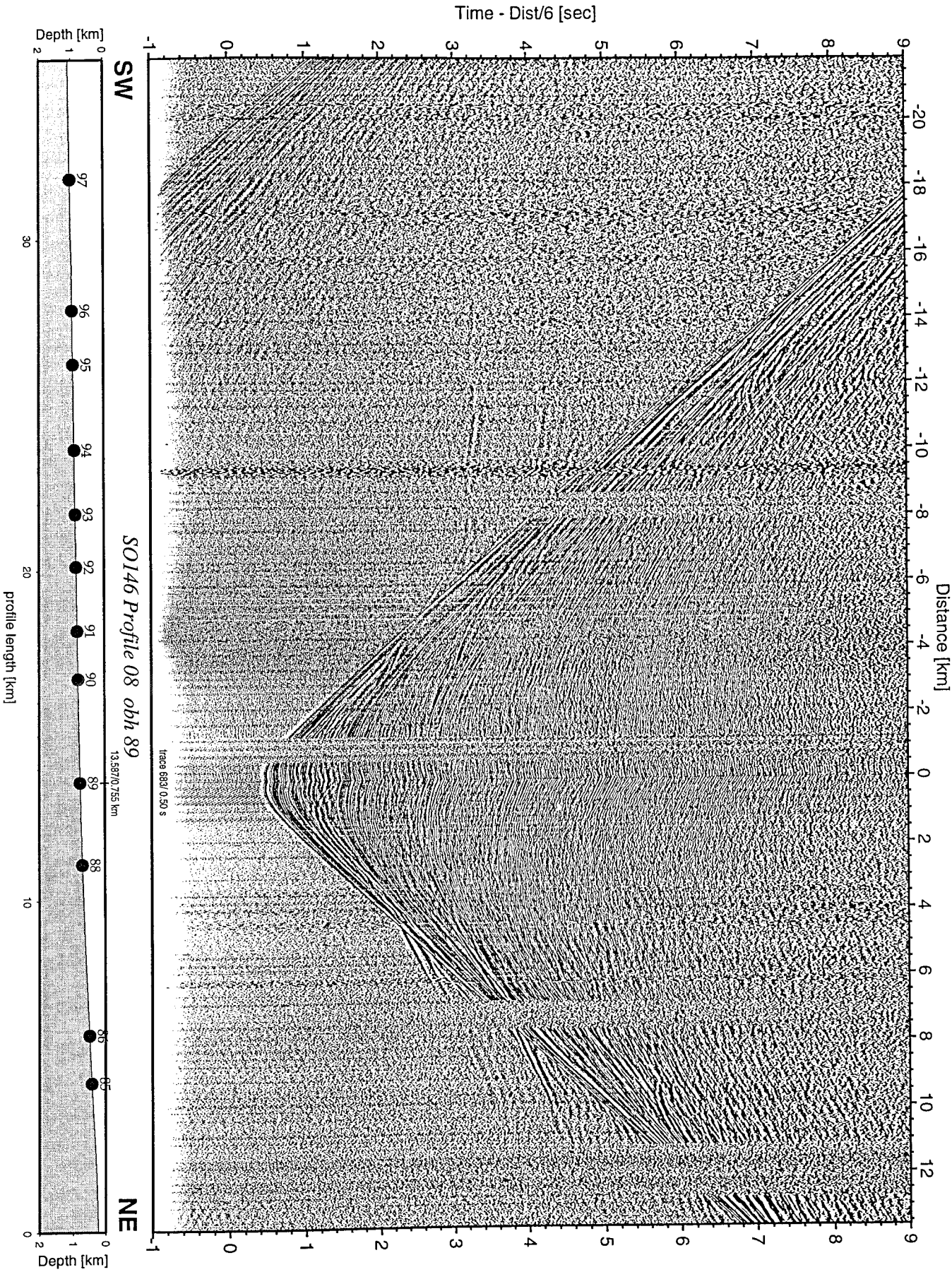

Figure 8.2.5: Record section from obh 89 , Profile 08.

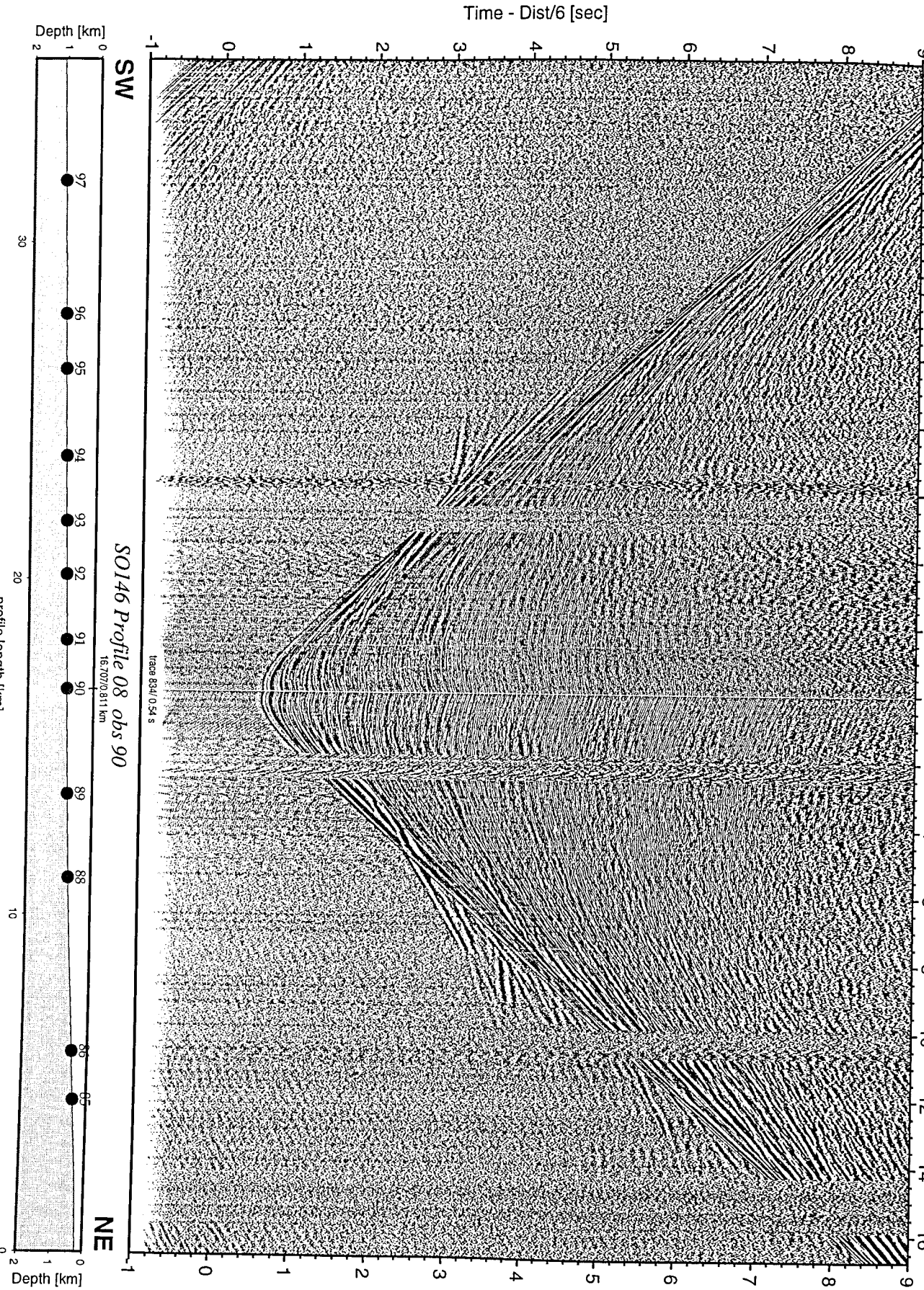

Figure 8.2.6: Record section from obs 90 hydrophone, Profile 08.

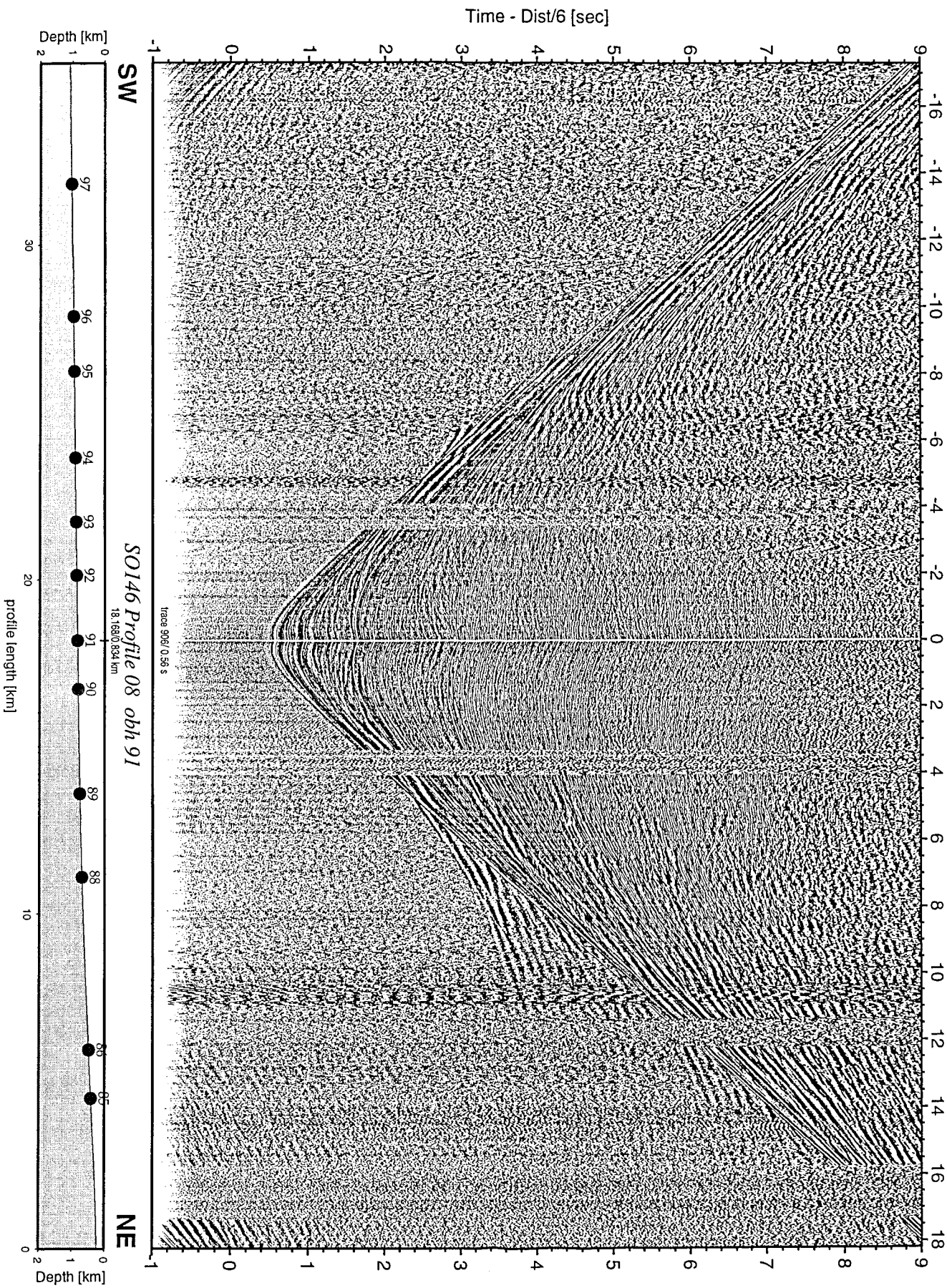

Figure 8.2.7: Record section from obh 91 , Profile 08.

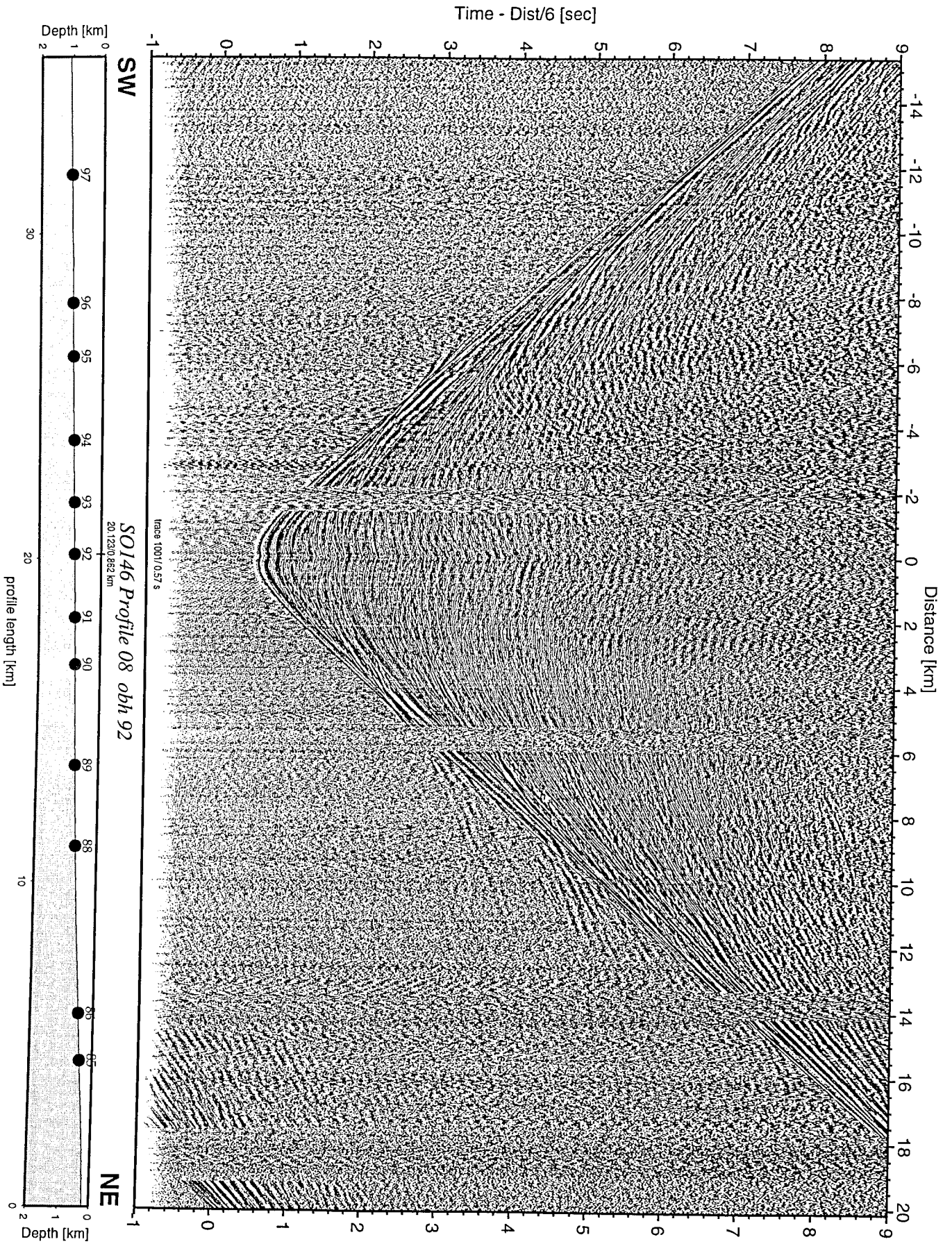

Figure 8.2.8: Record section from obh 92 , Profile 08.

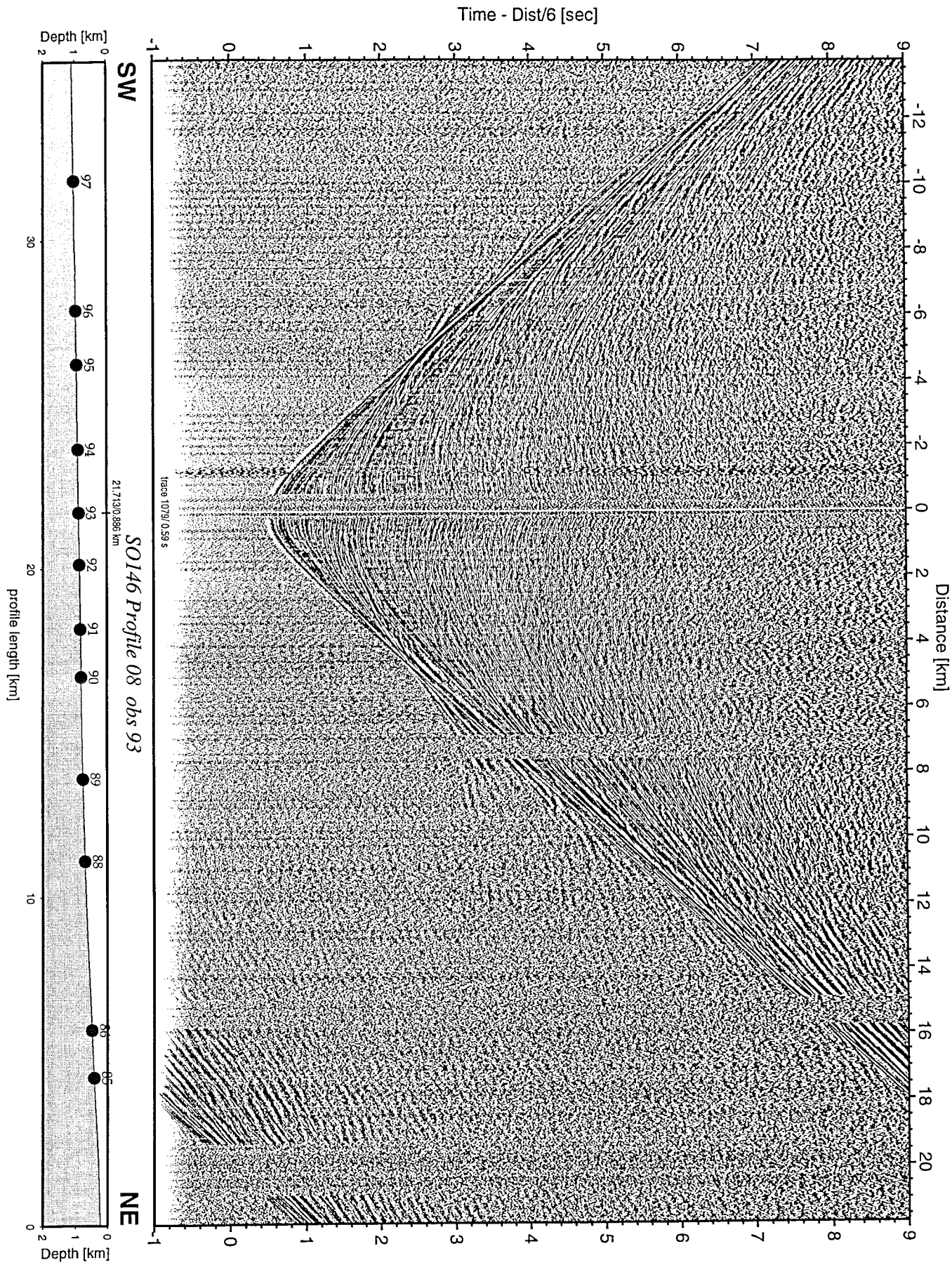

Figure 8.2.9: Record section from obs 93 hydrophone, Profile 08.

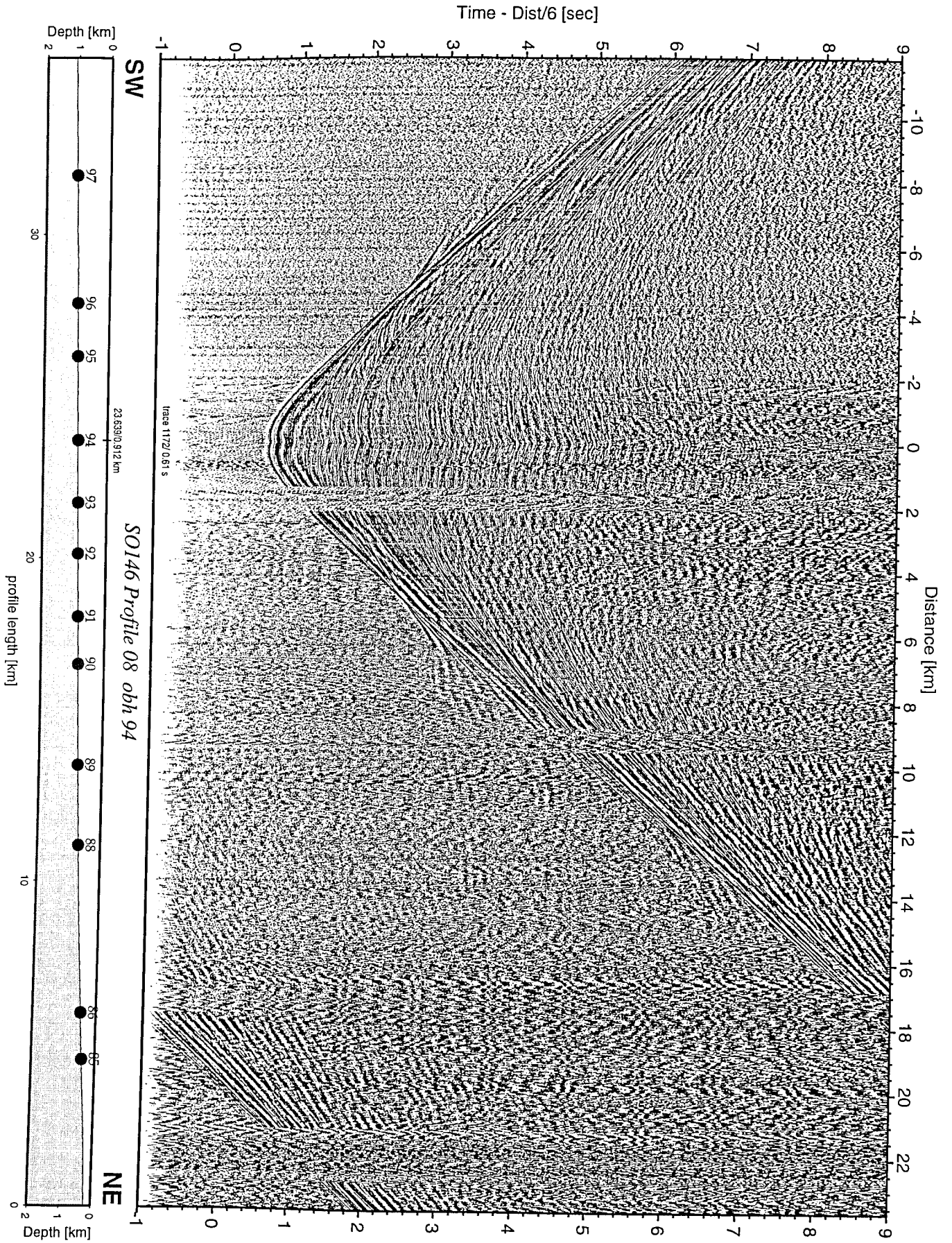

Figure 8.2.10: Record section from obh 94 , Profile 08.

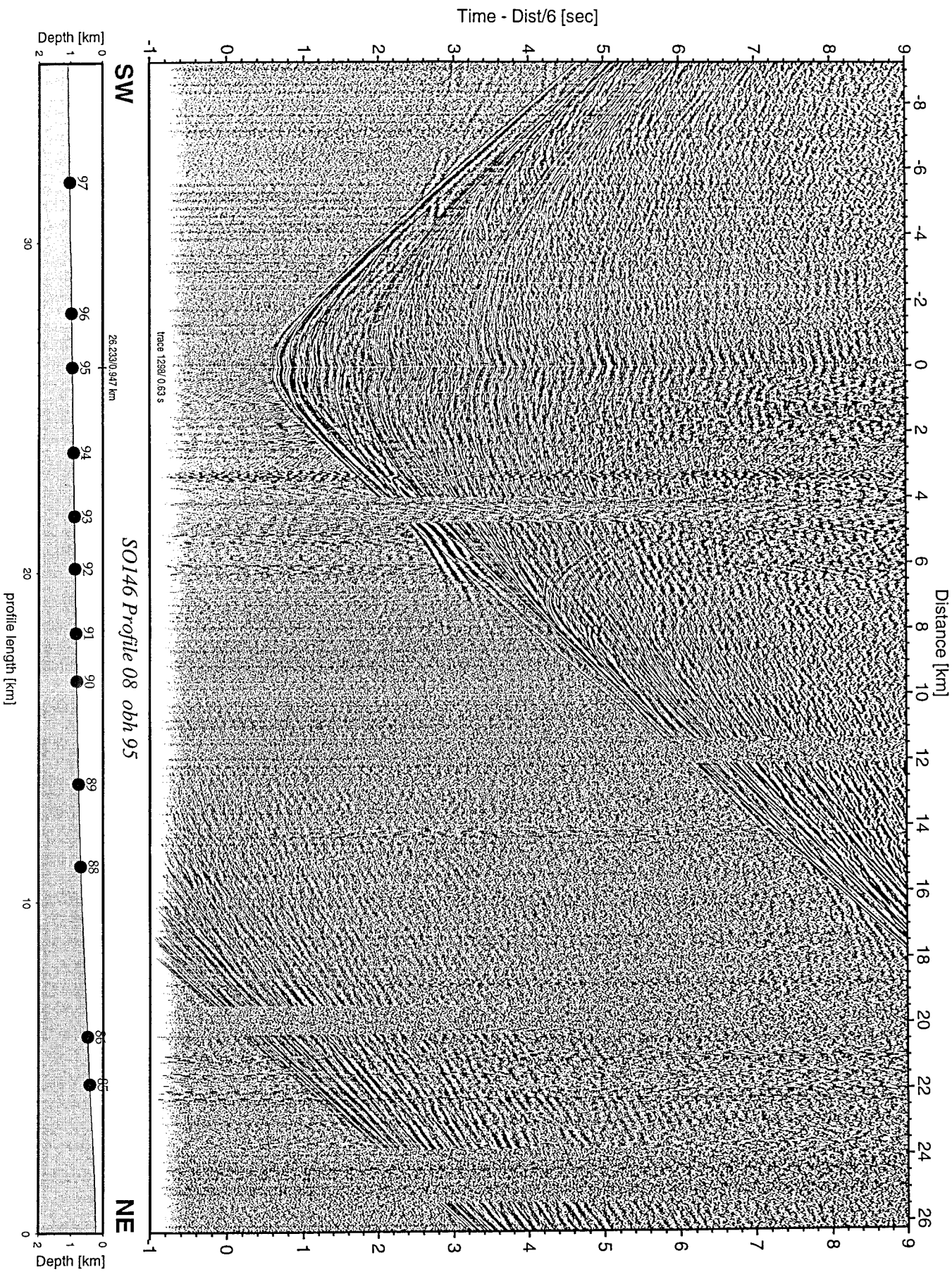

Figure 8.2.11: Record section from obh 95 , Profile 08.

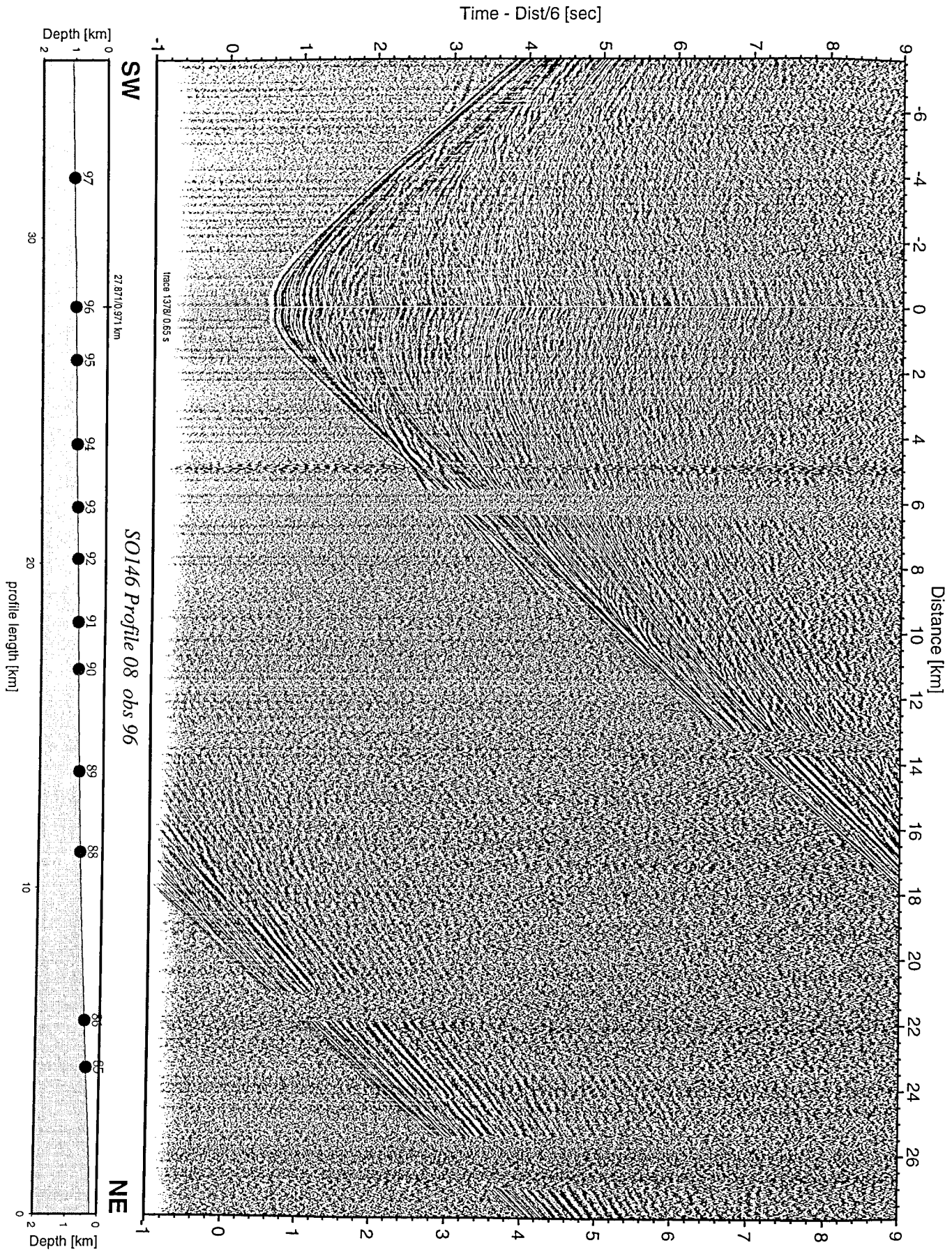

Figure 8.2.12: Record section from obs 96 hydrophone, Profile 08.

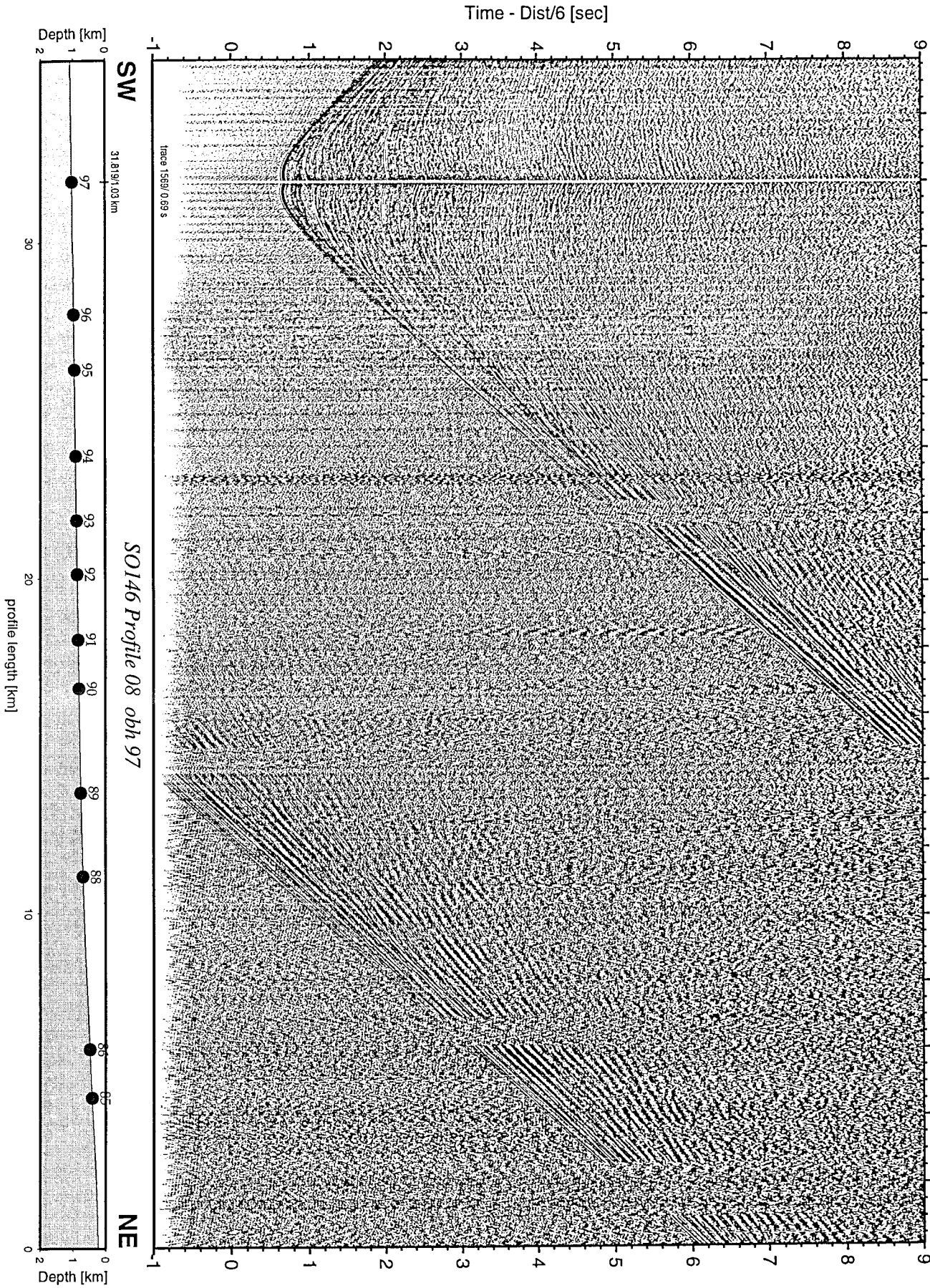

Figure 8.2.13: Record section from obh 97 , Profile 08.

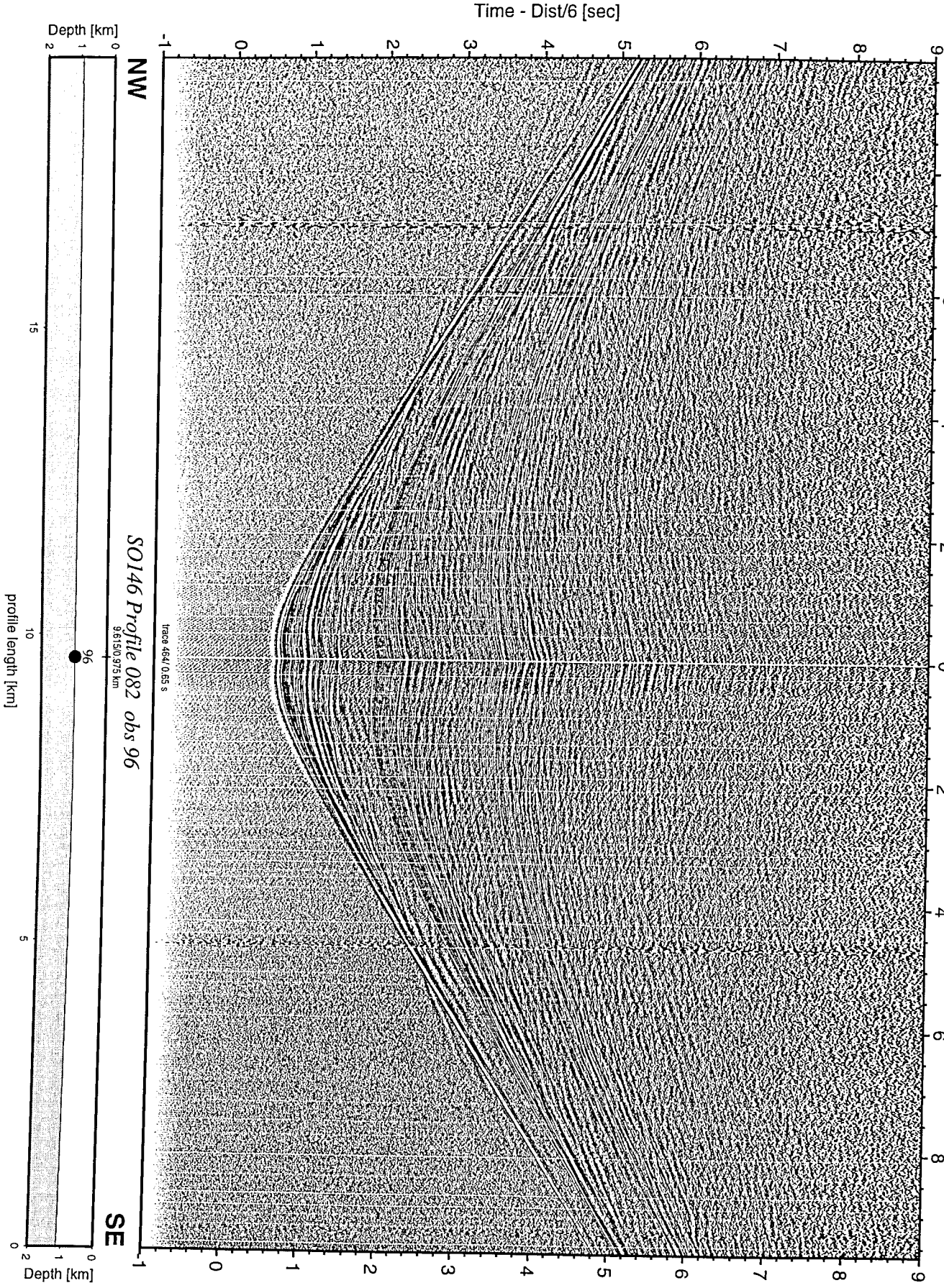

Figure 8.2.14: Record section from obs 96 hydrophone, Profile 082.

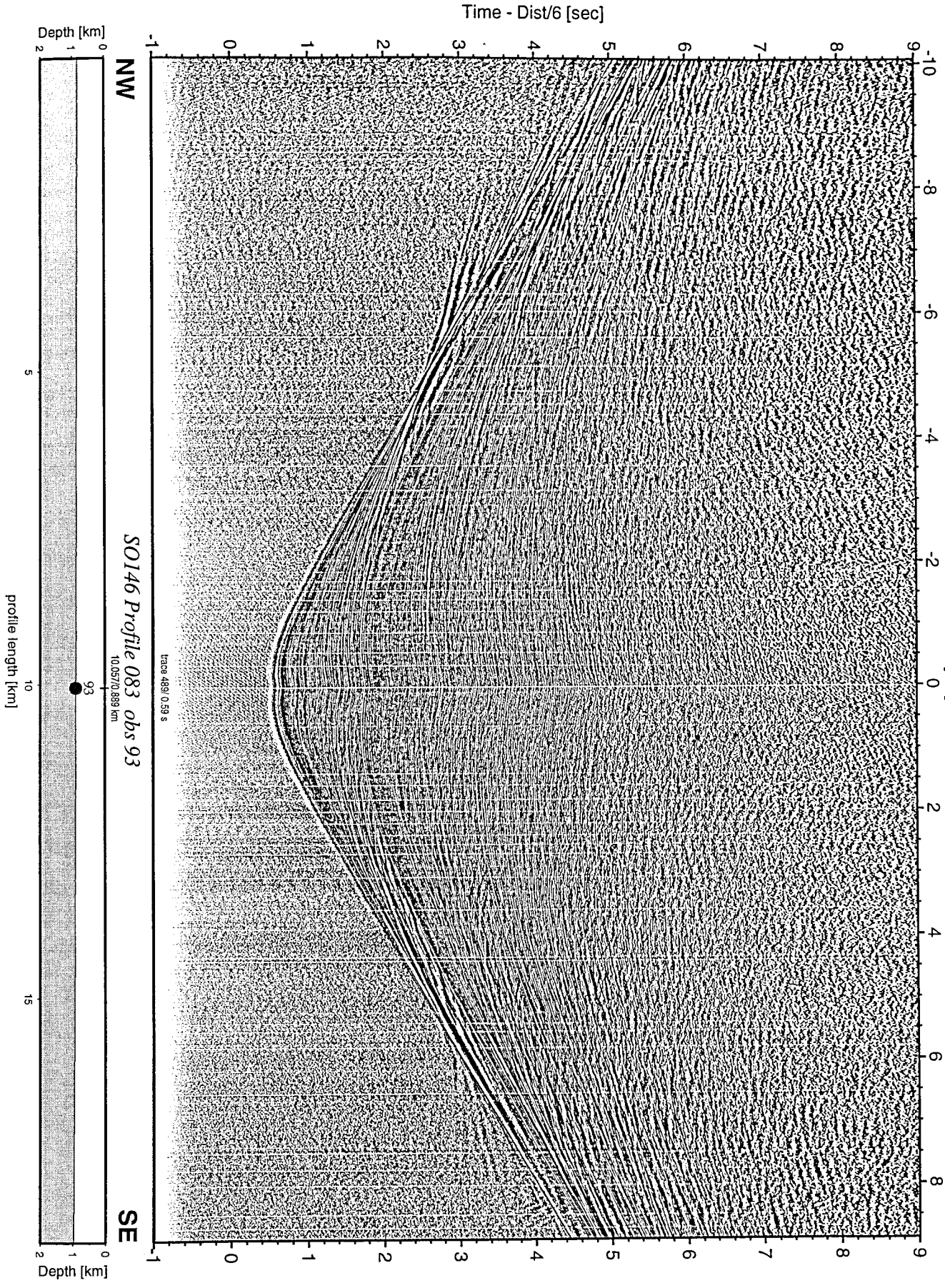

Figure 8.2.15: Record section from obs 93 hydrophone, Profile 083.

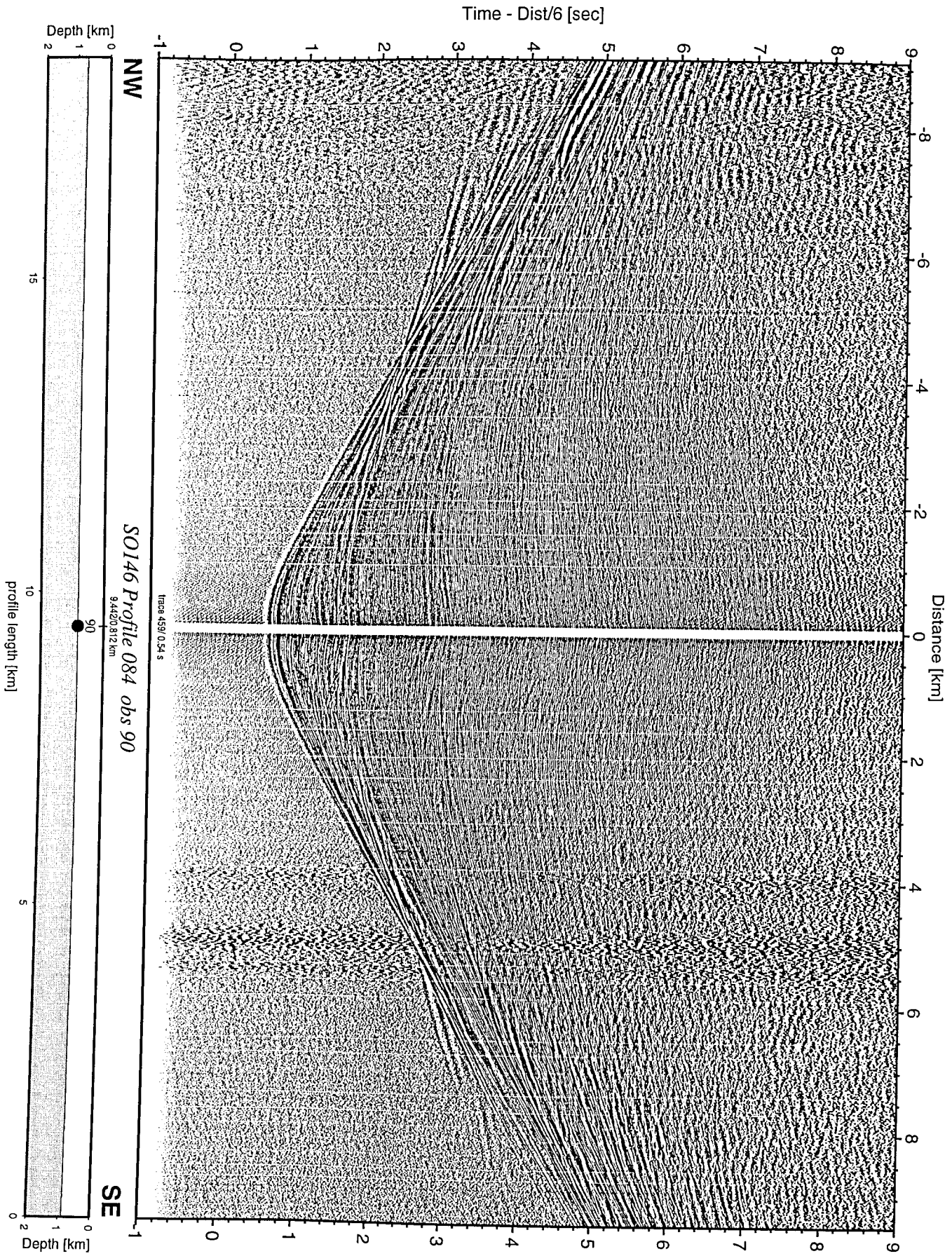

Figure 8.2.16: Record section from obs 90 hydrophone, Profile 084.

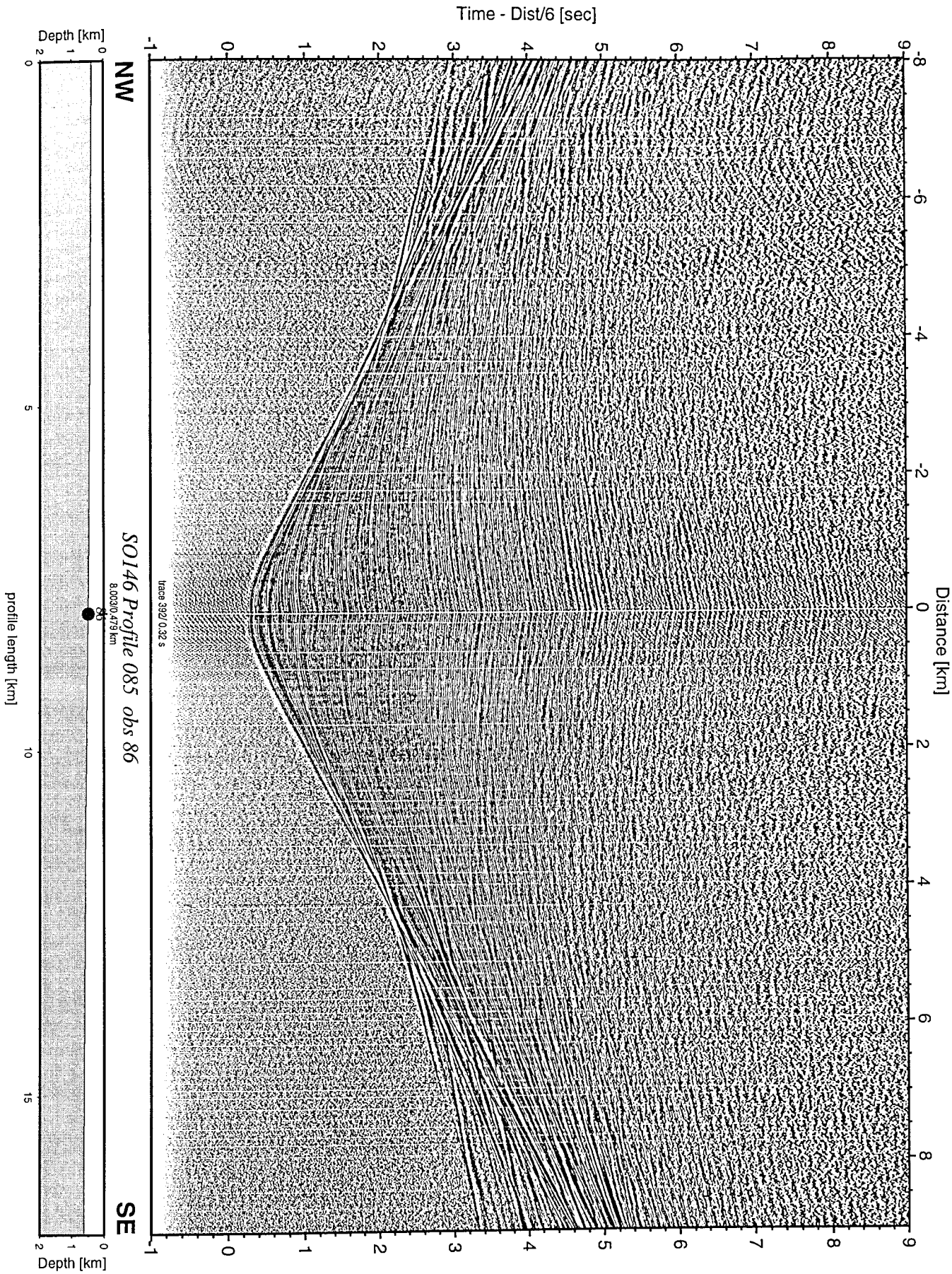

Figure 8.2.17: Record section from obs 86 hydrophone, Profile 085.

8.3 Parasound

(C. Hübscher and Shipboard Scientific Party)

The several Parasound sections presented in this report have been selected to give an overview about the quality and scientific usefulness of this kind of data. All depth values have been computed from traveltimes and assuming a constant velocity of 1500m/s. Each bar at the bottom of the sections represents a length of 1 km. Since different scales have been used, the vertical exaggerations are different for every section. The data is plotted time sequentially from the left to the right.

The first section shows the eroded shelf of the Yaquina basin. No Holocene sediment cover is present, which is indicative of strong coastal currents (Fig. 8.3.1). The slowly migrating mudwaves along line HH00-011 all have a constant wave length (Fig. 8.3.2). From which it can be assumed, according to the mathematical model presented by Hopfauf & Spiess (University of Bremen, in prep.), that the current has been stable over the entire depth and corresponding time span that has been imaged by the data. The hummocky seafloor structures on the right side in Fig. 8.3.3, part of line HH00-036, may be interpreted as chemoherm structures, like those observed in this area using the OFOS (s.b.). Where the wavy unconformity with the constant depth of approximately 960 m approaches the seafloor, gas migrates upwards toward the seafloor. The upper parallel reflections downlap onto that unconformity. The section from line HH00-043 which extends the WS/RS line 4 exhibits signal penetration depths of up to 100 m, suggesting that the sediments are of pelagic origin. The drape deposits covering the rough and hummocky basement is not resolved by this data.

Figs. 8.3.5-8 elucidate the relationship between OFOS observations and Parasound data. Shells and carbonates are present where certain layers pinch out on the step like seafloor (Figs. 8.3.5/6). For a first interpretation of the OFOS experiments see chapter 8.6 (this volume). The chemoherms named "Max and Moritz" are shown in Fig. 8.3.7. In areas where the signal penetration was significantly reduced, bacterial mats have been observed by the OFOS. Both observations suggest the presence of gases, such as methane and H_2S (from bacteria), which absorb seismic energy (Fig. 8.3.8).

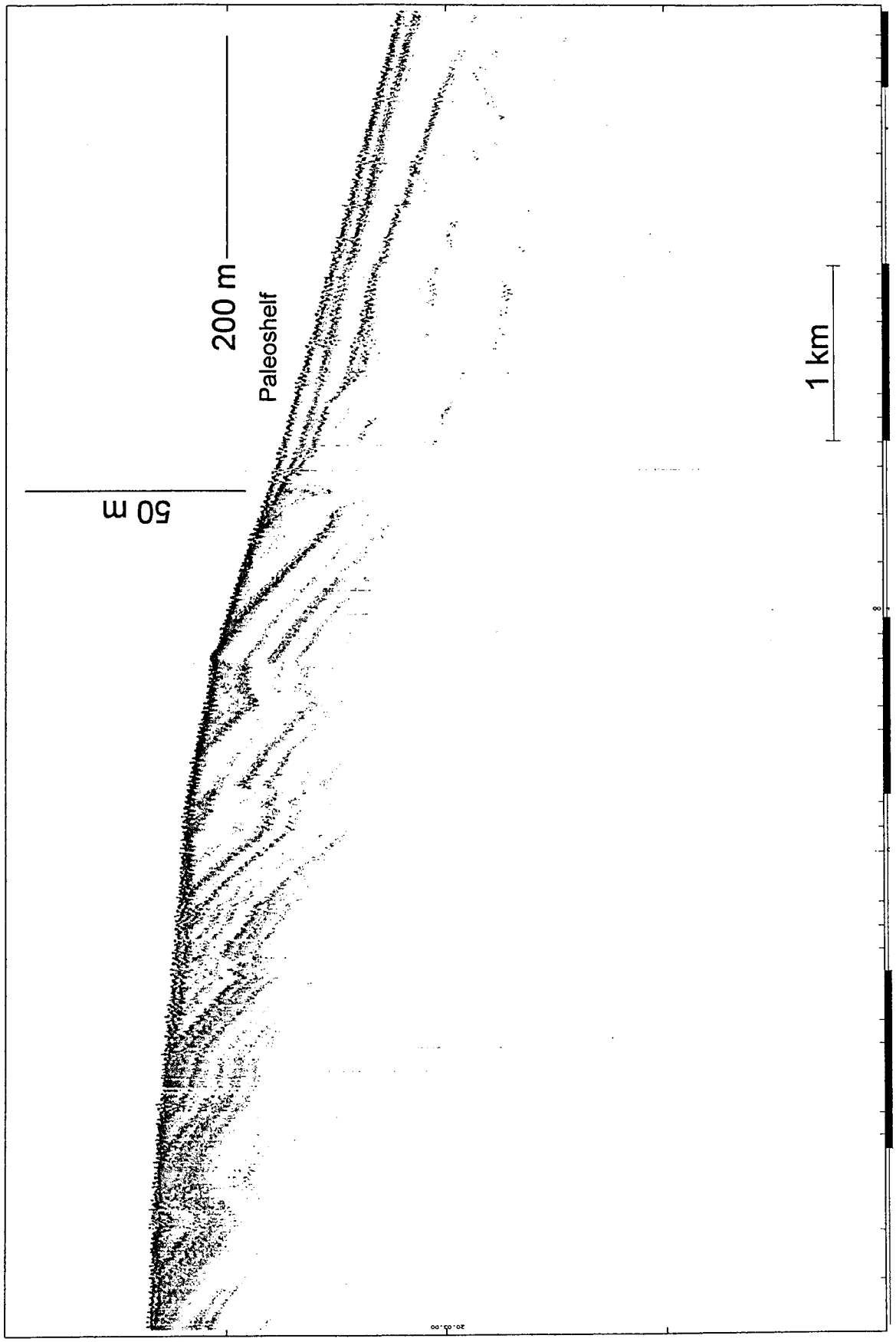

Fig. 8.3.1: Eroded layers at Yaquina Shelf. A paleo shelf may be present in a waterdepth of 200m.

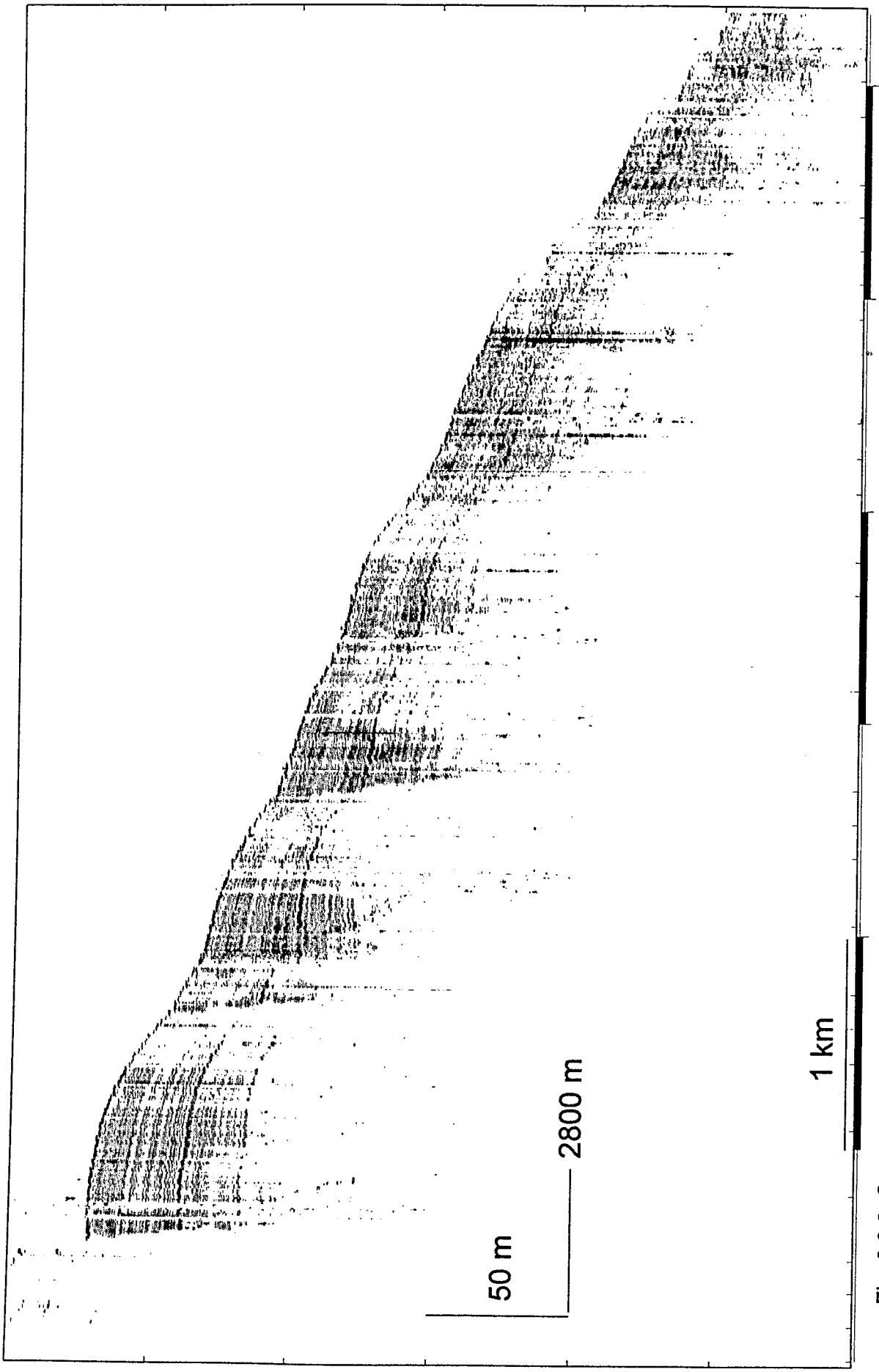

Fig. 8.3.2: Current generated mudwaves (line HH00-011).

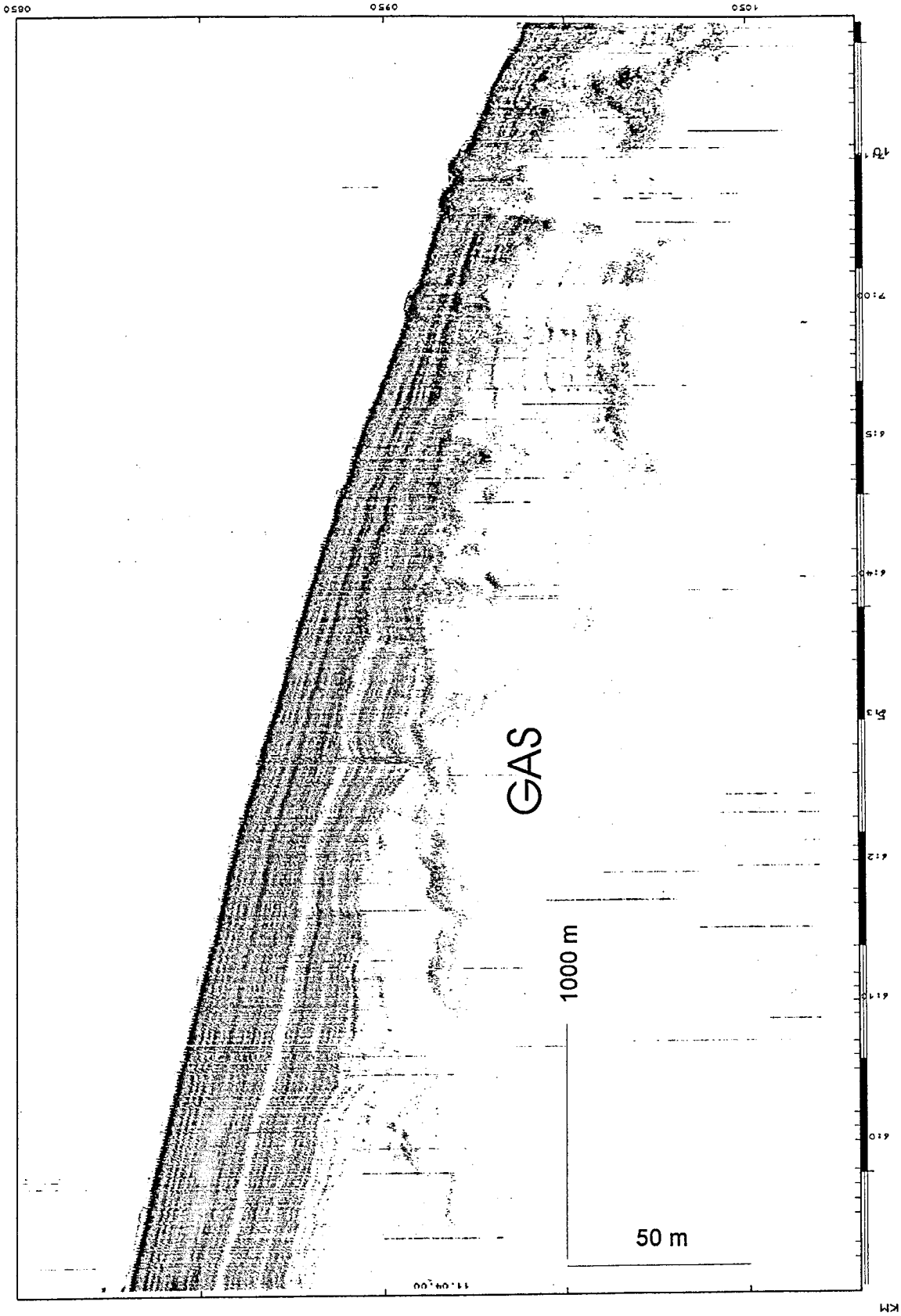

Fig. 8.3.3. A gas related reflection crosses the stratigraphy along line HH00-036.

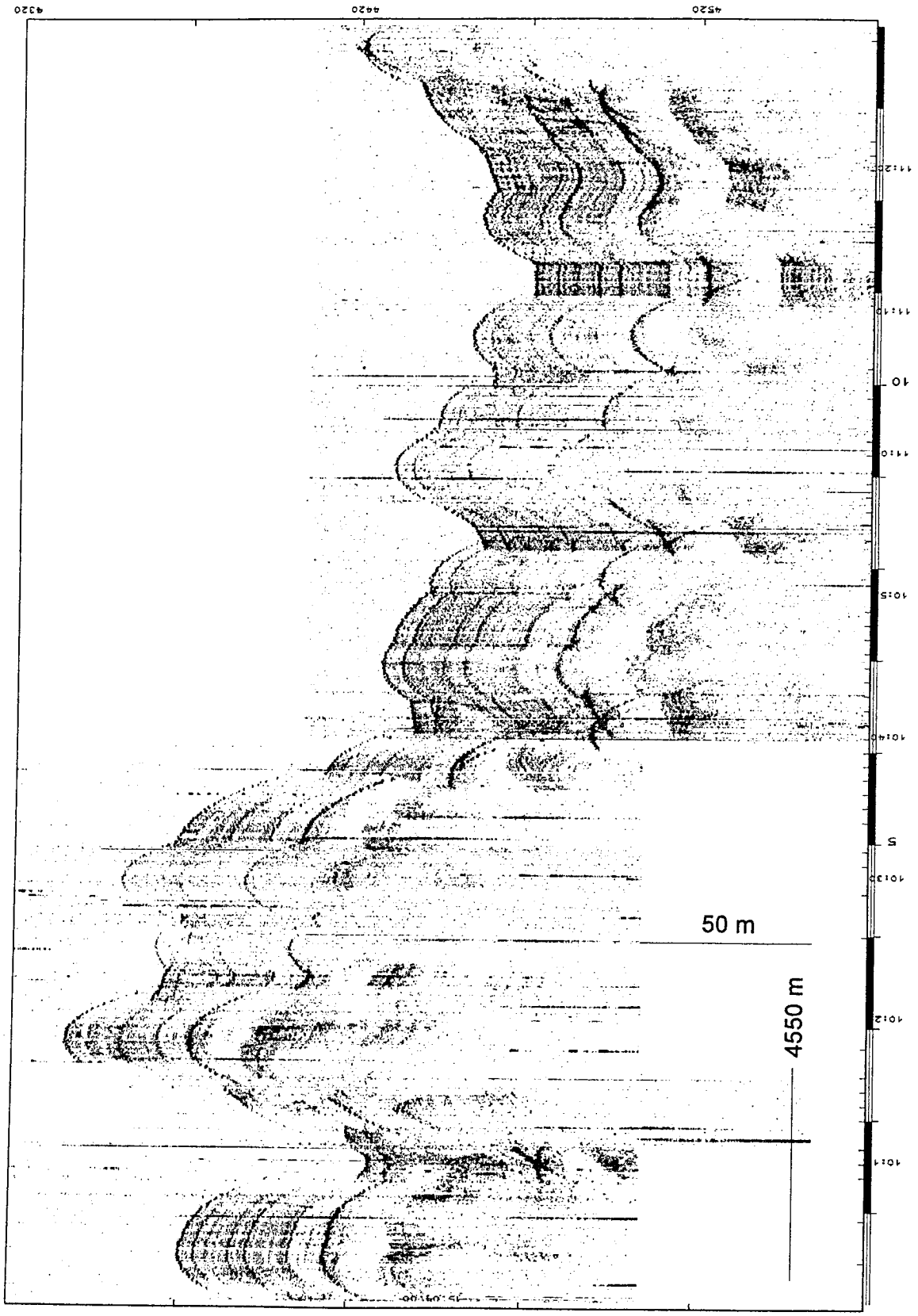

Fig.8.3.4: Hummocky but parallel layered sediments with high signal penetration along line HH00-043.

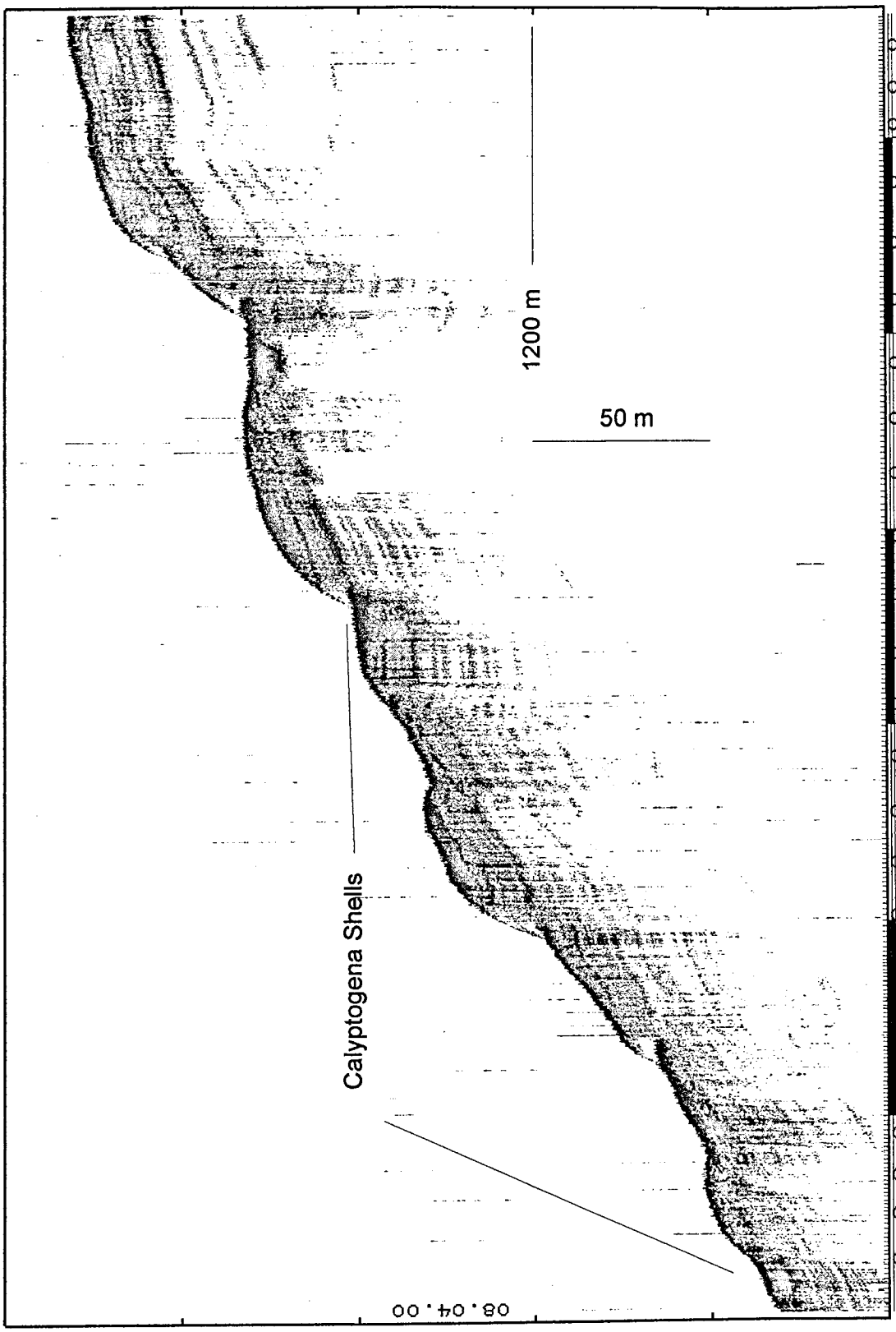

Fig. 8.3.5. Erosional truncated sediments along OFOS-1 transect (upper part).

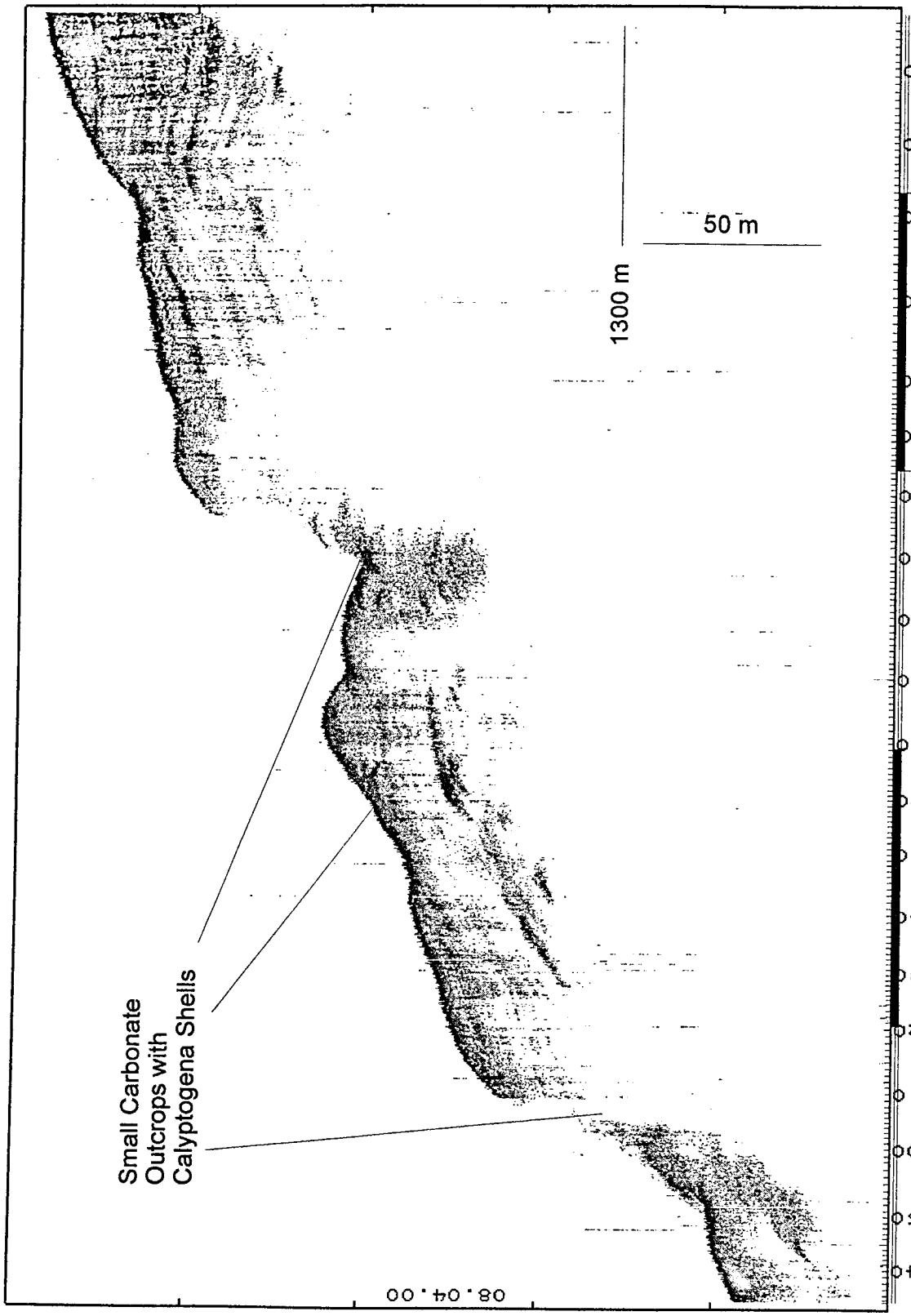

Fig. 8.3.6. Erosional truncation along OFOS-2 transect.

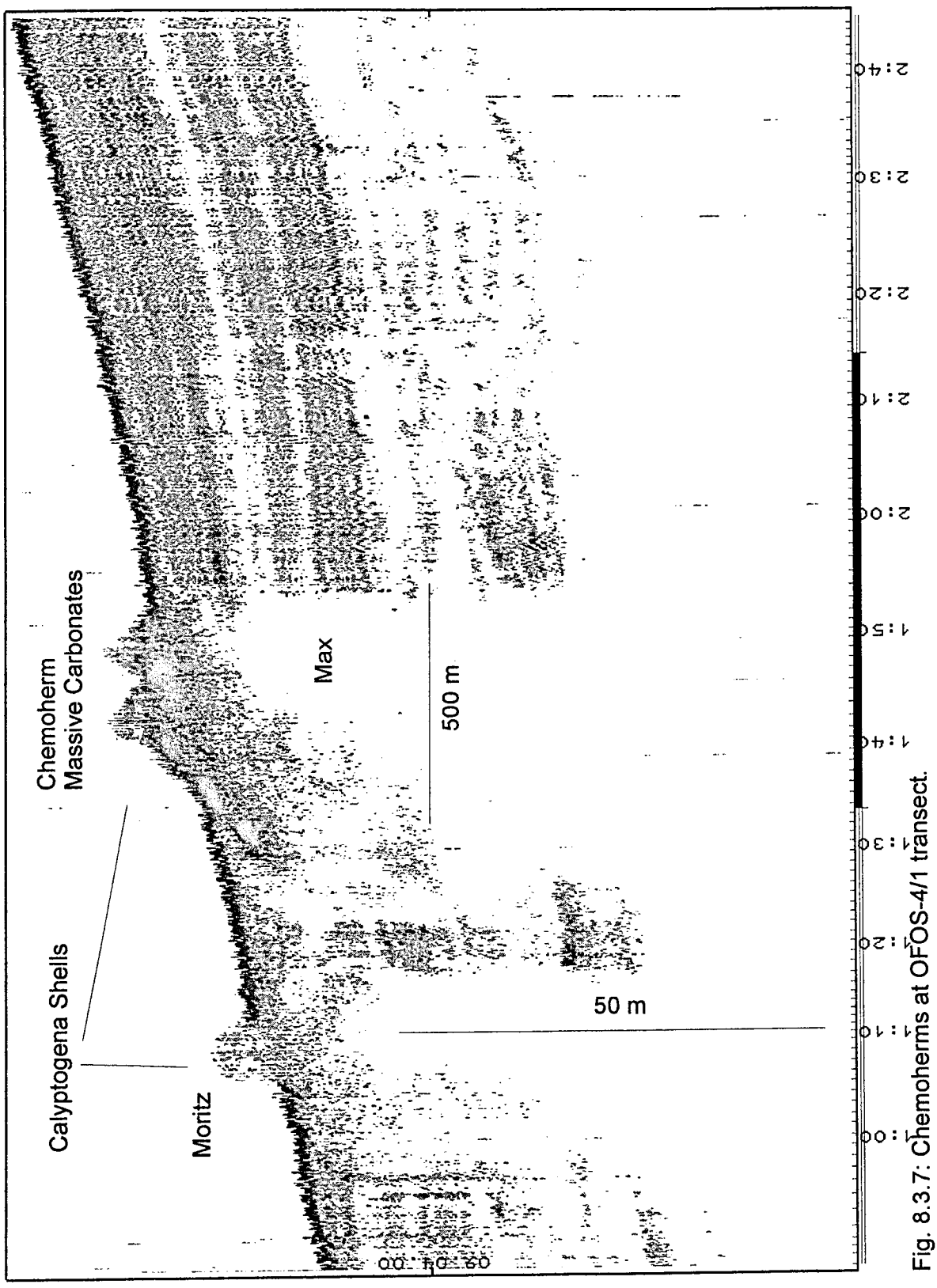

Fig. 8.3.7: Chemoherms at OFOS-4/1 transect.

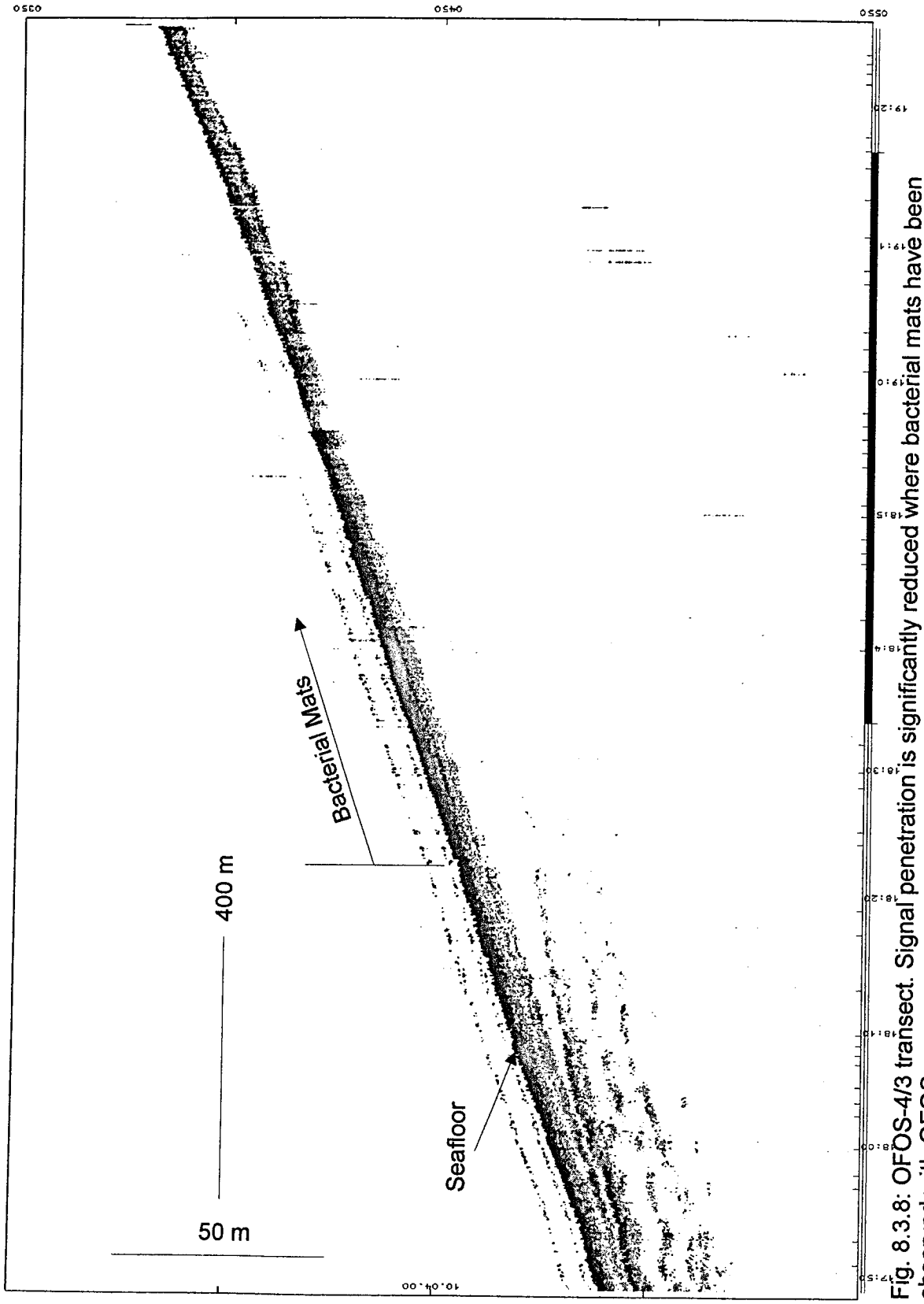

Fig. 8.3.8: OFOS-4/3 transect. Signal penetration is significantly reduced where bacterial mats have been observed with OFOS.

8.4 Yaquina basin, continental slope, and adjacent oceanic crust

(K. Huhn, N. Kukowski, J. Bohnert)

In the Yaquina working area (Figs. 8.4.1 and 8.4.2), HYDROSWEEP data were acquired simultaneously with wide angle and reflection seismic lines, transits between working areas, and during OFOS surveys. These data provide coverage over an area of about 18500 km^2 and include the ocean floor of the Nazca plate seaward of the trench, the trench itself and the lower slope and will allow morpho-tectonic interpretation of the area (Fig.8.4.3). Supplemented with French bathymetry data, acquired during the SEAPERC cruise of RV Jean Charcot in 1986, which covers an area just adjacent to our survey and another area west of our transit tracks between the Lima and Yaquina working areas, it will be possible to morphologically characterize large parts of the Peruvian margin. Additionally, several HYDROSWEEP tracks were completed to the north and south of OFOS tracks to get more complete coverage which enables regional correlations between tectonic structures identified from the video observations.

The surface morphology of the oceanic crust entering the Peru trench between 8°S and 9°S is very rough, much rougher than observed further to the south (Fig.8.4.4). It is characterized by a complex pattern of horsts and grabens with relief of up to more than 500 m. In the portion of the mapped area, where wide angle profile WS#4 is located, these structures are close to and parallel the trench. However, a bit further south, ridge-shaped linear structures enter the trench obliquely with angles up to 30°. Superimposed on these structures are other ridge-shaped linear features, best imaged in the 3D perspective view (Fig.8.4.5), which trend perpendicular to the trench axis. Still other linear but wider morphological highs and with much smoother topography are identified on the oceanic crust. Much of this morphology might be of older origin and inherited, e.g. in connection with sea floor spreading. However, close to the trench at least parts of the surface roughness seem to result from bending of the Nazca plate. Data acquired on our transits to and from the Paita area (Fig.8.4.2) suggest that this morphology is typical for the Nazca plate off large parts off northern Peru and different from what is observed in the seaward part of the Lima transect (cf chapter 9.5).

The oceanic trench is characterized by water depths of more than 6000 m. At the trench, the morphological style of the basement changes abruptly. All major features of the very steep lower slope trend trench-parallel. At the toe of the slope, a gently dipping trench parallel ridge is tentaively interpreted as offscraping of material from the oceanic plate accreted against the continent. The hinterlandward edge of the accretionary wedge is defined by a trench-parallel ridge. However, both of these ridges are much less prominent than accretionary ridges at truly accretionary margins, e.g. Cascadia or Makran. Locally, the morphology of the lower slope is quite variable with trench-parallel and north to south trending features. The latter direction coincides with that of some of the linear structures observed on Nazca plate. Between latitudes 8°10'S and 8° 20'S, a curved linear structure is visible at a location where the toe of the accretionary wedge retreats a few km.

Adjacent to the accretionary wedge is lower slope terrace. Here, the seafloor is cut by numerous narrow furrows and canyons which may result from mass wasting through surficial erosion (Fig.8.4.5). The landward edge of this part of the slope is marked by the 2500 m isobath. Further to the east, the slope, Yaquina basin and shelf dip quite gently.

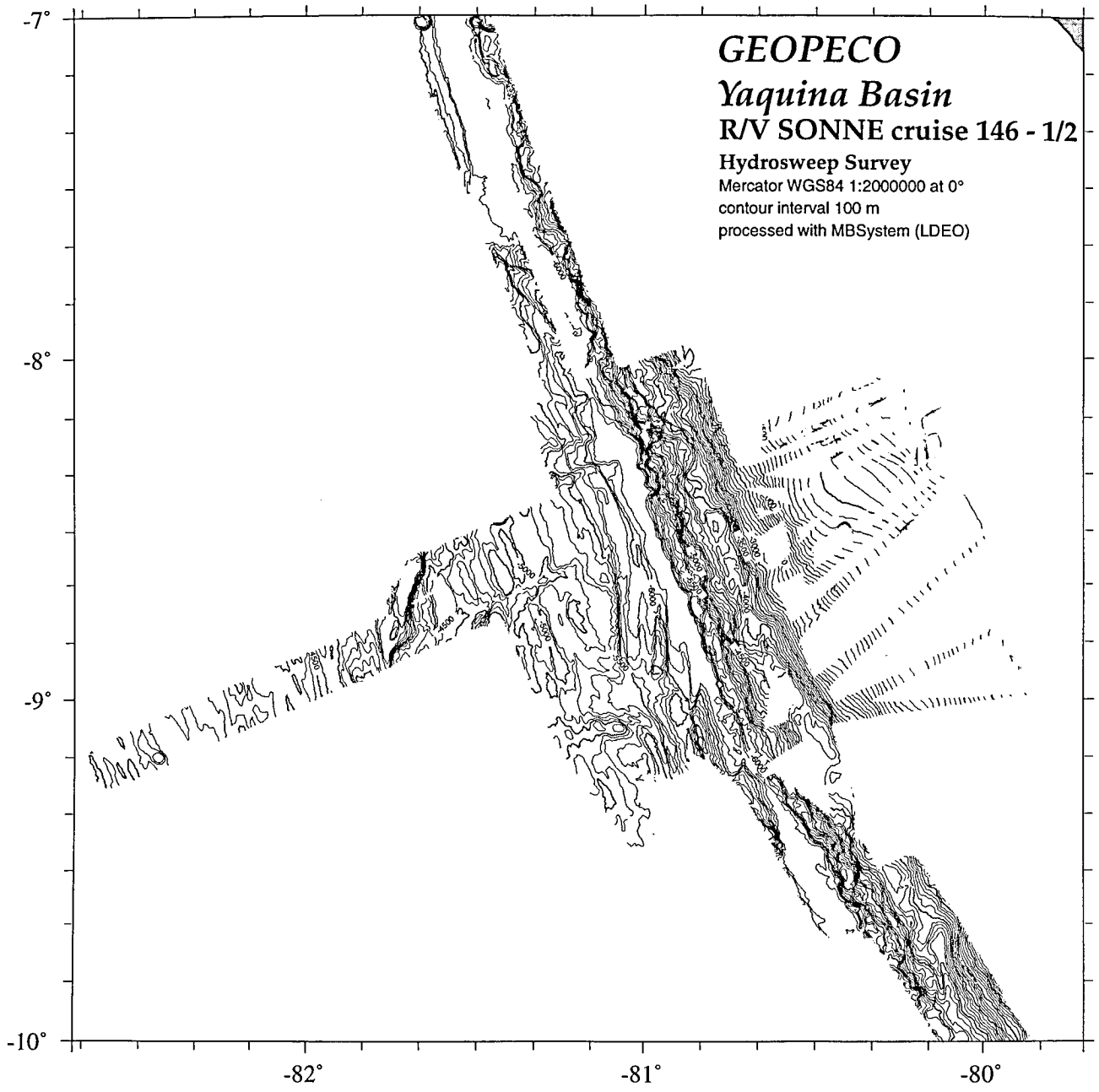

Figure 8.4.1: Bathymetric map of the Yaquina Basin off northern Peru. The part of the surveyed area, where coverage is complete, includes the oceanic Nazca Plate, the tench, and the lower slope shown in detail in Figure 8.4.3.

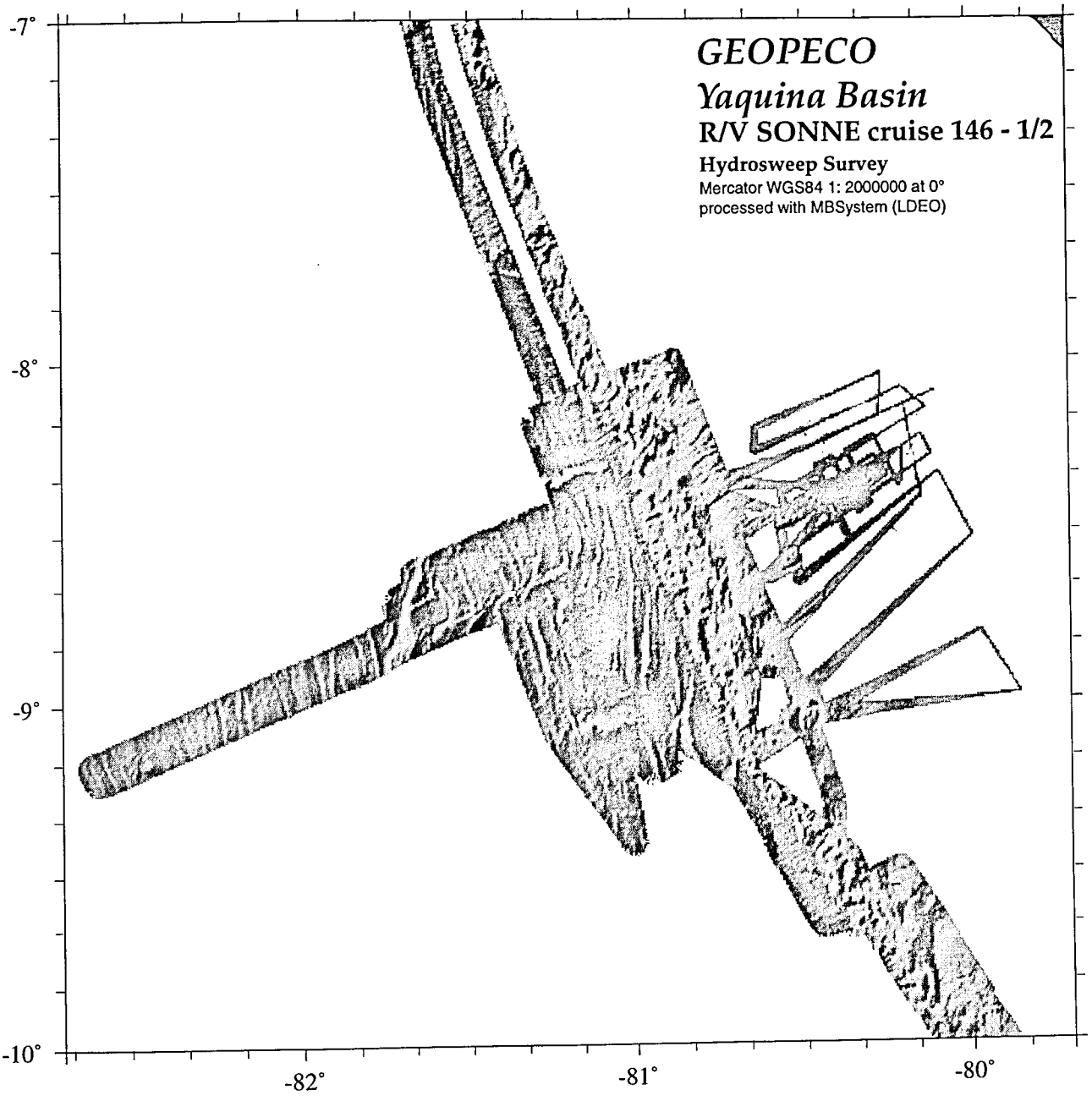

Figure 8.4.2: Grayscaled bathymetric map of the Yaquina Basin northern Peru. Illumination from northwest.

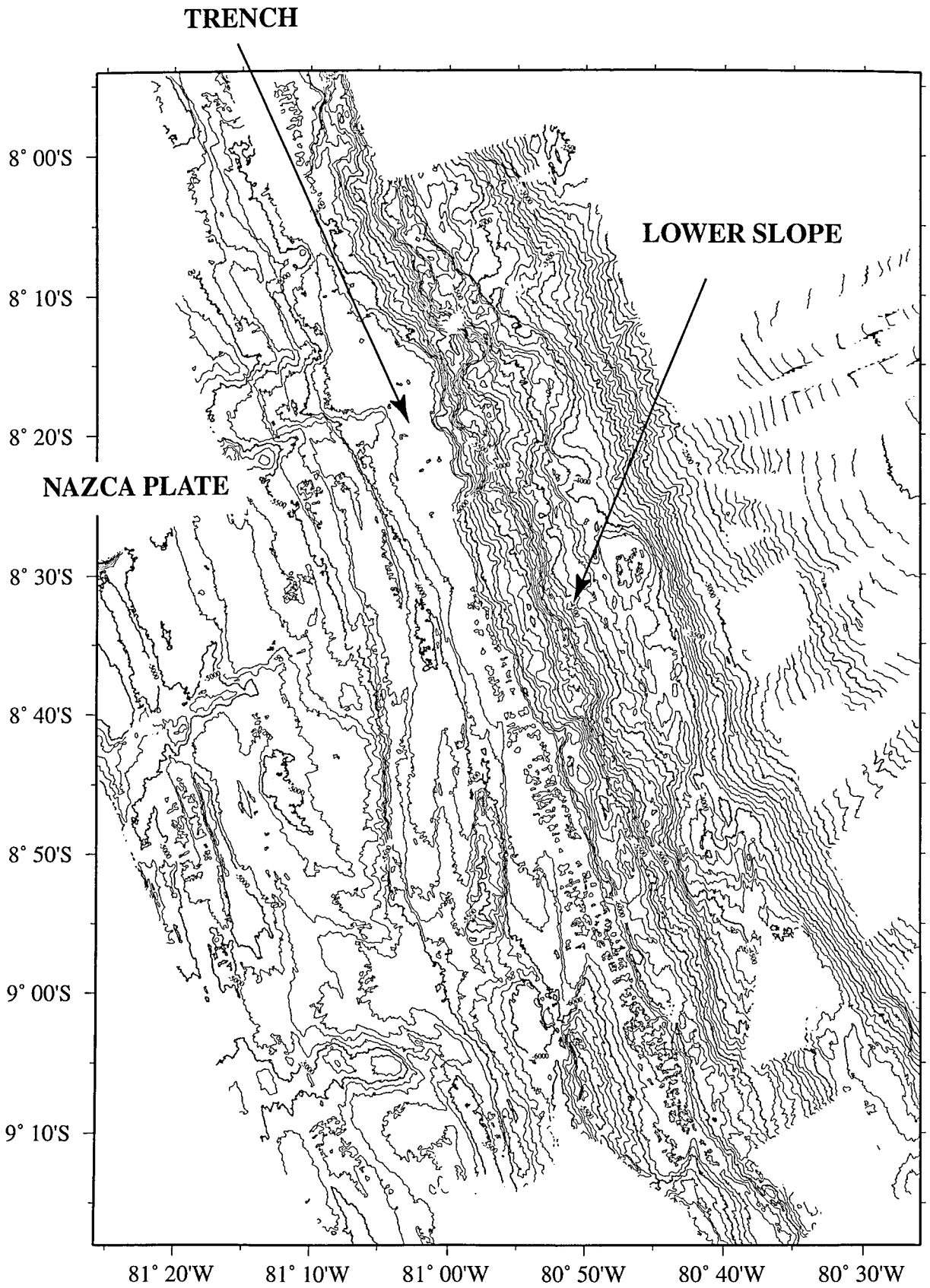

Figure 8.4.3: Bathymetric map of 115km x 164km large area offshore northern Peru. Data were recorded during SONNE cruise SO 146 - 1/2 (grid spacing of 200m). The map includes a part of the NAZCA Plate and the lower slope in the region of northern Peru.

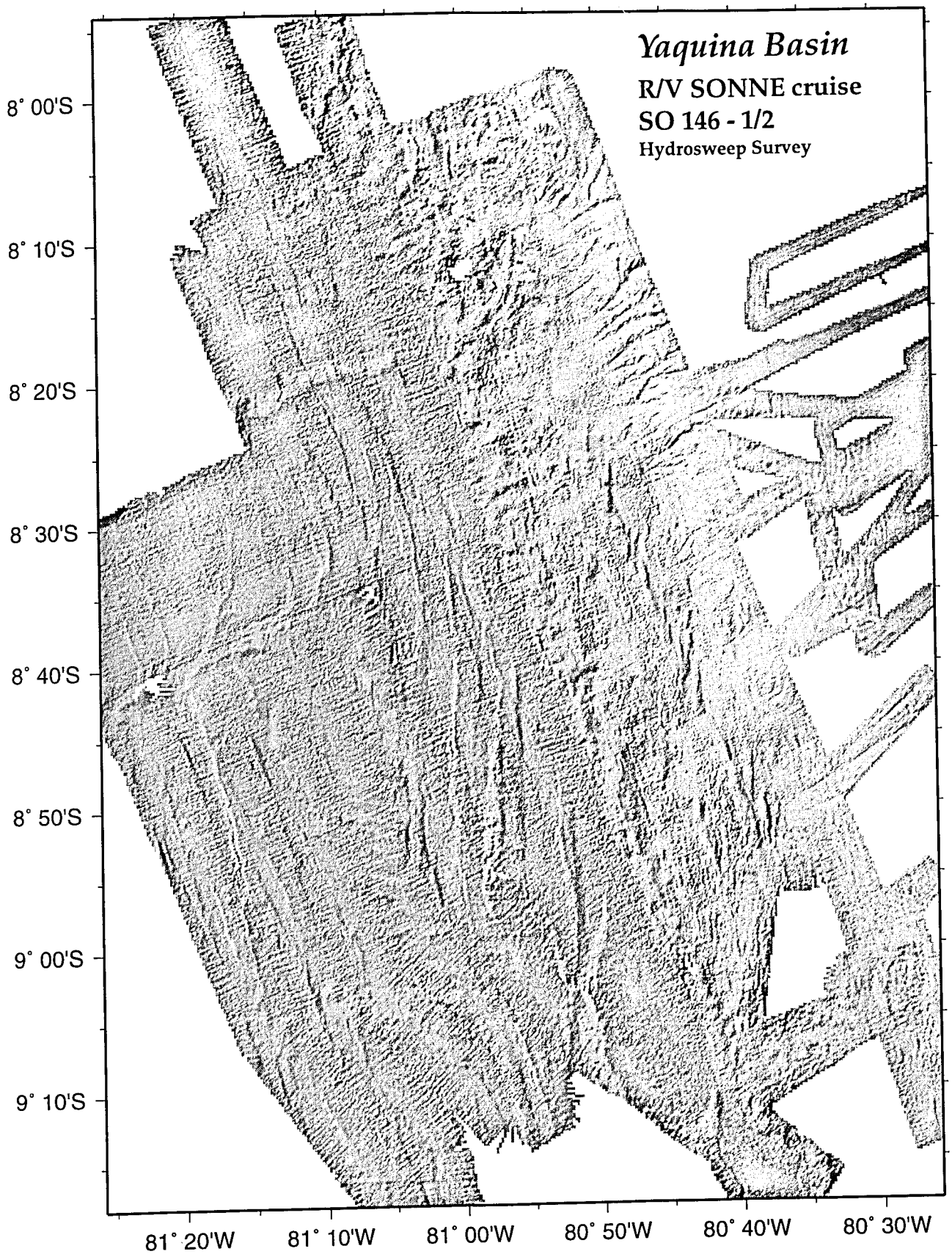

Figure 8.4.4: Grayscaled bathymetrical map of the Yaquina Basin. Shown is the same area as in figure 8.4.3.

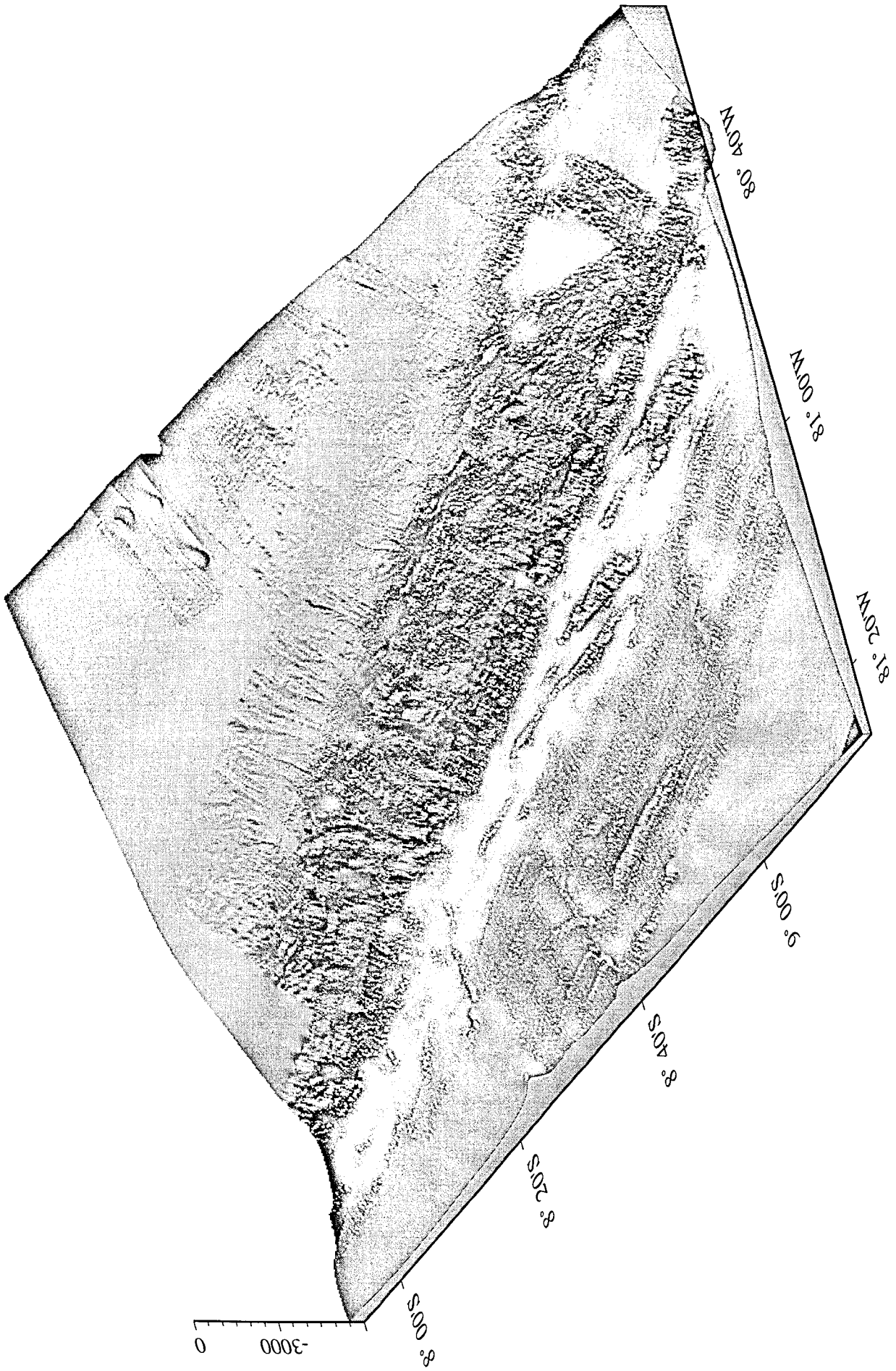

Figure 8.4.5: Perspective image of the Yaquima Basin and the lower slope. View from the Nazca Plate towards to the trench and the coastline of Peru.

8.5 Gravity and Magnetics in the Yaquina Transect

(G. A. Dehghani and R. Heinbockel)

The Free-air anomaly map of the region was constructed using all measured gravity profiles in the Yaquina Basin and the neighbouring trench area (Figure 8.5.1). Locations of ODP Sites 683, 684 and 685 are indicated as white circles. The map was produced using the GMT software package.

The Free-air anomaly field, of the Yaquina Basin and its surrounding, area varies between –180 mGal and 100 mGal. The the gravity field minimum coincides with the deepest part of the trench which trends NW.

The Free-air anomaly along the trench has a fairly high gradient (3 mGal/km) reaching values of –180 mGal along the trench axis. On the other side of the trench in the Yaquina Basin itself, landward of the trench, the Free-air anomaly is positive and relatively quiet. The shape and direction of this regional positive anomaly follows the morphology of the Yaquina Basin. Locally, gravity anomalies within the Yaquina Basin are not oriented parallel to the trench indicating the influence of active tectonics in the basin. However, the shape of the anomaly in the eastern part of the Yaquina Basin could be an artefact created by extrapolation of the available data. The positive anomaly in the southern part of the Yaquina Basin near the easternmost ODP site indicates the absence of Early Miocene sediments in this area.
Seaward of the trench the gravity anomaly is more typical of oceanic crust, with positive values and no strong disturbances.

The small lens-shaped local anomalies in this area are an artefact of vessel manoeuvring. We are confident that the signal quality will improve after post-processing. The gravity date will be combined with results from seismic experiments and drilling, and the dense distribution of acquired gravity data will allow the construction of 3-dimensional models.

Magnetic anomalies were recorded along some of the gravity profiles in the Yaquina Basin (Figure 8.5.2). The residual magnetic anomaly of profile 4c, crossing the peruvian trench with a SW trend possesses a length of 192 km. Seismic refraction and reflection data were also recorded along this profile. The most interesting feature of this profile are the two large anomalies associated with the oceanic crust and are most likely due to seafloor spreading.

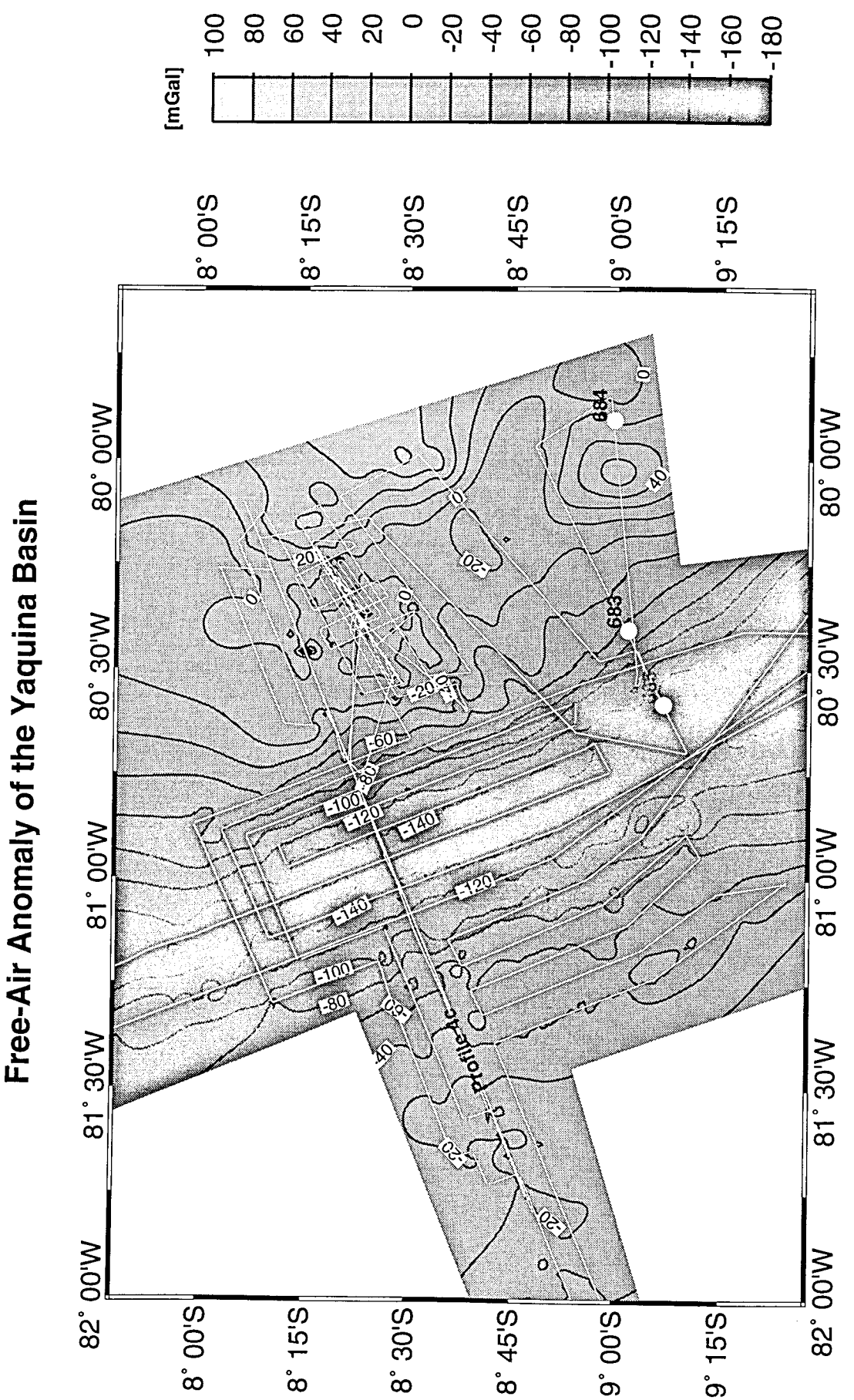
Free-Air Anomaly of the Yaquina Basin
[mGal]
100
80
60
40
20
0
-20
-40
-60
-80
-100
-120
-140
-160
-180
82° 00'W
81° 30'W
81° 00'W
80° 30'W
80° 00'W
8° 00'S
8° 15'S
8° 30'S
8° 45'S
9° 00'S
9° 15'S
Profile A-A'
684
683
685

Figure 8.5.1

Magnetic Residual Anomaly Along Profile 4c in the Yaquina Basin (preliminary)

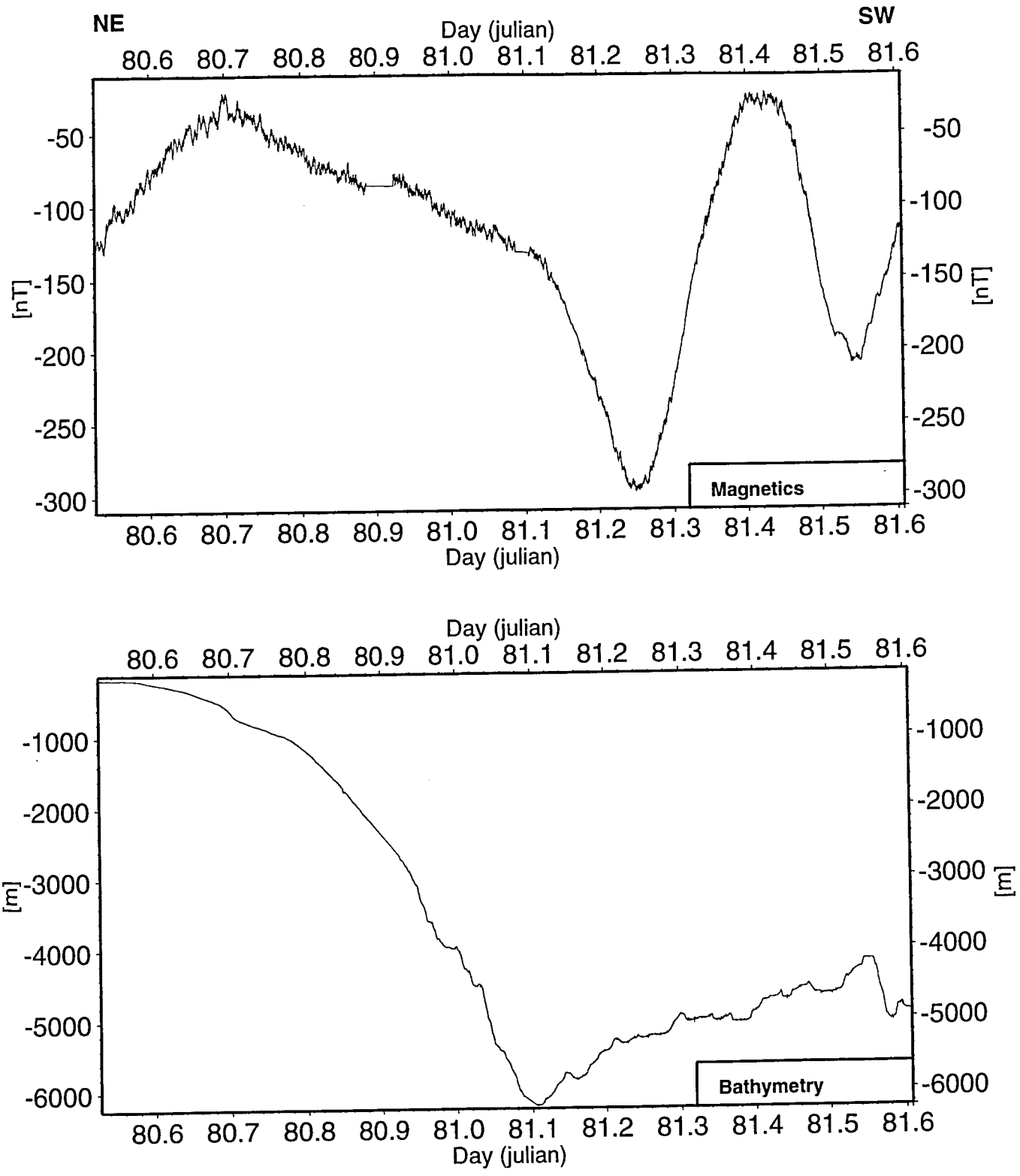

Figure 8.5.2

8.6 OFOS and TVG observations in Yaquina Basin

(J. Greinert, T. Nadler)

Seafloor observations with the OFOS sled were undertaken to investigate the occurrence of gas hydrate cropping out at the seafloor, as well as active or ancient cold vent sites in areas where BSR structures are observed in the seismic profiles. Latter studies can provide evidence of fluid pathways, but unfortunately the slow expulsion of upwardly migrating fluids without geochemical reactions at the seafloor can not be made by direct observations. Typical observations at cold vent areas are linked to fluids generated in deeper parts of the sediment column. Because of the higher concentrations of reduced chemical components these fluids are geochemically different from the pore water composition near the sediment surface. Typical components include hydrogen sulfide (H_2S) and methane (CH_4). H_2S is generated by sulfate reducing bacteria during the consumption of organic matter. Methane is derived either from CO_2-reduction by methanogenic bacteria (biogenic methane) or the maturation of organic matter (thermogenic methane). Both reduced chemical species, H_2S and CH_4, can be used indirectly as sign for active and inactive fluid venting and to determine the location of cold vent sites. Chemoautotrophic fauna, a symbioses of H_2S oxidizing bacteria, within the gills of clams (e.g. *calyptogena* or *acharax*) or tube worms, like pogonophora or *vestimentifera*, gives the most identifiable sign of H_2S-rich fluids. These fauna live in fields of some to several 100 individuals around 'focused' venting fluid sites. In particular the white clam *calyptogena*, which lives at the sediment surface, is known as common clam at cold vent sites at the peruvian continental margin (Olu et al., 1996). Bacteria's (e.g. *beggiatoa*) covering the sediment surface as white or orange colored mats using also H_2S and can be seen as sign of a more diffuse fluid expulsion.

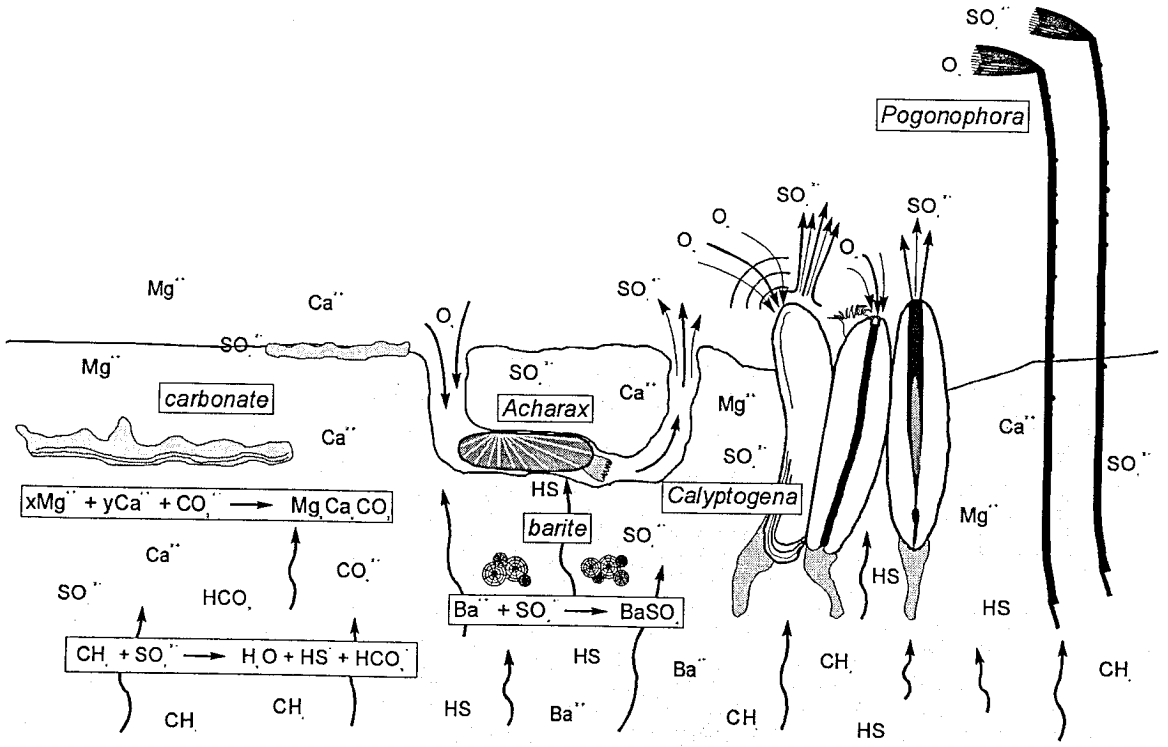

Figure 8.6.1: Geochemical mechanisms at methane and H_2S dominated cold vents. Beside the precipitation of carbonate, barite is formed if upward migrating dissolved Ba comes in contact with SO_4 from the pore or bottom water. This is the mechanism for the barite formation at the Paita area.

A typical result of methane expulsion at cold vents is the formation of authigenic carbonates. This formation is influenced by the diagenetic turnover of organic matter which also governs the total alkalinity as well as the isotopic composition of ΣCO_2 [Claypool and Kaplan, 1974; Whiticar, 1996]. Here, methane

generation via CO_2 reduction lowers the $\delta^{13}C_{CH4}$ to values < -80‰ PDB just below the sulfate reduction zone [Whiticar, 1996; Elvert et al., 1999]. However, typical $\delta^{13}C$ values from carbonates formed at methane-vents show values between -70 and -35 ‰ PDB [Ritger et al., 1987; Matsumoto, 1990; Kulm and Suess, 1990; Bohrmann et al., 1998]. These values are generated by methane oxidation via sulfate reduction of 'methanotrophic bacteria' and is thought to be the most important mechanism to increase alkalinity and favor the authigenic precipitation of carbonates at cold vents [Iversen and Jørgensen, 1985; Masuzawa et al., 1992; Whiticar, 1996; Ritger et al., 1987; Han and Suess, 1989; Kulm and Suess, 1990; Paull et al., 1992]. This process results in single carbonate blocks formed in a concretion-like mechanism within the sediment, slabs or sheets as sign of a diffuse methane flux (Aharon, 1994) as well as carbonate complexes – *chemoherms* - of more than 10 m high and several hundred meter in diameter formed at the sediment surface ult (e.g. Greinert et al., in review).

Yaquina Basin

OFOS observations at the Yaquina Basin were performed along seismic profile 'line 20' shot during SO146-1. We observed the seafloor at the upper, middle and lower slope during eight OFOS deployments (Table 8.6.1) and 4 TVG grab stations (see Table in chapter 11).

Table 8.6.1: Details to OFOS track in the Yaquina Basin

ship coordinates OFOS into water and on deck	OFOS coordinates bottom sight and from bottom	time / date UTC station start / end	water depth m OFOS	line 20 shot point
OFOS 1				
start 8°28.77' S / 80°31.88' W	8°28.853' S / 80°31.958' W	09:51 / 8.4.2000	1400	2250
end 8°26.17' S / 80°27.88' W	8°26.220' S / 80°27.947' W	15:50 / 8.4.2000	1040	1900
OFOS 2				
start 8°27.53' S / 80°31.88' W	8°27.552' S / 80°31.930' W	17:35 / 8.4.2000	1330	2206
end 8°22.89' S / 80°28.38' W	8°25.482' S / 80°28.418' W	20:58 / 8.4.2000	1045	1900
OFOS3-1				
start 8°23.75' S / 80°24.29' W	8°23.778' S / 80°24.360' W	10:56 / 9.4.2000	943	1595
end 8°22.89' S / 80°23.10' W	8°23.028' S / 80°23.166' W	12:47 / 9.4.2000	911	1483
OFOS 3-2				
start 8°23.62' S / 80°24.30' W	8°23.664' S / 80°24.348' W	13:51 / 9.4.2000	945	1593
end 8°23.12' S / 80°23.62' W	8°23.196' S / 80°23.643' W	15:06 / 9.4.2000	925	1532
OFOS 3-3				
start 8°23.18' S / 80°24.07' W	8°23.208' S / 80°24.072' W	16:03 / 9.4.2000	931	-
end 8°23.45' S / 80°23.64' W	8°23.436' S / 80°23.676' W	16:49 / 9.4.2000	929	-
OFOS 4-1				
start 8°19.07' S / 80°17.22' W	8°19.092' S / 80°17.202' W	10:40 / 10.4.2000	680	996
end 8°17.45' S / 80°14.85' W	8°17.496' S / 80°14.880' W	14:19 / 10.4.2000	481	794
OFOS 4-2				
start 8°17.06' S / 80°14.10' W	8°17.094' S / 80°14.112' W	14:58 / 10.4.2000	410	730
end 8°16.39' S / 80°12.72' W	8°16.392' S / 80°12.753' W	17:00 / 10.4.2000	265	614
OFOS 4-3				
start 8°17.57' S / 80°14.82' W	8°17.592' S / 80°14.841' W	17:49 / 10.4.2000	480	796
end 8°16.85' S / 80°13.84' W	8°16.884' S / 80°13.866' W	19.27 / 10.4.2000	377	700

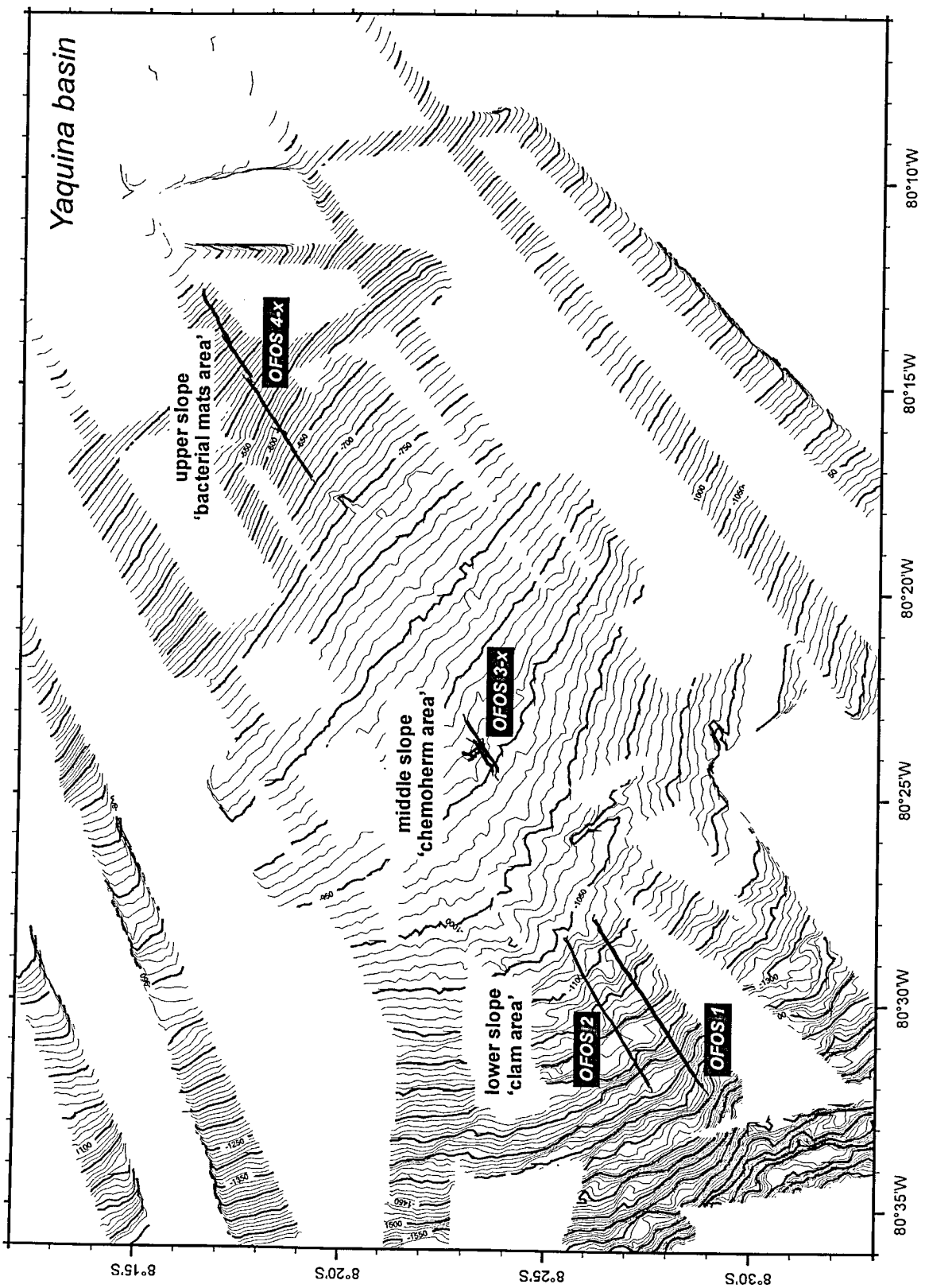

Figure8.6.2: OFOS tracks in the Yaquina Basin, SO146-2.

At the lower slope OFOS 1 and 2 were undertaken in the upslope direction showing clam fields of *calyptogena* shells and some living individuals. OFOS 3-1, 3-2 and 3-3 observed the area of the middle slope. Here, massive deposits of authigenic carbonate complexes, several 100 m in wide and up to 15 m in height, characterize the *Chemoherm-area* indicating a higher fluid flow of methane-rich fluids. In the upper slope, OFOS deployments 4-1, 4-2 and 4-3, show a wide area of current ripples and whitish bacterial mats of dm to m in size at water depths between 450 and 300m.

Lower slope; Clam-fields

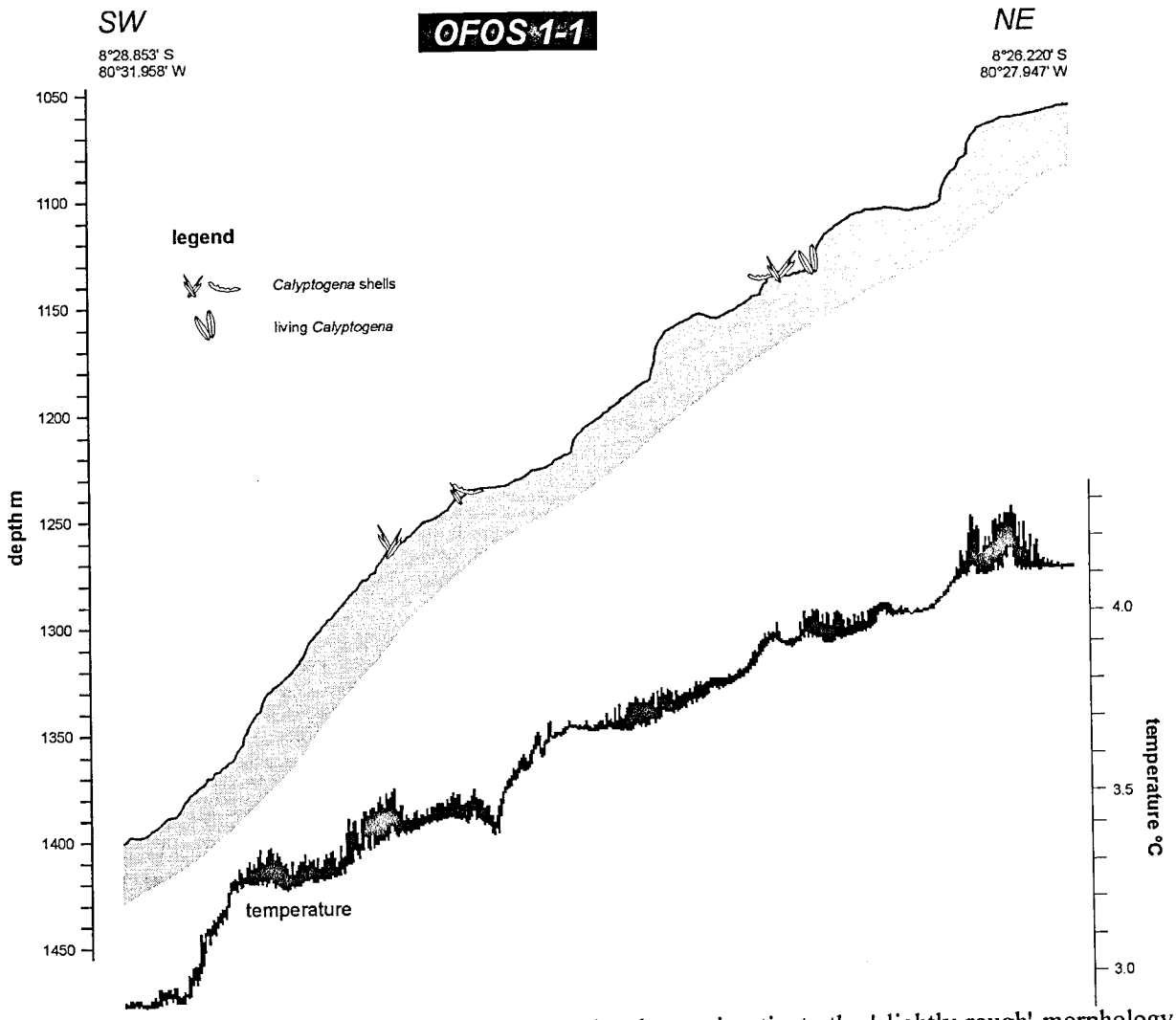

OFOS observations at the lower slope area were undertaken to inestigate the 'slightly rough' morphology occurring between 1400 and 1050 m water depth on line 20 (OFOS 1; Figure 8.6.3) and 1 Nm north of this line (OFOS 2; Figure 8.6.4). During both deployments bioturbated soft sediment was observed with brittle stars - sometimes more than 10 per m^2 -, crinoides and few sponges. These fauna represent 'normal' benthic organism community which live on or in the soft sediment. Their large quantity may be due to the brown fluffy layer on the sediment surface which is generated by a plankton bloom occurring during the time of our investigations.

Figure 8.6.3: Depth profiles from OFOS 1 with vent-related observations.

Bedrock cropping out or other geological structures were not observed along OFOS 1 and OFOS 2 tracks. Most striking were small fields of *calyptogena* shells during OFOS 1 and bigger clam shell fields with some living individuals during OFOS 2 (Figure 8.6.4). The most typical signs of fluid venting could be observed between 1300 and 1150 m water depth.

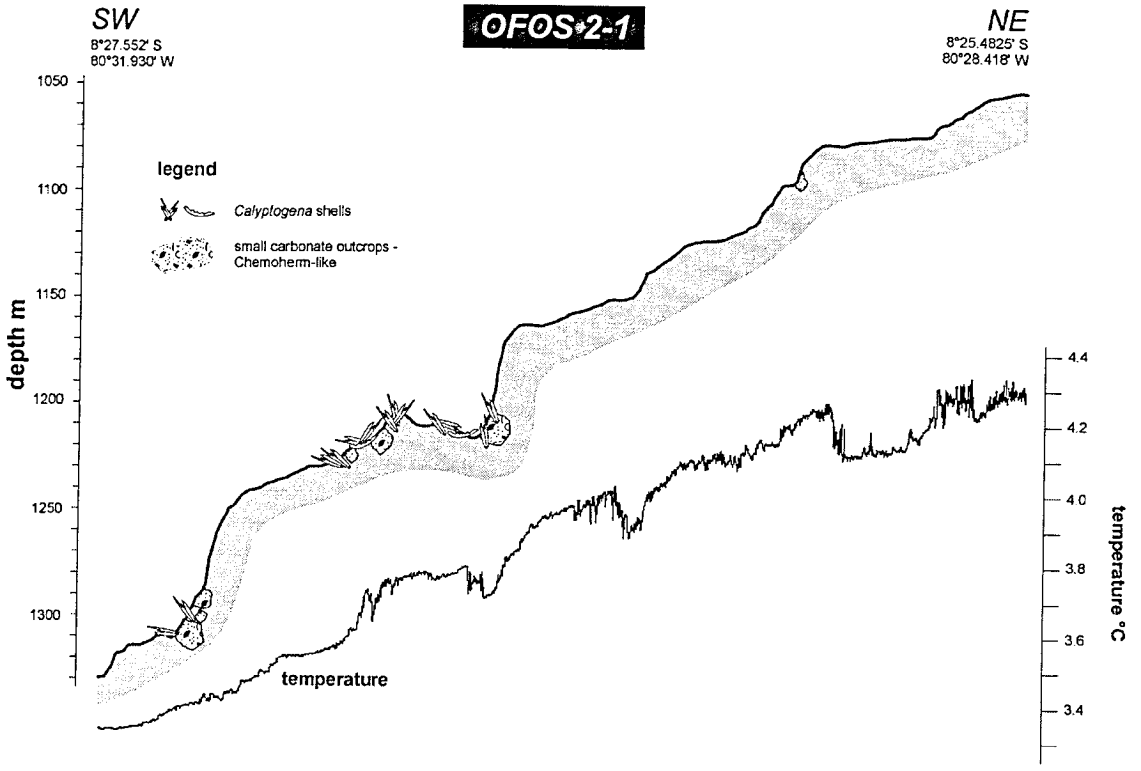

In addition small blocks tentatively identified as chemoherm-like carbonates associated with these clam observations were observed during OFOS 2.Even if only small indications of active fluide venting are observed, then the expulsion of H_2S and likely methane between 1300 and 1200 m indicate that 'focused' fluide flow is likely to occur in this area.

Figure 8.6.4: Depth profiles from OFOS 2 with vent-related observations.

Middle slope; Chemoherm area

OFOS observations at the middle slope were undertaken to observe the seafloor above the sudden termination of the BSR structure at shot point 1315 of seismic line 20. We planed to cover the seafloor between shot point 1600 - where two small mounts (named 'Max and Moritz') were seen in the seismic profile - and shot point 1200. We stopped OFOS 3-1 before the termination of the BSR was reached because we observed the massive chemoherm-like carbonate deposit (shot point 1560, 'Max') and sailed back to start a parallel track slightly north of OFOS track 3-1. During this track (OFOS 3-2) we again observed the 'Max' chemoherm. This chemoherm is up to 15m high and around 500 m wide in NE direction. To investigate the dimension of this complex we stopped OFOS 3-2 behind the NE end to undertake another OFOS track perpendicular to 3-1 and 3-2 oriented NW to SE. During the short transit to the starting point of this new track we observed another small mount NW of the 'Max' chemoherm. The southern end of this new mount (named 'Witwe Bolte') was recognized along OFOS 3-3 as small hill 4 m in height before we reached the 'Max' chemoherm (Figure 8.6.5).

The seafloor along OFOS 3-1 shows, in addition to the chemoherm, bioturbated soft sediment with brittle stars – although at a smaller frequency than during OFOS 1 and 2 - as 'normal' fauna. Between 940 and 935 m water depth (OFOS CTD depth) the - possible - southern edge of the 'Moritz' high was covered and shells were observed (Figure 8.6.4). Slides taken during the track will confirm if these shells are relic of unspecified bivalvia or of *calyptogena* and *acharax*.

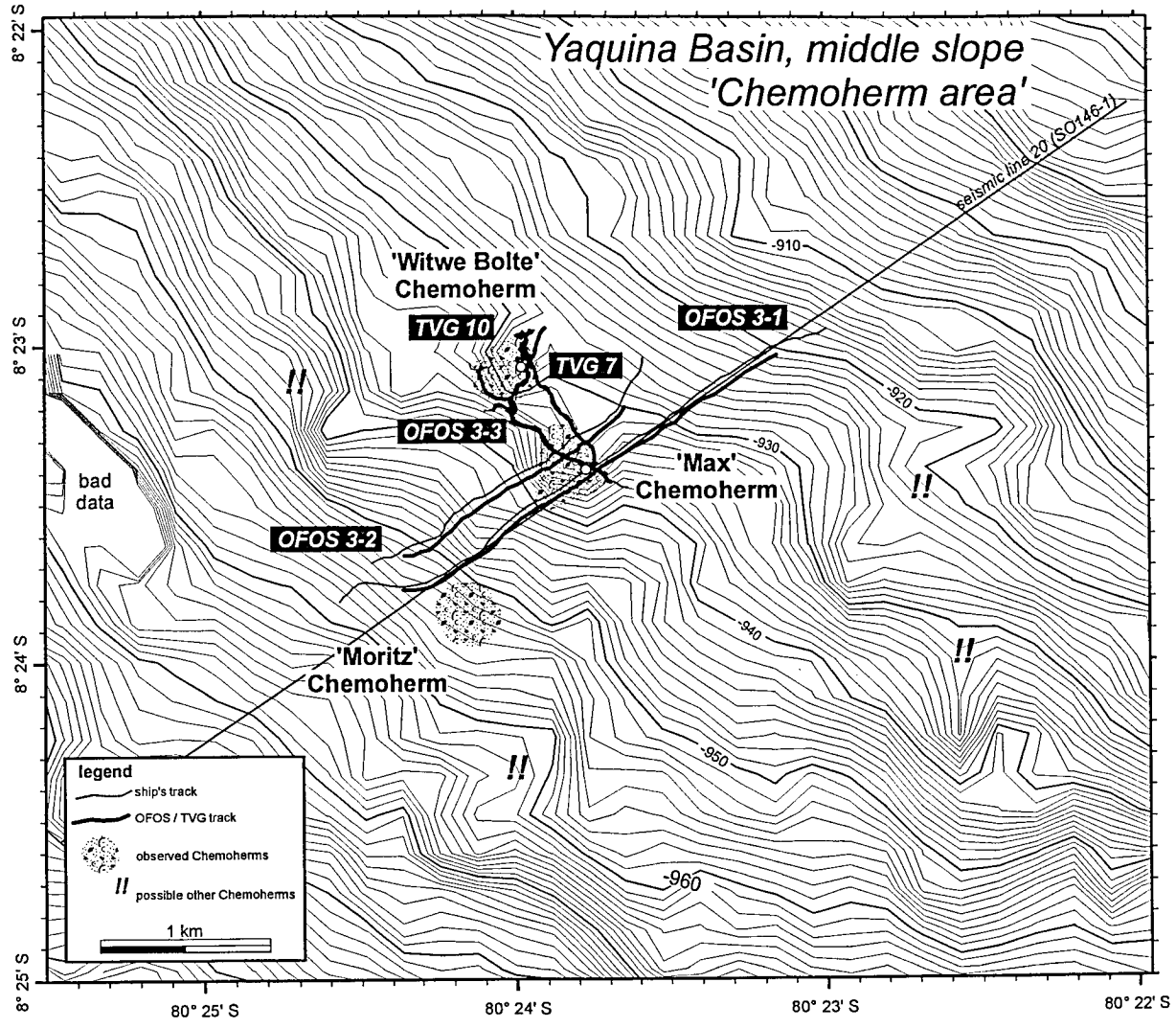

Figure 8.6.5: Bathymetric map of the 'Chemoherm area' at the middle slope of the Yaquina basin. TVG 7 was planed to observe 'Witwe Bolte' and take a sample at the 'Max' chemoherm. TVG 10 sampled the 'Witwe Bolte' chemoherm. At least four very likely chemoherm complexes can be mapped in addition based on the bathymetric information.

OFOS 3-2 showed clam shells in the same depth range as OFOS 3-1. These shells occur within an area of soft sediment with the normal bioturbation features and settlement with brittle stars as observed during OFOS 3-1. The southern flank of 'Max' along this track starts suddenly after some small patches of outcropping carbonates and a few clam shells. Along this track the chemoherm complex rises up to 10 m above the seafloor and shows a flat top before it ends after approximately 400m (Figure 8.6.5). Whitish bacterial mats of irregular shape, fields of *calyptogena* shells as well as clusters of *vestimentifera* indicate expulsing H_2S-rich fluids, whereas the irregular and porous carbonates themselves indicate methane as a major fluid component. The carbonates are typically covered with a thin sediment layer or show a thicker sediment layer on the top of the chemoherm (OFOS 3-1 and 3-3).

Along OFOS 3-3, which trends parallel to the slope, some fields of *calyptogena* shells were observed at the less steep flank of 'Max', only 5 m in hight. At the edge of the carbonate complex more shell fields were observed together with colored bacterial mats and abundant clusters of *vestimentifera*. Remarkably, the top of the chemoherm complex has a horizontal flat plateau of around 500 m in diameter (Figure 8.6.7).

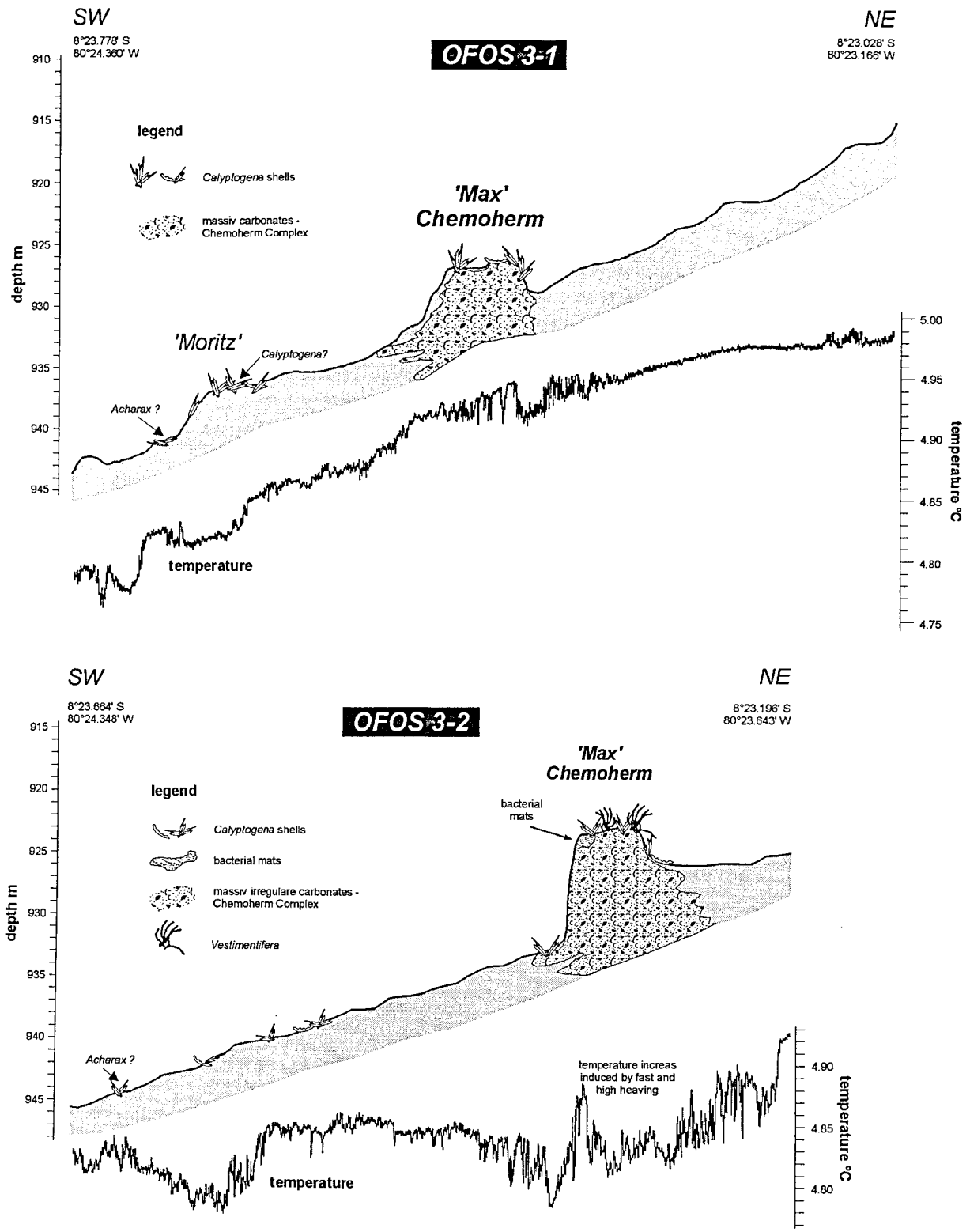

Figure 8.6.6: Depth profiles from OFOS 3-1 and 3-2.

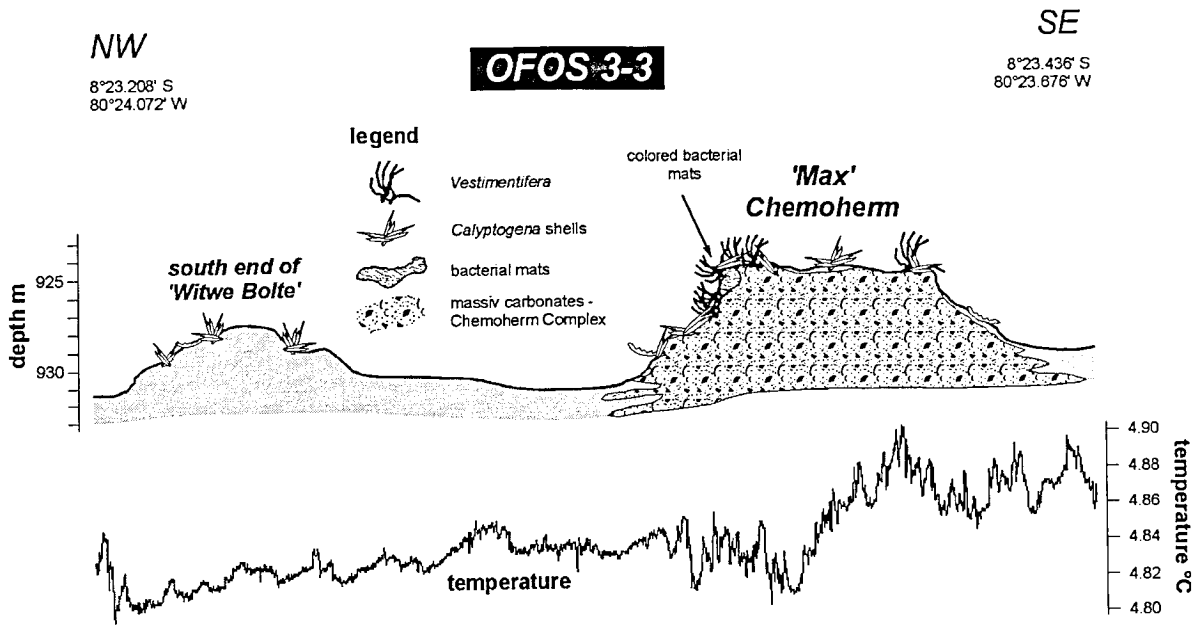

Figure 8.6.7: Depth profile from OFOS 3-3.

In addition to the OFOS observation, TVG 7 covered the 'Witwe Bolte' complex NW of 'Max'. This complex shows equivalent chemoherm structures with bacterial mats and *vestimentifera* clusters. Clams - unfortunately dead individuals - are abundant in areas with thicker sediment cover. Between both chemoherms the seafloor is composed of 'normal' sediment as described previously. This suggests that fluid flow occurred over longer time periods at local areas but without a visible sign of geochemical influences between these areas. A closer look at the 'Witwe Bolte' was taken during TVG 10. We tried to sample the carbonates nine times before the 10th drop, which recovered about 30 kg of carbonate. During sampling we observed clusters of *vestimentifera* and also small fields (around 30 individuals) of living *calyptogena.* These observations suggest that fluids migrate through the pore space of the chemoherm complexes and have been recently expulsed at the seafloor, even though wide areas of the chemoherms look 'dead'.

Upper slope; Bacterial area

At the upper slope, between 700 and 250 m water depth, three OFOS tracks were undertaken to observe a BSR structure cropping out between shot point 780 and 870 (line 20) in water depths between 600 to 475 m. Because of the unspectacular second half of the track, we stopped this track 1 hr before its planed end and sailed to OFOS 4-2 (Figure 8.6.8). Just at the bottom we saw a dense coverage of whitish bacterial mats on a sandy seafloor with current ripples. To get the exact border between this area of 'diffuse' venting and the area 'of nothing' from OFOS 4-1 we closed the gap with OFOS 4-3.

The seafloor along OFOS track 4-1 started with less bioturbated soft sediment before we reached the area between 660 and 620 m water depth. Here, widely distributed small bacterial mats were observed, as well as irregular rough patches which we tentatively identified as chemoherm-like carbonates. This conclusion needs to be confirmed by slides taken during the track (Figure 8.6.9). Seeing the bacterial mats, we anticipated seeing gas hydrate covered with a thin sediment layer (... we saw what we hoped to see). Later observations during TVG 8 proved that gas hydrate cropping out do not occur at this locality. Above 630 m, the abundance of brittle stars increased sudden and drastically (more than 30 per m^2) and a brown fluffy layer on the sediment surface was identified. In addition to brittle stars and in combination with them, we observed white 'sticks' on the sea floor bottom which increased in density.

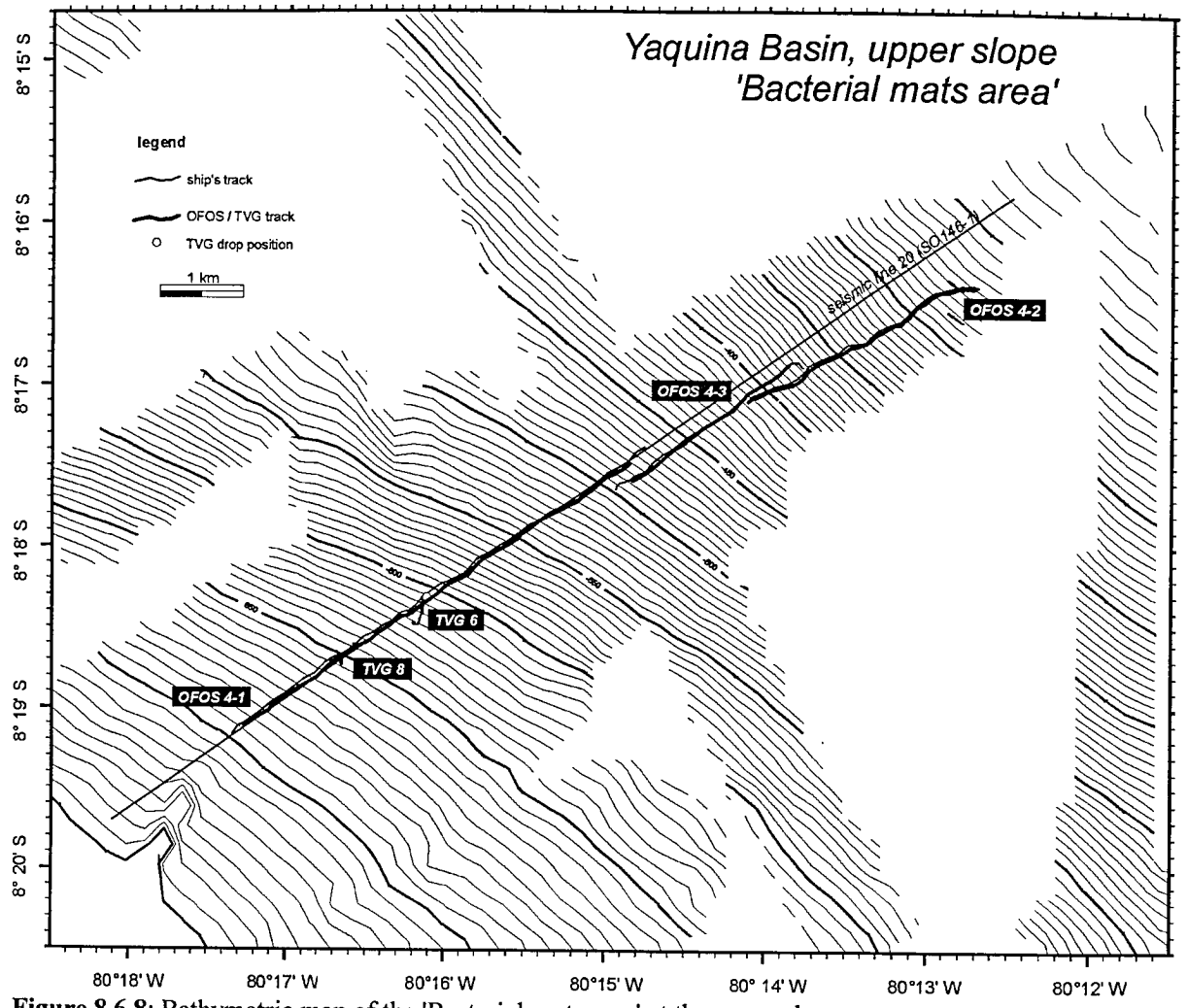

Figure 8.6.8: Bathymetric map of the 'Bacterial mats area' at the upper slope.

We assumed that we would see sediment buried *vestimentifera* but unfortunately these 'sticks' were identified as fish bones as sampled by TVG 6. At the end of this 'biologic' track a large number of red jelly fish like individuals were observed in the water column at around 520 water depth. No signs of gas hydrate or fluid venting were recognized up to the end of OFOS 4-1.

As mentioned previously, OFOS 4-2 starts in an area with sandy sediment characterized by current ripples of around 40 to 100 cm wave length. Whitish bacterial mats (rare red ones) of dm to m in size and irregular shape show dark spots at the center, a sign for high concentrations of organic carbon and authigenic sulfides formed by the reaction of expulsing H_2S with dissolved iron. Significantly, neither brittle stars nor other benthic organisms were recognized along the track, only few fish's were observed. Equivalent observations - no live, but bacterial mats - were made during OFOS 4-3 above 450 m water depth (Figure 8.6.10), whereas the lower section of OFOS 4-3 showed only sediment - slightly harder as usually - with patch-like rests of a fluffy layer.

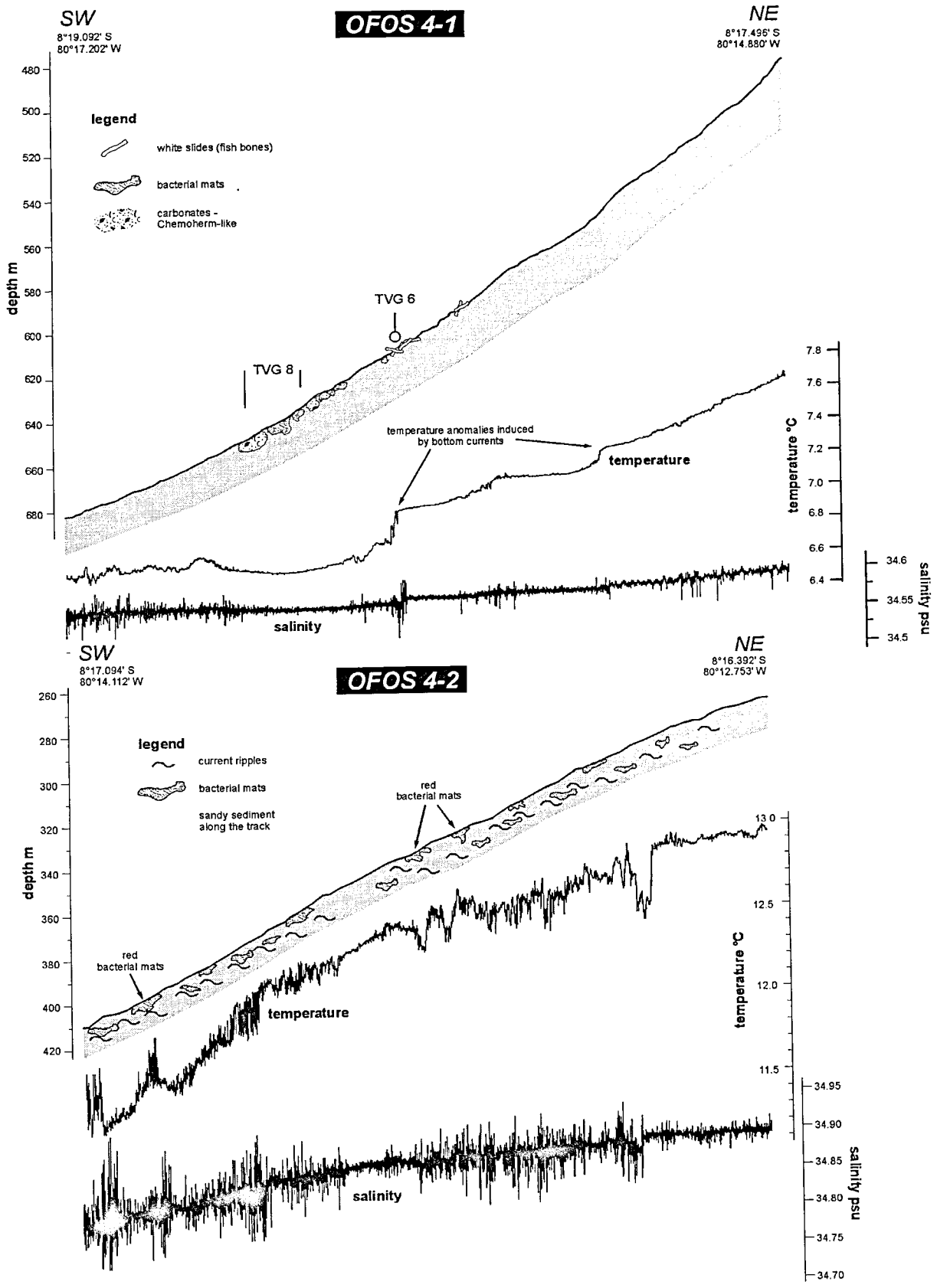

Figure 8.6.9: Depth profile of OFOS 4-1 and 4-2.

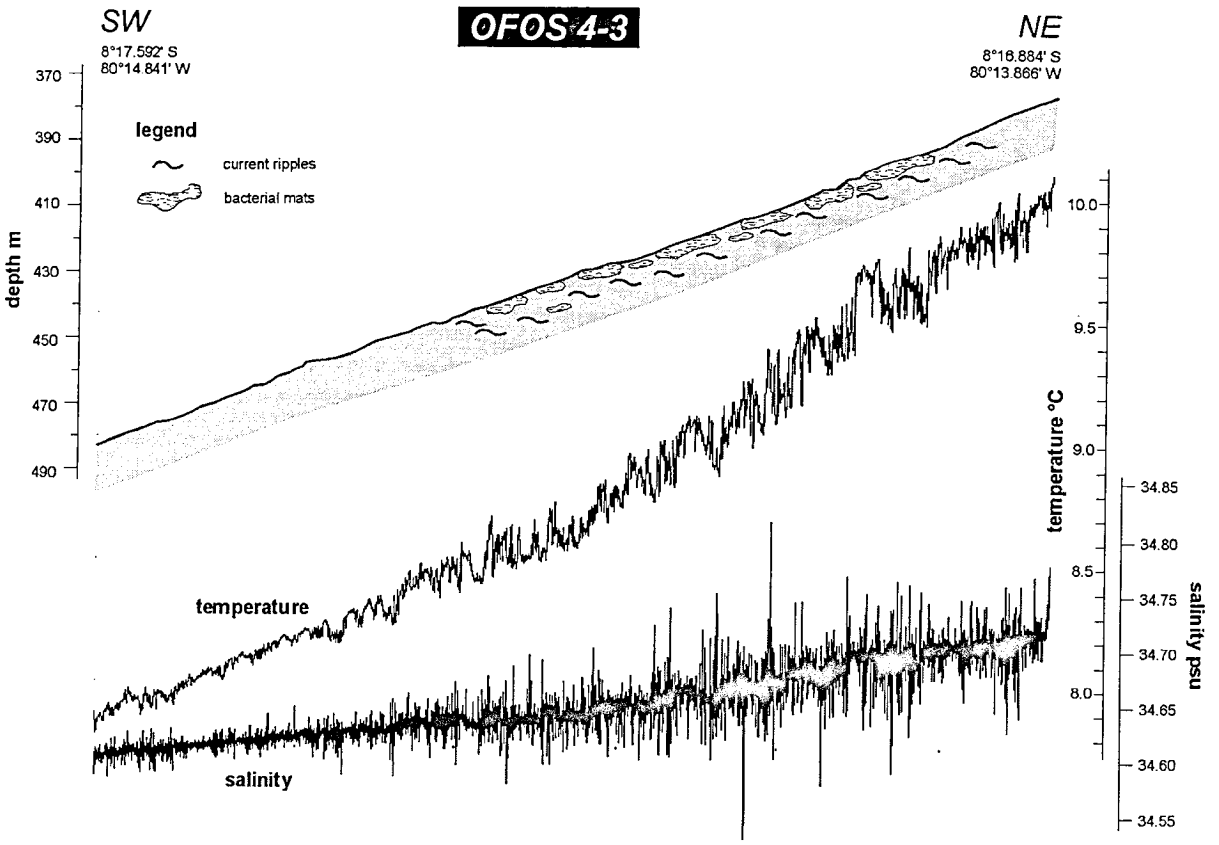

Figure 8.6.10: Depth profile of OFOS 4-3.

The observations made at the upper slope area of the Yaquina Basin suggest that in water depths shallower than about 450 m, a diffuse fluid flux of H_2S-rich fluids contaminate the bottom water for benthic organisms. The venting rates seem to be high enough to allow bacterial population to live but is not strong, focused or old enough for the settlement of vent organisms like *calyptogena* or *vestimentifera.*

8.7 Heat flow measurements: preliminary results

(N. Kaul, R.Harris, B. Heesemann)

The work of von Huene and Pecher (1999) provides the motivation for heat flow measurements in an area of vertical tectonic movement and occasional BSR occurrence.

Seven heat flow stations comprising 77 penetrations were attempted, 61 yielded successful heat flow measurements. Failure to penetrate the sea floor (16 attempts) is most likely due to exposed carbonates as observed during OFOS dives (sections 8.6 and 9.7) along heat flow station profiles. These carbonates are observed to occur as blocks or a closed cover.

The heat flow stations are positioned in 3 different areas. Three stations (HF0020, HF0021, and HF0022) are located on seismic line 20 (this survey) in Yaquina basin. A fourth station (HF0023) is located on seismic line 9 some 13 km NW of seismic line 20 (figure 8.7.1).

The second area of investigation is the Lima basin. Heat flow stations HF0024 and HF0025 (figure 8.7.5) are positioned on recent seismic line 26 and seismic line HIG13 (Hawaii Institute of Geophysics).

The third area lies across the Lima continental shelf. Heat flow station HF0026 is positioned on the basis of a seismic line shot by an exploration company (Shell 1018). This line was partially re-recorded during this cruise (line 101) for improved position control (figure 8.7.8).

A feature of regional interest is the low magnitude of heat flow observed on the continental margin offshore Peru. Most heat flow values fall between 30 and 50 mW/m^2, well below the expected heat flow of 70 – 80 mW/m^2 for 35 Ma old crust. This observation was first reported by Yamano and Uyeda (1990). As the area of investigation is an area of high sedimentation and tectonic activity, corrections need to be applied for sedimentation rates as well as tectonic subsidence or uplift.

Results of all heat flow stations are summarised in table VIII (appendix).

Temperature in the water column does not reach a constant value within the depth range where the heat flow stations are positioned. This makes it necessary to have CTD data available for calibrating the thermistor strings of the heat probe. One CTD cast is available, located near the south-western end profile 20 down to a water depth of 2700 m.

Yaquina Basin

Three heat flow targets in the Yaquina basin were identified on the basis of seismic line 20 and include areas where a strong BSR is present and areas where the BSR vanishes or is not easily identified.
Seismic line 20 is oriented south westerly (figure 8.7.1) and lies between the shelf break at about 200 m water depth and deeper environments at about 1500 m depth. Midslope a strong BSR is identified. Downslope the character of this BSR changes to a hummocky band of reflectors with a significantly reduced amplitude. Further downslope a sedimentary section is cut by normal faults which intersect the surface. Finally, a third area of interest is upslope of the prominent BSR where reflectors seem to cut through the sedimentary section and nearly reach the sea floor.

Three heat flow stations were positioned across the boundaries between these different areas. They are intended to test the hypothesis that , a) heat flow is constant over a BSR and is consistent with the depth to the BSR (HF0021), b) normal faulting provides fluid pathways resulting in a convective component of the heat flow signal (HF0020), and c) the upper limit of the gas hydrate stability zone is related to a BSR rising to the seafloor (HF0022). Finally, because the upper limit of the gas hydrate stability zone (GHSZ) is expected at this water depth, a correlation between the limit of the GHSZ and a thermal anomaly is tested.

Overall, acquired heat flow values range between 4 and 110 mW/m^2 with mean values for stations HF0020, HF0021, and HF0022 of 67.6 ± 16, 32.7 ± 7.8 and 22.9 ± 18 mW/m^2, respectively (figures 8.7.2c – 8.7.4c).

A slight trend is present from higher to lower heat flow values as one approaches the shelf edge. One value of 218 mW/m^2 (HF0022P05) is considered uncertain because of its high tilt (36.6°) and uncertain penetration. It should be noted, that no penetrations were possible in water depths shallower than 500 m, most probably due to sandy sediments near the shelf edge.

A short wavelength correlation exists between high heat flow values and the surface expression of normal faults for station HF0022. The penetration interval for this station was chosen to be 500 m in an attempt to avoid aliasing fault related effects. Variation of heat flow values is remarkably higher here than elsewhere in the working area (s.d 18 mW/m^2 corresponding to a variation of 78% of the mean). High values correspond to faults. This observation is consistent with the idea there is an additional convective component to observed heat flow values across the faults.

Station HF0023 is a 12 km long profile along a strong BSR on seismic line 9. The seismic image shows a faulted sediment layer above the BSR. These faults do not appear to penetrate the BSR but exist only near the surface. The seismic amplitude of the BSR decreases from a maximum at 2000 m water depth (shot point no 300 – 600) upslope (shot point no > 700). Measured heat flow is remarkably uniform with values of 37 mW/m^2 (s.d. 7.8 mW/m^2), figure 8.7.5c. Other trends are not observed in this data. The absence of a correlation between heat flow and surface faults strongly suggests purely conductive heat transport.

Thermal conductivity determinations were acquired from in-situ measurements approximately every second penetration point. This is reasonable, because thermal conductivity varies only slightly on a local scale. Observed thermal conductivity values are relatively low with harmonic ranging between 0.84 and 0.96 W/m*K with an overall mean of XX W/m*K. In figures 8.7.2b, 8.7.3b, 8.7.4b and 8.7.5b mean values of thermal conductivity are summarised as a function of position along heat flow station. The lowermost station (HF0020) depicts a reversed gradient of conductivities showing a decrease of values with increasing subbottom depth by some 0.06 W/m*K. Stations HF0021 and HF0022 show increasing values with depth. A distinct increase in thermal conductivity from 0.85 to 1.0 W/m*K at approximately 1.6 mbsf occurs at several penetrations.

Thermal conductivity along each is station is reasonably constant and variations in heat flow are attributed to variations in thermal gradient. Heat flow along profiles of undisturbed sediment sections is almost constant and can therefore be regarded as a background value. As a consequence, variations across inferred faults are interpreted as a convective component.

Yaquina Basin, SO146 Heat Flow Stations 20, 21, 22, 23

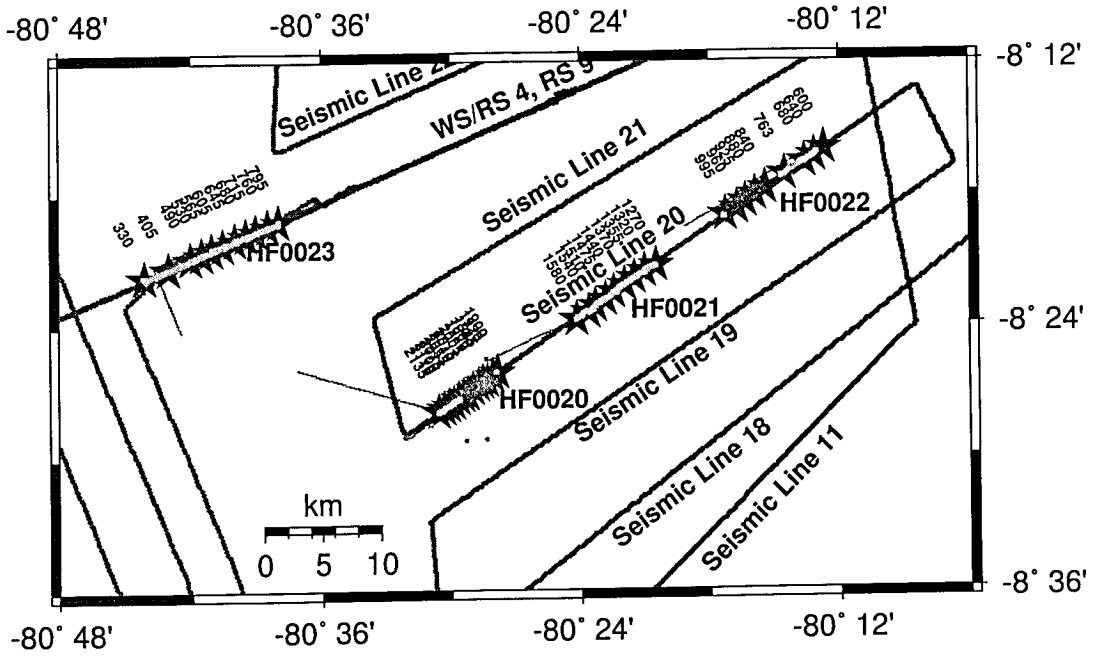

Figure 8.7.1: Location map of heat flow stations HF0020 - HF0023.

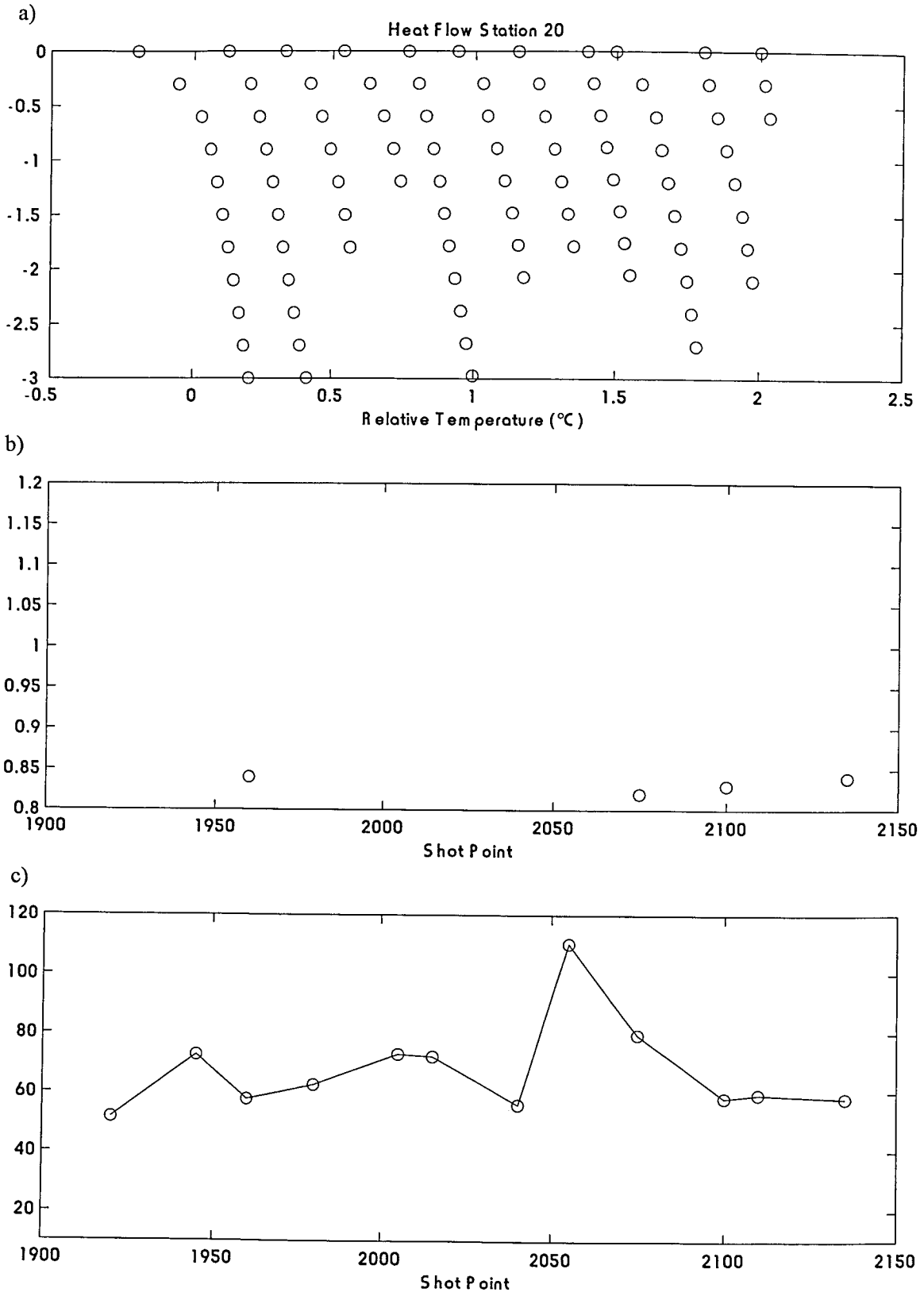

Figure 8.7.2: Results of heat flow station HF0020. Top: relative temperatures T(z), middle: vertical mean thermal conductivities, bottom: heat flow values plotted along seismic profile 20. Horizontal axis represents shot point numbers. 100 shot points represent 2.5 km distance.

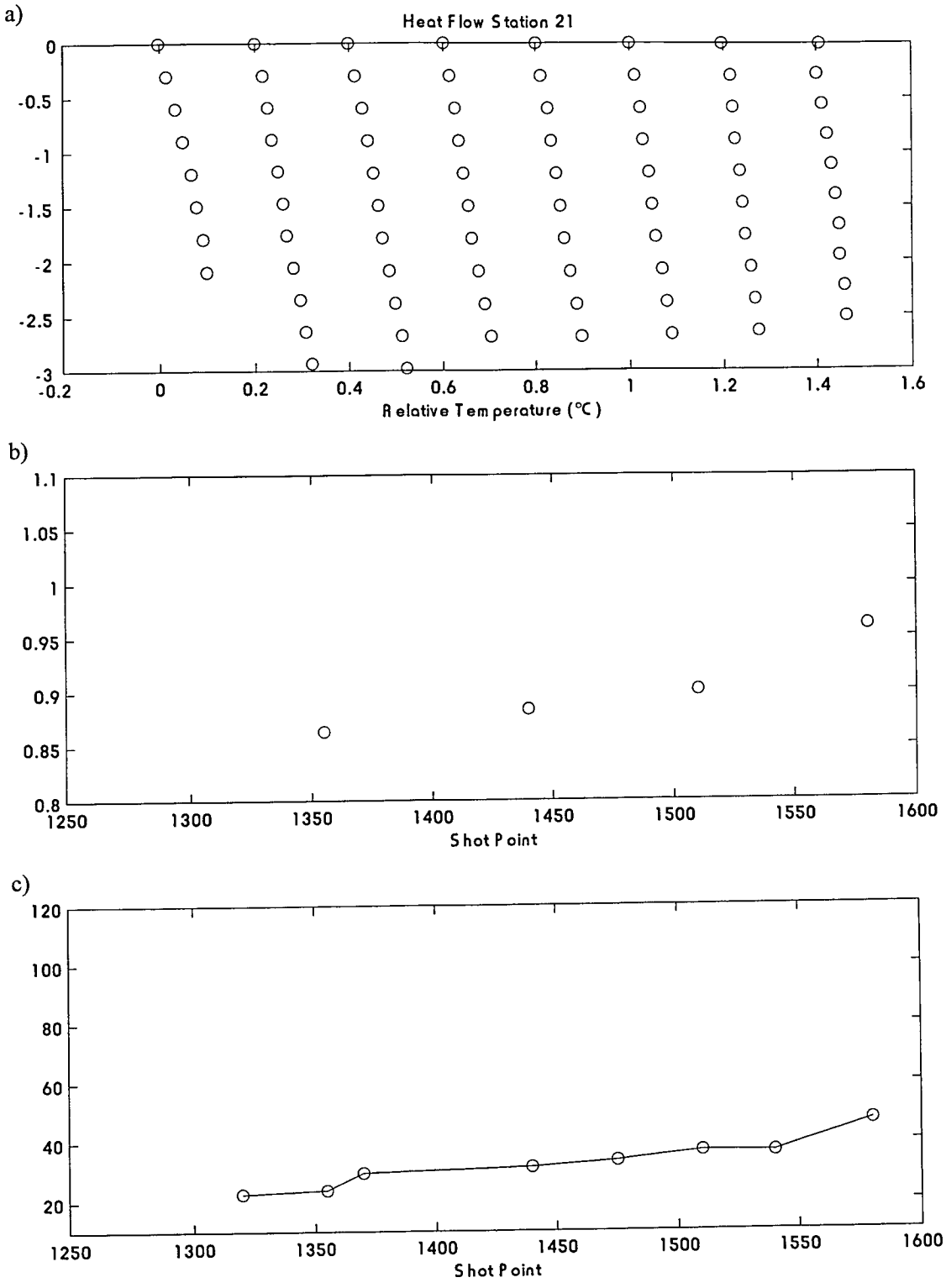

Figure 8.7.3: Results of heat flow station HF0021. Top: relative temperatures T(z), middle: vertical mean thermal conductivities, bottom: heat flow values plotted along seismic profile 20. Horizontal axis represents shot point numbers. 100 shot points represent 2.5 km distance.

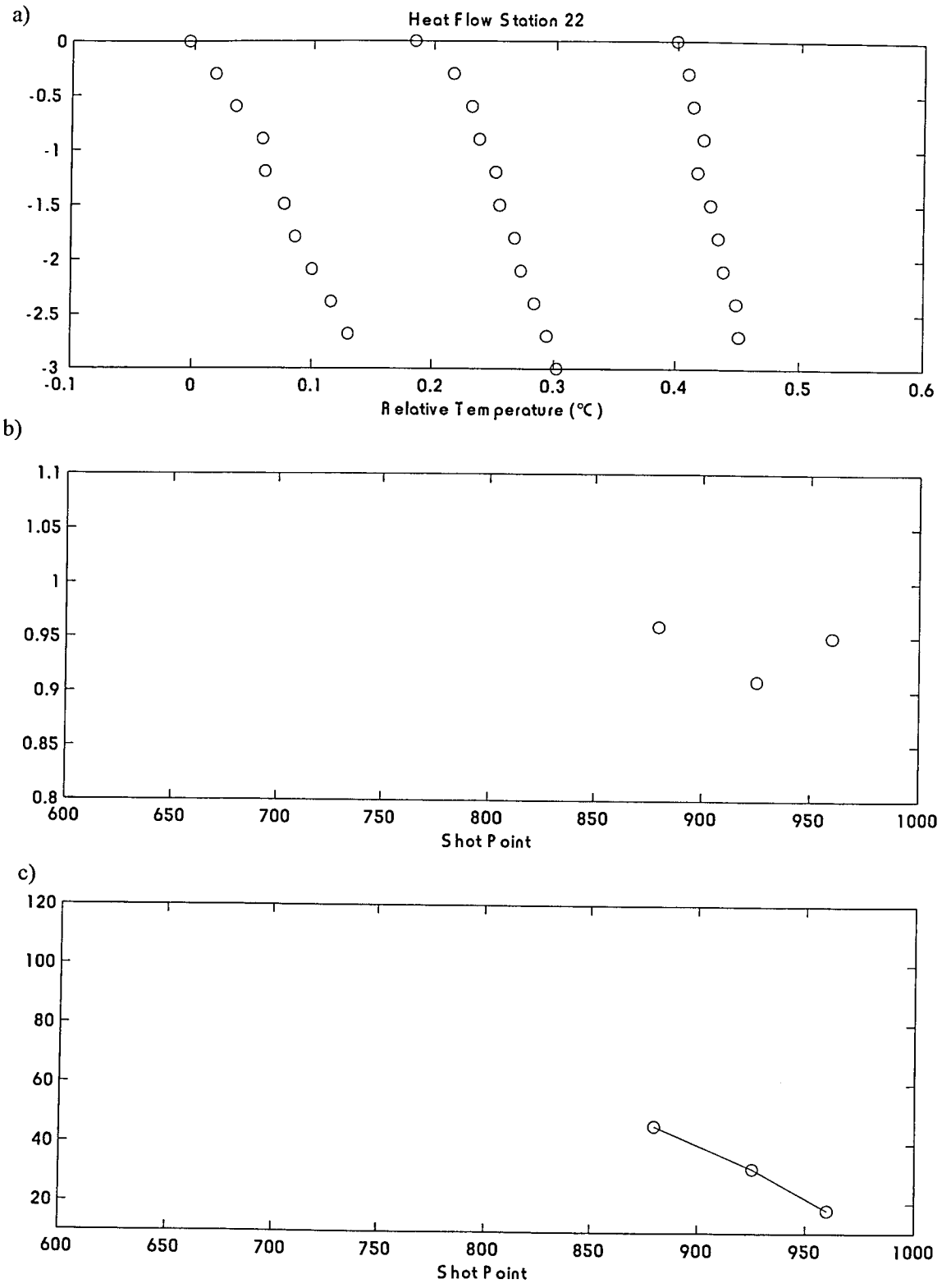

Figure 8.7.4: Results of heat flow station HF0022. Top: relative temperatures T(z), middle: vertical mean thermal conductivities, bottom: heat flow values plotted along seismic profile 20. Horizontal axis represents shot point numbers.

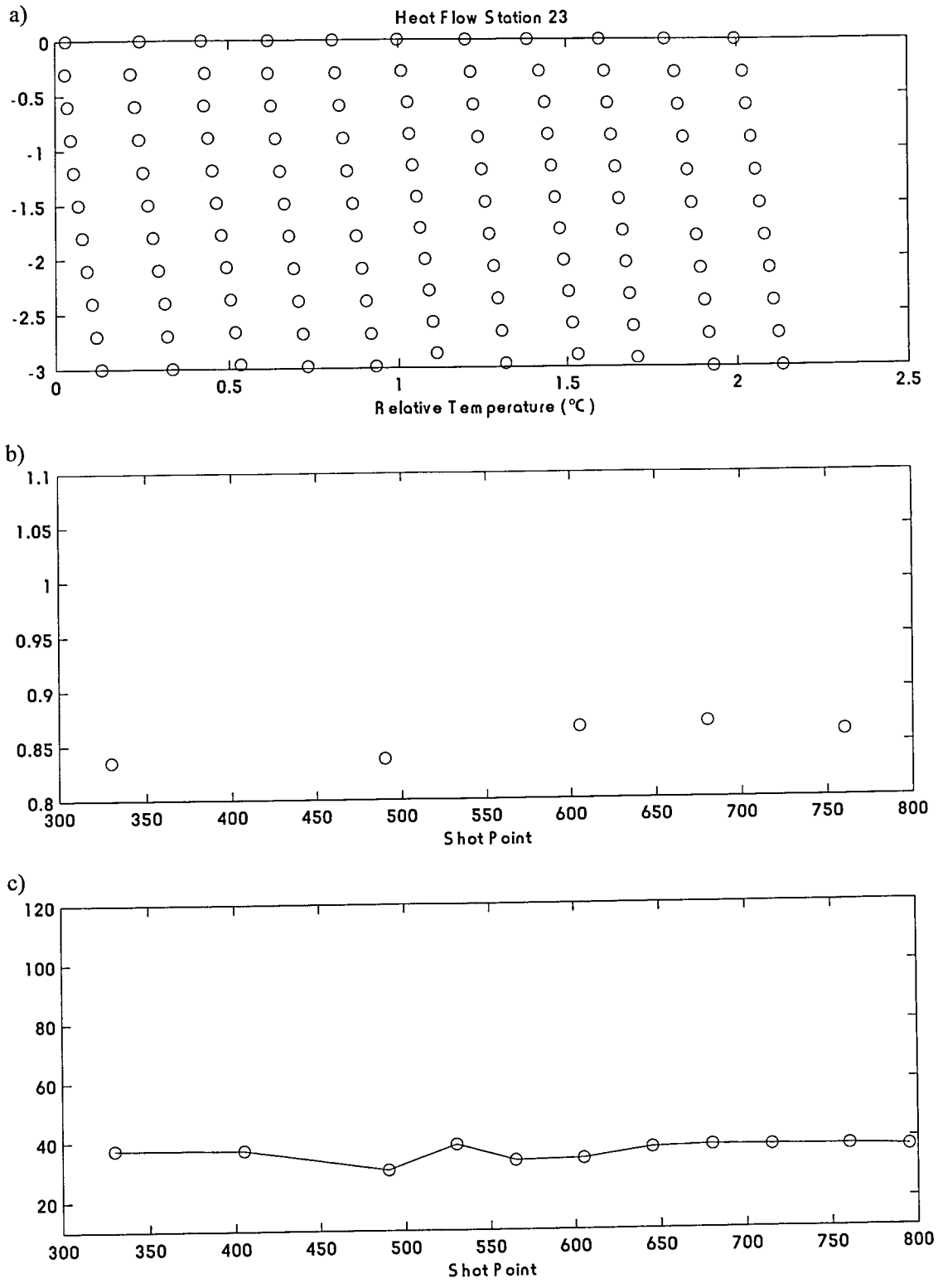

Figure 8.7.5: Results of heat flow station HF0023. Top: relative temperatures T(z), middle: vertical mean thermal conductivities, bottom: heat flow values plotted along seismic profile 9. Horizontal axis represents shot point numbers.

8.8 CTD water column observations and gas hydrate stability

(J. Greinert)

CTD investigations of the water column were completed with the Seabird 19 CTD on theOFOS sled during the OFOS deployments and with the Seabird 911 plus CTD at station CTD 2 in the Yaquina Basin. The main task was the modeling of sound velocity profiles needed for accurate bathymetric mapping.

Table 8.8.1: Stations of water column observations

station	date time (UTC)	latitude S	longitude W	HS water depth (m)
Yaquina Basin				
CTD 2	13/04/00 22:15	8°21.730'	80°44,090'	2703
OFOS 4-1, 4-2, 4-3	see table in the OFOS chapter			
Lima Basin				
OFOS 5-1, 5-2	see table in the OFOS chapter			
OFOS 6-1	see table in the OFOS chapter			

Both CTDs are in good agreement and can be correlated. Thus, the sound velocity profiles from OFOS deployments in the Lima Basin could be used for this region but as seen in Figure 8.8.1 no significant differences exist in sound velocities between both working areas.

Water column Yaquina Basin

Investigations at station CTD 2 show the typical strong temperature decrease from 23°C at the surface to 15°C in 30 m water depth (Figure 8.8.1). Parallel to the temperature profile the sound velocity decrease from around 1530 to 1505 m/s in the upper 30 m with a minimum of 1484 m/s in 1200 m. Below the sound velocity smoothly increases again to 1502 m/s in 2700 m water depth.

More smoothly decreasing is the salinity which starts by ca. 35.05 psu then drops to 34.55 psu at 800 m water depth and increases again to 34.667 psu. Nevertheless, this layer of lower salinity is sandwiched, the water column is stable as shown by the increasing density profile. Here, the steep gradient at the surface is induced by summer heating of the surface waters. An unexpected observation is the total oxygen consumption between 20 and 650 m water depth, likely induced by the remineralization of plankton. High amounts of plankton, probably a plankton plume, were indicated by brown colored surface water. The observation of a green-brown fluffy layer at the seafloor during OFOS tracks 4-1, 4-2 and 4-3 is consistent with this interpretation.

Gas hydrate stability

The occurrence of gas hydrate in the sediments of the study areas is indicated by strong BSR features. To calculate the shallowest depth for the occurrence of gas hydrate at the sediment surface, the CSMHYD program from Sloan (1998) and a salt correction of 0.0328 for 1 psu salinity after Dickens and Quinby-Hunt (1994) were used with data from CTD 2 (Figure 8.8.2). A gas phase of pure methane is assumed for the gas hydrate.
Both temperature profiles from CTD 2 and OFOS 5-2 show that gas hydrate is not stabile above 595 m water depth. Unfortunately no signs of outcropping gas hydrate could be observed below this depth.

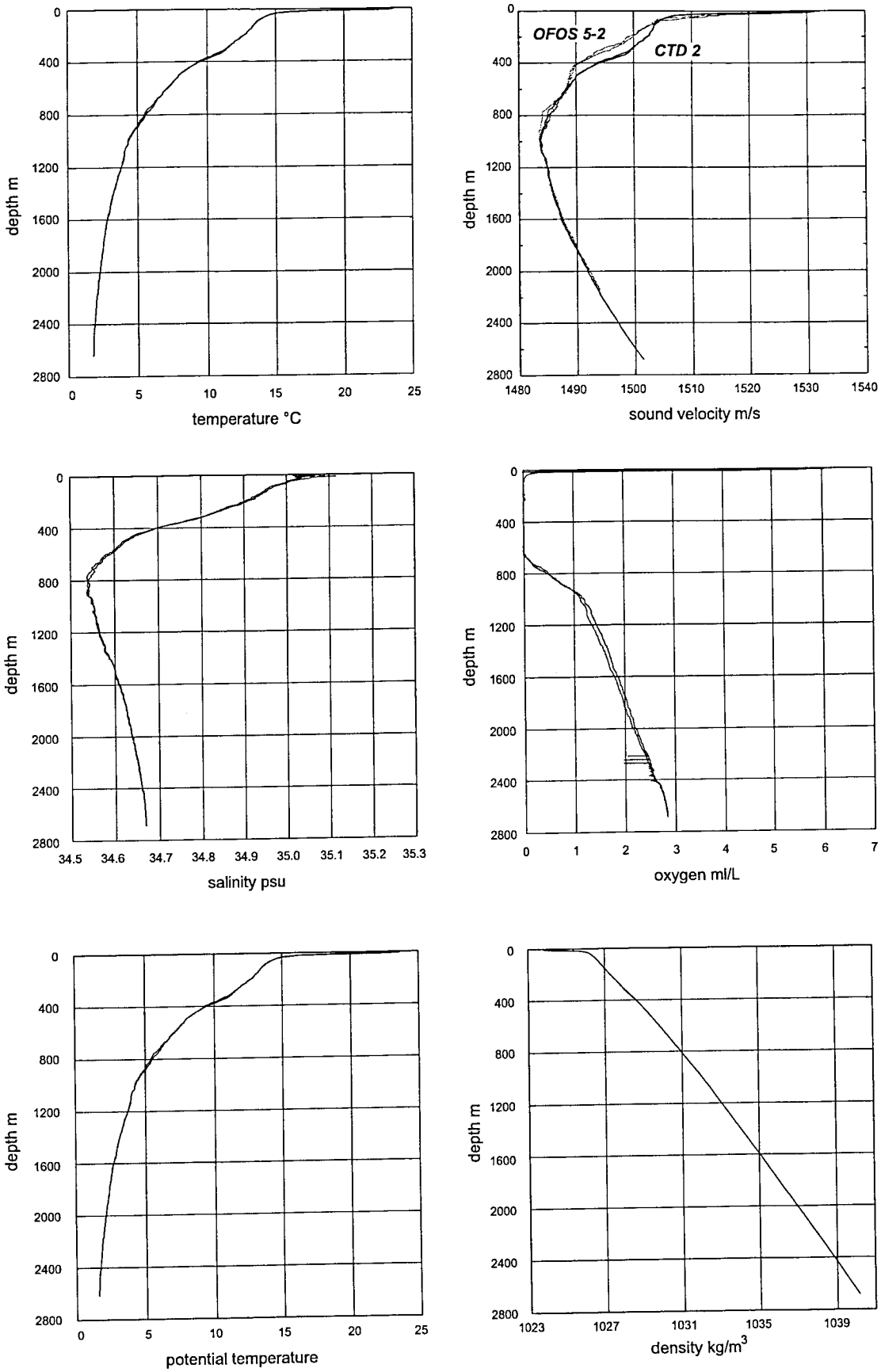

Figure 8.8.1: CTD profile from station CTD 2 in the Yaquina Basin. Differences of around 2 m/s can be observed between 100 and 600 m water depth relative to OFOS 5-2 from the Lima Basin; below 1000 m both profiles are identical.

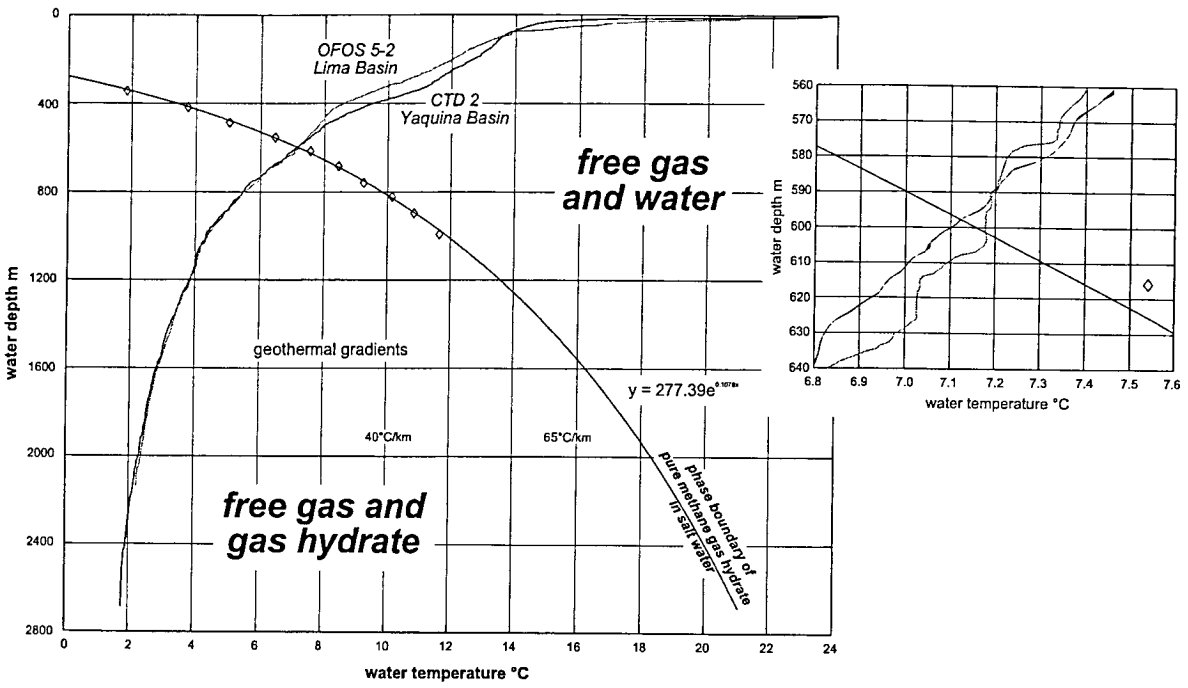

Figure 8.8.2: Gas hydrate stability diagram. Pressure and salinity from CTD 2 were taken for the transfer from pressure to water depth and the salt correction. To prove the calculated phase boundary ($y = 277.39\ e^{0.1078x}$) experimental data from Dickens and Quinby-Hunt (1994) are plotted as diamonds.

9. Lima Transect

Geologic framework

The second leg was largely dedicated to studying the gas hydrate system in Lima Basin and the adjacent lower slope. Lima Basin is underlain by metamorphic continental crust (e.g., Suess and von Huene, 1988). Drilling of ODP Leg 112, Site 679, provided control for a reconstruction of Lima Basin stratigraphy based mainly on data collected by the Hawaii Institute for Geophysics (HIG) in 1985 (Ballesteros et al., 1988). The sedimentary section on top of the metamorphic basement was not penetrated by drilling in Lima Basin. Seismic reflections from this sediment section, however, show similar patterns to Eocene sediments drilled in Yaquina Basin. It was therefore concluded that the metamorphic basement of Lima Basin is probably overlain by Eocene sediments. A truncation above the presumably Eocene sediments most likely corresponds to a regional Oligocene hiatus. Borehole 679E was drilled down to 360 m beneath the seafloor (mbsf), reaching mid-Miocene sediments. A prominent unconformity at 245 mbsf corresponds to a hiatus between 7-11 Ma in mid-Miocene time. It was caused by subaerial or shallow-water erosion probably due to uplift of the margin during subduction of Nazca Ridge (e.g., Suess and von Huene, 1988). This unconformity is often referred to as the floor of Lima Basin. Rapid subsidence at an average of about 500 m/m.y. started in mid-to-late Miocene times in the wake of the north-to-south migrating crest of Nazca Ridge along the margin.

Slope dip increases drastically seawards of Lima Basin along the middle slope, which is characterized by extensive faulting. At a water depth of about 3800 m, turbidite-filled basins stretch across the margin over about 15 km. These basins are commonly defined as the landward edge of the lower slope (e.g., von Huene and Miller, 1988), although some authors consider them as part of the middle slope (e.g., Hussong et al., 1988). Sediments appear to be trapped at the seaward edge of the basins by a regional high that rises by about 100 m and appears to be uplifted along a series of high-angled thrust faults (Hussong et al., 1988). Sidescan images from this region revealed a series of dark round features that were interpreted as mud volcanoes (Hussong, 1986). Seaward of this topographic high, slope dip increases and seismic images reveal landward dipping reflections which are interpreted as accreted trench fill (von Huene and Miller, 1988). The basement beneath the middle slope and the lower-slope basins appears to be metamorphic continental crust. It's seaward boundary is not well defined from seismic data, however, it appears to roughly coincide with the topographic high at the seaward edge of lower-slope basins (e.g., von Huene and Miller, 1988; von Huene et al., 1996). The recent geologic history at the lower slope along the Lima transect appears to be closely linked to a renewed build-up of an accretionary prism after a paleo-prism had been eroded during subduction of the crest of Nazca Ridge ~4 Ma. The formation of a new prism is believed to cause moderate uplift of the lower slope (e.g., von Huene and Pecher, 1999).

ODP Leg 112 Sites 682 and 688 drilled into the middle and lower slope. Site 682 was located above the lower-slope basins, Site 688 at their landward edge (where no BSR was present, which was considered a drilling hazard). At both sites, Eocene sediments were reached beneath an Oligocene hiatus. Gas hydrates were recovered at Site 688 from 141 mbsf mixed with fine silt and clay. Although no gas hydrates were sampled at Site 682, chlorinity profiles suggested a presence of gas hydrates at this site (Suess, von Huene, et al., 1988). A strong BSR is present beneath the lower-slope basins. It weakens and disappears landwards close to normal faults, which was interpreted as a possible indication for gas venting through faults (e.g., Pecher et al., 1996b). Seawards, the BSR disappears at the edge of the accretionary prism. This is explained by the low organic carbon content of the accreted trench fill sediments which does not favor biogenic methane and subsequent gas hydrate formation (von Huene and Pecher, 1999).

Nature of BSRs off Peru

The nature of BSRs beneath the lower-slope basins has been investigated with seismic waveform analyses (Miller and von Huene, 1991; Pecher et al., 1996a). It was found that these strong BSRs probably involve free gas at the base of gas hydrate stability (BGHS), which is in accordance to results from many similar studies of BSRs worldwide (e.g., Singh et al., 1993) as well as from drilling (Bangs et al., 1993, MacKay et al., 1994; Holbrook et al., 1996). It is not clear, however, if the gas is concentrated in a seismically thin layer (less than one wavelength) as predicted for the lower slope

from seismic waveform analysis (Miller and von Huene, 1991; Pecher et al., 1996a) or if it is dispersed over a thick zone as encountered during ODP Leg 164 on the Blake Ridge (Holbrook et al., 1996). Indirect analyses based on the study of seismic waveforms require an accurate background velocity model without which a thick zone of layers that contain free gas at very low concentrations may go unnoticed. Korenaga et al. (1997) demonstrated that without borehole information, the Blake Ridge BSR probably would also have been interpreted as a thin gas layer.

Formation of BSRs

Sediments on the Peru margin have a very high organic carbon content caused by the high primary production in this upwelling region. This provides an ideal environment for the biogenic generation of methane for gas hydrate formation. It is therefore likely that gas hydrates occur over most of the margin where they are stable. However, BSRs are absent beneath most of Lima Basin. This observation led to the hypothesis of a tectonic suppression of BSRs (Pecher et al., 1996b; von Huene and Pecher, 1999). Tectonic subsidence leads to an increase of pressure, a shift of methane hydrate stability towards higher temperatures, and hence, a downward movement of the BGHS with respect to the sediment column. Free gas beneath the BGHS is then absorbed into the gas hydrate stability zone (GHSZ) – the BSR disappears. Sedimentation, on the other hand, causes an upward movement of isotherms and hence, of the BGHS with respect to the sediment column. Then, gas hydrate dissociates to free gas. On the lower slope, strong sedimentation and a predicted moderate uplift due to the formation of an accretionary prism, both cause such an upward movement of the BGHS. This is consistent with the observation of strong BSRs. Quantification of subsidence and sedimentation effects on the vertical movement of the BGHS in Lima Basin, however, indeed suggests a net movement downward, which would explain the regional lack of BSRs.

BSRs have been observed in two small areas above topographic and probably structural highs (figs. 1.6 and 1.8). Apparent seafloor erosion would add to the downward movement of the BGHS caused by subsidence. Hence, the question now is, how can a BSR be sustained in such an environment? The above model of tectonic BSR formation is a "static" view of a gas hydrate system. Gas hydrate and BSR occurrences, however, appear to describe a "dynamic" steady-state equilibrium: On the one hand, gas hydrates dissociate even within their pressure-temperature stability field because pore waters of the uppermost sediments and the ocean water are usually undersaturated with methane. This causes diffusion of methane molecules out of the gas hydrate cages and a breakdown of the clathrate structure. On the other hand, gas hydrates form from a constant supply of methane. In this view, methane flux into the GHSZ plays a major role for BSR formation. Xu and Ruppel (1999) quantitatively concluded for the Blake Ridge that a minimum ("critical") methane flux is required to have free gas at the base of gas hydrate occurrence, i.e., to generate a BSR. Their quantification of the critical methane flux at the edge of a BSR on the Blake Ridge is in good agreement with other estimates of methane flux (Paull et al., 1996). A downward movement of the BGHS, in this context, may be viewed as a methane sink.

Transect P1-P3 to study physical properties of gas hydrate bearing sediments

A transect across P1-3 in Lima Basin (fig. 1.8) appears to be an ideal location to study gas-hydrate-bearing sediments. Most investigations of the effect of gas hydrates on the properties of sediments are thwarted by the lack of knowledge of the properties of the host sediments if they were gas-hydrate-free. A slight layer dip along this transect, however, provides us with a rare section of gas-hydrate-free reference sediments: Layers that are above the BGHS beneath P2 and P3, which –based on the observation of a strong BSR— most likely contain gas hydrates, are beneath the BGHS at P1. Gas strongly decreases Vp and therefore, gas-bearing sediments could not be used to obtain the seismic properties of the host sediment. However, the lack of a BSR beneath P1 suggests that the sediments are gas-free.

9.1. MCS Seismics

(I. Pecher, C. Hübscher, R. Coman, C. Herold)

9.1.1. Scientific Objectives of MCS and OBH/S Seismics

We planned to achieve the following objectives with the high-resolution MCS and OBH/S experiments in Lima Basin:

- To test the model of tectonic BSR suppression. Which role does vertical tectonism play in the development of BSRs? A stratigraphic reconstruction of Lima Basin that ties ODP Site 679 and the existing HIG data together with the high-resolution MCS data acquired during this cruise will allow us to constrain rates of subsidence, sedimentation, and erosion. Using a multiphase model of the gas hydrate system, we will quantify the effect of vertical tectonism on the observed distribution of BSRs.
- To measure the effect of gas hydrates on the seismic properties of sediments. Are gas hydrates detectable with remote seismic techniques? The P1-P3 transect offers us a rare gas-hydrate-free and gas-free reference site. Although quantification of the effect of gas hydrates on sediment properties requires drilling, we will for the first time be able to test in the field if we can resolve the differences in Vp and Vs caused by gas hydrates.
- To map the thickness of the free gas zone. Is the thick free gas zone on the Blake Ridge exceptional or are previous results e.g. from waveform inversion misleading? Thick free gas zones are reflected by low-velocity zones (LVZs), which are usually difficult to image. Because of the limited lateral extent of the BSR, however, we expect to be able to detect a possible LVZ beneath the BSR along the P1-P3 transect.
- To study the high-resolution plumbing system within and immediately beneath the gas hydrate zone. 2.5-D data acquired while locating OBH/Ss at the seafloor for the SeeBoSeis experiments (see 9.3.) will offer us rare high-resolution images of layers that cross the BSR and penetrate the GHSZ and may act as fluid and gas migration paths. Seismic attributes, in particular reflectivity and instantaneous frequency may indicate upward migrating gas, even within the GHSZ, as demonstrated, e.g., by Taylor et al. (2000) over the Blake Ridge Diapir. The dense line spacing will enable us to extrapolate from 2.5 D and obtain 3-D images of possible fluid migration paths.

Drilling related objectives are:

- To design a vertical seismic profile (VSP) experiment for measuring Vs in hydrate-bearing sediments. Measurement of Vs in the borehole is straight-forward with offset-VSPs, provided we can rely on sufficient P-to-S conversion. For the design of offset-VSPs, we need to know the optimum offset for recording P-to-S converted waves over the entire borehole.
- To ensure that the proposed boreholes penetrate the free gas zone. Drilling the entire thickness of the free gas zone will provide critical constraints on the size of the free gas reservoir, the nature of the deep biosphere, and the significance of upward migrating fluids into the GHSZ.
- To determine the best drilling locations for studying the model of tectonic BSR suppression. Our analysis will show where to position the drill sites to obtain optimum constraints for rates of subsidence, sedimentation, and erosion.

On the lower slope, we focused upon the following objectives:

- To study possible fluid migration paths through the gas hydrate stability zone. Several normal and thrust faults cut through both the gas hydrate zone and the BSR. We planned to investigate if anomalous amplitudes and "pull-ups" of the BSR may indicate fluid and gas migration through these faults. A decrease of BSR amplitude close to faults may also suggest the escape of gas through these faults.
- To study the lateral variability of BSRs and possible fluid migration paths. This is essential to avoid possible overpressures while drilling. On the Peruvian lower slope, BSRs are exceptionally

strong. Sediment permeability may be much higher than, e.g., on the Blake Ridge. Therefore, accidentally penetrating a topographic high of the BSR may lead to and escape of overpressured gas and fluids, jeopardize the success of drilling, and may even constitute a safety hazard.

9.1.2. Data

Lines HH00-026-033 where acquired while shooting over the OBH/Ss during OBH/S deployment P07 (fig. 9.1.1 for location maps, figs. 9.1.2-5; all figures show brute stacks). The data were acquired with two 105/105 in^3 (1.6 l) GI guns in harmonic mode. For a stratigraphic survey of Lima Basin (figs. 9.1.6-13), we originally planned to use an array of a 2 l, 2.5 l, and 3 l airgun in order to achieve deeper penetration. A shearing off of a trigger line during the first line (HH00-065a) forced us to go back to the GI gun configuration. Penetration with the GI guns, however, was excellent: Where the BSR is absent, we always achieved penetration down to the L5/L4 interface from late Miocene time according to the stratigraphy of Ballesteros et al. (1988) (fig. 9.1.2). In most profiles, the deeper mid-Miocene unconformity is also reached (fig. 9.1.6c). As expected, penetration beneath the BSRs was not as good as with the high-frequency signals generated by the GI-guns, however, we mostly reached the mid-Miocene unconformity. Hence, we have achieved sufficient penetration for our planned stratigraphic reconstruction of Lima Basin, particularly since we plan to focus on recent geology. Data quality of profiles HH00-033 should increase significantly after adequate processing to suppress strong 50-Hz noise. Data quality of all other profiles from Lima Basin is excellent even at this early processing stage.
Lines HH00-044-064 and HH00-075-091 were acquired with one 45/105 in^3 (0.7/1.6 l) GI gun while shooting over the OBH/Ss deployed for the SeeBoSeis experiments 1 and 2. The main purpose of these OBH/S lines is to locate the receivers on the seafloor. The 37 MCS lines, however, with an average spacing of 300 m will also produce excellent high-resolution 2.5 images of the subsurface in two areas, one with and one without a BSR. These data should therefore help us significantly to better understand the plumbing system through the GHSZ and beneath the BSR. The enhanced resolution of this high frequency source is demonstrated in fig. 9.1.14. A layer that cuts through the BSR at about FFN 800 appears to disrupt the BSR.

In the deep water over the lower slope, we had to reduce our shot interval for lines HH00-092-101 from typically 8-10 s to 12-14 s in order to be able to record both the primary and multiple seafloor reflections. This is important for calibration of reflection coefficients. The lower shot rate leads to larger lateral spacing of reflections, and hence, less lateral continuity of the images. Geometric dispersion of seismic energy increases with depth which is the cause for lower penetration. Nevertheless, we could easily penetrate the sediment section down to the BSR (figs. 9.1.15-17). We acquired three parallel seismic lines spaced at 500 m across a lower-slope basin (across proposed drill sites P4-6) as well as two perpendicular lines. Four OBHs were deployed along the center line across the basin. These data will allow us to study the lateral variability of BSR strength and possible fluid migration paths and would be a good basis for determining safe borehole locations.

Good lateral coverage was essential over the deepest study area close to proposed drill site P7 where the seafloor is very rough. We therefore decided not to record the water multiple (and hence, not to have the capability to calibrate the seafloor reflection coefficient) in order to be able to increase the shot rate and hence, significantly improve lateral coverage. We acquired three parallel and one perpendicular seismic lines across site P7. The objective of this study was, in addition to locating a safe possible drill site, to investigate a possible fluid migration path that appears to extend to the seaward edge of the BSR in line 1018 (Pecher, 1995). Current images of the brute-stack data are severely distorted by diffraction hyperbolas from the rough seafloor. Migration of the data using velocities that were previously obtained from line 1018 should help to collapse these diffraction hyperbolas and to significantly enhance the seismic images.

Lima-Basin

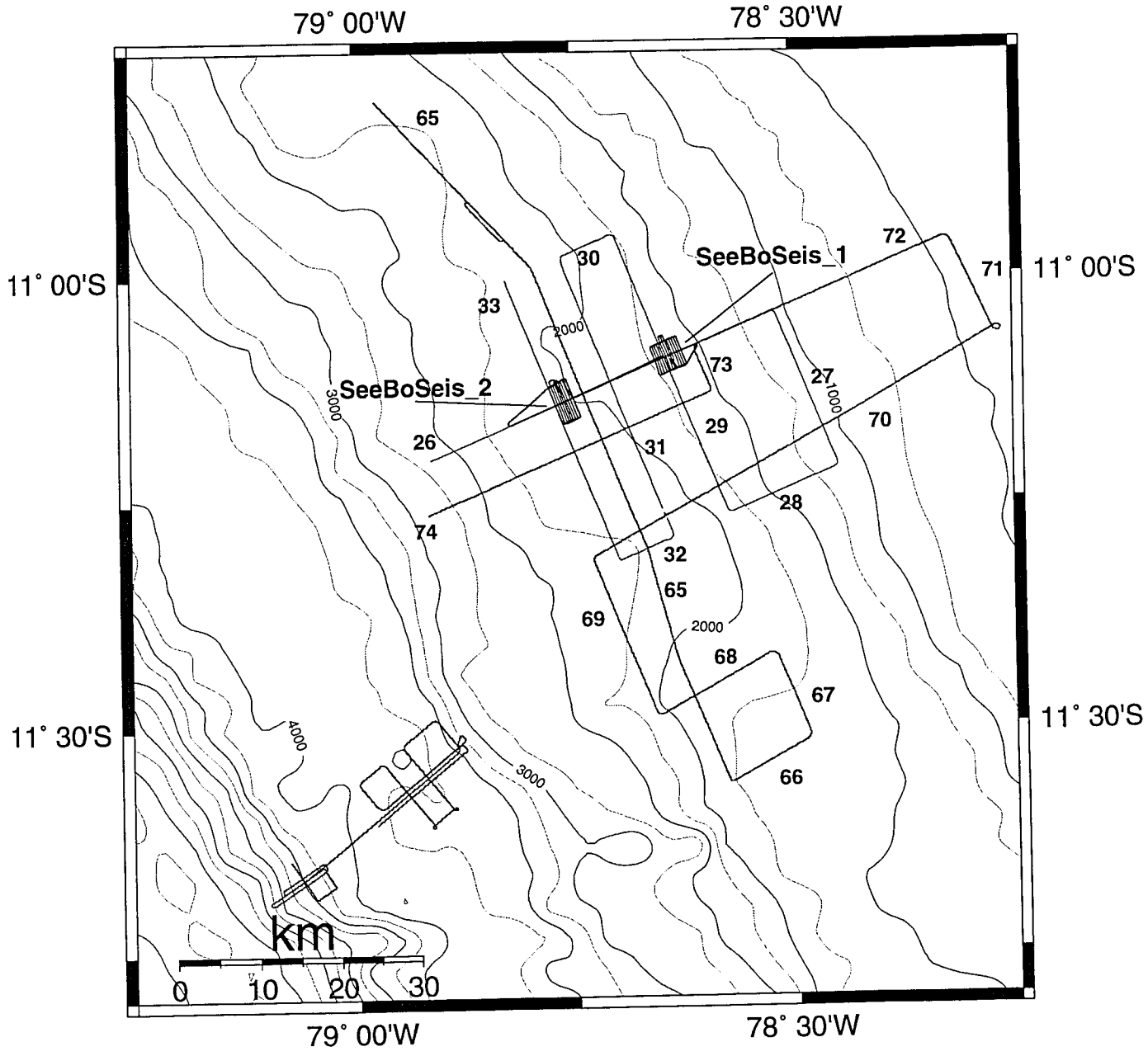

Figure 9.1.1a: Seismic lines Lima Basin

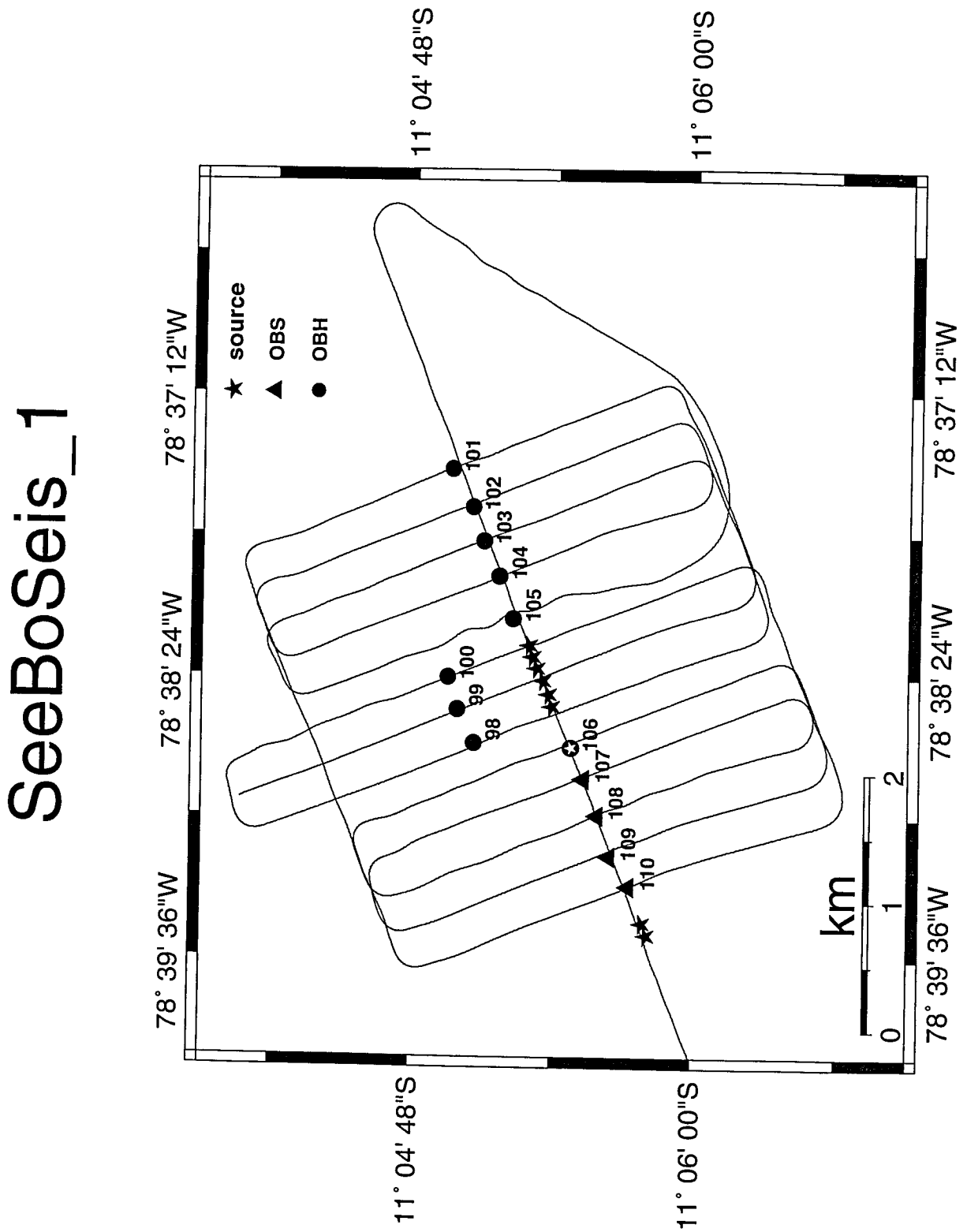

Figure 9.1.1b: Seismic lines SeeBoSeis_1

SeeBoSeis_2

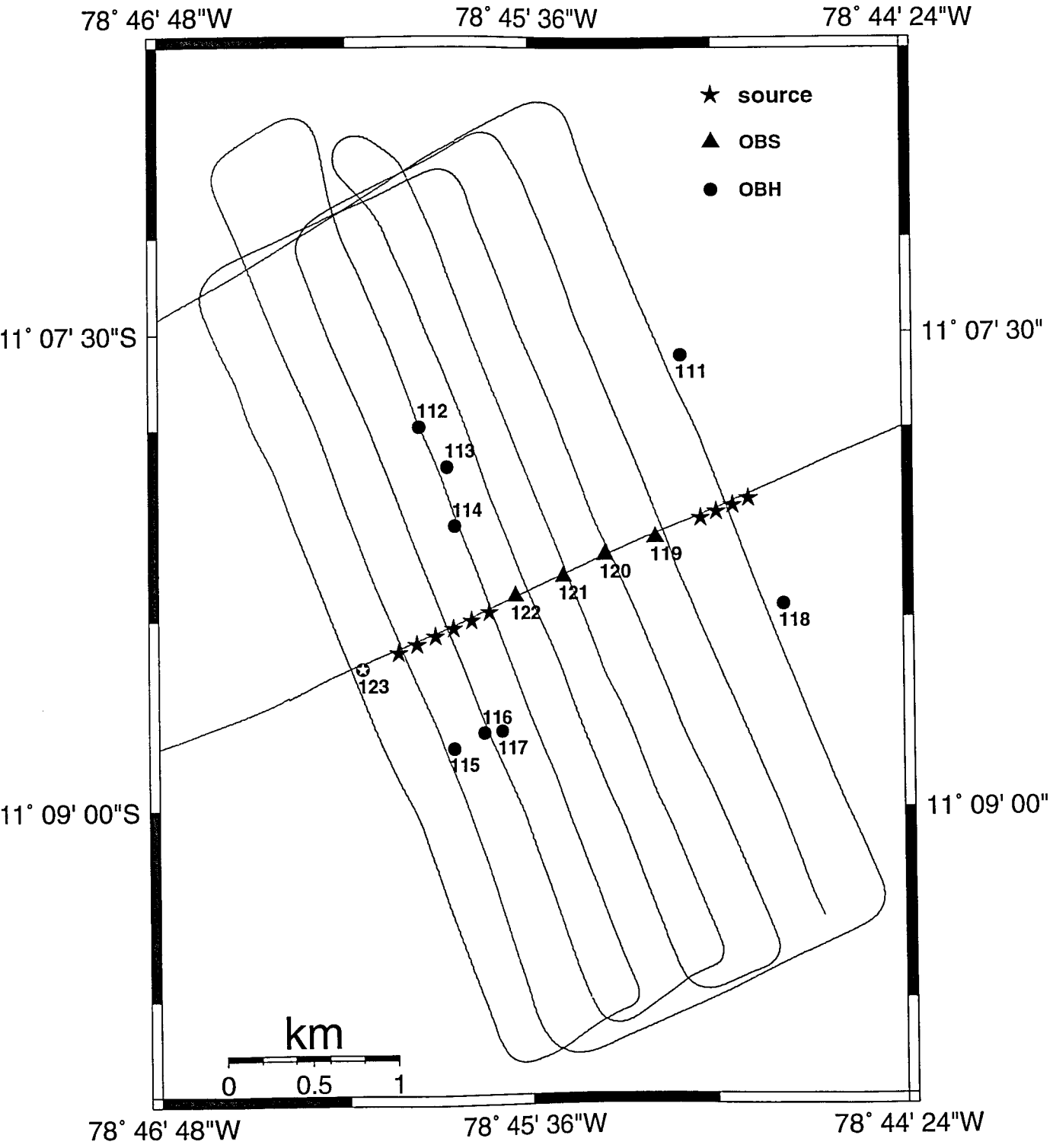

Figure 9.1.1c: Seismic lines SeeBoSeis_2

Lower Slope

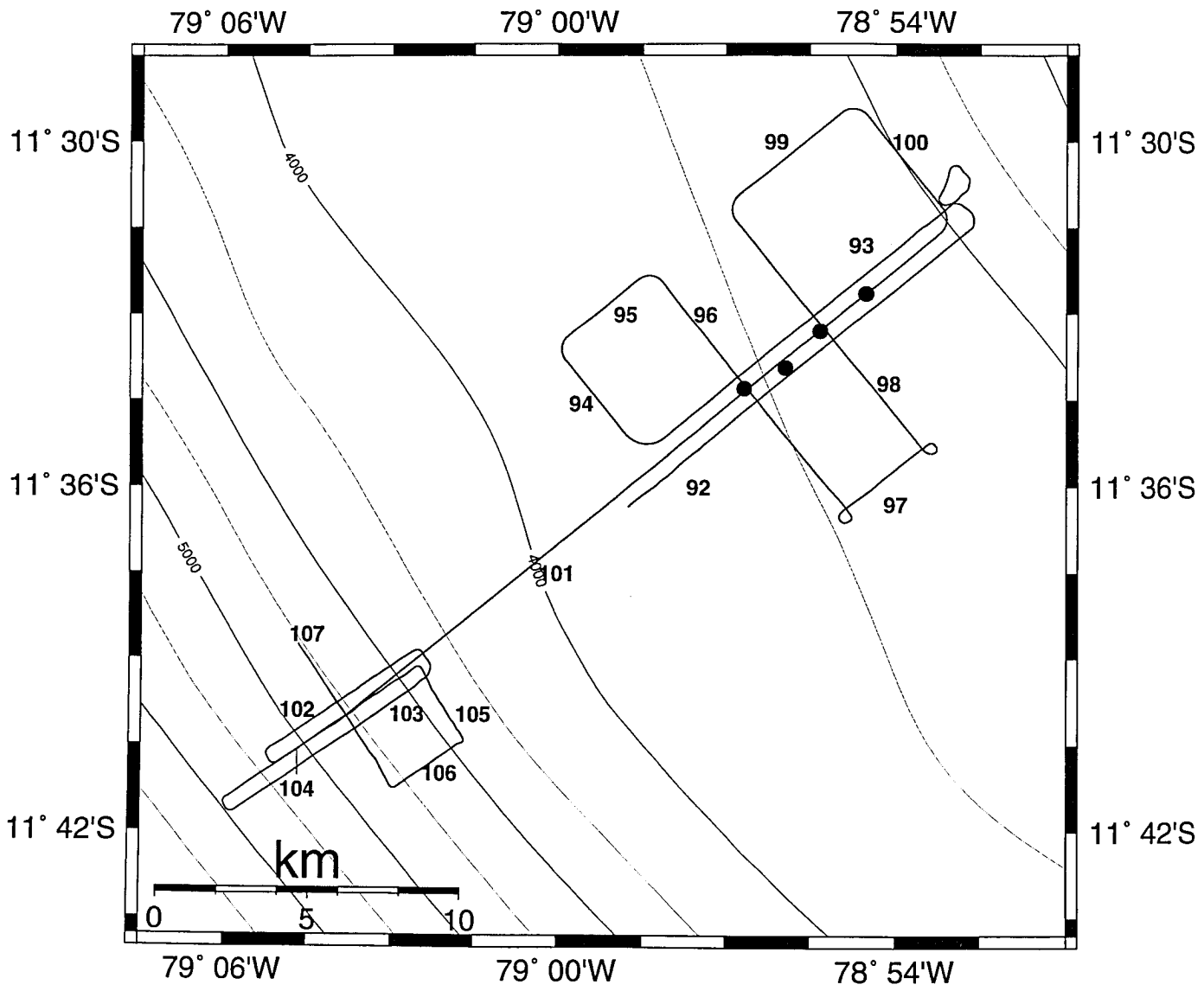

Figure 9.1.1d: Seismic lines Lower Slope

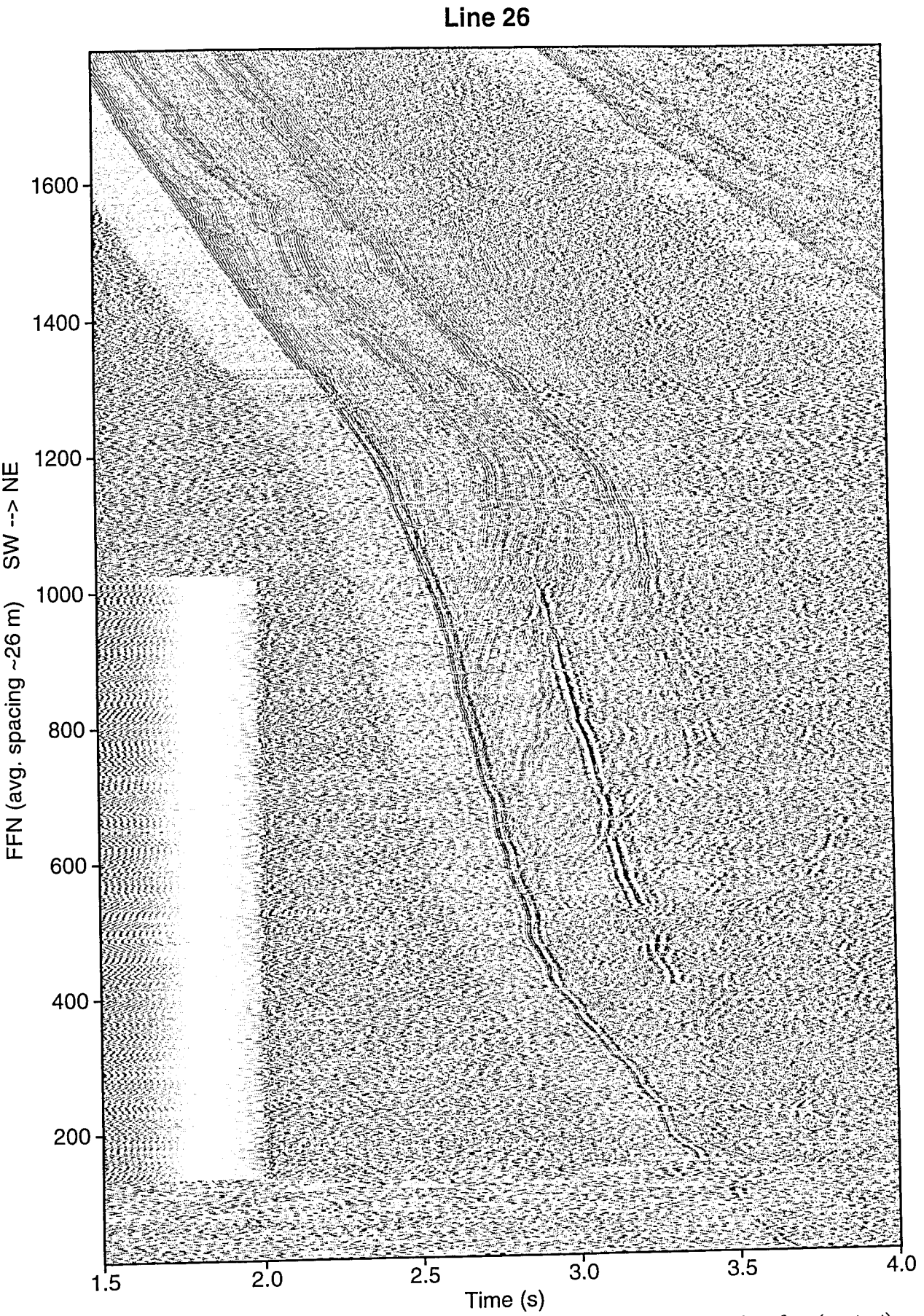

Fig. 9.1.2: MCS line 26. Top of reflections at ~2.2s, FFN 1600, are from L4/5 interface (see text). BP 10/25-150/200 Hz; Notch 30/50/80 Hz 1/0.1/1; Trace bal.; AGC 0.5 s.

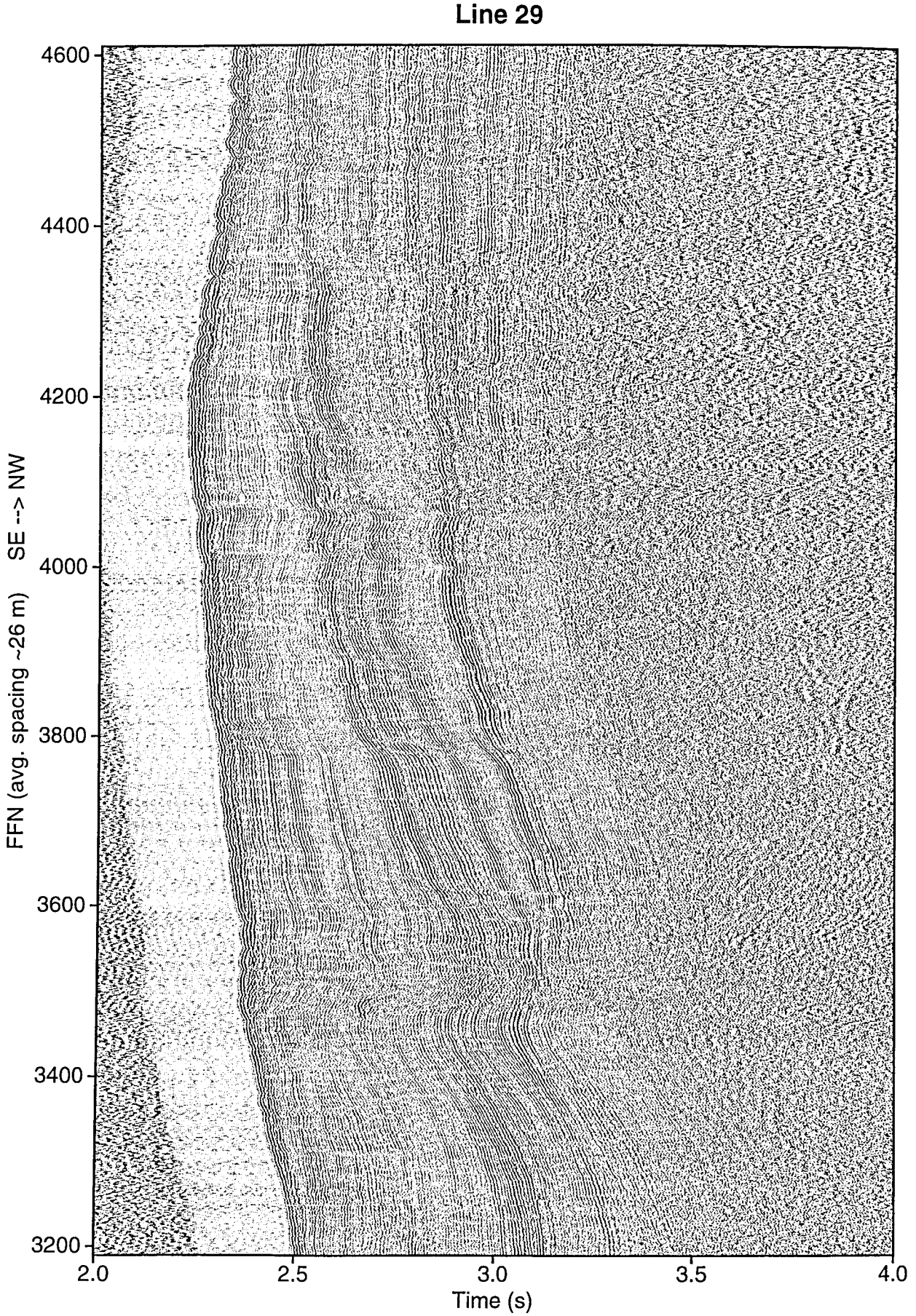

Fig. 9.1.3: MCS line 29. BP 10/25-150/200 Hz; Notch 30/50/80 Hz 1/0.1/1; Trace bal.; AGC 0.5 s

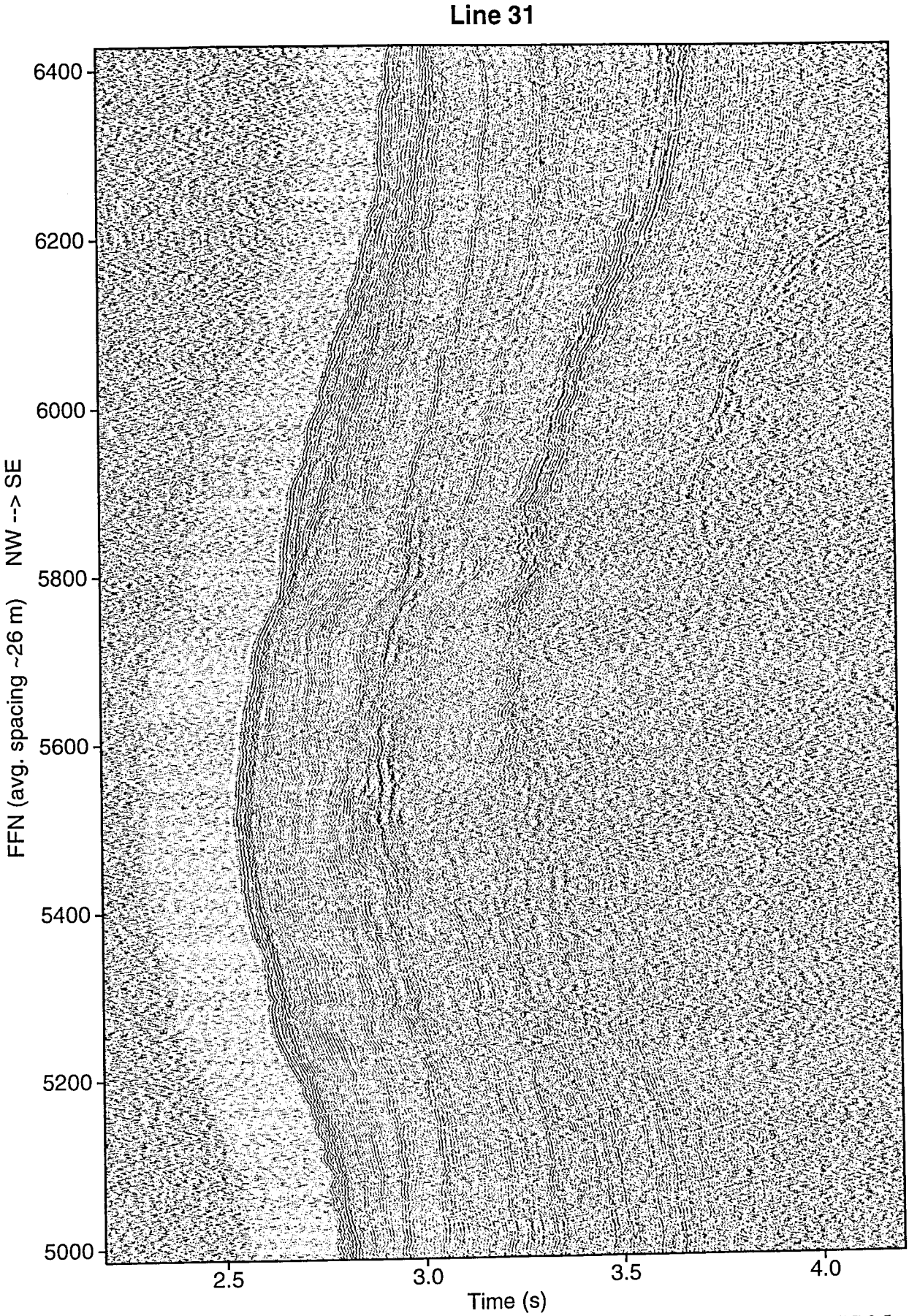

Fig. 9.1.4: MCS line 31. BP 10/25-150/200 Hz; Notch 30/50/80 Hz 1/0.1/1; Trace bal.; AGC 0.5 s.

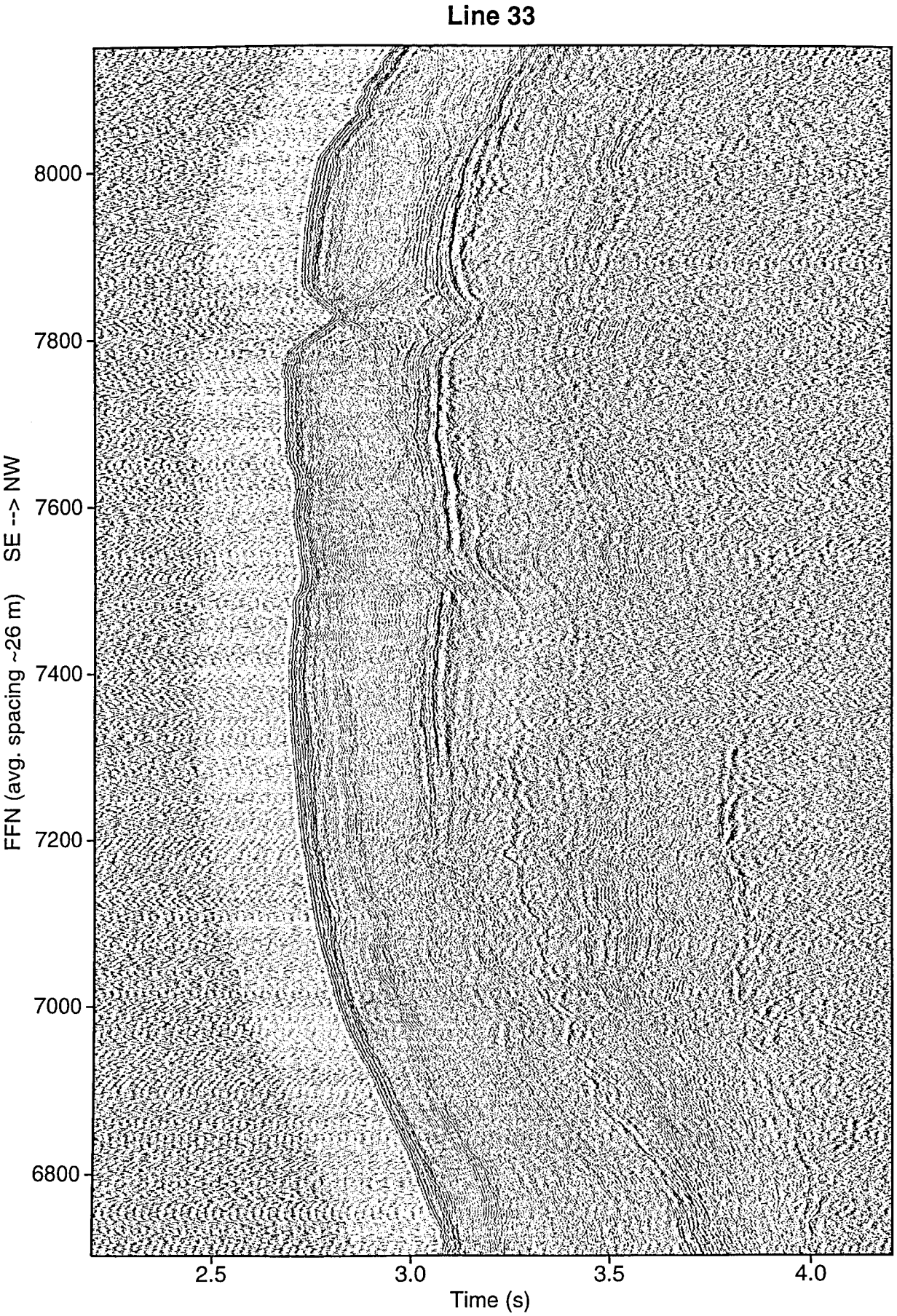

Fig. 9.1.5: MCS line 33. BP 10/25-150/200 Hz; Notch 30/50/80 Hz 1/0.1/1; Trace bal.; AGC 0.5 s.

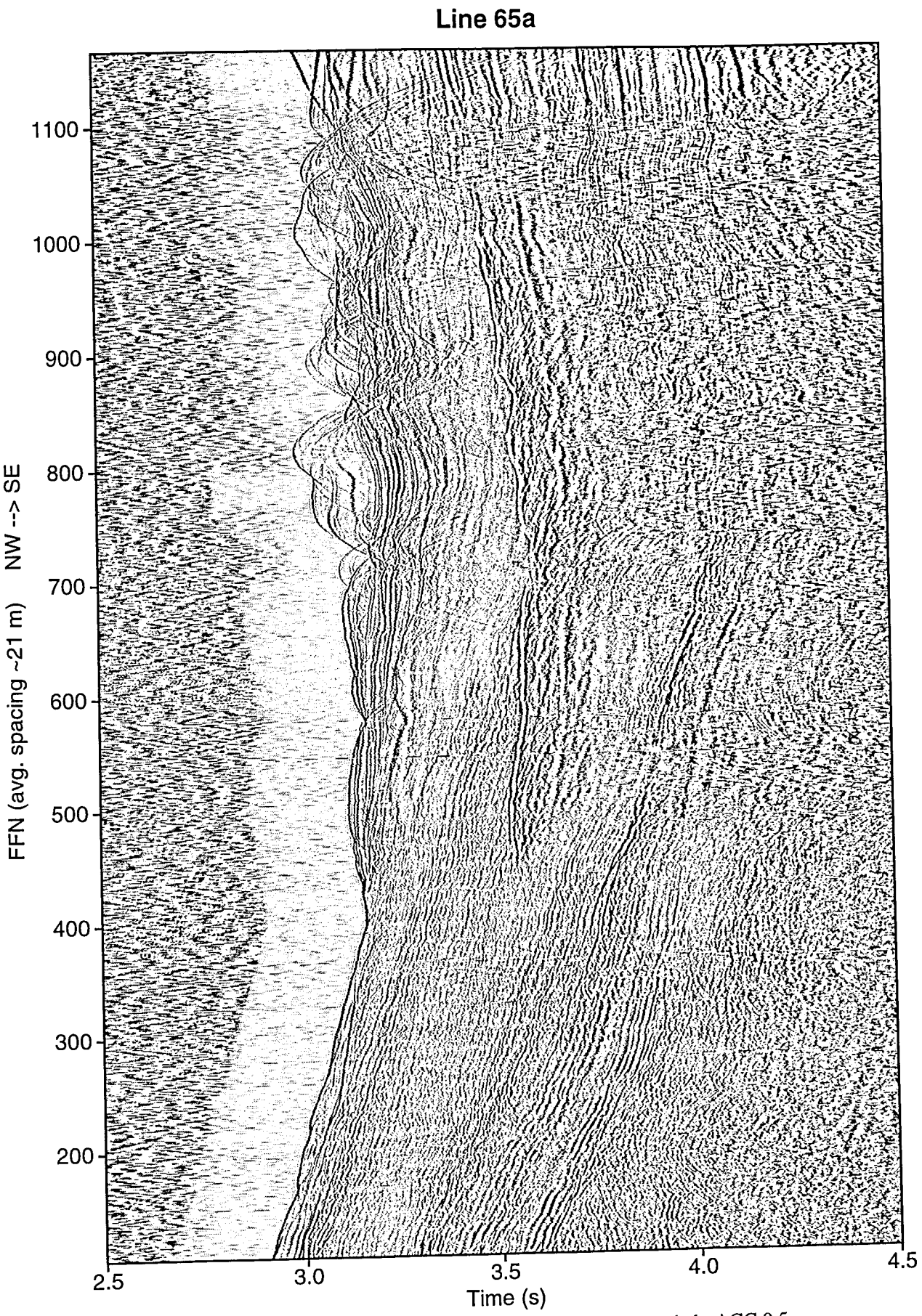

Fig. 9.1.6a: MCS line 65a. Airgun array. BP 5/15-150/200 Hz; Trace bal.; AGC 0.5 s.

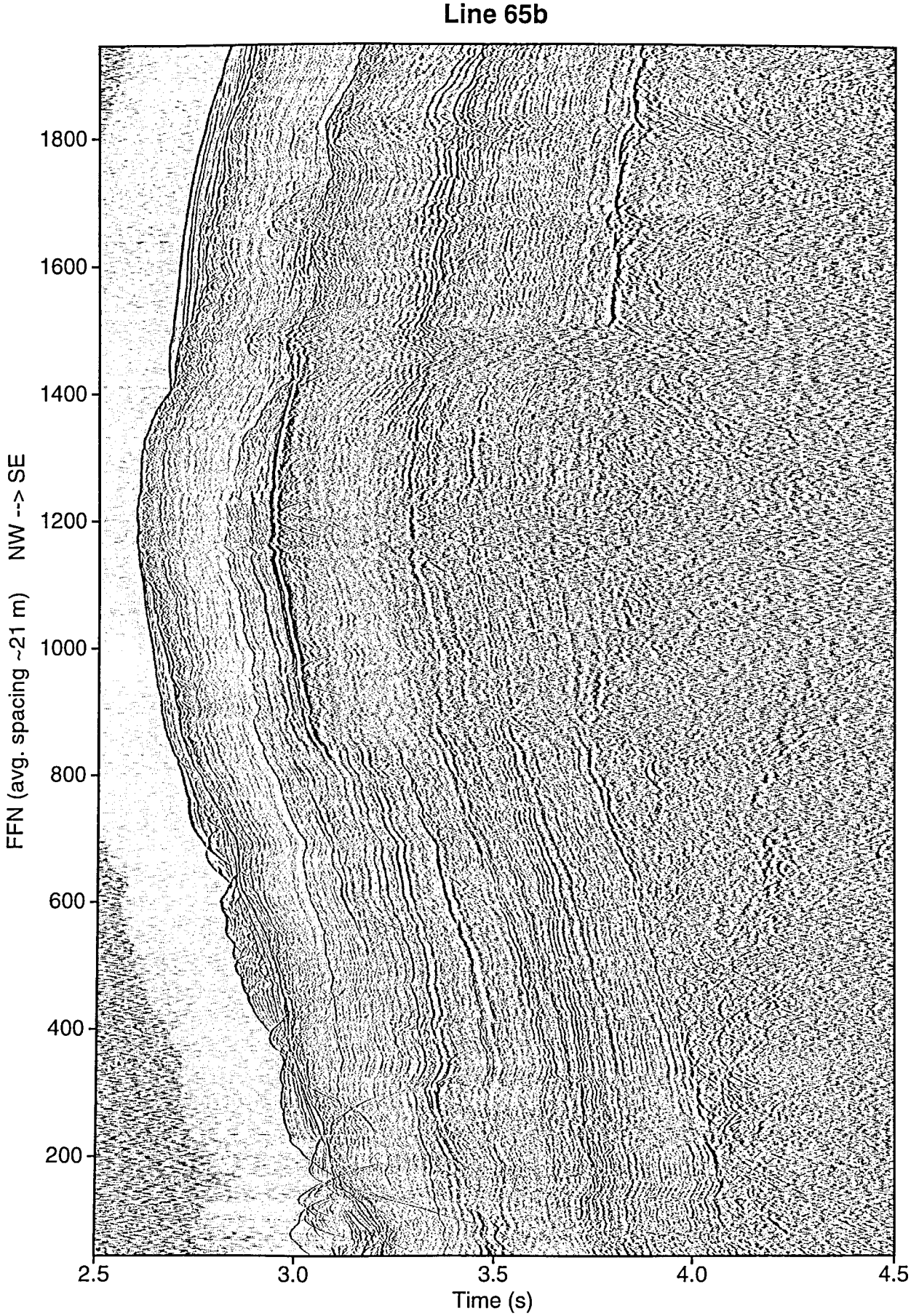

Fig. 9.1.6b: MCS line 65b. G/I gun array. BP 15/25-150/200 Hz; Trace bal.; AGC 0.5 s.

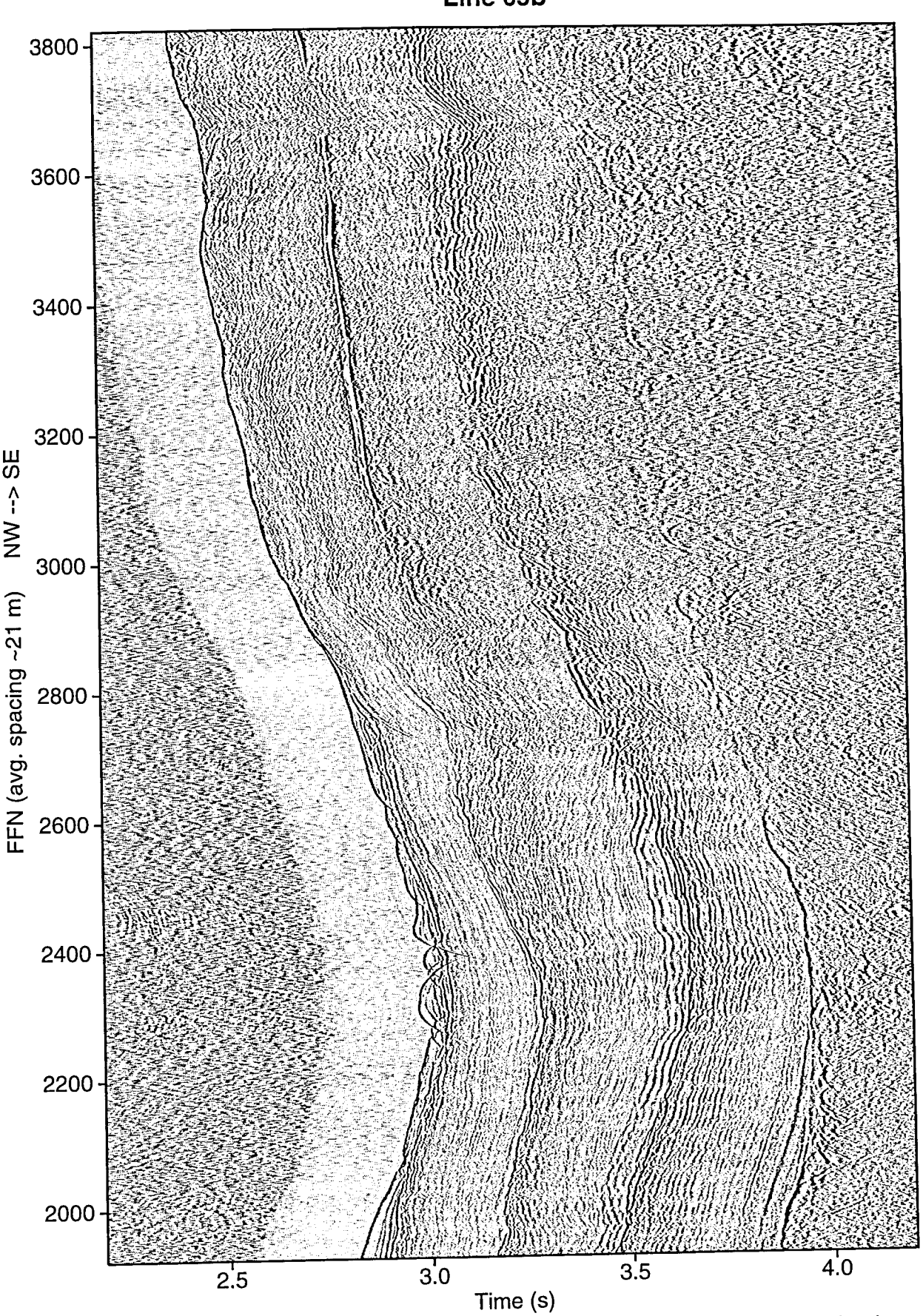

Fig. 9.1.6c: MCS line 65b. Reflection at ~3.9s, FFN 2400, is probably from mid-Miocene unconformity. BP 15/25-150/200 Hz; Trace bal.; AGC 0.5 s.

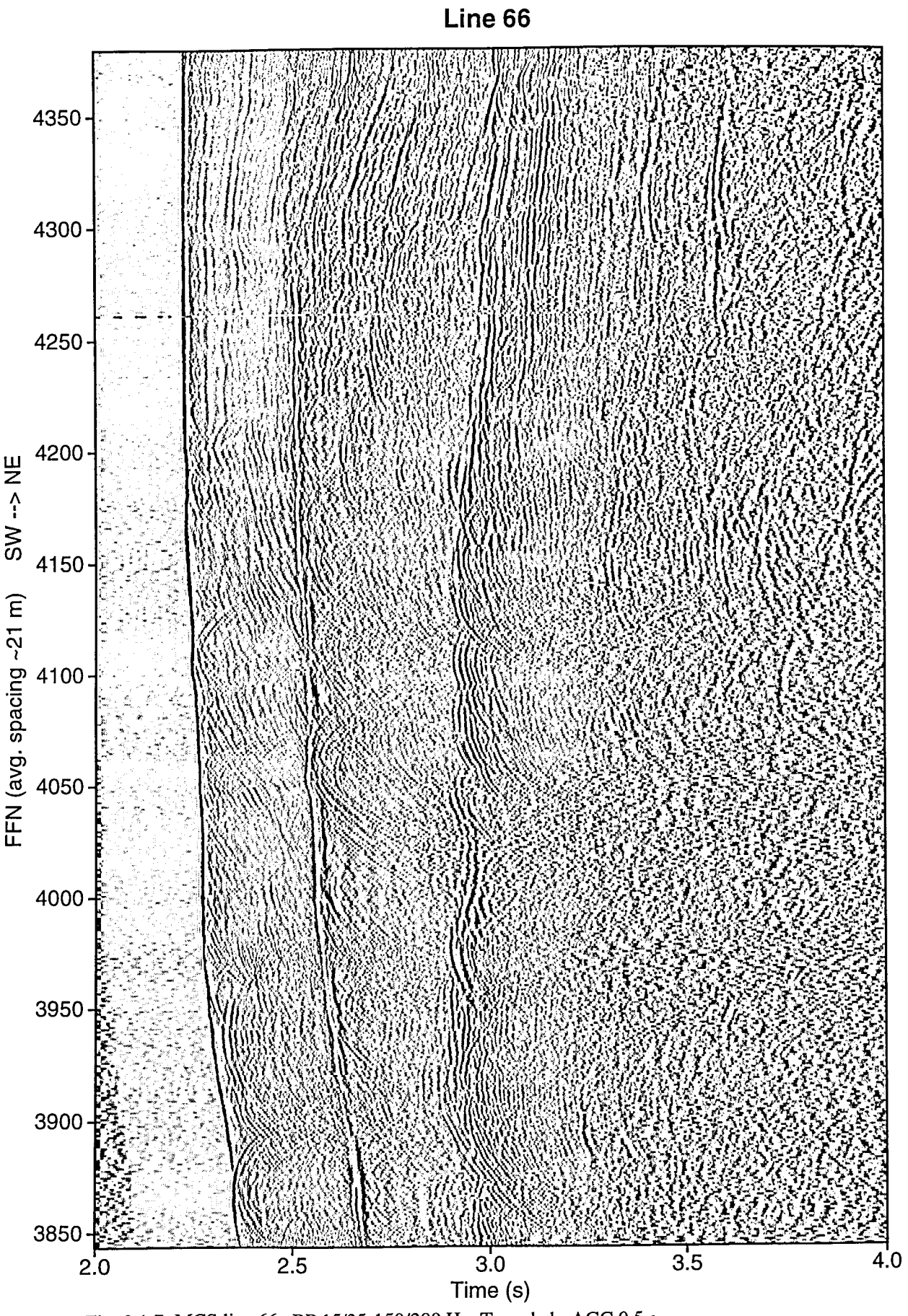

Fig. 9.1.7: MCS line 66. BP 15/25-150/200 Hz; Trace bal.; AGC 0.5 s.

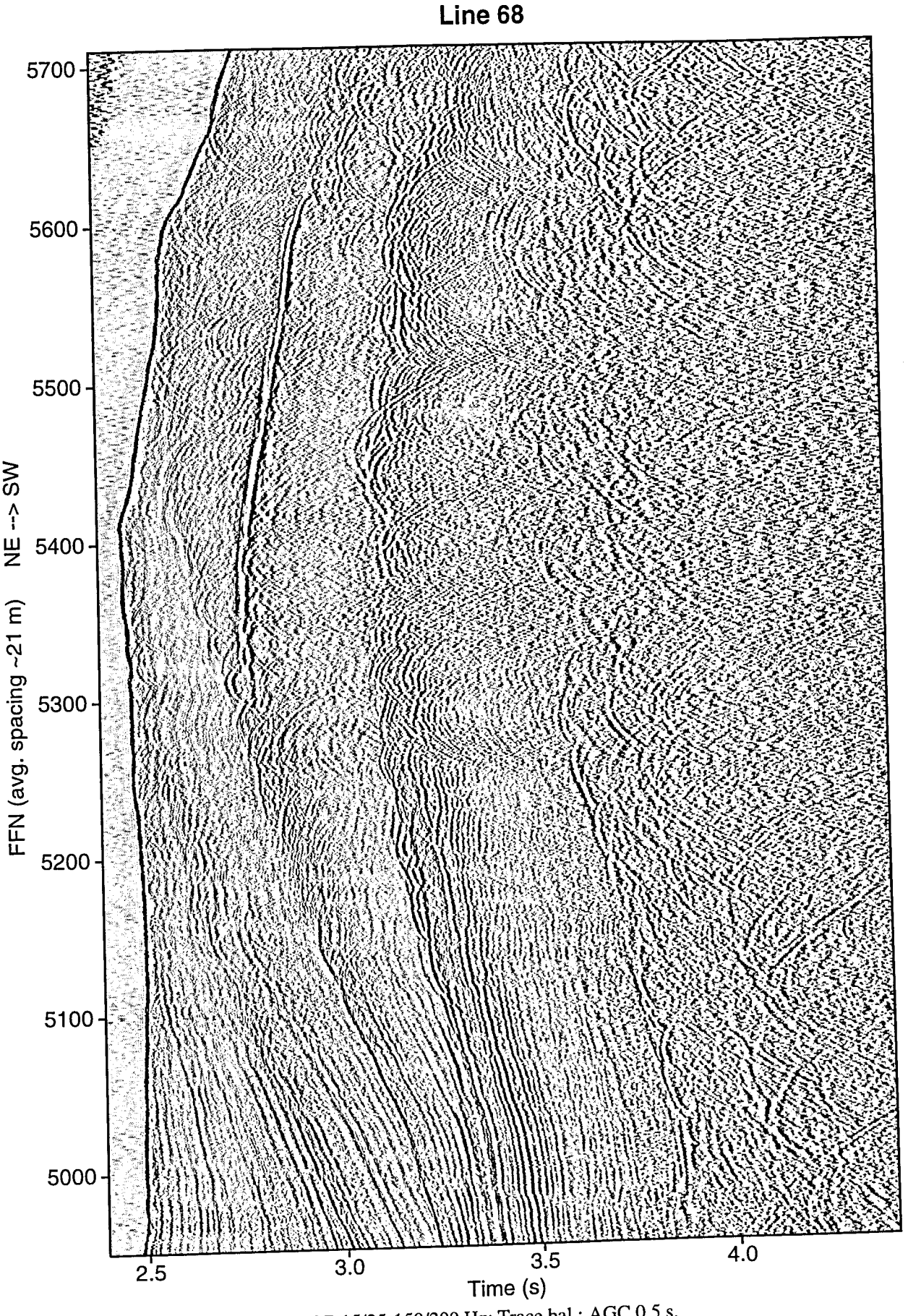

Fig. 9.1.8: MCS line 68. BP 15/25-150/200 Hz; Trace bal.; AGC 0.5 s.

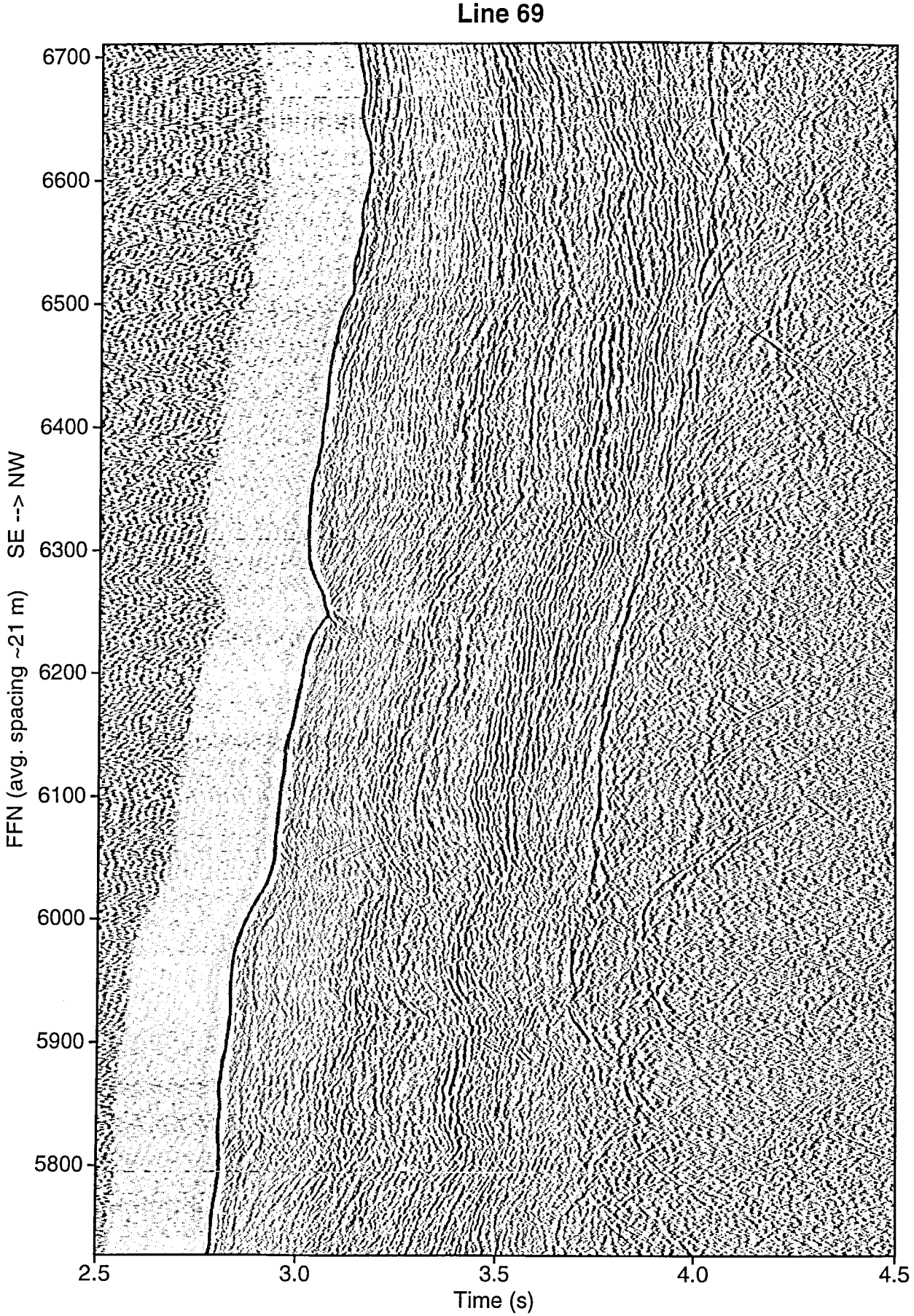

Fig. 9.1.9: MCS line 69. BP 15/25-150/200 Hz; Trace bal.; AGC 0.5 s.

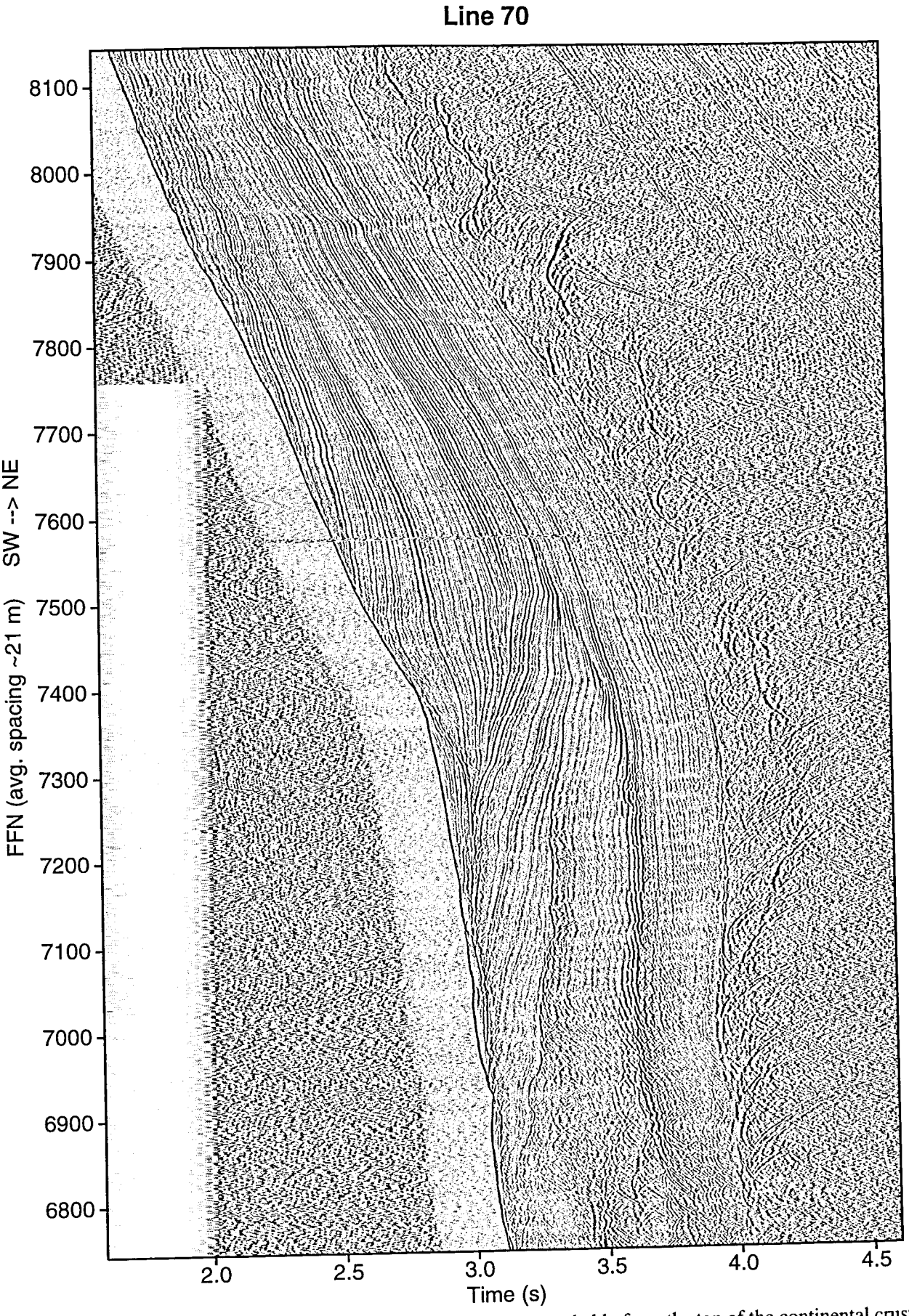

Fig. 9.1.10a: MCS line 70. Diffractions at ~3s, FFN 8100, are probably from the top of the continental crust. BP 15/25-150/200 Hz; Trace bal.; AGC 0.5 s.

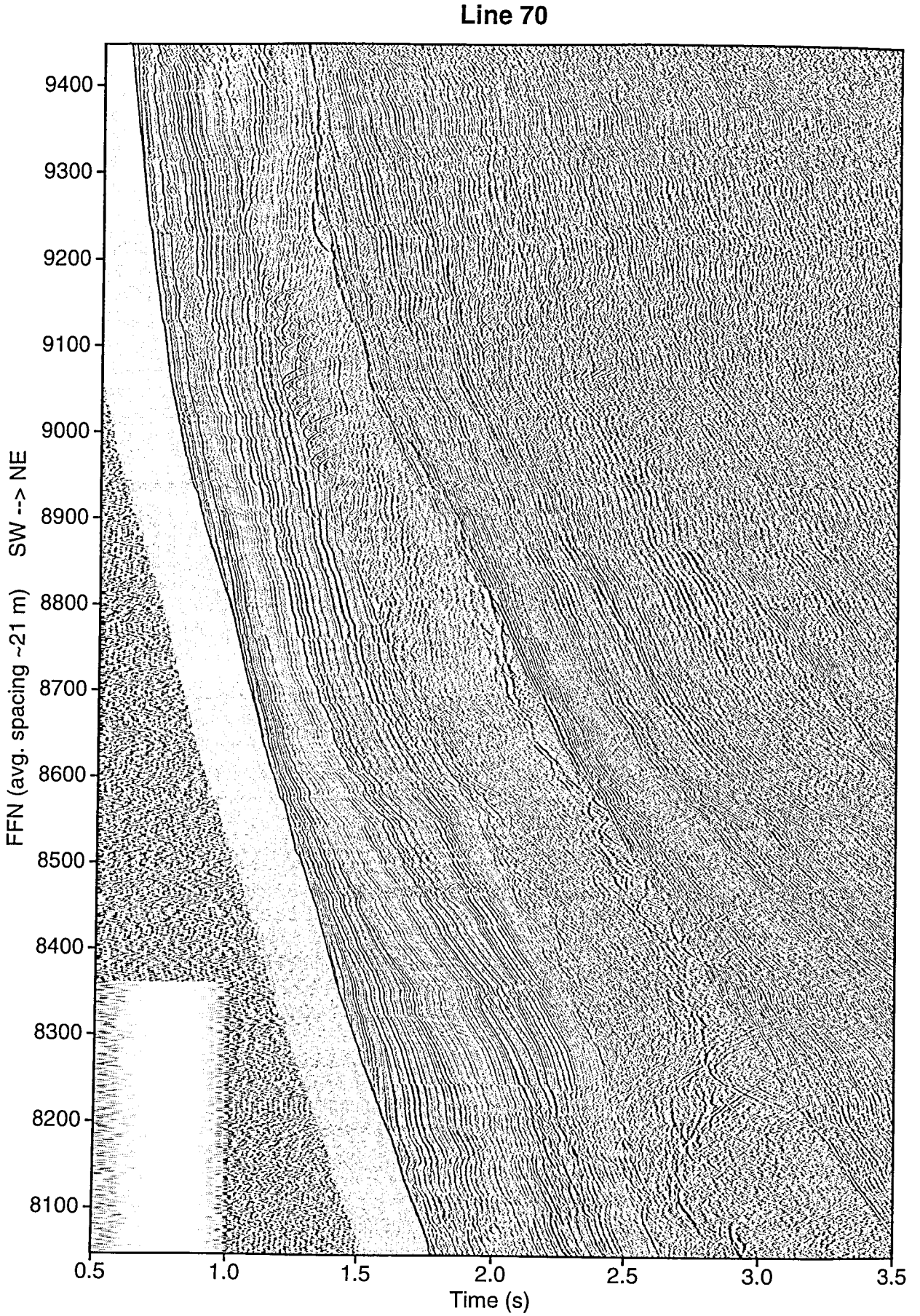

Fig. 9.1.10b: MCS line 70. Northeastern side crosses ODP Site 679.
BP 15/25-150/200 Hz; Trace bal.; AGC 0.5 s.

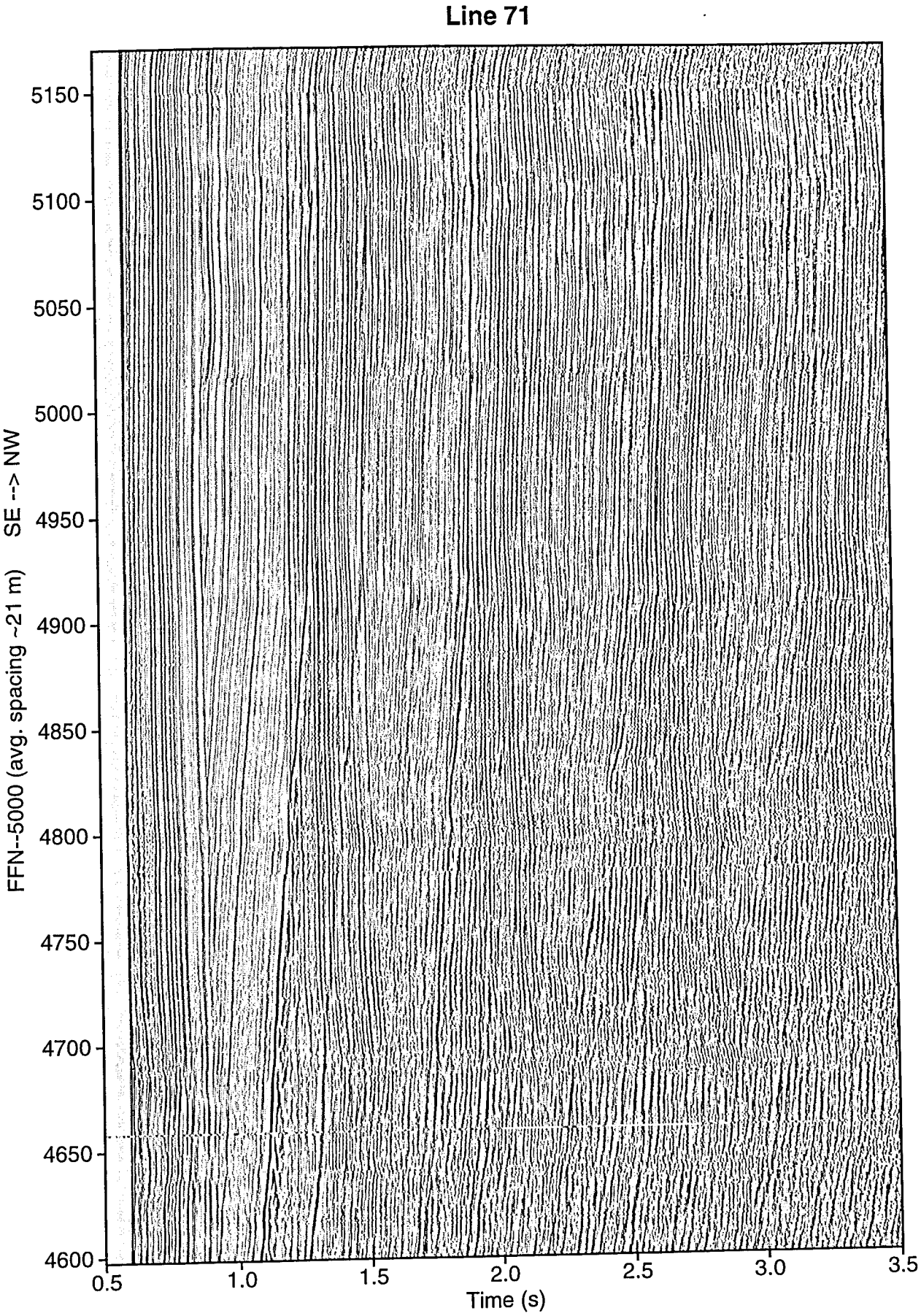

Fig. 9.1.11: MCS line 71. Southeastern side crosses ODP Site 679.
BP 15/25-150/200 Hz; Trace bal.; AGC 0.5 s.

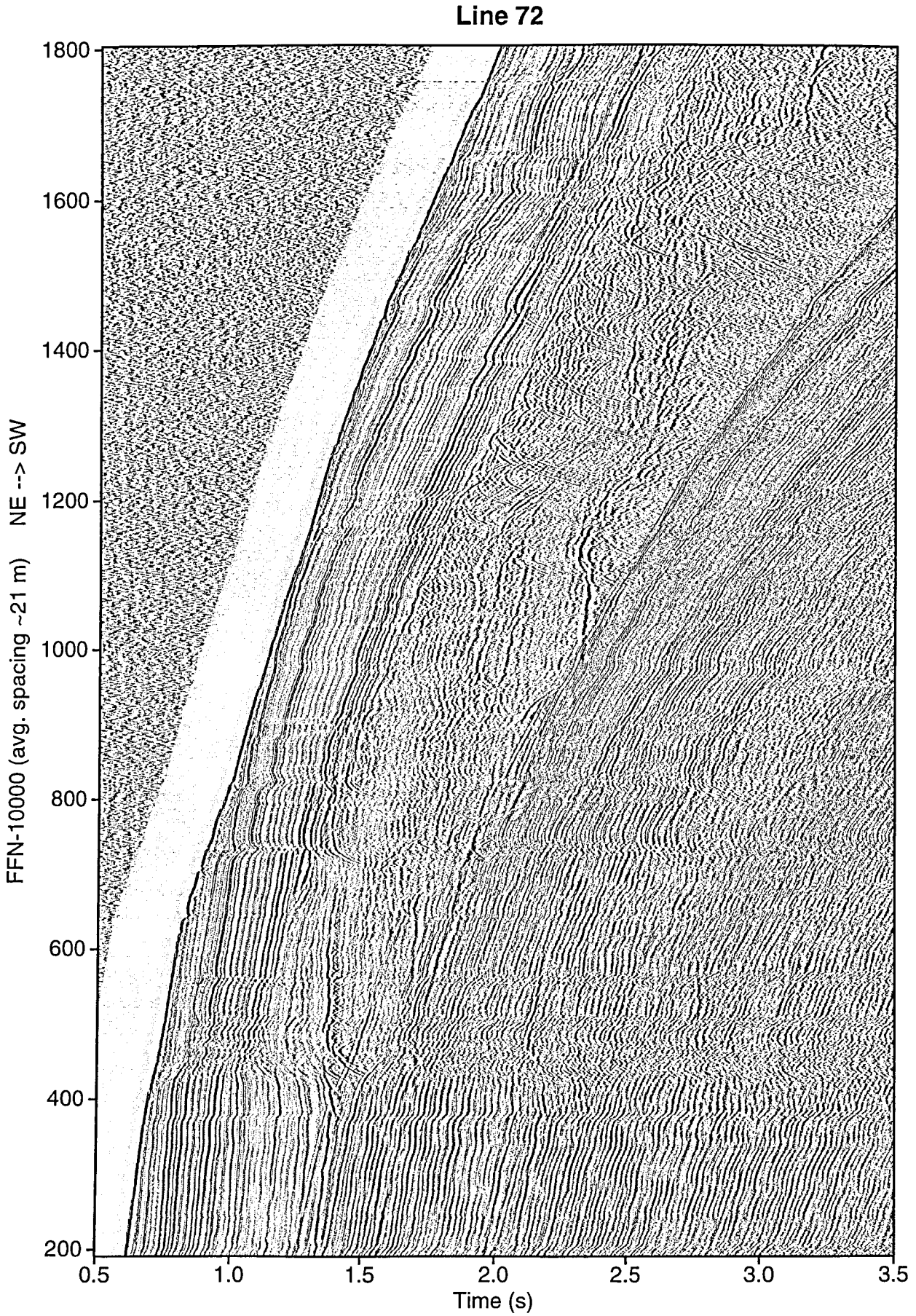

Fig. 9.1.12: MCS line 72. BP 15/25-150/200 Hz; Trace bal.; AGC 0.5 s.

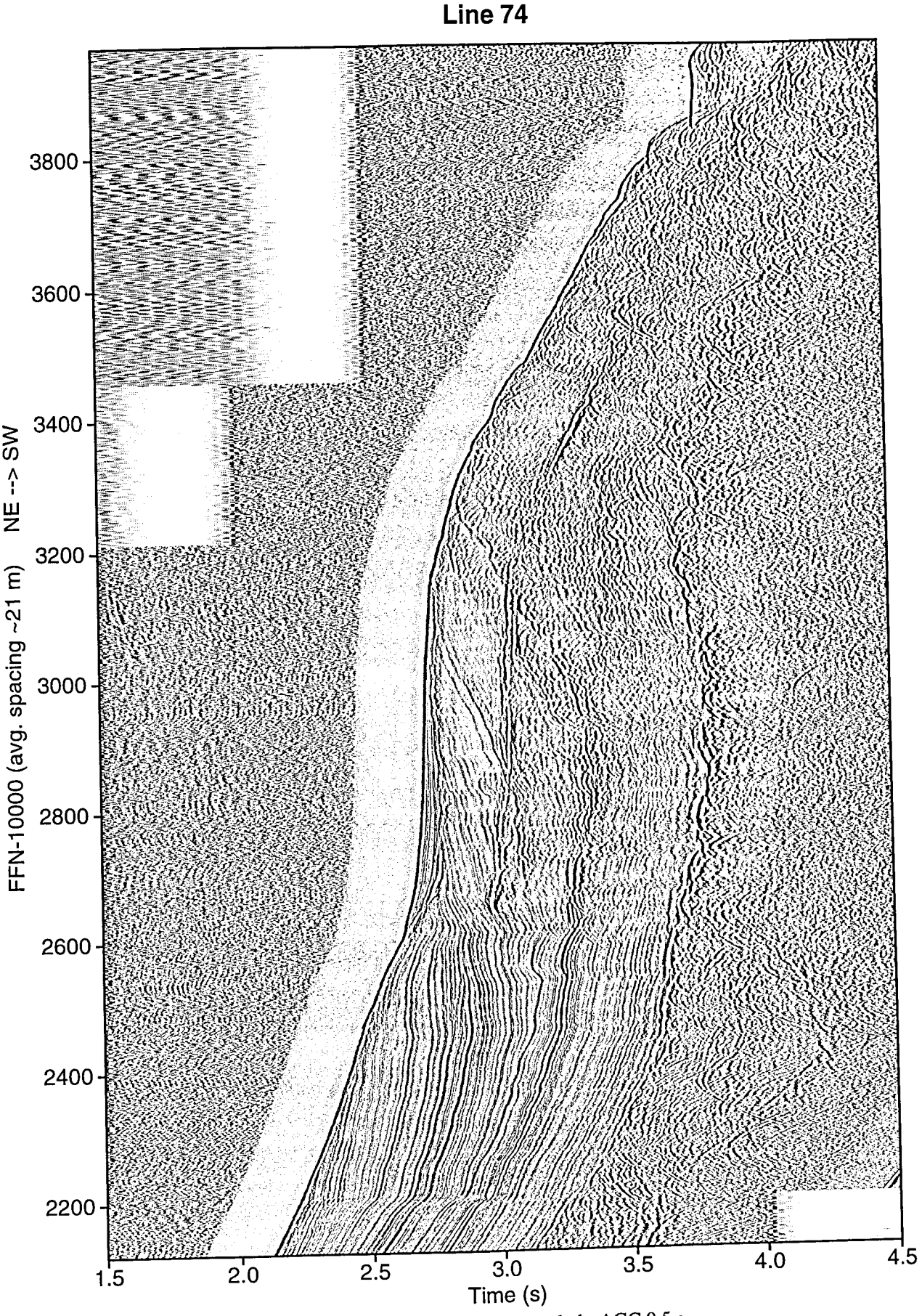

Fig. 9.1.13: MCS line 74. BP 15/25-150/200 Hz; Trace bal.; AGC 0.5 s.

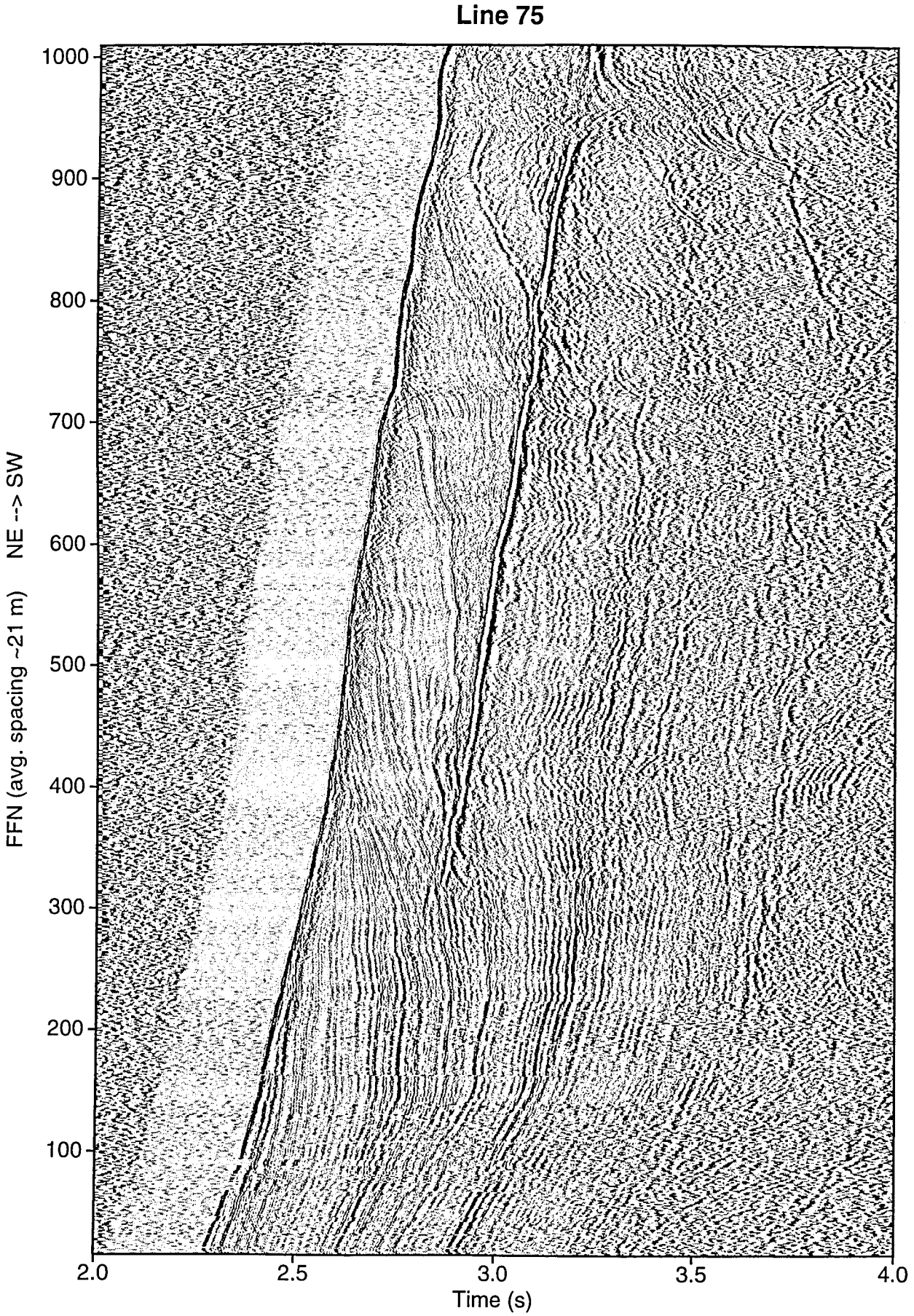

Fig. 9.1.14: MCS line 75. 45/105 cu-in G/I gun for 2.5-D survey.
BP 15/25-175/225 Hz; Trace bal.; AGC 0.5 s.

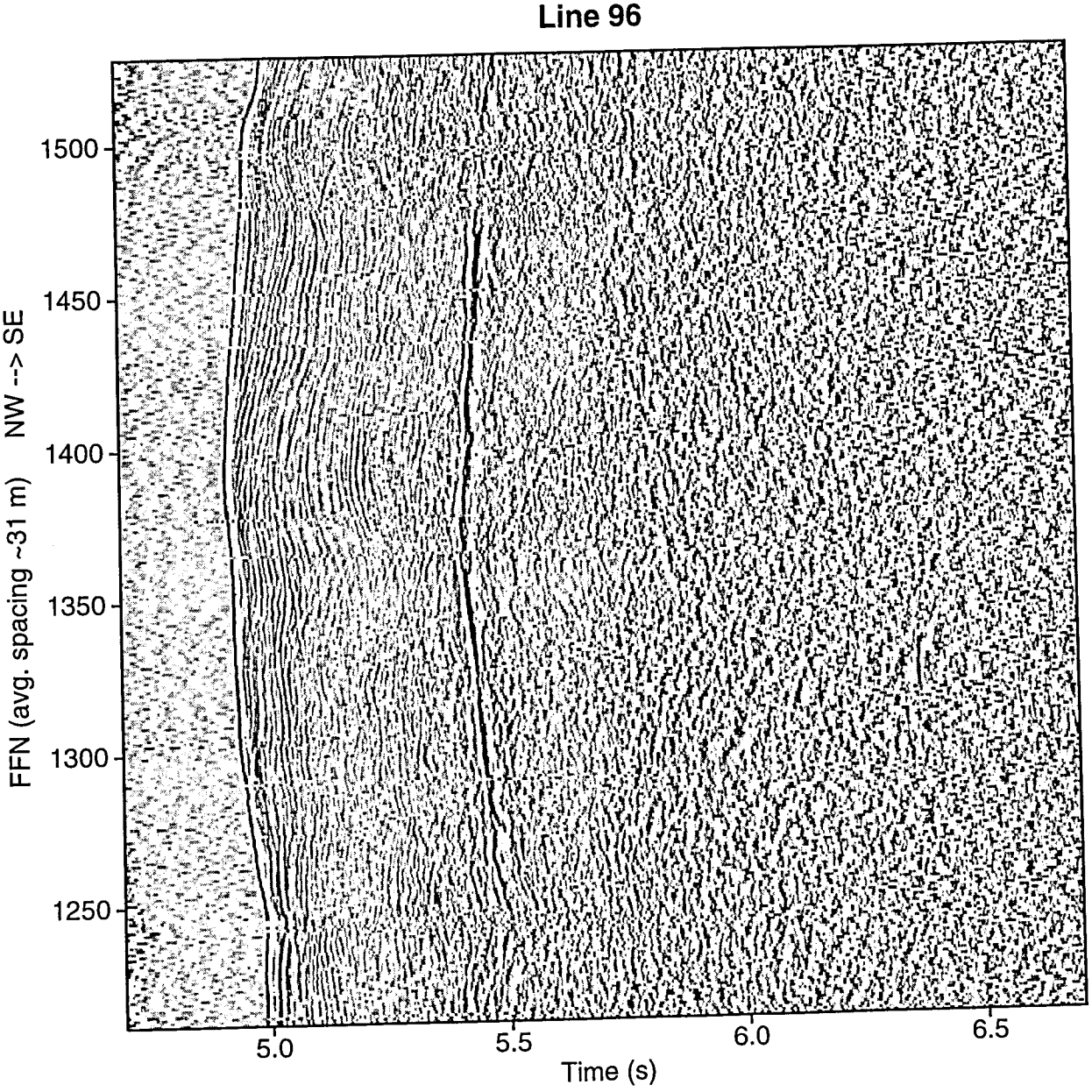

Fig. 9.1.15: MCS line 96. 2 105/105 cu-in G/I guns.
BP 10/20-150/200 Hz; Trace bal.; AGC 0.5 s.

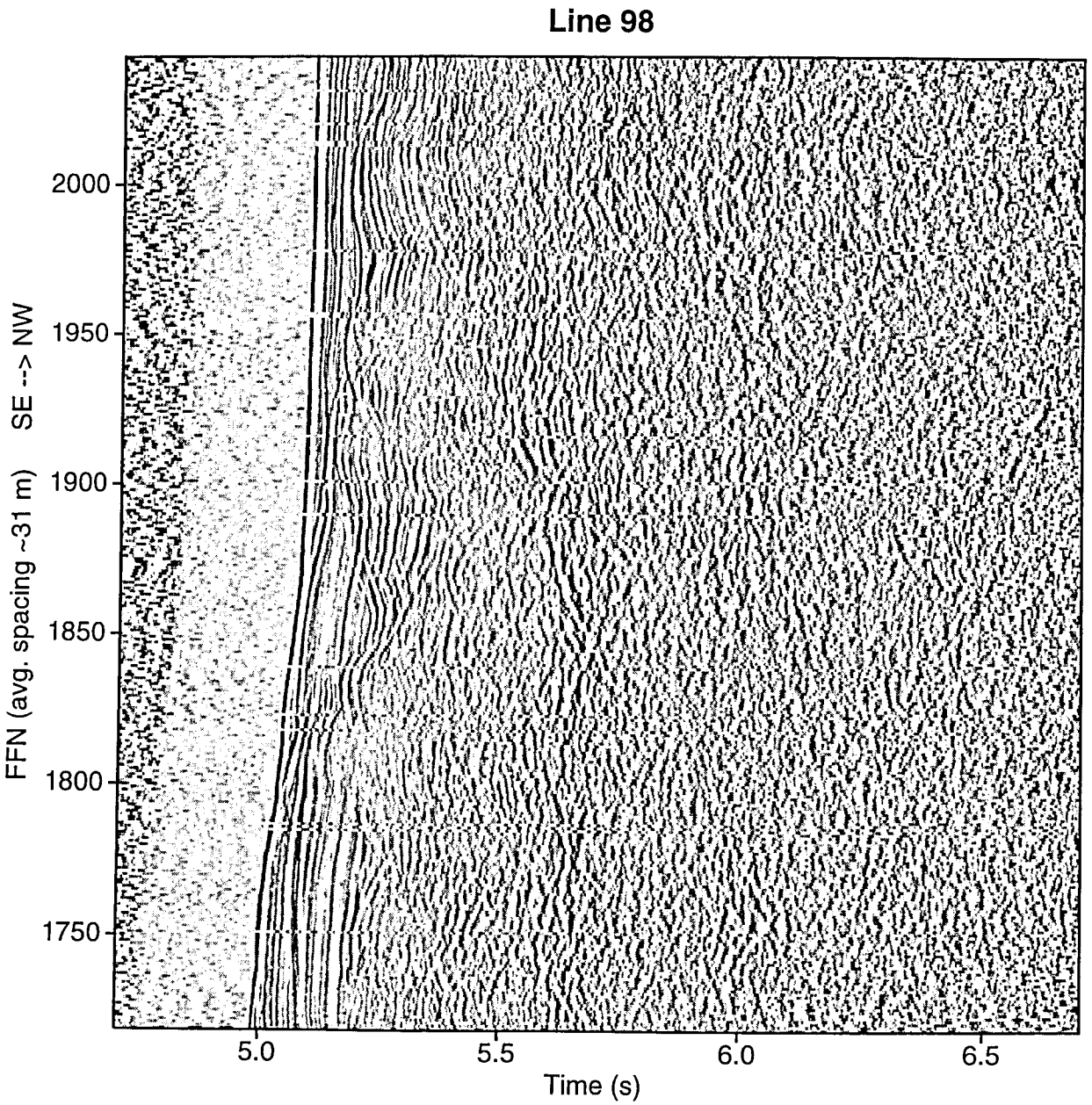

Fig. 9.1.16: MCS line 98. BP 10/20-150/200 Hz; Trace bal.; AGC 0.5 s.

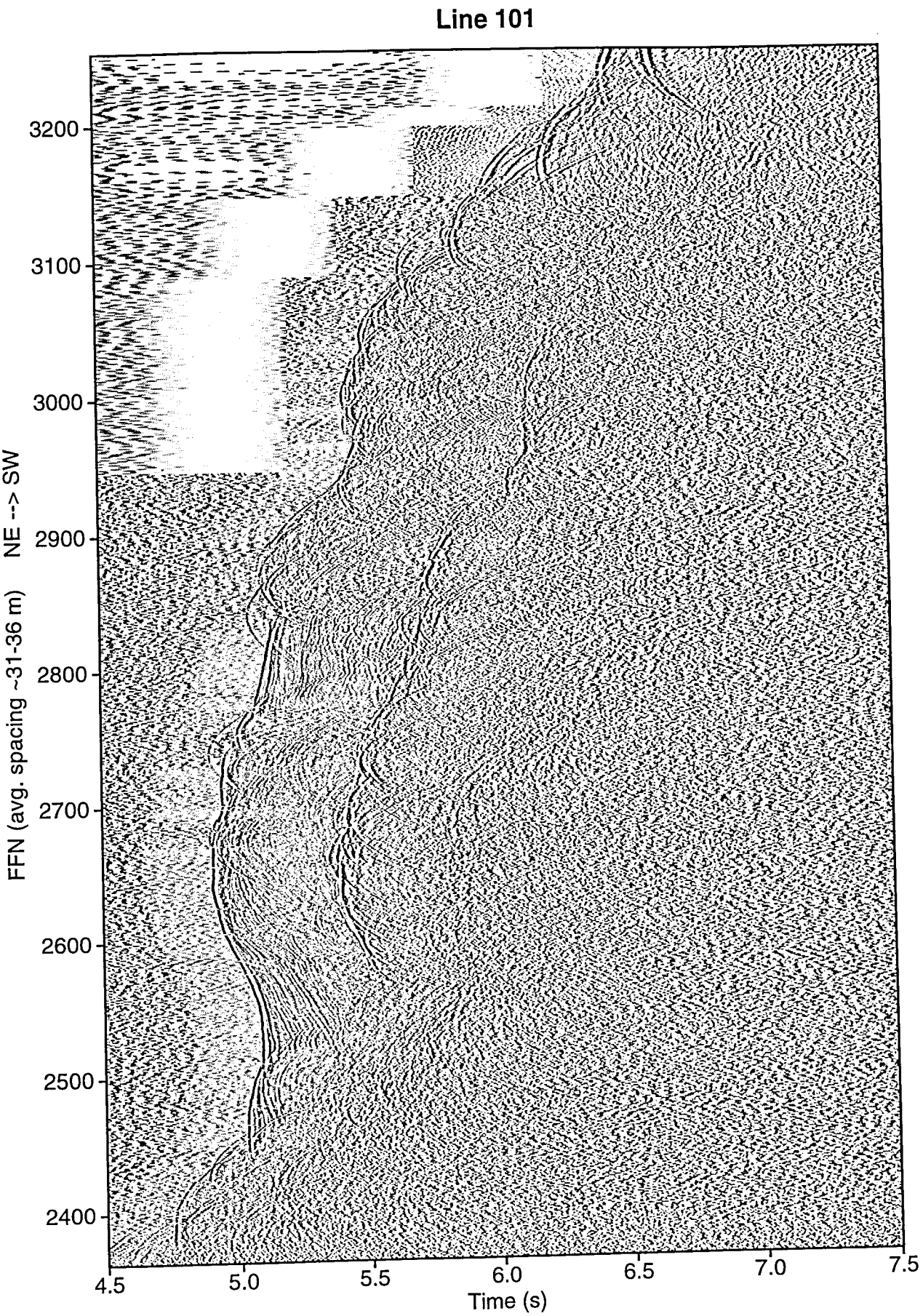

Fig. 9.1.17: MCS line 101. BP 10/20-150/200 Hz; Trace bal.; AGC 0.5 s.

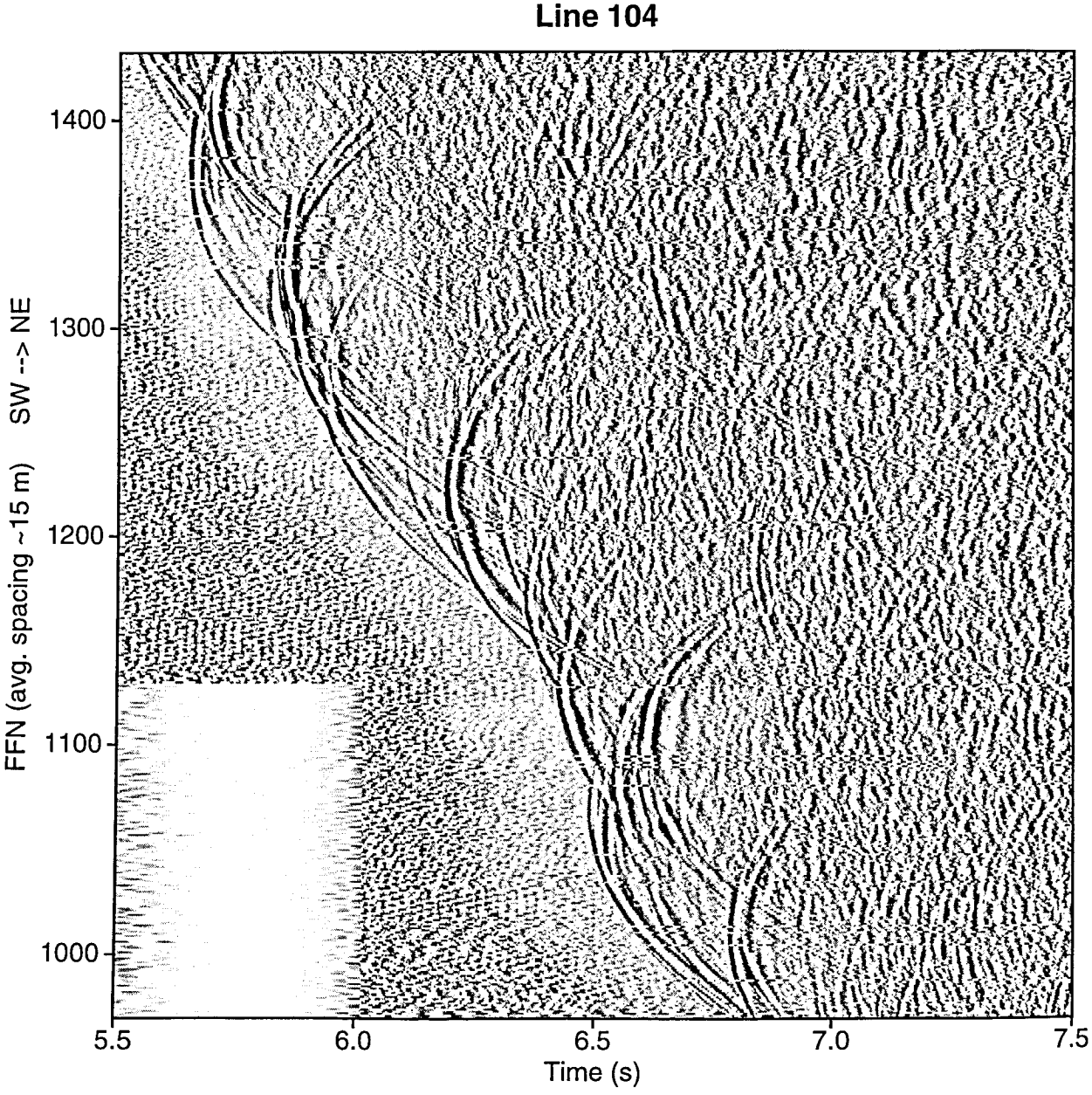

Fig. 9.1.18: MCS line 104. Most diffractions from the rough seafloor should collapse after seismic migration. BP 10/20-150/200 Hz; Trace bal.; AGC 0.5 s.

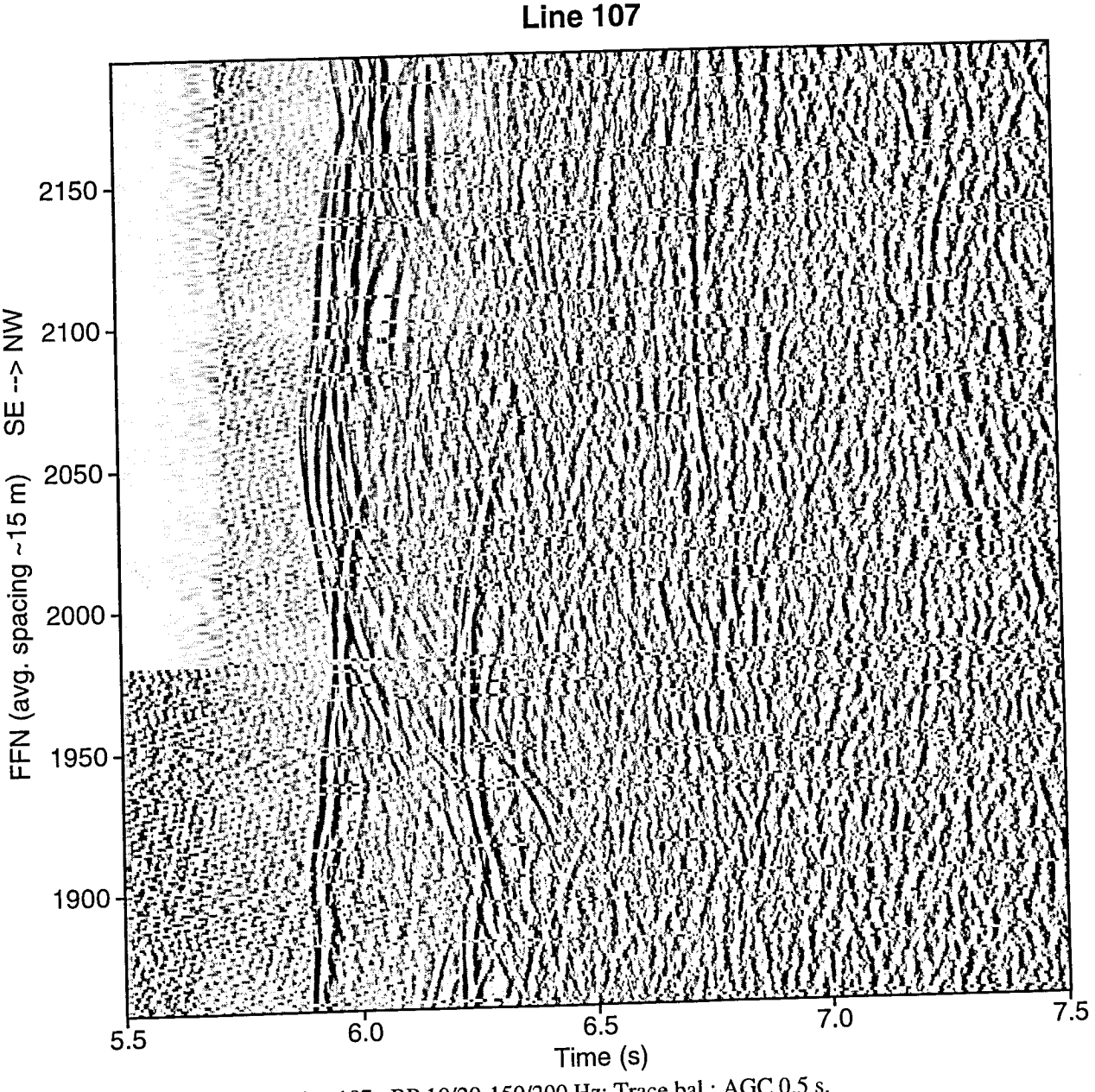

Fig. 9.1.19: MCS line 107. BP 10/20-150/200 Hz; Trace bal.; AGC 0.5 s.

9.2. OBH/S Seismics

(T. Leythaeuser, D. Klaeschen, I. Pecher, R. Coman)

9.2.1. Data

Two 105/105 in^3 (1.6/1.6 l) GI guns were used during P07 and P11 (MCS lines HH00 026-33 and 092-101, see 9.1.), one 45/105 in^3 (0.7/1.6 l) GI gun during P09 and P10 (MCS lines HH00 0044-064 and 0075-091; SeeBoSeis 1 and 2) (fig. 9.2.1). On P07 all records display wide-angle reflections (PiP) and refracted arrivals (Pn) from the metamorphic basement (figs. 9.2.2-25). The observation of strong P-to-S converted arrivals in OBS 76 and 80 demonstrates the excellent suitability of the OBSs for converted-wave studies. An apparently hard seafloor probably improved coupling. We observed both PS-arrivals (downgoing P-waves that are transmitted upon reflection and travel back to the seafloor as S-waves) and PSS-arrivals (downgoing P-waves that are converted at the seafloor upon transmission into S-waves and reflected on deeper horizons as S-waves). Because of the hard seafloor, some PSP-arrivals (PS-waves that are converted back to P-waves at the seafloor) may be present in the hydrophone sections. Further studies are necessary to unambiguously identify arrival types. The geophone sections of OBS 84 only display weak and noisy arrivals. We speculate that the geophones were not coupled sufficiently to the seafloor.

GI gun shots were recorded during deployments P09 and P10 primarily to be able to determine the location of the OBH/S on the seafloor. Due to the small GI gun used and the short offsets recorded, no clear Pn arrivals can be found on P09 and P10. Nevertheless, all records do show near-vertical reflections from the basement (figs 9.2.26-53). Data quality of these records in general is not optimum. The configuration of the instruments had been modified to record SeeBoSeis shots, which included changing the dynamic ranges, increasing the sampling rates from 1 kHz to mostly 2.5 kHz, and using different storage media in most instruments. At this point, we do not know which of the changes caused the deterioration of data quality. Blocks of traces with poor data quality appear at regular time intervals interbedded in blocks of excellent traces on those recorders sampling at 2.5 kHz. These time intervals may coincide with the data being flushed from memory to the harddisks that were used as storage media for the first time in this configuration. Our suspicions therefore focus around these harddisks. The poorer-quality traces, however, still recorded seismic signals and we are therefore confident that adequate data processing will allow us to fully evaluate the data from P09 and P10.

During deployment P11, located at the lower continental slope, two 105/105 in^3 (1.6/1.6 l) GI guns were used. The records show a clear near-vertical reflection corresponding to the BSR seen in the MCS data, where present. On OBH 126 and OBH 127 at 12-14 km offset and 6 seconds, a wide-angle reflection from the top of the subducted sediments is imaged (figs 9.2.54-56).

9.2.2. Correlation of Arrivals in the Different Data Sets – Example OBS 76

An unambiguous correlation of arrivals in the OBH/S data and the MCS reflection data is essential for our planned analysis of the sub-surface velocity structure. This can be easily achieved down to the L4/L5 interface (fig. 9.2.57). Further processing to eliminate the 50-Hz noise in the streamer records should enable us to identify deeper reflections. We will also be able to use HIG-13, which had been shot essentially along the same track as HH00-026, for an identification of arrivals down to the metamorphic basement.

9.2.3. 2-D Imaging with Densely Spaced OBH/S

The dense deployment of the OBH/Ss necessary for recording the SeeBoSeis shots (section 9.3.) should allow us to image the subsurface in 2-D. For this, we are planning to use a high-order NMO correction. This approach is demonstrated in fig. 9.2.58 using the OBH/S records from deployment P07.

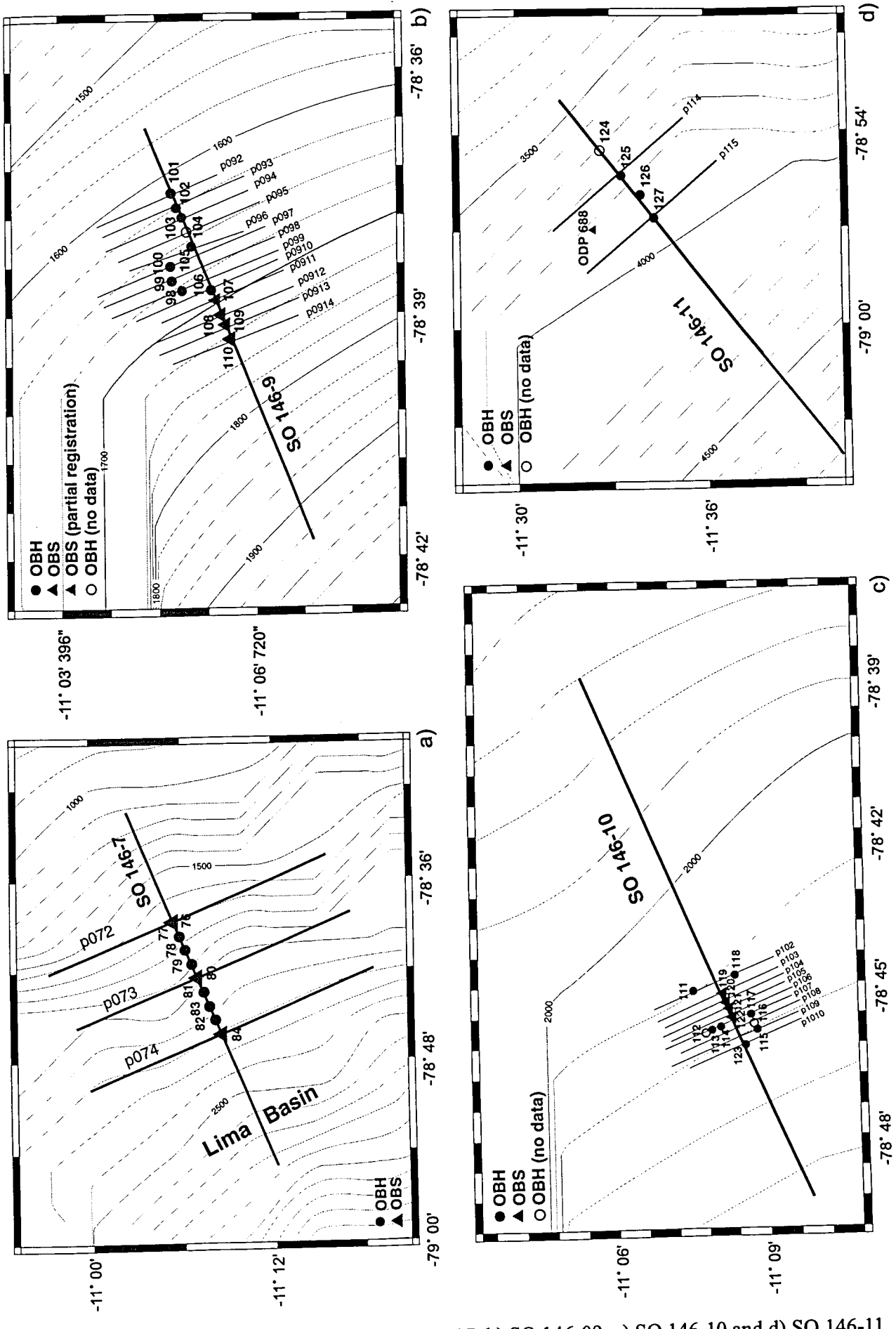

Figure 9.2.1: Location maps of profiles a) SO 146-07, b) SO 146-09, c) SO 146-10 and d) SO 146-11.

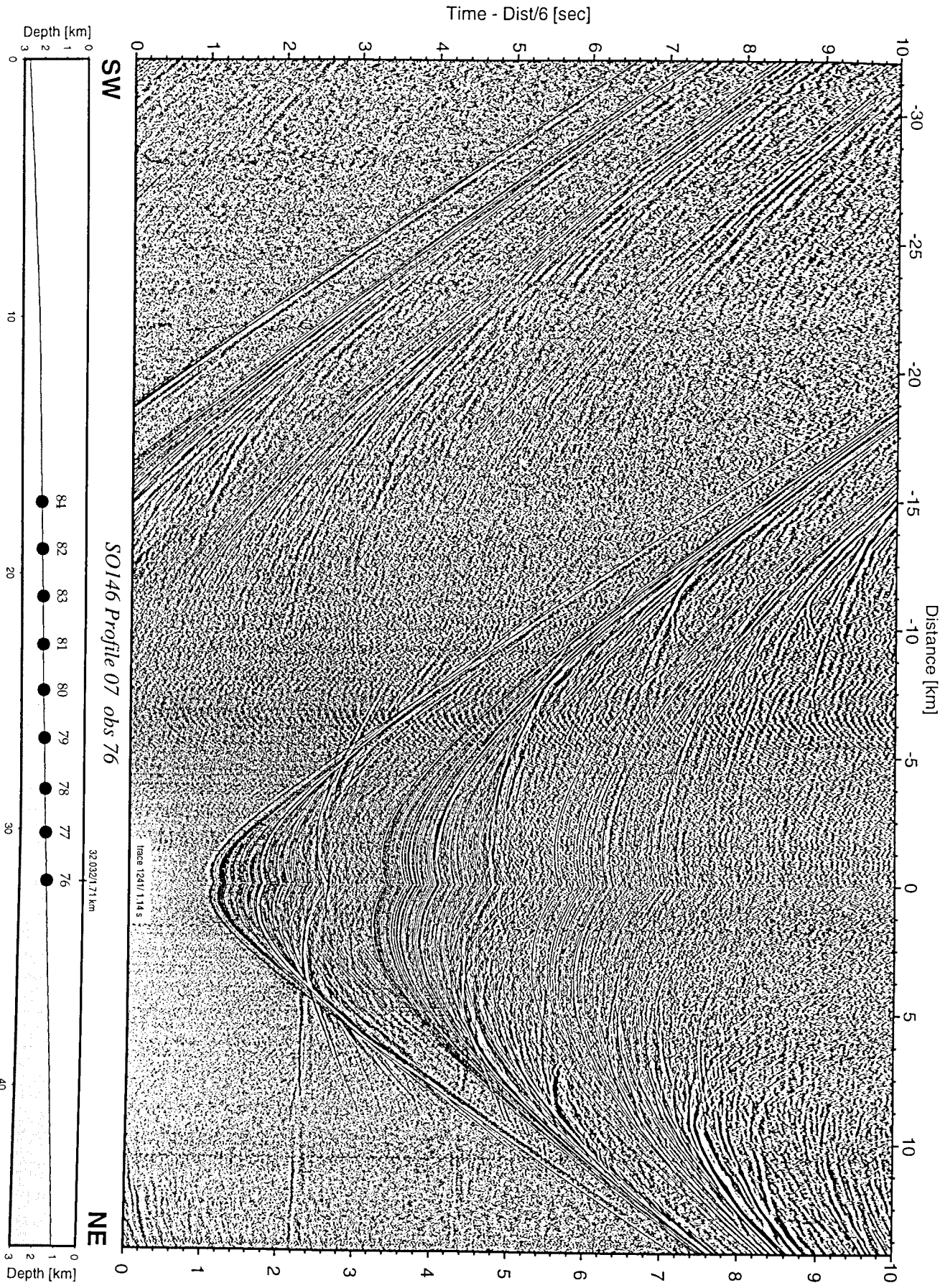

Figure 9.2.2: Record section from obs 76 hydrophone, Profile 07.

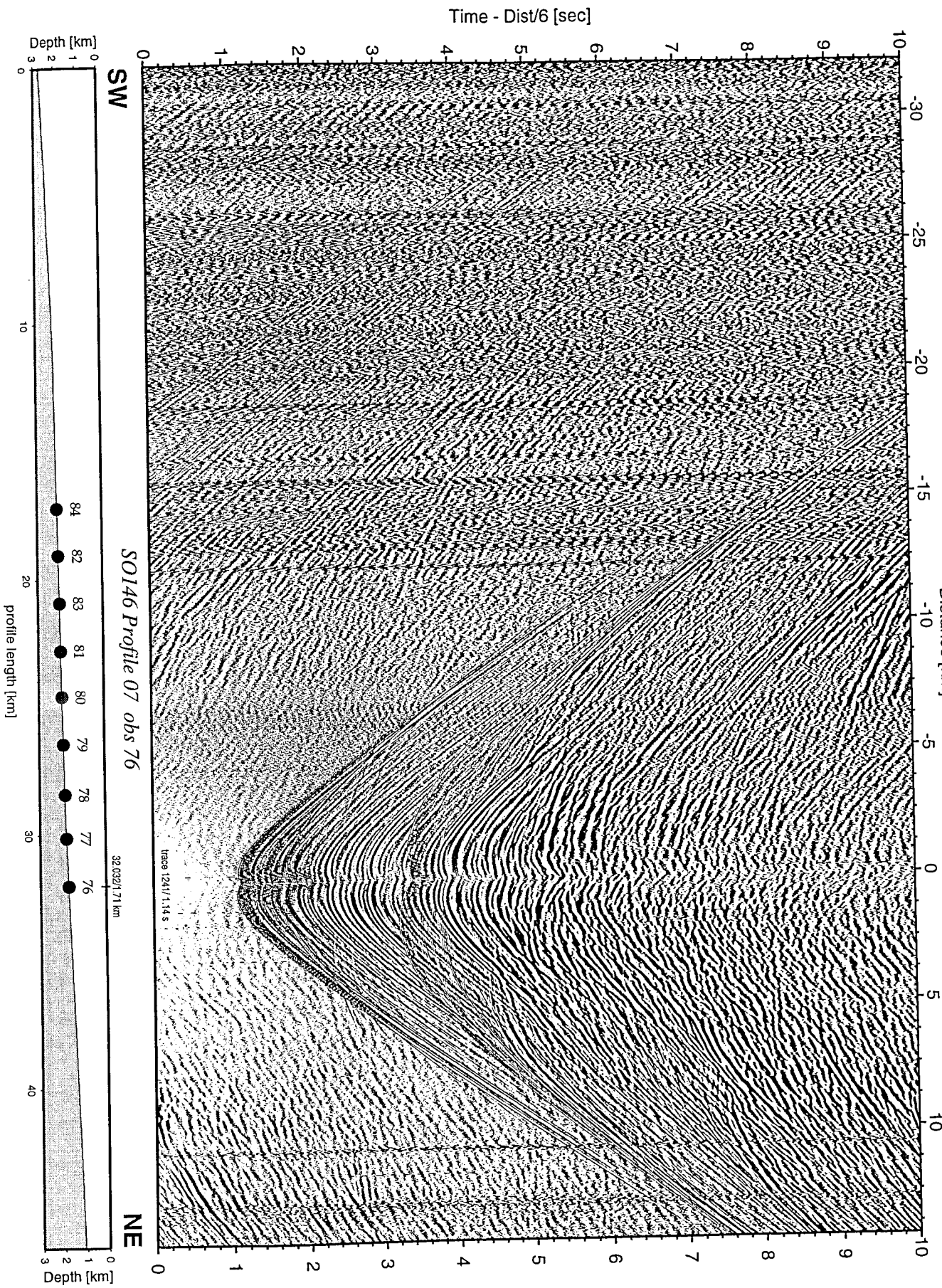

Figure 9.2.3: Record section from obs 76 horizontal component 1, Profile 07.

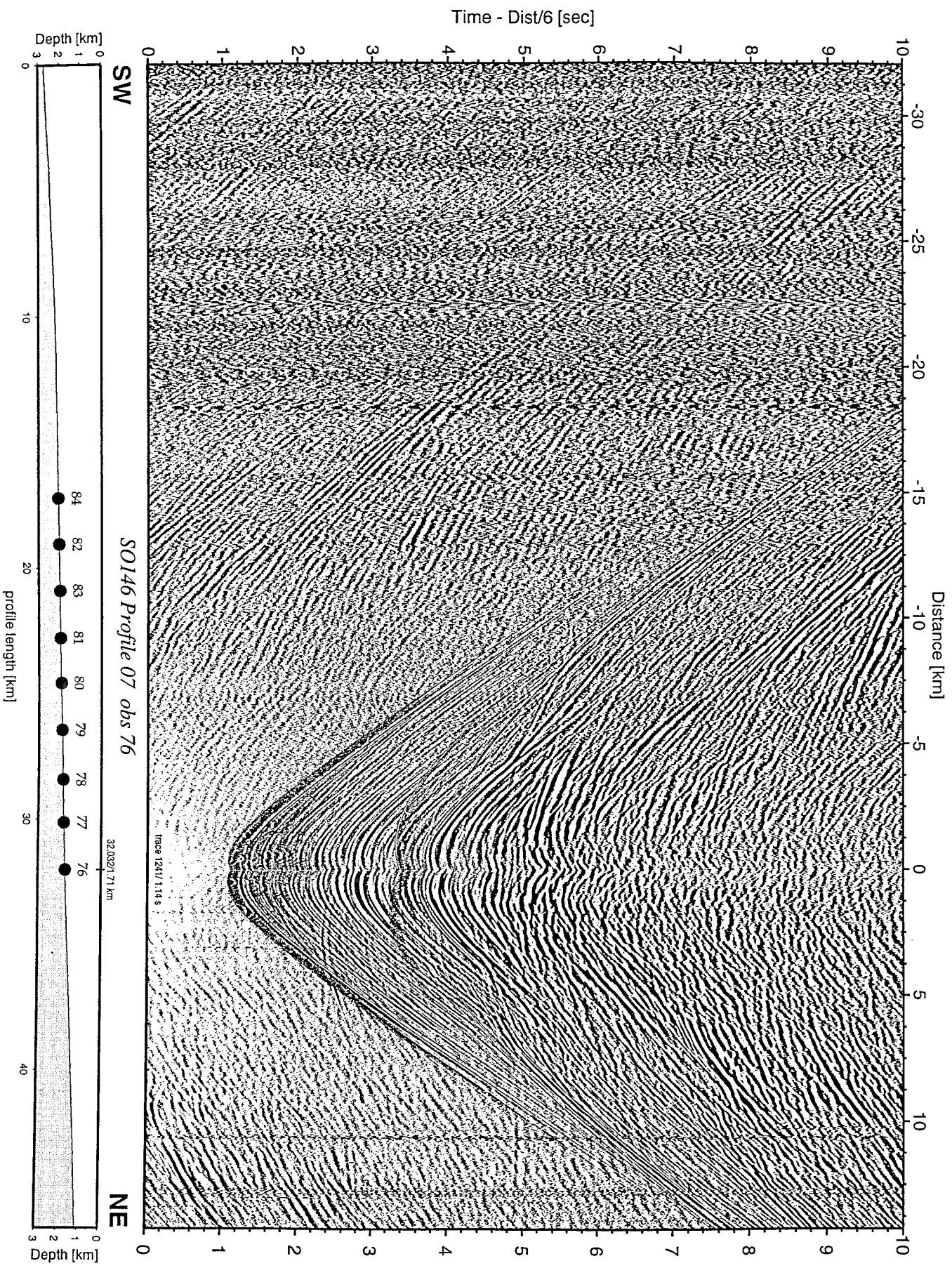

Figure 9.2.4: Record section from obs 76 horizontal component 2, Profile 07.

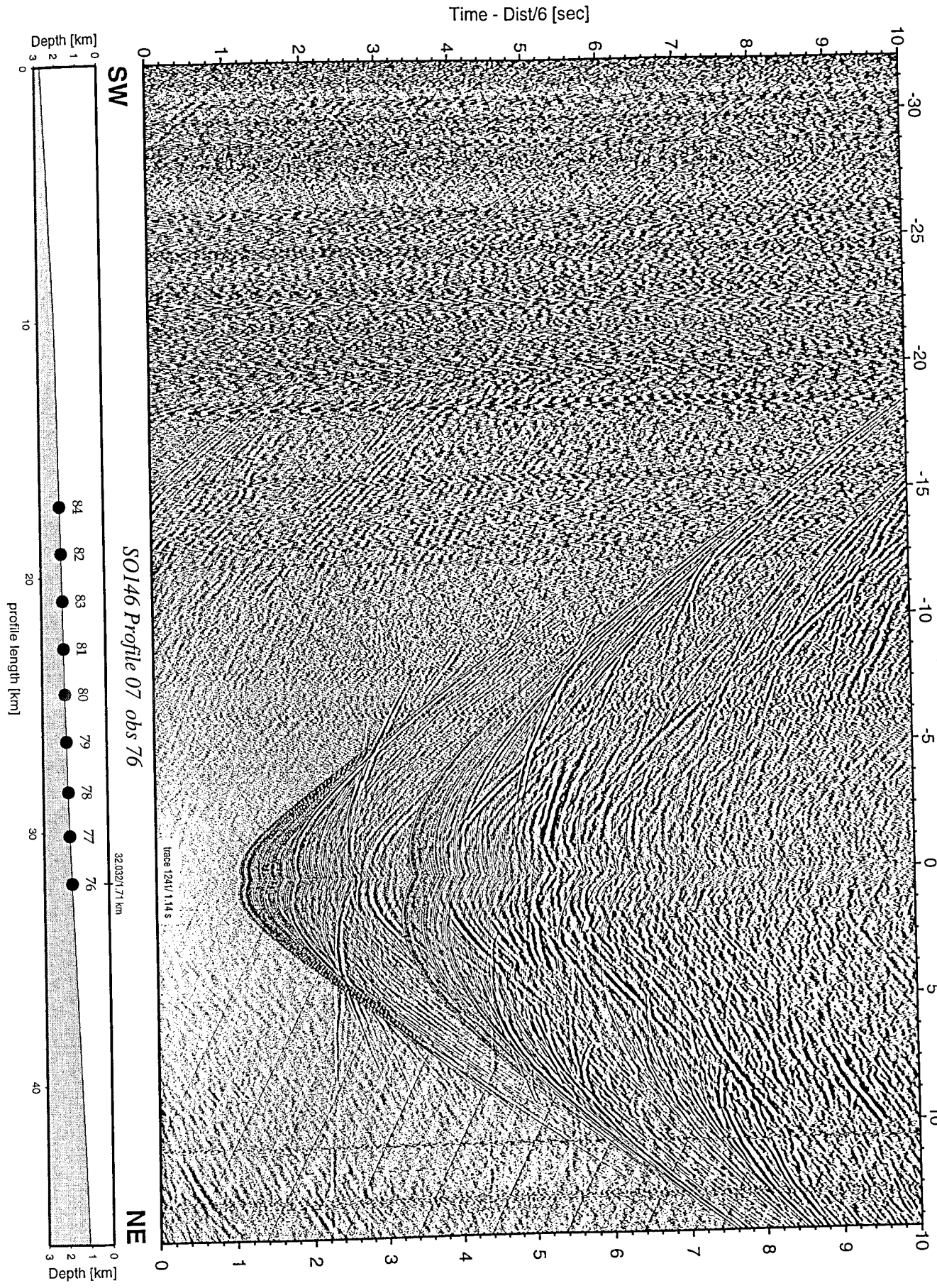

Figure 9.2.5: Record section from obs 76 vertical component, Profile 07.

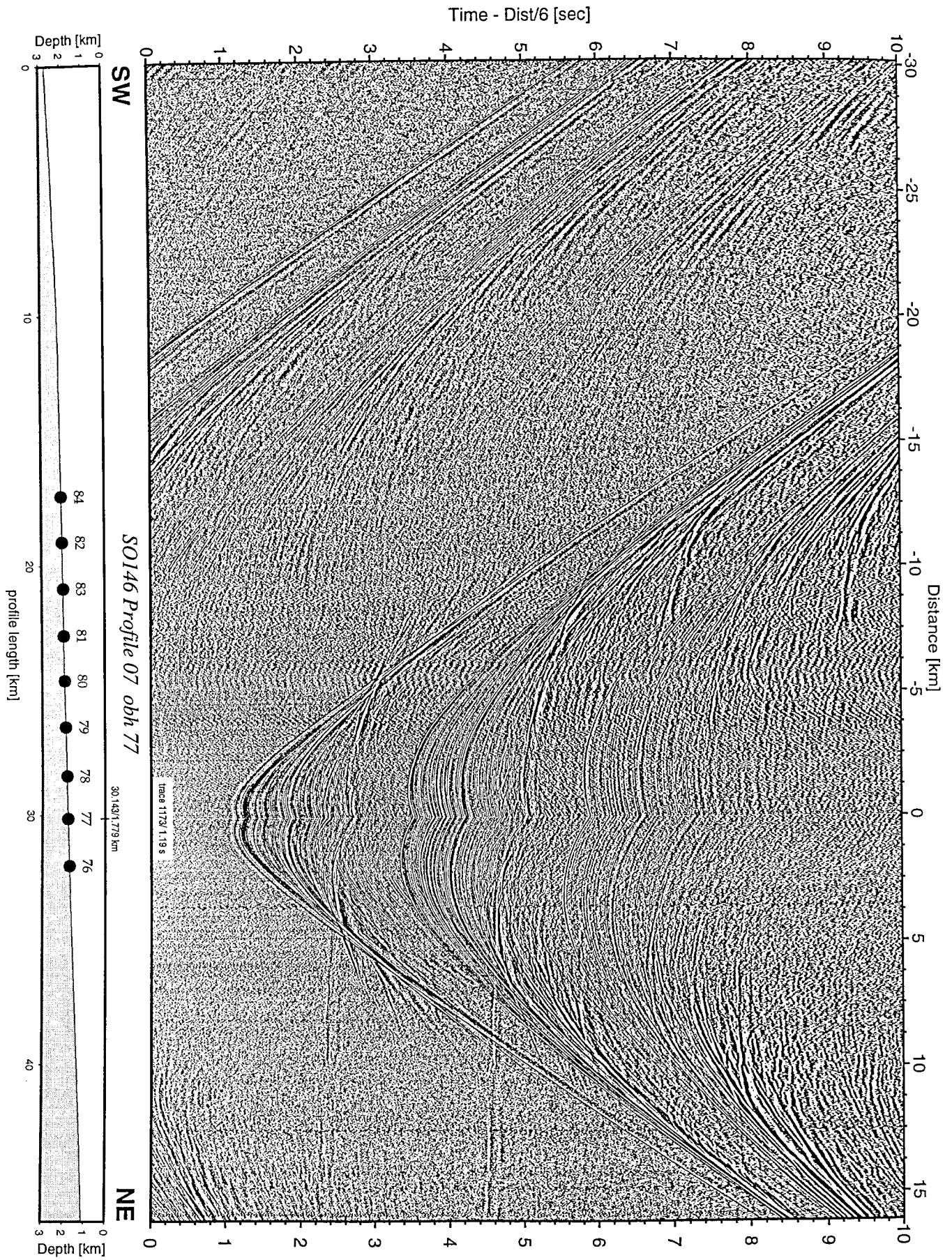

Figure 9.2.6: Record section from obh 77 , Profile 07.

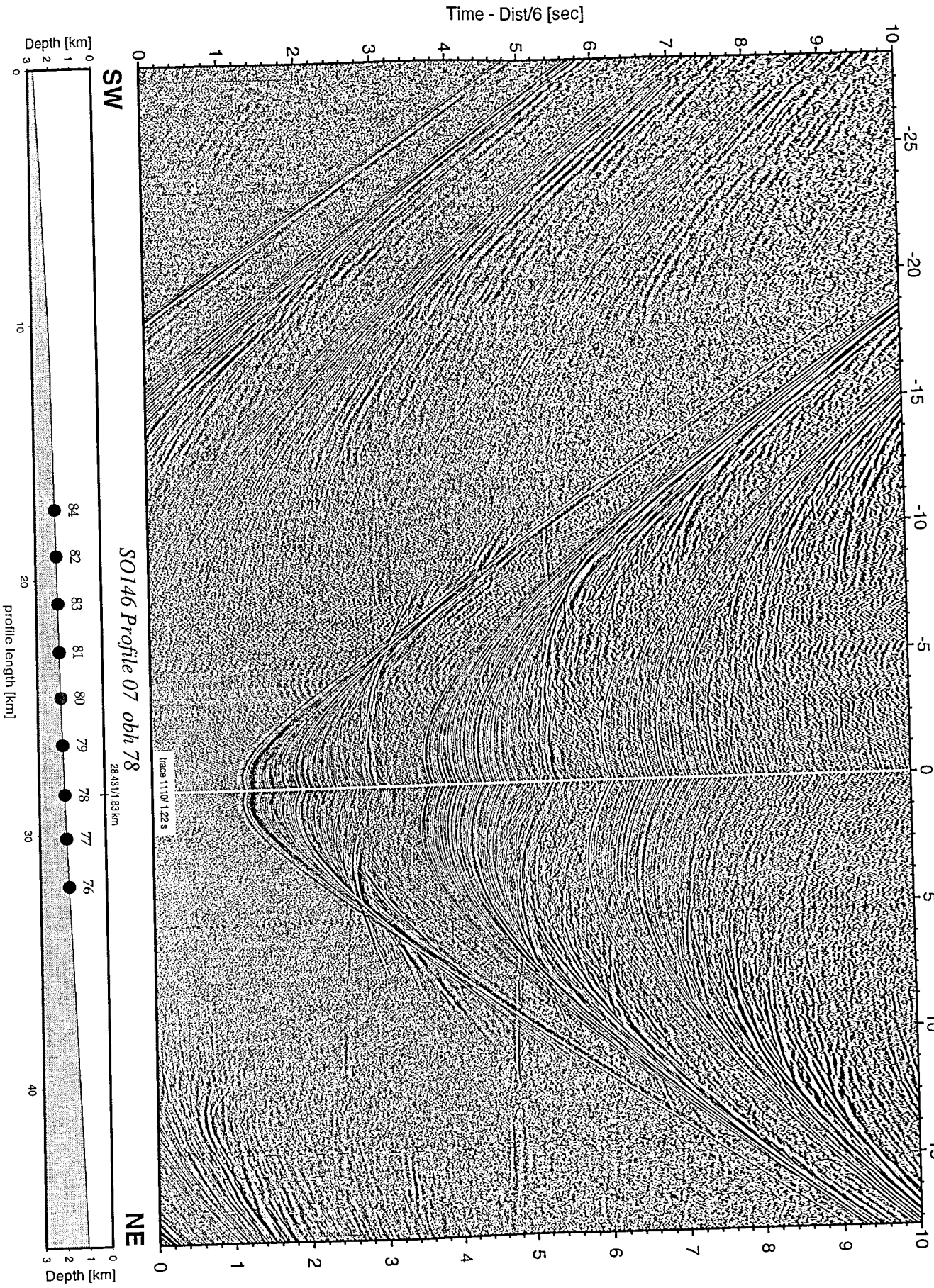

Figure 9.2.7: Record section from obh 78 , Profile 07.

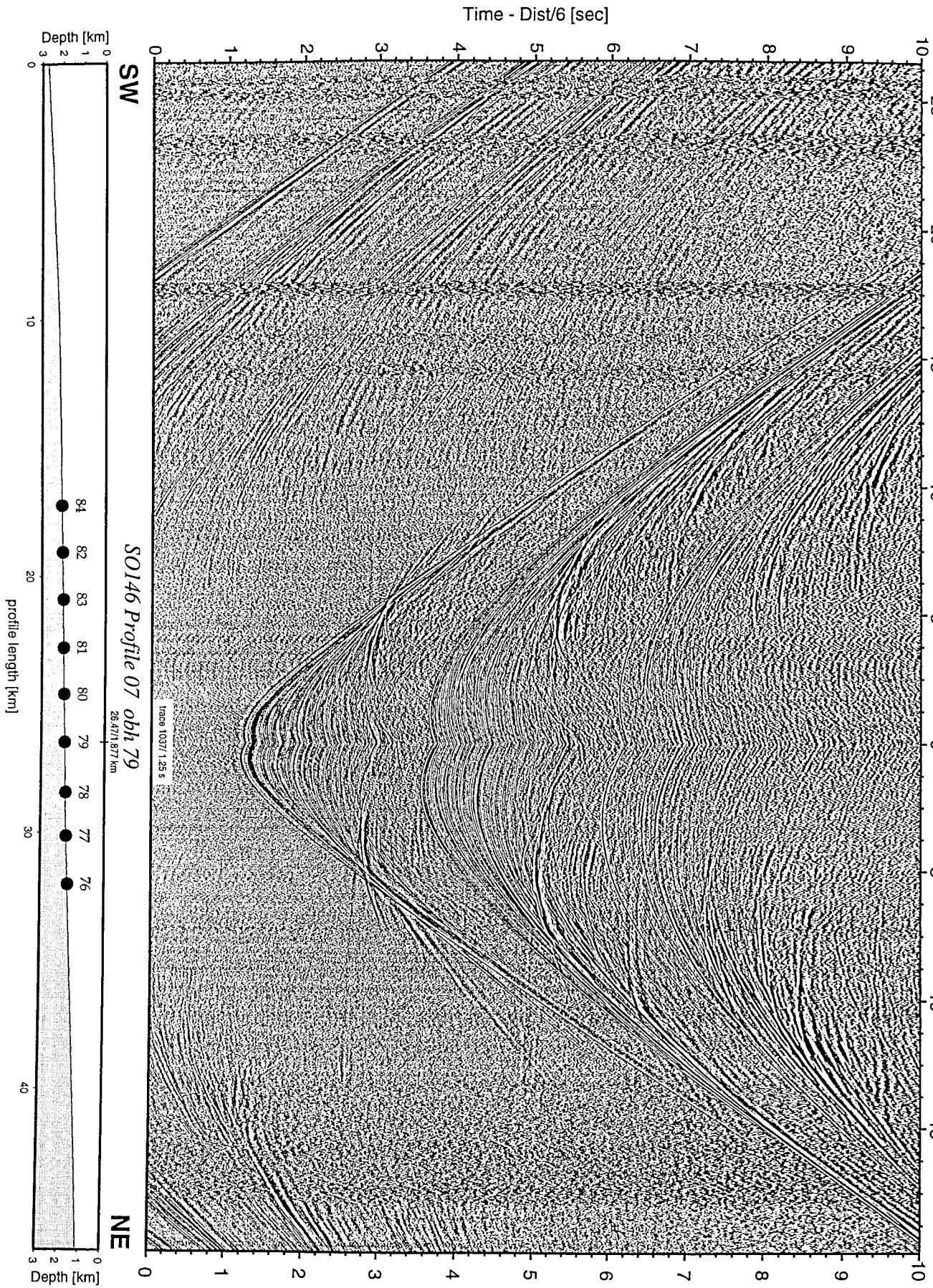

Figure 9.2.8: Record section from obh 79 , Profile 07.

Figure 9.2.9: Record section from obs 80 hydrophone, Profile 07.

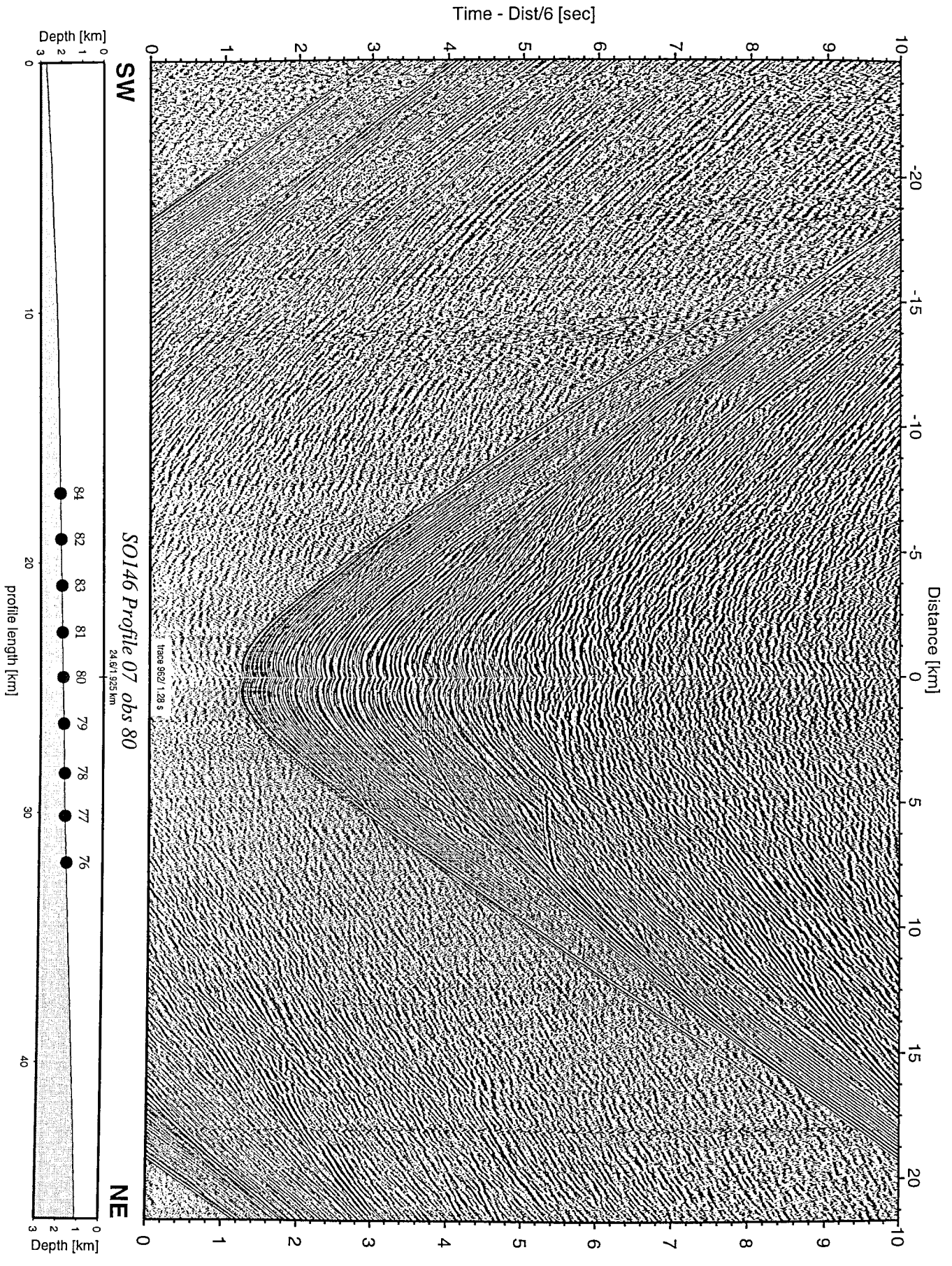

Figure 9.2.10: Record section from obs 80 horizontal component 1, Profile 07.

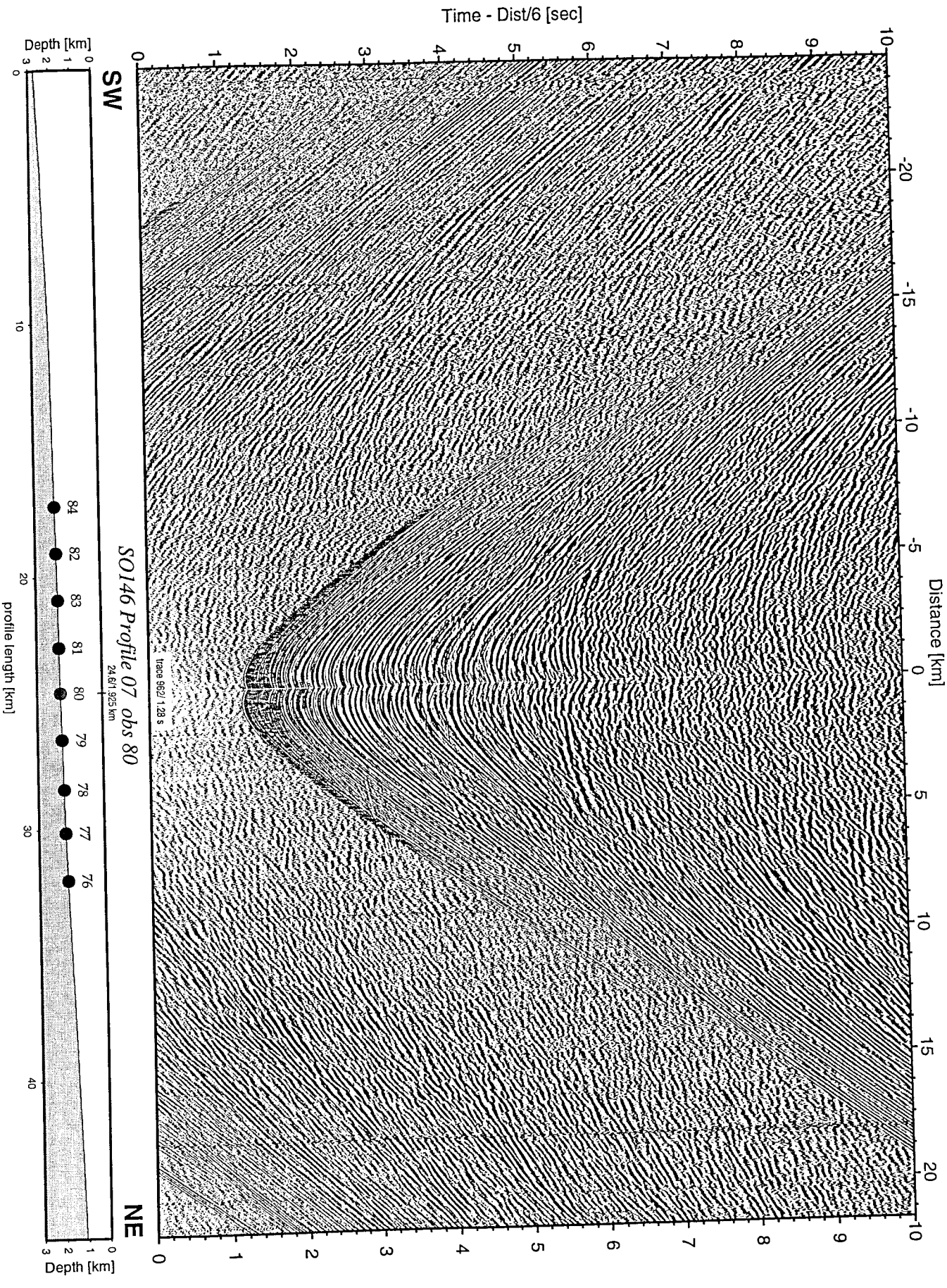

Figure 9.2.11: Record section from obs 80 horizontal component 2, Profile 07.

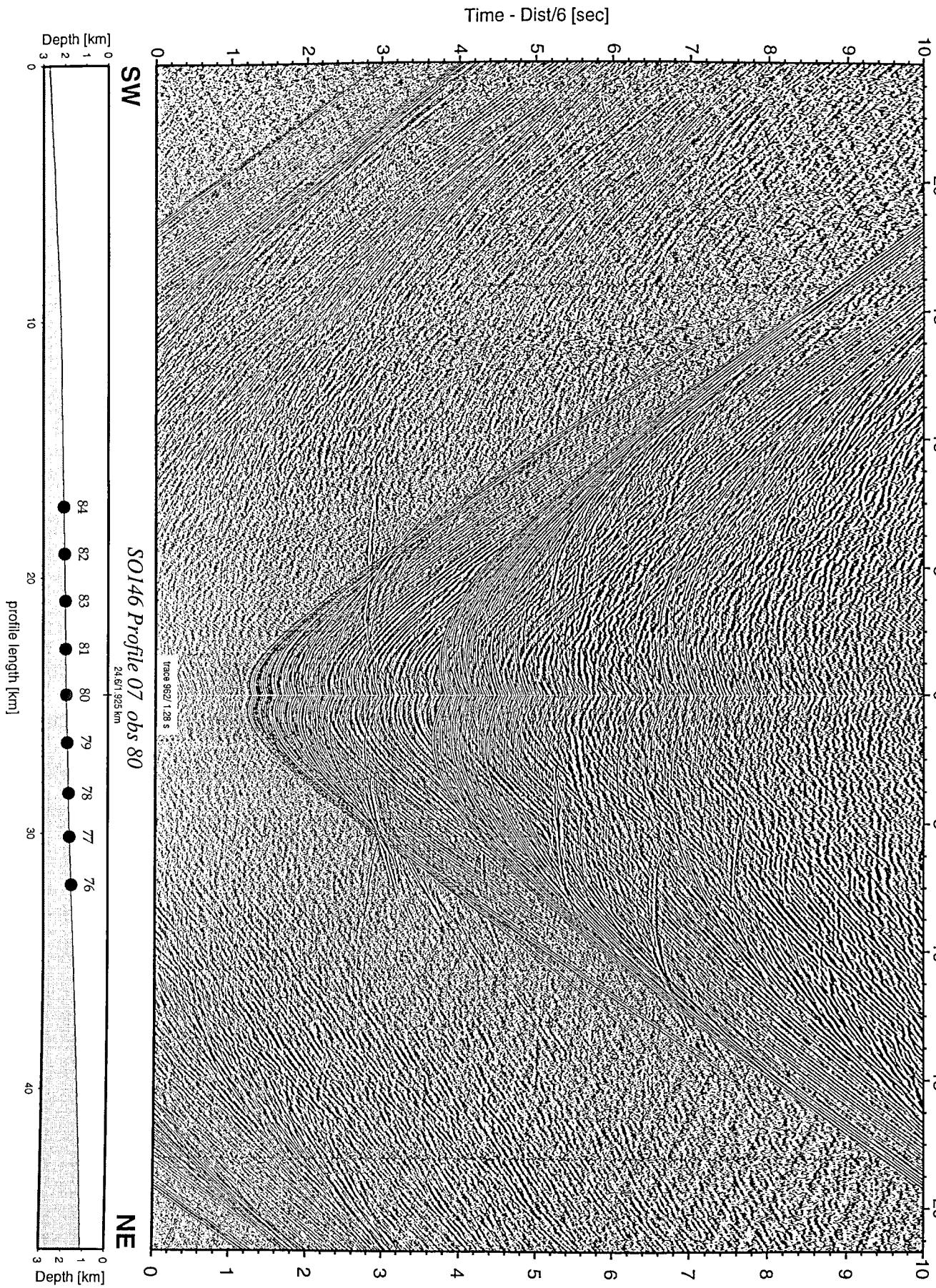

Figure 9.2.12: Record section from obs 80 vertical component, Profile 07.

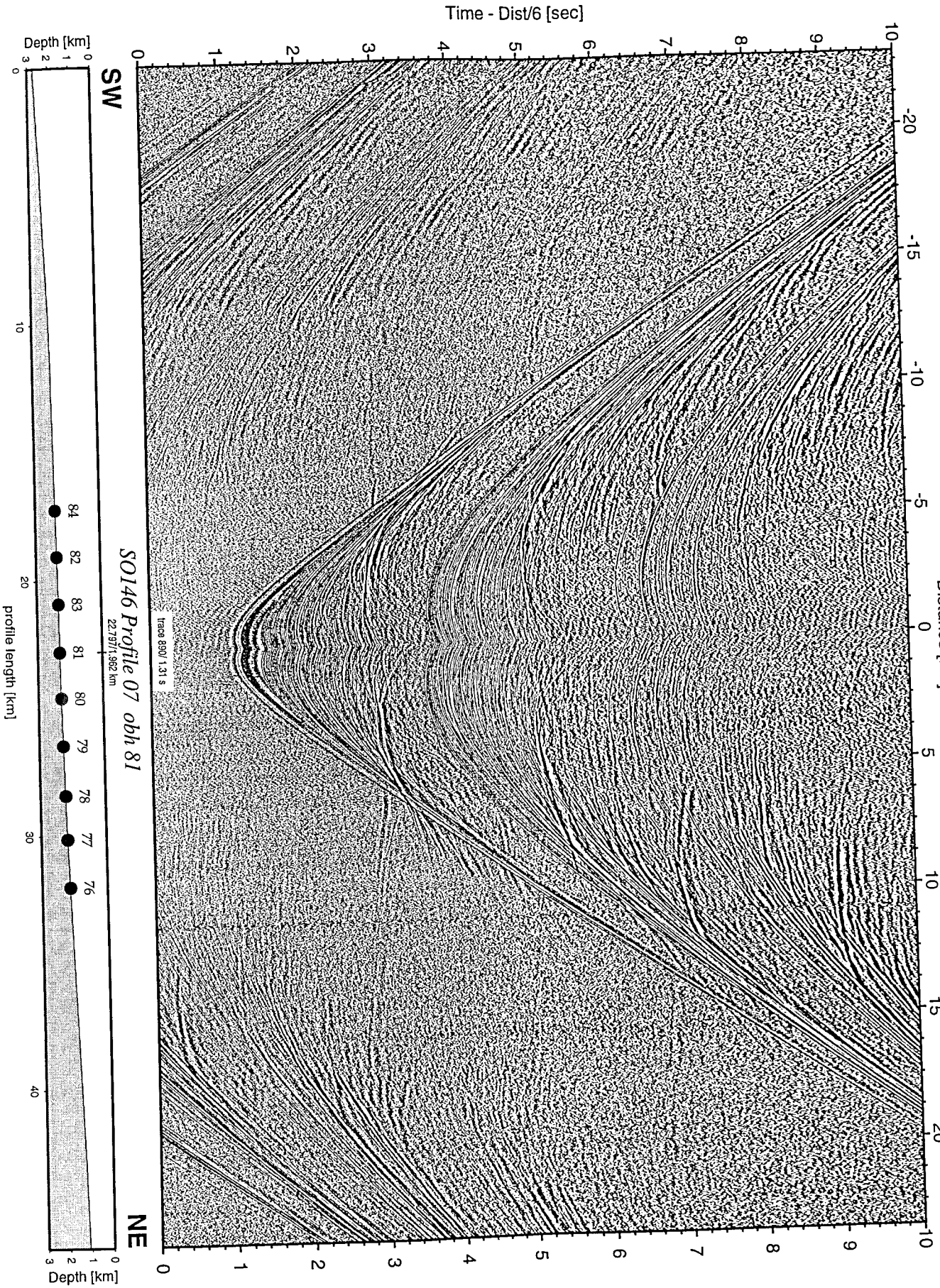

Figure 9.2.13: Record section from obh 81 , Profile 07.

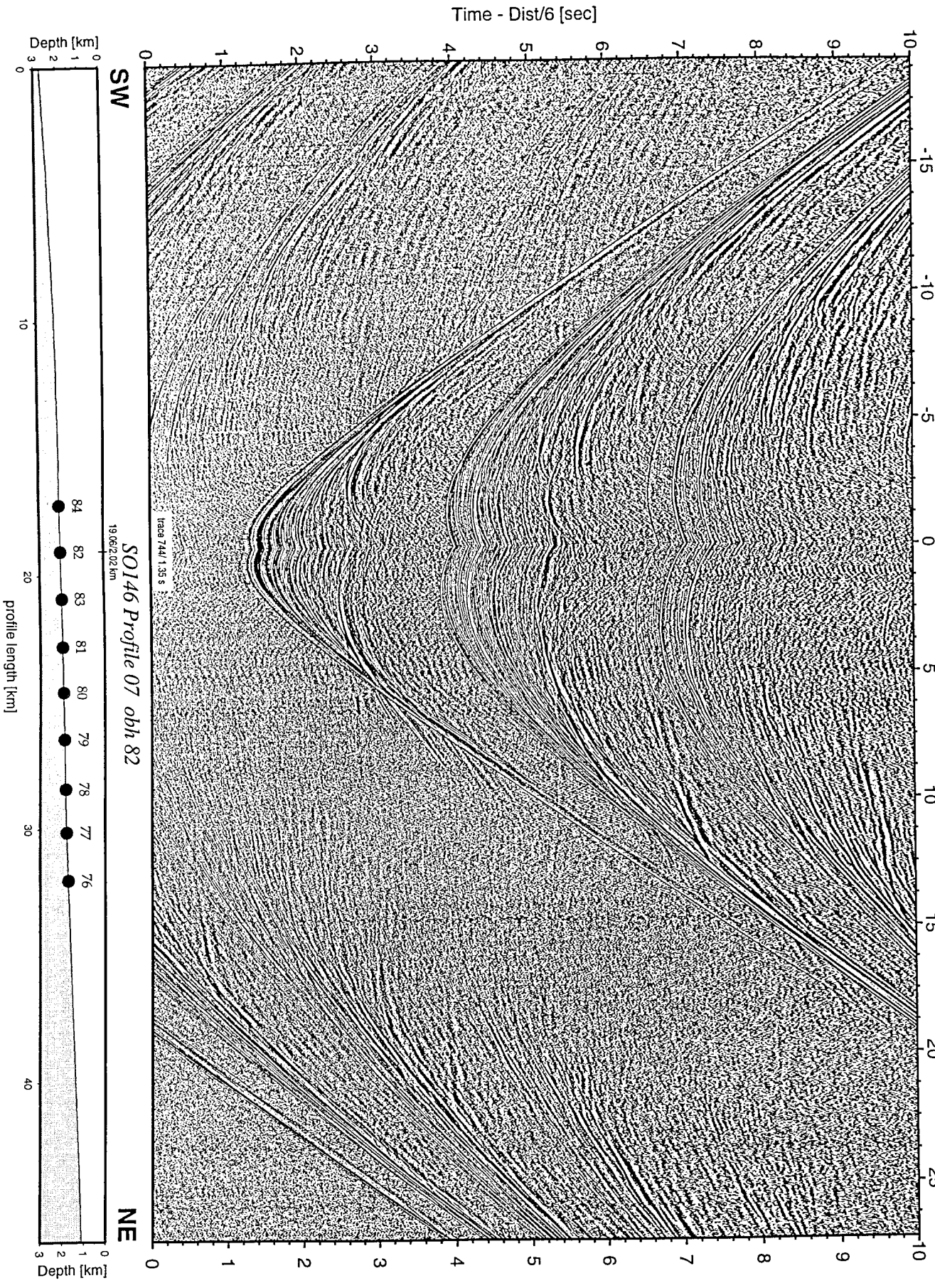

Figure 9.2.14: Record section from obh 82 , Profile 07.

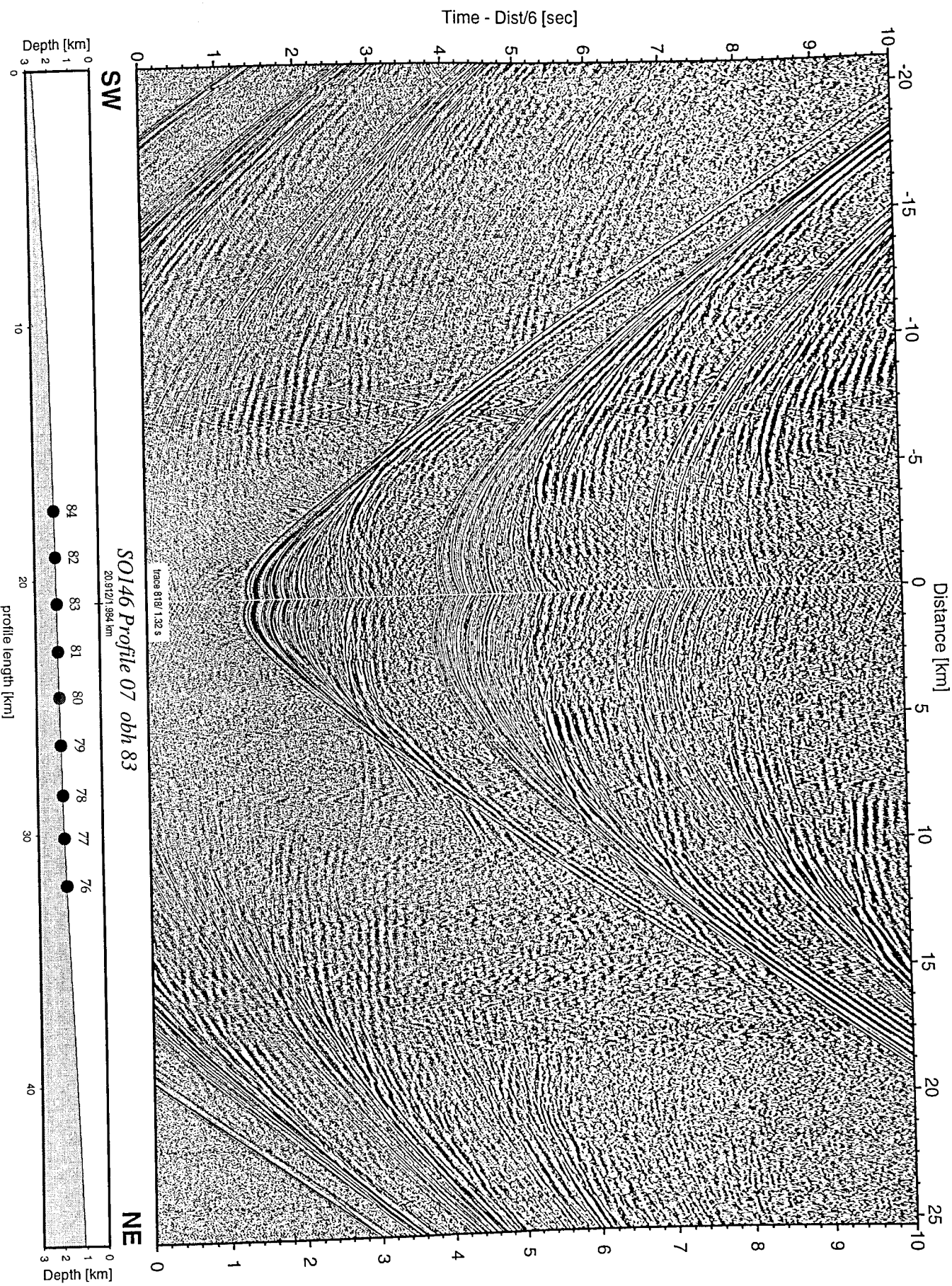

Figure 9.2.15: Record section from obh 83 , Profile 07.

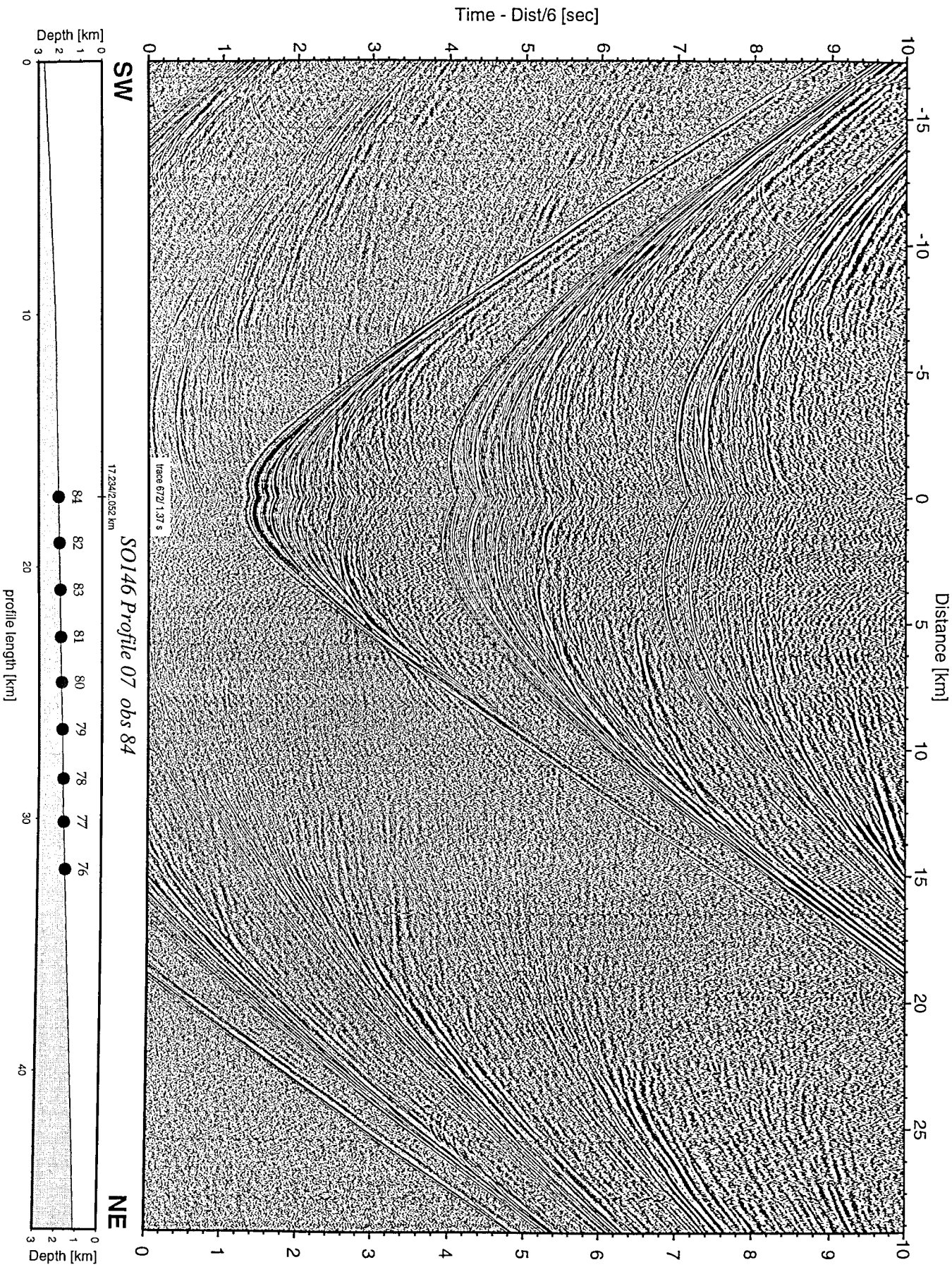

Figure 9.2.16: Record section from obs 84 hydrophone, Profile 07.

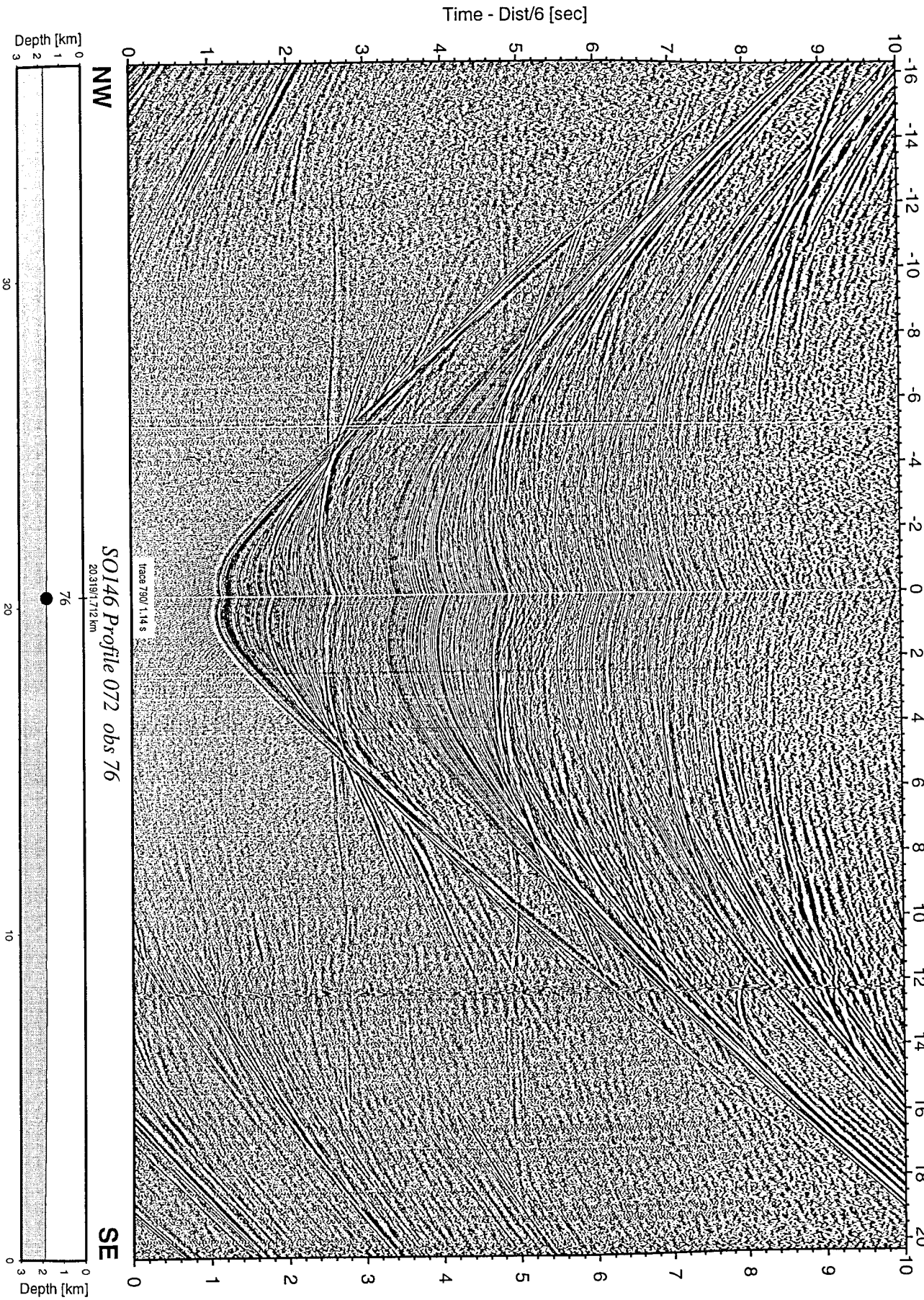

Figure 9.2.17: Record section from obs 76 hydrophone, Profile 072.

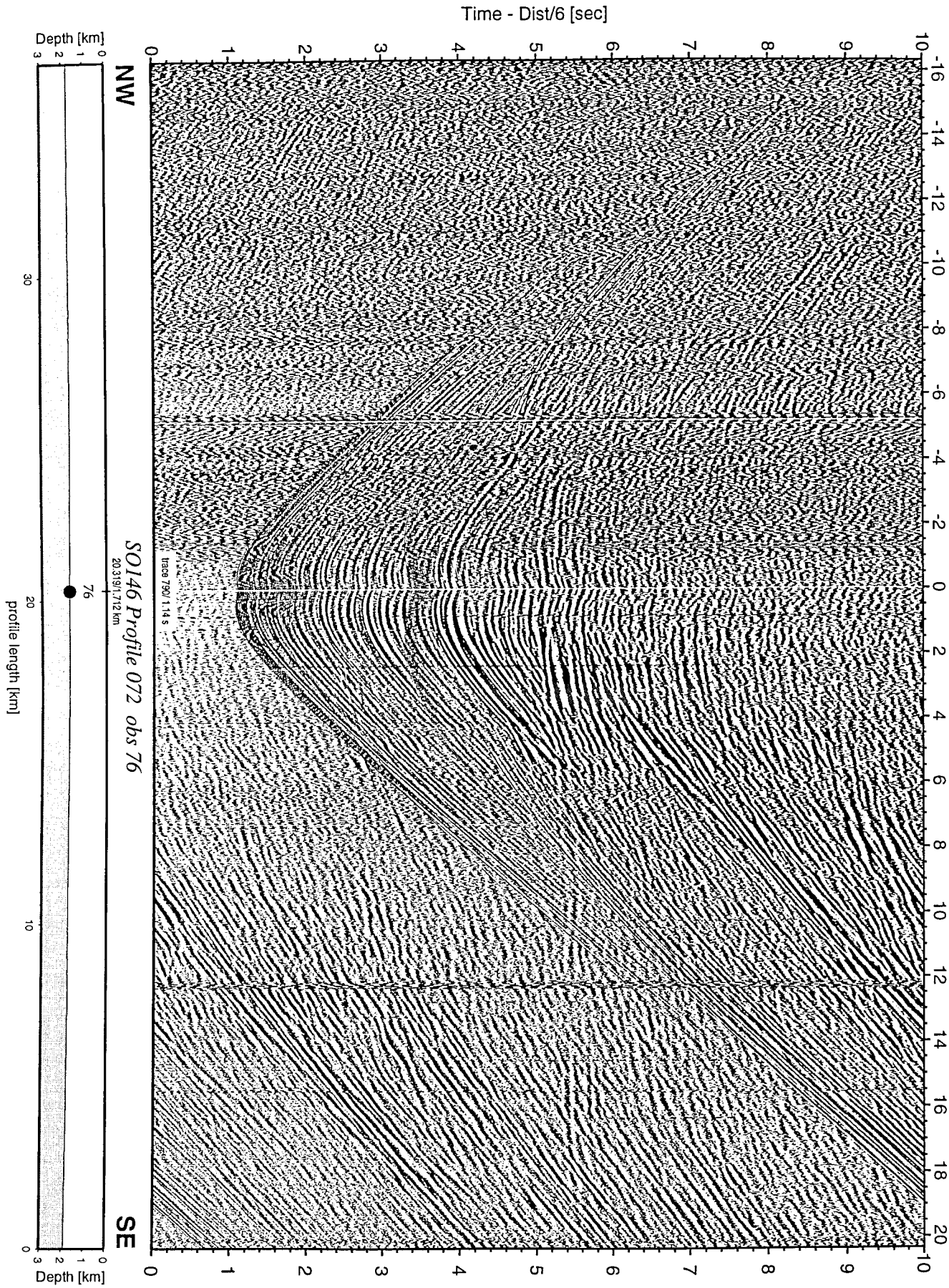

Figure 9.2.18: Record section from obs 76 horizontal component 1, Profile 072.

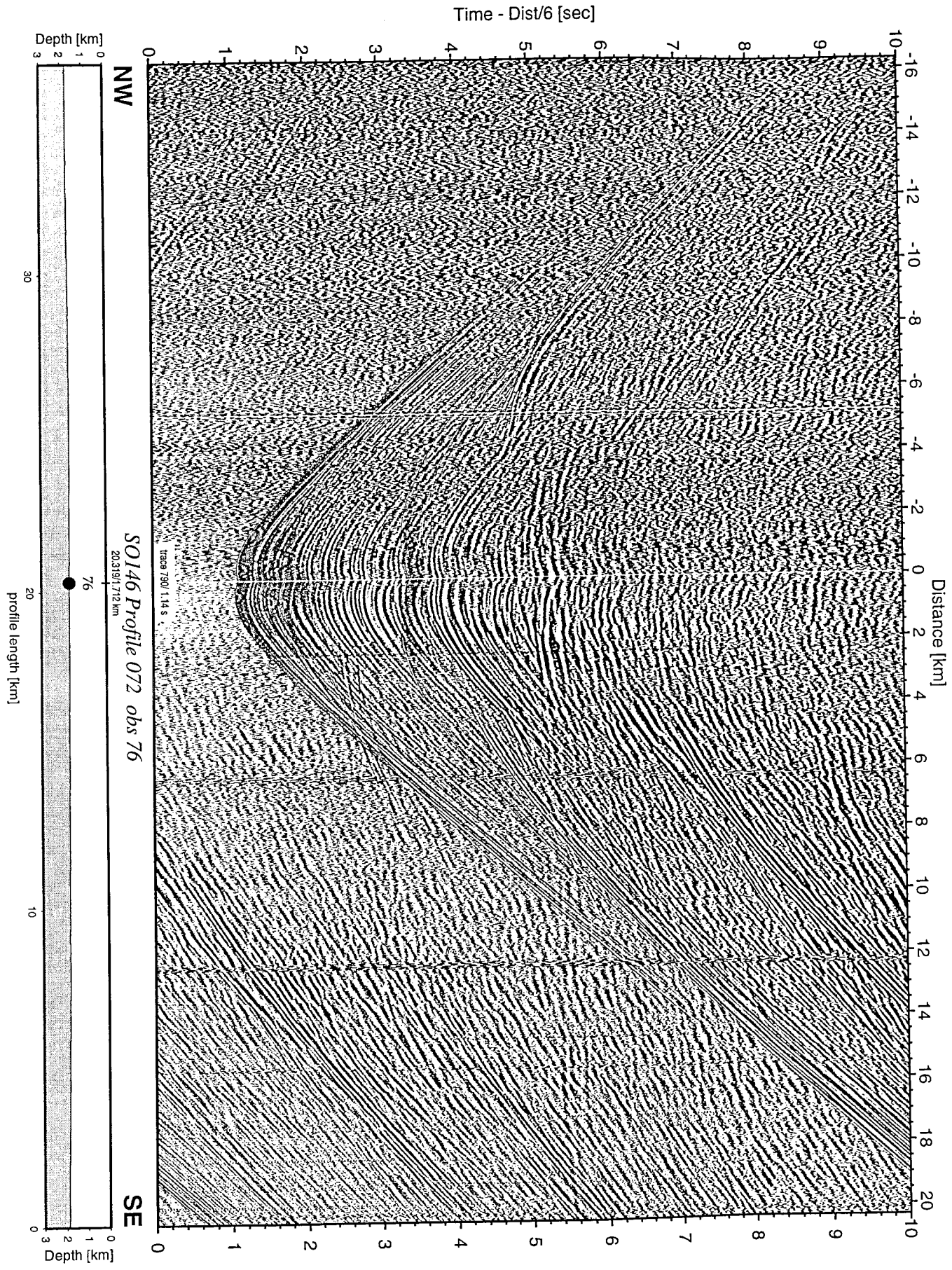

Figure 9.2.19: Record section from obs 76 horizontal component 2, Profile 072.

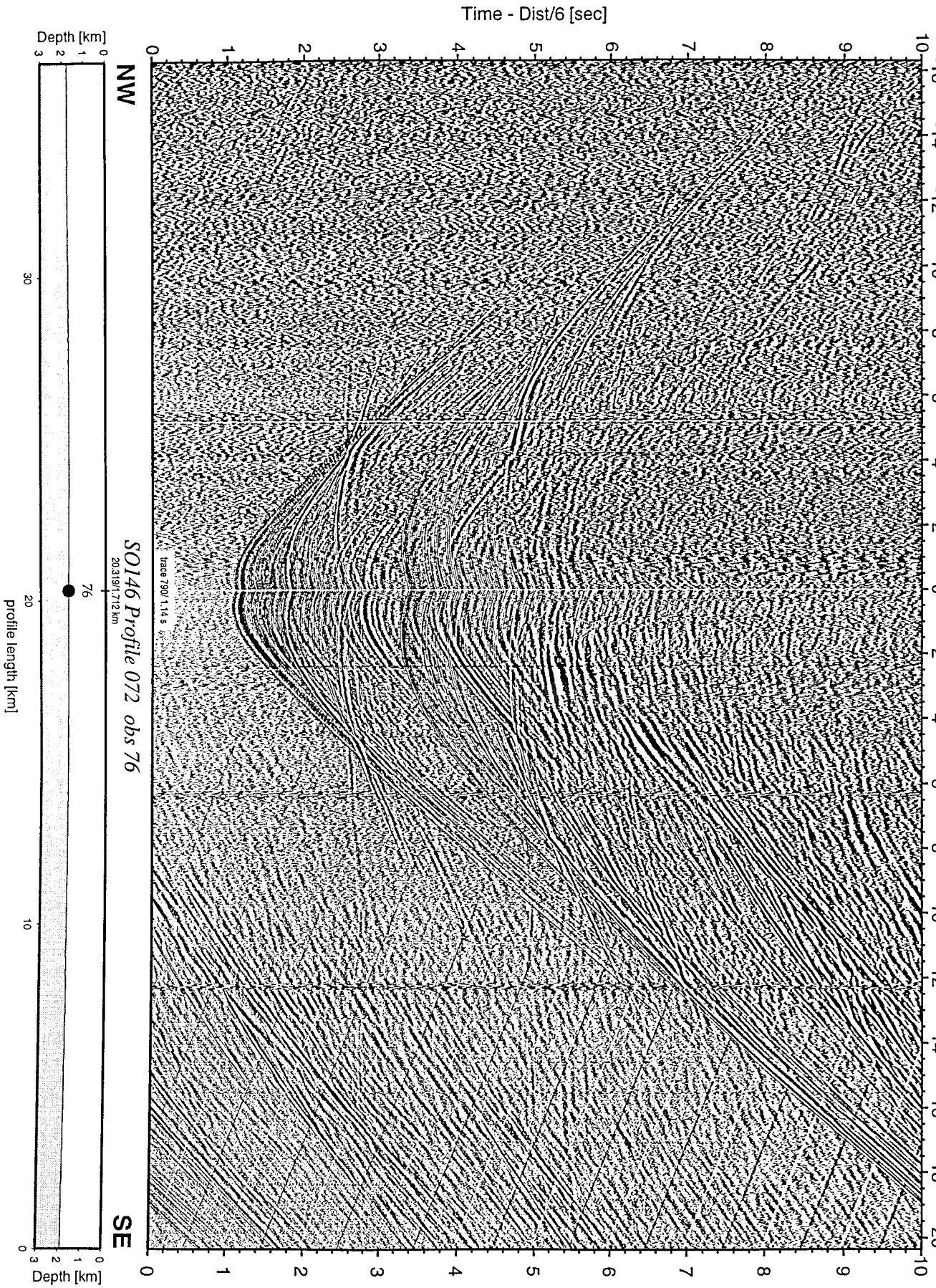

Figure 9.2.20: Record section from obs 76 vertical component, Profile 072.

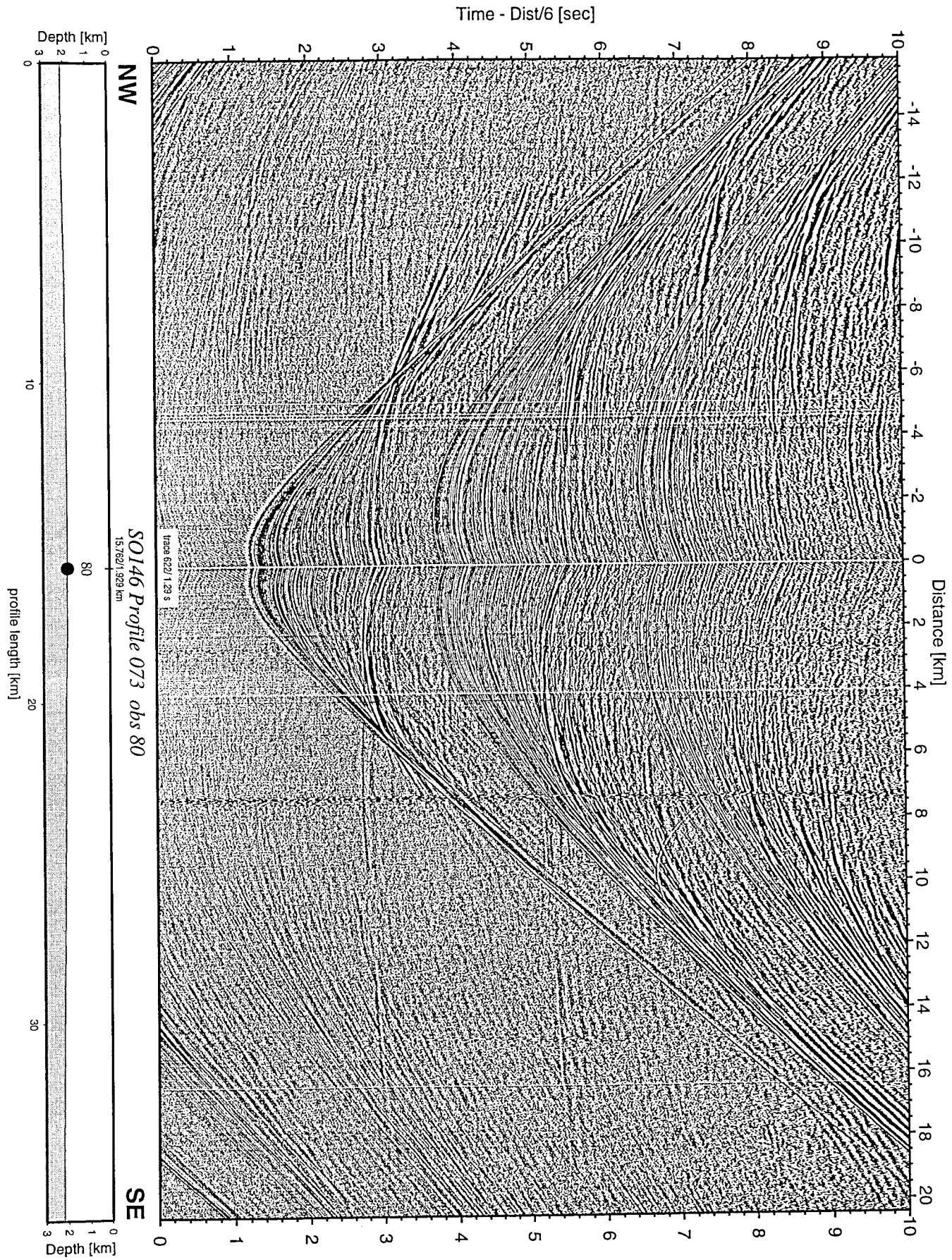

Figure 9.2.21: Record section from obs 80 hydrophone, Profile 073.

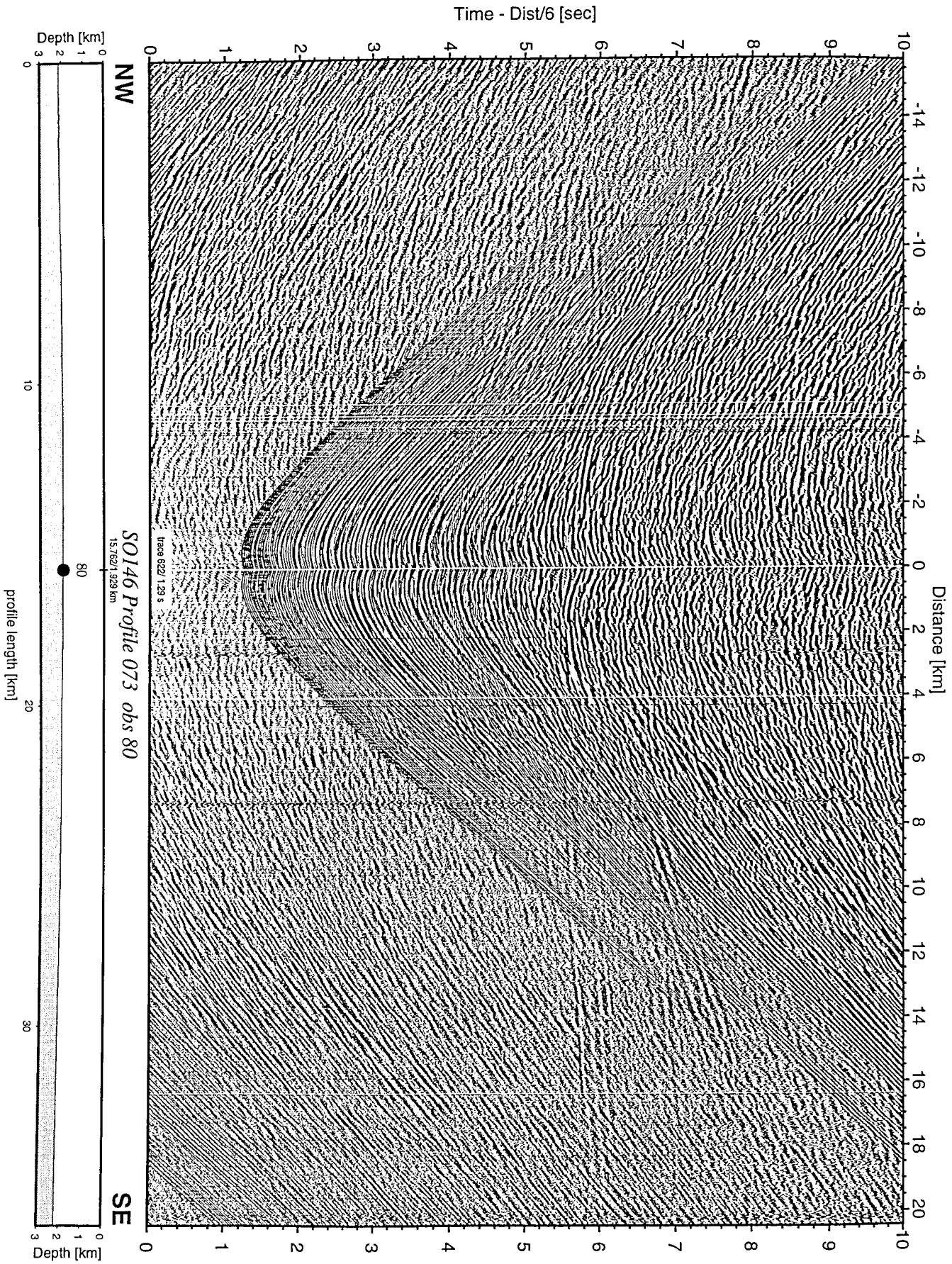

Figure 9.2.22: Record section from obs 80 horizontal component 1, Profile 073.

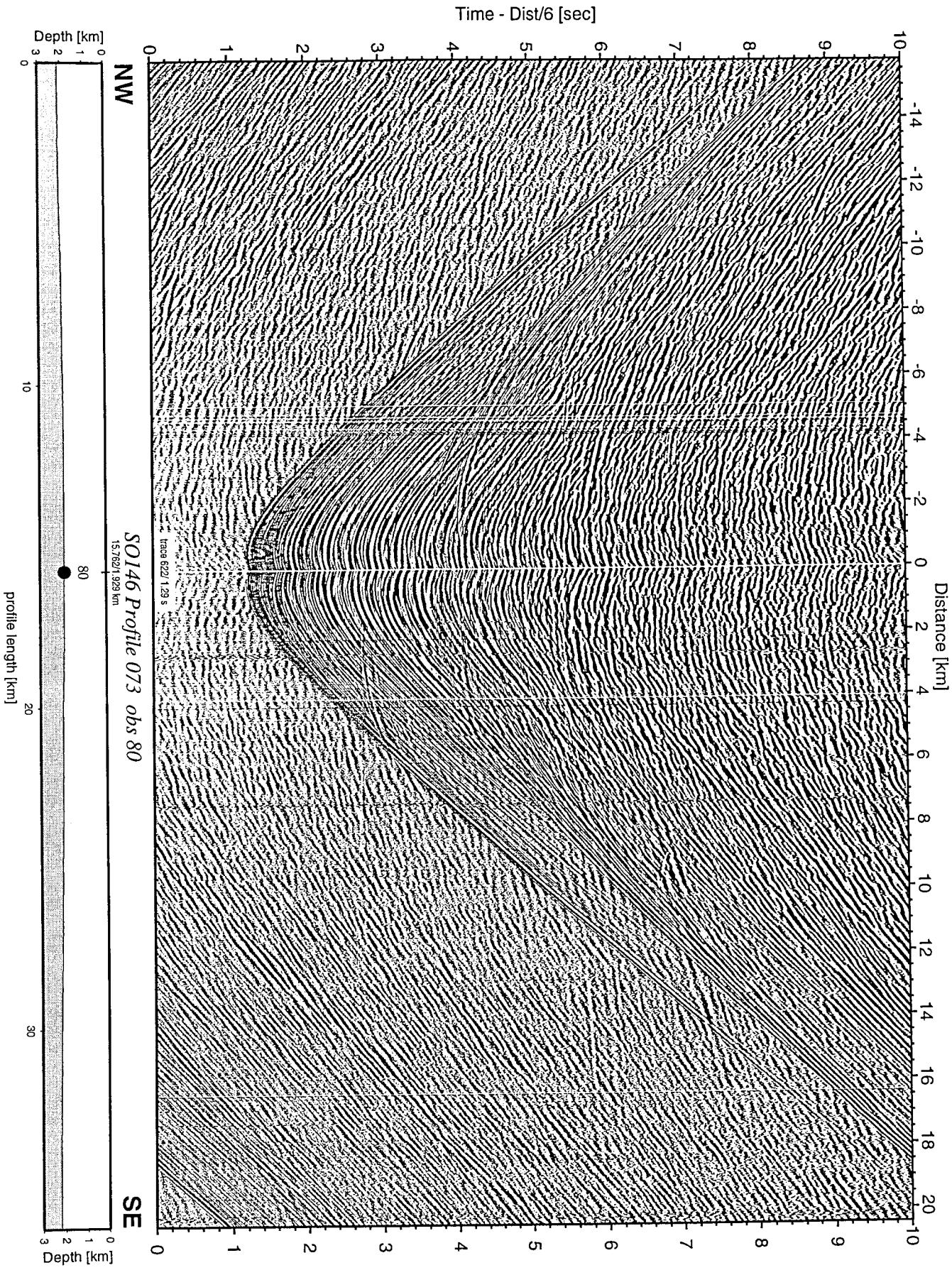

Figure 9.2.23: Record section from obs 80 horizontal component 2, Profile 073.

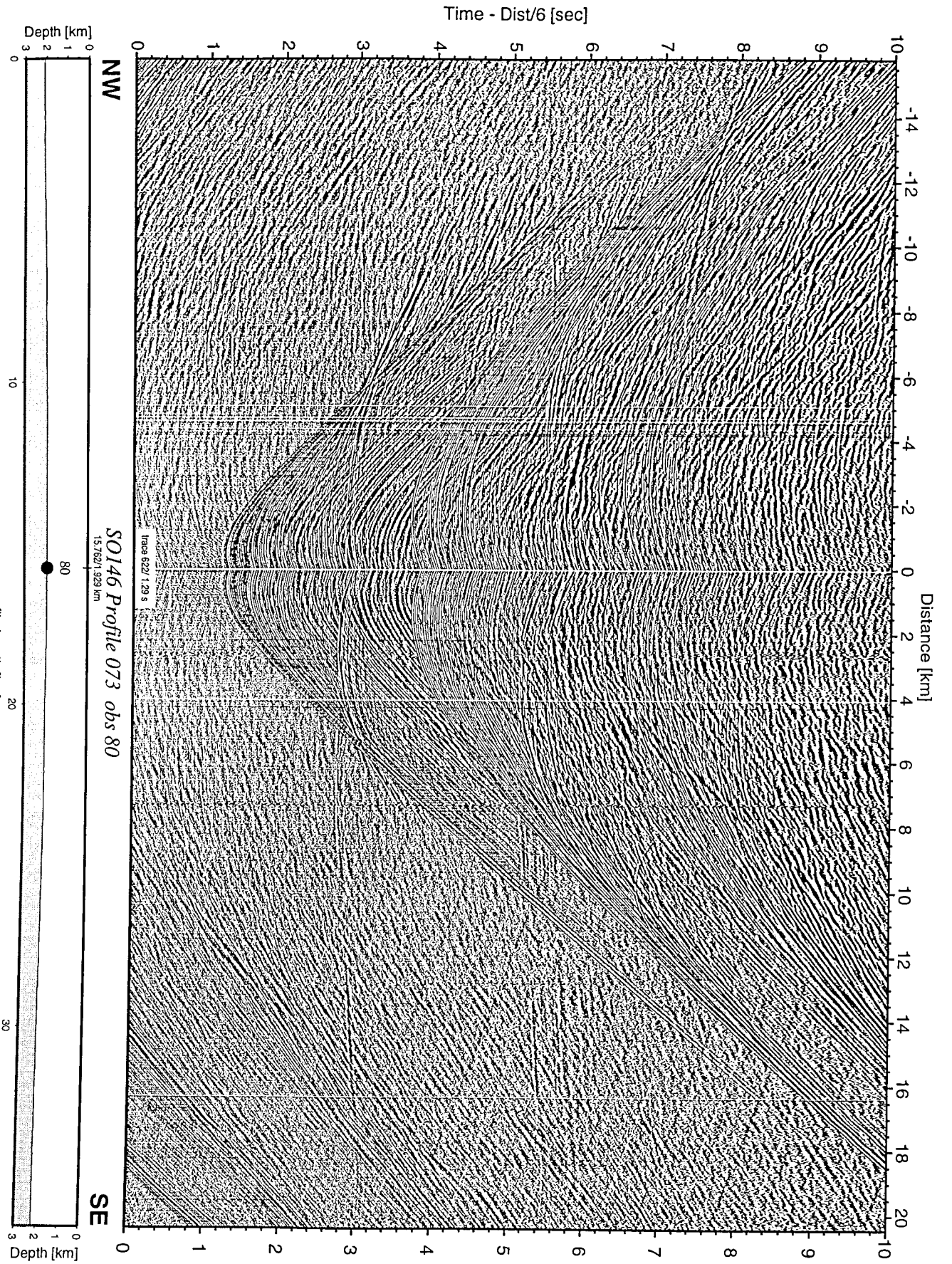

Figure 9.2.24: Record section from obs 80 vertical component, Profile 073.

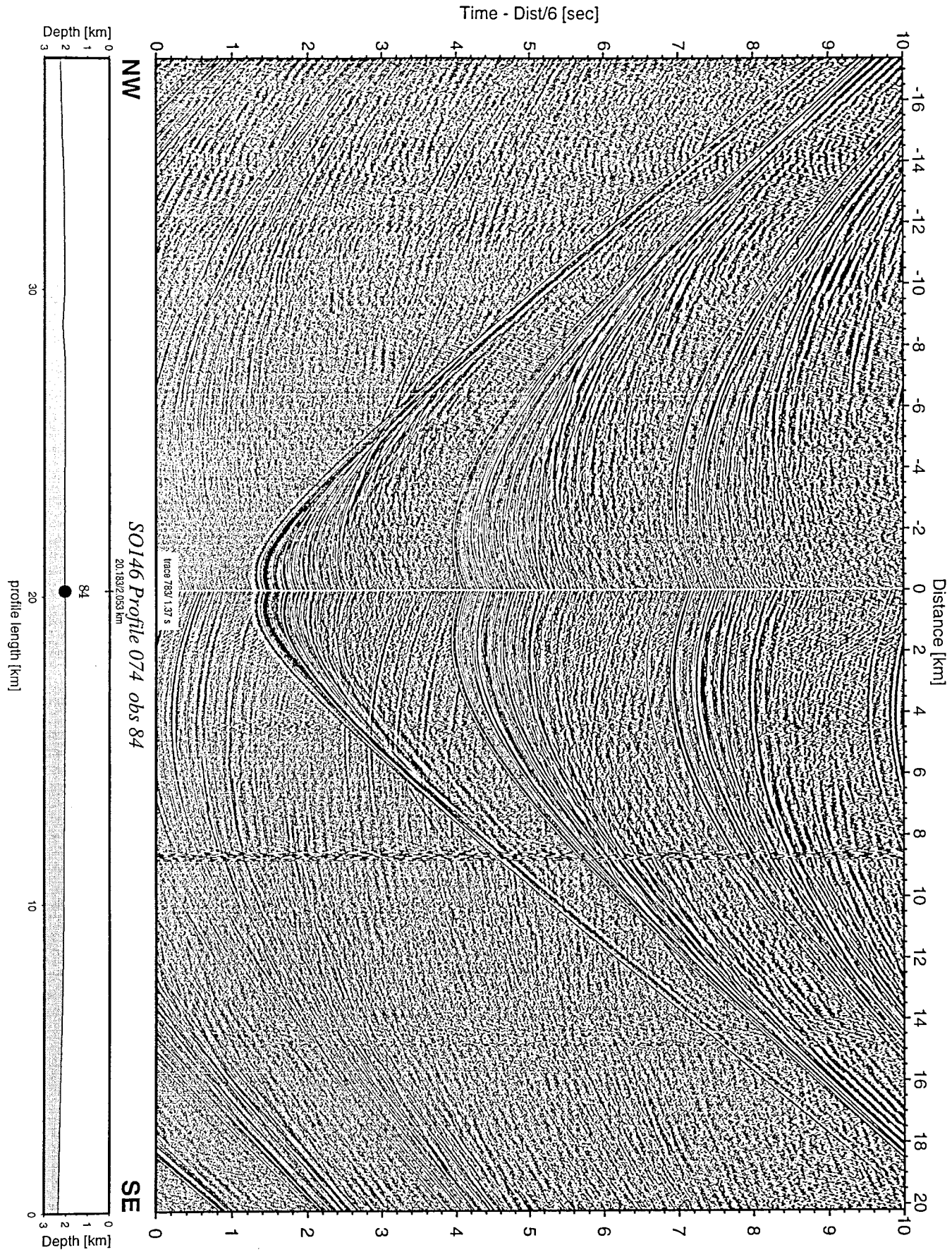

Figure 9.2.25: Record section from obs 84 hydrophone, Profile 074.

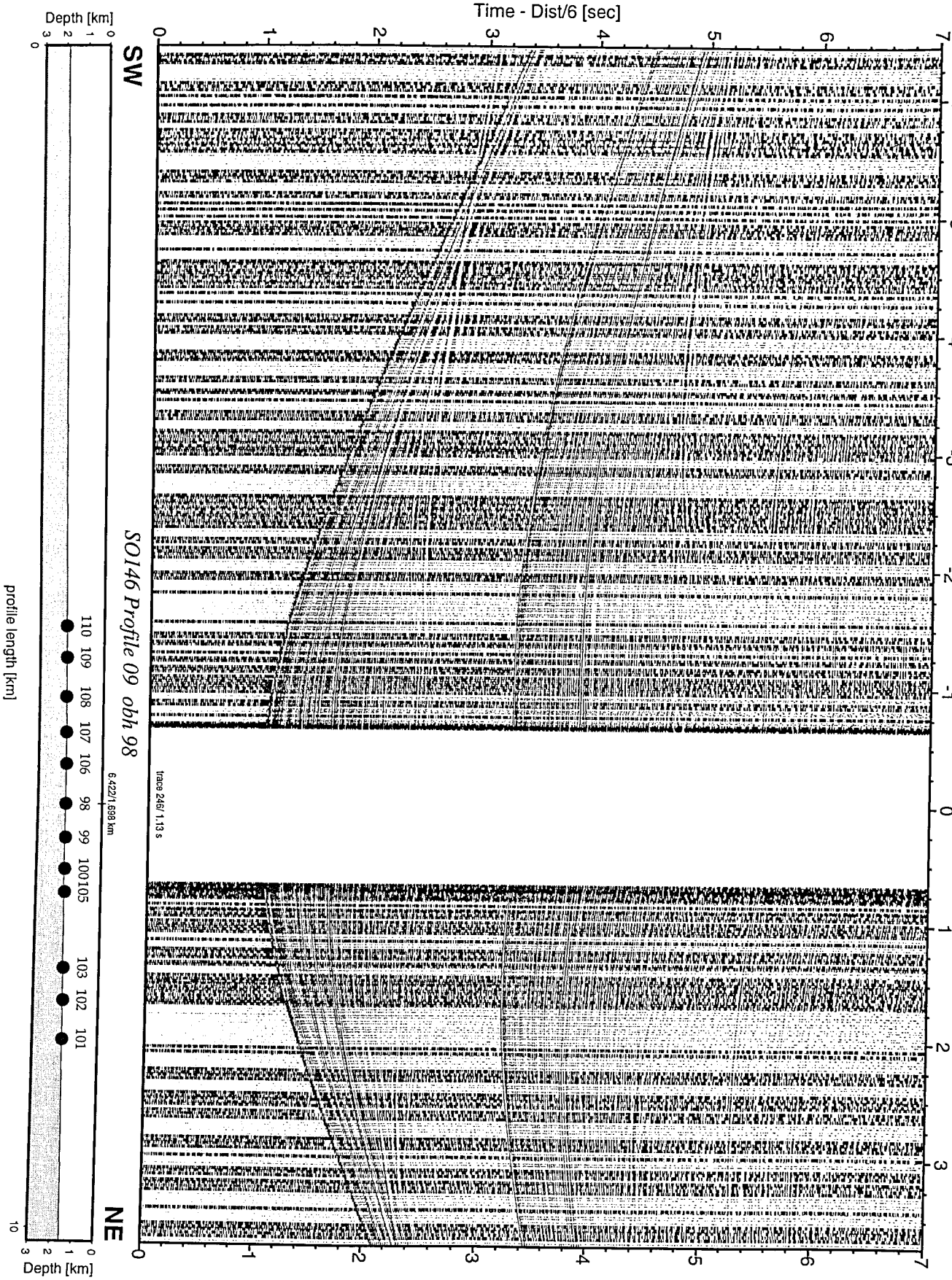

Figure 9.2.26: Record section from obh 98 , Profile 09.

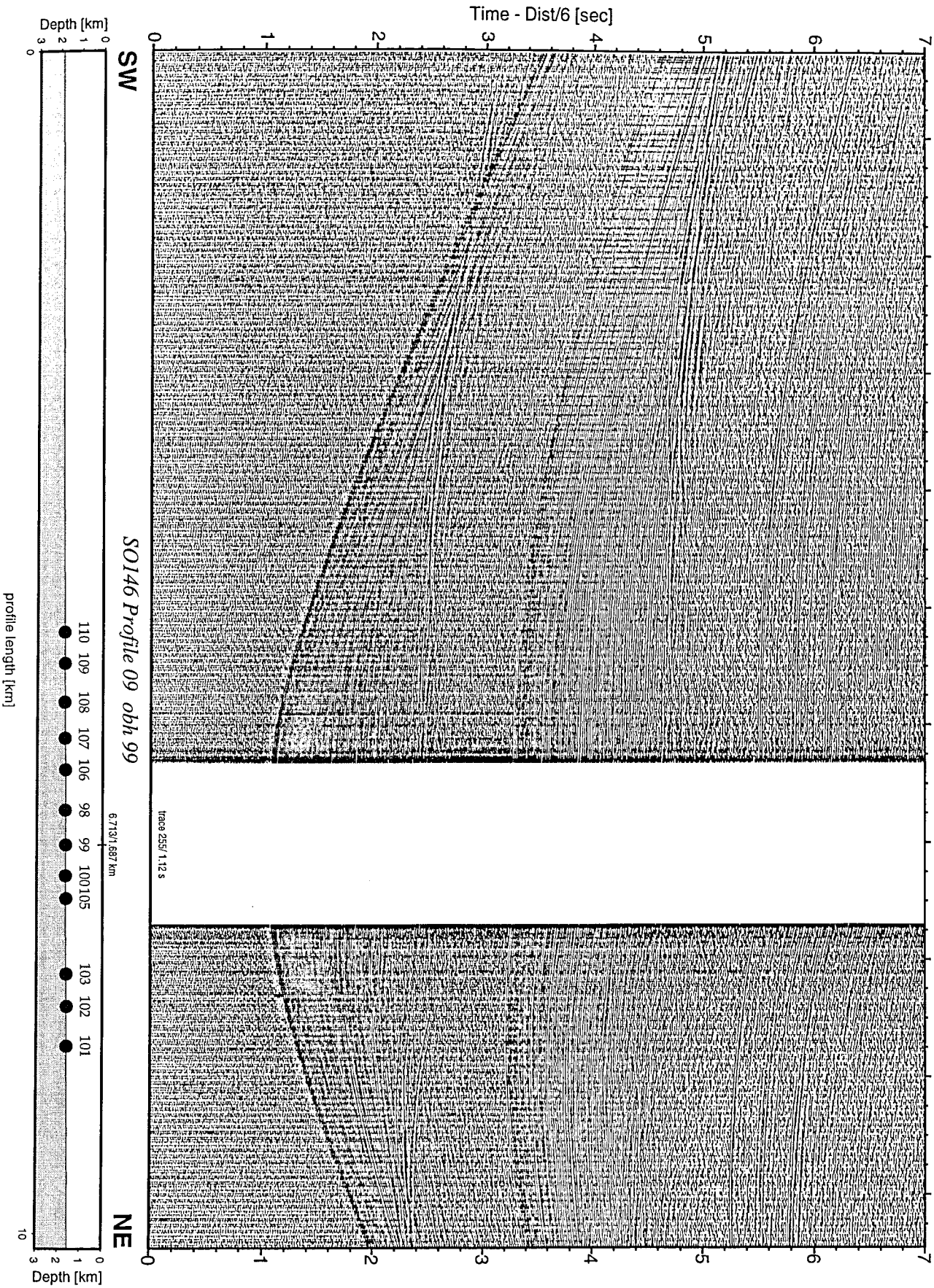

Figure 9.2.27: Record section from obh 99 , Profile 09.

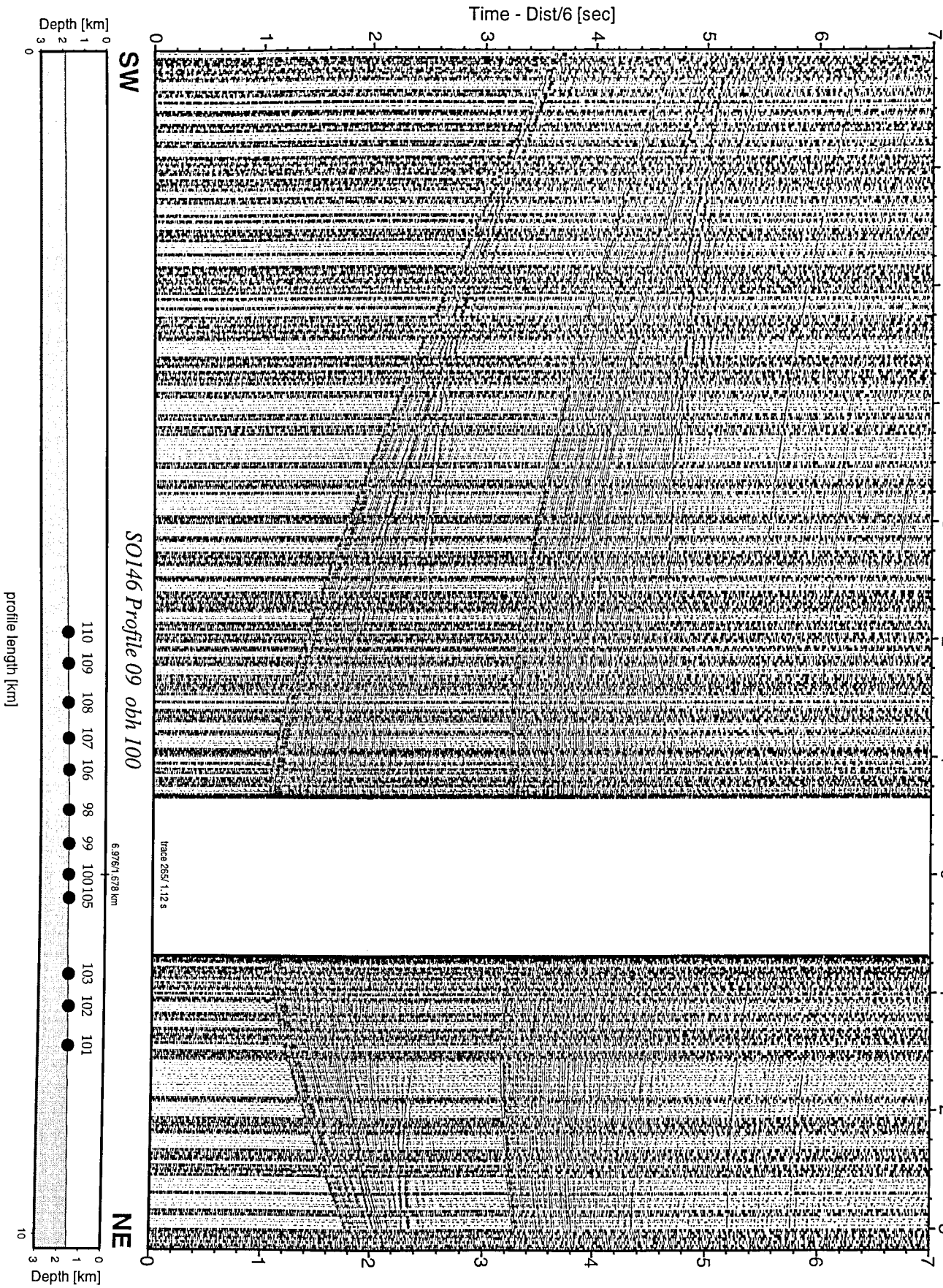

Figure 9.2.28: Record section from obh 100 , Profile 09.

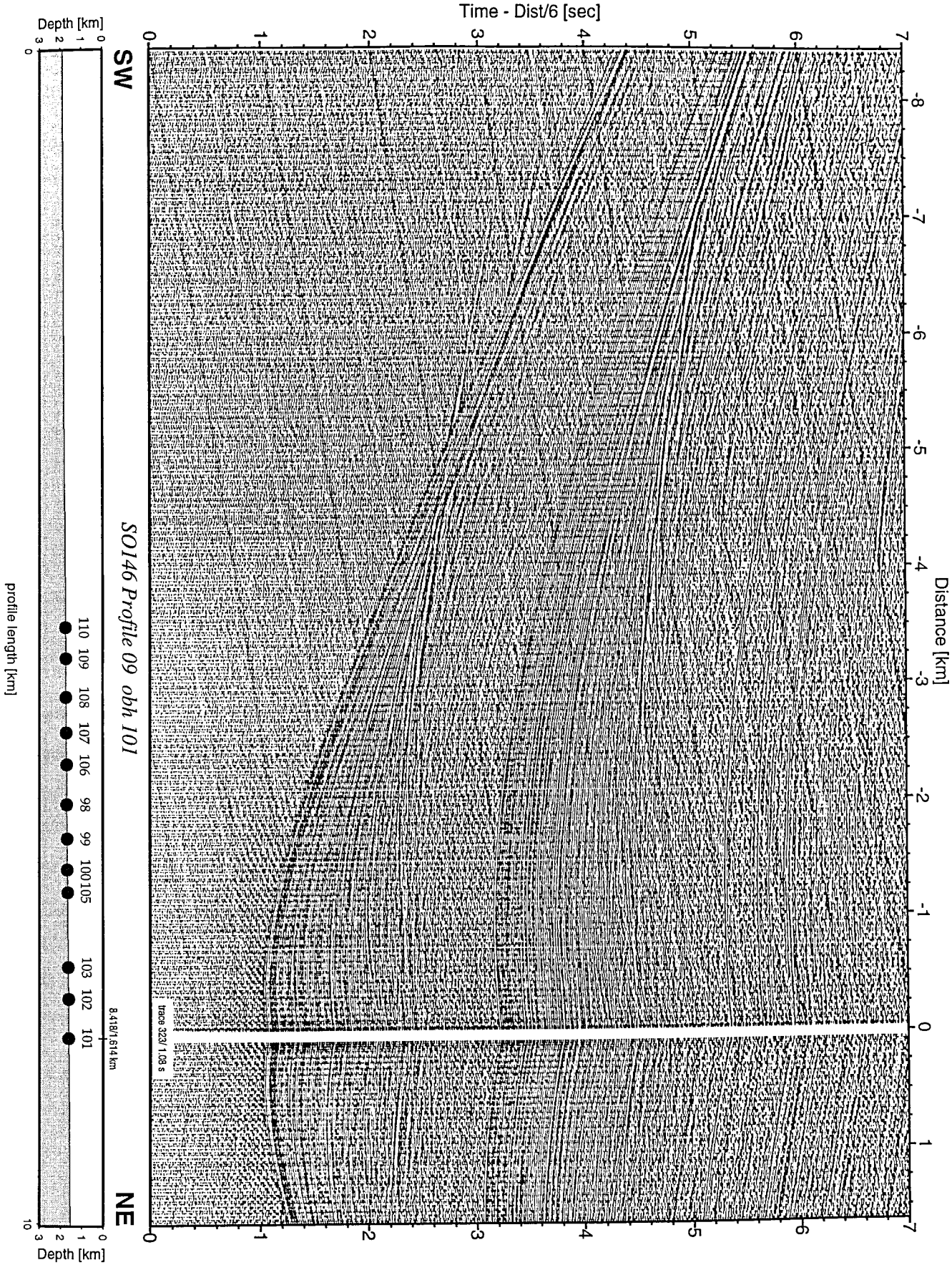

Figure 9.2.29: Record section from obh 101 , Profile 09.

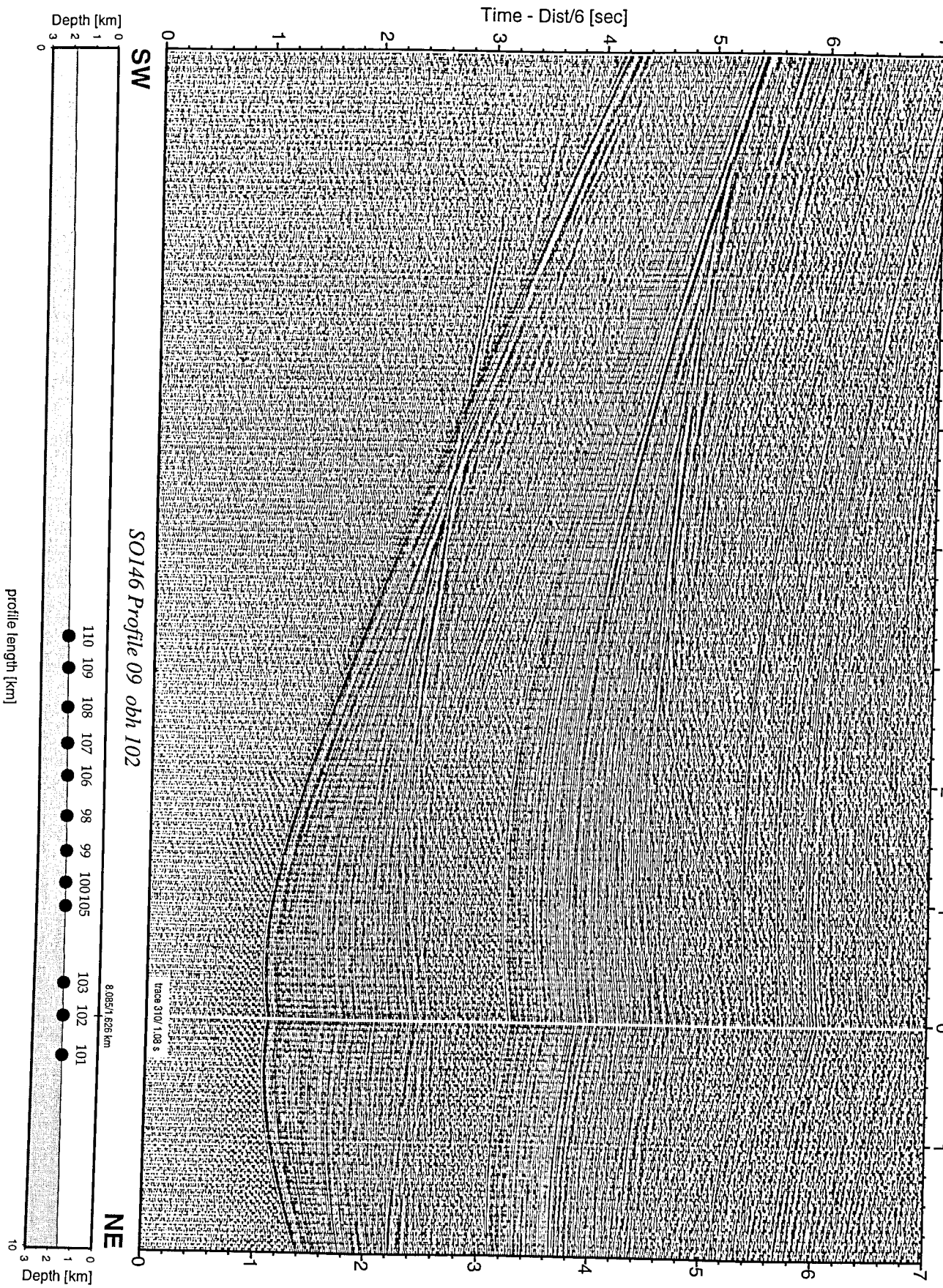

Figure 9.2.30: Record section from obh 102 , Profile 09.

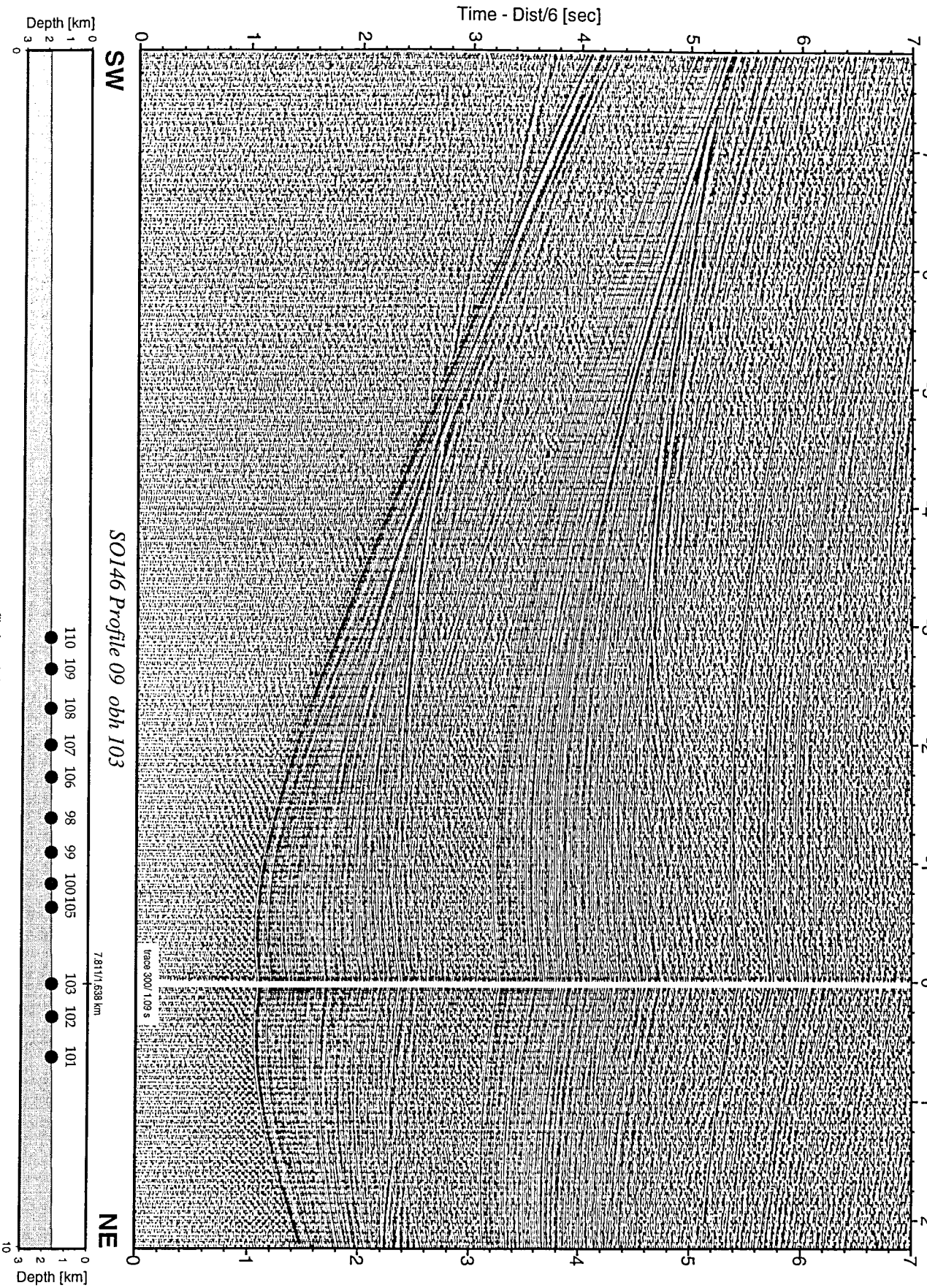

Figure 9.2.31: Record section from obh 103 , Profile 09.

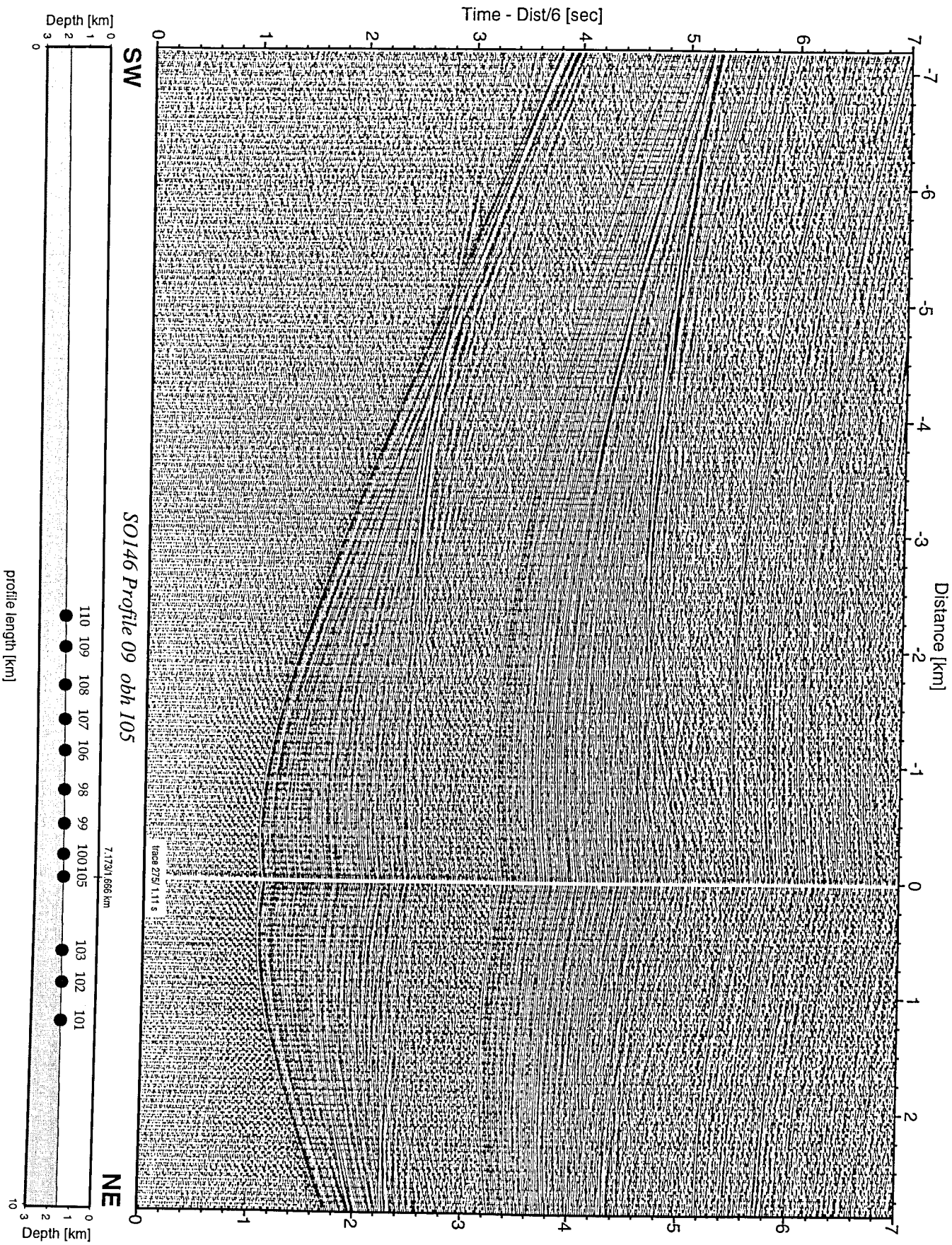

Figure 9.2.32: Record section from obh 105 , Profile 09.

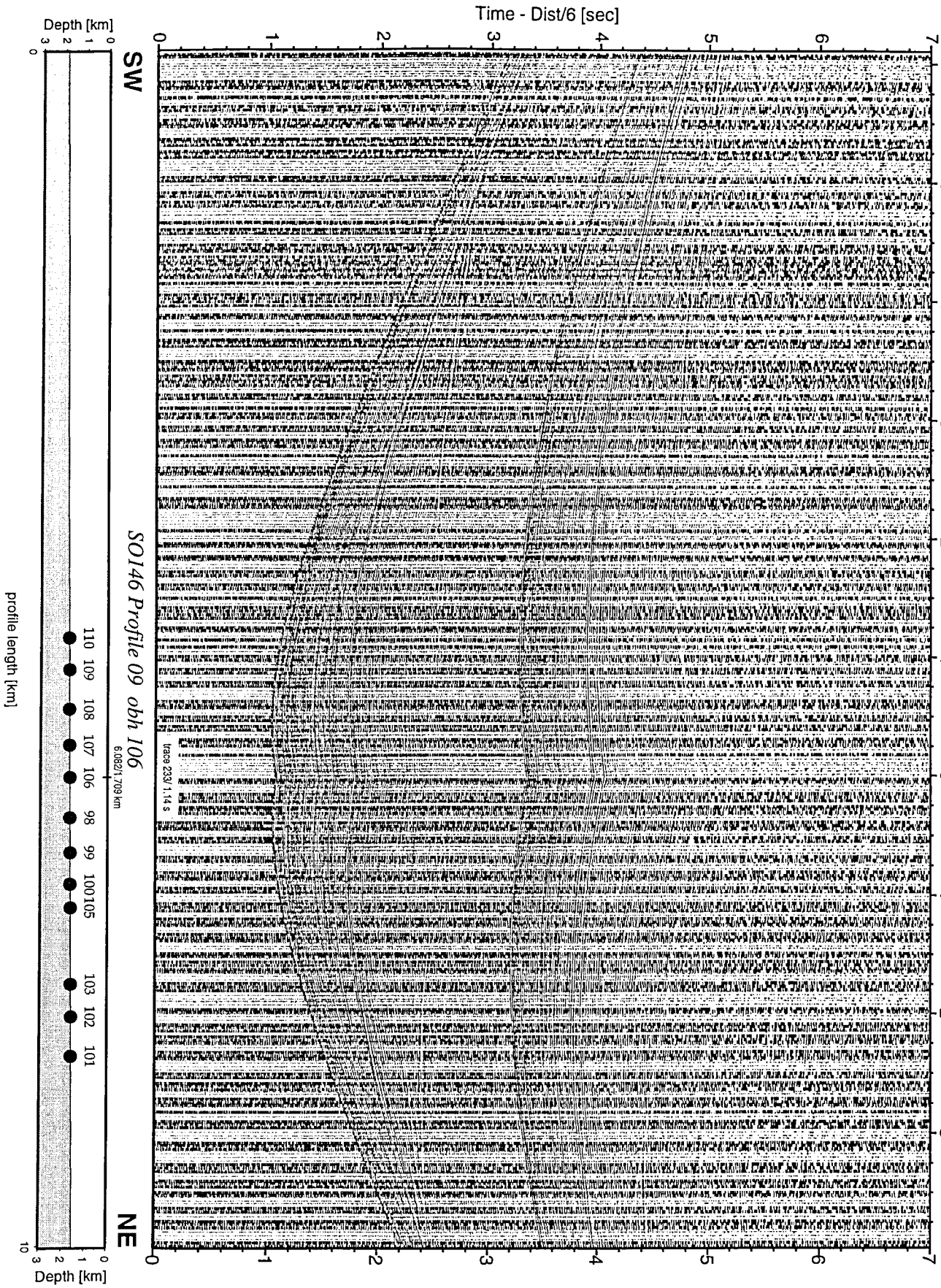

Figure 9.2.33: Record section from obh 106 , Profile 09.

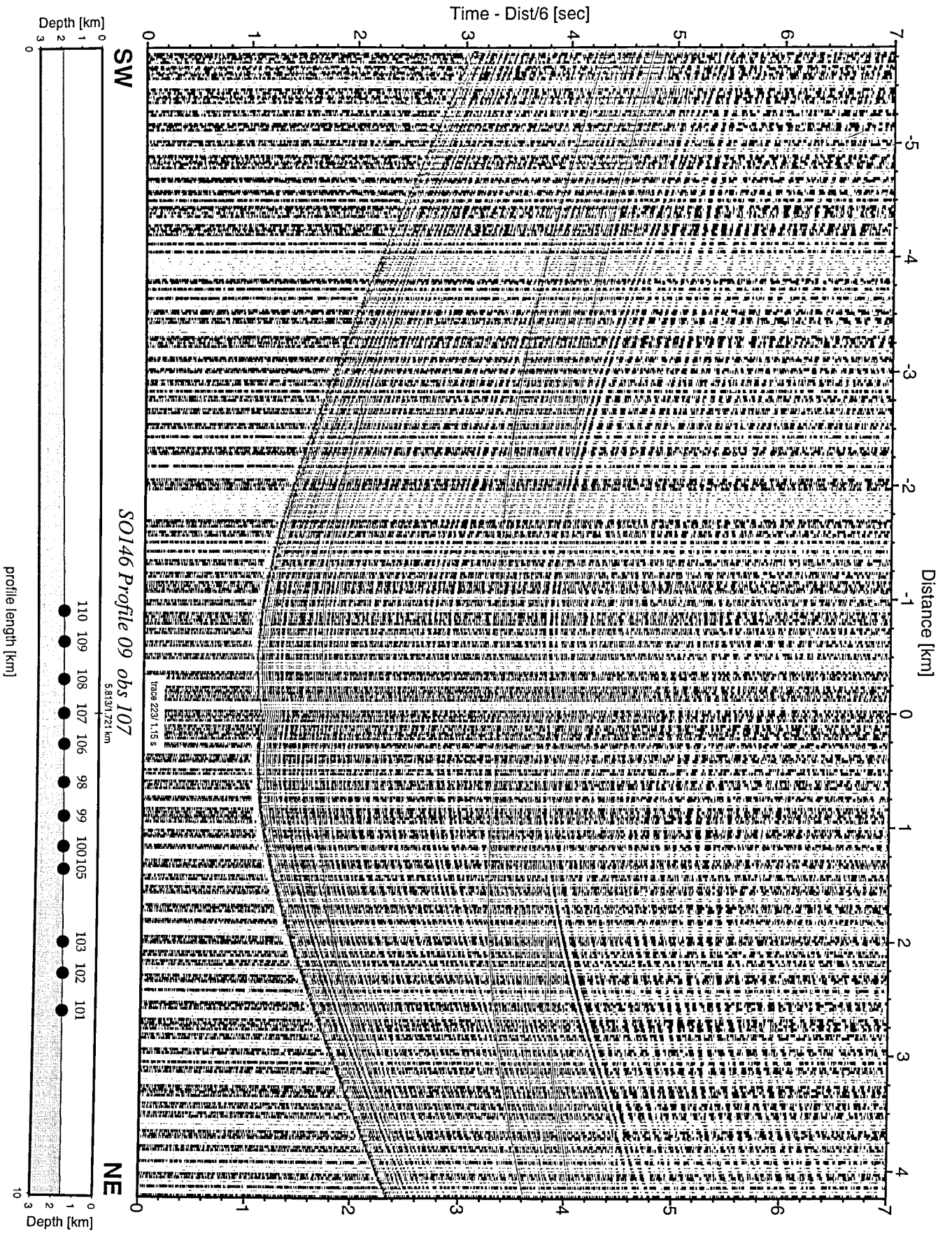

Figure 9.2.34: Record section from obs 107 horizontal component 1, Profile 09.

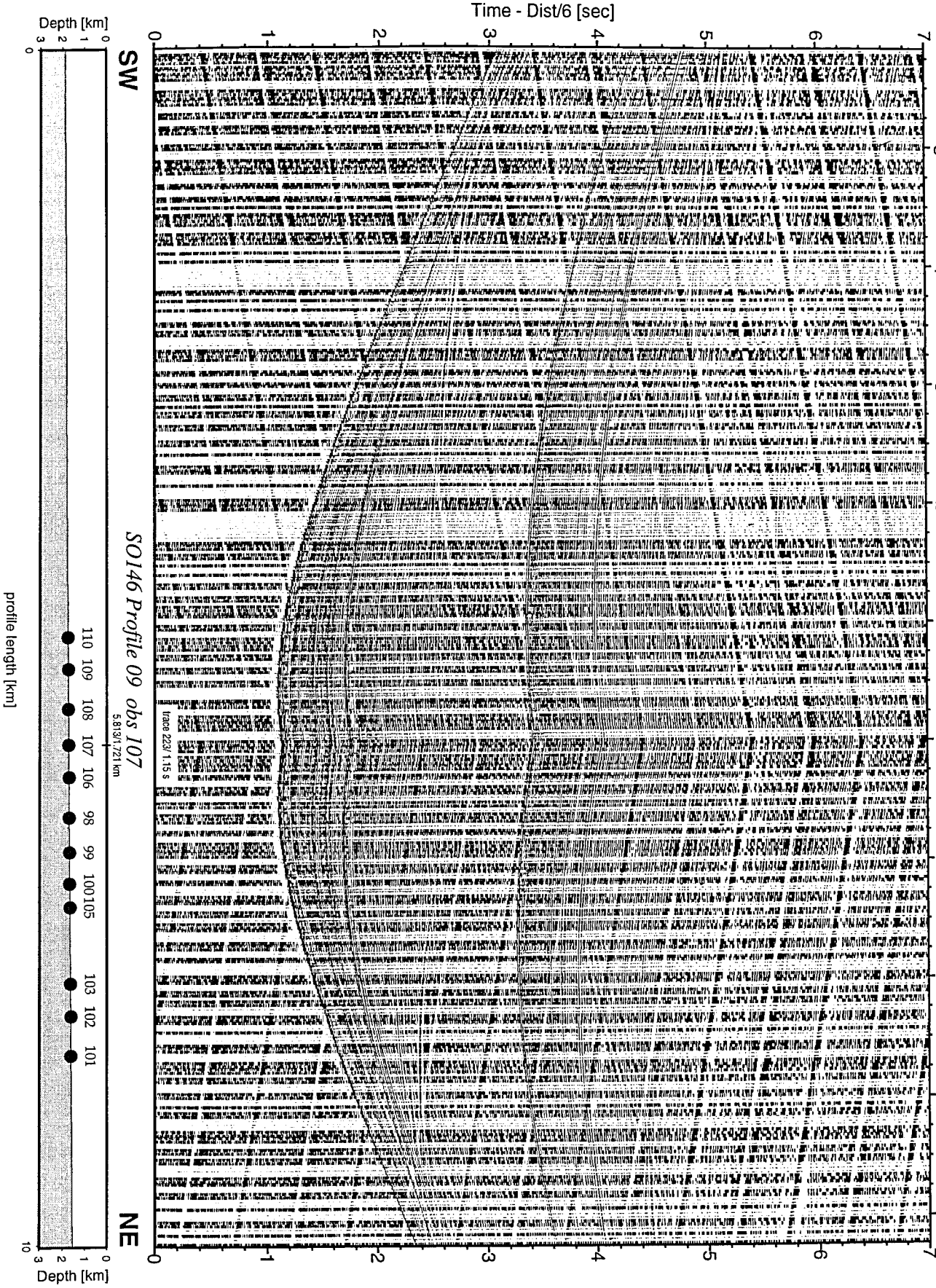

Figure 9.2.35: Record section from obs 107 vertical component, Profile 09.

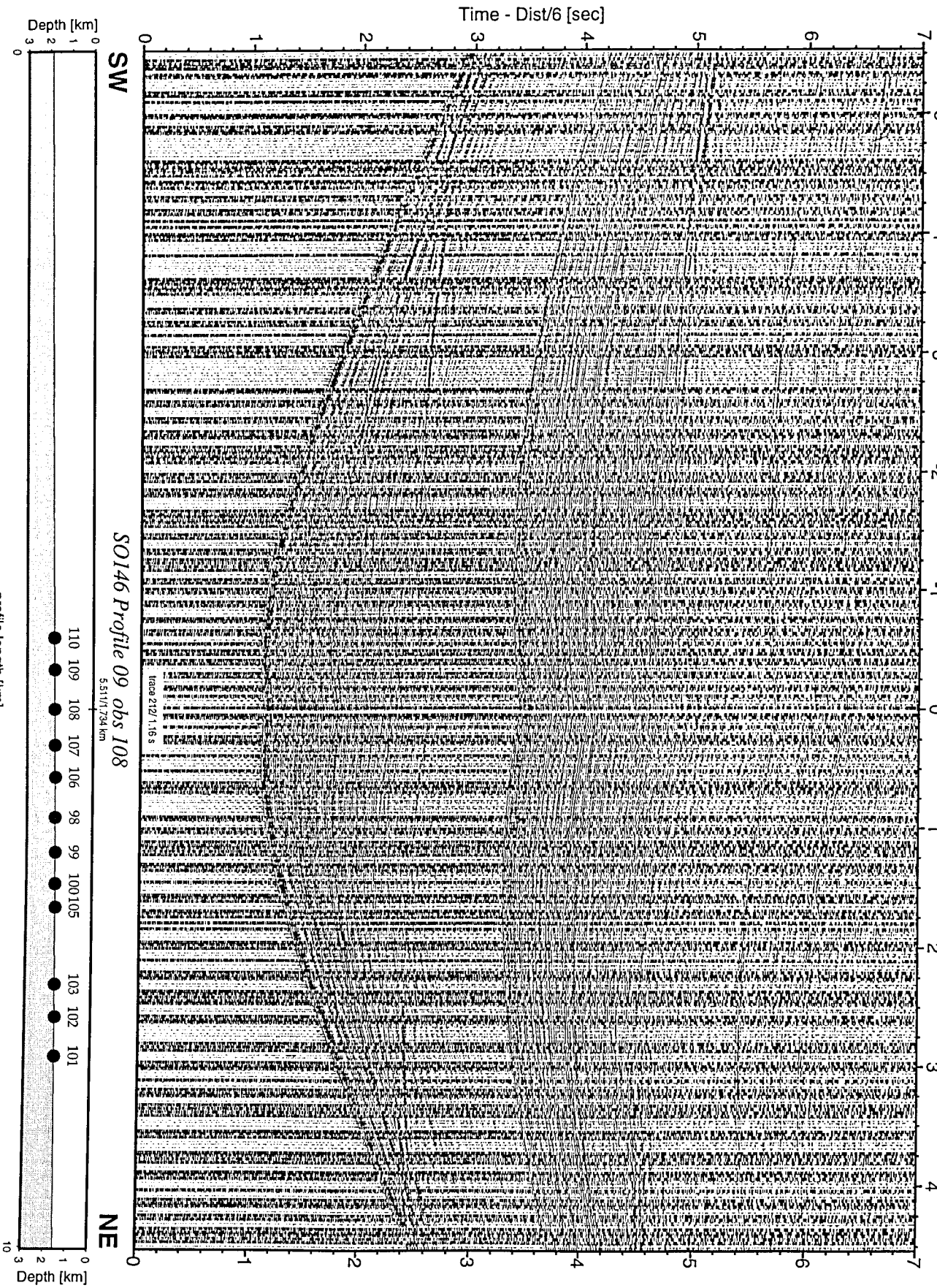

Figure 9.2.36: Record section from obs 108 hydrophone, Profile 09.

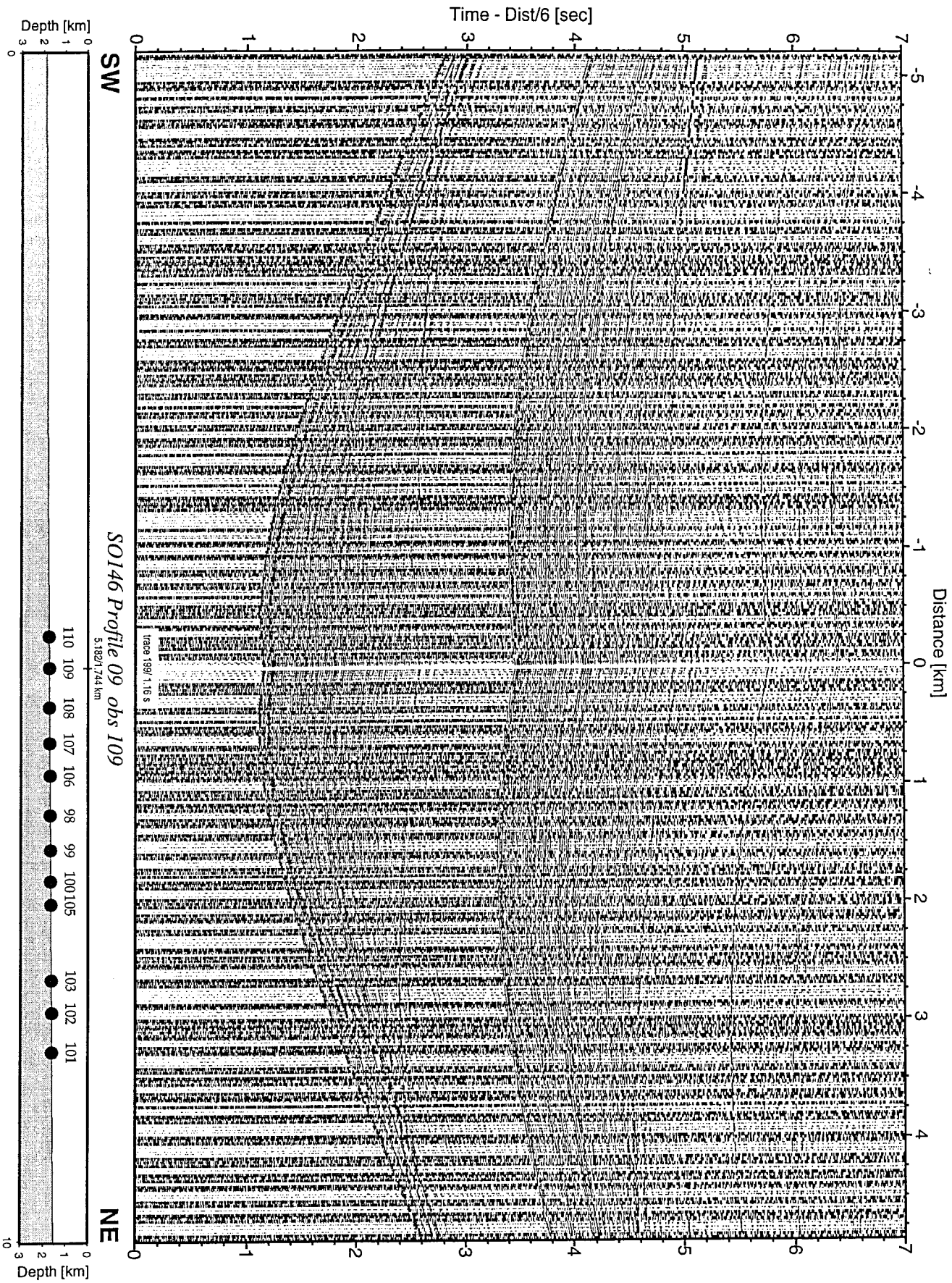

Figure 9.2.37: Record section from obs 109 hydrophone, Profile 09.

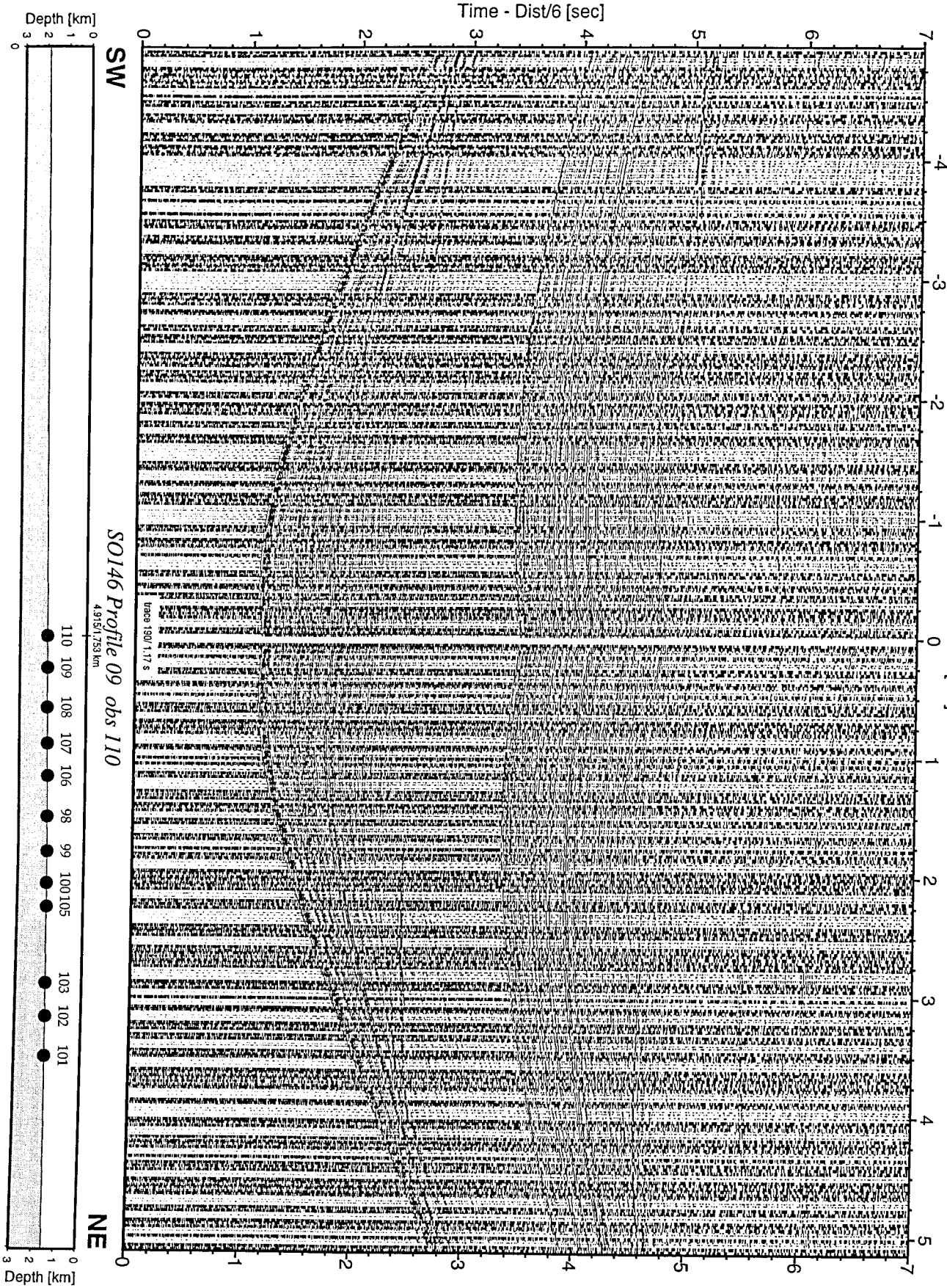

Figure 9.2.38: Record section from obs 110 hydrophone, Profile 09.

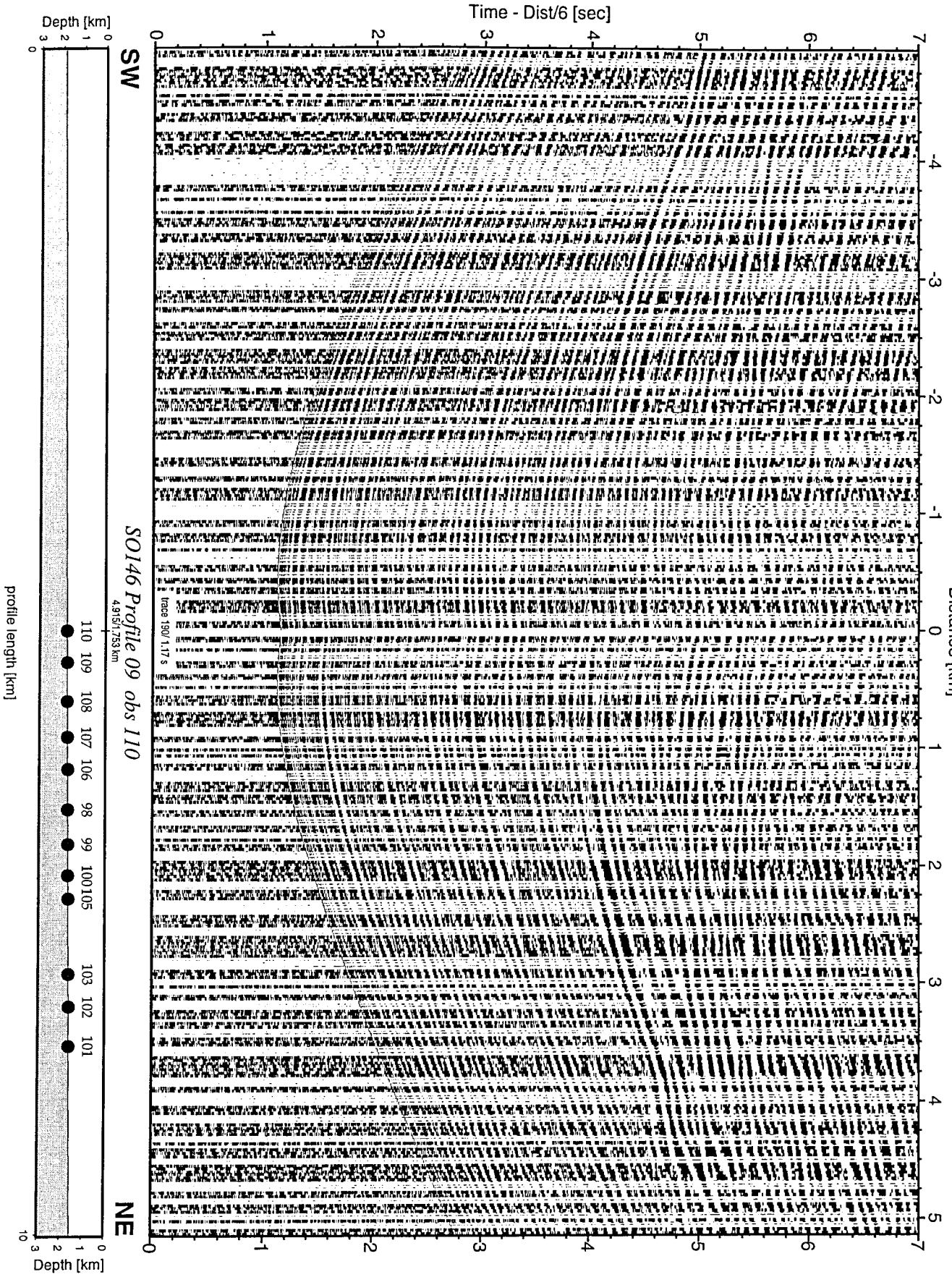

Figure 9.2.39: Record section from obs 110 horizontal component 1, Profile 09.

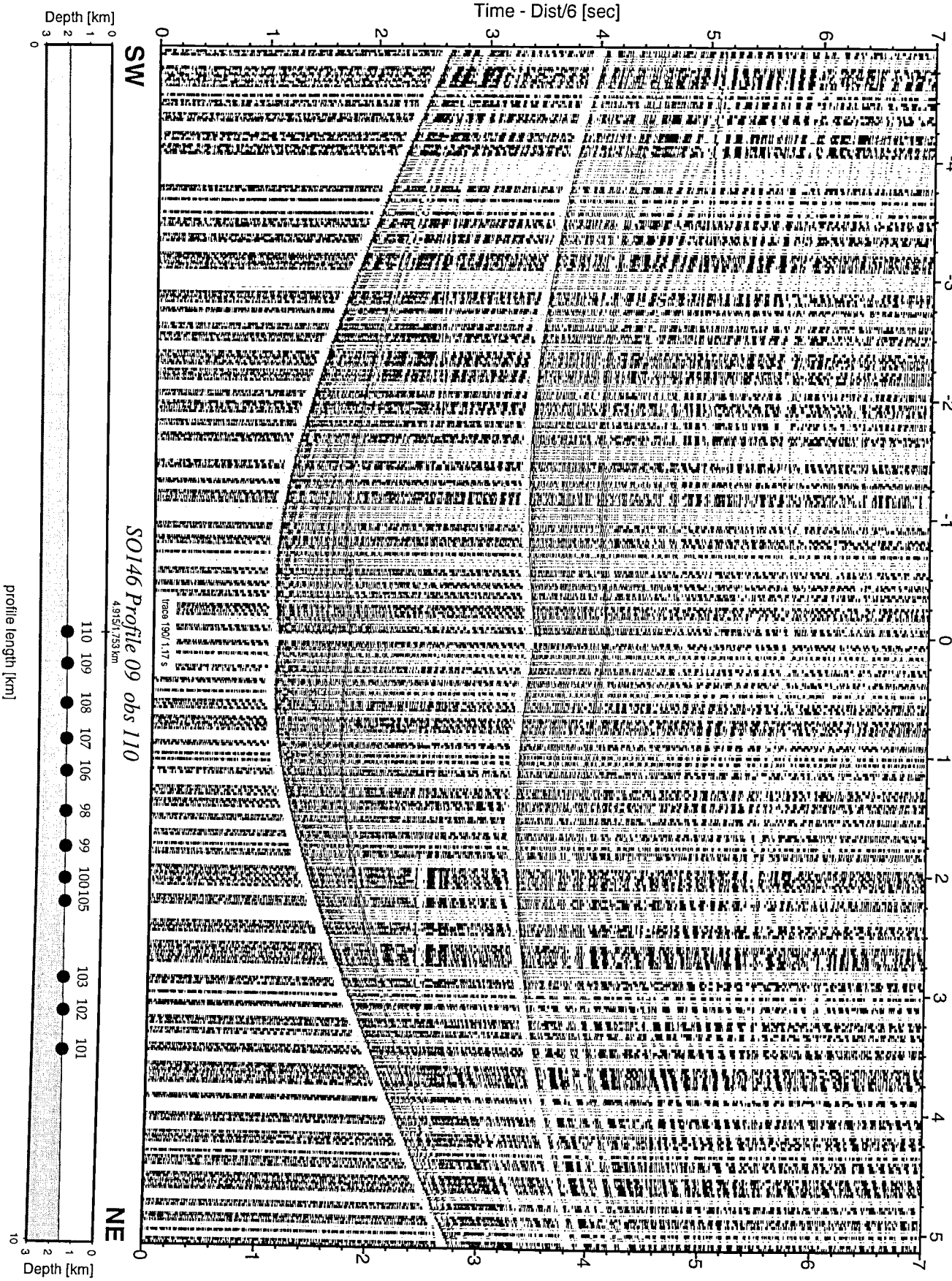

Figure 9.2.40: Record section from obs 110 vertical component, Profile 09.

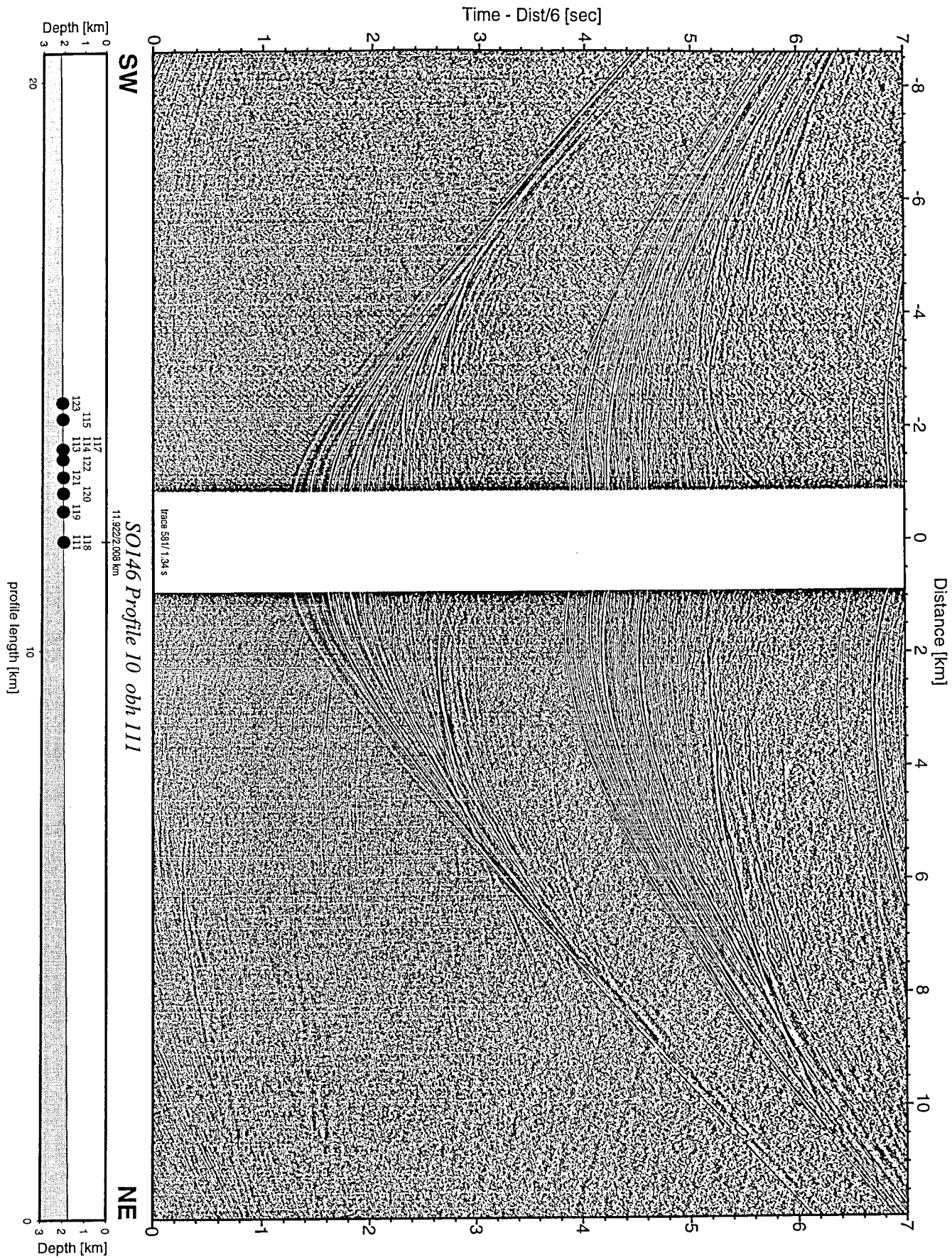

Figure 9.2.41: Record section from obh 111 , Profile 10.

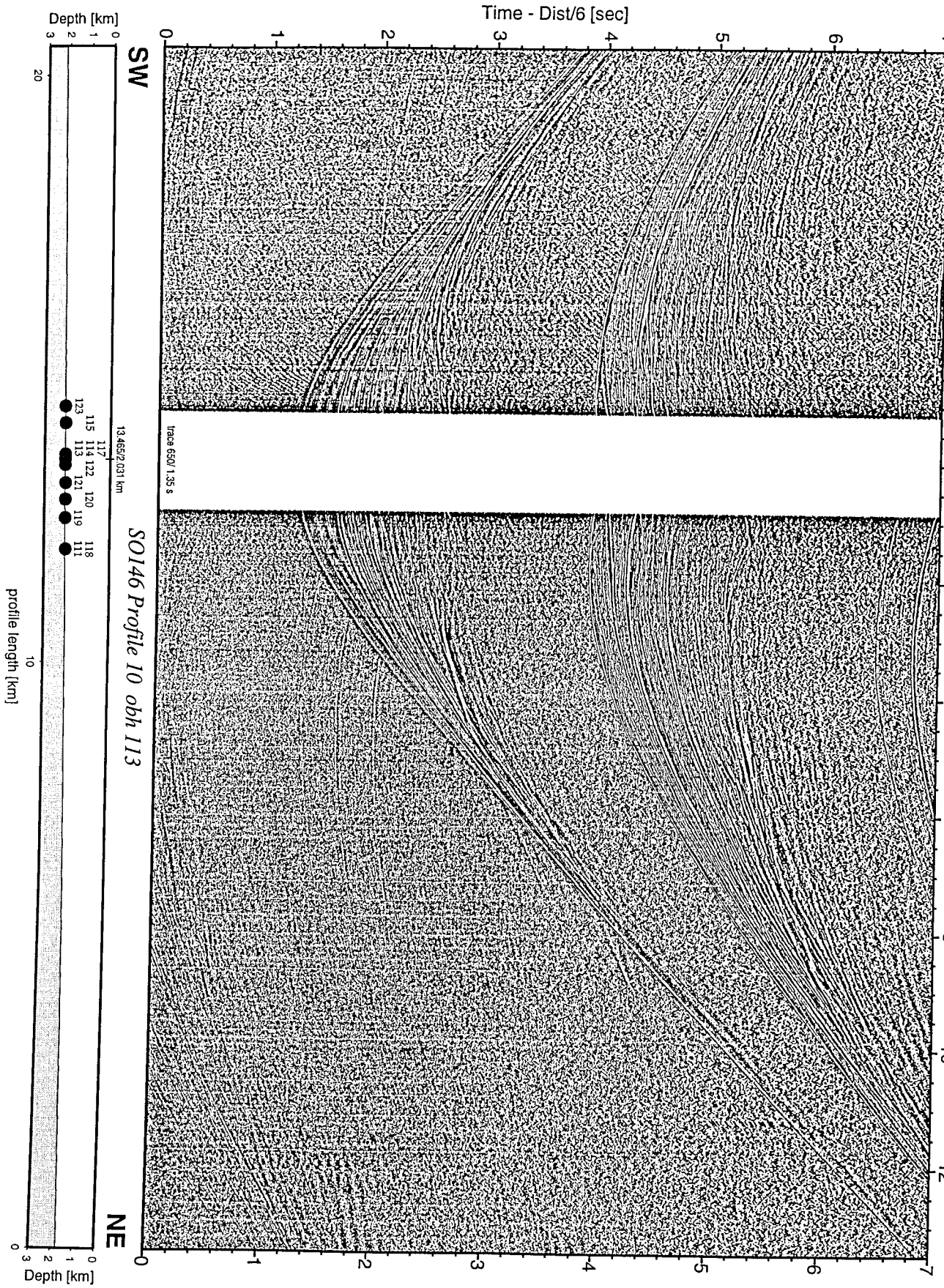

Figure 9.2.42: Record section from obh 113 , Profile 10.

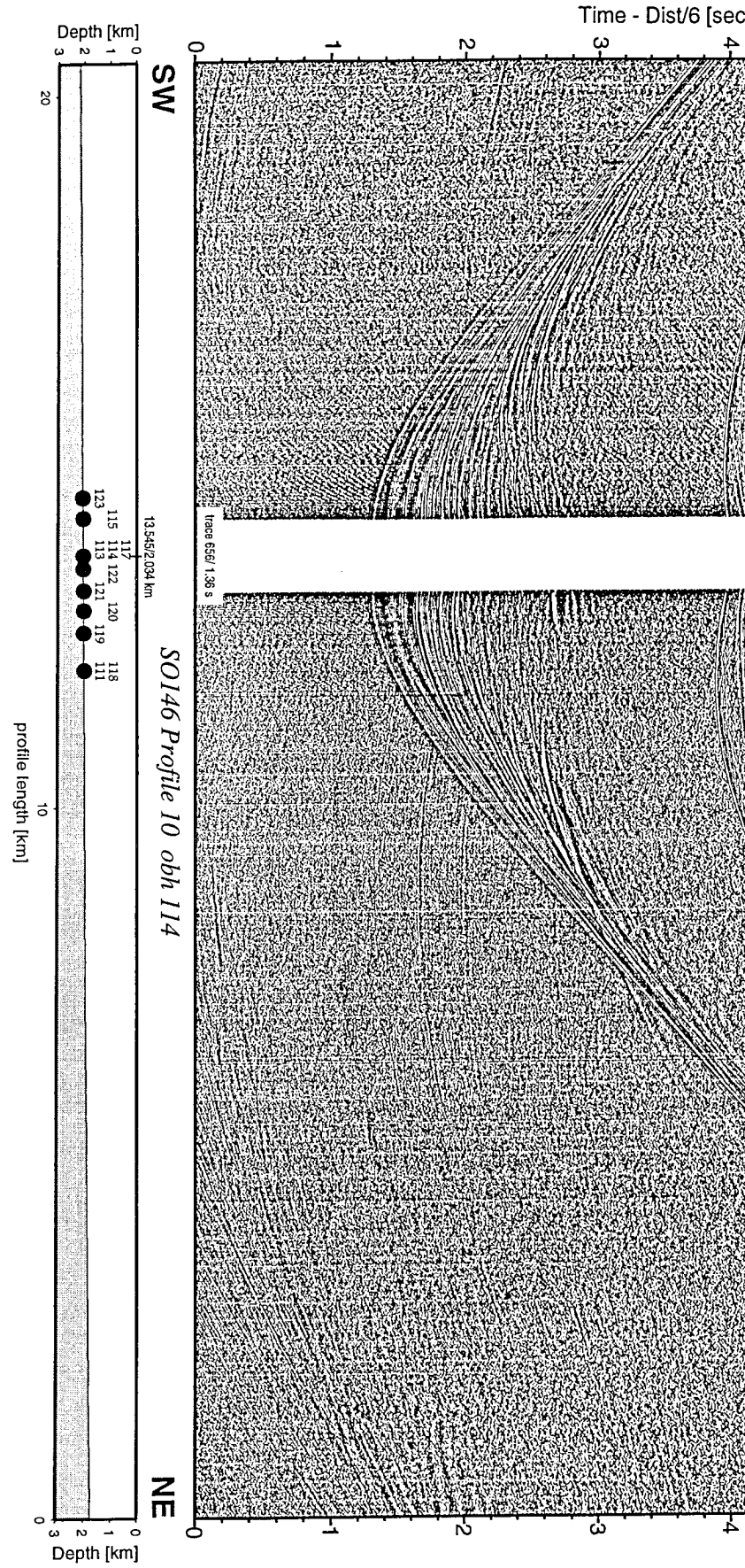

Figure 9.2.43: Record section from obh 114 ,

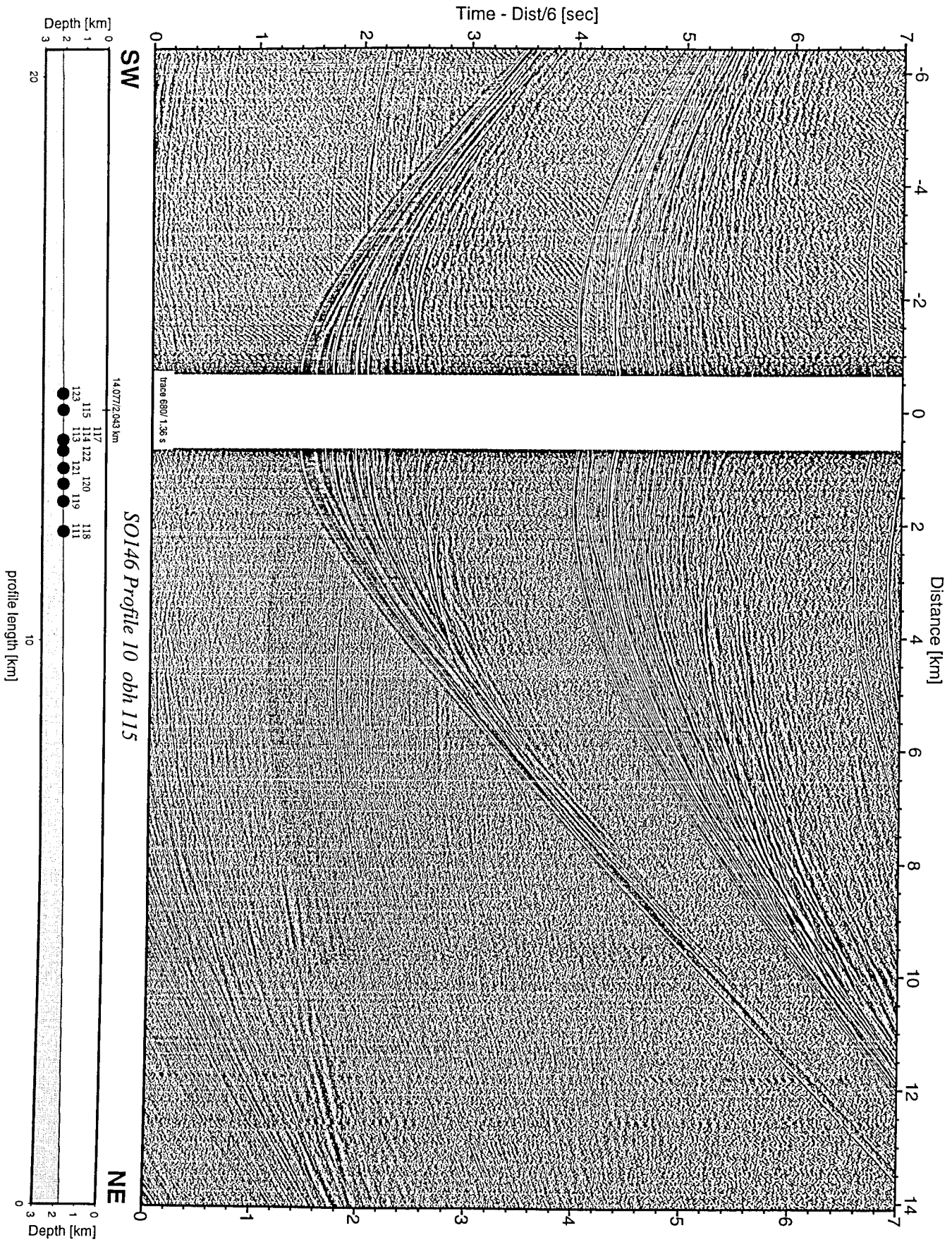

Figure 9.2.44: Record section from obh 115 , Profile 10.

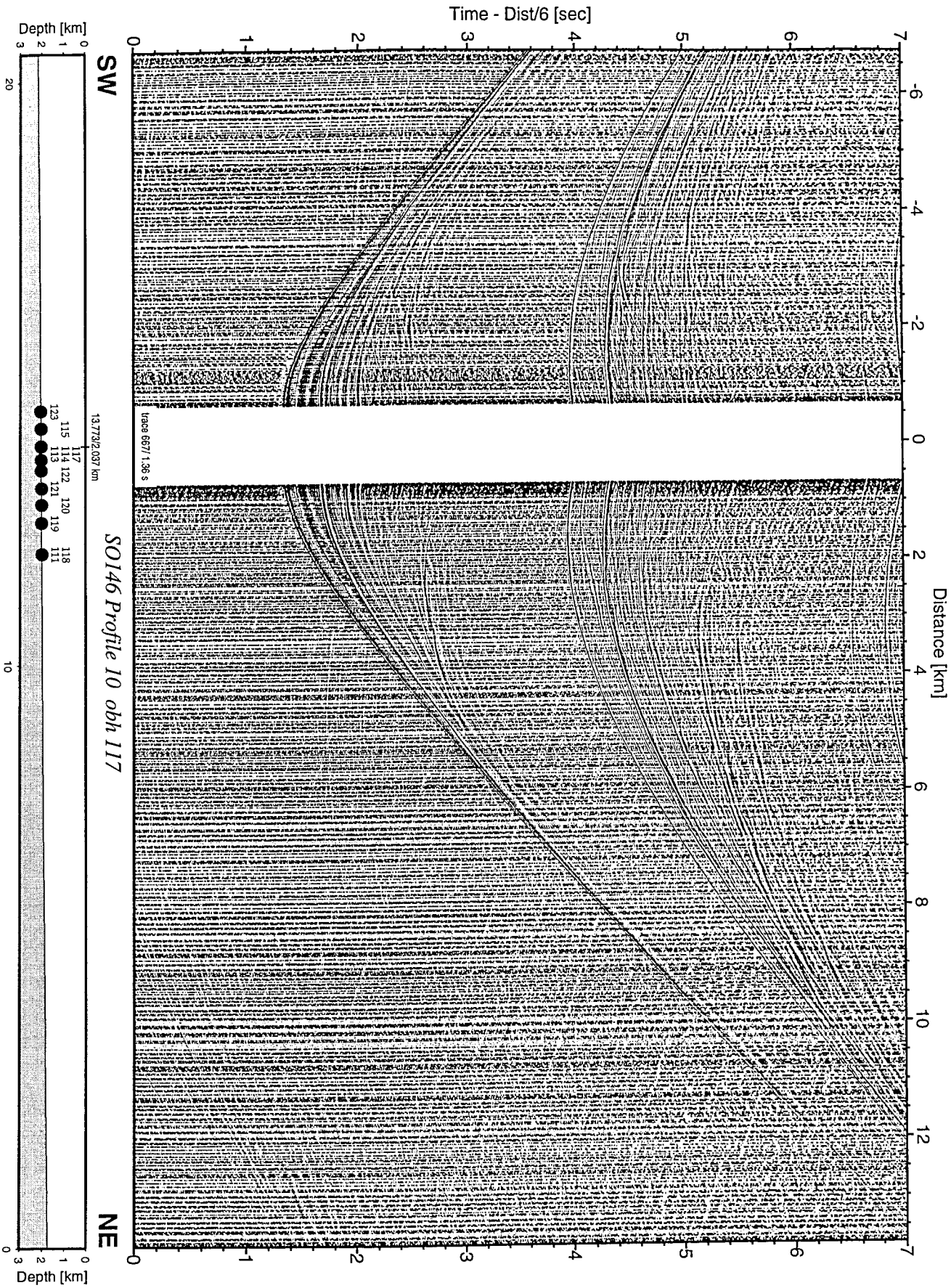

Figure 9.2.45: Record section from obh 117 , Profile 10.

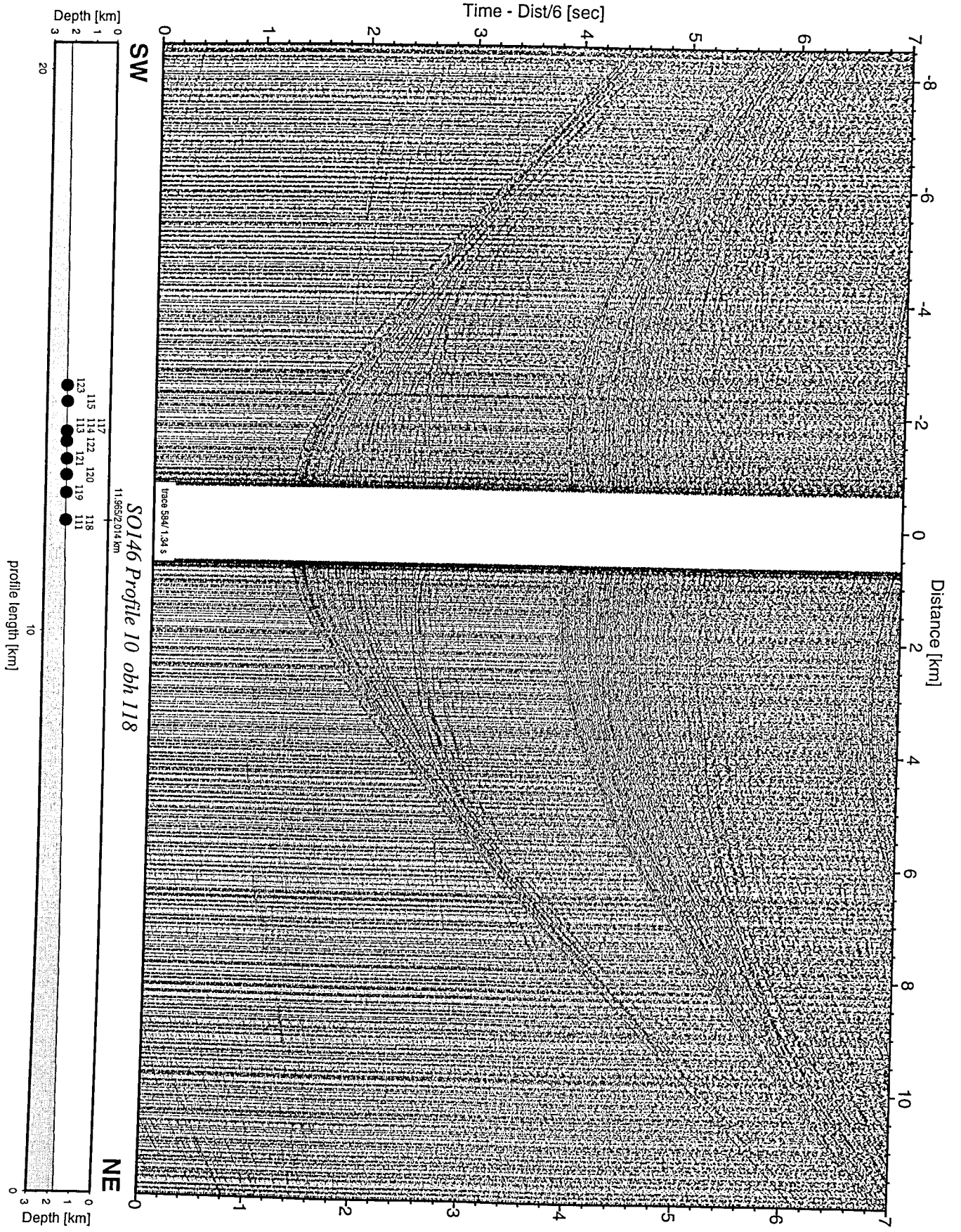

Figure 9.2.46: Record section from obh 118 , Profile 10.

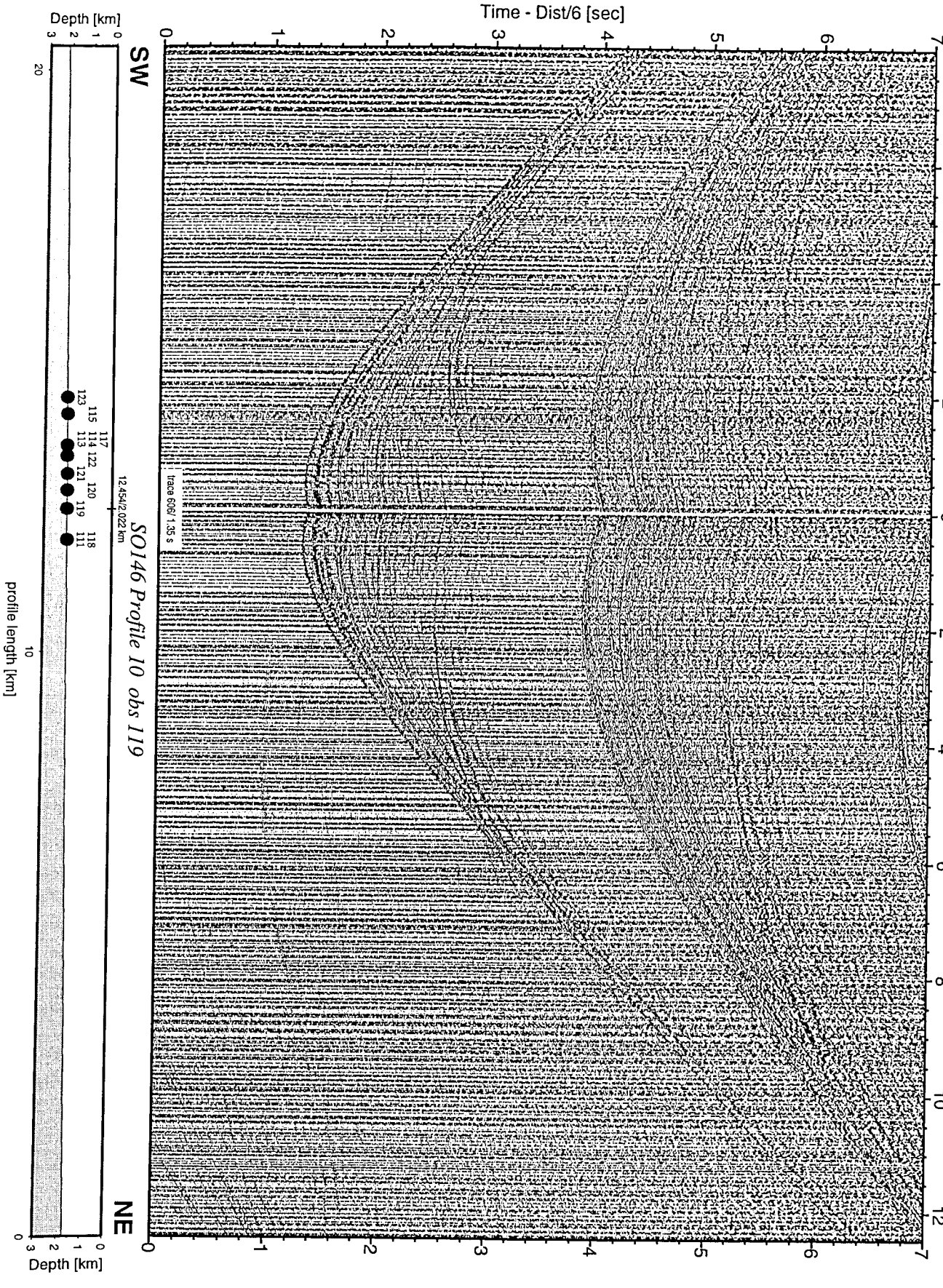

Figure 9.2.47: Record section from obs 119 hydrophone, Profile 10.

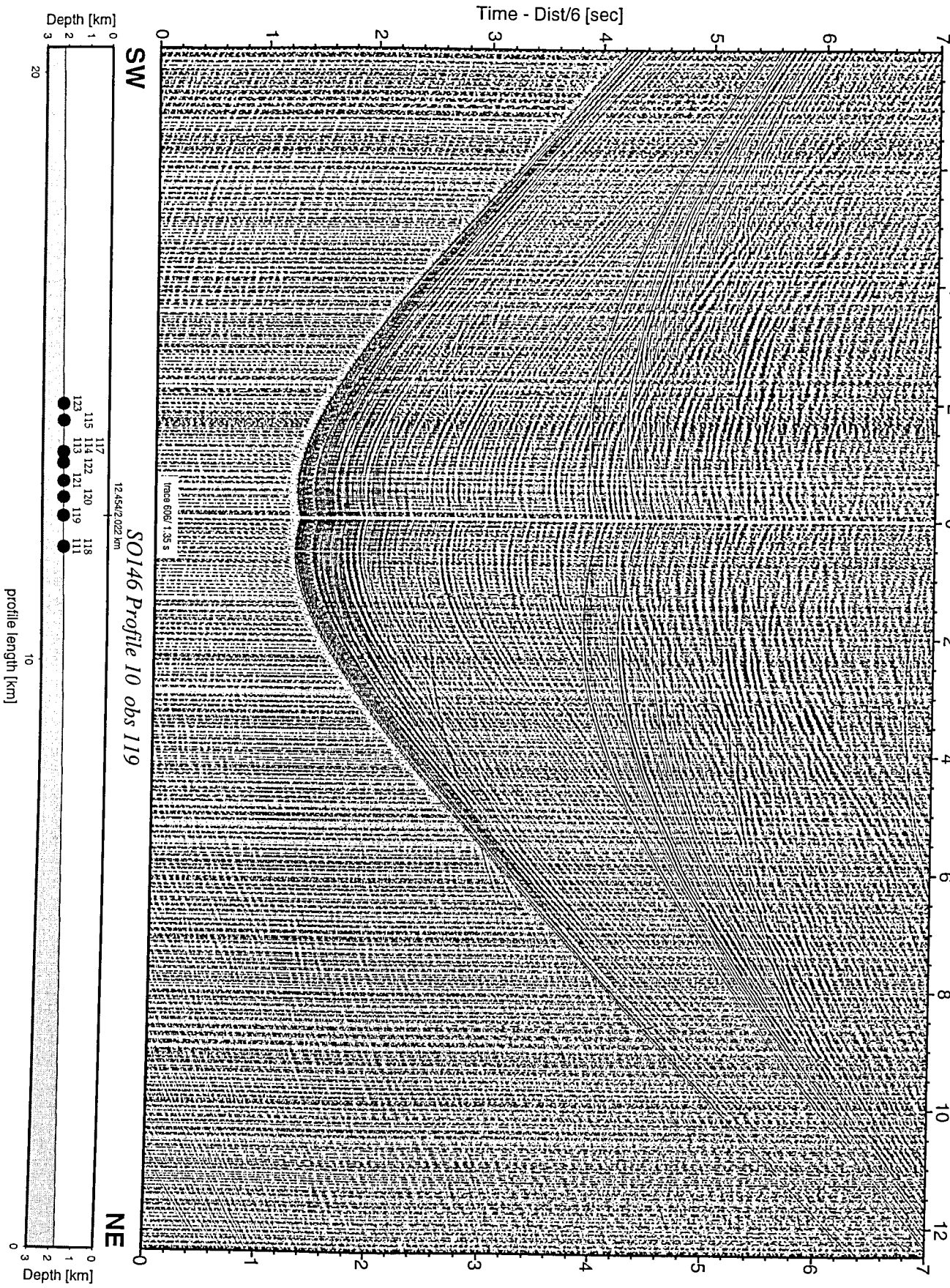

Figure 9.2.48: Record section from obs 119 horizontal component 1, Profile 10.

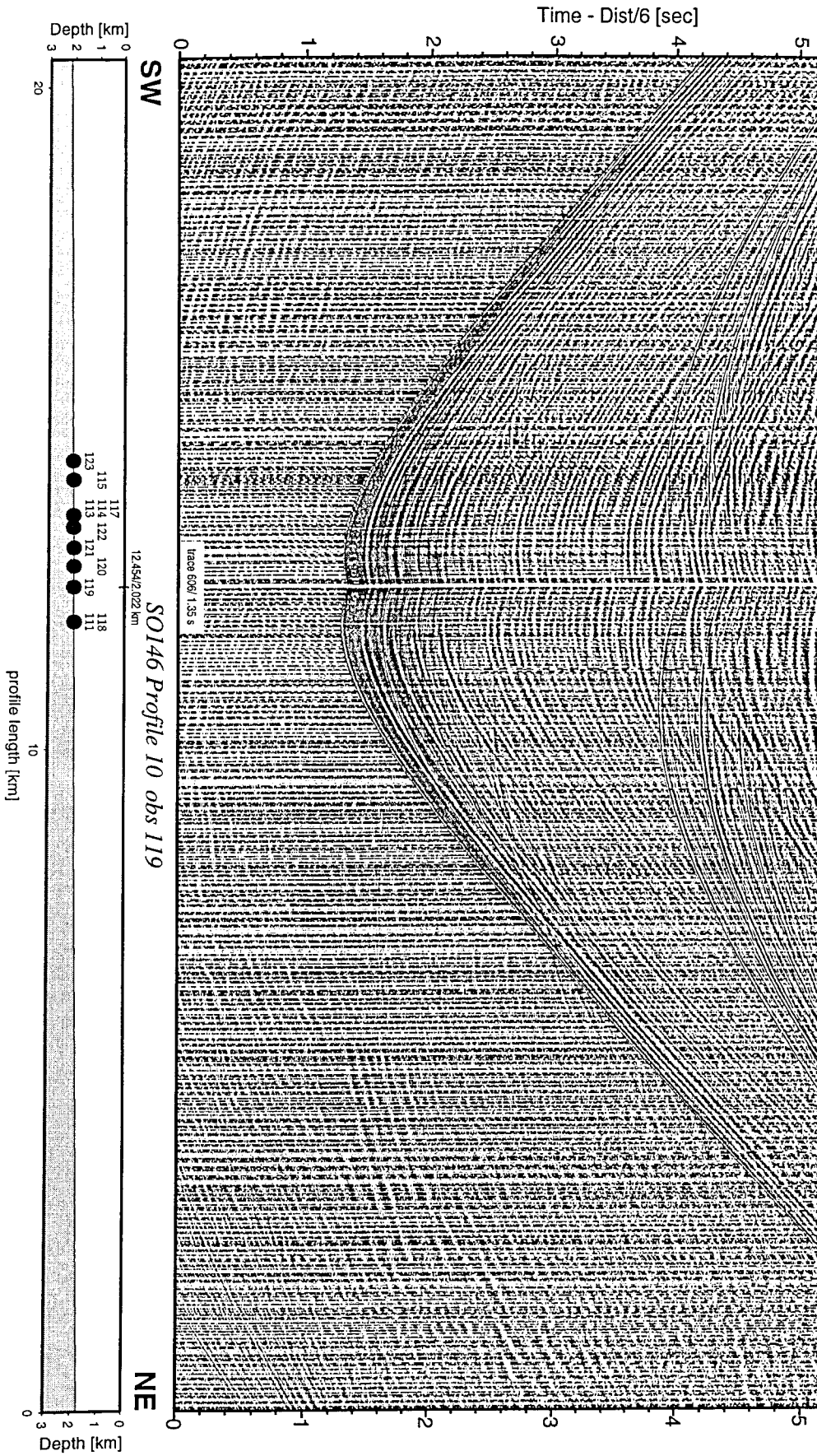

Figure 9.2.49: Record section from obs 119 horizontal co

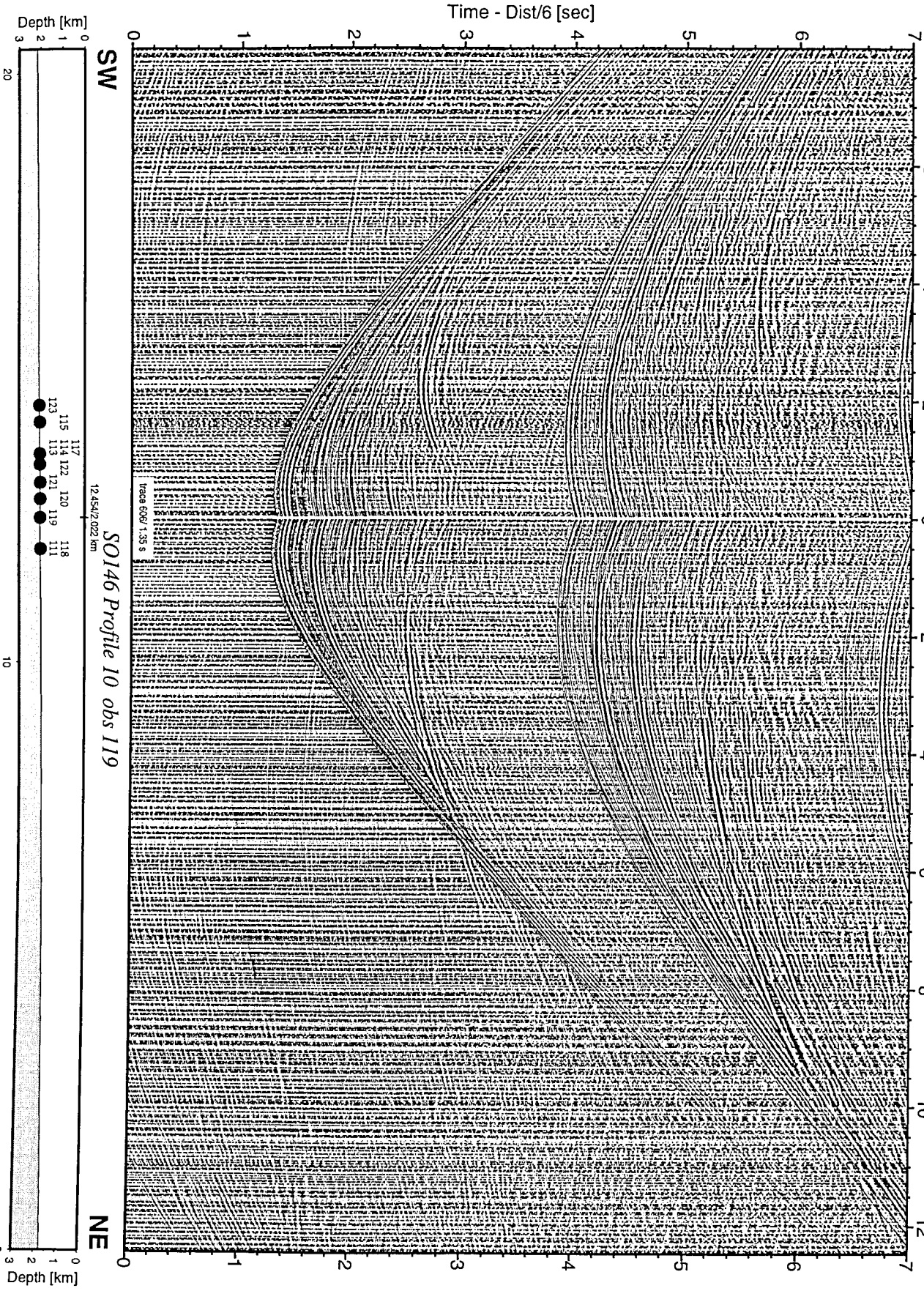

Figure 9.2.50: Record section from obs 119 vertical component, Profile 10.

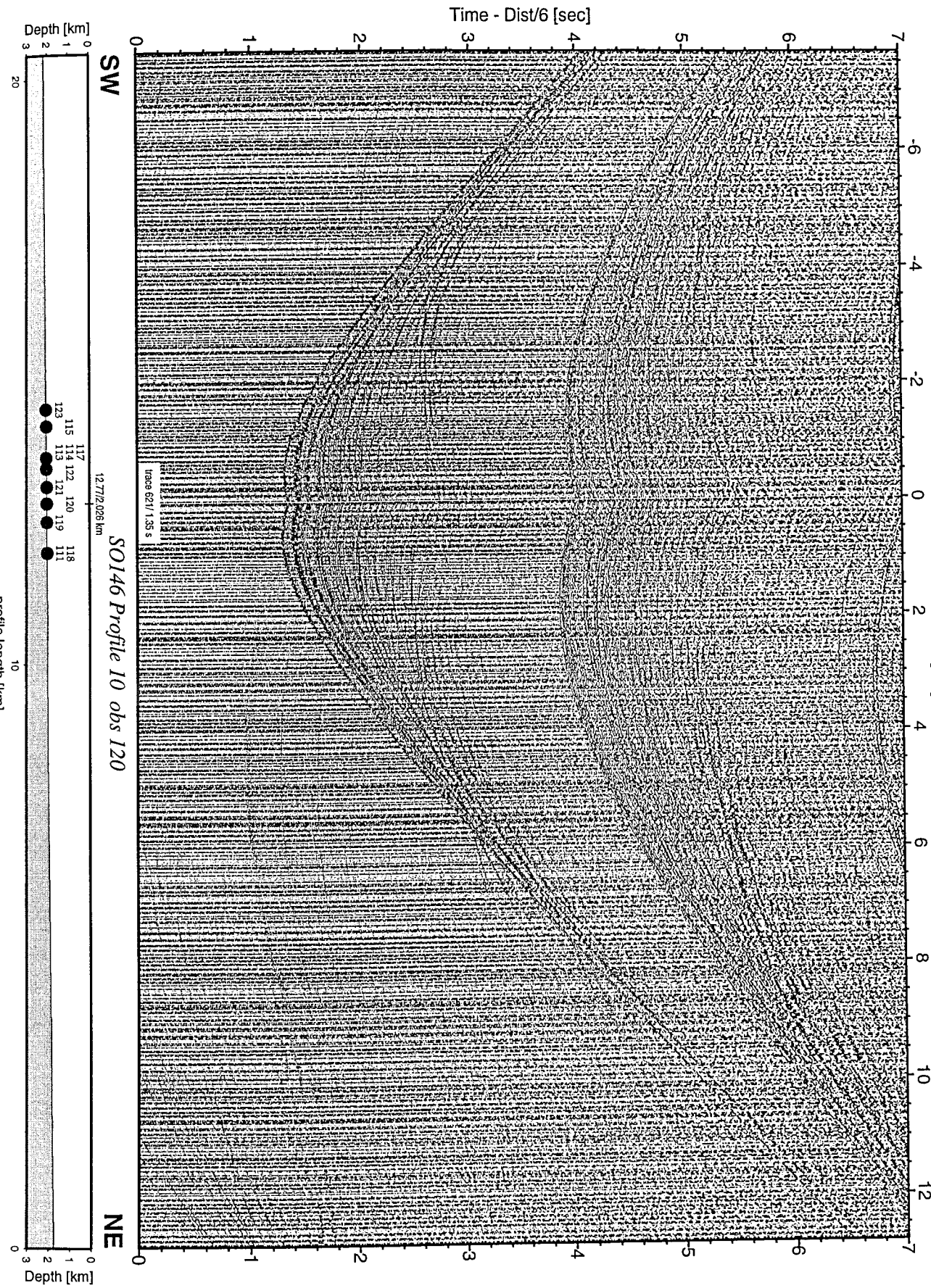

Figure 9.2.51: Record section from obs 120 hydrophone, Profile 10.

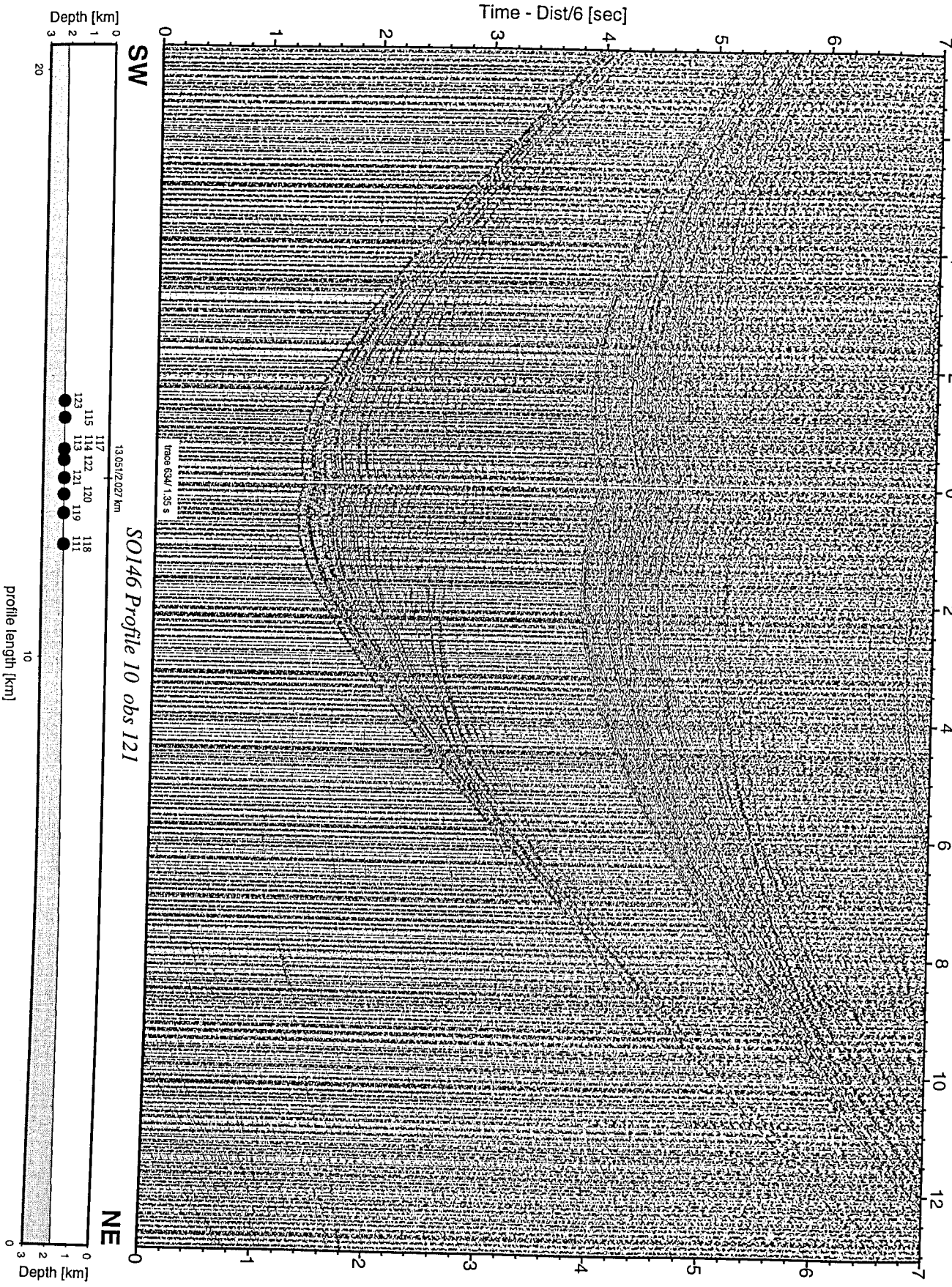

Figure 9.2.52: Record section from obs 121 hydrophone, Profile 10.

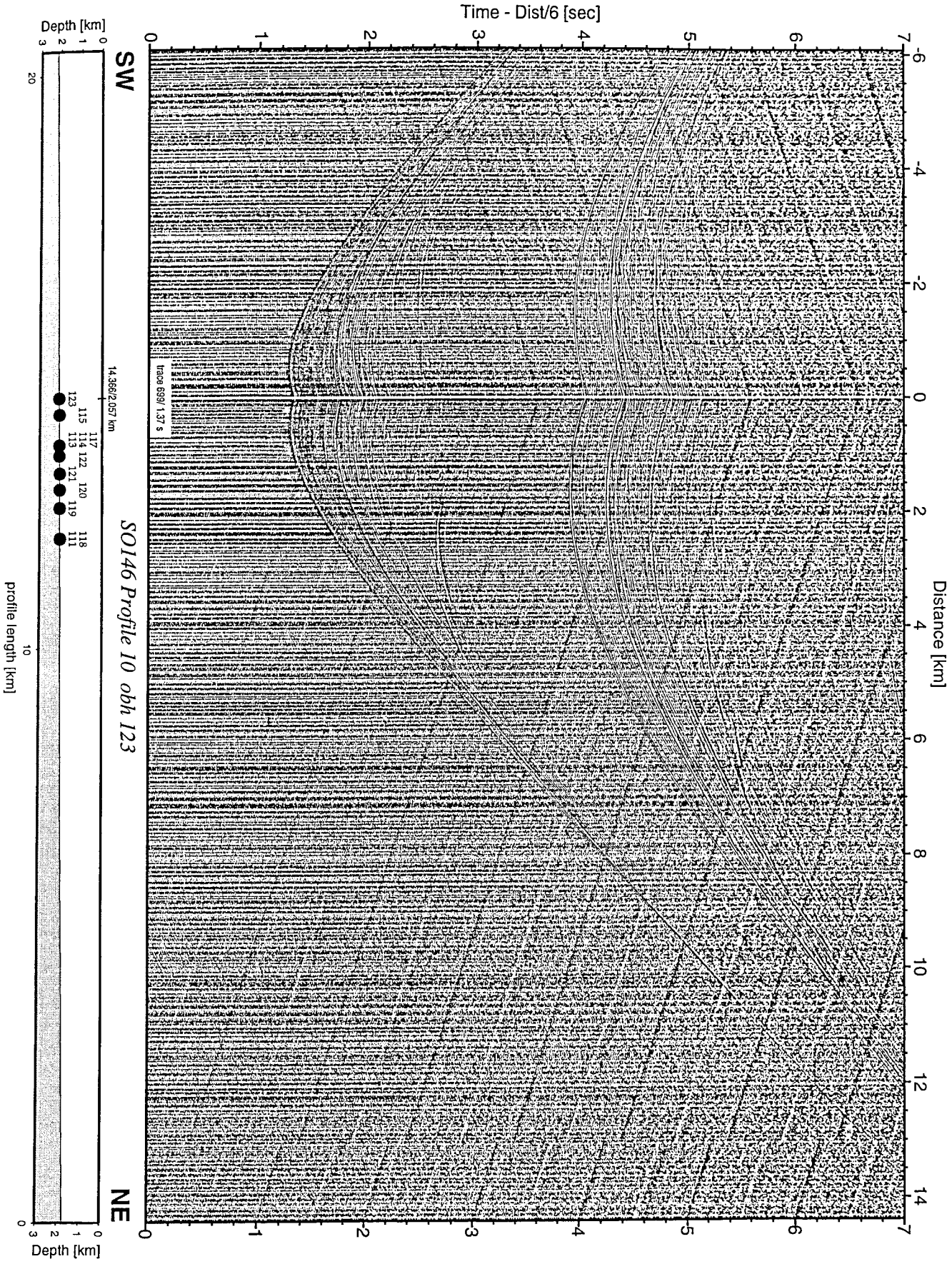

Figure 9.2.53: Record section from obh 123 , Profile 10.

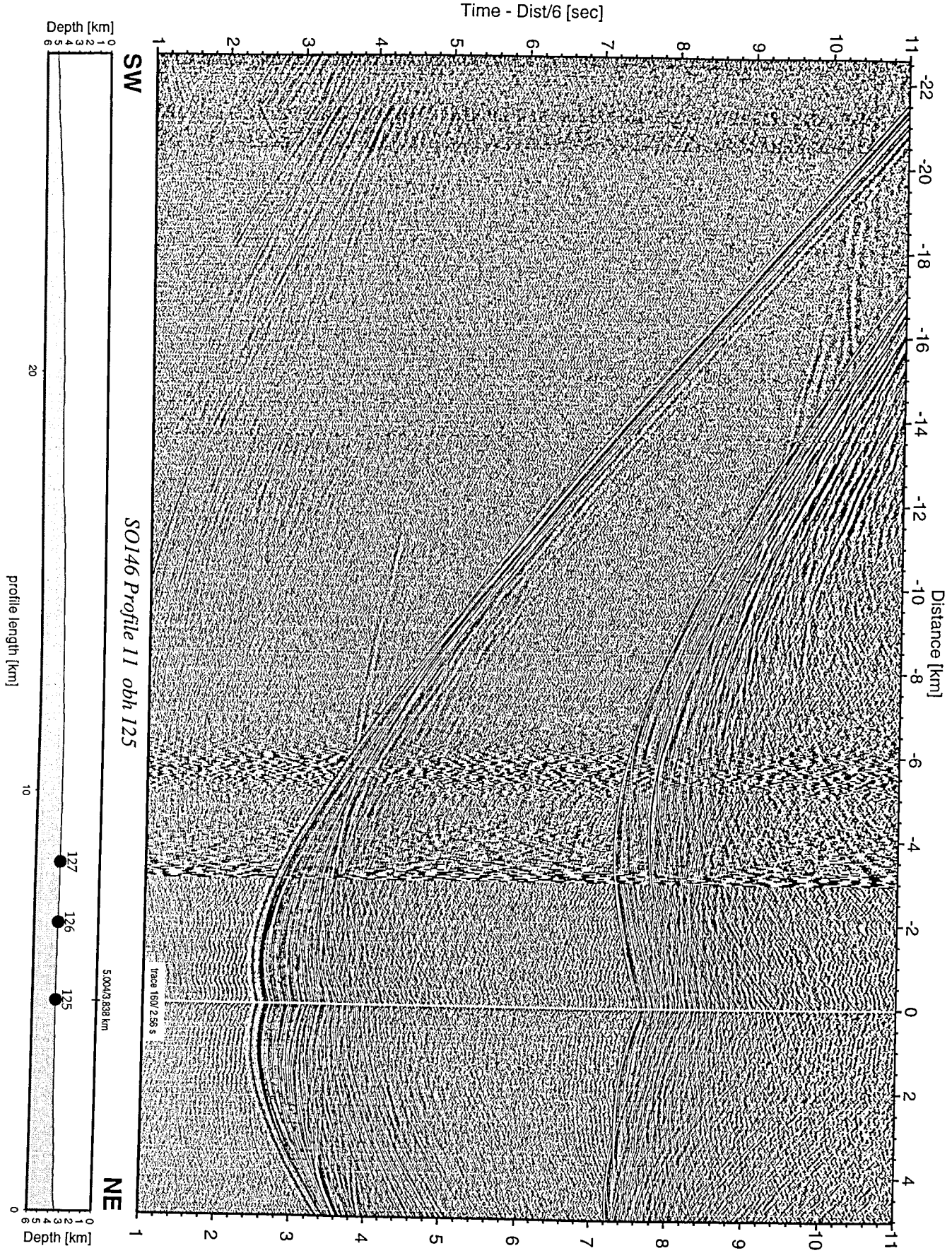

Figure 9.2.54: Record section from obh 125 , Profile 11.

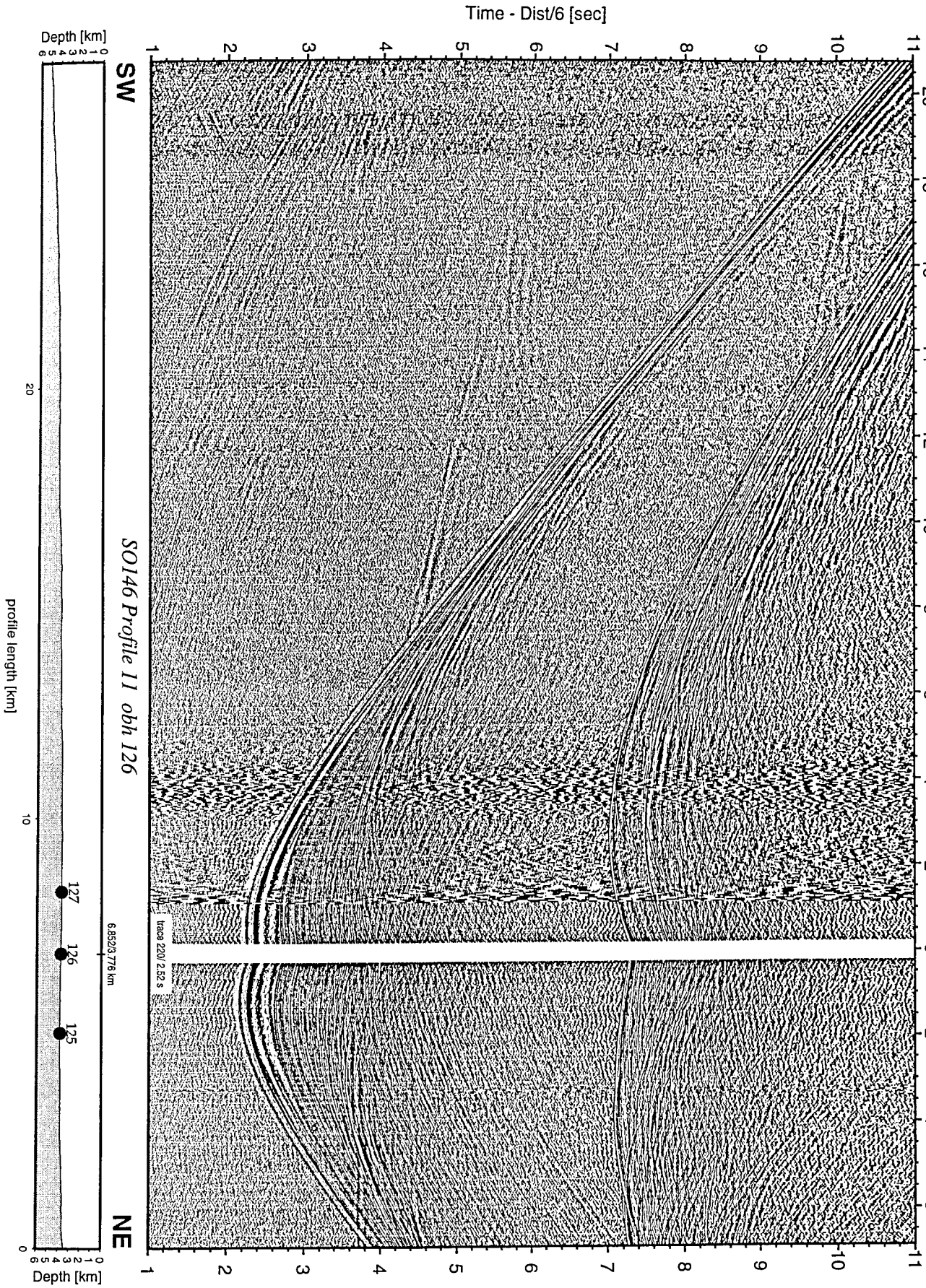

Figure 9.2.55: Record section from obh 126 , Profile 11.

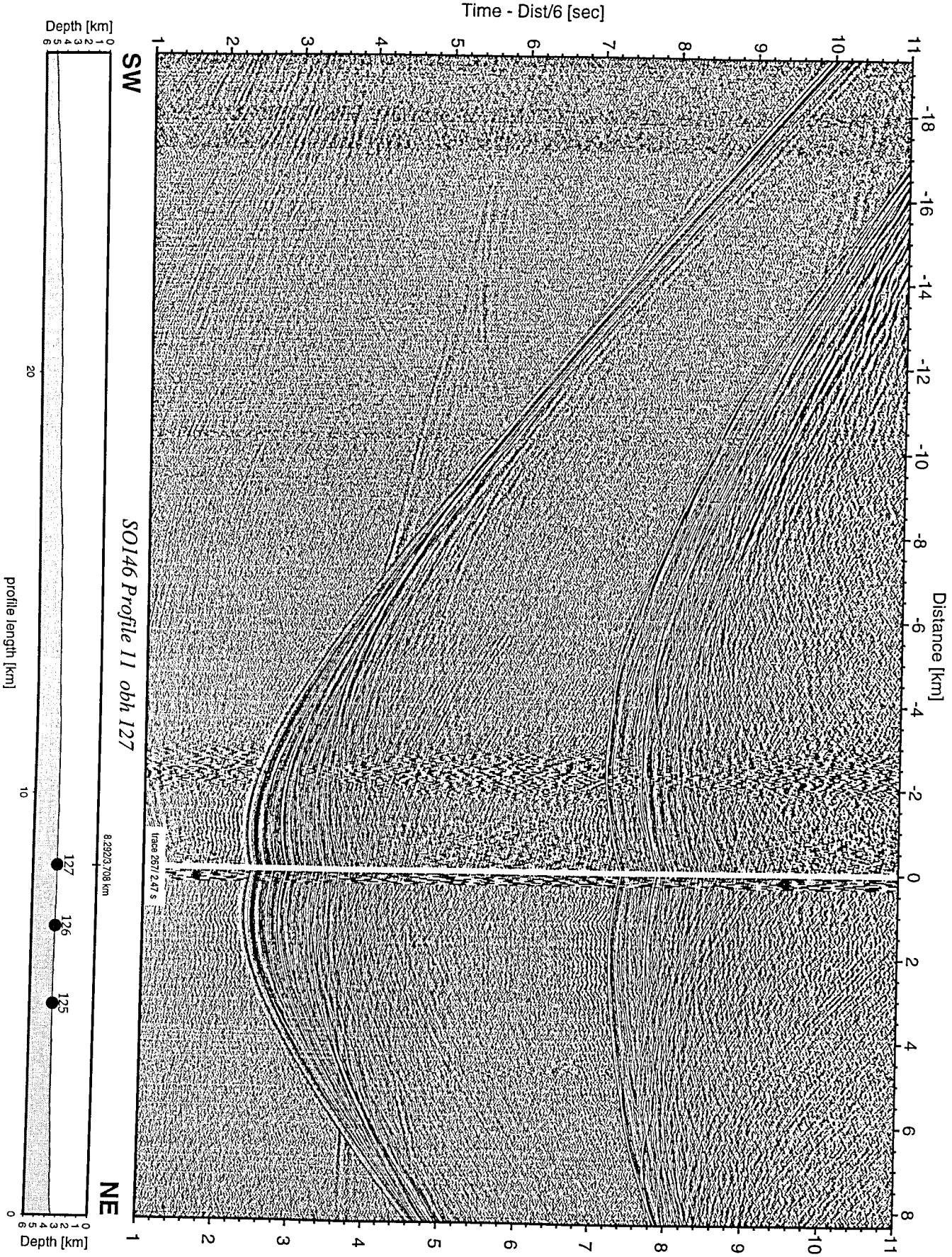

Figure 9.2.56: Record section from obh 127 , Profile 11.

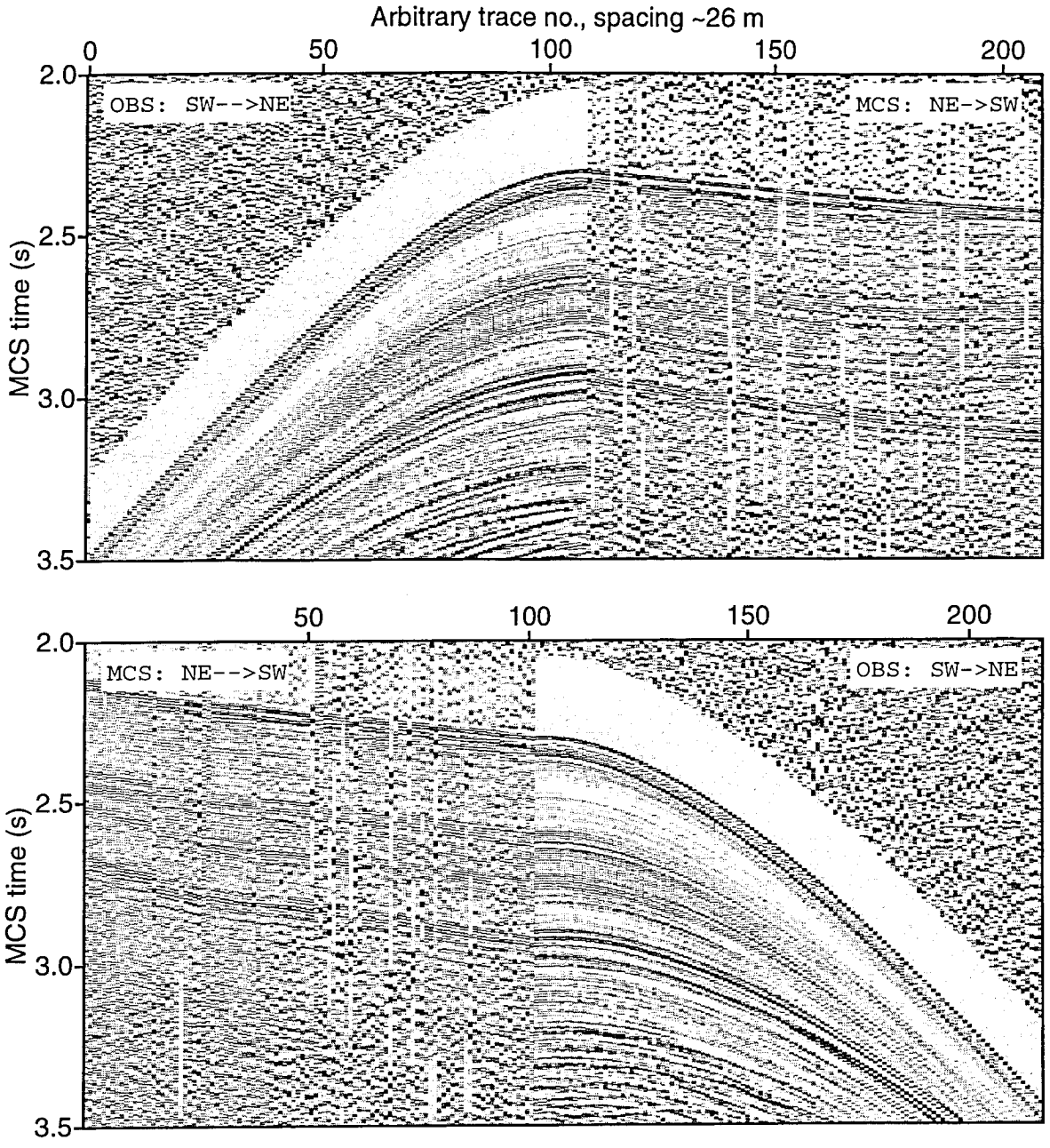

Fig. 9.2.57: Identification of arrivals in high-resolution wide-angle data, p07 OBS 76, MCS line 26. Top: SW branch of hydrophone record, shifted to MCS two-way traveltime (TWT), compared to flipped MCS section SW of OBS location. Bottom: Same plot with NE branches. Arrivals down to the L4/5 interface (fig. 9.1.2) can easily be correlated. Enhanced processing of line 26 and/or a similar correlation with reflections in line HIG-13, which was acquired essentially along the same track, should give us TWT constraints for velocity models through the entire sediment section down to the metamorphic basement.

Figure 9.2.58: OBH/S hydrophone image after downward continuation of the wavefield and high-order NMO. Top, OBS80, from left to right: Original gather, gather after downward continuation of wavefield, NMO corrected gather, V(z) function for NMO correction. Bottom: composite image of all OBH/S from P07. Note that we have almost achieved 2-D coverage at the basement. Compare to image from reflection seismic data, HIG 13 (figure 1.8).

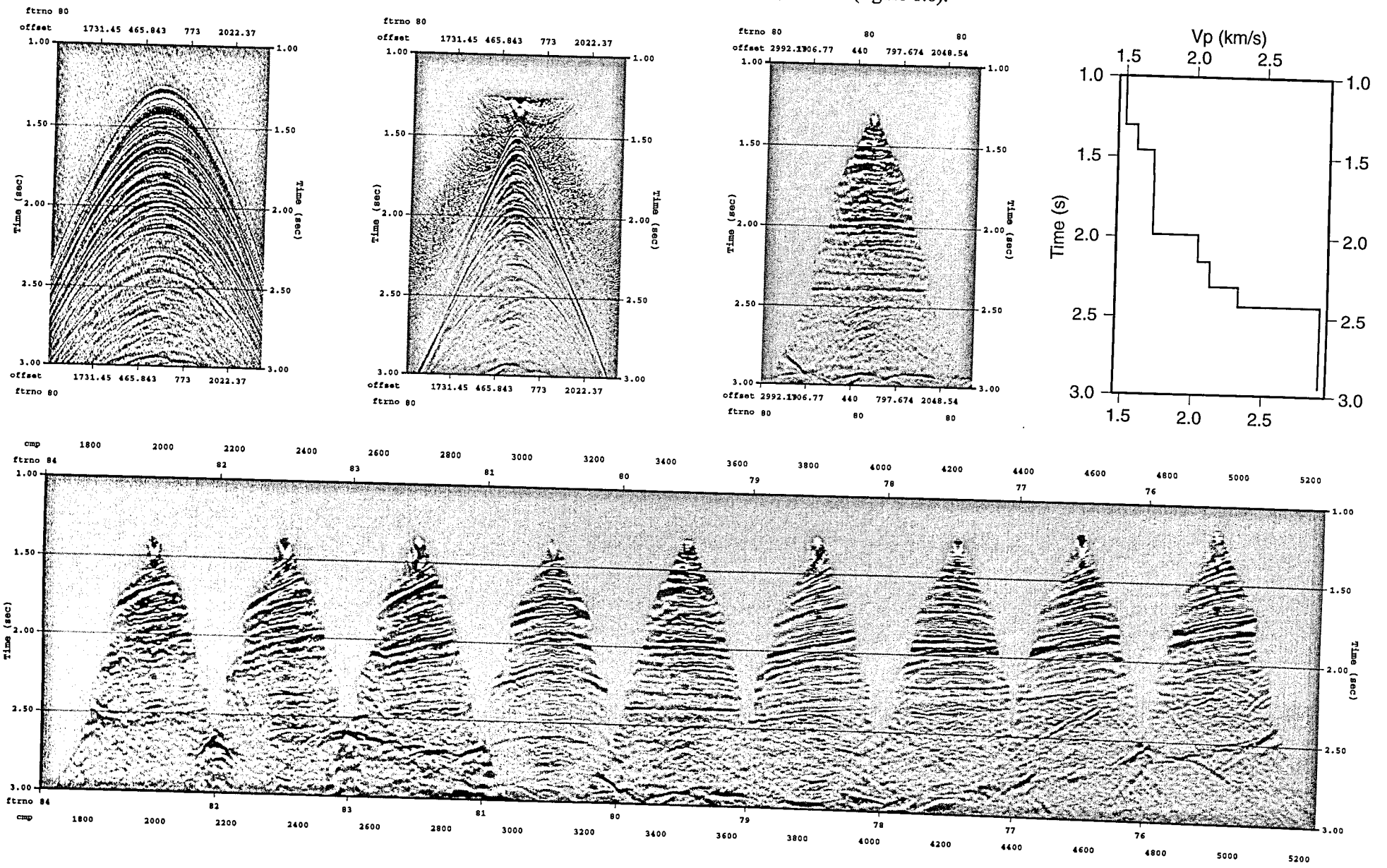

9.2.4. Planned Analyses of MCS and OBH/S Data

Tectonic suppression of BSRs. The HIG data will be re-processed including a velocity analysis and depth conversion. This velocity model will be interpolated in 3-D and used to also convert the new high-resolution MCS data to depth. We then plan to tie both the HIG data and the new MCS data into Site 679, which was crossed by HIG-14 and now by HH00-070 and HH00-071. Since no major truncation was found at Site 679 above the mid-Miocene unconformity, we should obtain full stratigraphic control from this site. We plan to apply one and two-dimensional backstripping to quantify the vertical motion of the seafloor. This, together with sedimentation and erosion rates, will form the input for a numerical steady-state model of the gas hydrate system. This numerical approach is currently being developed and is an extension of an earlier one-dimensional analytical model (Xu and Ruppel, 1999).

Physical properties of gas hydrate-bearing sediments; thickness of free gas zone: We plan to obtain a 1-D starting velocity/depth function by applying a higher-order NMO analysis (fig. 9.2.58), which is a novel approach for the analysis of high-resolution OBH/S data. For an extension into 2-D, we will utilize structural information from the MCS by adding an additional constraint to the modeling: Velocity models must meet the constraint that the two-way-traveltime at zero-offset to layer interfaces match those observed in the MCS data. We plan to use a modified version of the RayGUI ray-tracing package (Zelt and Smith, 1992, Loss et al., 1998). For a Vs analysis, the generally low Vs immediately beneath the seafloor causes near-vertical S-wave rays. This impedes conventional NMO analysis. We therefore plan a combination of higher-order NMO analyses and event correlation (PS-converters mostly are also good PP-reflectors). Event correlation will be facilitated by the dense spacing of OBSs during deployments P09 and 10.

9.3 SeeBoSeis

(R. Coman, C. Hübscher, R. Herber, C. Herold)

Overview
This is the first experiment where the SeeBoSeis system was used to conduct high resolution seafloor seismics. The main objective of the SeeBoSeis experiment was the characterization of near surface sediments in the Lima Basin in terms of velocity (P and S) and elastic parameters.

We performed two measurements: The first measurement was conducted in a region without a BSR, while the second was in a region with a BSR. Since similar sediment layers are present at both sites; both above and below the BSR, as well as in the area without a BSR, the experiments were intended to study the influence of gas on seismic attributes.

Another objective was to test the amplitudes, frequencies and reliability of the SeeBoSeis sources. Before the two above mentioned measurements were made, we performed two other tests with the SeeBoSeis sources. From the 24 total sources used in all experiments, 23 imploded. The water waves were strong and had peak energies between 400Hz and 1100Hz. However, the reflections were small because the high frequencies are absorbed.

SeeBoSeis setup
The SeeBoSeis system consists of two separate components: a broadband ocean-bottom recording system and an implosive source. For descriptions of the OBS/OBH instruments see chapter 4.3, and for the SeeBoSeis source see chapter 4.4.3.

Since the frequency of the SeeBoSeis sources was expected to be between 200 Hz and 800 Hz (Herber et al., 1998), the sampling rate was set to 2500 Hz for each OBS and for three of the OBHs. The others OBHs instrument was set to a sampling rate of 1000 Hz.

We also expected a high energy direct wave (water wave) and low energy reflections. As the direct wave is important for estimating the energy of the SeeBoSeis source, and the source signature is important for future processing and for source improvements, clipping of the direct wave was avoided by using two channels for registration with the OBH. The first channel used no amplification, while the second channel used a pre-amplifier.

Receivers and sources were deployed by free fall using Global Positioning System (GPS) to locate the dropping positions. The instrument locations on the seabed were further constrained using airgun shots collected while the ship navigated by GPS. During shooting to determine the position of the OBS/OBH instruments, we also acquired MCS data. For determination of the true shot locations we intend to use techniques and computer codes employed in local earthquake studies. For this reason, some OBH instruments were placed offline in both experiments.

SeeBoSeis tests

Before performing the measurements in Lima Basin we tested the SeeBoSeis sources in two experiments.

For the first test we deployed a cylindrical source with a coaxial cable to a water depth of 2000 m, with an OBH recording unit fixed 30 m above. To destabilize the glass hemisphere, we used small shot ammunition. The main results of these tests are:

- the glass hemisphere was completely broken (Figure 9.3.1);
- because of the high hydrostatic pressure, grains of shot were found inside the source after imploding;
- since the source was suspended on the cable, the cable vibration superimposed the source signal.

For the second test we dropped two spherical sources on reflection profile HH00-044 in the Yaquina Basin. The goals of this test were:

- to test the spherical SeeBoSeis source;
- to record the form of the signal and the signal frequency from the source at the sea floor;
- to observe the behavior of the SeeBoSeis source in shallow water, as the water depth was between 500 m and 700 m;
- to estimate the energy of the water wave and Scholte wave;

The position of this test was chosen so as to permit the identification of an anticipated Scholte wave. For about two minutes before the SeeBoSeis implosion and for three minutes after the implosion, the GI gun was not used.

The registration of shot number 1 is shown in Figure 9.3.2. The main results of this experiment are:

- both sources imploded;
- the frequency of both shots was greater than 200 Hz;
- both shots generated a Scholte wave, which propagated with velocities between 130 m/s and 200 m/s.

SeeBoSeis measurements

For the measurements made in the Lima Basin we used 4 OBS and 9 OBH. One of the OBS instruments used a 30 Hz sensors. We placed this OBS in a position with smaller offsets. For both measurements, we also performed a zero-offset shot. For this shot we attached a source on the anchor of one of the OBH instruments. We chose a vertical separation between the source and OBH of 50 m. This way, we could also register the source signatures from the GI guns.

We performed two measurements in the Lima Basin. The first experiment was placed in a region without a BSR, while the second experiment was placed in a region with a BSR. The occurrence of a BSR in the Lima Basin is known from former seismic measurement and also from MCS data collected during the profile HH00-026 (see chapter 9.1).

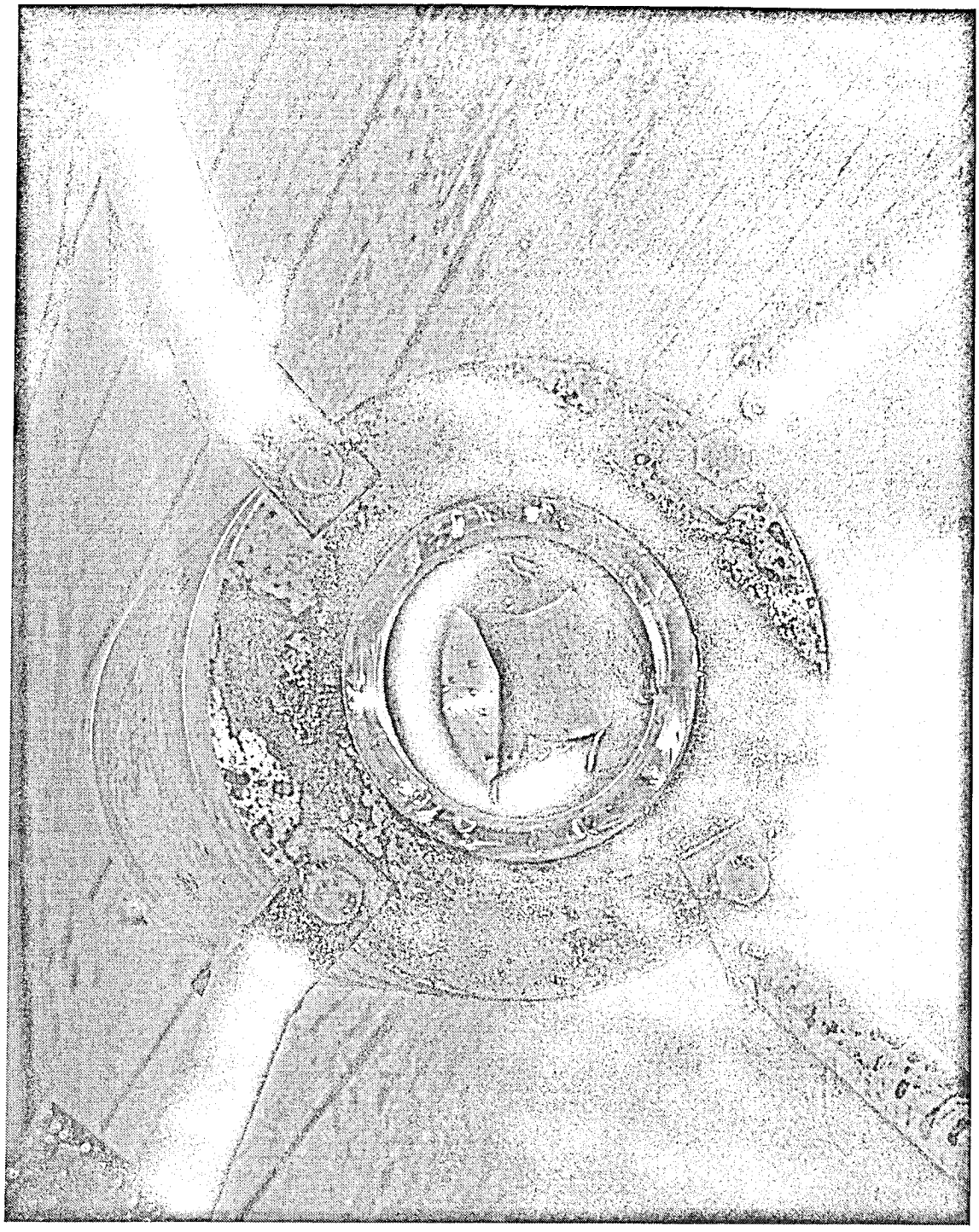

Figure 9.3.1 Cylindrical SeeBoSeis source after implosion. Half glass sphere is completly broken

For the SeeBoSeis_1 measurement we used 10 SeeBoSeis sources, 4 OBS and 9 OBH. Besides the 3 OBH which were offline, all other sources and receivers were along the main line. The lateral offset was 600 m. In general, the distance between receivers was 300 m and the distance between sources 100 m. The location of the SeeBoSeis_1 experiment with sources and receivers is shown in Figure 9.3.3. We designed this measurement not only to achieve high stratigraphic resolution in the region without a BSR, but also to test different SeeBoSeis constructions, to estimate the energy of the SeeBoSeis sources and to optimize the offset for the SeeBoSeis_2 experiment.

The characteristics of the sources used are given in Table 9.3.1, while the OBS/OBH characteristics are given in the appendix V. The zero-offset shot was located at OBH 106.

No.	Source Type	Destabilization Method	Time of Implosion	Remarks
1	Cylinder	Shot ammunition	22:00:00	Zero Offset
2	Alu-cylinder	Spring & bolt	22:05:00	
3	Alu-cylinder	Spring & bolt	22:10:00	#3 & #4 same position
4	Cylinder	Shot ammunition	22:15:00	
5	Sphere	Shot ammunition	21:55:00	
6	Cylinder	Shot ammunition	21:50:00	
7	Cylinder	Shot ammunition	21:45:00	
8	Cylinder	Shot ammunition	21:40:00	
9	Cylinder	Shot ammunition	21:35:00	
10	Cylinder	Shot ammunition	21:30:00	

Table 9.3.1

The main results of SeeBoSeis_1 measurement are:

- all sources imploded;
- the source signatures of the sources using shot ammunition are all very similar in terms of energy and frequency content (Figure 9.3.4);
- the water wave of the SeeBoSeis shots is characterized by frequencies ranging between 600Hz and 1100Hz;
- the source signals from SeeBoSeis sources using shot ammunition has higher amplitudes than signals from the sources using a spring and bolt;
- the amplitudes of the reflections are low. By considering only one trace, they are hard to localize. An example of a possible reflection is shown in Figure 9.3.5;
- the registration from some OBS/OBH has a strong bias or low frequency (1Hz-5Hz) noise;
- no Scholte wave was detected.

For SeeBoSeis_2 we used the experience from the first measurement and made the following changes:

- we avoided long offsets and increased the data density at near offsets (between 300 m and 1000 m);
- we only used SeeBoSeis sources with shot ammunition.

For the SeeBoSeis_2 measurement we deployed 11 SeeBoSeis sources plus 4 OBS and 9 OBH. The location of the SeeBoSeis_2 experiment with sources and receivers is shown in Figure 9.3.6. The characteristics of the sources used are given in Table 9.3.2, while the OBS/OBH characteristics are given in appendix V. The zero-offset shot was located at OBH 123.

From the 11 sources used, 10 imploded. The SeeBoSeis_2 experiment reconfirmed the above mentioned observations from SeeBoSeis_1.

No.	Source Type	Destabilization Method	Time of Implosion	Remarks
1	Alu-cylinder	Shot ammunition	16:50:00	Zero offset; 50m rope
2	Sphere	Shot ammunition	16:20:00	
3	Cylinder	Shot ammunition	16:40:00	
4	Cylinder	Shot ammunition	16:35:00	did not implode
5	Cylinder	Shot ammunition	16:30:00	
6	Cylinder	Shot ammunition	16:25:00	
7	Cylinder	Shot ammunition	16:45:00	
8	Sphere	Shot ammunition	16:15:00	
9	Sphere	Shot ammunition	16:10:00	
10	Sphere	Shot ammunition	16:05:00	
11	Alu-cylinder	Shot ammunition	16:55:00	

Table 9.3.2

High resolution plumbing system from 2.5-D seismic data: Starting with a large-scale 2-D velocity model from a combined analysis of the MCS and OBH/S records (see above), we plan to apply 2.5-D processing (such as migration) to the grid of MCS data acquired while locating the OBH/Ss used for the SeeBoSeis experiments. A reflectivity inversion will allow us to estimate the high-resolution 2.5-D velocity structure. This will be interpolated to 3-D and we will investigate if corrections for 3-D layer dips have to be applied. With this, we will obtaine a 3-D image of the subsurface structure. We will now investigate seismic attributes searching for high negative-amplitude events and the lowering of instantaneous frequencies that is typical beneath gas-bearing layers. Such events will be interpreted as possible fluid-migration paths. Comparison to the same layers at the site P1 will offer us a "baseline" for the attributes of the fully water-saturated layers.

Indications for gas migration through the GHSZ on the lower slope: We plan essentially the same analysis as above, although only in 2-D. Large-scale velocities will be provided from the four OBHs deployed in the lower-slope basins and from line 1018 around P7. We will particularly investigate lateral changes of the reflection coefficient of the BSR. A sudden decrease of BSR reflectivity close to faults may indicate venting of free gas from the BGHS through faults.

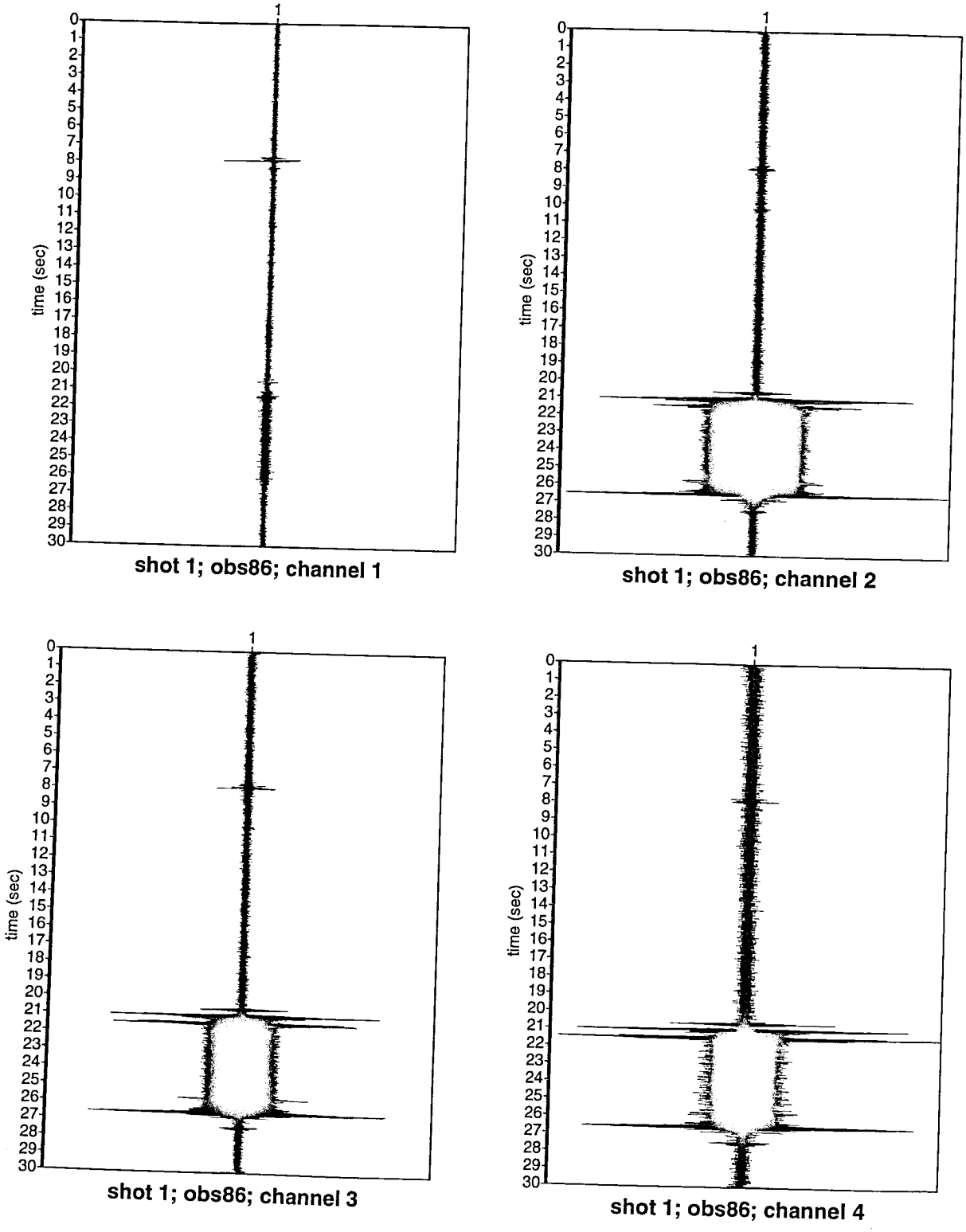

Figure 9.3.2 Registration of shot number 1 at OBS86
channel 1=hydrophone; channnel 2 and 3=horizontal component
channel 4=vertical component

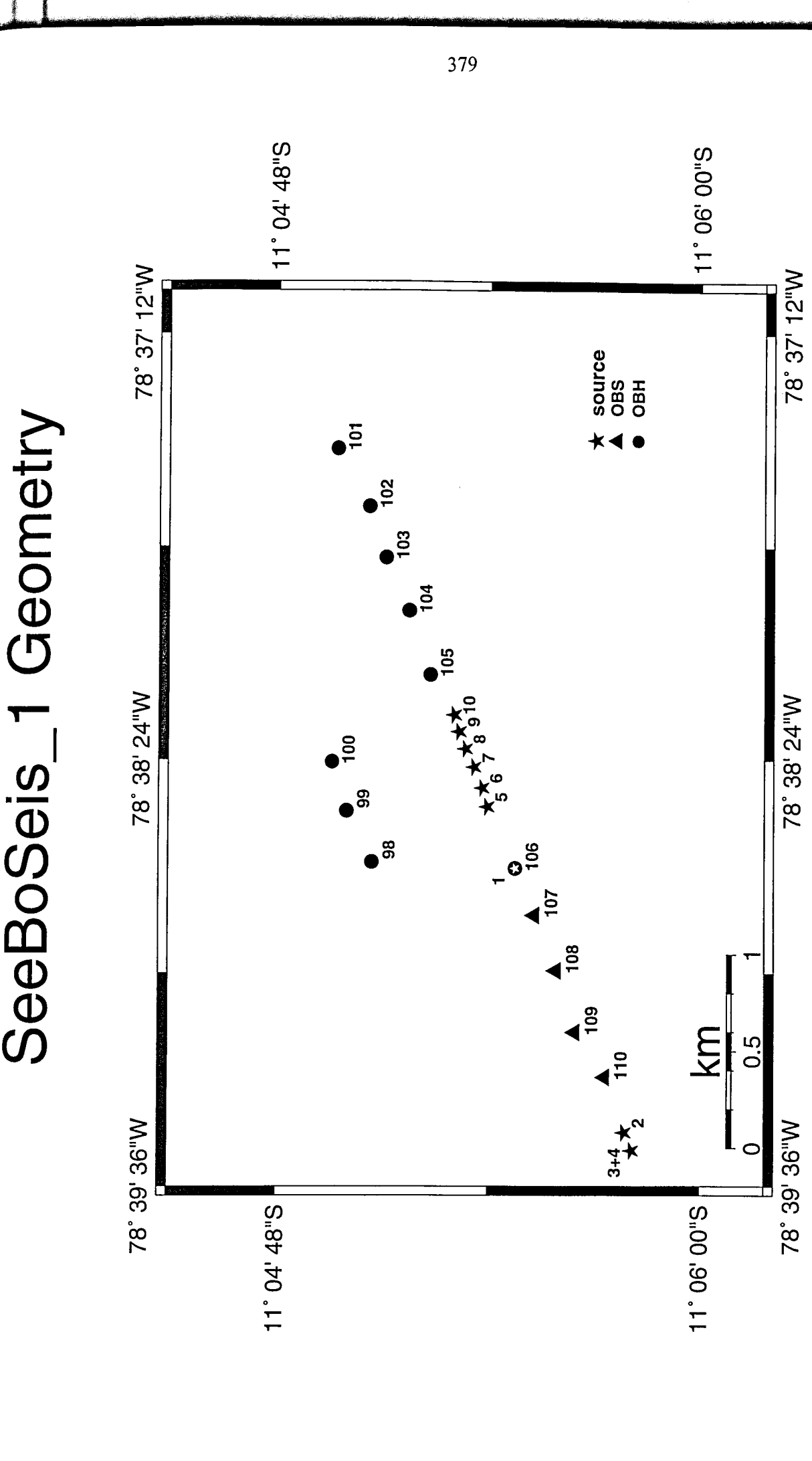

Figure 9.3.3 SeeBoSeis_1: sources and receivers

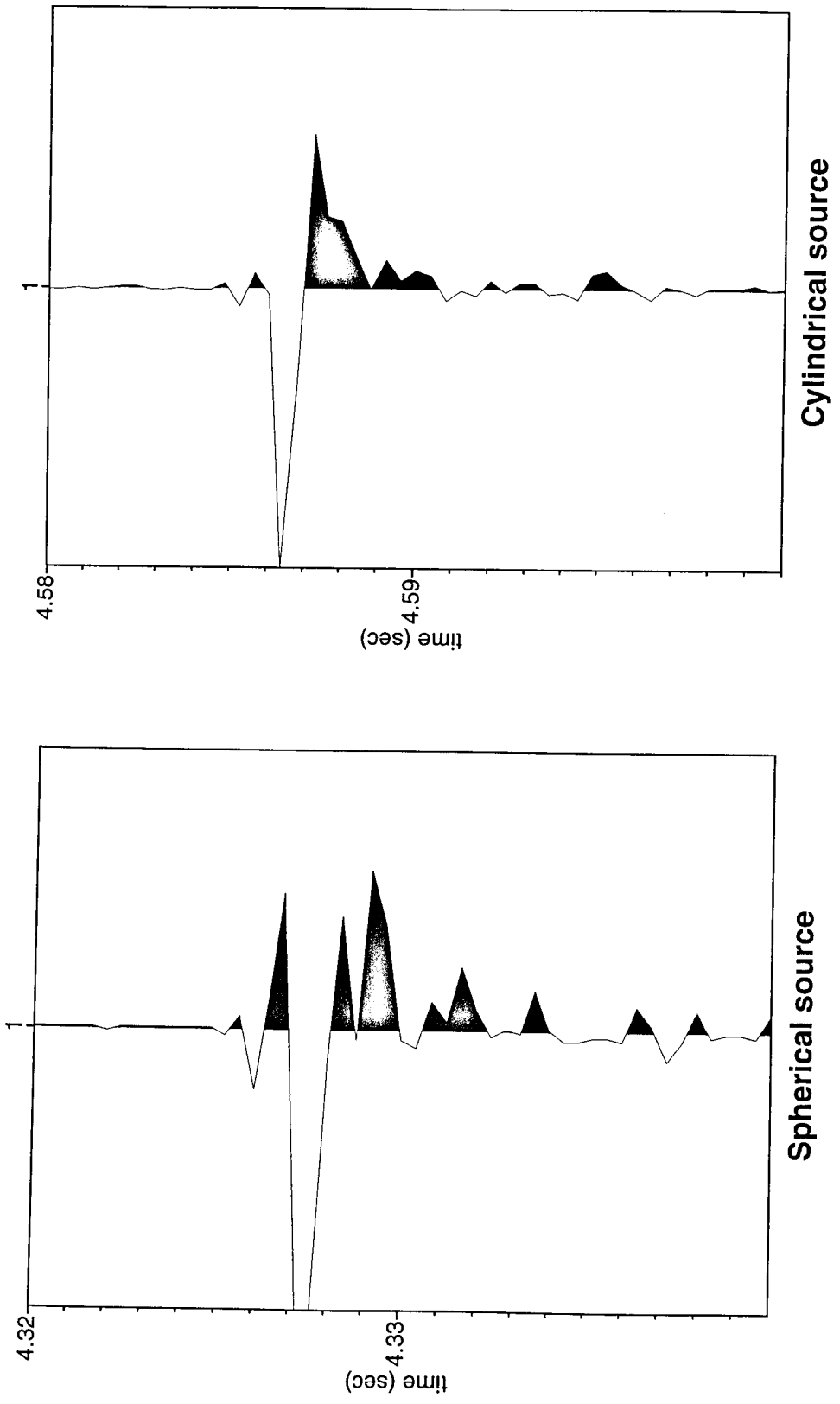

Figure 9.3.4 Source signature of spherical and cylindrical SeeBoSeis source

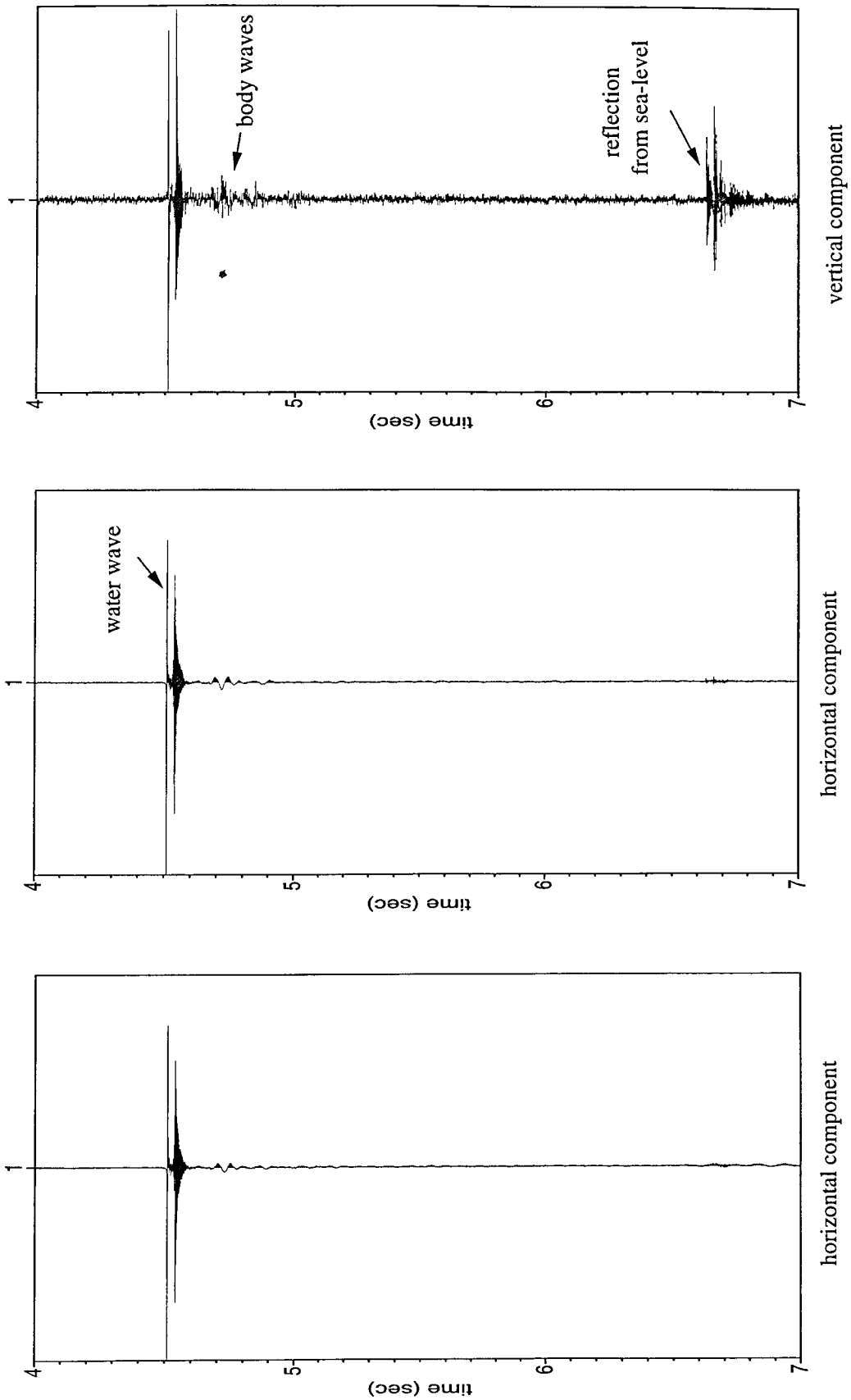

Figure 9.3.5 SeeBoSeis traces from OBS107, shot 1.

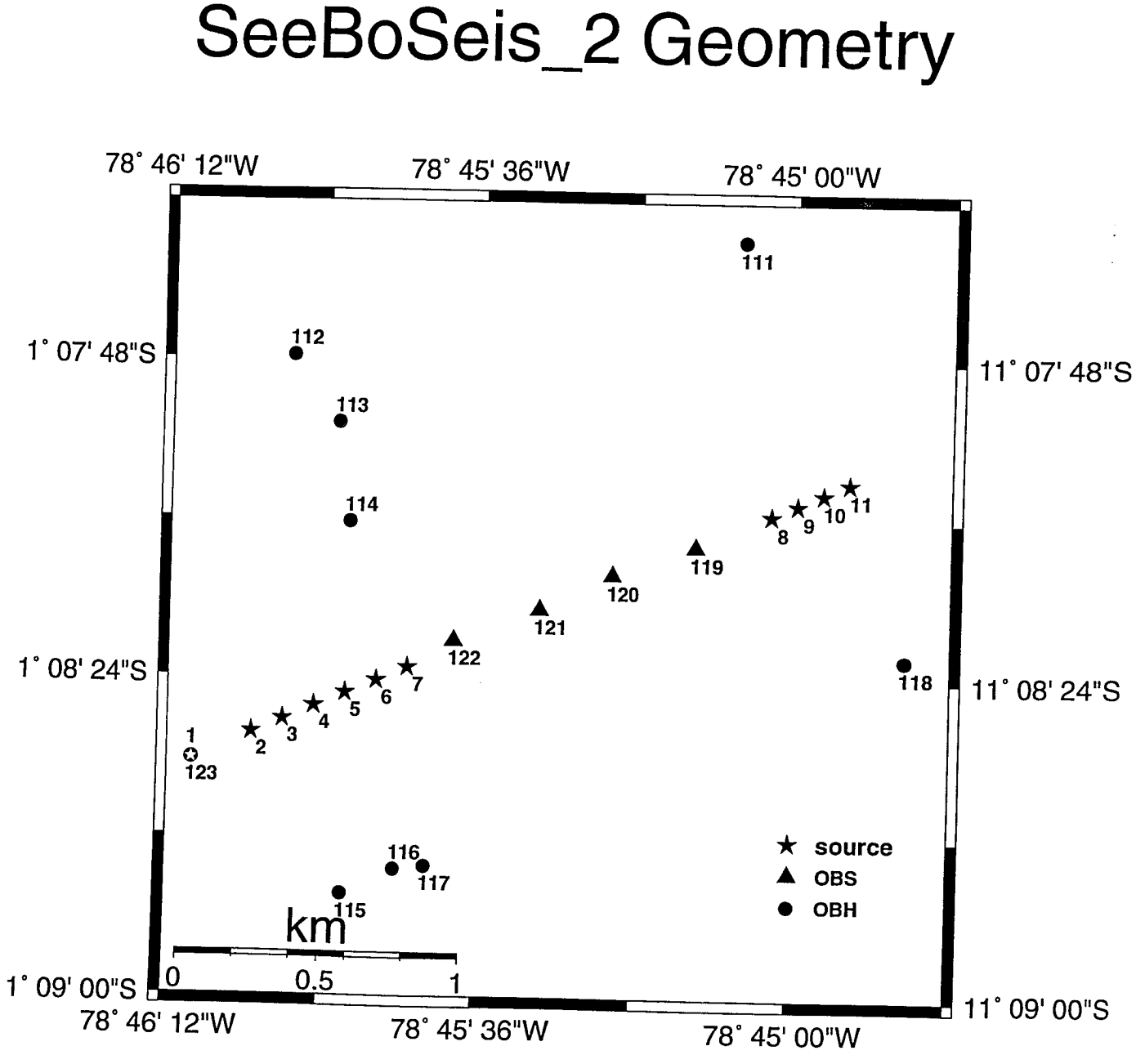

Figure 9.3.6 SeeBoSeis_2: sources and receivers

9.4 Parasound

(C. Hübscher and Shipboard Scientific Party)

The several Parasound sections presented in this report have been selected to give an overview of the quality and scientific usefulness of this kind of data. All depth values have been computed from traveltimes and an assumed constant travel velocity of 1500 m/s. Each bar at the bottom of a section corresponds to a length of 1 km. Since different scales have been used, the vertical exaggerations are different for every section. The data is plotted time sequentially from the left to the right.

On the shelf upslope of the Lima Basin, parallel reflector units are apparently disrupted by acoustic blanking (Fig. 9.4.1). This characteristic is well known (e.g., the Amazon shelf) in areas where gas is absorbing the seismic energy. The upper boundary of the blanked zones is not a lithological horizon, but results rather from bacteria which reduce methane. The presence of these methane consuming bacterium prevent gas from migrating further upward, and therefor halt the upward extension of the acoustic blanking. The SE Lima Basin is delimited downslope by a morphological high with landward dipping layers (Fig. 9.4.2). At a waterdepth of about 1000 m, line HH00-027 which runs parallel to the slope, elucidates the erosional seafloor with slumps resting above (Fig. 9.4.3). The topographic highs further downslope on line HH00-065 may represent gravity transported sediment blocks (slides), however it is also possible that these features are contourites (Fig. 9.4.4). A more steplike erosional surface characterizes the area of line HH00-070 (Fig. 9.4.5).

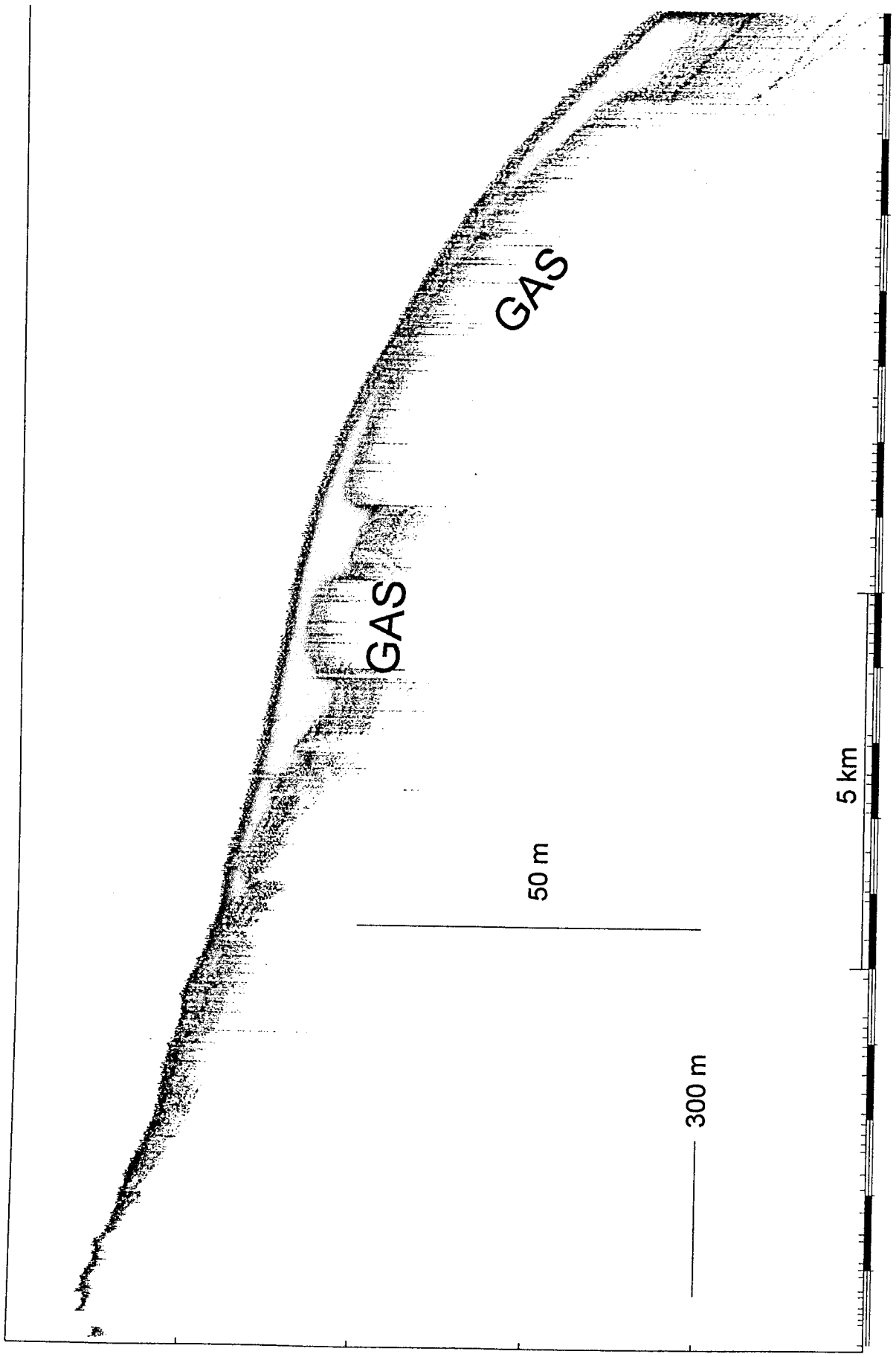

Fig. 9.4.1: Acoustic blanking at the shelf of Lima Basin.

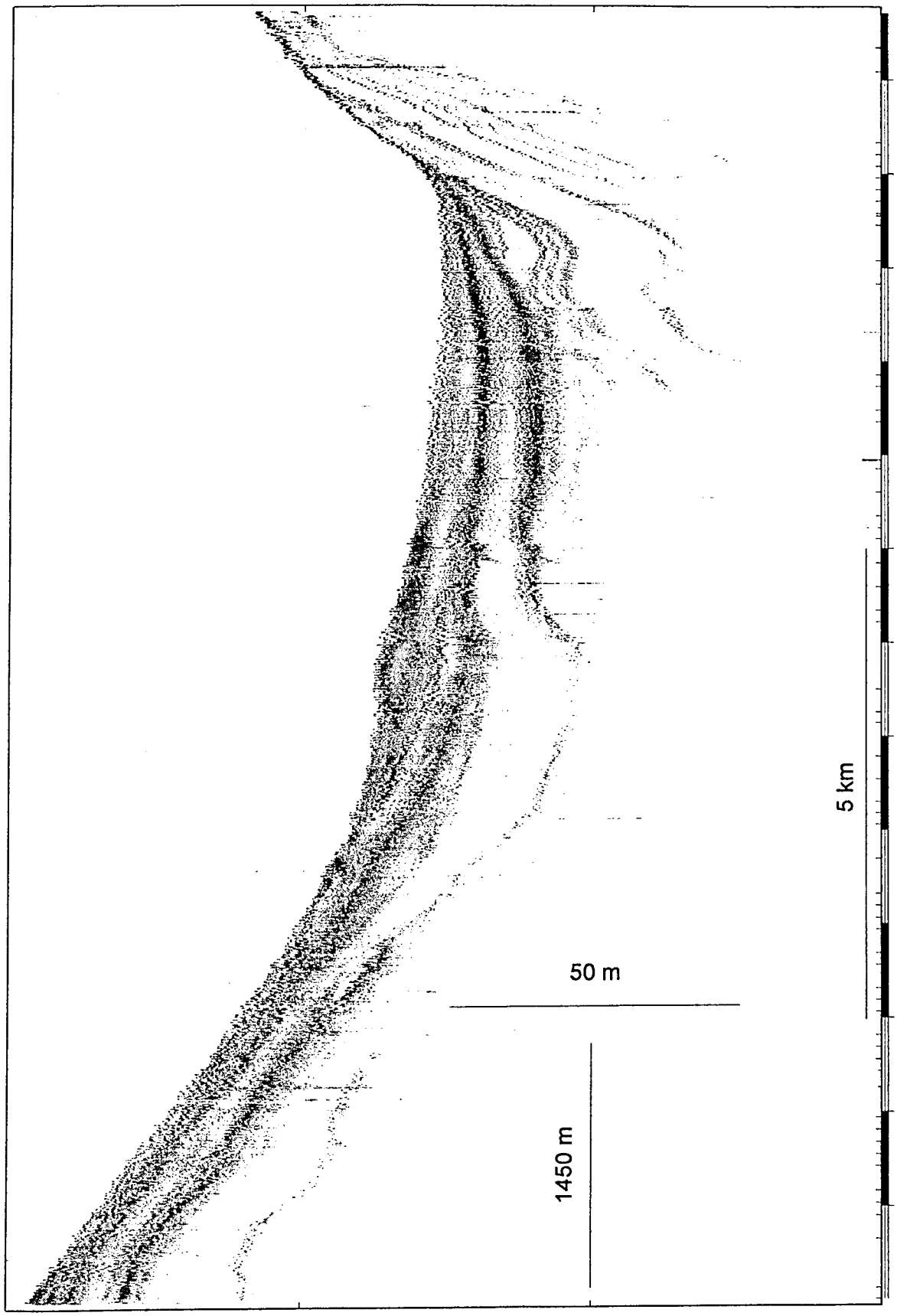

Fig. 9.4.2: Deposits in SE Lima Basin

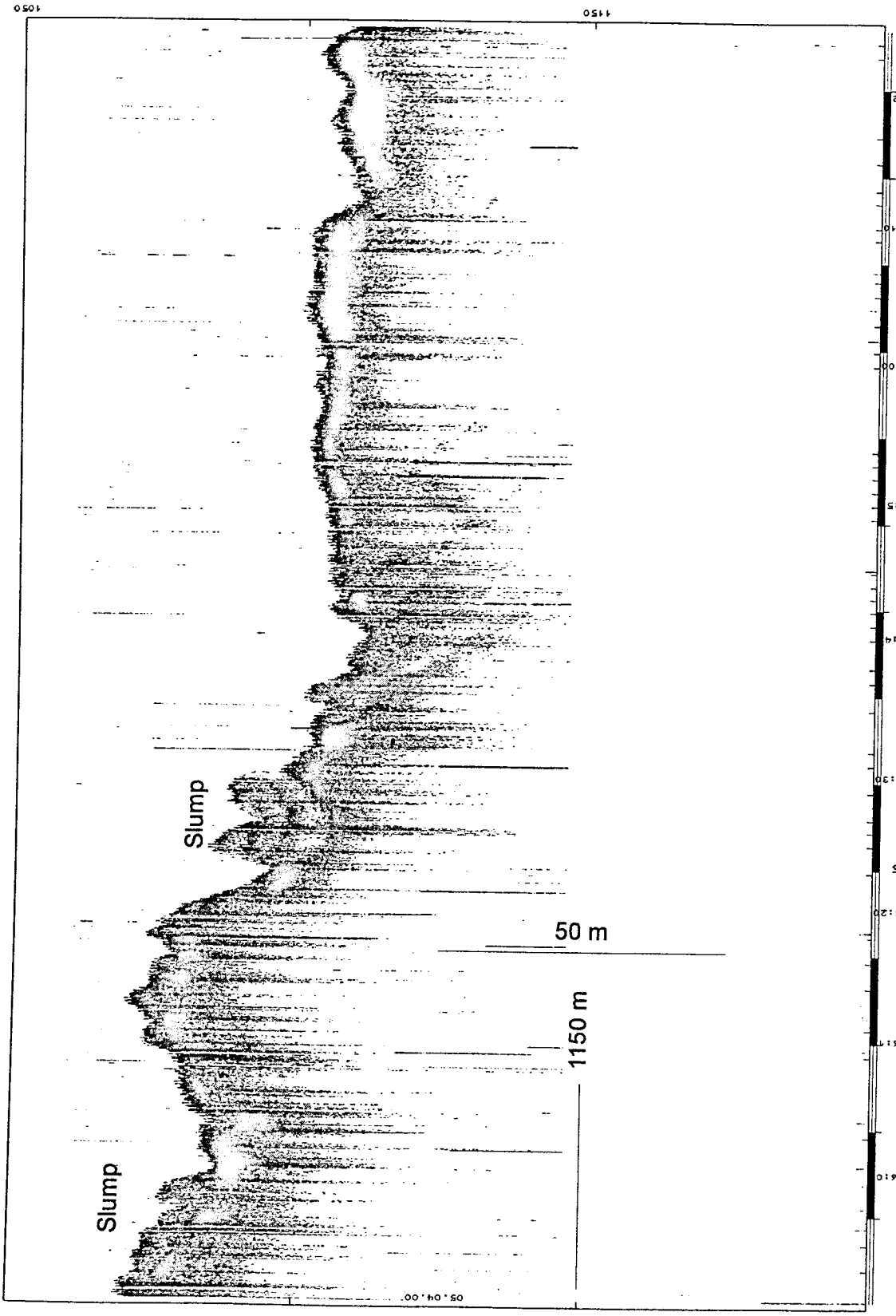

Fig. 9.4.3. The Parasound data from line HH00-027 shows an erosional seafloor with slumps.

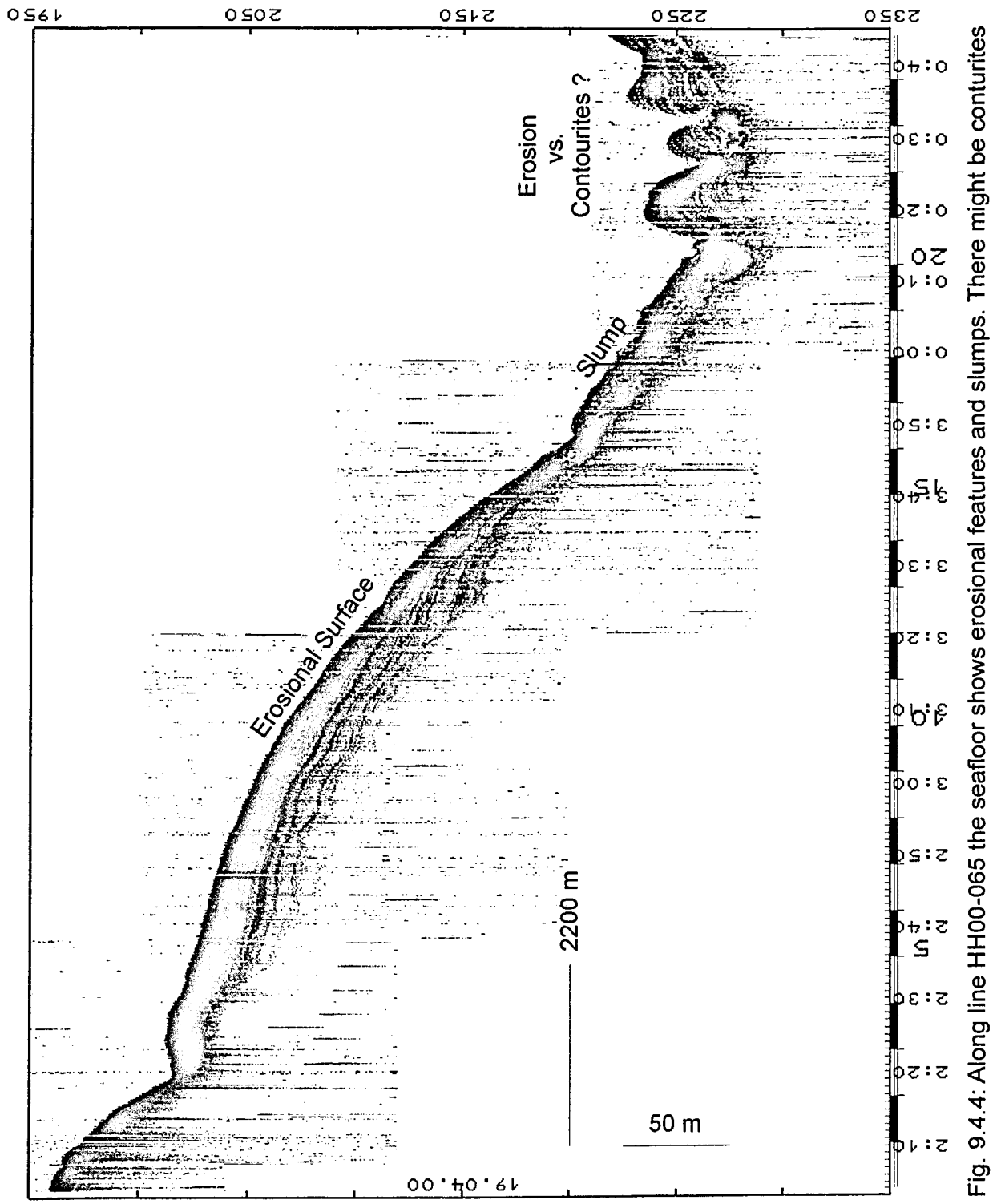

Fig. 9.4.4: Along line HH00-065 the seafloor shows erosional features and slumps. There might be conturites in a waterdepth of 2250 m.

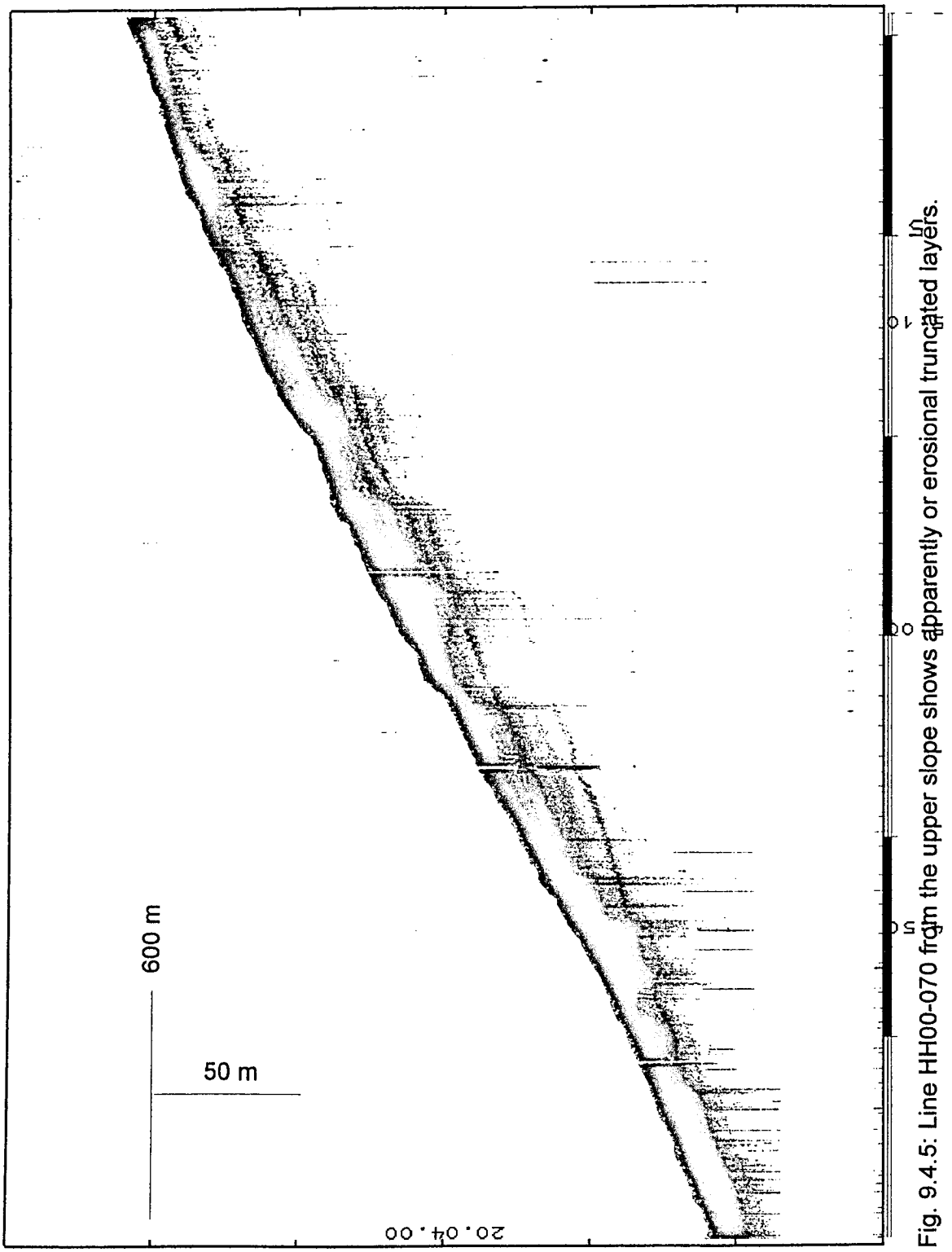

Fig. 9.4.5: Line HH00-070 from the upper slope shows apparently or erosional truncated layers.

9.5 Lima Basin

(N. Kukowski, J. Bohnert, K. Huhn)

In the Lima working area, while we did not complete systematic mapping, through intensive seismic work and several transits we came close to covering the area between 11°S and 12°S (Figure 9.5.1, 9.5.2). SeaMarc II data acquired in preparation for ODP Leg 112 will be used to supplement the bathymetric map in some areas.

The topography of the oceanic plate is much more subdued here than along the Yaquina transect. However, trench parallel linear features are observed here. The lower slope is remarkable steep and variable morphology at a local scale. However, the steep part of the slope only extends to the 4000m isobath, where an adjacent terrace dips gently towards the coast. One exception is a prominent step at water depths between 3500 m and 3000 m. The upslope edge of the central part of Lima Basin is marked by the 2000 m isobath which shows a significant curvature surrounding a depression.

To the north, in the surveyed area, our transits demonstrate that the lower slope becomes steeper and steeper towards the north and the terrace narrows. Therefore, we suggest that the Peruvian continental slope is characterized by a very steep and variable lower slope consistent with the structural images obtained from the wide angle seismics and in agreement with mechanical concepts.

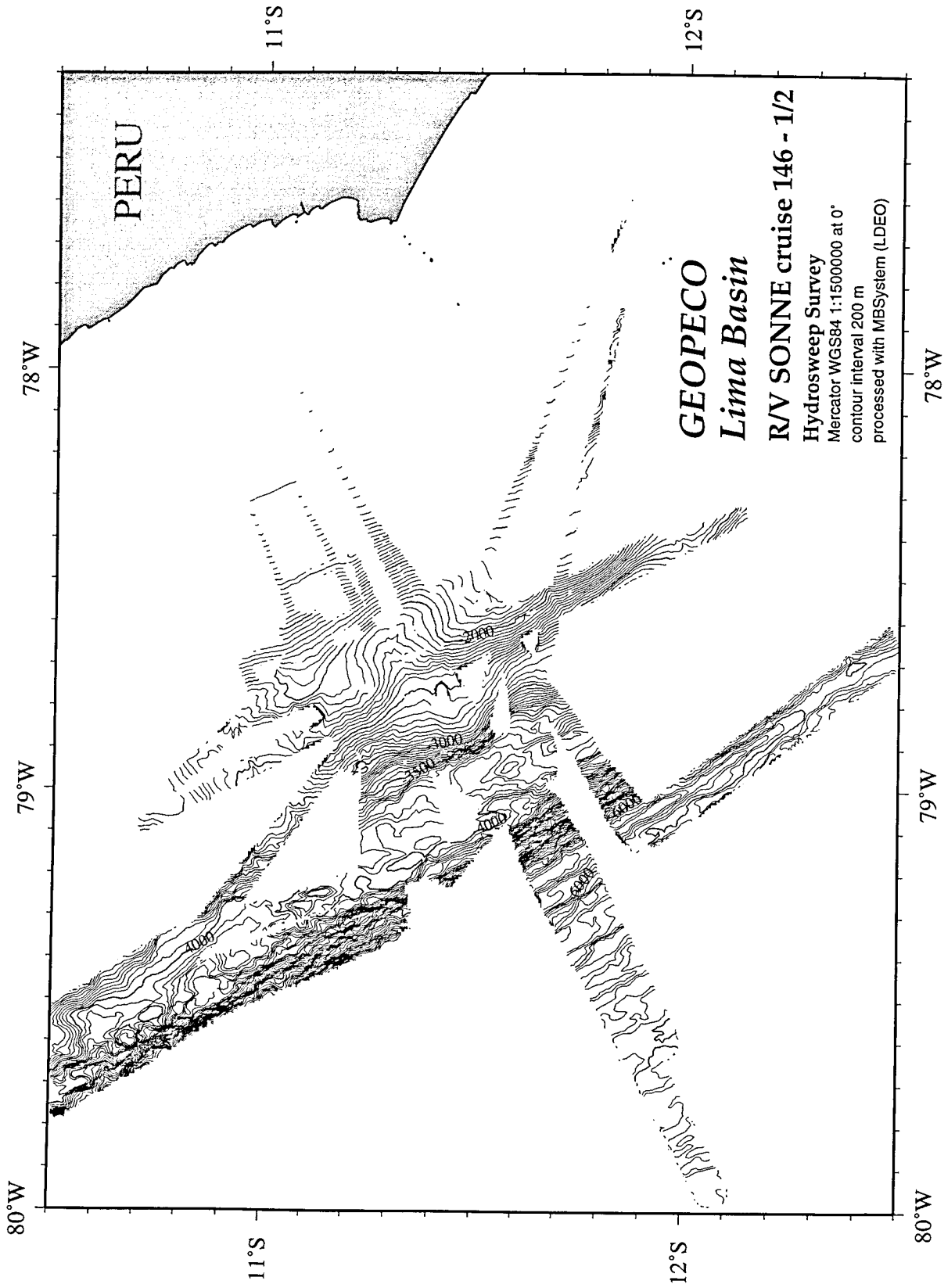

Figure 9.5.1: Bathymetric map of the Lima Basin reccorded during SO 146 - 1/2 (contour interval 200m).

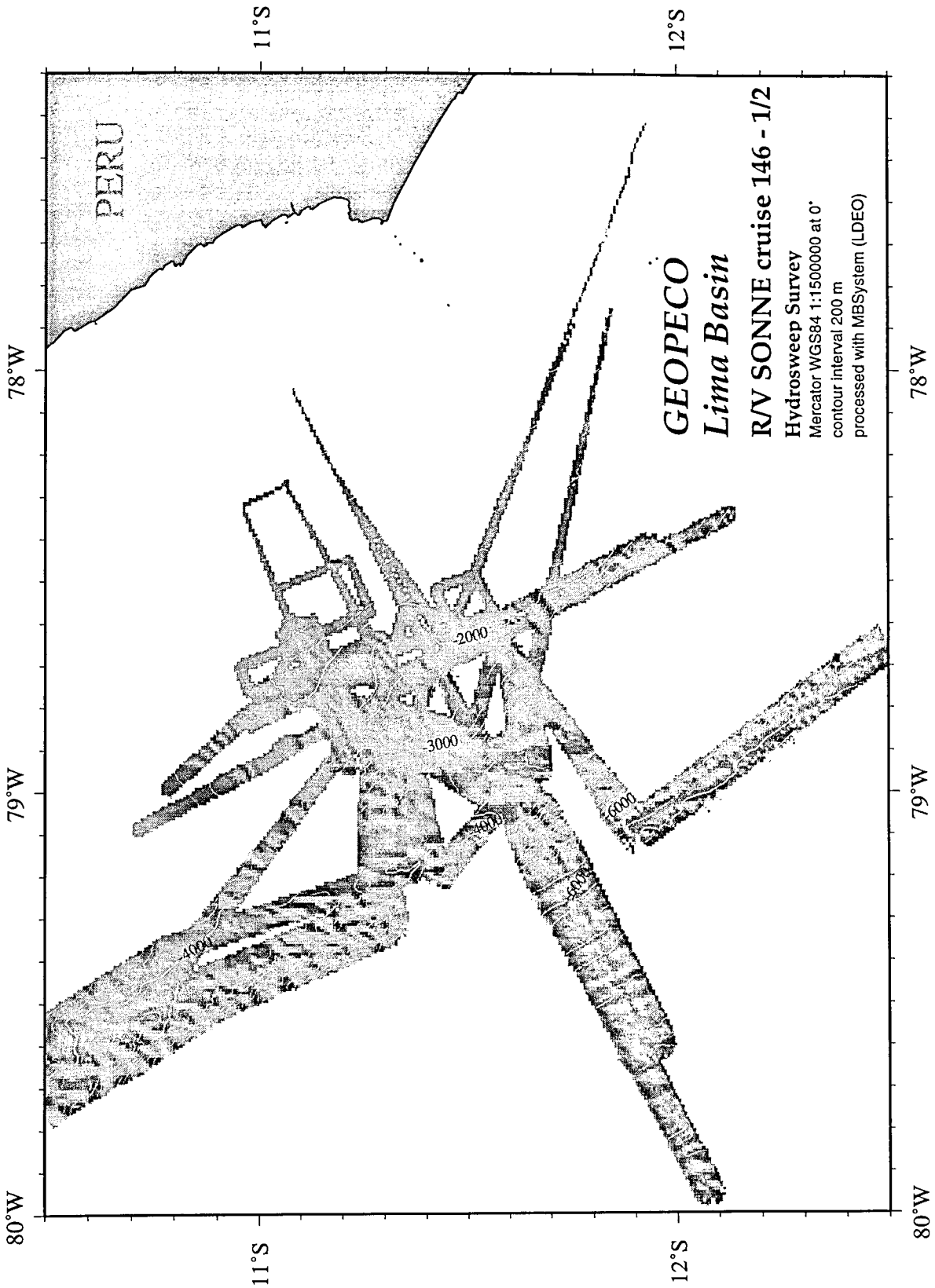

Figure 9.5.2: Bathymetry of the Lima Basin (isobath spacing).

9.6 Gravity and Magnetics in the Lima Transect

(G. A. Dehghani, R. Heinbockel)

The Free-air anomaly map of the Lima Basin (Figure 9.6.1) was produced using all measured gravity profiles in this area. The positions of all available ODP sites are plotted as white circles. This map was produced using the GMT software package.

The Free-air anomaly field has values between –180 and 40 mGal. A large negative Free-air anomaly associated with the trench dominates this map. The maximum gradient of the gravity anomaly is located over the seaward and landward wall of the trench.

The gravity anomaly in the Lima Basin is oriented mostly parallel to the trench axis. This indicates, contrary to the Yaquina Basin, that tectonics in the Lima Basin show no significant irregularities. The Free-air anomaly in the western part of the map increases from –140 to 40 mGal and represents the transition to typical oceanic.

A preliminary magnetic residual anomaly along Profile 5c in the Lima Basin (NE-SW direction, 225 km) is presented (Figure 9.6.2). The position of profile 5c is shown on the Free-air anomaly map (Figure 9.6.1). In contrast to the magnetic anomaly along profile 4c in the Yaquina Basin, the magnetic anomaly along profile 5c does not indicate significant sea floor spreading anomalies in the western part of the profile over the oceanic crust. A fairly large magnetic anomaly is observed over the continental slope, and is most probably caused by strong tectonic movement and intruded magmatic material.

Free-Air Anomaly of the Lima Basin

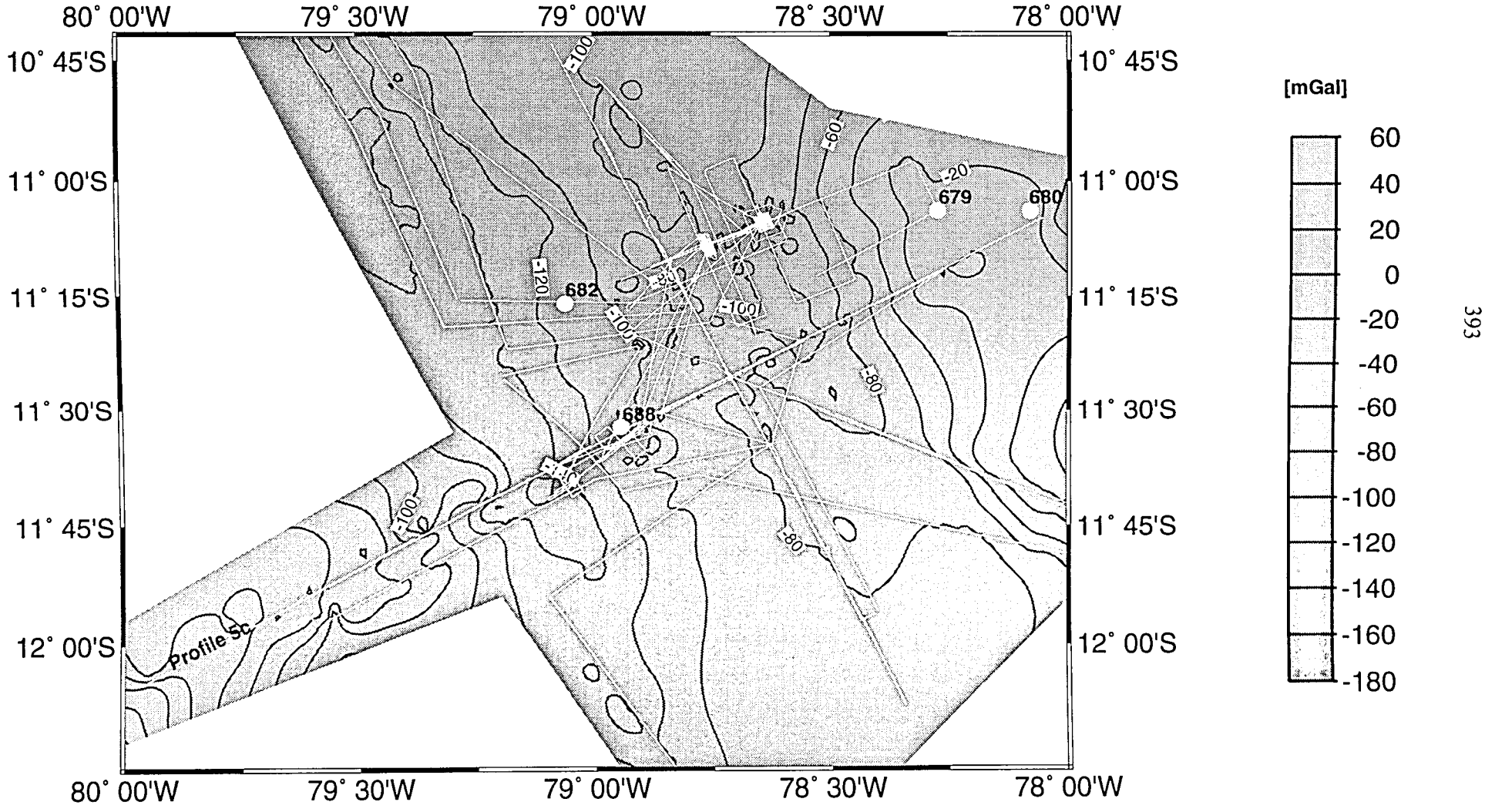

Figure 9.6.1

Magnetic Residual Anomaly Along Profile 5c in the Lima Basin (preliminary)

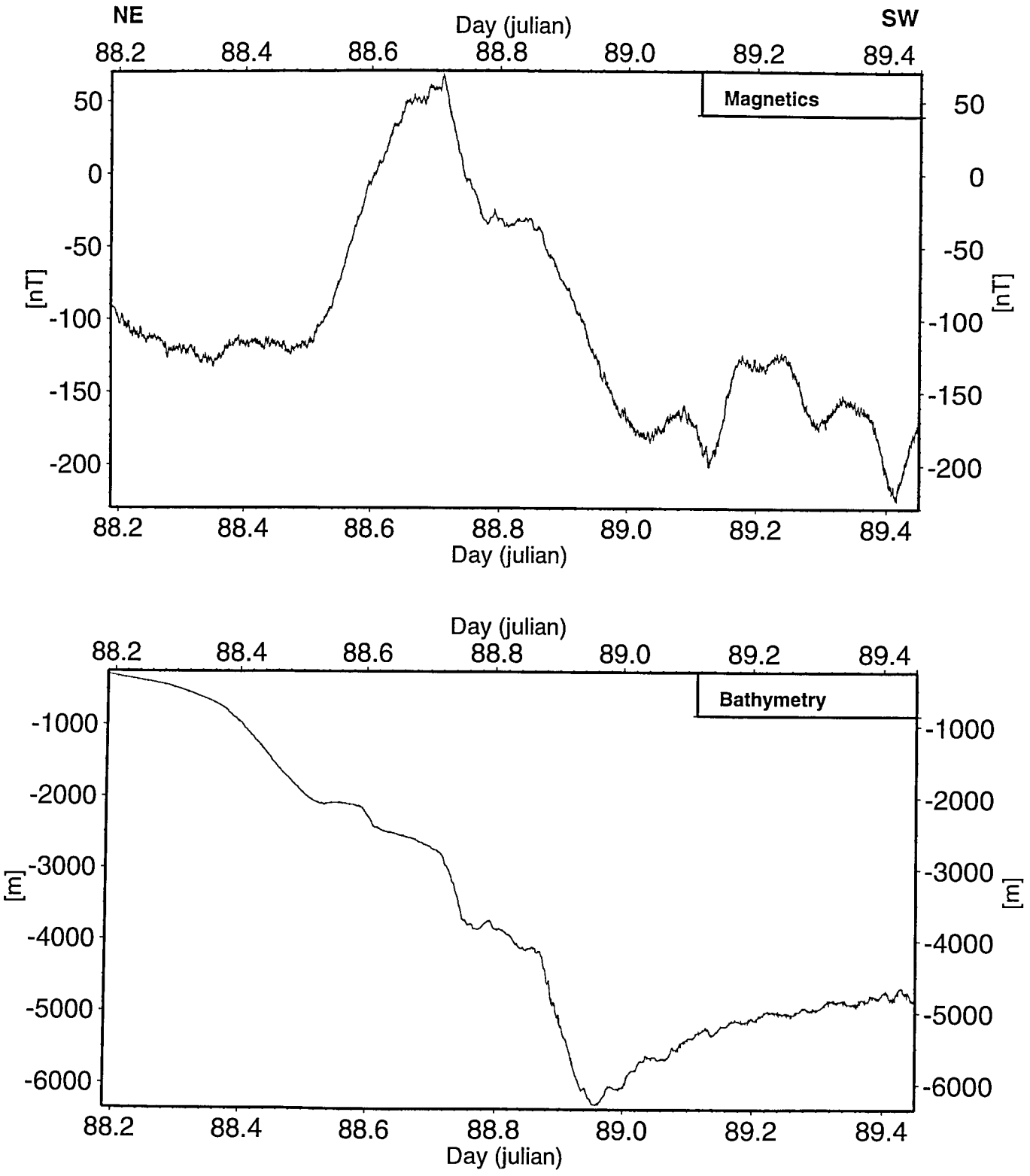

Figure 9.6.2

9.7 OFOS observations in Lima Basin an the Lima Lower Slope area

(J. Greinert, T. Nadler)

Sea floor observations in the Lima Basin were undertaken during two OFOS deployments (OFOS 5-1 and 5-2) on seismic line 26 (SO146-2). This area is known previously from HIG 13. The last OFOS track during SO146-2, OFOS 6-1 covered the Lower Slope at the Lima area along seismic line 101 (SO146-2), to observe the seafloor above 'the world strongest BSR'.

All OFOS profiles started to the SW and continued up the continental slopebecause of the wind and current conditions.

Table 9.7.1: Details to OFOS tracks in the Lima Basin and the Lower Slope area.

	ship coordinates OFOS into water and on deck	OFOS coordinates bottom sight and from bottom	time / date UTC station start / end	water depth m OFOS	line 26 / 101 shot point	
	OFOS 5-1					
start	11°08.01' S / 78°45.22' W	11°08.136' S / 78°45.240' W	17:14 / 18.04.2000	1990	(26)	768
end	11°06.16' S / 78°40.39' W	11°06.258' S / 78°40.518' W	01:37 / 19.04.2000	1810	(26)	1142
	OFOS 5-2					
start	11°09.83' S / 78°49.43' W	11°09.832' S / 78°49.357' W	04:12 / 21.04.2000	2140	(26)	452
end	11°08.04' S / 78°45.05' W	11°08.150' S / 78°45.176' W	11:52 / 21.04.2000	2008	(26)	772
	OFOS 6-1					
start	11°36.17' S / 78°58.93' W	11°36.234' S / 78°58.909' W	12:29 / 24.4.2000	3825	(101)	2802
end	11°31.66' S / 78°53.18' W	11°31.684' S / 78°53.176' W	23:23 / 24.4.2000	3545	(101)	2378

Lima Basin

OFOS 5-1 observed the area between water depths of 1990 and 1810 m where the BSR terminates on landward dipping sediment layers which crop out at the start of OFOS 5-1 (Figure 9.7.1). The area above the BSR is characterized by landward dipping layers which penetrate the BSR and induce a 'wave-like' morphology of 20 to 40 m high smooth steps at the seafloor. This feature was thought hold the highest potential for fluids transported along layers cropping out from blow the BSR.

Upon reaching the bottom during OFOS 5-1 we observed rounded massive blocks of dm to m in size covering the seafloor as single edifices or as patches of more than 10 m in length. Most of these blocks are dark at the surface but cross sections have a beige color typical of cemented sediment. In areas with a denser block coverage white spots (?) and shells are recognized between 1980 and 1940 m water depth (Figure 9.7.2). We assume the presence of *calyptogena* shells but this has to be confirmed by slides. Still speculating what kind of blocks we have had observed we investigated slab- and sheet-like crusts of several m in diameter which build a hard layer just below the sediment surface (1900 - 1880 m water depth).

These features are typical for a carbonate cementation of the sediment just below the surface induced by the diffuse expulsion of methane-rich fluids. This observation leads to the interpretation that the blocks are 'methane-derived diagentic' carbonates formed by a concretion like growth within the sediment column and exposed at the seafloor by sediment erosion. Similar blocks and slabs are well known from the Hydrate Ridge at the Oregon margin. Here they are related to upward migrating methane rich fluids proved by there $\delta^{13}C$ isotopic composition (e.g. Greinert et al., in review). The unintentional sampling of one small piece of these blocks with the heat flow equipment (see chapter 11) supports the assumption of carbonate cemented sediment.

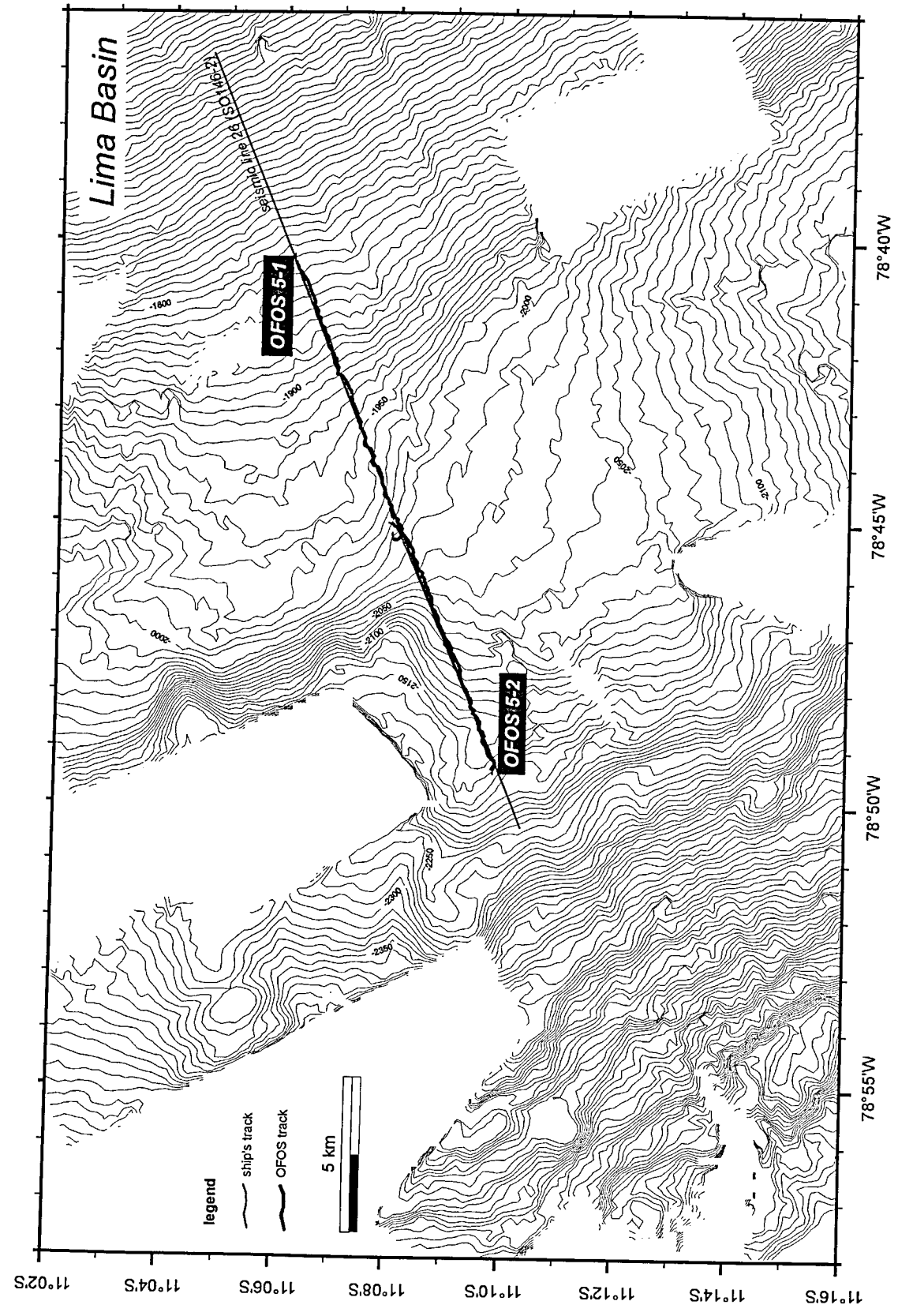

Figure 9.7.1: Bathymetric map with OFOS tracks in the Lima Basin.

OFOS 5-2 showed some similar blocks at the beginning of the track (Figure 9.7.2). Unfortunately the seafloor between 2120 and 2040 m water depth does not indicate signs of fluid venting or geological features which can be used for tectonical interpretations.

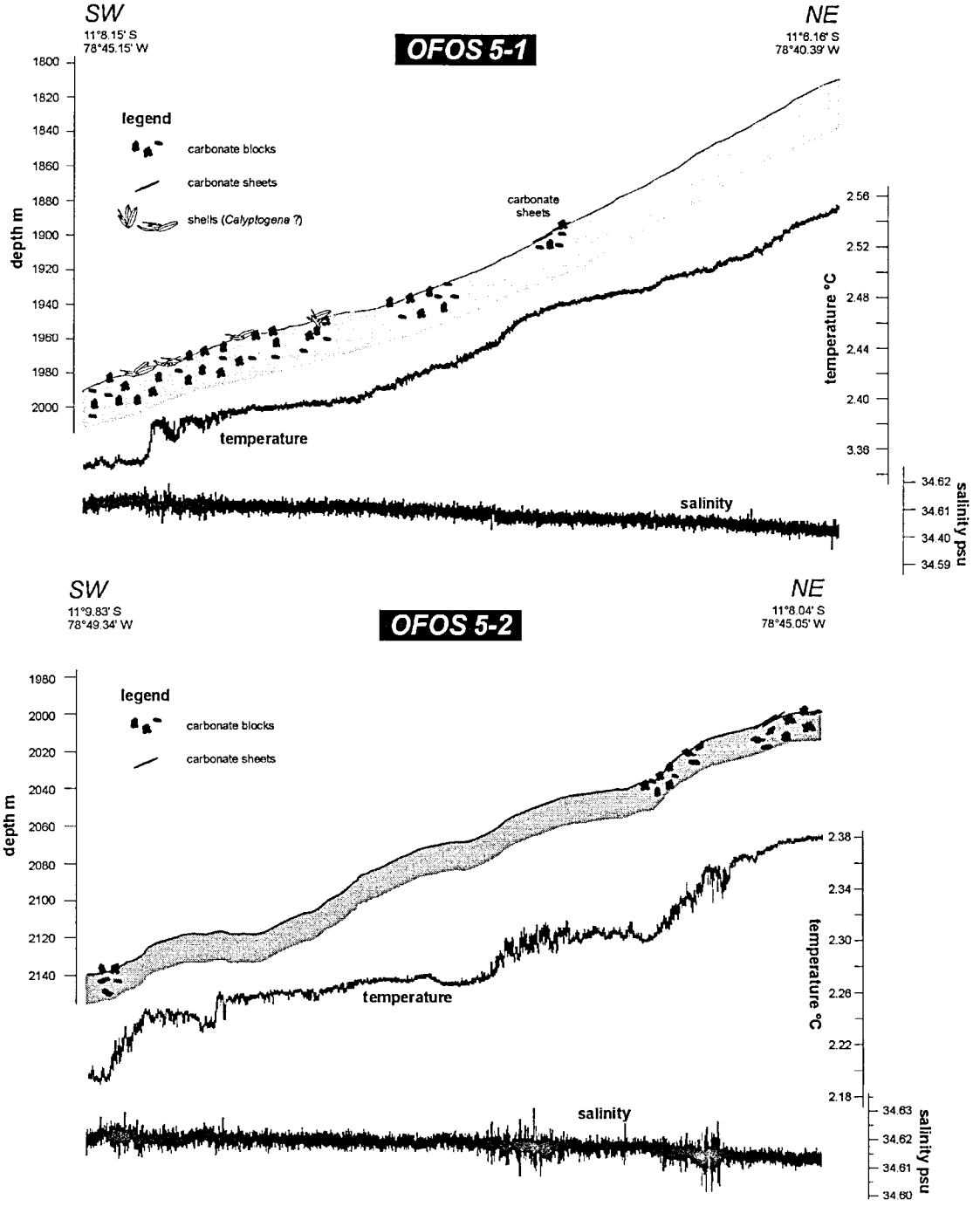

Figure 9.7.2: Depth profiles of OFOS 5-1 and 5-2.

Lima Lower Slope

Only one OFOS track could be completed at the Lima Lower Slope area because of winch and cable problems at the end of the cruise. OFOS 6-1 investigated the seafloor between 3825 and 3550 m water depth slightly south of the seismic line 101 from SO146-2 (Figure 9.7.3).

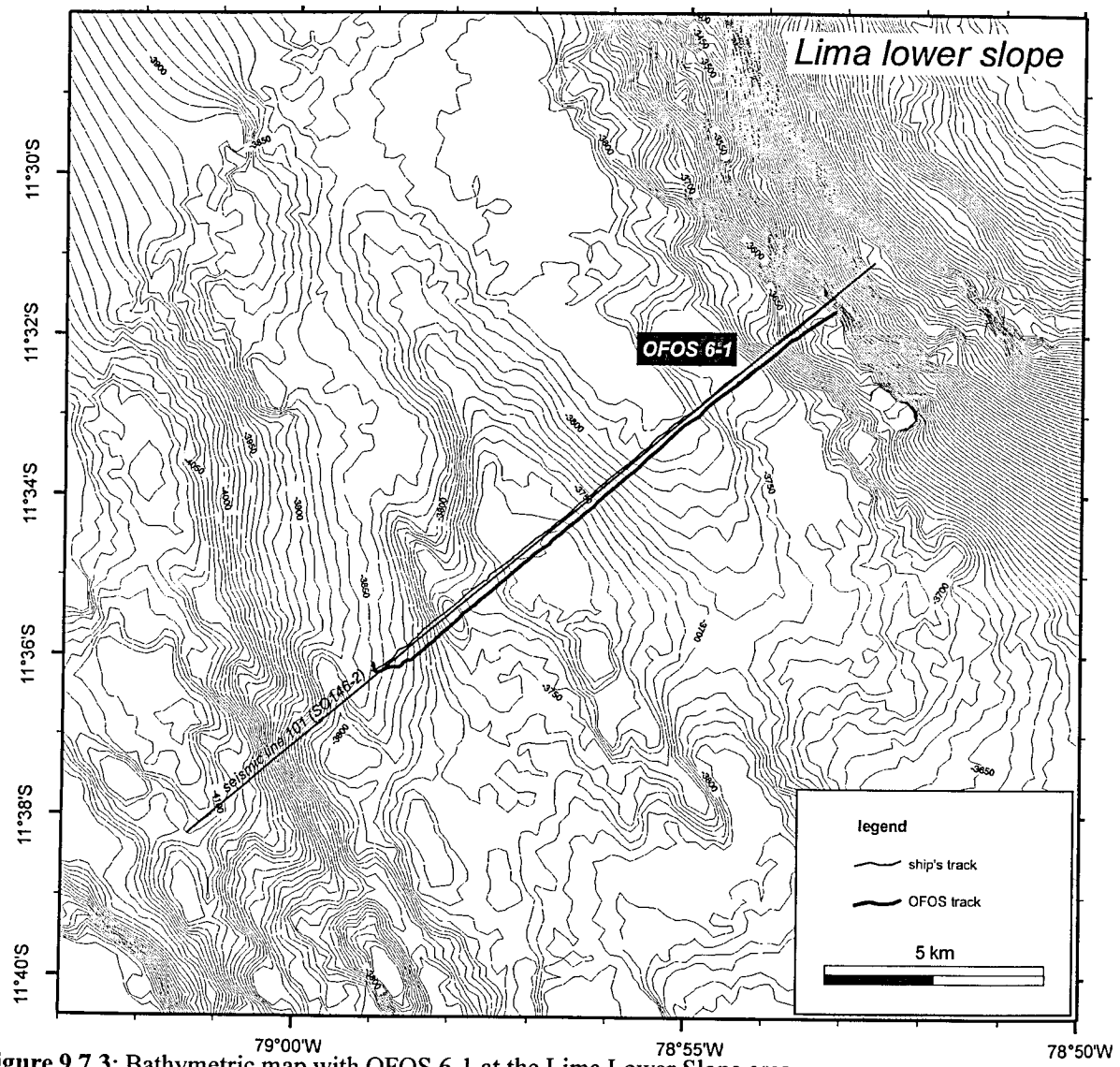

Figure 9.7.3: Bathymetric map with OFOS 6-1 at the Lima Lower Slope area.

Starting at a smooth rising flank, the seafloor consists of soft sediment with significantly less benthic organisms and may be due to the great water depth here. Dark, irregular patches of approximately 1 m in diameter and with lighter spots of bioturbation burrows were observed. The reason for this occurrence of likely stronger reducing conditions is unknown. A possible explanation are slow migrating fluids but 'normal' diagenetic processes without any relation to fluid venting are reasonable too.

Climbing upward, talus blocks of outcropping 'basement' were seen at the foot of a 50 m high pinnacle-like summit (Figure 9.7.4). Before we passed the top of this summit we thought we observed a single clam

shell, but this has yet to be confirmed. The 'basement' is slightly covered with soft sediment, showed no sedimentary bed cropping out or other features allowing a more sophisticated classification of these rock. Clear signs of venting could be observed at the top of the smooth summit between 3690 and 3650 m water depth just above the BSR given by the distributed occurrence of *calyptogena* shells and patches of them as well as the observation of two living individuals.

As expected, the downward going flank of this summit and the sediment filled basin in the NE showed no signs of fluid venting or other gas hydrate signs.

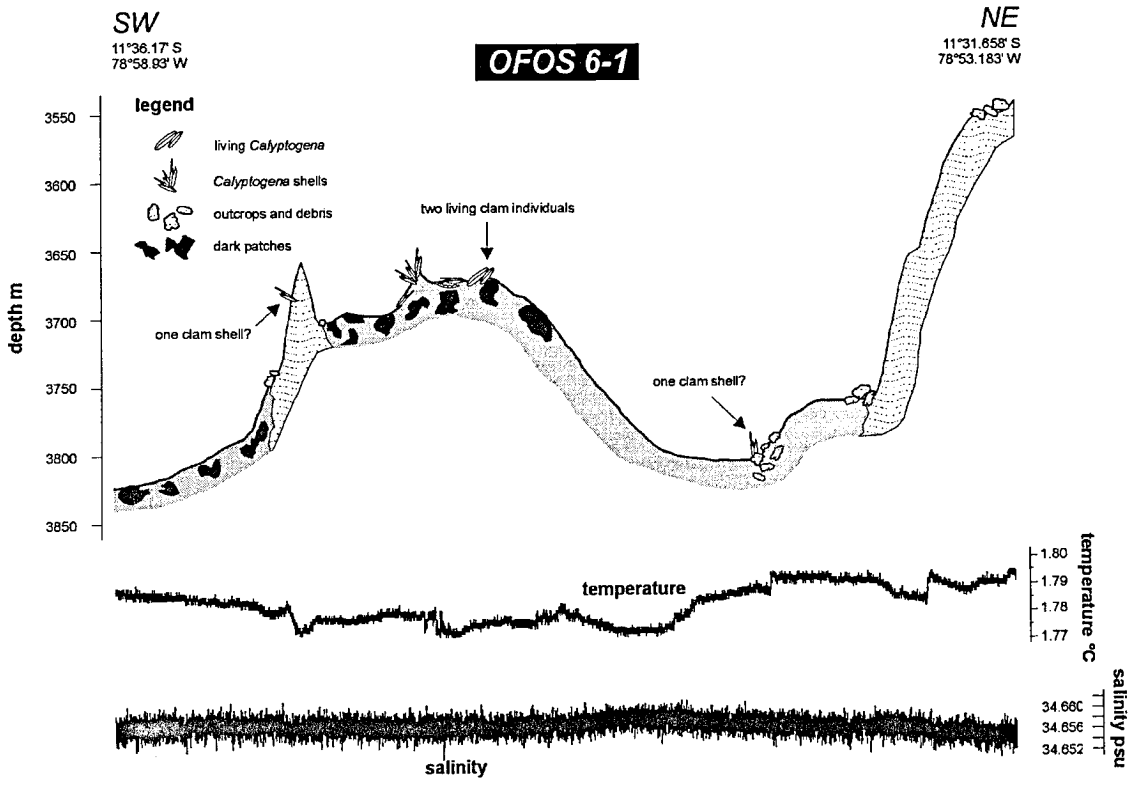

Figure 9.7.4: Depth profile of OFOS 6-1.

At the foot of the first 'step' we observed talus blocks and debris from the 'basement' edifice. They appear similar to those of the 'pinnacle-summit'. Again we may have observed a single clam shell before we started to climb upward along the sediment covered first step. At the edge of the last steep rising flank, consisting of sediment covered 'basement', we observed some debris fields before we climbed up to a small plateau in 3550 m water depth.

Even if no active and densely populated cold vent sites were observed, the investigation of clam shells at the top region of the smooth summit above the BSR clearly indicate the general occurrence of expulsion H_2S-rich fluids. Based on cold vents observations at the EDGE area (Aleutian accretionary prism; Suess et al., 1998; Greinert, 1999) we assume that active cold vents would be discovered by further OFOS tracks in this region.

9.8 Heat flow

Seismic line HIG 13 forms the basis for investigations in Lima basin. During this survey, seismic line 26 was acquired next to HIG 13 and across proposed ODP drill sites P1, P2 and P3-a. The target of this investigation is a BSR with a very large reflection amplitude, the strongest ever observed. This BSR can be traced for approximately 12 km, but farther downslope it vanishes abruptly. In upslope direction a sediment sequence with high reflectivity dominates the picture, resulting in an undetectable BSR.

Heat flow stations HF0024 and HF0025 are located across the lower and upper end of the BSR to observe the transition between zones of different BSR occurrence (figure 9.8.1).

Visual inspections of the seafloor was carried out ahead of heat flow station work (OFOS section 9.7). From video observations, an abundant occurrence of rocks and rocky coverage, inferred as carbonates, was observed.

As a consequence, these stations had the least success with six penetrations out of 15 attempts. Results are summarised in figures 9.8.2c and 9.8.3c. Just one penetration of station HF0024 gave a value of 59 mW/m^2 beyond the lower end of the observable BSR. Five values were determined upslope of the BSR yielding constantly values of 36.4 ± 2.6 mW/m^2. No heat flow values could be achieved over the BSR.

One sample stone was recovered during heat flow operation. This sample was identified as carbonate.

Thermal conductivity along stations HF0024 and HF0025 range from 1.1 to 0.9 W/m*K with a spatial trend (see figures 9.8.2b and 9.8.3b). Thermal conductivity decreases as the lateral distance to the BSR increases indicating a correlation between carbonate content, possibility of penetration and conductivity.

In contrast to stations HF0020 – HF0022 seismic profile 26 across Lima basin shows no indications for faulting. If degassing of Methane and Hydrogensulfide (H_2S) occurs on this profile, as indicated by carbonates and biological activity, it is likely diffusive. Increased heat flow due to convection is not suggested by the data.

Heat flow station HF0026 is located some 30 km south of Lima basin on the Lima lower slope. This location was chosen on seismic line 101 in the vicinity of ODP site 688 (figure 9.8.4). The station resembles the transition between BSR (shotpoint no > 2570) and undetectable BSR (shotpoint no < 2550). Heat flow values indicate a slowly varying trend between 42 and 55 mW/m^2 with a mean value of 48.8 ± 4.5 mW/m^2 (figure 9.8.5c). A topographic effect due to bathymetric changes of 150 m has to be considered. In this preliminary interpretation no correlation between the change in BSR occurrence and heat flow can be observed.

Thermal conductivity yields values of 0.87 W/m*K throughout the profile (figure 9.8.5b).

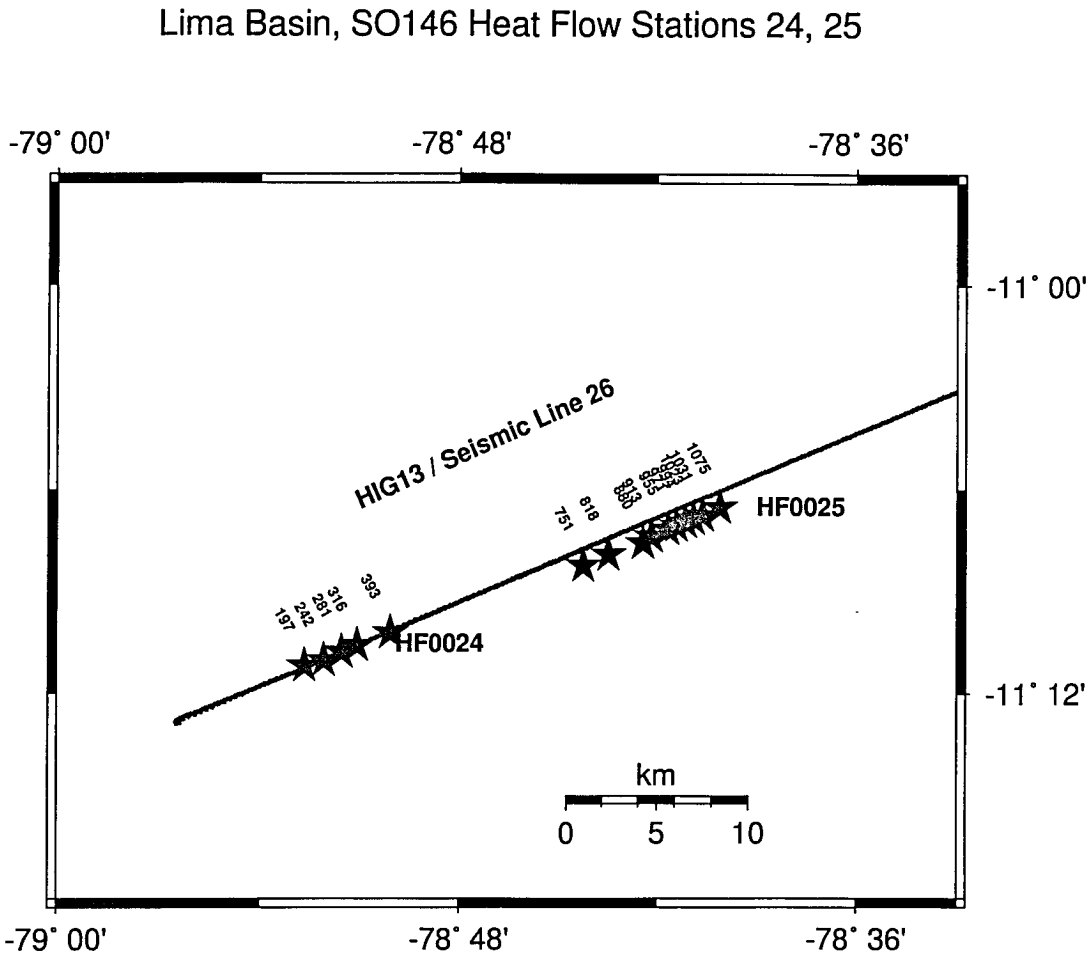

Figure 9.8.1: Location map of heat flow stations HF0024 - HF0025.

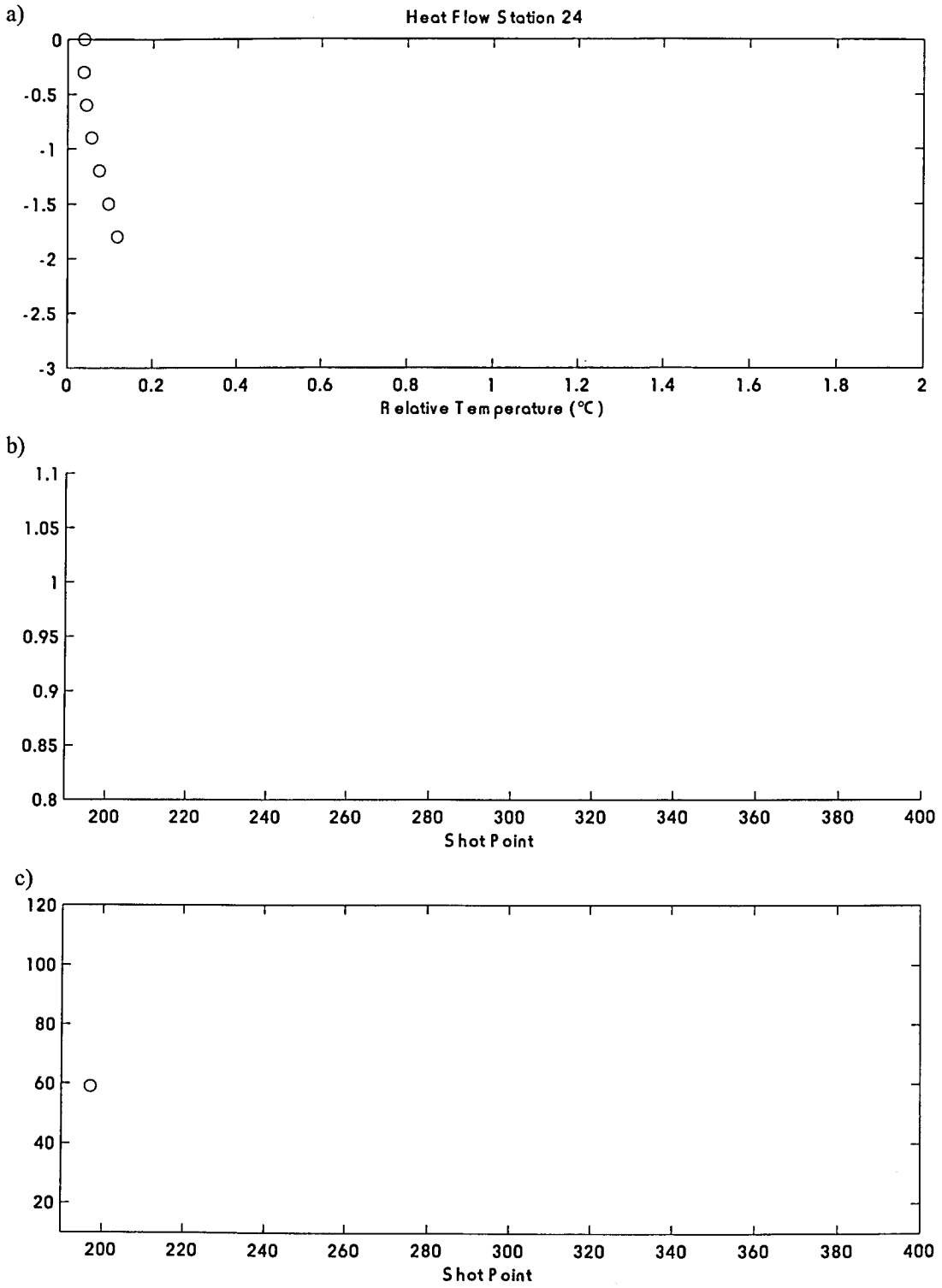

Figure 9.8.2: Results of heat flow station HF0024. Top: relative temperatures T(z), middle: vertical mean thermal conductivities, bottom: heat flow values plotted along seismic profile 26. Horizontal axis represents shot point numbers.. Just one out of five attempts succeeded with a penetration.

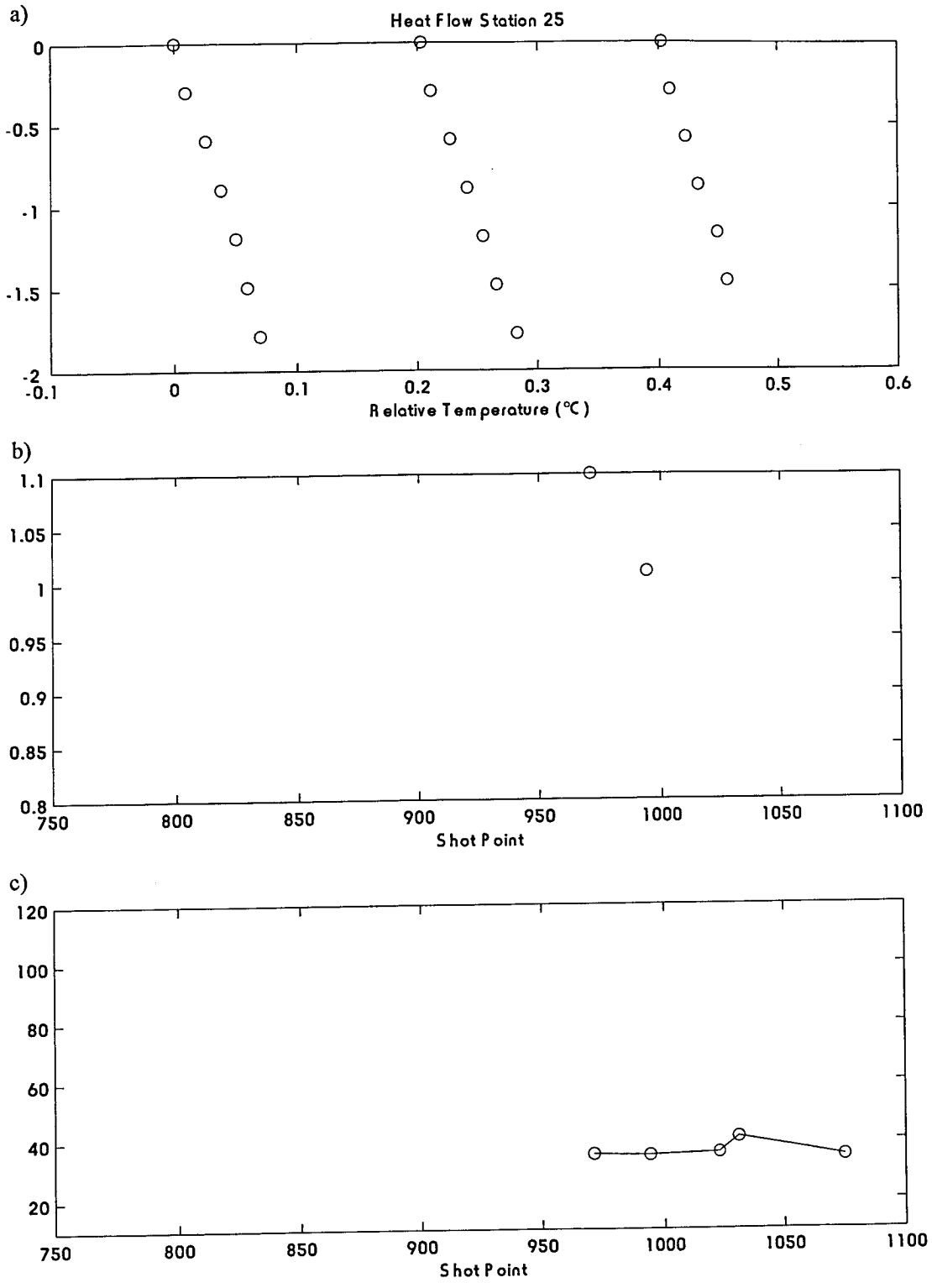

Figure 9.8.3: Results of heat flow station HF0025. Top: relative temperatures T(z), middle: vertical mean thermal conductivities, bottom: heat flow values plotted along seismic profile 26. Horizontal axis represents shot point numbers. Five out of ten attempts succeeded.

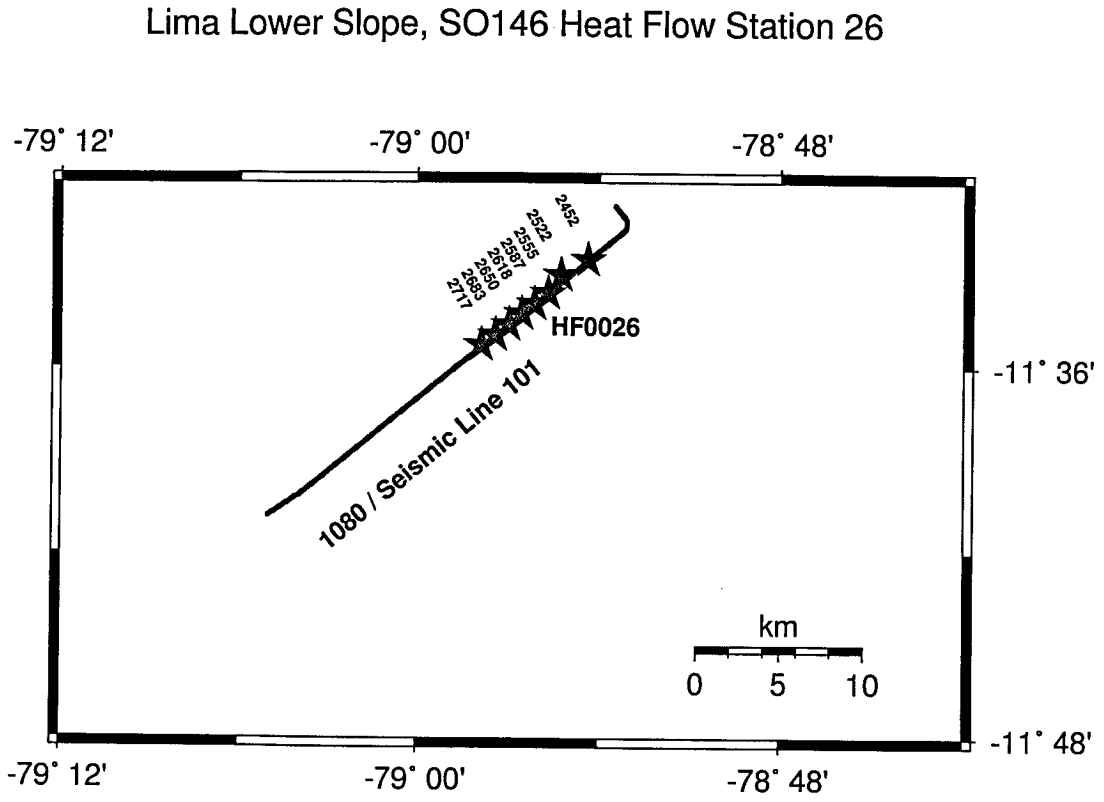

Figure 9.8.4: Location map of heat flow stations HF0026.

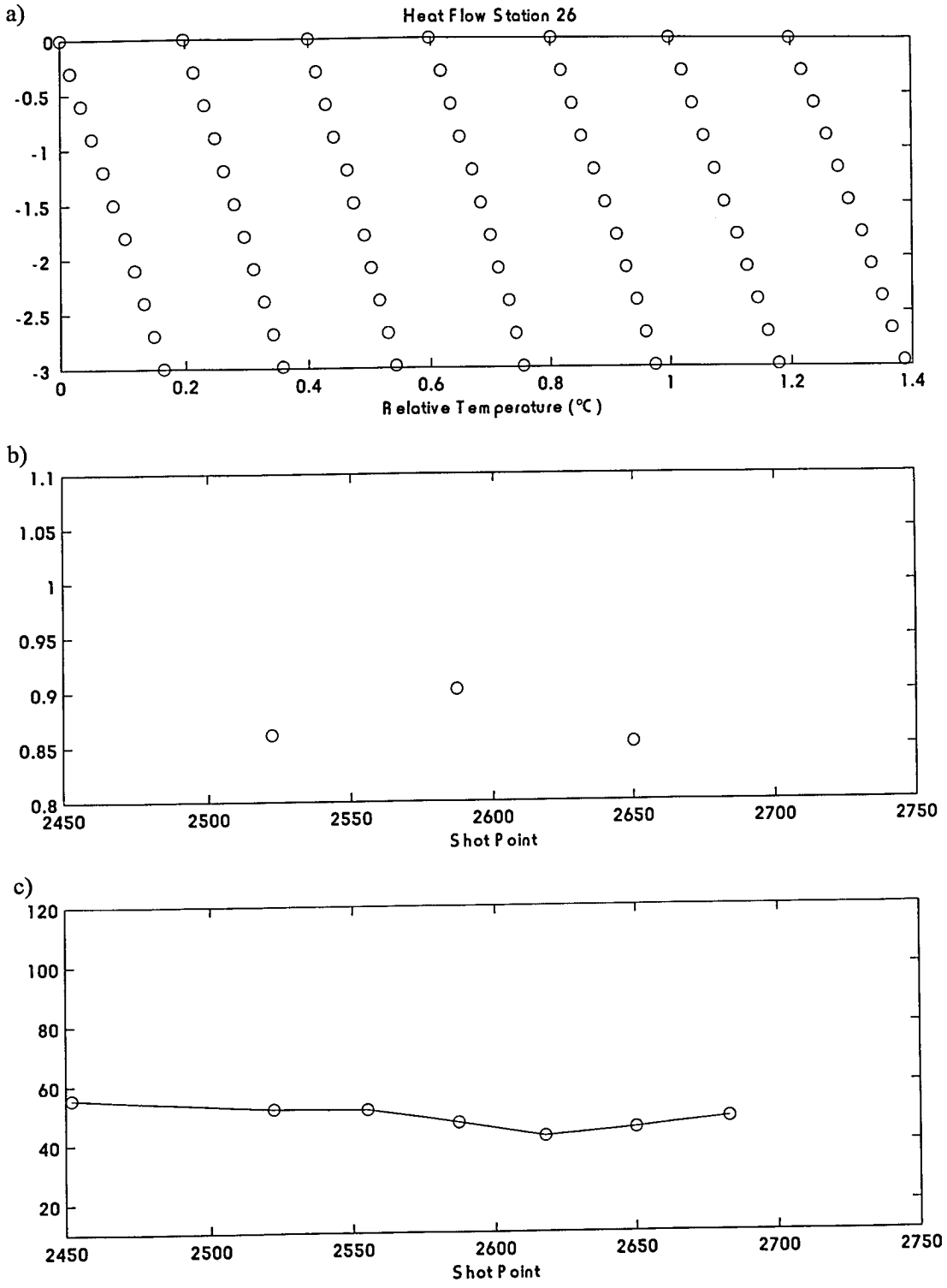

Figure 9.8.5: Results of heat flow station HF0026. Top: relative temperatures T(z), middle: vertical mean thermal conductivities, bottom: heat flow values plotted along seismic profile 101 across the Lima lower slope. Horizontal axis represents shot point numbers.

10. Observation of Natural Seismicity

(H. Letz, J. Bialas, E. Norabuena)

The Peruvian continental margin is characterized by high seismicity caused by the Nazca Plate subducting beneath the South American Plate. In the past, large earthquakes have led to massive destruction and loss of life. The most recent earthquake occurred in February 1996 had a magnitude of Mw 7.5 and was associated with a strong tsunami with measured run-up heights of about 1 – 5 meters along a coastline of 400 km (Heinrich et al., 1998).

To investigate the natural seismicity of the offshore research area, we installed a network of temporary stations, 'SEISMIO 1', at the margin of the Lima Basin. On 15 – 16 March, three OBS and two OBH were deployed. The array shaped like a 'cross' was evenly spaced with an interval of 18.8 km around the center station, OBS 39 (Figure 10.1). The distance between the coast and OBS 39 was approximately 118 km. The OBS and OBH equipment was retrieved on 27 March, after having been in operation at site for about twelve days. A summary of deployment details is given in Appendix VIII.

While the instruments where listening for earthquake events SONNE returned to Yaquina basin. Due to the exiting data retrieved there the working time was expanded and the instrument recovery was delayed. As batteries ran out meanwhile the amount of data recorded by each instrument differed slightly. While OBS 38, OBS 39 and OBS 40 recorded about 87 hours of data, the last instrument retrieved, OBH 37, recorded 153 hours. OBH 41 was returned with just 2.05 hours of data that contained not a single event. Over the period of deployment timing errors (skew) of the data-loggers ranged between 15ms and –22ms. The drift of the internal time-base is within limits for seismological applications. For a first inspection the data were converted into PASSCAL formatted data streams only. Cutout of time windows by use of program DIV (chapter 4.9.1) sets of time series were created at regular intervals which allowed to display all samples within SEG-Y format. By this all station recordings were visually checked for possible events. Automatic detection analysis will follow later on making use of dedicated software available from earlier seismological studies during CINCA cruise off Chile (Husen et al., 1999).

With exception of a few minor glitches, the quality of the data is generally good. All hydrophone channels recorded earthquakes but at a constantly changing background noise level (in amplitude and frequency) increasing or decreasing in periods that lasted for hours. Preferred channels to search for earthquakes were the horizontal components of the OBSs at channel 2, 3 and the vertical component at channel 4. However, numerous free oscillations of about 10 seconds duration were detected on the OBS 40's horizontal components, perhaps due to a misalignment of the seismometer at the ocean floor. The vertical component of OBS 39 produced a very weak signal throughout the entire length of recording, leaving only the horizontal channels for picking earthquakes. Channel 2,3, and 4 of OBS 38 were strongly attenuated so that channel 1 was used to screen for events, making it difficult to identify and pick S-phases. A common observation with regard to all three component seismometers was the presence of a notable 'DC' offset. OBH 37 recorded a few small local events. Unfortunately, these earthquakes have only been recorded at one or two stations within the array, thus making it impossible to locate them. Earthquakes picked on OBH 37 – OBS 40 are presented in chronological order in Appendix VIII. Seven earthquakes have been located. The Data presented in Table 10.1 is preliminary.

Four hypocenters are located beneath the Andes mountains at depths between 37 km to 43 km (Figure 10.2). Three earthquakes are located closer to the array: These events are (a) 16th March, 0720 UTC, at a distance of 80 km SE and a focal depth of 27 km; (b) 17th March, 18:58 UTC, at about 189 km SE of the array, at a focal depth of 21 km; and (c) 19th March, 02:40 UTC, at a distance of 118 km NW of the array at focal depth of 20 km. As an example of a local event, the trace of the earthquake was recorded on 16th March, at 07:21 UTC is shown in Figure 10.3.a. The other trace (fig. 10.3.b) is taken

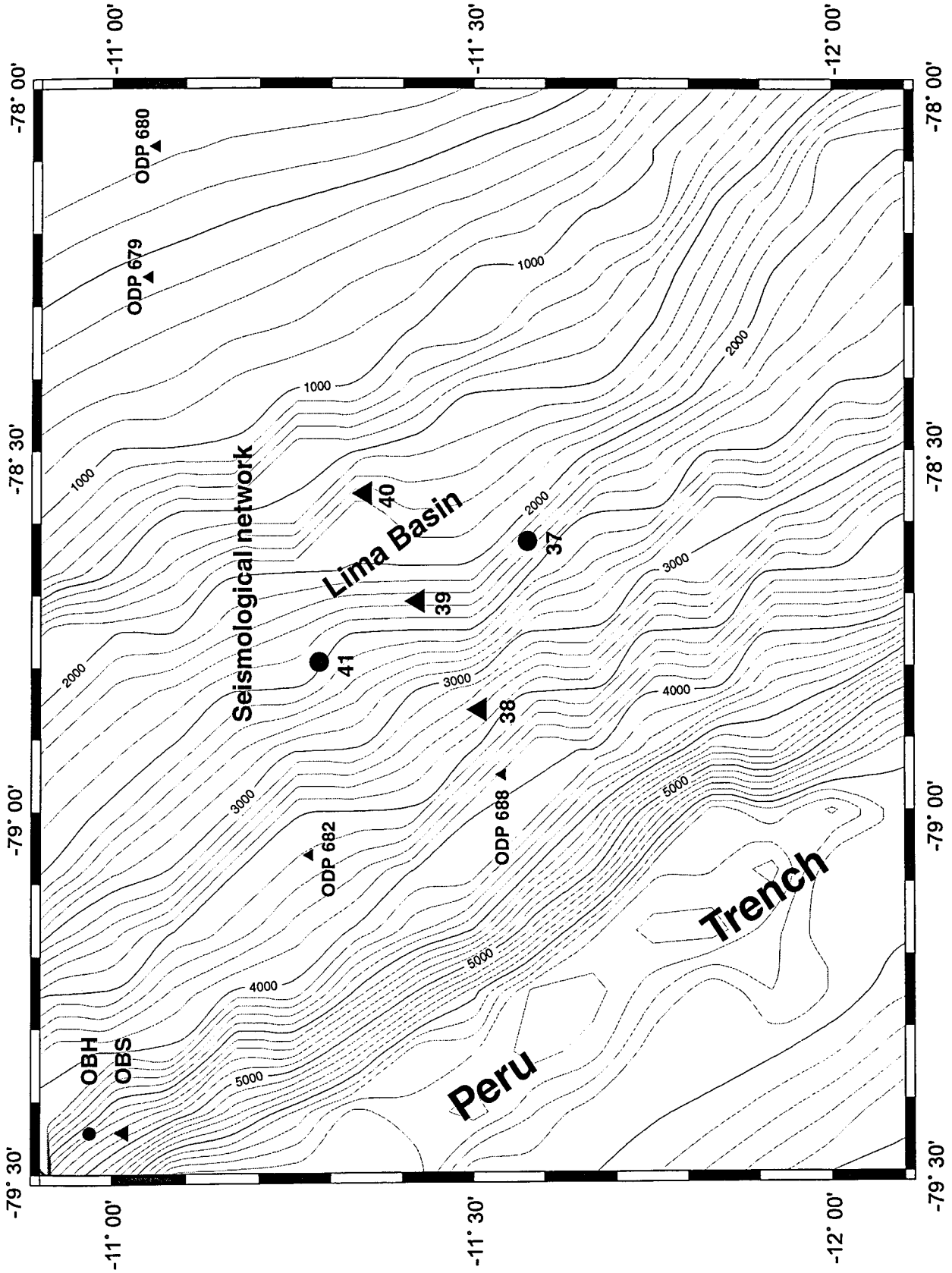

Figure 10.1: Location map of the seismological network in the Lima Basin.

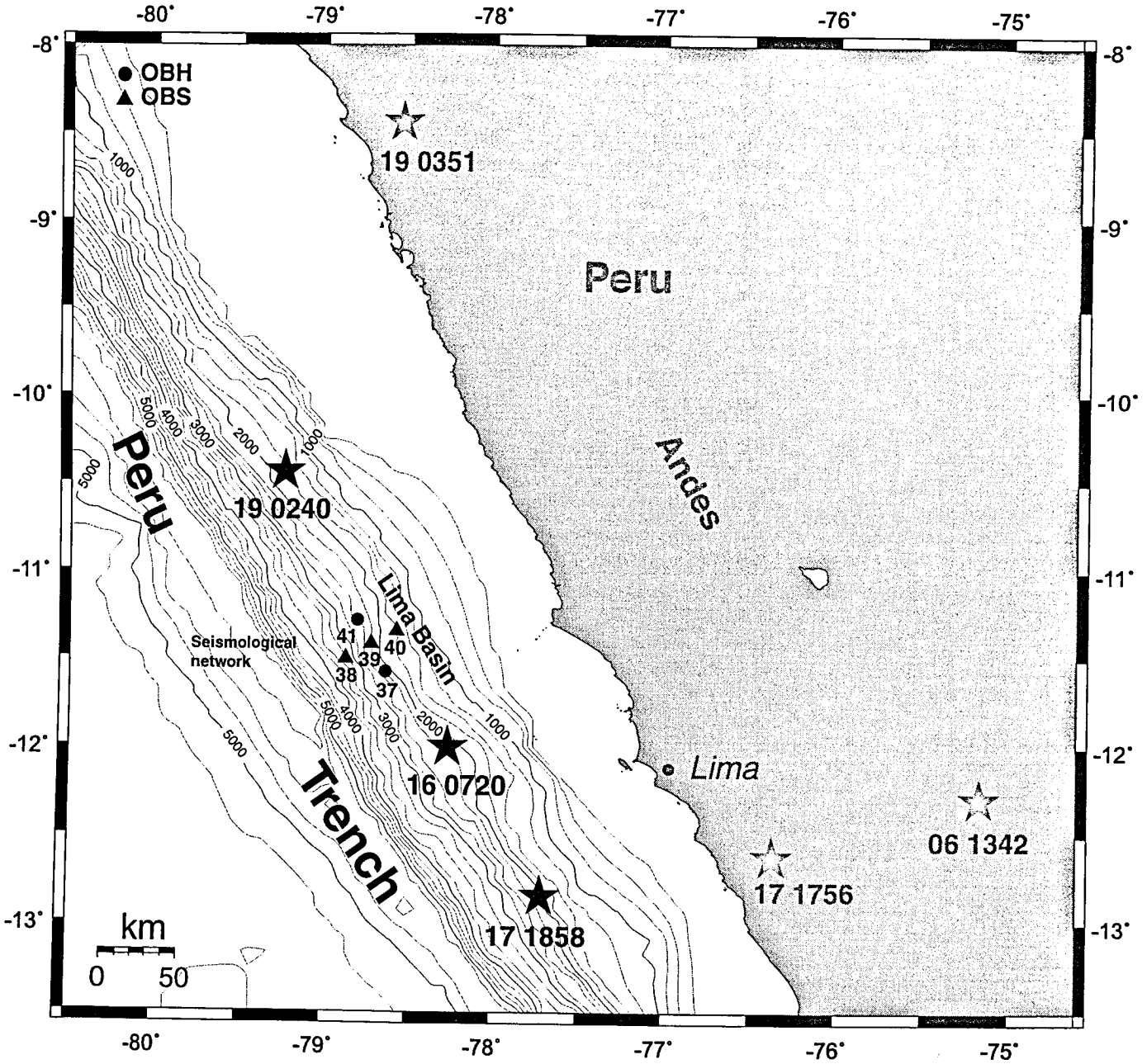

Figure 10.2: Located earthquakes of temporary marine network.
The earthquake of 18th March 2000 at 14:36 UTC is not included.

from an event recorded on 19th March, at 02:40 UTC. These earthquakes may represent the type of foreland seismicity we initially expected to locate but in greater numbers.

Date	Origin time UTC	Hypocenter Lat °S	Long °W	Depth km	Az °	Δ km
06.03.00	13:42:09.4	-12.29	-75.17	43	200	420
16.03.00	07:20:50	-12.00	-78.25	27	135	80
17.03.00	17:56:16.5	-12.62	-76.36	39	294	282
17.03.00	18:58:10	-12.84	-77.71	21	325	189
18.03.00	14:36:51	-12.93	-73.75	37	287	551
19.03.00	02:40:14.8	-10.44	-79.23	20	153	118
19.03.00	03:51:04	-08.44	-78.55	39	182	330

Table 10.1 Located earthquakes.

On 6th March at 13:42 UTC, shortly after the air gun shooting had ceased on profile SO146-01, a larger earthquake, originating from the Andes mountain range at an epicenter distance of 420 km, was recorded on all OBH/S that were operational across the Nazca Ridge (see chapter 6.2.1). The event was clearly picked at all channels (P and S phases) as shown in Figure 10.4. Table 10.2 presents the arrival times.

Station No.	Time (UTC) P-Phase	S-Phase
OBH01	EP 13 42 06.0	ES 42 46.8
OBH02	EP 13 42 05.6	ES 42 46.0
OBS03	EP 13 42 05.2	ES 42 45.6
OBH04	EP 13 42 04.3	ES 42 44.3
OBS05	EP 13 42 04.0	ES 42 43.6
OBH06	EP 13 42 04.0	ES 42 43.2
OBS07	EP 13 42 03.2	ES 42 42.8
OBH08	EP 13 42 03.2	
OBH09	EP 13 42 02.8	

Table 10.2 Arrival times of the earthquake of 6th March 2000 at 13:42 UTC.

This is the only well located earthquake on cruise SO146-01/02 with very low residuals for P- and S-phases. The error ellipse for the epicenter was calculated at x=3.28 km and y=11.54 km. The most distant earthquake was recorded on 18th March, 14:36 UTC, at a hypocenter distance of 552 km. The magnitude of all events can only be estimated to exceed ML >4 as the recording equipment was not calibrated.

We point out that all data needs to be reprocessed and arrival times checked. Phase picking of each event will be reviewed at GEOMAR. To increase our ability to discriminate earthquakes and display traces at a higher resolution different software will be applied. In addition, earthquake locations will significantly improve in accuracy if phase readings from Peruvian and Chilean monitoring networks can be obtained.

The number and distribution of earthquakes recorded with this small sized marine network ensures that sufficient events happen in this region to enable seismological studies in order to locate events

from the subducting oceanic plate. For future studies of Andean foreland seismicity, we recommend that the number of OBH/OBS instruments deployed be doubled thereby increasing the size of the seismic array. The distribution of hypocenters located during the first inspection of the raw data already demonstrates that events will not only be observed from underneath the continental slope but also from beneath the Andean mountains. For further improve of relocation techniques it is advisable to combine future marine networks with installation of onshore stations. This will ensure to cover a higher number of earthquakes with the deployed array and therefore reduces the relocation error (e.g. Hasegawara et al., 1994; Husen et al., 1999).

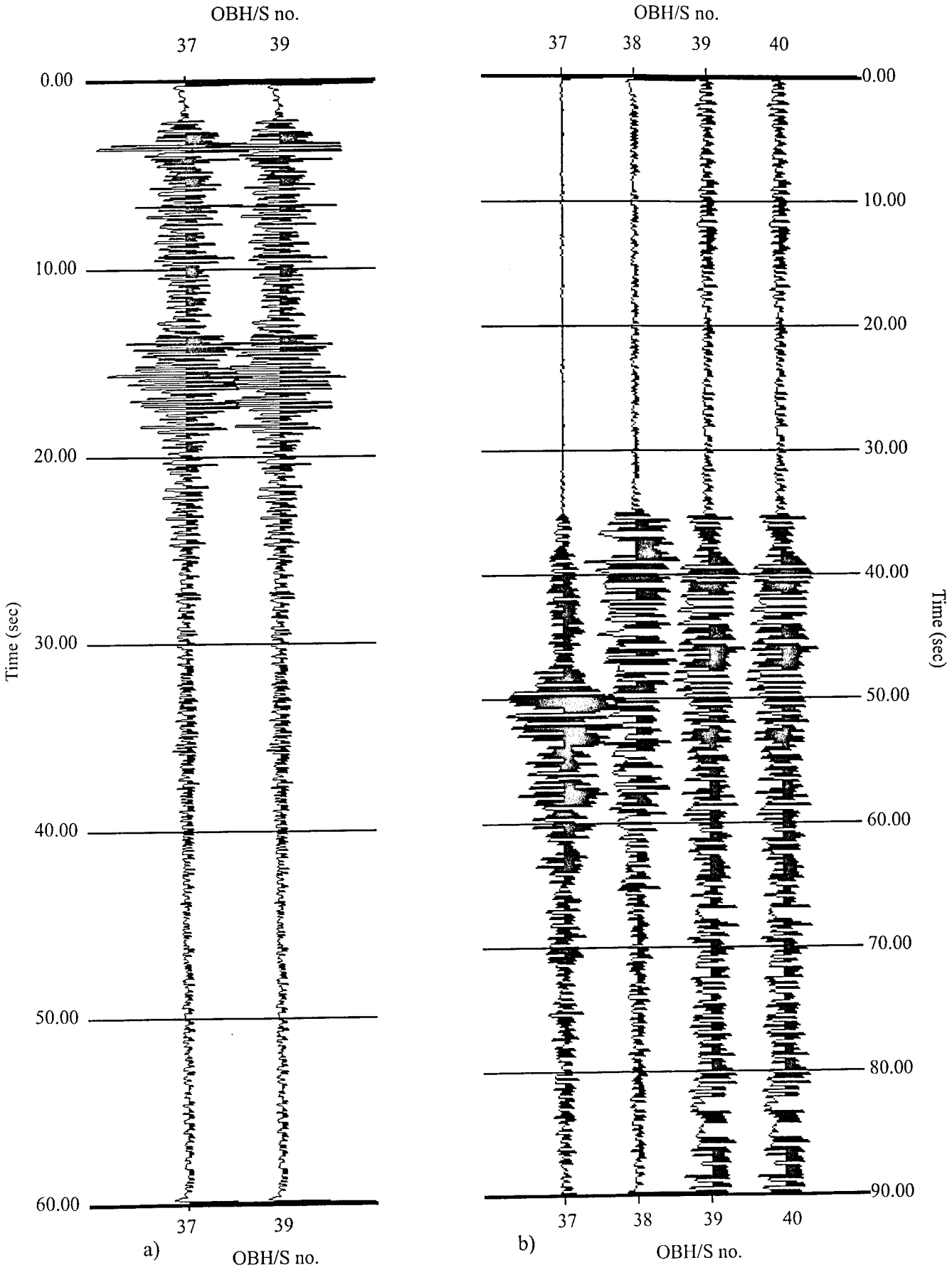

Figure 10.3.: Earthquake examples recorded within the marine seismic network at Lima basin Amplitudes are normalized to median trace values for display.
a) recording time : 16. March 2000 - 07:21 UTC
b) recording time: 19. March 2000 - 02:40 UTC

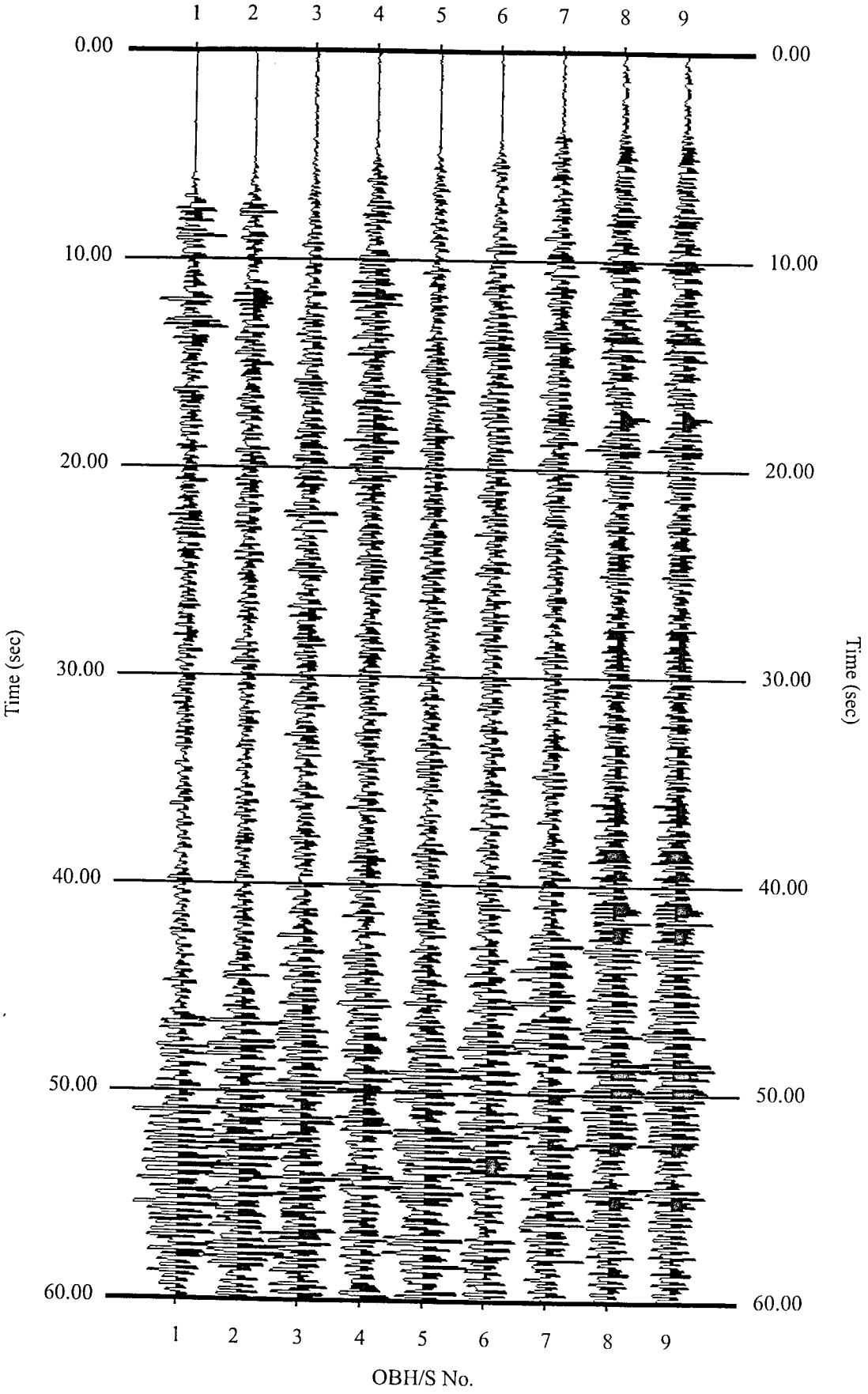

Figure 10.4.: Earthquake observation along line 1 accross Nazca Ridge
Amplitudes are normalized to median trace value for display.
recording time: 06. March 2000 - 13:42 hrs UTC

11 Geological sampling at Paita and Yaquina Basin

11.1 Barite sampling at the Paita area (SO 146-1)

S. Bollwerk

During expedition SO 146-1, the TVG occupied two stations, TVG-1 and TVG-2 (Table 11.1.1) at the Paita area along the Peruvian active margin, between 5° 35'S to 5° 36'S and 81° 38'W to 81° 39'W (Figure 11.1.1). The scientific objectives were to obtain authigenic barite deposits associated with clams and *vestimentifera* communities on active cold fluid expulsing vent sites.

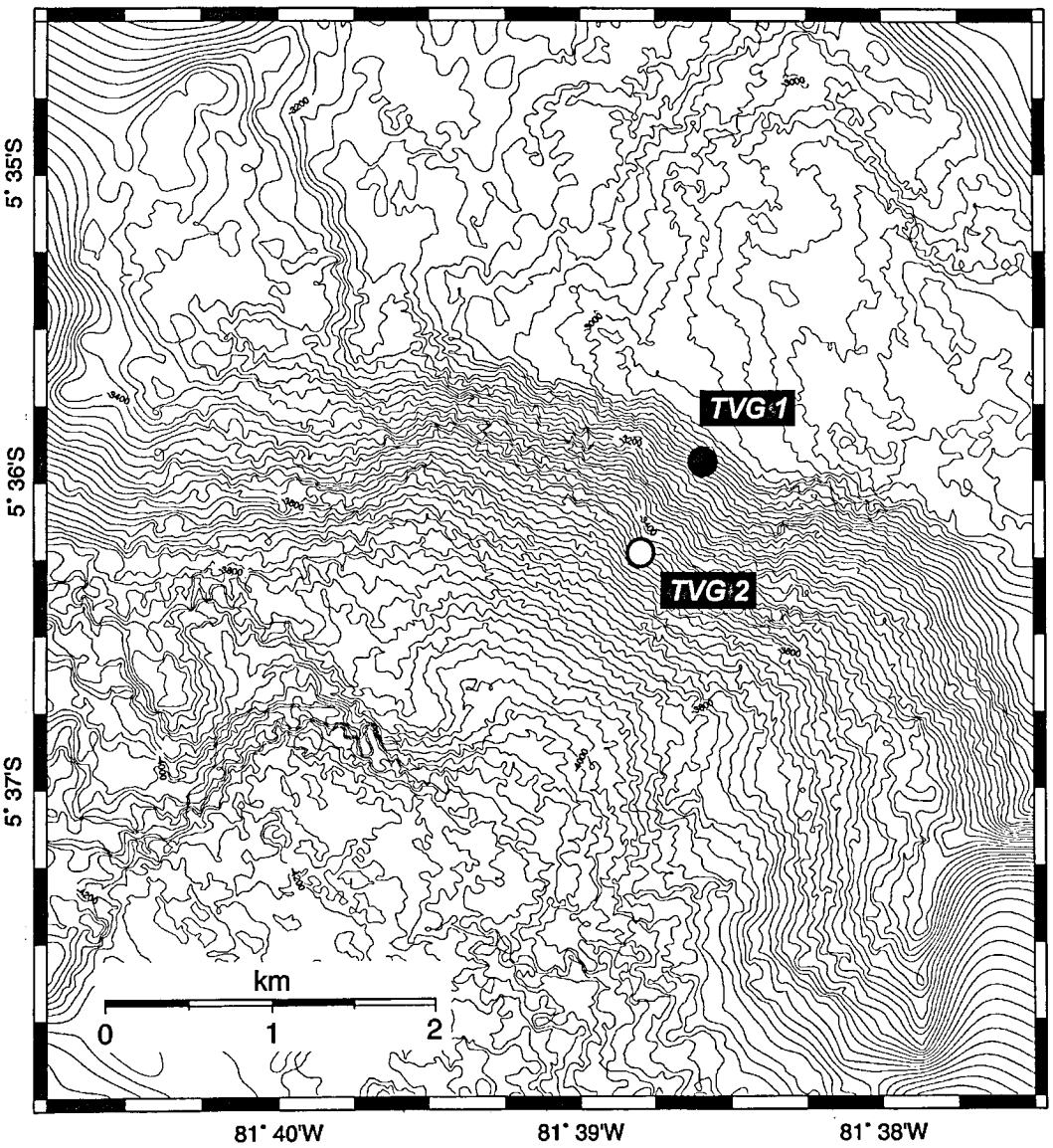

Figure 11.1.1: Bathymetry of the Paita area from the HYDROSWEEP survey during SO146-1 including TVG-1 grab positions.

Table 11.1.1: Details of the TVG stations during SO146-1

station	date	time (UTC)	latitude S	longitude W	water depth (m)
TVG-1 start	17.03.2000	19:00	5°35.774'	81°38.758'	3082
1. grab		21:14	5°36.093'	81°38.515'	3186
2. grab/ end		21:54	5°35.934'	81°38.636'	3124
TVG-2 start	18.03.2000	01:25	5°36.310'	81°38.860'	3620
end		05:01	5°36.140'	81°38.610'	3314

Motivation for the TVG-operation at TVG-1 was stemed from detailed OFOS surveys during cruise SO78 (Peruvent; Suess, 1992). The coordinates for the TVG-2 station were based on the work of Olu et al. (1996), who postulated a very high clam density between 1-1000 individuals per m^2 and the occurrence of barite deposits. Both TVG tracks were documented on video and the Geo-protocol. The ship and TVG tracks from both stations are shown in figure 11.1.2. Unfortunately, only TVG-1 was successful recovering sediment, clams and chunks of barite precipitates after a second attempt.

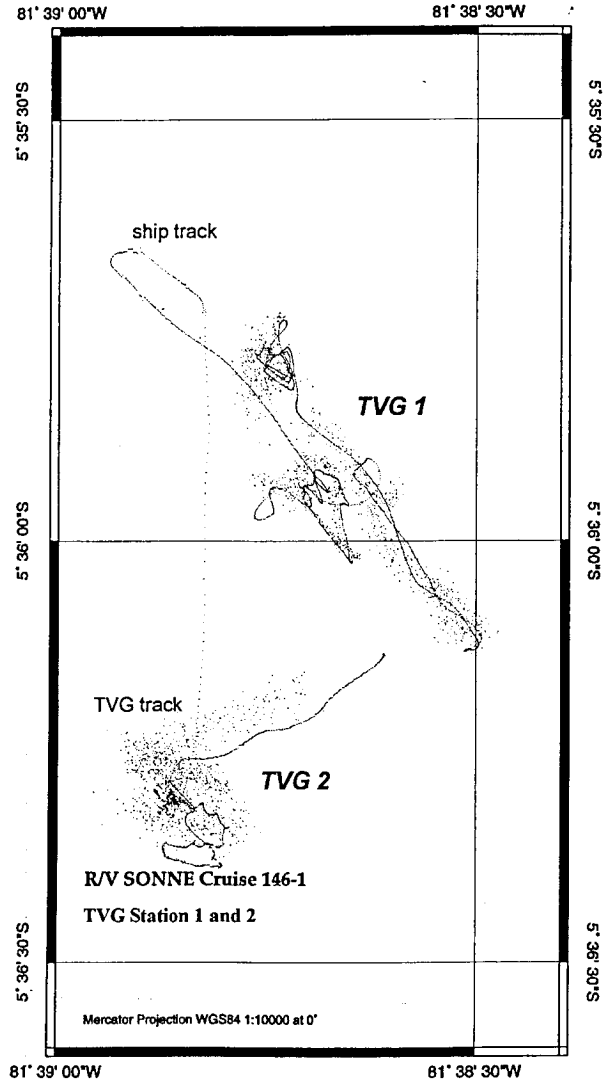

Figure 11.1.2: Cruise track and TVG position during TVG-1 and TVG-2

TV observations showed a very steep and rough terrain (Figure 11.1.1). Both, numerous living and dead clam communities, and some serpulids were observed. The fact that the unsuccessful TVG-2 observations are not in agreement with the evidence of Olu et al. (1996) possibly indicates a dynamic vent system and a shifting of venting fluids in space and time.

When TVG-1 was brought back on deck we detected a strong odor of H_2S. The temperature of the sediment was measured immediately after heaving of the TVG and provided a value of about 5°C. The contents of the TVG were both photographed and described. The benthic fauna (two species of *Calyptogena sp.*) were collected from the surface and stored in alcohol. Separate push cores for subsampling were pushed into the still closed grab where the sediment surface appeared to be the least disturbed. This allows a depth dependent sampling of pore water and sediment. After opening the grab, solidified sediments with thin barite crust (Figure 11.1.3) were found within the gray and black muddy sediment. The solidified sediment also showed many tracks made by benthic organism.

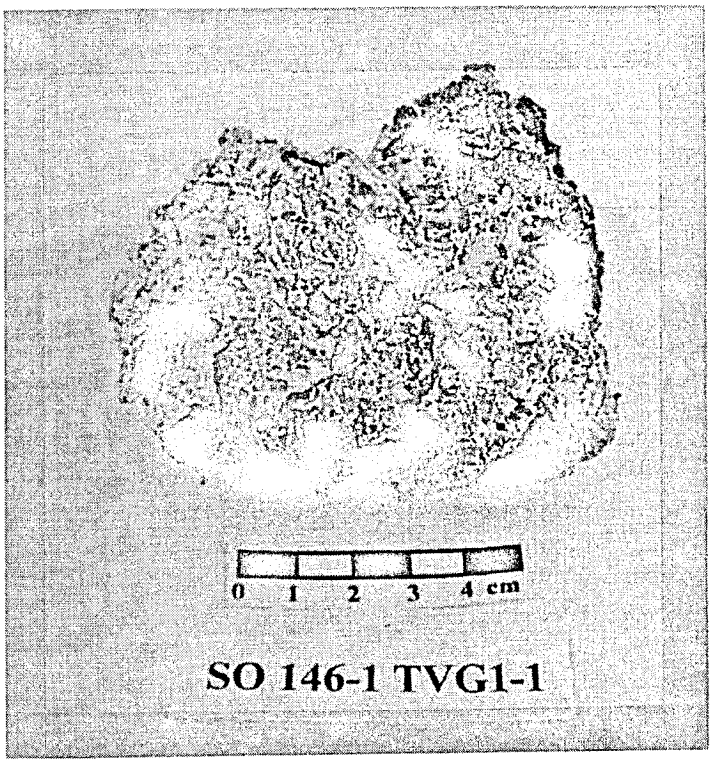

Figure 11.1. 3: Solidified sediment with thin barite crust from TVG-1.

Pore water and sediment sampling

Pore water and sediment samples were subsampled from the push cores (subcore A and D). The sediment was segmented in the cold-room (4°C) and pore water was extracted from a sediment volume of 50 ml at each sampled depth with a centrifuge (Hettich Universal). Up to a depth of 11 cm, slices of 2 cm were cut, from 11 cm to 21 cm, slices of 3 cm were made, and below 21 cm to the bottom of the core, slices of 5 cm were cut, and all were centrifuged for pore water. In all, the sampling obtained between 3 and 6 ml of pore water (Table 11.1.2).

No geochemical analyses were done on board but will be carried out at GEOMAR. For trace element analyses a volume of 2 ml was acidified with 25 µl of 37 % HCl suprapur.

Table 11.1.2: Subsampling from TVG-1.

subcore	core recovery (cm)	No. of sediment samples	No. of pore water samples	No. of pore water samples with HCl
TVG-1 A	40	16	16	16
TVG-1 D	38	16	16	16

Biological samples

The sampled clams consisted of 58 living individuals of two species of *Calyptogena sp.* ranging between 2.5 to 12 cm in length. Some shells were found from *Acharax sp.* and also from *Calyptogena sp.*. These organisms are the typical biological community at H_2S- and methane-rich fluid expulsion sites and are already known from the Paita area (Olu et al., 1996).

11.2 Sampling in the Yaquina Basin (SO146-2)

(J. Greinert, T. Nadler)

TV grab sampling in the Yaquina Basin was attempted during four TVG stations (Table 11.2.1); TVG 6 and 8 at the upper part of the seismic line 20 (SO146-2); TVG 7 and 10 at the chemoherm complexes located at the middle part of line 20. The tracks are shown on the maps in the OFOS chapter.

TVG 6

This grab station was undertaken to sample an area where heat flow measurements could not penetrate the sediment and white 'sticks' - preliminarily interpreted as *vestimentifera* - could be observed during OFOS 4-1. The 0.2 Nm long track covers the area at 650 m water depth which was investigated during OFOS 4-1. The same white 'sticks' could be observed just before the TV grab was dropped but neither *vestimentifera* nor outer signs of fluid venting (e.g. H_2S odor) were found in the recovered sediment. This extremely homogenous sediment consists of greenish mud containing 15 to 20 % foraminiferas. The white 'sticks' are very likely fish bones which were found in the sediment after opening of the grab on deck. Compared to the observations during OFOS 4-1 we suggest a mass extinction of fish possibly induced by the plankton bloom and a strong oxygen consumption consistent with CTD 2. Some sediment samples were taken for mineral and foraminifera analyses and few organisms - worms and tube worms - were collected as well.

TVG 7

The objective of the 0.5 Nm long track of TVG 7 was the sampling of carbonates at the chemoherm called 'Max' observed by OFOS 3-2 and 3-3. This track was planed to cover an area where a chemoherm-like morphologic structure was observed, during a ship turn from the end of OFOS 3-2 to OFOS 3-3. This morphological high 'Witwe Bolte' should be investigated before the sampling at the 'Max' chemoherm. In fact, soon after the TVG has reached the bottom we observed another chemoherm complex with similar authigenic carbonate precipitates, *vestimentifera* and even small fields with living *calyptogena* (see OFOS chapter for description). Reaching the 'Max' chemoherm, we tried to sample the massive carbonates but without success. The grab turned over or could not close properly. We took a sample in a dense sediment covered area just beside the chemoherm. Sediment with strong H_2S odor, shells from *calyptogena* and a

second kind of bivalvia could be recovered. Also several soft concretions of cm size were found. They show bioturbation cast-like or irregular shape and holes of borrowing organisms. Their initially carbonate cementation was indicated through an acid testing.
The observations just before the sample was taken, the H_2S smell, and the soft carbonate concretions in the sampled area are all consistent with a rim facies of the focused fluid flow regime of the chemoherm complexes.
Mineralogical, isotopic and chemical analyses of the soft concretions will indicate if the cementation is also methane related as we suggest for the chemoherm carbonates from TVG 10.

Table 11.2.1: Details of TVG sampling in the Yaquina Basin

	ship coordinates TVG into water and on deck	TVG coordinates bottom sight and from bottom	HS water depth m ship / dropped TVG	time / date UTC station begin / end
TVG 6				
start	8°18.307 S / 80°16.160 W	8°18.414 S / 80°16.154 W	611	07:06 / 12.4.2000
end	8°18.323 S / 80°16.112 W	8°18.333 S / 80°16.136 W	605	07:20 / 12.4.2000
dropped	8°18.320 S / 80°16.130 W	8°18.333 S / 80°16.136 W	606	07:13 / 12.4.2000
TVG 7				
start	8°23.007 S / 80°24.110 W	8°23.073 S / 80°24.096 W	942	09:29 / 12.04.2000
end	8°23.473 S / 80°23.782 W	8°23.374 S / 80°23.795 W	939	12:21 / 12.04.2000
dropped	8°23.370 S / 80°23.800 W	8°23.374 S / 80°23.795 W	910	11:44 / 12.04.2000
TVG 8				
start	8°18.71 S / 80°16.607 W	8°18,717 S / 80°16.668 W	653	14:07 / 12.04.2000
end	8°18.60 S / 80°16.580 W	8°18.609 S / 80°16.578 W	943	14:55 / 12.04.2000
dropped	-	-	-	-
TVG 10				
start	8°22.977 S / 80°23.959 W	8°22.960 S / 80°23.973 W	935	10:04 / 14.4.2000
end	8°22.949 S / 80°23.874 W	8°23.066 S / 80°23.978 W	934	11:45 / 14.4.2000
dropped	8°23.072 S / 80°23.960 W	8°23.066 S / 80°23.978 W	930	11:14 / 14.4.2000

TVG 8

TVG 8 was undertaken based on the observation of 'one' possible small gas hydrate field during OFOS 4-1. Unfortunately, the presence of gas hydrate at the sediment surface was not confirmed. Thus, we didn't drop the TV grab no sample was taken.

TVG 10

A second sampling at the chemoherm complexes at the middle slope area was undertaken by TVG 10, this time at the 'Witwe Bolte' chemoherm. On nine attempts we could not penetrate the hard and massive carbonates, the TV grab turned over or could not close properly. Finally, the tenth drop recovered several irregular carbonate chunks (30 kg) of cm to some dm in size. They show a greenish gray color of cemented sediment and white to light-yellow pore and rim cements of zoned aragonite layers with botryoidal structure. White tubes from serpulides, incorporated shell fragments and few pre-cemented mud clasts induce a breccia-like texture. However, compared to authigenic carbonates from Hydrate Ridge at the Oregon Margin (Greinert et al., in review) these carbonates represent a new lithologic type of chemoherm carbonates. Detailed mineralogical and isotopic investigations will elucidate the formation mechanisms but an influence of methane rich fluids expulsing at the seafloor is very likely.

11.3 Sampling in the Lima-Basin

No sediment or carbonate sampling could be undertaken in the Lima Basin using real sampling equipment. Nevertheless, during the heat flow profile HF 24-5 (11°10.20 S 78°50.09 W; 2224 m water depth) the device turned over several times due to the hardness of the cemented sediment and one small chunk (2 x 5 cm) could be recovered from the weight of the device. Tests with acid indicate that the beige sediment matrix is cemented by carbonate. Mineralogical and isotopic investigations at GEOMAR will give further clues on the origin of these - methane-related ? - carbonate. We suggest that this small chunk is a part of one of the bigger blocks observed during OFOS 5-1 and 5-2 and thus can hopefully serve as a suitable 'representative' sample.

12. ACKNOWLEDGEMENTS

Cruise SO 146-1&2 was funded by the German Ministery of Education, Research, Science, and Technology (BMBF) under project No. 03G0146A to GEOMAR within the continued and generous most commendable support for marine sciences with an outstanding research vessel such as SONNE. We also gratefully acknowledge the support of NSF (grant No. OCE-9906891) to Ingo Pecher of University of Texas.

We most warmly thank master H. Papenhagen and his crew for their excellent support in all work done and for the splendid and efficient working atmosphere throughout the entire highly ambitious working program.

13. REFERENCES

Ballesteros, M.W., G.F. Moore, B. Taylor, and S. Ruppert, 1988: Seismic stratigraphic framework of the Lima and Yaquina forearc basins. In: E. Suess and R. von Huene, et al., Proc. ODP, Init. Repts., 112. College Station, TX (Ocean Drilling Program), 77-90.

Bangs, N.L., D.S. Sawyer, X. Golovchenko 1993: Free gas at the base of the gas hydrate zone in the vicinity of the Chile triple junction. Geology 21, 905-908.

Beck, S.L., and L.J. Ruff, 1989: Great earthquakes and subduction along the Peru trench. Phys. Earth Planet. Int. 57, 199 – 224.

Bialas, J., and E. R. Flueh, 1999: Ocean Bottom Seismometers; Sea Technology, 40, 4, 41-46.

Blondel, P., and B.J. Murton, 1997: Handbook of Seafloor Sonar Imagery, John Wiley and Sons, Chichester, 314.

Bullard, E.C., 1993: Heat flow in South Africa, Proc. R. Soc. London Series A, 173, 474-503.

Cande, S.C., 1985: Nazca-South American plate interactions since 50 mybp. In: Peru continental margin, D.M. Hussong, S.P. Dang, L.D. Kulm, R.W. Couch and T.W.C Hilde. Marine Sciences International, Woods Hole, MA.

Caress, D.W., and D.N. Chayes, 1996: Improved processing of Hydrosweep DS multibeam data on the R/V Maurice Ewing. Mar. Geophys. Res. 18, 631 - 650.

Davis, D.M., J. Suppe, and F.A. Dahlen, 1983. Mechanics of fold-and-thrust-belts and accretionary wedges. J. Geophys. Res. 88, 1153 – 1172.

Domenico, S.N., 1977: Elastic properties of unconsolidated porous sand reservoirs. Geophysics 42, 1339-1368.

Flueh, E. R., and J. Bialas, 1996: A digital, high data capacity ocean bottom recorder for seismic investigations; Int. Underwater Sytems Design, 18(3), 18-20.

Grant, J.A., and R. Schreiber, 1990: Modern swath sounding and sub-bottom profiling technology for research applications: The Atlas Hydrosweep and Parasound systems. Mar. Geophys. Res. 12, 9 -19.

Gutscher, M.-A., N. Kukowski, J. Malavieille and S.E. Lallemand, 1998a: Material transfer in accretionary wedges from analysis of a systematic series of analog experiments. - J. Struct. Geol., 20, 407 - 416.

Gutscher, M.-A., N. Kukowski, J. Malavieille and S.E. Lallemand, 1998b: Episodic imbricate thrusting and underthrusting; analog experiments and mechanical analysis applied to the Alaskan accretionary wedge. - J. Geophys. Res., Vol.103, 10161 - 10176.

Hartzell, S., and C. Langer, 1993: Importance of model parametrisation on finite fault inversions: application to the 1974 M_W 8.0 Peru earthquake. J. Geophys. Res. 98, 22123-22134.

Hasegawa, A., S. Horiuchi, and N. Umino, 1994: Seismic structure of the northeastern Japan margin: A synthesis; J. Geophys. Res., 99, B11, 22295-22311.

Heinrich, P., F. Schindele, S. Guibourg and P. Ihmle, 1998: Modeling of the February 1996 Peruvian tsunami Geophysical Research Letter 25, 2687 - 2690.

Herber, R., Grevemeyer, I., Exner, O., Villinger, H. and Weigel, W., 1998: An implosive seismoacoustic source for seismic experiments on the ocean floor, Mar. Geophys. Res. 20: 239-247.

Holbrook, W.S., H. Hoskins, W.T. Wood, R.A. Stephen, D. Lizarralde and the Leg 164 Scientific Party 1996: Methane hydrate and free gas on the Blake Ridge from vertical seismic profiling. Science 273, 1840-1843.

Hsu, J.T., 1992: Quaternary uplift of the Peruvian coast related to the subduction of the Nazca Ridge: 13.5 to 15.6 degrees South latitude. Quaternary International 15/16, 87 – 97.

Huene, R. von, E. Suess and Leg 112 Shipboard Scientists, 1988: Ocean Drilling Program Leg 112, Peru continental margin: Part 1, Tectonic history. Geology 16, 934 – 938.

Huene, R. von, and J. Miller, 1988: Migrated multichannel seismic-reflection records across the Peru continental margin. In: E. Suess and R. von Huene, et al., Proc. ODP, Init. Repts., 112. College Station, TX (Ocean Drilling Program), 109-124.

Huene, R. von, I.A. Pecher and M.-A. Gutscher, 1996: Material flux in the Peru subduction zone due to the subduction of Nazca ridge and development of the accretionary prism. Tectonics 15, 19-33.

Huene, R. von, and I.A. Pecher, 1999: Vertical tectonics and the origin of BSRs along the Peru margin. Earth Planet. Sci. Lett. 166, 47 – 55.

Husen, S., E. Kissling, E. Flueh, and G. Asch, 1999: Accurate hypocenter determination in the of the Nazca subduction zone in Northern Chile using a combined on-/offshore network. Geophys. J. Int., 138, 687-701.

Hussong, D.M., 1986: Mud volcanoes. In: Yearbook of Science and Technology: McGraw-Hill, New York, 286-289.

Hussong, D.M., T.B. Reed IV and W.A. Bartlett, 1988: SEAMARC II sonar imagery and bathymetry of the Nazca Plate and Peru Forearc, ODP Leg 112. In: E. Suess and R. von Huene et al., Proc. ODP, Init. Repts., 112. College Station, TX (Ocean Drilling Program), 125-130.

Hyndman, R.D., K. Wang, T. Yuan and G.D. Spence (1993): Tectonic sediment thickening, fluid expulsion, and the thermal regime of subduction zone accretionary prisms: the Cascadia margin off Vancouver Island. J. Geophys. Res. 98, 21865-21876.

Kastner, M., H. Elderfield, J.B. Martin, E. Suess, K. A. Kvenvolden, R.E. Garrison 1990: Diagenesis and interstitial-water chemistry at the Peruvian continental margin - major constituents and strontium isotopes. Proc. ODP, Sci. Res. 112, 413 - 440.

Knickmeyer, E.T., 1996: Hochgenaues Differential-GPS, Proc. 11th Annual Meeting of the German Hydrographic Society, Glücksburg, 3.-5.6.

Korenaga, J., W.S. Holbrook, S.C. Singh and T.A. Minshull, 1997: Natural gas hydrates on the southeast US margin: constraints from full waveform inversion and traveltime inversion of wide-angle seismic data. J. Geophys. Res., 102, 15345-15365.

Kukowski, N., R. von Huene, J. Malavieille and S.E. Lallemand, 1994: Sediment accretion against a buttress beneath the Peruvian continental margin at 12° S as simulated with sandbox modeling. Geologische Rundschau 83, 822-831.

Kukowski, N., and I.A. Pecher, 1999: Thermo-hydraulics of the Peruvian accretionary complex at 12°S. J. Geodynamics, 27, 373 – 402.

Kulm, L.D., T.M. Thornburg, E. Suees, J. Resig and P. Fryer, 1988: Clastic, diagenetic, and metamorphic lithologies of a subsiding continental block: central Peru forearc. In: E. Suess and R. von Huene, et al., Proc. ODP, Init. Repts., 112. College Station, TX (Ocean Drilling Program), 91-107.

Kvenvolden, K.A., 1993: Gas hydrates - geologic perspective and global change. Rev. of Geophysics, v. 31, no. 2, p. 173-187.

Kvenvolden, K. A., and M. Kastner 1990: Gas hydrates of the Peruvian outer continental margin. Proc. ODP, Sci. Res. 112, 517 - 526.

Lallemand, S.E., P. Schnürle, J. Malavieille, 1994: Coulomb theory applied to accretionary and non-accretionary wedges: possible causes for tectonic erosion and/or frontal accretion. J. Geophys. Res. 99, 12033-12055.

Linke, P., E. Suess, M. Torres, V. Martens, W.D. Rugh, W. Ziebis, and L.D. Kulm, 1994: In situ measurements of fluid flow from cold seeps at active continental margins. Deep Sea Research 41, 721 - 739.

Loss, J., I.A. Pecher, U.S. ten Brink, 1998: RayGUI – A graphical user interface for interactive raytracing (rayinvr). U.S. Geol. Survey, Open File Report, 98-203.

Luetgert, J., 1992: Interactive two-dimensional seismic raytracing for the Macintosh, USGS Open File Report, 43.

MacKay, M.E., R.D. Jarrard, G.K., Westbrook and R.D. Hyndman, 1994: Origin of bottom simulating reflectors: Geophysical evidence from the Cascadia accretionary prism. Geology 22, 459-462.

Marsters, J.C., and H.A. Christian, 1990: Hydraulic conductivity of diatomaceous sediment from the Peru continental margin obtained during ODP Leg 112. in: E. Suess, R. von Huene et al.: Ocean Drilling Program, Scientific Results, Washington (U.S. Printing Office) 112, 633 - 639.

Miller, J.J., W.L. Myung and R. von Huene, 1991: An analysis of a reflection from the base of a gas hydrate zone off Peru. Am. Assoc. Petrol. Geol. Bull. 75, 910-924.

Müller, R. D., W.R. Roest, J.-Y. Royer, L.M. Gahagan and J.G. Sclater, 1995: A digital age map of the ocean floor. SIO Reference Series 93-30.

Paull, C.K., R. Matsumoto, P.J. Wallace et al., 1996: Proceedings of the Ocean Drilling Program, Initial Reports, Texas A &M University, 164, 623 p.

Pecher, I.A., 1995: Seismic studies of bottom simulating reflectors at theconvergent margins offshore Peru and Costa Rica. Dissertation, U. Kiel, GEOMAR Report 47, 159 p.

Pecher, I.A., T. A. Minshull, S.C. Singh and R. von Huene, 1996a: Free gas at a bottom simulating reflector offshore Peru: results from full waveform inversion. Earth and Planetary Science Letters 139, 459 - 469.

Pecher, I.A., R. von Huene, C.R. Ranero , N. Kukowski, T.A. Minshull and S.C. Singh, 1996b: Formation mechanisms of free gas beneath the hydrate stability zone at convergent margins - geophysical evidence from bottom simulating reflectors at the Peruvian and Pacific Costa Rica margins. - Proceedings of the 2nd International Conference on Natural Gas Hydrates, Toulouse, 593 - 600.

Pecher, I.A., N. Kukowski, C.R. Ranero and R. von Huene, 2000: Gas hydrates along the Peru and middle America trench systems. AGU Monograph Series, subm.

Pilger, R.H., 1985: Cenozoic plate kinematics, subduction and magmatism: South American Andes. J. Geol. Soc. London 141, 793 - 802.

Rempel, A., and B.A. Buffett, 1997: Formation and accumulation of gas hydrate in porous media, J. Geophys. Res. 102 151-10, 164.

Schreiber, R., H.W. Schencke, 1990: Efficient hydrographic surveying of EEZ with new multibeam echosounder technology for shallow and deep water. Ocean resouces 1, 73 - 87.

Sclater, J.G., C. Jaupart and D. Galson, 1980: The heat loss through oceanic and continental crust and the heat loss of the earth. Reviews of Geophysics and Space Physics 18, 269 - 311.

Seeber, G., 1996: Stand und Einsatzmöglichkeiten von GPS - ein Überblick, Proc. 11th Annual Meeting of the German Hydrographic Society, Glücksburg, 3.-5.6.

Shi, Y., C.-Y. Wang, and R. von Huene, 1990: Modeling pore pressure, central Peru margin. In: E. Suess, R. von Huene et al.: Ocean Drilling Program, Scientific Results, Washington (U.S. Printing Office) 112, 517-526.

Singh, S.C., T.A. Minshull and G.D. Spence, 1993: Velocity structure of a gas hydrate reflector. Science, 260, 204-207.

Spence, W., C., Mendoza, E.R. Engdahl, G.L. Choy and E. Norabuena, 1999: Seismic subduction of the Nazca Ridge as shown by the 1996-97 Peru earthquakes. Pure appl. Geophys. 154, 753-776.

Suess, E., R. von Huene et al., 1988: Proceedings of the Ocean Drilling Program, Initial Reports, Texas A &M University, 112, 738 p.

Suess, E., R. von Huene and Leg 112 Shipboard scientists, 1988: Ocean Drilling Program Leg 112, Peru continental margin: Part 2, Sedimentary history and diagenesis in a coastal upwelling environment. Geology 16, 939 - 943.

Swenson, J.L., and S.L. Beck, 1999: Source characteristics of the 12 November 1996 M_w 7.7 Peru subduction zone earthquake Pure appl. Geophys. 154, 731 – 751.

Taylor, MH, WP Dillon, and IA Pecher, 2000. Trapping and migration of methane associated with the gas hydrate stability zone at the Blake Ridge Diapir: New insights from seismic data. Mar. Geol., 164, 37-51.

Villinger, H., and E. Davis, 1987: A new reduction algorithm for marine heat flow measurements. J. Geophys. Res., 92, 12846 - 12856.

Weinrebe, W., 1997: Fahrtbericht SO112 HIRESBAT GEOMAR Report 64.

Yamano, M., and S. Uyeda, 1990: Heat flow studies in the Peru Trench subduction zone. In: E. Suess et al.: Ocean Drilling Program, Scientific Results, Washington (U.S. Printing Office) 112, 667-682.

Xu, W., C. Ruppel, 1999: Predicting the occurrence, distribution, and evolution of methane gas hydrates in porous marine sediments. – J. Geophys. Res. 104, 5081 - 5095.

Zelt, C.A., and R.B. Smith, 1992: Seismic traveltime inversion for 2-D crustal velocity structure. Geophys. J. Int. 108, 16-34.

Stationsprotokoll F.S. "S O N N E" Reise SO 146/1

Eingesetzte Geräte

HS	Hydrosweep
PS	Parasound
OBH/OBS	Ocean Bottom Hydrofone und Seismograph
GD	Gradiometer
GV	Gravimeter
Streamer	
3 x 32 Liter – airgun-array	
2 x GI-airguns	
GTVA	Fernsehgreifer Typ A
CTD/ROS	CTD-Sonde

Eingesetzte Winden :

Winde	*D/M*	*Typ*	*RF-Nr*	*SO 146/1 Einsatz*	*Gesamt Einsatz*	*SO 146/1 S`länge*	*Gesamt S`länge*	*Zust.*
W 1	18,2	LWL	816233	031 h	0913 h	11573 m	259504 m	2
W 2	18,2	LWL	000000	000	0000	00000	000000	0
W 4	11,0	NSW	817141	000	0222	03000	139383	3
W 5	11,0	NSW	817164	004	0034	11653	041317	2
W 6	18,2	DRAKO	814150	010	0898	15100	748388	3

Winde	*SO 146/1 gefierte max.Länge*	*jemals gefierte max.Länge*
W 1	3582 m	6474 m
W 2	0000	6545
W 4	0000	6100
W 5	5200	5200
W 6	6800	7900

Geräteverluste : 1 OBS ; 1 Streamer abgerissen, geborgen

Abkürzungen im Stationsprotokoll:

z.W.	zu Wasser
a.D.	an Deck
Boko	Bodenkontakt
Bosi	Bodensicht
SL(max.)	(maximale)Seillänge
LT	Lottiefe nach Hydrosweep
W x	eingesetzte Winde
HS	Hydrosweep
PS	Parasound
XPNDR	Transponder

Zeit : UTC - 05 Stunden

03.03.2000

Profil 01 HS/PS/GV

0523	Beginn Profil		18 23,76 S 72 19,38 W	
1020	Ende Profil		17 49,26 S 73 00,00 W	052 sml

Station 01 releaser-Test W 6

1024	Beginn Station	LT = 6314 m	17 49,31 S 73 00,29 W
1038	releaser z.W.		
1231	Slmax = 5500 m	LT = 6299 m	17 49,33 S 73 00,14 W
1246	Beginn hieven		
1435	releaser a.D.	Ende Station	

Profil 02 HS/PS/GV

1438	Beginn Profil	17 49,26 S	73 00,00 W
1930	Abbruch Profil	17 21,90 S	73 45,00 W
2113	Fortsetzung Profil	17 25,21 S	74 06,12 W
2400		17 04,68 S	74 28,68 W

04.03.2000

1030	Ende Profil	15 47,00 S	75 49,10 W	191 sml

Station 02 CTD/ROS W 5

1036	Beginn Station	LT = 5220 m	15 47,00 S 75 49,10 W
1045	CTD z.W.		
1230	Slmax = 5200 m	LT = 5245 m	15 46,86 S 75 48,93 W
1454	CTD a.D.		15 46,82 S 75 48,90 W
1458	Ende Station		

Profil 03 HS/PS/GV

1458	Beginn Profil	15 46,82 S	75 48,90 W	
1710		16 02,00 S	76 06,50 W	023 sml
1828		15 53,00 S	76 18,00 W	014 sml
1847		15 55,75 S	76 19,25 W	003 sml
2006		16 04,25 S	76 07,88 W	014 sml
2022		16 06,50 S	76 09,50 W	003 sml
2141	Ende Profil	15 58,00 S	76 21,00 W	014 sml

Auslegung OBH/OBS auf Profil 01 WS/RS

2208 – 2214	Test OBH		
2215	OBH 01 z.W.	LT = 3241 m	16 01,18 S 76 24,03 W
2311	OBH 02 z.W.	LT = 3211 m	15 56,40 S 76 30,03 W

05.03.2000

0010	OBH 03 z.W.	LT = 3083 m	15 51,88 S 76 35,99 W
0105	OBH 04 z.W.	LT = 2928 m	15 46,80 S 76 42,01 W
0200	OBH 05 z.W.	LT = 2994 m	15 41,99 S 76 48,00 W
0256	OBH 06 z.W.	LT = 2931 m	15 37,20 S 76 54,20 W

0351	OBH 07 z.W.	LT = 2904 m	15 32,60 S 77 00,00 W
0446	OBH 08 z.W.	LT = 2983 m	15 27,79 S 77 06,00 W
0545	OBH 09 z.W.	LT = 3026 m	15 22,99 S 77 12,00 W

Profil 04 HS/PS/GV

0600	Beginn Profil	15 22,00 S 77 11,00 W	
0717	Ende Profil	15 14,00 S 77 21,50 W	013 sml

Profil WS/RS 01 v = 4,0 kn über Grund

0753	Beginn aussetzen	15 10,96 S 77 27,13 W	
0810	STb airgun z.W.		
0828	Bb airgun z.W.		
0903	Beginn Profil	15 13,38 S 77 24,14 W	
0925	Bb airgun z.W.		
0937	streamer z.W.	l = 050 m	
0952	Gradiometer z.W.	l = 220 m	
1126	Bb airgun z.W.		
2400		15 50,91 S 76 36,93 W	
06.03.2000			
0756	Ende Profil	16 10,70 S 76 12,00 W	090 sml
0757	streamer a.D.		
0808	Gradiometer a.D.		
0821	Stb airgun a.D.		
0832	Bb air gun a.D.		

Profil 05 HS/PS

0837	Beginn Profil	16 12,07 S 76 10,22 W	
0910		16 09,20 S 76 07,00 W	009 sml
1213		15 48,20 S 76 19,00 W	021 sml
1304	Ende Profil	15 55,50 S 76 24,00 W	003 sml

Aufnahme OBH/OBS von Profil 01 WS/RS

1317	OBH 01 ausgelöst	1353	gesichtet	1407	a.D.	16 01,32 S 76 24,29 W
1432	OBH 02	1509		1518		15 56,49 S 76 30,23 W
1545	OBH 03	1633		1642		15 51,64 S 76 36,13 W
1707	OBH 04	1748		1756		15 46,84 S 76 42,18 W

1821 – 2000 Releaser test mit W 6 SL max = 2800 m LT = 2930 m

2108	OBH 06	2137	2156	15 37,23 S 76 54,42 W
2222	OBH 07	2315	2325	15 32,72 S 77 00,09 W
2352	OBH 08	0030	0039	15 27,80 S 77 06,15 W
07.03.2000				
0125	OBH 09	0203	0213	15 23,00 S 77 12,07 W

Profil HS/PS 06

0234	Beginn Profil	15 22,51 S 77 09,00 W	
0502	Ende Profil	15 38,00 S 76 49,00 W	025 sml

FS SONNE Stationsprotokoll SO 146/1

Auslegung OBH/OBS für das Profil WS/RS 02

0540	OBH 10 z.W.	LT = 2927 m	15 35,50 S 76 43,20 W
0635	OBS 11 z.W.	LT = xxxx m	15 29,99 S 76 38,40 W
0725	OBH 12 z.W.	LT = xxxx m	15 24,04 S 76 33,60 W
0814	OBH 13 z.W.	LT = 3898 m	15 18,04 S 76 28,79 W
0900	OBH 14 z.W.	LT = 4983 m	15 12,07 S 76 23,91 W
0927	OBH 15 z.W.	LT = 4686 m	15 09,09 S 76 21,42 W
1002	OBS 16 z.W.	LT = 3597 m	15 06,06 S 76 18,91 W
1037	OBH 17 z.W.	LT = 2544 m	15 01,52 S 76 15,17 W
1111	OBH 18 z.W.	LT = 2186 m	14 58,05 S 76 12,33 W
1135	OBH 19 z.W.	LT = 2152 m	14 55,70 S 76 10,35 W
1155	OBH 20 z.W.	LT = 1683 m	14 54,05 S 76 09,01 W
1225	OBH 21 z.W.	LT = 0563 m	14 50,81 S 76 06,41 W
1252	OBH 22 z.W.	LT = 0266 m	14 48,01 S 76 04,09 W

Profil WS/RS 02 v = 4,0 kn über Grund

1356	Beginn Profil ; M-airgun z.W.		14 40,91 S 75 58,33 W
1404	Stb airgun z.W.		
1415	Bb airgun z.W.		
1428	Streamer z.W.	L = 30 m	
1445	Gradiometer z.W.	L = 220 m	
2400		15 12,36 S 76 24,09 W	

08.03.2000

1358	Ende Profil	15 56,00 S 77 00,00 W	096 sml
1408	Streamer a.D.		
1413	Gradiometer a.D.		
1418	M-airgun a.D.		
1427	Stb-airgun a.D.		
1436	Bb-airgun a.D.		

Profil HS/PS 07

1448	Beginn Profil	15 57,23 S 76 59,33 W	
1640	Ende Profil	15 43,00 S 76 46,75 W	018 sml

Aufnahme OBS 05

1618	OBS ausgelöst
1653	gesichtet
1705	a.D.

Profile HS/PS 08 bis 15 und Aufnahme OBH/OBS

1731	Beginn Profil 08	15 41,22 S 76 44,66 W	
1939	Ende Profil 08	15 54,04 S 76 26,60 W	034 sml
1958	Beginn Profil 09	15 51,48 S 76 24,70 W	
2203	Ende Profil 09	15 38,75 S 76 42,28 W	021 sml
2208	OBH 10 ausgelöst	2241 gesichtet 2258 a.D.	
2326	Beginn Profil 10	15 35,72 S 76 39,43 W	

09.03.2000

0131	Ende Profil 10	15 49,00 S 76 22,80 W	021 sml
0149	Beginn Profil 11	15 46,26 S 76 21,19 W	

0347	Ende Profil 11	15 33,62 S	76 37,05 W	020 sml
0353	OBH 11 ausgelöst	0442 a.D.		
0452	Beginn Profil 12	15 30,00 S	76 38,40 W	
0856	Ende Profil 12	15 55,28 S	76 04,47 W	040 sml
0917	Beginn Profil 13	15 52,67 S	76 01,90 W	
0929	GI-airguns z.W.			
0936	streamer z.W.			
0943 – 1315	Test der GI-airguns	v = 5,0 kn		
1322	airguns a.D.			
1329	streamer a.D.			
1513	Ende Profil 13	15 28,39 S	76 32,78 W	048 sml
1520	OBS 12 ausgelöst	1613 gesichtet	1621 a.D.	
1626	Beginn Profil 14	15 24,00 S	76 33,00 W	
2030	Ende Profil 14	15 50,38 S	76 00,00 W	037 sml
2059	Beginn Profil 15	15 47,63 S	76 75,57,08 W	
2400		15 26,44 S	76 22,34 W	

10.03.2000

0040	Ende Profill15	15 22,00 S	76 27,55 W	039 sml

Profil GI 02 RS

0128	GI-airguns z.W.			
0137	streamer z.W.	L = 300 m		
0144	Beginn Profil	v = 5,0 kn	15 24,42 S	76 33,94 W
1206	Ende Profil		14 43,00 S	76 00,00 W 054 sml
1214	airguns a.D.			
1222	streamer a.D.			

Einholen OBH/OBS 22 bis 13

1305	OBH 22 ausgelöst	1305 gesichtet	1320	a.D.	14 48,06 S 76 04,17 W
1343	OBH 21	1349	1400		14 50,87 S 76 06,45 W
1419	OBH 20	1441	1452		14 5,22 S 76 09,03 W
1452	OBH 19	1516	1523		14 55,84 S 76 10,32 W
1528	OBH 18	1608	1616		14 58,18 S 76 12,21 W
1618	OBH 17	1644	1652		15 01,25 S 76 14,98 W
1709	OBH 16	1810	1822		15 06,29 S 76 18,96 W
1840	OBH 15	1934	1954		15 09,29 S 76 21,54 W
2011	OBH 14	2116	2129		15 11,99 S 76 24,16 W
2158	OBH 13	2240	2302		15 18,11 S 76 29,00 W

Profile HS/PS 16 und 17

2351	Beginn Profil 16	15 12,00 S 76 24,00 W

11.03.2000

1206	Profilwechsel 16/17	13 37,50 S 77 45,00 W123 sml
1416	Ende Profil 17	13 51,50 S 78 02,00 W022 sml

Ausbringen OBS/OBH auf WS/RS Profil 03

1447	OBH 23 z.W.	LT = 4827 m	13 47,98 S 78 05,12 W
1547	OBH 24 z.W.	LT = 5112 m	13 42,00 S 77 58,23 W
1642	OBS 25 z.W.	LT = 5610 m	13 35,99 S 77 51,28 W

1717	OBH 26 z.W.	LT = 4967 m	13 33,00 S 77 47,83 W
1751	OBS 27 z.W.	LT = 3912 m	13 30,00 S 77n 44,36 W
1821	OBH 28 z.W.	LT = 3702 m	13 26,97 S 77 40,93 W
1909	OBH 29 z.W.	LT = 3211 m	13 22,48 S 77 35,74 W
1954	OBS 30 z.W.	LT = 2258 m	13 18,00 S 77 30,54 W
2027	OBH 31 z.W.	LT = 1775 m	13 15,00 S 77 27,06 W
2103	OBH 32 z.W.	LT = 1438 m	13 11,99 S 77 23,60 W
2136	OBS 33 z.W.	LT = 1387 m	13 09,00 S 77 20,17 W
2210	OBH 34 z.W.	LT = 1417 m	13 05,98 S 77 16,69 W
2306	OBH 35 z.W.	LT = 1057 m	13 00,00 S 77 09,74 W
12.03.2000			
0004	OBH 36 z.W.	LT = 0394 m	12 54,00 S 77 02,88 W

Profil WS/RS 03

0115	Beginn Aussetzen	12 46,01 S 76 53,74 W
0124	Stb airgun z.W.	
0134	Bb airgun z.W.	
0142	M airgun z.W.	
0154	streamer z.W. l = 100 m	
0154	Gradiometer z.W. l = 220 m	
0154	Beginn Profil v = 4,0 kn	12 47,38 S 76 55,29 W
0710	Stb airgun a.D.	
0820	Stb airgun z.W.	
1200		13 14,27 S 77 26,21 W
2400		13 46,34 S 78 03,23 W
13.03.2000		
0509	Ende Profil	14 00,00 S 78 19,00 W109 sml
0515	streamer a.D.	
0521	Gradiometer a.D.	
0530	M airgun a.D.	
0541	Stb airgun a.D.	
0550	Bb airgun a.D.	

Aufnahme OBH/S von WS/RS-Profil 03

0702	OBH 23 ausgelöst	0751 gesichtet	0808	a.D.	13 47,63 S 78 05,16 W
0850	OBH 24	0956	1006		13 41,62 S 77 58,63 W
1006	OBS 25	1126	1142		13 35,56 S 77 51,50 W
1204	OBH 26	1302	1312		13 32,76 S 77 48,00 W
1313	OBS 27	1418	1426		13 29,82 S 77 49,48 W
1427	OBH 28	1512	1520		13 26,81 S 77 41,03 W
1541	OBH 29	1617	1625		13 22,31 S 77 35,88 W
1655	OBS 30	1732	1741		13 17,35 S 77 30,66 W

Profil RS-GI 03

1750	Beginn aussetzen GI guns	13 18,00 S 77 30,52 W
1756	airguns z.W.	
1800	streamer z.W.	
1800	Beginn Profil	13 17,63 S 77 30,13 W
1812	Gradiometer z.W.	

2400		12 57,32 S	77 06,70 W
14.03.2000			
0109	ä.K. auf 57 Grad	12 54,00 S	77 02,90 W
0158	überfahren DDP-site 687	12 51,78 S	76 59,43 W
0210	Ende Profil 03	12 51,23 S	76 58,58 W 36 sml

Profil RS-GI 04 / 05

0254	Beginn Profil	12 50,82 S	76 59,75 W
0306	überfahren DDP-site 687		
0651	Profilwechsel 04 / 05	13 09,60 S	76 52,80 W020 sml
1200		13 11,65 S	77 19,12 W
1451	Ende Profil 05	13 12,75 S	77 33,70 W040 sml
1507	streamer a.D.		
1505	Gradiometer a.D.		
1513	airguns a.D.		

Aufnahme OBH/S von Profil 05

1838	OBH 36 ausgelöst	1840	gesichtet	1849	a.D.	12 54,02 S 77 02,96 W
1942	OBH 35	1951		1957		13 00,04 S 77 09,80 W
2056	OBH 34	2115		2137		13 05,97 S 77 16,86 W
2206	OBS 33	2231		2242		13 09,10 S 77 20,25 W
2304	OBH 32	2320		2328		13 12,07 S 77 23,71 W
2351	OBH 31	0015		0024		13 15,03 S 77 27,10 W

15.03.2000

Profile HS/PS 18 und 19

0307	Beginn Profil 18	13 30,60 S	77 52,20 W
1507	Profilwechsel 18 / 19	11 54,00 S	79 06,00 W 120 sml
1828	Ende Profil 19	11 34,5 S	78 37,5 W 034 sml

Auslegung OBH/S 37 bis 41

1836	OBH 37 z.W.	LT = 2127 m	11 34,53 S	78 37,52 W
2002	OBS 38 z.W.	LT = 2957 m	11 30,60 S	78 51,55 W
2105	OBS 39 z.W.	LT = 2391 m	11 25,72 S	78 42,48 W
2207	OBH 40 z.W.	LT = 2032 m	11 20,85 S	78 33,55 W
2332	OBH 41 z.W.	LT = 2352 m	11 17,00 S	78 47,54 W

Profile HS/PS 20 bis 23

2332	Beginn Profil 20	11 17,00 S	78 47,54 W
16.03.2000			
0242	Profilwechsel 20 / 21	11 19,00 S	79 19,00 W 031 sml
0525	Profilwechsel 21 / 22	10 54,00 S	79 30,00 W 027 sml
1416	Ende Profil 22	09 39,00 s	80 18,00 W 088 sml
1431	Beginn Profil 23	09 39,00 S	80 21,00 W
17.03.2000			
0017	Ende Profil 23	08 15,00 S	81 11,20 W 060 sml

Station GTVA-1 W 2

1456	Beginn Station	LT = 3070 m	05 35,76 S 81 38,75 W

1500	GTV z.W.			
1627	Bosi SL = 3038 m	LT = 3096 m	05 35,77 S	81 38,73 W
	Kurs = 144 Grad v = 0,5 kn			
1715	1. Griff SL = 3193 m	LT = 3194	05 36,09 S	81 38,51 W
1722	Greifer entleert			
1754	2. Griff SL = 3186 m	LT = 3136 m	Sub 05 36,06 S	81 38,53 W
1755	hieven ein			
2019	GTVA a.D.			
2035	Ende Station			

Station GTVA 2W 2

2124	Beginn Station	LT = 3633 m	05 36,29 S	81 38,88 W
2126	GTV z.W.			
2231	Bosi SL = 3582 m	LT = 3608 m	05 36,31 S	81 38,86 W
	div. Kurse v = 0,5 kn			
18.03.2000				
0100	hieven ein SL = 3374 m	LT = 3318 m	05 36,13 S	81 38,60 W
0244	GTVA a.D.			
0245	Ende Station			

Profile HS/PS 24 bis 31

1756	Beginn Profil 24	08 10,75 S	81 03,75 W	
2245	Ende Profil 24	08 59,00 S	80 44,75 W	51 sml
2314	Beginn Profil 25	08 57,00 S	80 40,75 W	
19.03.2000				
0337	Ende Profil 25	08 12,75 S	80 58,50 W	48 sml
0358	Beginn Profil 26	08 11,30 S	80 55,25 W	
0813	Ende Profil 26	08 54,00 S	80 38,00 W	46 sml
0834	Beginn Profil 27	08 54,00 S	80 34,75 W	
1340	Profilwechsel 27 / 28	08 06,50 S	80 54,00 W	51 sml
1536	Profilwechsel 28 / 29	08 14,25 S	81 11,90 W	19 sml
1655	Profilwechsel 29 / 30	08 26,75 S	81 07,00 W	13 sml
2015	Ende Profil 30	08 38,50 S	81 15,79 W	30 sml

Ausbringen OBH/S auf Profil WS/RS 04

2049	OBH 42 z.W.	LT = 4559 m	08 42,44 S	81 33,01 W
2253	OBH 43 z.W.	LT = 5238 m	08 34,31 S	81 13,75 W
20.03.2000				
0044	OBH 43 z.W.	LT = 5523 m	08 27,06 S	80 56,51 W
0112	OBH 45 z.W.	LT = 4605 m	08 25,88 S	80 53,75 W
0150	OBH 46 z.W.	LT = 3920 m	08 23,89 S	80 49,00 W
0240	OBH 47 z.W.	LT = 2419 m	08 20,93 S	80 42,00 W
0323	OBS 48 z.W.	LT = 1556 m	08 18,39 S	80 36,00 W
0436	OBH 49 z.W.	LT = 0738 m	08 13,76 S	80 25,00 W
0538	OBH 50 z.W.	LT = 0256 m	08 09,96 S	80 16,01 W

Profil WS/RS 04

0646	Beginn Aussetzen	08 05,79 S	80 06,11 W
0655	Stb airgun z.W.		

0707	Bb airgun z.W.			
0714	M airgun z.W.			
0731	Gradiometer z.W.	L = 220 m		
0726	Streamer z.W.	L = 200 m		
0745	Beginn Profil	08 07,00 S	80 09,00 W	103 sml
2400		08 32,52 S	81 09,42 W	

21.03.2000

0934	Ende Profil	08 47,50 S	81 45,00 W	
0948	Gradiometer a.D.			
0949	Streamer a.D.			
100	M airgun a.D.			
1010	Stb airgun a.D..			
1019	Bb airgun a.D.			

Aufnahme OBH/S 42 – 46 von WS/RS Profil 04

1136	OBH 42 ausgelöst	1234	gesichtet	1243	a.D.	08 42,29 S	81 33,24 W
1414	OBH 43	1513		1522		08 34,08 S	81 13,98 W
1644	OBH 44	1746		1754		08 26,89 S	80 56,66 W
1747	OBH 45	1845		1853		08 25,78 S	80 53,90 W
1858	OBH 46	1944		1953		08 23,82 S	80 49,08 W

Profile RS 06 bis 25

1953	Beginn Profil	08 23,82 S	80 49,08 W	
2008	Streamer z.W.	L = 300 m		
2017	airguns z.W.			
2035	Gradiometer z.W.	L = 220 m		

22.03.2000

0414	Profilwechsel 06 / 07	08 08,00 S	80 11,50 W	40 sml
0728	Profilwechsel 07 / 08	08 24,00 S	80 08,50 W	16 sml
1600	Profilwechsel 08 / 09	08 54,25 S	80 39,00 W	43 sml
1910	Profilwechsel 09 / 10	09 10,30 S	80 42,00 W	16 sml

23.03.2000

0458	Profilwechsel 10 / 11	08 48,10 S	79 58,00 W	49 sml
0727	Profilwechsel 11 / 12	08 59,00 S	79 51,00 W	13 sml
1520	Ende Profil 12	09 02,96 S	80 30,60 W	39 sml

1525 – 1550 holen alles a.D. Reperatur air guns

1700 – 1725 bringen airguns, streamer und Gradiometer aus

1725	Beginn Profil 13	08 57,53 S	80 28,64 W	

24.03.2000

0058	Profilwechsel 13 / 14	08 31,20 S	79 59,41 W	38 sml
0331	Profilwechsel 14 / 15	08 19,80 S	80 05,42 W	13 sml
0945	Profilwechsel 15 / 16	08 19,83 S	80 05,40 W	31 sml
1057	Profilwechsel 16 / 17	08 32,79 S	80 31,03 W	06 sml
1644	Profilwechsel 17 / 18	08 16,78 S	80 06,62 W	29 sml
1734	Profilwechsel 18 / 19	08 13,21 S	80 08,42 W	04 sml
2309	Profilwechsel 19 / 20	08 29,02 S	80 32,19 W	28 sml

25.03.2000

0017	Profilwechsel 20 / 21	08 23,61 S	80 33,60 W	05 sml
0615	Profilwechsel 21 / 22	08 00,60 S	80 07,51 W	30 sml

0720	Profilwechsel 22 / 23	08 05,01 S 80 11,98 W	06 sml
0824	Unterbrechung Profil 23	08 07,06 S 80 16,86 W	
0825 – 0846	holen streamer und airguns ein		
0846 – 0915	Schleife		
0920	streamer z.W.		
0924	airguns z.W.		
0927	Fortsetzung Profil 23	08 06,67 S 80 50,93 W	
1412	Profilwechsel 23 / 24	08 16,01 S 80 38,05 W	28 sml
1500	Profilwechsel 24 / 25	08 12,01 S 80 38,00 W	04 sml
1933	Ende Profil 25	08 03,01 S 80 16,82 W	23 sml
1945	streamer a.D.		
1947	Gradiometer a.D.		
1951	airguns a.D.		

Aufnahme OBS/H 50 bis 47

2100	OBH 50 ausgelöst	2103 gesichtet	2111 a.D.	08 09,97 S 80 16,07 W
2205	OBH 49	2213	2222	08 13,82 S 80 25,03 W
2320	OBS 48	2342	2400	08 18,13 S 80 36,29 W

26.03.2000

0001	OBH 47	0027	0049	08 20,73 S 80 42,37 W

Profile HS/PS 31 bis 37

0111	Beginn Profil 31	08 23,0 S 80 45,0 W	
0431	Profilwechsel 31 / 32	08 55,0 S 80 32,0 W	34 sml
0651	Profilwechsel 32 / 33	09 18,0 S 80 24,5 W	24 sml
0759	Profilwechsel 33 / 34	09 30,0 S 80 24,5 W	12 sml
0850	Profilwechsel 34 / 35	09 36,5 S 80 18,5 W	09 sml
0913	Profilwechsel 35 / 36	09 37,0 S 80 14,5 W	04 sml
1743	Profilwechsel 36 / 37	10 52,0 S 79 26,75 W	88 sml
2010	Profilwechsel 37 / 38	11 15,5 S 79 17,25 W	25 sml
2304	Profilende 38	11 16,0 S 78 48,0 W	

Aufnahme OBH/S 37 bis 41

2249	OBH 41	ausgelöst 2312	gesichtet 2323	a.D.	11 16,96 S 78 47,57 W

27.03.2000

0015	OBS 38	0055	0106	11 30,54 S 78 51,67 W
0137	OBS 39	0207	0225	11 25,68 S 78 42,56 W
0306	OBS 40	0340	0355	11 20,87 S 78 33,62 W
0453	OBH 37	0515	0529	11 34,51 S 78 37,60 W

Profile HS/PS 39 und 40

0530	Beginn Profil 39	11 34,50 S 78 37,60 W	
0743	Profilwechsel 39 / 40	11 39,00 S 79 00,00 W	23 sml
1123	Ende Profil 40	11 57,50 S 79 35,50 W	39 sml

Auslegung OBH/S auf WS/RS-Profil 05

1150	OBH 51 z.W.	LT = 5006 m	11 53,84 S 79 36,63 W
1337	OBH 52 z.W.	LT = 5497 m	11 46,71 S 79 23,02 W
	OBH am Seil ; L = 600 m		

1508	OBH 53 z.W.	LT = 5498 m	11 39,04 S	79 08,31 W
1532	OBH 54 z.W.	LT = 4412 m	11 37,31 S	79 05,06 W
1604	OBS 55 z.W.	LT = 3956 m	11 34,94 S	79 00,53 W
1636	OBH 56 z.W.	LT = 3842 m	11 32,54 S	78 56,06 W
1709	OBH 57 z.W.	LT = 2900 m	11 30,24 S	78 51,51 W
1742	OBH 58 z.W.	LT = 2571 m	11 27,88 S	78 47,00 W
1830	OBS 59 z.W.	LT = 2415 m	11 25,55 S	78 42,54 W
1848	OBH 60 z.W.	LT = 2083 m	11 23,21 S	78 38,03 W
1920	OBS 61 z.W.	LT = 2032 m	11 20,80 S	78 33,52 W
1953	OBH 62 z.W.	LT = 1587 m	11 18,42 S	78 29,05 W
2025	OBH 63 z.W.	LT = 1040 m	11 16,11 S	78 24,57 W
2124	OBH 64 z.W.	LT = 0496 m	11 11,38 S	78 15,56 W

Profil WS/RS 05

2240	Beginn aussetzen		11 04,83 S	78 03,11 W
2249	Stb airgun z.W.			
2256	Bb airgun z.W.			
2306	M airgun z.W.			
2317	Streamer z.W.	l = 250 m		
2322	Gradiometer z.W.	l = 220 m		
2346	Beginn Profil		11 06,60 S	78 06,60 W120 sml
28.03.2000				
1200			11 29,76 S	78 50,67 W
2400				
29.03.2000				
0545	Ende Profil		12 03,25 S	79 54,52 W
0600	Streamer a.D.			
0611	Gradiometer a.D.			
0621	M airgun a.D.			
0632	Stb airgun a.D.			
0640	Bb airgun a.D.			

Aufnahme OBH/S von Profil WS/RS 05

0819	OBH 51	ausgelöst	0922	gesichtet	0927	a.D.	11 53,71 S 79 36,67 W
1023	OBH 52		1116		1125		11 46,64 S 79 23,04 W
1301	OBH 53		1402		1410		11 39,02 S 79 08,29 W
1403	OBS 54		1500		1505		11 37,29 S 79 05,09 W
1442	OBS 55		1548		1555		11 34,86 S 79 05,97 W
1548	OBH 56		1627		1635		11 32,48 S 79 56,16 W
1630	OBS 57		1717		1726		11 30,23 S 79 51,61 W
1754	OBH 58		1808		1820		11 27,84 S 78 47,12 W
1820 – 2008		div. Auslöseversuche OBS 59 ; ohne Erfolg					
2027	OBH 60		2051		2102		11 23,19 S 78 38,21 W
2128	OBS 61		2138		2158		11 20,85 S 78 33,80 W
2228	OBH 62		2247		2256		11 18,47 S 78 29,11 W
2326	OBH 63		2337		2348		11 16,14 S 78 24,55 W
30.03.2000							
0040	OBH 64		0045		0057		11 11,42 S 78 16,60 W

HS/PS Profile 41bis 43

0100	Beginn Profil 41	11 11,47 S	78 15,70 W	
0346	Profilwechsel 41 / 42	11 27,00 S	78 39,00 W	28 sml
0659	Profilwechsel 42 / 43	11 56,00 S	78 24,00 W	32 sml
0711	Profilende 43	11 56,97 S	78 26,05 W	10 sml

Auslegung OBH/S auf Profil WS/RS 06

0721	OBH 65 z.W.	LT = 2477 m	11 56,96 S	78 26,07 W
0823	OBH 66 z.W.	LT = 2394 m	11 48,08 S	78 30,76 W
0919	OBH 67 z.W.	LT = 2235 m	11 39,03 S	78 35,54 W
0949	OBS 68 z.W.	LT = 2163 m	11 34,56 S	78 37,90 W
1020	OBH 69 z.W.	LT = 2259 m	11 30,05 S	78 40,30 W

Station GTVA 03 W 2 Bergungsversuch OBH 59

1111	Beginn Station		LT = 2434 m	11 25,44 S	78 42,71 W
1114	GTV z.W.				
1158	Bosi	SL = 2398 m	LT = 2423 m	11 25,48 S	78 42,58 W
1740	Boko	SL = 2391 m	LT = 2412 m	11 25,56 S	78 42,50 W
1743	hieven ein				
1843	GTV a.D.				
1850	Ende Station				

Auslegung OBH/S auf Profil WS/RS 06 ff

1857	OBS 70 z.W.	LT = 2419 m	11 25,57 S	78 42,66 W
1936	OBH 71 z.W.	LT = 2494 m	11 21,06 S	78 45,04 W
2009	OBS 72 z.W.	LT = 2318 m	11 16,58 S	78 47,41 W
2045	OBH 73 z.W.	LT = 2293 m	11 12,13 S	78 49,74 W
2142	OBH 74 z.W.	LT = 2424 m	11 03,25 S	78 54,45 W
2242	OBH 75 z.W.	LT = 2464 m	10 54,31 S	78 59,19 W

31.03.2000

Profil WS/RS 06

0042	Beginn aussetzen	10 43,08 S	70 05,14 W
0050	Stb airgun z.W.		
0058	Bb airgun z.W.		
0105	M airgun z.W.		
0111	streamer z.W.		
0116	Beginn Profil	10 44,70 S	79 04,25 W
0729	hieven streamer ein		
0735	streamer a.B. abgerissen		
0754	Unterbrechung Profil	11 08,09 S	78 51,88 W30 sml
0825	alles ein		
0830 – 0930	Bergung Rest-streamer		
1007	alle airguns z.W.		
1007	Fortsetzung Profil 06 als WS-Profil	11 03,94 S	78 54,07 W70 sml
1146	Gradiometer z.W. l = 220 m		
2400		11 53,38 S	78 27,96 W

01.04.2000

FS SONNE Stationsprotokoll SO 146/1

0332	Ende Profil 06	12 05,94 S	78 21,30 W
0333	Beginn einholen		
0407	alles a.D.		

Aufnahme OBH/S von Profil WS/RS 06

0548	OBH 65 ausgelöst	0619	gesichtet	0629 a.D.	11 56,99 S 78 26,09 W
0713	OBH 66	0741		0751	11 48,10 S 78 30,76 W
0828	OBH 67	0855		0900	11 39,05 S 78 35,57 W
0901	OBS 68	0934		0941	11 34,52 S 78 37,91 W
0944	OBH 69	1008		1014	11 30,01 S 78 40,32 W
1016	OBS 70	1055		1102	11 25,47 S 78 42,72 W
1018	OBS 59 ausgelöst, ohne Erfolg				
1103	OBH 71	1128		1144	11 20,79 S 78 45,25 W
1145	OBS 72	1225		1233	11 16,53 S 78 47,40 W
1234	OBH 73	1325		1330	11 12,12 S 78 49,65 W
1404	OBH 74	1432		1440	11 03,20 S 78 54,39 W
1509	OBH 75	1536		1541	10 54,31 S 78 59,18 W

Station GTVA 04 W 02

1901	Beginn Station	LT = 2427 m	11 25,45 S 78 42,58 W
1904	GTVA z.W.		
1948	Bosi SL = 2389 m	LT = 2424 m	11 25,52 S 78 42,55 W
02.04.2000			
0222	Boko SL = 2391 m	LT = 2412 m	11 25,53 S 78 42,51 W
0256	brechen ab, hieven ein		
0350	GTVA a.D.		
0400	Ende Station		

Insgesamt wurden gefahren :
1 CTD
2 GTVA zur Probennahme
2 GTVA zur Bergung OBH 59

HS/PS-Profile	= 1754 sml	mit Gravimeter
WS/RS-Profile	= 0548 sml	mit Gradiometer und Gravimeter
WS Profile	= 0070 sml	mit Gradiometer und Gravimeter
RS Profile	= 0605 sml	mit Gradiometer und Gravimeter

0453 GI-guns a.D.

Bergung OBH/S von Profil 07

0555	OBH 76	ausgelöst	0622 gesichtet	0640 a.D.	11 05,43 S 78 38,56 W
0641	OBH 77		0703	0714	11 05,83 S 78 39,56 W
0714	OBH 78		0738	0748	11 06,24 S 78 40,42 W
0746	OBH 79		0806	0810	11 06,66 S 78 41,36 W
0808	OBS 80		0838	0844	11 06,97 S 78 42,32 W
0840	OBH 81		0900	0907	11 07,42 S 78 43,27 W
0903	OBH 82		0924	0932	11 07,79 S 78 44,21 W
0932	OBH 83		0952	1000	11 08,21 S 78 45,13 W
0955	OBS 84		1027	1039	11 08,58 S 78 46,05 W

Profile HS/PS 43 bis 50

1045	Beginn Profil 43	11 08,57 S 78 46,19 W	08 sml
1130	Profilwechsel 43 / 44	11 13,5 S 78 52,0 W	41 sml
1526	Profilwechsel 44 / 45	10 48,0 S 79 25,0 W	87 sml
2347	Profilwechsel 45 / 46	09 34,5 S 80 13,5 W	14 sml
07.04.00			
0106	Profilwechsel 46 / 47	09 39,0 S 80 26,5 W	54 sml
0612	Profilwechsel 47 / 48	08 52,0 S 80 52,75 W	45 sml
1025	Profilwechsel 48 / 49	08 10,0 S 81 08,75 W	17 sml
1205	Profilwechsel 49 / 50	08 03,0 S 80 44,5 W	22 sml
1412	Ende Profil 50	08 23,5 S 80 44,5 W	

Stationen HF 01 bis 13 W 1

1535 Beginn Station 01 LT = 1253 m 08 27,94 S 80 30,58 W

1537 HF z.W.

Profilkurs = 56 Grad v = 1,0 kn Dist. zw. den Messpunkten := 0,27 sml

1607	Boko HF 01	SL = 1269 m	LT = 1253 m	08 27,92 S	80 30,58 W
1654	Boko HF 02	SL = 1258 m	LT = 1240 m	08 27,77 S	80 30,33 W
1738	Boko HF 03	SL = 1230 m	LT = 1216 m	08 27,64 S	80 30,12 W
1842	Boko HF 04	SL = 1142 m	LT = 1181 m	08 27,5o S	80 29,89 W
1931	Boko HF 05	SL = 1215 m	LT = 1174 m	08 27,33 S	80 29,67 W
1935	hieven a.D.				
2050	HF z.W.				
2120	Boko HF 05/2	SL = 1178 m	LT = 1173 m	08 27,33 S	80 29,67 W
2210	Boko HF 06	SL = 1169 m	LT = 1158 m	08 27,17 S	80 29,44 W
2248	Boko HF 07	SL = 1150 m	LT = 1153 m	08 27,03 S	80 29,22 W
2328	Boko HF 08	SL = 1123 m	LT = 1140 m	08 26,87 S	80 28,99 W
08.04.00					
0015	Boko HF 09	SL = 1120 m	LT = 1122 m	08 26,72 S	80 28,74 W
0054	Boko HF 10	SL = 1130 m	LT = 1114 m	08 26,57 S	80 28,53 W
0142	Boko HF 11	SL = 1094 m	LT = 1080 m	08 26,41 S	80 28,32 W
0219	Boko HF 12	SL = 1088 m	LT = 1075 m	08 26,27 S	80 28,07 W
0301	Boko HF 13	SL = 1079 m	LT = 1069 m	08 26,11 S	80 27,85 W
0340	HF a.D. Ende Station				

Station OFOS 01 W 1

0419 Beginn Station LT = 1446 m 08 28,97 S 80 31,14 W

0422	OFOS z.W.			
0452	Bosi	SL = 1420 m	LT = 1421 m	08 28,76 S 80 31,88 W
	Kurs = 56 Grad	v = 1,0 kn		
1051	hieven	SL = 1078 m	LT = 1044 m	08 26,17 S 80 27,88 W
1119	OFOS a.D.	Ende Station		

Station OFOS 02 W 1

1158	Beginn Station		LT = 1344 m	08 27,65 S 80 32,09 W
1200	OFOS z.W.			
1235	Bosi	SL = 1336 m	LT = 1342 m	08 27,53 S 80 31,88 W
	Kurs = 59 Grad	v = 0,8 kn		
1800	hieven ein	SL = 1054 m	LT = 1065 m	08 25,46 S 80 28,37 W
1825	OFOS a.D.	Ende Station		

Stationen HF 14 bis 22 W 01

1900	HF z.W.		LT = 958 m	08 23,74 S 80 24,21 W
1925	Boko HF 14	SL = 964 m	LT = 954 m	08 23,69 S 80 24,16 W
2044	Boko HF 15	SL = 949 m	LT = 941 m	08 23,37 S 80 23,61 W
2136	Boko HF 16	SL = 934 m	LT = 930 m	08 23,11 S 80 23,26 W
2246	Boko HF 17	SL = 926 m	LT = 915 m	08 22,82 S 80 22,82 W
2350	Boko HF 18	SL = 910 m	LT = 901 m	08 22,50 S 80 22,41 W
09.04.00				
0101	Boko HF 19	SL = 892 m	LT = 887 m	08 22,18 S 80 21,90 W
0203	Boko HF 20	SL = 878 m	LT = 871 m	08 21,87 S 80 21,45 W
0302	Boko HF 21	SL = 862 m	LT = 856 m	08 21,57 S 80 20,99 W
0358	Boko HF 22	SL = 851 m	LT = 842 m	08 21,31 S 80 20,47 W
0433	HF a.D.	Ende der HF-Messungen		

Station OFOS 03 W 1

0505	Beginn Station		LT = 964 m	08 23,85 S 80 24,50 W
0533	OFOS z.W.			
0556	Bosi	SL = 955 m	LT = 958 m	08 23,75 S 80 24,29 W
	Kurs = 56 Grad	v = 0,8 kn		
0747	Ende Bosi	SL = 929 m	LT = 927 m	08 22,98 S 80 23,11 W
0813	OFOS a.D.	Ende Station		

Station OFOS 04 W 1

0831	Beginn Station		LT = 962 m	08 23,67 S 80 24,46 W
0832	OFOS z.W.			
0852	Bosi	SL = 948 m	LT = 957 m	08 23,62 S 80 24,29 W
	Kurs = 59 Grad	v = 0,8 kn		
1006	Ende Bosi	SL =		08 23,12 S 80 23,62 W
1025	OFOS a.D.	Ende Station		

Station OFOS 05 W 1

1041	Beginn Station		LT = 943 m	08 23,21 S 80 24,06 W
1042	OFOS z.W.			
1103	Bosi	SL = 931 m	LT = 942 m	08 23,18 S 80 24,06 W
	Kurs = 153 Grad	v = 0,8 kn		

Appendix I Captains Report (continued)

RF Reedereigemeinschaft
Forschungsschiffahrt GmbH

Stationsprotokoll F.S. "S O N N E" Reise SO 146/2

Eingesetzte Geräte		Einsätze	/ Seemeilen
HS	Hydrosweep		1234
PS	Parasound		1234
OBH/OBS	Ocean Bottom Hydrofone und Seismograph	52	
GD	Gradiometer		
GV	Gravimeter		
Streamer			
HF	Wärmemesssonde	65	
2 x GI-airguns	Seismik		0634
OFOS	Unterwasser-Observierungs-System	12	
GTVA	Fernsehgreifer Typ A	08	
CTD/ROS	CTD-Sonde	01	

Eingesetzte Winden :

Winde	*D/M*	*Typ*	*RF-Nr*	*SO 146/2 Einsatz*	*Gesamt Einsatz*	*SO 146/2 S`länge*	*Gesamt S`länge*	*Zust.*
W 1	18,2	LWL	816233	161 h	1074 h	43614 m	303118 m	3
W 2	18,2	LWL	000000	000	0000	00000	000000	0
W 4	11,0	NSW	817141	000	0222	03000	139383	3
W 5	11,0	NSW	817164	005	0039	04690	046007	3
W 6	18,2	DRAKO	814150	006	0904	07900	756288	3

Winde	*SO 146/2 gefierte max.Länge*	*jemals gefierte max.Länge*
W 1	3000 m	6474 m
W 2	0000	6545
W 4	0000	6100
W 5	2690	5200
W 6	7900	7900

Geräteverluste : keine

Abkürzungen im Stationsprotokoll:

z.W.	zu Wasser
a.D.	an Deck
Boko	Bodenkontakt
Bosi	Bodensicht
SL(max.)	(maximale)Seillänge
LT	Lottiefe nach Hydrosweep
W x	eingesetzte Winde
HS	Hydrosweep
PS	Parasound
XPNDR	Transponder

FS SONNE Stationsprotokoll SO 146/2

Zeit : UTC - 05 Stunden

04.04.2000

Station GTVA 05 W 01

1700	Beginn Station	LT = 2423 m	11 25,54 S	78 42,51 W
1748	Bosi SL = 2389 m	LT = 2418 m	11 25,54 S	78 42,51 W
1905	OBS 59 touchiert			
1910	Hydrofonmessung zeigt daß OBS aufsteigt			
1935	OBS 59 aufgetaucht			
1942	GTVA a.D.			
1951	OBS 59 a.D.		11 25,55 S	78 42,56 W
1955	Ende Station			

Releaser-Test W 01

2120	Beginn Station	LT = 3226 m	11 20,0 S 78 55,7 W
2123	Releaser z.W.		
2218	Slmax = 3000 m	LT = 3224 m	11 19,9 S 78 55,7 W
2218 – 2230	testen releaser mit Hydrofon		
2327	Releaser a.D.		
2328	Ende Station		

05.04.00

Auslegung OBH/S auf Profil WS/RS 07

0134	OBH 76 z.W.	LT = 1711 m	11 05,47 S 78 38,67 W
0152	OBH 77 z.W.	LT = 1781 m	11 05,86 S 78 39,63 W
0209	OBH 78 z.W.	LT = 1832 m	11 06,24 S 78 40,55 W
0228	OBH 79 z.W.	LT = 1879 m	11 06,63 S 78 41,50 W
0242	OBS 80 z.W.	LT = 1929 m	11 07,01 S 78 42,44 W
0308	OBH 81 z.W.	LT = 1966 m	11 07,39 S 78 43,37 W
0326	OBH 82 z.W.	LT = 1983 m	11 07,78 S 78 44,31 W
0343	OBH 83 z.W.	LT = 2022 m	11 08,18 S 78 45,25 W
0415	OBS 84 z.W.	LT = 2054 m	11 08,57 S 78 46,20 W

Profil WS/RS 07

0520	Beginn aussetzen	11 12,77 S	78 56,42 W	
0527	streamer z.W. L = 300 m			
0541	GI-guns z.W.			
0551	Gradiometer z.W. L = 250 m			
0600	Beginn Profil	11 11,67 S	78 53,69 W	24 sml
1044	ä.K. auf 158 Grad	11 02,40 S	78 31,20 W	11 sml
1303	ä.K. auf 247 Grad	11 12,78 S	78 26,86 W	08 sml
1437	ä.K. auf 337 Grad	11 15,88 S	78 34,36 W	20 sml
1834	ä.K. auf 247 Grad	10 57,13 S	78 42,15 W	04 sml
1930	ä.K. auf 157 Grad	10 58,68 S	78 45,90 W	20 sml
2333	ä.K. auf 247 Grad	11 17,44 S	78 38,11 W	04 sml

06.04.00

0022	ä.K. auf 337 Grad	11 18,98 S	78 41,86 W	22 sml
0423	Ende Profil	11 00,23 S	78 49,65 W	
0434	Gradiometer a.D.			
0448	Streamer a.D.			

0453 GI-guns a.D.

Bergung OBH/S von Profil 07

0555	OBH 76	ausgelöst	0622 gesichtet	0640 a.D.	11 05,43 S 78 38,56 W
0641	OBH 77		0703	0714	11 05,83 S 78 39,56 W
0714	OBH 78		0738	0748	11 06,24 S 78 40,42 W
0746	OBH 79		0806	0810	11 06,66 S 78 41,36 W
0808	OBS 80		0838	0844	11 06,97 S 78 42,32 W
0840	OBH 81		0900	0907	11 07,42 S 78 43,27 W
0903	OBH 82		0924	0932	11 07,79 S 78 44,21 W
0932	OBH 83		0952	1000	11 08,21 S 78 45,13 W
0955	OBS 84		1027	1039	11 08,58 S 78 46,05 W

Profile HS/PS 43 bis 50

1045	Beginn Profil 43	11 08,57 S 78 46,19 W	08 sml
1130	Profilwechsel 43 / 44	11 13,5 S 78 52,0 W	41 sml
1526	Profilwechsel 44 / 45	10 48,0 S 79 25,0 W	87 sml
2347	Profilwechsel 45 / 46	09 34,5 S 80 13,5 W	14 sml
07.04.00			
0106	Profilwechsel 46 / 47	09 39,0 S 80 26,5 W	54 sml
0612	Profilwechsel 47 / 48	08 52,0 S 80 52,75 W	45 sml
1025	Profilwechsel 48 / 49	08 10,0 S 81 08,75 W	17 sml
1205	Profilwechsel 49 / 50	08 03,0 S 80 44,5 W	22 sml
1412	Ende Profil 50	08 23,5 S 80 44,5 W	

Stationen HF 01 bis 13 W 1

1535 Beginn Station 01 LT = 1253 m 08 27,94 S 80 30,58 W

1537 HF z.W.

Profilkurs = 56 Grad v = 1,0 kn Dist. zw. den Messpunkten := 0,27 sml

1607	Boko HF 01	SL = 1269 m	LT = 1253 m	08 27,92 S	80 30,58 W
1654	Boko HF 02	SL = 1258 m	LT = 1240 m	08 27,77 S	80 30,33 W
1738	Boko HF 03	SL = 1230 m	LT = 1216 m	08 27,64 S	80 30,12 W
1842	Boko HF 04	SL = 1142 m	LT = 1181 m	08 27,5o S	80 29,89 W
1931	Boko HF 05	SL = 1215 m	LT = 1174 m	08 27,33 S	80 29,67 W
1935	hieven a.D.				
2050	HF z.W.				
2120	Boko HF 05/2	SL = 1178 m	LT = 1173 m	08 27,33 S	80 29,67 W
2210	Boko HF 06	SL = 1169 m	LT = 1158 m	08 27,17 S	80 29,44 W
2248	Boko HF 07	SL = 1150 m	LT = 1153 m	08 27,03 S	80 29,22 W
2328	Boko HF 08	SL = 1123 m	LT = 1140 m	08 26,87 S	80 28,99 W
08.04.00					
0015	Boko HF 09	SL = 1120 m	LT = 1122 m	08 26,72 S	80 28,74 W
0054	Boko HF 10	SL = 1130 m	LT = 1114 m	08 26,57 S	80 28,53 W
0142	Boko HF 11	SL = 1094 m	LT = 1080 m	08 26,41 S	80 28,32 W
0219	Boko HF 12	SL = 1088 m	LT = 1075 m	08 26,27 S	80 28,07 W
0301	Boko HF 13	SL = 1079 m	LT = 1069 m	08 26,11 S	80 27,85 W
0340	HF a.D. Ende Station				

Station OFOS 01 W 1

0419 Beginn Station LT = 1446 m 08 28,97 S 80 31,14 W

0422	OFOS z.W.			
0452	Bosi	SL = 1420 m	LT = 1421 m	08 28,76 S 80 31,88 W
	Kurs = 56 Grad	v = 1,0 kn		
1051	hieven	SL = 1078 m	LT = 1044 m	08 26,17 S 80 27,88 W
1119	OFOS a.D.	Ende Station		

Station OFOS 02 W 1

1158	Beginn Station		LT = 1344 m	08 27,65 S 80 32,09 W
1200	OFOS z.W.			
1235	Bosi	SL = 1336 m	LT = 1342 m	08 27,53 S 80 31,88 W
	Kurs = 59 Grad	v = 0,8 kn		
1800	hieven ein	SL = 1054 m	LT = 1065 m	08 25,46 S 80 28,37 W
1825	OFOS a.D.	Ende Station		

Stationen HF 14 bis 22 W 01

1900	HF z.W.		LT = 958 m	08 23,74 S 80 24,21 W
1925	Boko HF 14	SL = 964 m	LT = 954 m	08 23,69 S 80 24,16 W
2044	Boko HF 15	SL = 949 m	LT = 941 m	08 23,37 S 80 23,61 W
2136	Boko HF 16	SL = 934 m	LT = 930 m	08 23,11 S 80 23,26 W
2246	Boko HF 17	SL = 926 m	LT = 915 m	08 22,82 S 80 22,82 W
2350	Boko HF 18	SL = 910 m	LT = 901 m	08 22,50 S 80 22,41 W
09.04.00				
0101	Boko HF 19	SL = 892 m	LT = 887 m	08 22,18 S 80 21,90 W
0203	Boko HF 20	SL = 878 m	LT = 871 m	08 21,87 S 80 21,45 W
0302	Boko HF 21	SL = 862 m	LT = 856 m	08 21,57 S 80 20,99 W
0358	Boko HF 22	SL = 851 m	LT = 842 m	08 21,31 S 80 20,47 W
0433	HF a.D.	Ende der HF-Messungen		

Station OFOS 03 W 1

0505	Beginn Station		LT = 964 m	08 23,85 S 80 24,50 W
0533	OFOS z.W.			
0556	Bosi	SL = 955 m	LT = 958 m	08 23,75 S 80 24,29 W
	Kurs = 56 Grad	v = 0,8 kn		
0747	Ende Bosi	SL = 929 m	LT = 927 m	08 22,98 S 80 23,11 W
0813	OFOS a.D.	Ende Station		

Station OFOS 04 W 1

0831	Beginn Station		LT = 962 m	08 23,67 S 80 24,46 W
0832	OFOS z.W.			
0852	Bosi	SL = 948 m	LT = 957 m	08 23,62 S 80 24,29 W
	Kurs = 59 Grad	v = 0,8 kn		
1006	Ende Bosi	SL =		08 23,12 S 80 23,62 W
1025	OFOS a.D.	Ende Station		

Station OFOS 05 W 1

1041	Beginn Station		LT = 943 m	08 23,21 S 80 24,06 W
1042	OFOS z.W.			
1103	Bosi	SL = 931 m	LT = 942 m	08 23,18 S 80 24,06 W
	Kurs = 153 Grad	v = 0,8 kn		

1148	Ende Bosi	SL = 932 m	LT = 944 m	08 23,45 S 80 23,64 W
1214	OFOS a.D.	Ende Station		

Station TEST SeeBoSei W 5

1410	Beginn Station		LT = 2702 m	08 38,30 S 80 36,0 W
1418	Schuss-unit z.W.			
1506	Slmax = 2000 m			
1509	Auslösung Schuss registriert			
1512	hieven ein			
1606	Gerät a.D.	Ende Station		

Profile HS/PS 51 und 52

1634	Beginn Profil 51		08 36,69 S 80 32,20 W	08 sml
1722	Profilwechsel 51 /52		08 28,38 S 80 34,10 W	32 sml
1905	Profilende 52		08 18,92 S 80 17,92 W	

Stationen HF 23 bis 31

1950	HF z.W.			
2001	Boko HF 23	SL = 266 m	LT = 250 m	08 16,03 S 80 12,71 W
2106	Boko HF 24	SL = 303 m	LT = 286 m	08 16,34 S 80 13,14 W
2157	Boko HF 25	SL = 351 m	LT = 338 m	08 16,65 S 80 13,58 W
2320	Boko HF 26	SL = 466 m	LT = 440 m	08 17,20 S 80 14,52 W
10.04.00				
0035	Boko HF 27	SL = 548 m	LT = 534 m	08 17,84 S 80 15,42 W
0126	Boko HF 28	SL = 590 m	LT = 583 m	08 18,17 S 80 15,89 W
0224	Boko HF 29	SL = 640 m	LT = 624 m	08 18,45 S 80 16,34 W
0331	Boko HF 30	SL = 673 m	LT = 659 m	08 18,75 S 80 16,77 W
0421	Boko HF 31	SL = 695 m	LT = 687 m	08 19,03 S 80 17,15 W
0454	HF a.D.	Ende Station		

Station OFOS 06 W 1

0505	Beginn Station			
0520	OFOS z.W.		LT = 700 m	08 19,16 S 80 17,34 W
0540	Bosi	SL = 696 m	LT = 692 m	08 19,07 S 80 17,22 W
	Kurs = 56 Grad	v = 0,8 kn		
0917	Ende Bosi, hieven	SL = 483 m	LT = 479 m	08 17,48 S 80 14,88 W
0917	OFOS a.D.	Ende Station		

Station OFOS 07 W 1

0945	Beginn Station		LT = 420 m	08 17,15 S 80 14,22 W
0947	OFOS z.W.			
0958	Bosi	SL = 403 m	LT = 406 m	08 17,06 S 80 14,10 W
	Kurs = 56 Grad	v = 0,8 kn		
1200	hieven ein	SL = 286 m	LT = 286 m	08 16,38 S 80 12,74 W
1213	OFOS a.D.	Ende Station		

Station OFOS 08 W 1

1235	Beginn Station			
1237	OFOS z.W.		LT = 494 m	08 17,63 S 80 14,94 W

FS SONNE Stationsprotokoll SO 146/2

1249	Bosi	SL = 480 m	LT = 483 m	08 17,56 S 80 14,82 W
	Kurs = 54 Grad	v = 0,8 kn		
1428	hieven ein	SL = 365 m	LT = 372 m	08 16,85 S 80 13,83 W
1439	OFOS a.D.	Ende Station		

Auslegung OBH/S 85 bis 97

1508	OBH 85 z.W.	LT = 411 m	08 17,04 S 80 14,86 W
1524	OBS 86 z.W.	LT = 480 m	08 17,47 S 80 14,86 W
1545	OBH 87 z.W.	LT = 611 m	08 18,35 S 80 16,16 W
1602	OBH 88 z.W.	LT = 720 m	08 19,02 S 80 17,21 W
1618	OBH 89 z.W.	LT = 752 m	08 19,64 S 80 18,31 W
1634	OBS 90 z.W.	LT = 810 m	08 20,70 S 80 19,74 W
1649	OBH 91 z.W.	LT = 833 m	08 21,14 S 80 20,40 W
1704	OBH 92 z.W.	LT = 861 m	08 21,72 S 80 21,28 W
1718	OBS 93 z.W.	LT = 884 m	08 22,20 S 80 22,00 W
1734	OBH 94 z.W.	LT = 913 m	08 22,78 S 80 22,87 W
1753	OBH 95 z.W.	LT = 948 m	08 23,57 S 80 24,07 W
1806	OBS 96 z.W.	LT = 971 m	08 24,06 S 80 24,82 W
1831	OBH 97 z.W.	LT = 1227 m	08 25,23 S 80 26,60 W

Profil WS/RS 08

1925	Beginn Ausbringen Geräte		08 30,55 S 80 21,83 W	
1933	Streamer z.W.			
1936	airguns z.W.			
1949	Gradiometer z.W.			
2002	Beginn Profil		08 28,65 S 80 22,70 W	11 sml
2245	ä.K. auf 59 Grad		08 21,52 S 80 26,00 W	04 sml
2340	ä.K. auf 135 Grad		08 17,34 S 80 24,39 W	10 sml
11.04.00				
0221	ä.K. auf 55 Grad		08 26,89 S 80 19,74 W	03 sml
0301	ä.K. auf 335 Grad		08 25,37 S 80 17,50 W	10 sml
0534	ä.K. auf 60 Grad		08 16,05 S 80 21,86 W	06 sml
0655	ä.K. auf 154 Grad		08 13,25 S 80 16,95 W	09 sml
0919	ä.K. auf 59 Grad		08 21,88 S 80 12,68 W	01 sml
1053	ä.K. auf 337 Grad		08 16,13 S 80 11,74 W	05 sml
1102	ä.K. auf 236 Grad		08 15,56 S 80 11,98 W	19 sml
1218	1 SeeBoSeis-Kugel z.W.		08 18,15 S 80 15,88 W	
1312	2. dito z.W.		08 20,15 S 80 18,90 W	
1555	Ende Profil		08 26,21 S 80 28,06 W	
1623	alles ein			

Aufnahme OBH/S 97 bis 85

1642	OBH 97 ausgelöst	1652 gesichtet	1657 a.D.	08 25,29 S 80 26,66 W
1658	OBS 96	1717	1722	08 28,16 S 80 24,87 W
1722	OBH 95	1733	1738	08 23,65 S 80 24,09 W
1740	OBH 94	1752	1801	08 22,87 S 80 22,89 W
1742 – 1824	lösen OBS 93 aus, steigt nicht			
1825	OBH 92	1836	1847	08 21,86 S 80 21,30 W
1847	OBH 91	1900	1912	08 21,28 S 80 20,42 W
1913	OBS 90	1929	1941	08 20,84 S 80 19,77 W

FS SONNE Stationsprotokoll SO 146/2

1942 OBH 89	1952	2009	08 19,96 S	90 18,30 W
2010 OBH 88	2015	2040	08 19,35 S	80 17,23 W
2055 OBH 87	2103	2114	08 18,59 S	80 16,14 W
2116 OBS 86	2128	2149	08 17,86 S	80 14,80 W
2150 OBH 85	2155	2225	08 17,65 S	80 14,13 W

2318 – 2400 OBS 93 eingemessen

12.04.00

0000 – 0100 OBS 93 eingemessen

Station GTVA 06 W 01

0148	Beginn Station	LT = 620 m	08 18,46 S	80 16,21 W
0150	GTV z.W.			
0207	Bosi SL = 604 m	LT = 605 m	08 18,37 S	80 16,15 W
0214	Griff SL = 605 m	LT = 605 m	08 18,32 S	80 16,13 W
0236	GTV a.D.			
0245	Ende Station			

Profil HS/PS 52

0300	Beginn Profil	08 17,28 S	80 15,81 W	02 sml
0311	ä.K. auf 234 Grad	08 18,85 S	80 15,34 W	08 sml
0400	Ende Profi l	08 23,82 S	80 22,25 W	

Station GTVA 07 W 1

0425	Beginn Station	LT = 939 m	08 23,05 S	80 24,14 W
0428	GTV z.W.			
0448	Bosi SL = 928 m	LT = 939 m	08 23,07 S	80 24,11 W
0618	Boko SL = 924 m	LT = 934 m	08 23,28 S	80 23,79 W
0644	Griff SL = 930 m	LT = 935 m	08 23,37 S	80 23,79 W
0722	GTV a.D.			
0726	Ende Station			

Profil HS/PS 53

0743	Beginn Profil	08 21,84 S	80 24,69 W	08 sml
0837	Ende Profil	08 17,16 S	80 17,31 W	

Station GTVA 08 W 1

0855	Beginn Station	LT = 653 m	08 18,72 S	80 16,66 W
0907	GTV z.W.			
0922	Bosi SL = 644 m	LT = 652 m	08 18,71 S	80 16,67 W
0955	hieven SL = 636 m	LT = 642 m	08 18,60 S	80 16,58 W
	keine Probennahme			
1012	GTV a.D. Ende Station			

Profil HS/PS 54

1100	Beginn Profil	08 23,82 S	80 22,25 W	01 sml
1105	ä.K. auf 54 Grad	08 24,48 S	80 21,92 W	08 sml
1200	ä.K auf 233 Grad	08 20,62 S	80 15,00 W	10 sml
1255	ä.K. auf 336 Grad	08 25,90 S	80 22,53 W	03 sml
1313	Ende Profil	08 23,22 S	80 23,80 W	

Station GTVA 09 Bergungsversuch OBS 93 W 1

1330	Beginn Station		LT = 887 m	08 22,34 S 80 21,94 W
1331	GTV z:w.			
1352	Bosi	SL = 874 m	LT = 885 m	08 22,27 S 80 21,98 W
1445	hieven vor			
1515	schneiden long line			
1544	Bosi	SL = 872 m	LT = 886 m	08 22,23 S 80 22,00 W
2122	Griff	SL = 882 m	LT = 877 m	08 22,20 S 80 22,03 W
			Sub	08 22,25 S 80 22,01 W
2210	Griff		Sub	08 22,21 S 80 22,01 W
2212	hieven ein			
2239	GTV a.D.	kein Erfolg	Ende Station	

Profil HS/PS 55

2300	Beginn Profil	08 21,52 S 80 24,48 W	17 sml
13.04.00			
0043	ä.K. auf 337 Grad	08 30,30 S 80 40,00 W	10 sml
0140	Ende Profil	08 21,36 S 80 43,63 W	

Profil HF 32 bis 42 W 1

0215	Beginn Station		LT = 1831 m	08 19,24 S 80 38,01 W
0216	HF z.W.			
0302 - 0315	Boko HF 32	SL = 1841 m	LT = 1839 m	08 19,25 S 80 38,01 W
0416 – 0431	Boko HF 33	SL = 1916 m	LT = 1916 m	08 19,44 S 80 38,51 W
0529 – 0537	Boko HF 34	SL = 1983 m	LT = 1989 m	08 19,66 S 80 39,04 W
0642 – 0656	Boko HF 35	SL = 2060 m	LT = 2068 m	08 19,86 S 80 39,54 W
0758 – 0804	Boko HF 36	SL = 2130 m	LT = 2136 m	08 20,01 S 80 40,03 W
0859 – 0915	Boko HF 37	SL = 2201 m	LT = 2203 m	08 20,26 S 80 40,51 W
1012 – 1018	Boko HF 38	SL = 2269 m	LT = 2277 m	08 20,45 S 80 41,18 W
1105 – 1112	Boko HF 39	SL = 2343 m	LT = 2368 m	08 20,70 S 80 41,53 W
1208 – 1222	Boko HF 40	SL = 2401 m	LT = 2430 m	08 20,84 S 80 41,96 W
1357 – 1403	Boko HF 41	SL = 2558 m	LT = 2548 m	08 21,29 S 80 42,96 W
1545 – 1558	Boko HF 42	SL = 2697 m	LT = 2720 m	08 21,67 S 80 44,00 W

Station CTD 02 W 5

1709	Beginn Station	LT = 2707 m	08 21,71 S 80 44,07 W
1819	Slmax = 2690 m	LT = 2709 m	08 21,71 S 80 44,09 W
1945	CTD a.D.	Ende Station	08 21,73 S 80 44,09 W

Station GTVA 10 Bergung OBS 93 W 1

2157	Beginn Station		LT = 889 m	08 22,22 S 80 21,96 W
2200	GTV z.W.			
2220	Bosi	SL = 874 m	LT = 889 m	08 22,20 S 80 22,00 W
14.04.00				
0310	Griff OBS	SL = 861 m	LT = 887 m	08 22,20 S 80 22,02 W
0316	hieven ein			
0418	GTV a.D.			
0421	OBS 93 a.D.			

0429	Ende Station			

Station GTVA 11 W 10500

0500	Beginn Station		LT = 936 m	08 23,00 S 80 23,97 W
0504	GTV z.W.			
0525	Bosi	SL = 920 m	LT = 936 m	08 22,98 S 80 23,96 W
0536	1. Griff	SL = 925 m	LT = 931 m	08 23,01 S 80 22,97 W
0613	2. Griff	SL = 890 m	LT = 930 m	08 23,07 S 80 23,98 W
0647	GTV a.D.			
0651	Ende Station			

Profile HS/PS 56 bis 62

0837	Beginn Profil 56	08 21,36 S 80 43,63 W	24 sml
0845	Gradiometer z.W.		
1115	Profilwechsel 56 / 57	07 59,00 S 80 52,40 W	28 sml
1416	Profilwechsel 57 / 58	08 10,60 S 81 18,00 W	16 sml
1558	Profilwechsel 58 / 59	08 25,75 S 81 12,00 W	29 sml
1911	Profilwechsel 59 / 60	08 37,00 S 81 40,00 W	03 sml
1930	Profilwechsel 60 / 61	08 39,75 S 81 39,00 W	05 sml
2002	Profilwechsel 61 / 62	08 42,00 S 81 43,75 W	05 sml
2035	Ende Profil 62	08 46,50 S 81 42,00 W	

Profil WS/RS 09

2035	Beginn Profil	08 46,50 S 81 42,00 W	59 sml
2049	GI-guns z.W.		
2059	streamer z.W.		
15.04.00			
0825	Ende Profil	09 09,99 S 82 36,51 W	
0837	Gradiometer a.D.		
0843	GI-guns a.D.		
0854	streamer a.D.		

Profile HS/PS 63 bis 00

0918	Gradiometer z.W.		
0922	Beginn Profil 63	09 13,48 S 82 35,04 W	77 sml
1730	Profilwechsel 63 / 64	08 42,75 S 81 23,50 W	25 sml
2009	Profilwechsel 64 / 65	09 06,0 S 81 14,0 W	22 sml
2234	Ende Profil 65	09 24,0 S 81 00,5 W	
2246	Beginn Profil 66	09 24,0 S 81 00,5 W	10 sml
2348	Profilwechsel 66 / 67	09 14,5 S 81 02,0 W	13 sml
16.04.00			
0112	Profilwechsel 67 / 68	09 04,0 S 81 10,0 W	25 sml
0354	Profilwechsel 68 / 69	08 41,0 S 81 19,5 W	04 sml
0420	Profilwechsel 69 / 69	08 39,25 S 81 16,0 W	25 sml
0657	Profilwechsel 69 / 70	09 02,0 S 81 06,5 W	14 sml
0824	Profilwechsel 70 / 71	09 12,0 S 80 57,0 W	04 sml
0851	Profilwechsel 71 / 72	08 58,8 S 81 03,5 W	14 sml
1025	Profilwechsel 72 / 73	09 10,0 S 80 53,7 W	15 sml
1245	Profilwechsel 73 / 74	08 38,0 S 81 12,5 W	04 sml

1312	Profilwechsel 74 / 75	08 36,0 S 81 08,75 W	22 sml
1532	Profilwechsel 75 / 76	08 56,0 S 81 00,0 W	10 sml
1636	Ende Profil 77	09 03,8 S 80 54,0 W	
1648	Gradiometer a.D.		

17.04.00

Auslegung OBH/S

1305	OBH 98	z.W.	LT = 1698 m	11 05,06 S 78 38,69 W
1313	OBH 99	z.W.	LT = 1688 m	11 05,00 S 78 38,54 W
1319	OBH 100	z.W.	LT = 1677 m	11 04,96 S 78 38,40 W
1335	OBH 101	z.W.	LT = 1619 m	11 04,97 S 78 37,53 W
1344	OBH 102	z.W.	LT = 1632 m	11 05,05 S 78 37,68 W
1353	OBH 103	z.W.	LT = 1644 m	11 05,10 S 78 37,83 W
1400	OBH 104	z.W.	LT = 1657 m	11 05,17 S 78 37,98 W
1407	OBH 105	z.W.	LT = 1666 m	11 05,23 S 78 38,13 W
1427	OBH 106	z.W.	LT = 1717 m	11 05,48 S 78 38.,69 W
1442	OBS 107	z.W.	LT = 1726 m	11 05,53 S 78 38,84 W
1505	OBS 108	z.W.	LT = 1738 m	11 05,60 S 78 39,00 W
1524	OBS 109	z.W.	LT = 1745 m	11 05,66 S 78 39,14 W
1539	OBS 110	z.W.	LT = 1760 m	11 05,73 S 78 39,29 W
1551	1 SeeBoSeis	z.W.	LT = 1772 m	11 05,78 S 78 39,45 W
1559	2 SeeBoSeis	z.W.	LT = 1775 m	11 05,81 S 78 39,50 W

1638 – 1643 Auslegung 6 SeeBoSeis Positionen siehe Druckerprotokoll

Profil HS/PS 78

1707	Beginn Profil	11 04,73 S 78 35,48 W	02 sml
1719	ä.K. auf 248	11 06,59 S 78 36,14 W	04 sml
1743	ä.K. auf 337	11 07,90 S 78 39,43 W	05 sml
1809	ä.K. auf 070	11 04,21 S 78 40,96 W	04 sml
1834	ä.K. auf 126	11 03,00 S 78 37,63 W	01 sml
1845	Ende Profil	11 03,70 S 78 36,14 S	

Profil WS 10

1856	Sreamer z.W.		
1915	Schlepphydrofon z.W.		
1930	Beginn Profil	11 04,99 S 78 37,52 W	02 sml
2005	Ende Profil	11 05,70 S 78 39,28 W	

Profil WS 11

2017	Schlepphydrofon a.D.	
2040	GI-guns z.W.	
2056	Beginn Profil	11 06,62 S 78 41,64 W
2201	ä.K. auf 203	11 04,66 S 78 36,57 W
2222	dito 248	11 05,92 S 78 37,12 W
2229	dito 338	11 06,16 S 78 37,76 W
2255	dito 068	11 04,29 S 78 38,49 W

2300	dito	158	11 04,18 S 78 38,21 W	
2324	dito	247	11 06,04 S 78 37,45 W	
2335	dito	338	11 06,34 S 78 38,17 W	15 sml
18.04.00				
0004	dito	071	11 04,11 S 78 39,08 W	
0010	dito	158	11 04,01 S 78 38,78 W	
0038	dito	247	11 06,23 S 78 37,90 W	
0047	dito	337	11 06,52 W 78 38,60 W	
0112	dito	066	11 04,66 S 78 39,37 W	
0115	dito	158	11 04,53 S 78 39,07 W	
0141	dito	248	11 06,40 S 78 38,30 W	
0146	dito	338	11 06,58 S 78 38,76 W	
0210	dito	067	11 04,72 S 78 39,52 W	
0214	dito	158	11 04,60 S 78 39,20 W	
0239	dito	246	11 06,45 S 78 38,45 W	
0245	dito	338	11 06.65 S 78 38,91 W	
0309	dito	066	11 04,79 S 78 39,67 W	
0331	dito	158	11 04,11 S 78 38,05 W	
0355	dito	246	11 05,97 S 78 37,29 W	
0359	dito	337	11 06,10 S 78 37,59 W	
0423	dito	065	11 04,25 S 78 38,35 W	
0430	dito	157	11 04,05 S 78 37,90 W	
0454	dito	247	11 05,91 S 78 37,13 W	
0506	dito	338	11 06,28 S 78 38,02 W	
0535	Ende Profil WS 11		11 04,06 S 78 38,93 W	27 sml
0542	GI-guns a.D.			
0552	streamer a.D.			

Aufnahme OBH/S 98 bis 110

0552	OBH 98	ausgelöst 0612	gesichtet 0625	a.D.	11 05,10 S 78 38,69 W
0621	OBH 99	0640	0649		11 05,08 S 78 38,52 W
0645	OBH 100	0704	0714		11 05,02 S 78 38,39 W
0712	OBH 101	0728	0745		11 05,05 S 78 57,56 W
0730	OBH 102	0753	0805		11 05,10 S 78 37,68 W
0753	OBH 103	0810	0826		11 05,14 S 78 37,84 W
0819	OBH 104	0840	0852		11 05,20 S 78 37,95 W
0845	OBH 105	0905	0912		11 05,27 S 78 38,11 W
0906	OBH 106	0922	0928		11 05,54 S 78 38,70 W
0923	OBS 107	0949	0957		11 05,62 S 78 38,80 W
0949	OBS 108	1018	1026		11 05,67 S 78 38,95 W
1019	OBS 109	1049	1059		11 07,73 S 78 39,10 W
1049	OBS 110	1118	1127		11 05,74 S 78 39,27 W

Station OFOS 09 W 1

1212	Beginn Station	LT = 2016 m	11 08,10 S 78 45,20 W
1252	Bosi SL = 2001 m	LT = 2018 m	11 08,15 S 78 45,15 W
	Kurs = 67 Grad v = 0,7 kn		
2000	hieven SL = 1827 m	LT = 1829 m	11 06,16 S 78 40,38 W
2039	OFOS a.D. Ende Station		

Stationen HF 43 bis 52

2115	HF z:W.		LT = 2008 m	11 08,18 S	78 44,24 W
2206	Boko HF 43 umgefallen	SL = 2014 m	LT = 2013 m	11 08,25 S	78 44,23 W
2315 – 2319	Boko HF 44	SL = 1994 m	LT = 1987 m	11 07,92 S	78 43,47 W
19.04.00					
0012 – 0020	Boko HF 45	SL = 1981 m	LT = 1967 m	11 07,75 S	78 43,00 W
0138	Boko HF 46 umgefallen	SL = 1939 m	LT = 1929 m	11 07,39 S	78 42,17 W
0233	Boko HF 47 umgefallen	SL = 1894 m	LT = 1903 m	11 07,19 S	78 41,73 W
0241	Boko 2 umgefallen	SL = 1894 m	LT = 1894 m	11 07,23 S	78 41,65 W
0317 – 0331	Boko HF 48	SL = 1884 m	LT = 1880 m	11 07,08 S	78 41,41 W
0406 – 0420	Boko HF 49	SL = 1870 m	LT = 1871 m	11 06,98 S	78 41,18 W
0455 – 0510	Boko HF 50	SL = 1862 m	LT = 1860 m	11 06,88 S	78 40,93 W
0545 – 0600	Boko HF 51	SL = 1851 m	LT = 1848 m	11 06,78 S	78 40,66 W
0648 – 0707	Boko HF 52	SL = 1826 m	LT = 1822 m	11 06,57 S	78 40,13 W
0708	hieven ein				
0746	HF a.D.	Ende HF-Stationen			

Profie I GI 65 - 74

1017	Beginn ausbringen	10 47,19 S	78 59,64 W	
1021	Stremer z.W.			
1034	airguns z.W.			
1036	Beginn Profil	10 47,66 S	78 59,02 W	
1042	Gradiometer z.W			
1053	Beginn Profil	10 48,47 S	78 58,20 W	
1258	Ausfall airguns	10 56,15 S	78 50,88 W	15 sml
1313	Gradiometer a.D.			
1325	airguns a.D.			
1325 – 1414	Schleife über Stb			
1418	GI-guns z.W.			
1425	Gradiometer z.W. Fortsetzung Profil	10 55,64 S	78 51,38 W	
1528	ä.K. auf 157 Grad	10 59,44 S	78 47,78 W	16 sml
1927	ä.K. auf 164 Grad	11 18,19 S	78 39,98 W	20 sml
2055	ä.K. auf 157 Grad	11 25,56 S	78 37,97 W	08 sml
2240	Gradiometer vorgehievt			
2242	Profilwechsel 65 / 66	11 33,86 S	78 34,52 W	09 sml
2246	Gradiometer volle Länge			
2350	Gradiometer vorgehievt			
2400	Profilwechsel 66 / 67	11 30,68 S	78 29,06 W	06 sml
20.04.00				
0008	Gradiometer volle Länge			
0109	Gradiometer vorgehievt			
0112	Profilwechsel 67 / 68	11 23,04 S	78 31,33 W	06 sml
0021	Gradiometer volle Länge			

0253	Gradiometer vorgehievt			
0257	Profilwechsel 68 / 69	11 29,36 S	78 39,34 W	09 sml
0304	Gradiometer volle Länge			
0508	Gradiometer vorgehievt			
0512	Profilwechsel 69 / 70	11 18,76 S	78 43,76 W	11 sml
0519	Gradiometer volle Länge			
1116	Gradiometer vogehievt			
1119	Ende Profil 70	11 03,78 S	78 26,34 W	21 sml
1137	Beginn Profil 71	11 03,78 S	78 16,35 W	
1146	Gradiometer volle Länge			
1258	Gradiometer vorgehievt			
1302	Profilwechsel 71 / 72	10 57,46 S	78 19,30 W	07 sml
1310	Gradiometer volle Länge			
1639	Gradiometer vorgehievt			
1642	Profilwechsel 72 / 73	11 04,69 S	78 36,76 W	19 sml
1721	Profilwechsel 73 / 74	11 07,72 S	78 35,45 W	03 sml
1727	Gradiometer volle Länge			
2125	Ende Profil 74	11 15,68 S	78 54,75 W	21 sml
2155	alles a.D.			

Station OFOS 10 W 1

2300	Beginn Station	LT = 2171 m	11 09,80 S	78 49,42 W
2309	OFOS z.W.			
2350	Bosi SL = 2145 m	LT = 2171 m	11 09,83 S	78 49,34 W
	Kurs = 67 Grad v = 0,7 kn			
21.04.00				
0611	Ende Bosi SL = 1997 m	LT = 2001 m	11 08,03 S	78 45,04 W
0651	OFOS a.D.			
0655	Ende Station			

Auslegung OBH/S

0711	OBH 111 z.W.	LT = 1990 m	11 07,58 S	78 45,15 W
0730	OBH 112 z.W.	LT = 2027 m	11 07,79 S	78 45,96 W
0741	OBH 113 z.W.	LT = 2027 m	11 07,93 S	78 45,90 W
0751	OBH 114 z.W.	LT = 2027 m	11 08,10 S	78 45,86 W
0807	OBH 115 z.W.	LT = 2044 m	11 08,82 S	78 45,89 W
08818	OBH 116 z.W.	LT = 2042 m	11 08,76 S	78 45,75 W
0834	OBH 117 z.W.	LT = 2042 m	11 08,81 S	78 45,60 W
0850	OBH 118 z.W.	LT = 2024 m	11 08,38 S	78 44,43 W
0916	OBS 119 z.W.	LT = 2020 m	11 08,15 S	78 45,18 W
0929	OBS 120 z.W.	LT = 2023 m	11 08,20 S	78 45,35 W
0945	OBS 121 z.W.	LT = 2027 m	11 08,27 S	78 45,49 W
0957	OBS 122 z.W.	LT = 2032 m	11 08,33 S	78 45,65 W
1013	OBS 123 z.W.	LT = 2054 m	11 08,57 S	78 46,19 W

Auslegung SBS

1032	SBS 11 z.W.	LT = 2042 m	11 08,49 S	78 45,98 W
1033	SBS 12 z.W.	LT = 2040 m	11 08,47 S	78 45,96 W
1034	SBS 13 z.W.	LT = 2039 m	11 08,46 S	78 45,93 W

1035	SBS 14	z.W.	LT = 2037 m	11 08,44 S	78 45,87 W
1036	SBS 15	z.W.	LT = 2036 m	11 08,42 S	78 45,82 W
1037	SBS 16	z.W.	LT = 2034 m	11 08,39 S	78 45,77 W
1048	SBS 17	z.W.	LT = 2012 m	11 08,08 S	78 45,03 W
1049	SBS 18	z.W.	LT = 2012 m	11 08,06 S	78 44,98 W
1050	SBS 19	z.W.	LT = 2008 m	11 08,05 S	78 44,93 W
1051	SBS 20	z.W.	LT = 2007 m	11 08,02 S	78 44,88 W

GI-Profile 75 bis 87

1210	streamer z.W.			
1215	GI-guns z.W.			
1215	Beginn Profil 75	11 05,27 S	78 38,62 W	
1433	Profilwechsel 75 / 76	11 09,88 S	78 49,32 W	
1518	Profilwechsel 76 / 77	11 07,38 S	78 46,67 W	
1535	Profilwechsel 77 / 78	11 06,81 S	78 45,47 W	
1607	Profilwechsel 78 / 79	11 09,27 S	78 44,47 W	
1622	Profilwechsel 79 / 80	11 09,75 S	78 45,51 W	
1657	Ende Profil 80	11 07,00 S	78 46,44 W	
1702	Beginn Profil 81	11 06,86 S	78 46,34 W	
1739	Profilwechsel 81 / 82	11 09,63 S	78 45,22 W	
1745	Profilwechsel 82 / 83	11 09,82 S	78 45,65 W	
1815	Profilwechsel 83 / 84	11 07,39 S	78 46,66 W	
1829	Profilwechsel 84 / 85	11 07,00 S	78 45,85 W	
1901	Ende Profi 85	11 09,43 S	78 44,80 W	
1905	Beginn Profil 86	11 09,57 S	78 45,01 W	
1937	Ende Profil 86	11 07,14 S	78 46,09 W	
1946	Beginn Profil 87	11 06,99 S	78 46,01 W	
2019	Profilwechsel 87 / 88	11 09,49 S	78 44,97 W	
2025	Profilwechsel 88 / 89	11 09,70 S	78 45,35 W	
2058	Profilwechsel 89 / 90	11 07,22 S	78 46,37 W	
2108	Profilwechsel 90 / 91	11 06,90 S	78 45,67 W	
2140	Ende Profil 91	11 09,35 S	78 44,66 W	46 sml
2148	airguns a.D.			
2200	streamer a.D.			

Aufnahme OBS/H 123 bis111

2152 OBH 123	ausgelöst	2215 gesichtet	2233 a.D.	11 08,63 S	78 46,28 W
2227 OBH 122		2301	2312	11 08,42 S	78 45,67 W
2303 OBH 121		2335	2345	11 08,37 S	78 45,45 W
2336 OBS 120					
22.04.00					
		0011	0023	11 08,32 S	78 45,36 W
0012 OBS 119		steigt nicht auf			
0044 OBS 118		0110	0118	11 08,45 S	78 44,86 W
0111 OBH 117		0136	0145	11 08,80 S	78 45,61 W
0137 OBH 116		0203	0215	11 08,82 S	78 45,79 W
0204 OBH 115		0226	0232	11 08,90 s	78 45,88 W
0227 OBH 114		0254	0304	11 08,14 S	78 45,88 W
0255 OBH 113		0316	0324	11 08,00 S	78 45,93 W

0318	OBH 112	0342	0349	11 07,89 S 78 45,96 W
0343	OBH 111	0408	0415	11 07,68 S 78 45,15 W

Stationen HF 53 bis XX W 01

0507	Beginn Station		LT = 2455 m	11 11,09 S 78 52,63 W
0509	HF z.W.			
0603	Boko HF 53	SL = 2453 m	LT = 2456 m	11 11,20 S 78 52,59 W
0615	hieven			
0723	HF a.D. HF und Kabel defekt			
0725 – 0816	Reparatur HF			
0818	HF z.W.			
0909	Boko HF 54 umgefallen	SL = 2417 m	LT = 2419 m	11 01,01 S 78 52,09 W
1012	Boko HF 55 umgefallen	SL = 2385 m	LT = 2375 m	11 10,80 S 78 51,56 W
1105	Boko HF 56 umgefallen	SL = 2321 m	LT = 2330 m	11 10,59 S 78 51,09 W
1242	Boko HF 57	SL = 2252 m	LT = 2225 m	11 10,20 S 78 50,09 W
1250	Beginn hieven			
1346	HF a.D.			
1347	Ende Station			

Klarierung LWL-Kabel W 01

1558	Beginn Ausstecken	LT = 3794 m	11 32,36 S 78 54,55 W
1640	Slmax = 2430 m, hieven wieder ein		
1740	Dummy a.D.		

Auslegung OBH 124 bis 127

1741	OBH 124	z.W.	LT = 3795 m	11 32,64 S 78 54,52 W
1756	OBH 125	z.W.	LT = 3835 m	11 33,23 S 78 55,26 W
1820	OBH 126	z.W.	LT = 3796 m	11 33,75 S 78 55,94 W
1834	OBH 127	z.W.	LT = 3713 m	11 34,29 S 78 56,65 W

GI-Profile 92 bis 103

1914	streamer z.W.		
1918	airguns z.W.		
1920	Beginn Profil 92	11 36,49 S 78 56,95 W	
2054	Ende Profil 92	11 31,61 S 78 52,79 W	08 sml
2130	Beginn Profil 93	11 31,03 S 78 52,97 W	
2251	Profilwechsel 93/94	11 35,26 S 78 58,22 W	07 sml
2320	Profilwechsel 94/95	11 33,79 S 78 59,89 W	02,4 sml
2345	Profilwechsel 95/96	11 32,35 S 78 58,49 W	02,2 sml
23.04.00			
0053	Ende Profil 96	11 36,39 S 78 54,85 W	05,4 sml
0102	Beginn Profil 97	11 36,39 S 78 54,85 W	
0122	Ende Profil 97	11 35,32 S 78 53,32 W	02,7 sml
0131	Beginn Profil 98	11 35,32 S 78 53,52 W	
0236	Profilwechsel 98/99	11 31,14 S 78 57,00 W	05,4 sml
0309	Profilwechsel 99/100	11 29,30 S 78 54,71 W	

FS SONNE Stationsprotokoll SO 146/2

0339	Profilwechsel 100/101	11 31,39 S 78 52,96 W	
0350	Magnetometer z.W.	11 32,07 S 78 53,83 W	
0622	Magnetometer ein	11 40,00 S 79 03,80 W	
0646	Ende Profil 101	11 40,84 S 79 05,08 W	13,6
0652	Beginn Profil 102	11 40,62 S 79 05,23 W	
0755	Ende Profil 102	11 38,90 S 79 02,62 W	03,0 sml
0808	Beginn Profil 103	11 39,35 S 79 02,38 W	
0925	Ende Profil 103	11 41,61 S 79 05,75 W	04,0 sml
0934	Beginn Profil 104	11 41,39 S 79 05,90 W	
1050	Profilwechsel 104/105	11 39,15 S 79 02,52 W	04,0 sml
1125	Profilwechsel 105/106	11 40,40 S 79 01,66 W	01,5 sml
1156	Profilwechsel 106/107	11 41,25 S 79 02,94 W	01,5 sml
1259	Ende Profil 107	11 38,74 S 79 04,66 W	03,0 sml
1324	airguns und Streamer a.D.		

Aufnahme OBH 124 bis 127

1353	OBH 127	ausgelöst 1440	gesichtet 1447	a.D.	11 34,35 S 78 56,57 W
1423	OBH 126	1504	1513		11 33,86 S 78 55,82 W
1450	OBH 125	1537	1545		11 33,28 S 78 55,13 W
1514	OBH 124	1602	1610		11 32,69 S 78 54,41 W

Station GTVA 12 Bergung OBS 119 W 1

1825 – 1932	Einmessung OBS			
1940	Beginn Station		LT = 2020 m	11 08,13 S 78 45,22 W
1942	GTV z.W.			
2018	Bosi	SL = 1993 m	LT = 2019 m	11 08,14 S 78 45,18 W
24.04.00				
0230	OBS hakt fest, hieven			
0428	GTVA und OBS 119	a. D.		
0430	Ende Station			

Station OFOS 11 W 1

0726	Beginn Station		LT = 3855 m	11 36,06 S 78 58,98 W
0727	OFOS z.W.			
0834	Bosi	SL = 3823 m	LT = 3852 m	11 36,17 S 78 58,93 W
	Kurs = 50 Grad	v = 0,9 kn		
1200				11 34,44 S 78 56,79 W
1824	hieven	SL = 3580 m	LT = 3310 m	11 31,29 S 78 52,91 W
1834	Spulprobleme, ä.K. auf 170 Grad			
2019	fieren bis SL 0 3490 m			
2028	hieven			
2156	OFOS a.D.			
2157	Ende Station			

Stationen HF 58 bis 64 W 1

2235	Beginn Station		LT = 3744 m	11 35,03 S 78 57,83 W
2237	HF z.W.			
2353 – 0007	Boko HF 58	SL = 3729 m	LT = 3717 m	11 35,27 S 78 57,90 W
25.04.00				
0127 – 0133	Boko HF 59	SL = 3719 m	LT = 3720 m	11 35,00 S 78 57,45 W

0247 – 0300	Boko HF 60	SL = 3699 m	LT = 3702 m	11 34,67 S 78 57,05 W
0358 – 0404	Boko HF 61	SL = 3712 m	LT = 3713 m	11 34,37 S 78 56,69 W
0516 – 0531	Boko HF 62	SL = 3752 m	LT = 3766 m	11 34,00 S 78 56,23 W
0636 – 0643	Boko HF 63	SL = 3810 m	LT = 3816 m	11 33,59 S 78 55,73 W
0750 – 0804	Boko HF 64	SL = 3841 m	LT = 3833 m	11 33,27 S 78 55,29 W
0940 – 0947	Boko HF 65	SL = 3832 m	LT = 3790 m	11 32,74 S 78 54,59 W

0947 hieven a.D.
1104 HF a.D. Ende Station

Station OFOS 12 W 1

1318 Beginn Station LT = 4313 m 11 38,60 S 79 04,03 W
1345 SL = 1321 m Winde stop
1345 – 1528 Austausch Kulissenstein Spulwagen W 1
1448 WTD stellt Schaden an der Verbindung LWL-Kabel zum OFOS fest
1528 hieven ein 1604 OFOS a.D. Ende Station

Profile HS/PS 79 bis 83

1707	Beginn Profil 79	11 31,5 S 79 00,0 W	10 sml
1807	Profilwechsel 79/80	11 21,9 S 78 54,3 W	18 sml
1945	Profilwechsel 80/81	11 25,8 S 79 11,7 W	10 sml
2046	Profilwechsel 81/82	11 33,0 S 79 03,5 W	10 sml
2140	Profilwechsel 82/83	11 40,5 S 78 56,5 W	10 sml
2233	Ende Profil 83	11 38,5 S 78 47,0 W	

26.04.00

Profile HS/PS 84 bis 96

1442	Beginn Profil 84	12 25,0 S 77 22,0 W	74 sml
2054	Profilwechsel 84 / 85	13 36,0 S 77 42,0 W	126 sml
27.04.			
0800	Profilwechsel 85 / 86	15 12,0 S 76 18,5 W	008 sml
0841	Profilwechsel 86 / 87	15 18,5 S 76 23,0 W	040 sml
1212	Profilwechsel 87 / 88	15 45,3 S 75 52,5 W	029 sml
1441	Profilwechsel 88 / 89	16 07,8 S 76 12,0 W	039 sml
1800	Profilwechsel 89 / 90	15 44,3 S 76 44,0 W	005 sml
1827	Profilwechsel 90 / 91	15 48,5 S 76 47,0 W	046 sml
2244	Profilwechsel 91 / 92	16 17,8 S 76 10,0 W	012 sml
2400	Profilwechsel 92 / 93	16 10,0 S 76 00,0 W	009 sml
28.04.00			
0050	Profilwechsel 93 / 94	16 01,5 S 75 57,3 W	010 sml
0149	Profilwechsel 94 / 95	15 54,0 S 75 50,0 W	005 sml
0216	Profilwechsel 95 / 96	15 57,3 S 75 46,3 W	018 sml
0400	Ende Profil 96	16 10,0 S 76 00,0 W	

Appendix II

GEOPECO SO146 - PROFILE 01

INSTRUMENT	LAT (S)	LON (W)	DIST. TO	DEPTH	RELEASER-	ANT.	RECORDER	SKEW	REMARKS
	D:M	D:M	NEXT (nm	(m)	CODE	CH.	NUMBER	(ms)	
OBH 01	16:01.16	76:24.03	7.48	3240	6959	D	980907	1	
OBH 02	15:56.40	76:30.03	7.48	3210	6969	C	971202	-6	
OBS 03	15:51.59	76:35.99	7.53	3082	6A24	D	980906	6	auftauchen=50 min
OBH 04	15:46.80	76:42.03	7.48	2925	C679	C	980401	-2	
OBS 05	15:41.996	76:47.995	7.66	2992	4979	C	971201	-7	only hydrophone
OBH 06	15:37.201	76:54.20	7.23	2933	4A49	D	980402	0	
OBS 07	15:32.603	76:59.999	7.5	2902	5929	C	980901	12	0
OBH 08	15:27.792	77:06.002	7.5	2986	D674	D	990901	-6	
OBH 09	15:22.994	77:11.993		3045	5924	D	980902	1	

Appendix II

GEOPECO SO146 - Profile 02

INSTRUMENT	LAT (S)	LON (W)	DIST. TO	DEPTH	RELEASER-	ANT.	RECORDER	SKEW	REMARKS
	D:M	D:M	NEXT (nm)	(M)	CODE	CH.	NUMBER	(ms)	
OBS 05	15:41.996	76:47.995	5,78	2992	4979	C	971201	-7	2 cards empty
OBH 10	15:38.499	76:43.207	9,66	2930	5924	C	980905	3	not blinking
OBH 11	15:29.99	76:38.40	7,56	3211	d674	D	980902	2	
OBS 12	15:24.01	76:33.575	7,53	3408	6A24	C	9809006	9	
OBH 13	15:18.039	76:28.791	7,59	3898	6495 (Md. B)	A	980402	10	No Data !
OBH 14	15:12.071	76:23.914	3,82	4984	C679	C	980970	3	
OBH 15	15:09.091	76:21.420	3,84	4687	6969	D	971202	-14	No Data !
OBS 16	15:06.0917	76:18.923	5,87	3598	5929	A	990712	5	2 cards unread
OBH 17	15:01.40	76:15.25	7,35	2537	6959	D	990901	-10	
OBS 18	14:58.046	76:12.314	2,98	2186	B495	D	980901	19	2 Flashcards
OBH 19	14:55.585	76:10.5700	2,15	2150	C444	C	980401	-4	
OBH 20	14:54.054	76:09.003	4,09	1684	D654	C	991294	-10	
OBH 21	14:50.814	76:06.414	3,58	562	4949	B	980403	-3	
OBH 22	14:48.014	76:04.098		349	D634	D	991202	-3	

Appendix II

GEOPECO SO146-PROFILE 03

INSTRUMENT	LAT (S)	LON (W)	DIST. TO	DEPTH	RELEASER	ANT.	RECORDE	SKEW	REMARKS
	D:M	D:M	NEXT (nm)	(m)	CODE	CH.	NUMBER	(ms)	
OBH23	13: 47,934	78: 05.043		4828	4A49	C	980402	0	mode B, interruptions
OBH24	13: 41,943	77: 58.154	9.0	5113	C679	D	980902	1	
OBS25	13: 35,945	77: 51.288	9.0	5615	4979	C	980906	7	
OBH26	13: 32,994	77: 47.831	4.5	4963	6969	D	980905	2	
OBS27	13: 29,994	77: 44.368	4.5	3918	B495	C	980401	-4	poor coupling
OBH28	13: 26,966	77: 40.925	4.2	3700	6959	C	990901	-6	
OBS29	13: 22,483	77: 35.742	6.7	3214	C444	D	980907	0	
OBS30	13: 18,005	77: 30.534	6.7	2257	6A24	C	980908	3	
OBH31	13: 14,999	77: 27.062	4.5	1771	D654	C	980401	-4	
OBH32	13: 12.000	77: 23.612	4.5	1439	4949	A	971202	-12	interruptions
OBS33	13: 09.011	77: 20.154	4.5	1387	5929	D	980901	17	
OBH34	13: 05.984	77: 16.672	4.5	1416	D634	D	991294	-11	
OBH35	12: 59.987	77: 09.770	9.0	1058	D674	D	980403	-4	ohne Flaggentuch
OBH36	12: 54.008	77: 02.885	9.0	396	5924	C	991202	-3	Hydrophone defekt?

Appendix II

GEOPECO SO146 - PROFILE 04

INSTRUMENT	LAT (N)	LON (W)	DIST. TO	DEPTH	RELEASER-	ANT.	RECORDER	SKEW	REMARKS
	D:M	D:M	NEXT (nm)	(m)	CODE	CH.	NUMBER	(ms)	
OBH42	8 : 42,441	81 : 33,014		4562	D654	C	980902	0	-
OBH43	8 : 34,320	81 : 13,748	20.72	5238	4949	D	980402	0	-
OBH44	8 : 22,046	80 : 56,518	20.99	5536	5924	C	980901	10	-
OBH45	8 : 25,884	80 : 53,769	4.69	4596	C444	D	991294	-6	-
OBH46	8 : 23,892	80 : 49,010	5.12	3815	6959	D	980401	-3	blinking fast
OBH47	8 : 20,732	80 : 42,000	7.63	2420	6969	D	991293	-16	disk write error
OBS48	8 : 18,391	80 : 36,003	6.39	1556	5929	C	971202	-23	not blinking
OBH49	8 : 13,740	80 : 24,963	11.89	741	C679	C	980908	4	-
OBH50	8 : 09,957	80 : 16,016	9.64	256	4A49 (B)	C	980403	-8	-

Appendix II

GEOPECO SO146 - PROFILE 05

INSTRUMENT	LAT (N)	LON (W)	DIST. TO	DEPTH	RELEASER-	ANT.	RECORDER	SKEW	REMARKS
	D:M	D:M	NEXT (nm)	(m)	CODE	CH.	NUMBER	(ms)	
OBH51	11 : 53,830	79 : 36,620		5007	D634	C	980905	2	
OBH52	11 : 46,710	79 : 23,030	15.09	5492	D674	D	980902	2	600 m lead rope
OBH53	11 : 39,013	79 : 08,260	16.39	5498	6969	C	980402	0	2 interruptions
OBH54	11 : 37,310	79 : 05,060	3.57	4416	C679	D	980907	2	
OBS55	11 : 34,940	79 : 00,530	5.03	3957	B495	C	971202	-8	3K twisted up
OBH56	11 : 32,540	78 : 56,060	5.00	3848	4A49 (B)	D	980901	12	
OBS57	11 : 30,250	78 : 51,510	5.02	2909	5929	C	971201	-4	
OBH58	11 : 27,880	78 : 47,010	5.01	2571	6959	D	991244	3	sample rate=200 Hz
OBS59	11 : 25,542	78 : 42,538	4.97	2413	6A24	C	990901	x	does not rise
OBH60	11 : 23,200	78 : 38,020	5.01	2082	C444	C	991293	-7	
OBH61	11 : 20,493	78 : 33,697	5.03	2029	4979	D	991202	-3	
OBH62	11 : 18,410	78 : 29,050	5.01	1586	5924	C	980906	x	14 error messages
OBH63	11 : 16,100	78 : 24,560	4.98	1040	4949	D	980406	x	not blinking
OBH64	11 : 11,345	78 : 15,513	10.07	497	D654	C	980908	1	

Appendix II

GEOPECO SO146 - PROFILE 06

INSTRUMENT	LAT (N)	LON (W)	DIST. TO	DEPTH	RELEASER-	ANT.	RECORDER	SKEW	REMARKS
	D:M	D:M	NEXT (nm)	(m)	CODE	CH.	NUMBER	(ms)	
OBH65	11 : 56,960	78 : 26,070	10,07	2477	D654	C	980905	2	-
OBH66	11 : 48,080	78 : 30,760	10,07	2393	5924	D	990902	12	-
OBH67	11 : 39,030	78 : 35,540	5,03	2233	C444	C	980907	1	-
OBS68	11 : 34,560	78 : 37,900	5,04	2163	4979	D	971202	-7	-
OBH69	11 : 30,078	78 : 40,280	5,06	2259	6959	C	980902	2	-
OBS70	11 : 25,570	78 : 42,660	5,04	2421	5929	D	971201	-4	-
OBH71	11 : 21,060	78 : 45,040	5,04	2495	4A49 (B)	D	980402	0	-
OBS72	11 : 16,580	78 : 47,410	5,03	2316	B495	C	991202	-2	-
OBH73	11 : 12,117	78 : 49,737	9,94	2293	C679	D	980908	3	-
OBH74	11 : 03,270	78 : 54,433	10,08	2426	6969	C	991244	-2	-
OBH75	10 : 54,305	78 : 59,190		2465	D674	D	991204	-5	-

Appendix II

GEOPECO SO146 - PROFILE 07

INSTRUMENT	LAT (N)	LON (W)	DIST. TO	DEPTH	RELEASER-	ANT.	RECORDER	SKEW	REMARKS
	D:M	D:M	NEXT (nm)	(m)	CODE	CH.	NUMBER	(ms)	
OBH76	11 : 05,465	78 : 38,679	0.96	1713	3495	D	980901	-4	
OBH77	11 : 05,638	78 : 39,635	1.02	1784	6A24	D	980402	0	
OBH78	11 : 06,190	78 : 40,513	1.06	1837	6959	D	980902	1	
OBH79	11 : 06,628	78 : 41,495	1.01	1881	C679	D	980907	0	
OBH80	11 : 07,008	78 : 42,447	0.97	1913	4979	D	991202	-1	
OBH81	11 : 07,392	78 : 43,358	1.02	1964	6969	C	980905	1	ca. 250 m rope
OBS82	11 : 07,783	78 : 44,314	1.00	1984	4A49(B)	D	991294	-3	In position of OBH83
OBH83	11 : 08,178	78 : 45,249	0.99	2025	5924	C	980908	2	In position of OBH82
OBH84	11 : 08,561	78 : 46,174		2054	5929	C	9711201	-3	

Appendix II

GEOPECO SO146 - PROFILE 08

INSTRUMENT	LAT (N)	LON (W)	DIST. TO	DEPTH	RELEASER-	ANT.	RECORDER	SKEW	REMARKS
	D:M	D:M	NEXT (nm)	(m)	CODE	CH.	NUMBER	(ms)	
OBH85	8 : 17,050	80 : 14,198		452	5924	C	980905	-1	-
OBS86	8 : 17,461	80 : 14,852	0.77	478	D654	D	990901	-3	-
OBH87	8 : 18,345	80 : 16,158	1.57	610	4A49 (B)	C	982401	-1	No data
OBH88	8 : 19,010	80 : 17,198	1.23	687	6969	D	980901	105	-
OBH89	8 : 19,765	80 : 18,322	1.34	752	C679	C	980907	0	-
OBS90	8 : 20,698	80 : 19,741	1.69	810	5929	D	971202	80	3K didn't release
OBH91	8 : 21,136	80 : 20,403	0.79	834	6959	C	980902	1	-
OBH92	8 : 21,722	80 : 21,291	1.06	861	6A24	C	991294	-3	-
OBS93	8 : 22,200	80 : 22,012	0.86	885	B495	D	991202	-3	disk full 14/4 13:09
OBH94	8 : 22,779	80 : 22,885	1.04	911	C444	C	980402	0	-
OBH95	8 : 23,554	80 : 24,065	1.40	948	D634	C	980908	1	-
OBS96	8 : 24,044	80 : 24,809	0.88	971	4979	C	971201	-3	-
OBH97	8 : 25,228	80 : 26,601	2.13	1028	D674	D	991293	-3	-

Appendix II

GEOPECO SO146 - PROFILE 11

INSTRUMENT	LAT (N)	LON (W)		DIST. TO	DEPTH	RELEASER-	ANT.	RECORDER	SKEW	REMARKS
	D:M	D:M		NEXT (nm)	(m)	CODE	CH.	NUMBER	(ms)	
OBH124	11 : 32,641	78	54,523		3795	D634	C	991294		Gerät defekt
OBH125	11 : 33,297	78	55,315	1.015	3835	C444	D	980908	1	300 m Seil
OBH126	11 : 33,928	78	55,928	0.870	3792	6A24	C	980402	0	
OBH127	11 : 34,290	78	56,656	0.800	3722	6959	D	980902	0	

Appendix III GEOPECO SO146-1 - 32 l SEISMIC SOURCES

PROFILE NO.	DATE UTC	TIME UTC	LAT (S) D:M	LON (W) D:M	PULSE INT.	GUN POSITION	REMARKS
1	05.03.00	12:05	15 : 11,286	77 : 26,736	60	S	first shot
		12:31	15 : 12,110	77 : 25,799	60	S, P	
		13:22	15 : 14,185	77 : 23,153	60	S	
		15:29	15 : 19,560	77 : 16,382	60	S, P	
		20:31	15 : 33,580	77 : 00,480	60	S, P	P looses air
	06.03.00	12:10	16 : 11,290	76 : 11,280	60	S, P	last shot
2	07.03.00	17:59	14 : 41,170	75 : 58,596	60	M	first shot
		18:14	14 : 41,634	75 : 58,947	60	S, M	
		18:23	14 : 42,040	75 : 59,238	60	S, M, P	
		20:38	14 : 49,000	76 : 04,970	60	S, M, P	M looses air
	08.03.00	18:09	15 : 56,370	77 : 00,250	60	S, M, P	last shot
3	12.03.00	05:24	12 : 46,250	76 : 54,060	60	S	first shot
		05:34	12 : 46,530	76 : 54,340	60	S, P	
		05:43	12 : 46,890	76 : 54,740	60	S, M, P	
		11:10	13 : 01,420	77 : 11,450	60	M, P	S onboard
	13.03.00	07:22	13 : 55,258	78 : 13,328	60	M, P	last shot
4	20.03.00	11:57	8 : 05,950	80 : 06,460	60	S	first shot
		12:11	8 : 06,070	80 : 06,810	60	S, P	
		12:16	8 : 06,220	80 : 07,240	60	S, M, P	
	21.03.00	14:34	8 : 47,530	81 : 45,900	60	S, M, P	last shot
5	28.03.00	03:50	11 : 04,970	78 : 03,500	60	S	first shot
		03:57	11 : 05,100	78 : 03,780	60	S, P	
		04:07	11 : 05,330	78 : 04,210	60	S, M, P	
		17:11	11 : 30,050	78 : 51,240	60	S, M, P	M looses air
	29.03.00	10:46	12 : 03,280	79 : 54,580	60	S, M, P	last shot
6	31.03.00	05:51	10 : 43,420	79 : 04,990	60	S	first shot
		05:59	10 : 43,770	79 : 04,790	60	S, P	
		06:05	10 : 44,120	79 : 04,590	60	S, M, P	
		12:58	11 : 08,190	78 : 51,830	60	S, M, P	last shot
		14:57	11 : 03,340	78 : 54,320	60	S	first shot
		15:02	11 : 03,640	78 : 54,230	60	S, P	
		15:08	11 : 04,000	78 : 54,090	60	S, M, P	
	01.04.	08:44	12 : 06,480	78 : 20,990	60	S, M, P	last shot

*P: portside 32 l, M: mid 32 l, S: starboard 32 l

Appendix IV

High-resolution multichannel seismic (University of Hamburg)

Please cite lines like HH00-xyz, e.g., HH00-012 is line 12 in the table.

Profile	Start Coord.	End Coord.	Start Time	End Time	FFN	Tape	Source
HH1 WS/RS1	77° 22.17' W 15° 14.96' S	76° 12.13' W 16° 10,59' S	5/3/2000 13:39	6/3/2000 11:53	1-1343	1	2 x 32 l BOLT
HH2 WS/RS2	75°59.49' W 14° 42.37' S	77° 0.04' W 15° 56.05' S	7/3/2000 18:31	8/3/2000 17:59	1-1423	2	3 x 32l BOLT
HH3	76° 34.22' W 15°24.77 S	75°59.94' W 14°42.93' S	10/3/2000 5:39	10/3/2000 16:06	1-3427	4-5	GI (45/105) GI (25/25)
HH4 WS/RS3	77° 17.39' W 13° 06.58' S	78° 19.00' W 13° 59.99' S	12/3/2000 13:07	13/3/2000 9:09	1-1209	(6)-7	3 x 32l BOLT
HH5	77° 30.19' W 13° 17.59' S	76°59.40' W 12° 51.76' S	13/3/2000 22:02	14/3/2000 06:10	1-2949	8-9	GI (45/105) GI (25/25)
HH6	76° 59.90' W 12° 50.45' S	76° 52.87' W 13° 09.64' S	14/3/2000 06:49	14/3/2000 10:52	3169-4618	10	GI (45/105) GI (25/25)
HH7	76° 52.87' W 13° 09.64' S	77° 33.68' W 13° 12.75' S	14/3/2000 10:52	14/3/2000 18:41	4618-7497	10-12	GI (45/105) GI (25/25)
HH8 WS/RS4	80° 8.08' W 8° 6.62' S	81° 45.09 W 8° 47.53' S	20/3/2000 12:30	21/3/2000 14:34	3-1573	13	3 x 32l BOLT
HH9	80° 48.08' W 8° 23.47' S	80° 11.52' W 8° 8.02' S	22/3/2000 1:19	22/3/2000 9:14	7-2845	14-15	2 x GI (45/105)
HH10	80° 11.52' W 8° 8.02' S	80° 8.48' W 8° 24.00' S	22/3/2000 9:14	22/3/2000 12:30	2845-4025	15	2 x GI (45/105)
HH11	80° 8.48' W 8° 24.00' S	80° 39.00' W 8° 54.27' S	22/3/2000 12:30	22/3/2000 21:00	4025-7071	15-17	2 x GI (45/105)
HH12	80° 39.00' W 8° 54.27' S	80° 41.52' W 9° 10.05' S	22/3/2000 21:00	23/3/2000 00:15	7071-8145	17-18	2 x GI (45/105)
HH13	80° 41.52' W 9° 10.05' S	79° 58.08' W 8° 58.76' S	23/3/2000 00:15	23/3/2000 9:56	8145-11396	18-19	2 x GI (45/105)
HH14	79° 58.08' W 8° 58.76' S	79° 51.14' W 8° 58.76' S	23/3/2000 9:59	23/3/2000 12:26	11414-12297	19-20	2 x GI (45/105)
HH15	79° 51.32' W 8°58.02' S	80° 30.38' W 9° 2.94' S	23/3/2000 12:30	23/3/2000 20:17	12324-15085	20-21	2 x GI (45/105)
HH16	80° 28.19' W 8° 57.00' S	79° 59.69' W 8° 31.46' S	23/3/2000 22:16	24/3/2000 5:52	6-2736	22-23	2 x GI (45/105)
HH17	79° 59.69' W 8° 31.46' S	80° 5.33' W 8° 19.96' S	24/3/2000 5:52	24/3/2000 8:28	2736-3673	23	2 x GI (45/105)
HH18	80° 5.59' W 8°19.96' S	80° 30.43' W 8° 38.70' S	24/3/2000 8:32	24/3/2000 14:45	3693-5930	23-24	2 x GI (45/105)
HH19	80° 30.91' W 8° 32.75' S	80° 6.69' W 8° 16.84 S	24/3/2000 15:58	24/3/2000 21:43	6373-8433	24-25	2 x GI (45/105)
HH20	80° 8.58' W 8° 13.32' S	80° 8.58' W 8° 28.86' S	24/3/2000 22:33	25/3/2000 4:09	245-2260	26-27	2 x GI (45/105)
HH21	80° 33.51' W 8° 23.55' S	80° 7.71' W 8° 8.72' S	25/3/2000 5:17	25/3/2000 11:12	2672-4798	27-28	2 x GI (45/105)
HH22	80° 12.11' W 8° 5.64' S	80° 36.16' W 8° 15.93' S	25/3/2000 12:22	25/3/2000 19:13	5225-7678	28-29	2 x GI (45/105)
HH23	80° 37.98' W 8° 12.02' S	80° 17.01' W 8° 3.10' S	25/3/2000 20:00	26/3/2000 00:33	7959-9584	29-30	2 x GI (45/105)
HH24 WS/RS5	78° 4.96' W 11° 5.72' S	79° 54.48' W 12° 3.22' S	28/3/2000 4:18	29/3/2000 10:43	5-1829	31	3 x 32l BOLT
HH25 WS/RS6	No	Data					
HH26	78° 54.77' W 11° 12.11' S	78° 31.34' W 11° 1.46' S	5/4/2000 10:46	5/4/2000 15:46	33-1796	35	2 x GI (105/105)
HH27	78° 31.34' W 11° 1.46' S	78° 20.96' W 11° 72.65' S	5/4/2000 15:46	5/4/2000 18:00	1796-2600	35-36	2 x GI (105/105)
HH28	78° 20.96' W 11° 72.65' S	78° 34.50' W 11° 15.55' S	5/4/2000 18:00	5/4/2000 19:39	2600-3190	36	2 x GI (105/105)

HH29	78° 34.50' W 11° 15.55' S	78° 42.48' W 10° 57.22' S	5/4/2000 19:39	5/4/2000 23:40	3190- 4642	36-37	2 x GI (105/105)
HH30	78° 42.48' W 10° 57.22' S	78° 45.68' W 10° 58.64'S	5/4/2000 23:40	6/4/2000 00:31	4642- 4943	37	2 x GI (105/105)
HH31	78° 45.66' W 10° 59.24'S	78° 38.64' W 11° 17.66' S	6/4/2000 00:31	6/4/2000 04:38	4986- 6425	37-38	2 x GI (105/105)
HH32	78° 38.64' W 11° 17.66' S	78° 41.68' W 11° 18.91'S	6/4/2000 04:38	6/4/2000 05:20	6425- 6674	38	2 x GI (105/105)
HH33	78° 41.68' W 11° 18.91'S	78° 49.65' W 11° 0.26' S	6/4/2000 05:20	6/4/2000 09:23	6674- 8149	38-39	2 x GI (105/105)
HH34	80° 22.09' W 8° 29,.84' S	80° 27.11' W 8° 19.15' S	11/4/2000 00:42	11/4/2000 03:39	3- 1063	40	2 x GI (105/105)
HH35	80° 27.11' W 8° 19,.15' S	80° 24.40' W 8° 17.37' S	11/4/2000 3:39	11/4/2000 4:42	1063- 1440	40	2 x GI (105/105)
HH36	80° 24.40' W 8° 17.37' S	80° 14.86' W 8° 26.63' S	11/4/2000 4:42	11/4/2000 7:15	1441- 2358	40-41	2 x GI (105/105)
HH37	80° 14.54' W 8° 26.80' S	80° 22.09' W 8° 29.84' S	11/4/2000 7:23	11/4/2000 7:56	2408- 2605	41	2 x GI (105/105)
HH38	80° 17.70' W 8° 24.97' S	80° 21.77' W 8° 16.24' S	11/4/2000 8:07	11/4/2000 10:32	2669- 3542	41	2 x GI (105/105)
HH39	80° 21.64' W 8° 15.91' S	80°17.07' W 8° 13.32' S	11/4/2000 10:37	11/4/2000 11:55	3572- 4036	41-42	2 x GI (105/105)
HH40	80°16.72' W 8° 13.66' S	80°12.63' W 8° 21.97' S	11/4/2000 12:03	11/4/2000 14:19	4087- 4906	42	2 x GI (105/105)
HH41	80°11.98' W 8° 21.39' S	80°11.81' W 8° 15.97' S	11/4/2000 14:38	11/4/2000 15:51	5014- 5450	42	2 x GI (105/105)
HH42	80°12.14' W 8° 15.61' S	80°28.05' W 8° 26.20' S	11/4/2000 16:06	11/4/2000 20:55	5550- 7233	42-43	2 x GI (105/105)
HH43	81°43.56' W 8° 47.15' S	81°44.33' W 8° 47.48' S	15/4/2000 2:00	15/4/2000 2:09	6- 55	44 ?	1 x GI (45/105)
HH43b	81°44.63' W 8° 47.63' S	82°36.53' W 9° 10.00' S	15/4/2000 2:12	15/4/2000 13:25	105- 4138	45-46	2 x GI (45/105)
HH44 SeBo	78°41.71' W 11° 6.68' S	78°36.56' W 11° 4.62' S	18/4/2000 1:57	18/4/2000 3:01	61- 448	48	1 x GI (45/105)
HH45	78°36.56' W 11° 4.62' S	78°37.6' W 11° 5.93' S	18/4/2000 3:01	18/4/2000 3:21	449- 572	48	1 x GI (45/105)
HH46	78°37.6' W 11° 5.93' S	78°37.78' W 11° 6.12' S	18/4/2000 3:01	18/4/2000 3:29	573- 616	48	1 x GI (45/105)
HH47	78°38.01' W 11° 5.78' S	78°38.49' W 11° 4.34' S	18/4/2000 3:35	18/4/2000 3:55	654- 772	48	1 x GI (45/105)
HH48	78°38.19' W 11° 4.22' S	78°37.49' W 11° 6.03' S	18/4/2000 4:02	18/4/2000 4:25	813- 950	48	1 x GI (45/105)
HH49	78°37.64' W 11° 6.11' S	78°38.16' W 11° 6.31' S	18/4/2000 4:27	18/4/2000 4:34	963- 1003	48	1 x GI (45/105)
HH50	78°38.28' W 11° 6.20' S	78°39.06' W 11° 4.13' S	18/4/2000 4:36	18/4/2000 5:03	1015- 1178	48	1 x GI (45/105)
HH51	78°38.72' W 11° 4.15' S	78°37.94' W 11° 6.25' S	18/4/2000 5:11	18/4/2000 5:38	1225- 1387	48	1 x GI (45/105)
HH52	78°38.09' W 11° 6.32' S	78°38.59' W 11° 6.50' S	18/4/2000 5:40	18/4/2000 5:46	1400- 1439	48	1 x GI (45/105)
HH53	78°38.71' W 11° 6.39' S	78°39.35' W 11° 4.70' S	18/4/2000 5:49	18/4/2000 6:11	1455- 1584	48	1 x GI (45/105)
HH54	78°39.02' W 11° 4.65' S	78°36.31' W 11° 6.43' S	18/4/2000 6:17	18/4/2000 6:40	1623- 1764	48-49	1 x GI (45/105)
HH55	78°38.88' W 11° 6.44' S	78°39.33' W 11° 4.64' S	18/4/2000 6:47	18/4/2000 7:12	1804- 1955	49	1 x GI (45/105)
HH56	78°39.06' W 11° 4.95' S	78°38.57' W 11° 6.50' S	18/4/2000 7:19	18/4/2000 7:39	1994- 2115	49	1 x GI (45/105)
HH57	78°38.57' W 11° 6.50' S	78°38.93' W 11° 6.63' S	18/4/2000 7:39	18/4/2000 7:45	2116- 2154	49	1 x GI (45/105)
HH58	78°38.03' W 11° 6.53' S	78°38.65' W 11° 4.84' S	18/4/2000 7:48	18/4/2000 8:08	2165- 2291	49	1 x GI (45/105)
HH59	78°39.61' W 11° 4.76' S	78°38.06' W 11° 4.14' S	18/4/2000 8:10	18/4/2000 8:30	2299- 2424	49	1 x GI (45/105)
HH60	78°38.03' W 11° 4.18' S	78°37.32' W 11° 5.94' S	18/4/2000 8:32	18/4/2000 8:55	2430- 2567	49	1 x GI (45/105)

HH61	78°37.66' W 11° 6.03' S	78°38.29' W 11° 4.21' S	18/4/2000 9:00	18/4/2000 9:23	2597- 2744	49	1 x GI (45/105)
HH62	78°37.86' W 11° 4.11' S	78°37.17' W 11° 5.91' S	18/4/2000 9:29	18/4/2000 9:50	2782- 2924	49	1 x GI (45/105)
HH63	78°37.28' W 11° 5.97' S	78°37.98' W 11° 6.26' S	18/4/2000 9:55	18/4/2000 10:05	2933- 2990	49	1 x GI (45/105)
HH64	78°38.04' W 11° 6.21' S	78°38.94' W 11° 4.06' S	18/4/2000 10:07	18/4/2000 10:35	3000- 3170	49	1 x GI (45/105)
HH65a	78°58.40' W 10° 48.29' S	78°50.31' W 10° 56.77' S	19/4/2000 15:48	19/4/2000 18:10	106- 1165	50	3 x Prakla (2.5 / 3 / 2)
HH65b	78°51.70' W 10° 55.32' S	78°34.47' W 11° 33.79' S	19/4/2000 19:20	20/4/2000 3:44	45- 3821	51-52	2 x GI (105/105)
HH66	78°34.28' W 11° 33.73' S	78°29.08' W 11° 30.82' S	20/4/2000 3:47	20/4/2000 4:57	3844- 4379	52	2 x GI (105/105)
HH67	78°29.06' W 11° 30.59' S	78°31.23' W 11° 25.35' S	20/4/2000 5:00	20/4/2000 6:11	4398- 4928	52	2 x GI (105/105)
HH68	78°31.62' W 11° 25.23' S	78°39.31' W 11° 29.23' S	20/4/2000 6:13	20/4/2000 7:56	4950- 5710	52-53	2 x GI (105/105)
HH69	78°39.46' W 11° 29.09' S	78°43.66' W 11° 18.78' S	20/4/2000 7:58	20/4/2000 10:09	5728- 6710	53	2 x GI (105/105)
HH70	78°43.59' W 11° 18.66' S	78°16.37' W 11° 03.80' S	20/4/2000 10:13	20/4/2000 16:19	6743- 9447	53-55	2 x GI (105/105)
HH71	78°16.44' W 11° 03.80' S	78°19.50' W 10° 57.60' S	20/4/2000 16:40	20/4/2000 18:02	9598- 10170	55-56	2 x GI (105/105)
HH72	78° 19.74' W 10° 57.63' S	78° 36.48' W 11° 04.62' S	20/4/2000 18:04	20/4/2000 21:40	10192- 11804	56	2 x GI (105/105)
HH73	78°36.60' W 11° 04.84' S	78°35.56' W 11° 7.53' S	20/4/2000 21:43	20/4/2000 22:18	11830- 12090	56	2 x GI (105/105)
HH74	78° 35.70' W 11° 7.81' S	78° 55.05' W 11° 15.81' S	20/4/2000 22:22	21/4/2000 2:29	12119- 13968	56-57	2 x GI (105/105)
HH75 SeeBo 2	78° 38.89' W 11° 5.39' S	78° 49.31' W 11° 09.87' S	21/4/2000 17:18	21/4/2000 19:32	16- 1009	58	1 x GI (45/105)
HH76	78° 49.19' W 11° 09.45' S	78° 46.66' W 11° 07.38' S	21/4/2000 19:40	21/4/2000 20:18	1069- 1350	58	1 x GI (45/105)
HH77	78° 46.66' W 11° 07.38' S	78° 45.51' W 11° 06.78' S	21/4/2000 20:18	21/4/2000 20:34	1351- 1476	58	1 x GI (45/105)
HH78	78° 45.45' W 11° 06.85' S	78° 44.48' W 11° 09.32' S	21/4/2000 20:35	21/4/2000 21:07	1485- 1716	58	1 x GI (45/105)
HH79	78° 44.63' W 11° 09.41' S	78° 45.53' W 11° 09.75' S	21/4/2000 21:10	21/4/2000 21:21	1737- 1823	58	1 x GI (45/105)
HH80	78° 45.63' W 11° 09.54' S	78° 46.61' W 11° 06.97' S	21/4/2000 21:24	21/4/2000 21:57	1845- 2096	58	1 x GI (45/105)
HH81	78° 46.25' W 11° 07.06' S	78° 46.61' W 11° 06.97' S	21/4/2000 22:06	21/4/2000 19:32	2146- 2395	58-59	1 x GI (45/105)
HH82	78° 45.48' W 11° 09.74' S	78° 45.63' W 11° 09.80' S	21/4/2000 22:42	21/4/2000 22:44	2417- 2435	59	1 x GI (45/105)
HH83	78° 45.72' W 11° 09.72' S	78° 46.65' W 11° 7.35' S	21/4/2000 22:45	21/4/2000 23:16	2440- 2676	59	1 x GI (45/105)
HH84	78° 6.99' W 11° 7.28' S	78° 45.91' W 11° 06.99' S	21/4/2000 23:18	21/4/2000 23:27	2689- 2762	59	1 x GI (45/105)
HH85	78° 45. 85' W 11° 7.03' S	78° 44.83' W 11° 9.50' S	21/4/2000 23:29	22/4/2000 00:02	2778- 3018	59	1 x GI (45/105)
HH86	78° 45.05' W 11° 9.45' S	78° 46.11' W 11° 07.13' S	22/4/2000 00:06	22/4/2000 00:38	3035- 3290	59	1 x GI (45/105)
HH87	78° 45.99' W 11°07.03'S	78°44.99 W 11°09.47' S	22/4/2000 00:48	22/4/2000 01:19	3361- 3602	59	1 x GI (45/105)
HH88	78° 45.15' W 11° 09.58' S	78° 45.32' W 11° 09.68' S	22/4/2000 01:22	22/4/2000 01:25	3620- 3644	59	1 x GI (45/105)
HH89	78° 45.40' W 11° 09.62' S	78° 46.36' W 11° 07.23' S	22/4/2000 01:27	22/4/2000 01:58	3656- 3890	59	1 x GI (45/105)
HH90	78° 46.29' W 11° 07.13' S	78° 45.72' W 11° 06.88' S	22/4/2000 02:00	22/4/2000 02:07	3904- 3959	59	1 x GI (45/105)
HH91	78° 45.68' W 11° 06.92' S	78° 44.63' W 11° 09.40' S	22/4/2000 02:09	22/4/2000 02:41	3975- 4214	59	1 x GI (45/105)
HH92	78° 58.65' W 11° 36.30' S	78° 52.67 W 11° 31.52 S	23/4/2000 00:24	23/4/2000 01:56	13- 462	60	2 x GI (105/105)

HH93	78° 53.13' W 11° 31.17' S	78° 58.26' W 11° 35.26' S	23/4/2000 02:35	23/4/2000 03:55	541- 939	60	2 x GI (105/105)
HH94	78° 58.81 W 11° 35.07 S	78° 59.92 W 11° 33.64 S	23/4/2000 04:00	23/4/2000 04:22	964- 1074	60	2 x GI (105/105)
HH95	78° 59.77 W 11° 33.34 S	78° 58.80 W 11° 32.35 S	23/4/2000 04:27	23/4/2000 04:45	1096- 1190	60	2 x GI (105/105)
HH96	78° 58.23 W 11° 32.36 S	78° 55.02 W 11° 36.17 S	23/4/2000 04:49	23/4/2000 05:53	1211- 1528	60	2 x GI (105/105)
HH97	78° 54.02 W 11° 36.30 S	78° 53.39 W 11° 35.24 S	23/4/2000 06:02	23/4/2000 06:23	1577- 1675	60	2 x GI (105/105)
HH98	78° 53.55 W 11° 35.30 S	78° 56.87 W 11° 31.10 S	23/4/2000 06:32	23/4/2000 07:35	1719- 2042	60	2 x GI (105/105)
HH99	78° 56.83 W 11° 31.00 S	78° 54.80 W 11° 29.43 S	23/4/2000 07:37	23/4/2000 08:06	2049- 2197	60	2 x GI (105/105)
HH100	78° 54.65 W 11° 29.44 S	78° 53.11 W 11° 31.33 S	23/4/2000 08:09	23/4/2000 08:36	2213- 2353	60	2 x GI (105/105)
HH101	78° 53.15 W 11° 31.50 S	79° 05.07 W 11° 40.83 S	23/4/2000 08:39	23/4/2000 11:47	2363- 3253	60-61	2 x GI (105/105)
HH102	79° 05.14 W 11° 40.54 S	79° 02.59 W 11° 38.88 S	23/4/2000 11:55	23/4/2000 12:55	30- 388	62	2 x GI (105/105)
HH103	79° 02.45 W 11° 39.40 S	79° 05.77 W 11° 41.62 S	23/4/2000 13:08	23/4/2000 14:25	466- 916	62	2 x GI (105/105)
HH104	79° 05.87 W 11° 41.39 S	79° 05.77 W 11° 41.62 S	23/4/2000 14:34	23/4/2000 15:51	970- 1432	62	2 x GI (105/105)
HH105	79° 02.41 W 11° 39.14 S	79° 01.68 W 11° 40.37 S	23/4/2000 15:53	23/4/2000 16:24	1442- 1630	62	2 x GI (105/105)
HH106	79° 01.76 W 11° 40.47 S	79° 02.94 W 11° 41.24 S	23/4/2000 16:28	23/4/2000 16:58	1652- 1825	62	2 x GI (105/105)
HH107	79° 03.10 W 11° 41.04 S	79° 04.68 W 11° 38.73 S	23/4/2000 17.24	23/4/2000 17:59	1858- 2194	62	2 x GI (105/105)

GEOPECO SO146 - PROFILE09 - SeeBoSeis_1

INSTRUMENT	LAT (S)	LON (W)	DIST. TO	DEPTH	RELEASER-	ANT.	RECORDER	SKEW	REMARKS
	D:M	D:M	NEXT (nm)	(m)	CODE	CH.	NUMBER	(ms)	
OBH98	11 : 05,072	78 38,693		1699	5924	D	991294	-2	
OBH99	11 : 05,001	78 38,548	0.159	1689	4A49	C	980907	1	
OBH100	11 : 04,959	78 38,41	0.142	1677	6969	D	980402	-1	
OBH101	11 : 04,969	78 37,527	0.136	1619	C679	C	980908	1	
OBH102	11 : 05,055	78 37,689	0.181	1631	6959	D	980905	1	
OBH103	11 : 05,106	78 37,83	0.148	1644	6A24	C	980901	71	
OBH104	11 : 05,171	78 37,938	0.124	1657	C444	D	980906	3	
OBH105	11 : 05,232	78 38,151	0.218	1670	D634	C	980902	0	
OBH106	11 : 05,476	78 38,703	0.595	1716	D674	D	991293	-1	
OBS107	11 : 05,656	78 38,494	0.269	1731	4979	C	971202	58	
OBS108	11 : 05,589	78 38,995	0.496	1737	5929	D	971201	-2	
OBS109	11 : 05,647	78 39,166	0.178	1747	B495	C	990901	-1	
OBS110	11 : 05,727	78 39,291	0.146	1759	D654	C	991202	-1	
TRIGGER									

SBS1	11 : 05,476	78	38,706							SBS=SeeBoSeis
SBS2	11 : 05,785	78	39,444							
SBS3	11 : 05,806	78	39,498							
SBS4	11 : 05,806	78	39,498							
SBS5	11 : 05,397	78	38,532							
SBS6	11 : 05,382	78	38,478							
SBS7	11 : 05,358	78	38,418							
SBS8	11 : 05,332	78	38,364							
SBS9	11 : 05,315	78	38,322							
SBS10	11 : 05,301	78	38,274							

APPENDIX V

GEOPECO SO146 - PROFILE 10 -SeeBoSeis_2

INSTRUMENT	LAT (N)	LON (W)	DIST. TO	DEPTH	RELEASER-	ANT.	RECORDER	SKEW	REMARKS
	D:M	D:M	NEXT (nm)	(m)	CODE	CH.	NUMBER	(ms)	
OBH111	11 : 07,585	78 45,14		1987	D634	D	980902	1	
OBH112	11 : 07,796	78 45,968	0.841	2025	C444	C	980907	0	
OBH113	11 : 07,934	78 45,908	0.149	2029	6A24	D	980908	1	
OBH114	11 : 08,106	78 45,851	0.180	2029	6959	C	980905	1	
OBH115	11 : 08,823	78 45,894	0.715	2044	C679	D	980901	70	
OBH116	11 : 08,759	78 45,753	0.153	2040	6969	C	980906	3	
OBH117	11 : 08,710	78 45,598	0.160	2042	4A49	D	991294	-2	
OBH118	11 : 08,378	78 44,837	0.818	2024	5924	C	980402	0	
OBS119	11 : 08,149	78 45,184	0.410	2018	5929	D	971201		late recovery
OBS120	11 : 08,204	78 45,349	0.171	2024	B495	C	990901		recorder dead
OBS121	11 : 08,270	78 45,488	0.152	2027	D654	D	991202	0	
OBS122	11 : 08,330	78 45,648	0.168	2032	4979	C	971202	41	
OBH123	11 : 08,573	78 46,193	0.588	2054	D674	C	991293	0	
TRIGGER									

SBS1	11 : 08,556	78 46,152							SBS=SeeBoSeis
SBS2	11 : 08,502	78 46,032							
SBS3	11 : 08,478	78 45,972							
SBS4	11 : 08,454	78 45,912							
SBS5	11 : 08,424	78 45,852							
SBS6	11 : 08,400	78 45,792							
SBS7	11 : 08,376	78 45,732							
SBS8	11 : 08,088	78 45,042							
SBS9	11 : 08,064	78 44,988							
SBS10	11 : 08,046	78 44,94							
SBS11	11 : 08,022	78 44,892							

APPENDIX VI

List of Magnetic Profiles

(G. Ali Dehghani and Raffaela Heinbockel)

Profile	Start		End		Length [km]
	Longitude	Latitude	Longitude	Latitude	
1	77° 20.18' W	15° 16.54' S	76° 12.09' W	16° 10.62' S	157
2	76° 00.42' W	14° 43.52' S	76° 59.99' W	15° 56.00' S	171
3	76° 55.51' W	12° 47,55' S	78° 19.08' W	14° 00.08' S	202
3c	77° 29.40' W	13° 16.94' S	76° 58.55' W	12° 51.19' S	73
4b	76° 58.53' W	12° 51.17' S	76° 52.80' W	13° 09.56' S	35
5b	76° 52.80' W	13° 09.57' S	77° 32.90' W	13° 12.69' S	73
5c	78° 05.61' W	11° 06.07' S	79° 54.64' W	12° 03.31' S	225
6c	79° 03.82' W	10° 45.50' S	78° 21.35' W	12° 05.84' S	167
7-1c	78° 53.78' W	11° 11.70' S	78° 31.35' W	11° 02.46' S	44
7-2c	78° 31.35' W	11° 02.46' S	78° 26.96' W	11° 12.62' S	20
7-3c	78° 26.96' W	11° 12.64' S	78° 34.19' W	11° 15.80' S	14
7-4c	78° 34.22' W	11° 15.80' S	78° 42.34' W	10° 57.22' S	37
7-5c	78° 42.35' W	10° 57.22' S	78° 45.73' W	10° 58.90' S	7
7-6c	78° 45.73' W	10° 58.92' S	78° 38.20' W	11° 17.29' S	37
7-7c	78° 38.20' W	11° 17.29' S	78° 41.77' W	11° 18.93' S	7
7-8c	78° 41.78' W	11° 18.93' S	78° 49.63' W	11° 00.29' S	37
4c	80° 08.68' W	08° 06.87' S	81° 45.06' W	08° 47.52' S	192
6b	80° 46.64' W	08° 22.88' S	80° 11.68' W	08° 08.08' S	70
7b	80° 11.66' W	08° 08.07' S	80° 08.48' W	08° 24.04' S	30
8b	80° 08.48' W	08° 24.06' S	80° 39.01' W	08° 54.29' S	79
9b	80° 39.01' W	08° 54.30' S	80° 41.92' W	09° 09.89' S	29
10b	80° 41.92' W	09° 09.91' S	79° 57.99' W	08° 48.09' S	90
11b	79° 57.98' W	08° 48.10' S	79° 51.14' W	08° 58.84' S	23
12b	79° 51.14' W	08° 58.85' S	80° 31.17' W	09° 02.88' S	74
13b	80° 27.38' W	08° 56.30' S	79° 59.76' W	08° 31.52' S	68
14b	79° 59.75' W	08° 31.51' S	80° 05.28' W	08° 20.03' S	23
15b	80° 05.30' W	08° 20.00' S	80° 30.53' W	08° 38.58' S	58
16b	80° 30.54' W	08° 38.56' S	80° 30.99' W	08° 33.00' S	10
17b	80° 30.99' W	08° 32.99' S	80° 06.66' W	08° 16.74' S	54
18b	80° 06.66' W	08° 16.72' S	80° 08.42' W	08° 13.31' S	7
19b	80° 08.44' W	08° 13.30' S	80° 32.07' W	08° 28.87' S	52
20b	80° 32.08' W	08° 28.87' S	80° 33.57' W	08° 23.68' S	10
21b	80° 33.57' W	08° 23.67' S	80° 07.70' W	08° 08.69' S	55
22b	80° 07.69' W	08° 08.68' S	80° 11.94' W	08° 05.05' S	10
23b	80° 11.95' W	08° 05.05' S	80° 38.15' W	08° 15.94' S	52
24b	80° 38.16' W	08° 15.93' S	80° 37.98' W	08° 12.02' S	7
25b	80° 37.97' W	08° 12.00' S	80° 17.39' W	08° 03.23' S	41
8-1c	80° 22.48' W	08° 28.98' S	80° 27.28' W	08° 18.74' S	21
8-2c	80° 27.28' W	08° 18.73' S	80° 26.04' W	08° 17.79' S	3
8-3c	80° 24.05' W	08° 17.97' S	80° 19.90' W	08° 26.58' S	18
8-4c	80° 19.24' W	08° 26.55' S	80° 18.00' W	08° 25.71' S	3
8-5c	80° 17.89' W	08° 24.56' S	80° 21.59' W	08° 16.64' S	16
8-6c	80° 21.14' W	08° 15.63' S	80° 17.76' W	08° 13.71' S	7
8-7c	80° 16.60' W	08° 13.96' S	80° 12.43' W	08° 22.12' S	17

APPENDIX VI

List of Magnetic Profiles

(continued)

(G. Ali Dehghani and Raffaela Heinbockel)

Profile	Start		End		Length [km]
	Longitude	Latitude	Longitude	Latitude	
8-8c	80° 12.42' W	08° 22.12' S	80° 11.74' W	08° 16.24' S	11
8-9c	80° 11.74' W	08° 16.24' S	80° 27.95' W	08° 26.14' S	35
56a	80° 44.39' W	08° 19.42' S	80° 52.32' W	07° 59.23' S	40
57a	80° 52.34' W	07° 59.21' S	81° 17.86' W	08° 10.57' S	51
58a	81° 17.87' W	08° 10.59' S	81° 12.00' W	08° 25.77' S	30
59a	81° 11.99' W	08° 25.80' S	81° 39.80' W	08° 37.08' S	55
60a	81° 39.81' W	08° 37.10' S	81° 39.14' W	08° 39.40' S	4
61a	81° 39.14' W	08° 39.44' S	81° 43.55' W	08° 42.12' S	9
62a	81° 43.55' W	08° 42.16' S	81° 43.52' W	08° 47.12' S	9
9c	81° 43.53' W	08° 47.13' S	82° 36.61' W	09° 10.03' S	106
63a	82° 34.12' W	09° 13.08' S	81° 23.49' W	08° 42.82' S	141
64a	81° 23.47' W	08° 42.83' S	81° 14.10' W	09° 05.84' S	46
65a	81° 14.09' W	09° 05.87' S	81° 00.45' W	09° 24.08' S	42
66a	81° 00.43' W	09° 24.10' S	81° 01.99' W	09° 14.59' S	18
67a	81° 01.99' W	09° 14.57' S	81° 10.00' W	09° 03.95' S	24
68a	81° 10.01' W	09° 03.93' S	81° 19.35' W	08° 41.41' S	45
69a	81° 19.36' W	08° 41.39' S	81° 16.04' W	08° 39.33' S	7
70a	81° 16.01' W	08° 39.34' S	81° 06.46' W	09° 02.02' S	45
71a	81° 06.44' W	09° 02.04' S	80° 56.99' W	09° 12.01' S	25
72a	80° 56.97' W	09° 12.03' S	80° 53.81' W	09° 09.91' S	7
73a	80° 53.84' W	09° 09.87' S	81° 03.48' W	08° 58.54' S	27
74a	81° 03.52' W	08° 58.49' S	81° 12.41' W	08° 38.11' S	41
75a	81° 12.41' W	08° 38.08' S	81° 08.86' W	08° 36.06' S	8
76a	81° 08.81' W	08° 36.06' S	80° 59.98' W	08° 56.05' S	40
77a	80° 59.98' W	08° 56.05' S	80° 53.91' W	09° 03.89' S	18
64b	78° 58.35' W	10° 48.34' S	78° 51.00' W	10° 56.05' S	20
65b	78° 51.16' W	10° 55.89' S	78° 34.92' W	11° 32.89' S	74
66b	78° 33.70' W	11° 33.42' S	78° 30.37' W	11° 31.63' S	7
67b	78° 29.34' W	11° 29.83' S	78° 30.94' W	11° 25.99' S	8
68b	78° 32.36' W	11° 25.60' S	78° 38.23' W	11° 28.77' S	12
69b	78° 39.78' W	11° 28.34' S	78° 43.33' W	11° 19.79' S	17
70b	78° 42.92' W	11° 18.31' S	78° 17.16' W	11° 04.24' S	54
71b	78° 16.76' W	11° 02.91' S	78° 18.79' W	10° 58.56' S	9
72b	78° 20.40' W	10° 57.92' S	78° 35.71' W	11° 04.26' S	30
74b	78° 36.37' W	11° 08.11' S	78° 54.54' W	11° 15.60' S	36

Appendix VII

Summary of heat flow measurements. Asterisks denotes values not available
"DNP" stands for "did not penetrate".

Pen #	Latitude	Longitude	Water Depth	Tilt	Temp.	Thermal cond.		Q		RMS error	Shot #
	Dec Deg	Dec Deg	m	Deg	°C	W/m/K		mW/m^2			
HF020P01	-8,4565	-80,5097	1254	1,7	3,7	0,84	11	58,1	9	0,0064	2135
HF020P02	-8,4627	-80,5055	1240	3,3	3,7	0,85	0	59,5	9	0,0023	2110
HF020P03*	-8,4605	-80,5020	1216	2,1	***	0,83	11	58,3	9	***	2100
HF020P04	-8,4583	-80,4982	1181	2,3	3,9	0,82	0	79,7	6	0,0079	2075
HF020P05	-8,4553	-80,4943	1172	7,8	3,9	0,88	0	110,3	4	0,0086	2055
HF020P06	-8,4531	-80,4908	1160	7,8	3,9	0,85	11	56,0	8	0,0015	2040
HF020P07	-8,4515	-80,4874	1150	9,7	3,9	0,82	0	72,2	7	0,0049	2015
HF020P08	-8,4481	-80,4833	1124	7,2	4,0	0,82	0	73,0	6	0,0045	2005
HF020P09	-8,4453	-80,4792	1122	11,8	4,2	0,82	0	62,6	8	0,0031	1980
HF020P10	-8,4428	-80,4758	1114	7,3	4,1	0,84	0	57,7	8	0,0031	1960
HF020P11	-8,4418	-80,4720	1094	2,6	4,2	0,82	0	72,7	8	0,0064	1945
HF020P12	-8,4380	-80,4680	1088	7,9	4,4	0,94	3	51,6	3	0,0011	1920
HF020P13	-8,4353	-80,4643	1079	7,5	***	***	***	0	***	***	1900
HF021P01	-8,3953	-80,4025	957	3,9	4,8	0,96	8	47,0	8	0,0036	1580
HF021P02	-8,3897	-80,3935	942	12,2	4,9	0,90	0	36,4	11	0,0023	1540
HF021P03	-8,3852	-80,3882	931	6,8	5,0	0,90	11	36,8	11	0,0020	1510
HF021P04	-8,3805	-80,3803	915	5,4	5,1	0,91	0	33,6	9	0,0029	1475
HF021P05	-8,3748	-80,3737	902	4,1	5,1	0,88	10	31,5	10	0,0020	1440
HF021P06	-8,3697	-80,3585	886	8,2	5,2	0,91	0	29,7	10	0,0019	1370
HF021P07	-8,3645	-80,3577	870	12,0	5,3	0,86	10	23,9	10	0,0033	1355
HF021P08	-8,3595	-80,3500	856	21,6	5,5	0,91	0	22,8	10	0,0042	1320
HF021P09	-8,3552	-80,3413	851	28,0	DNP	***	***	0	***	***	1270
HF022P01	-8,3953	-80,4025	249	DNP	***	***	***	0	***	***	600
HF022P02	-8,3897	-80,3935	287	DNP	***	***	***	0	***	**	640
HF022P03	-8,3852	-80,3882	338	DNP	***	***	***	0	***	***	680
HF022P04	-8,3895	-80,3803	440	DNP	***	***	***	0	***	***	763
HF022P05	-8,2975	-80,2570	530	36,6	7,3	0,97	0	218,6	5	0,0164	840
HF022P06	-8,3022	-80,2645	578	6,5	7,4	0,96	10	46,0	10	0,0040	880
HF022P07	-8,3075	-80,2723	625	1,9	7,1	0,91	11	31,8	11	0,0068	925
HF022P08	-8,3123	-80,2788	659	0,9	6,8	0,95	0	17,8	10	0,0031	960
*HF022P09	-8,3171	-80,2874	690	4,70	***	0,85	9	4,1	9		*** 995
HF023P01	-8,3207	-80,6335	1839	0,9	2,7	0,86	0	37,1	7	0,0013	795
HF023P02	-8,3240	-80,6420	1923	1,3	2,5	0,86	11	37,7	10	0,0033	760
HF023P03	-8,3278	-80,6623	1951	9,3	2,4	0,86	0	37,7	9	0,0016	715
HF023P04	-8,3310	-80,6588	2067	6,2	2,4	0,87	11	37,9	10	0,0015	680
HF023P05	-8,3343	-80,6673	2137	5,6	2,3	0,86	0	37,3	10	0,0020	645
HF023P06	-8,3382	-80,6767	2202	17	2,2	0,87	11	33,9	10	0,0025	605
HF023P07	-8,3415	-80,6835	2277	8,5	2,2	0,86	0	33,3	11	0,0016	565
HF023P08	-8,3448	-80,6922	2366	15,5	2,1	0,86	0	38,9	11	0,0071	530
HF023P09	-8,3483	-80,7008	2439	13	2,1	0,84	11	30,4	11	0,0016	490
HF023P10	-8,3553	-80,7177	2555	10,2	2,0	0,86	0	37,2	11	0,0046	405
HF023P11	-8,3620	-80,7350	2713	11,8	1,9	0,84	11	37,4	11	0,0028	330
HF024P01	-11,1865	-78,8781	2456	0,1	2,0	0,9	7,0	59,1	5,0	0,0	197

HF024P02	-11,1845 -78,8682	2422	DNP	***	***	***	0	***	***	242
HF024P03	-11,1797 -78,8593	2377	DNP	***	***	***	0	***	***	281
HF024P04	-11,1765 -78,8515	2321	DNP	***	***	***	0	***	***	316
HF024P05	-11,1701 -78,8348	2224	DNP	***	***	***	0	***	***	393
HF025P01	-11,1375 -78,7373	2013	DNP	***	***	***	0	***	***	751
HF025P02	-11,1320 -78,7245	1989	DNP	***	***	***	0	***	***	818
HF025P03	-11,1262 -78,7070	1968	DNP	***	***	***	0	***	***	880
HF025P04	-11,1232 -78,7030	1930	DNP	***	***	***	0	***	***	913
HF025P05	-11,1195 -78,6945	1893	DNP	***	***	***	0	***	***	955
HF025P06	-11,1180 -78,6902	1870	12,2	***	1,10	5	35,4	5	***	971
HF025P07*	-11,1161 -78,6859	1871	10,8	***	1,01	7	35,0	7	***	994
HF025P08	-11,1145 -78,6820	1859	7,1	2,7	0,90	0	35,9	7	0,0022	1023
HF025P09	-11,1128 -78,6773	1848	9,7	2,7	0,90	0	41,1	7	0,0021	1031
HF025P10	-11,1088 -78,6688	1827	13,6	2,6	0,90	0	34,7	6	0,0023	1075
HF026P01	-11,5877 -78,9649	3270	0,1	***	***	***	0	***	***	2717
HF026P02	-11,5827 -78,9574	3721	2,8	1,9	0,87	11	48,4	10	***	2683
HF026P03	-11,5771 -78,9502	3705	6,1	1,9	0,85	11	45,1	9	***	2650
HF026P04	-11,5712 -78,9432	3712	6,7	1,9	0,87	11	42,3	10	***	2618
HF026P05	-11,5659 -78,9362	3758	4,3	1,9	0,90	11	47,1	10	***	2587
HF026P06	-11,5599 -78,9289	3818	5,0	1,9	0,87	11	51,7	10	***	2555
HF026P07	-11,5707 -78,9218	3835	6,2	1,9	0,86	11	52,0	11	***	2522
HF026P08	-11,5418 -78,9065	3777	9,9	1,9	0,87	11	55,4	11	***	2452

Appendix VIII

Details of OBS/OBH deployment on profile SEISMO 1

OBH 37	
Released	15 March 2000 at 2235 UTC
Drop-off coordinates	11° 34.53'S, 78° 37.52'W
Recovered	27 March 2000 at 0929 UTC
Pick-up coordinates	11° 34.51'S, 78° 37.60'W
Averaged position	11° 34.52'S, 78° 37.56'W
Water depth	2125 m
OBS 38	
Released	16 March 2000 at 0000 UTC
Drop-off coordinates	11° 30.60'S, 78° 51.55'W
Recovered	27 March 2000 at 0500 UTC
Pick-up coordinates	11° 30.54'S, 78° 51.67'W
Averaged position	11° 30.57'S, 78° 51.61'W
Water depth	2956 m
OBS 39	
Released	16 March 2000 at 0106 UTC
Drop-off coordinates	11° 25.72'S, 78° 42.48'W
Recovered	27 March 2000 at 0625 UTC
Pick-up coordinates	11° 25.68'S, 78° 42.56'W
Averaged position	11° 25.30'S, 78° 42.52'W
Water depth	2389 m
OBS 40	
Released	16 March 2000 at 0208 UTC
Drop-off coordinates	11° 20.86'S, 78° 33.54'W
Recovered	27 March 2000 at 0706 UTC
Pick-up coordinates	11° 20.87'S, 78° 33.62'W
Averaged position	11° 20.86'S, 78° 33.58'W
Water depth	2031 m
OBH 41	
Released	16 March 2000 at 0332 UTC
Drop-off coordinates	11° 17.00'S, 78° 47.54'W
Recovered	27 March 2000 at 0400 UTC
Pick-up coordinates	11° 16.96'S, 78° 47.57'W
Averaged position	11° 16.98'S, 78° 47.55'W
Water depth	2355 m

The sample rate of all channels was set to 250 Hz.

Appendix VIII (continued)

Earthquake arrival times recorded on SEISMO 1

Date	OBH 41	OBS 40	OBS 39	OBS 38	OBH 37
16.03.00		EP 01 58 17			
			EP 06 52 16	EP 06 52 18	EP 06 52 15.5
	No Data		ES 06 52 57	ES 06 52 45	ES 06 52 45
			EP 07 21 04		IP 07 21 01.5
			ES 07 21 14		
		EP 08 08 20.5			
		EP 11 50 40			
		ES 11 50 44			
					EP 15 48 09
			EP 16 44 37		
			ES 16 45 04		
					EP 17 13 11
					EP 18 04 15

17.03.00					EP 02 03 25
				IP 04 10 53.5	EP 04 10 55.3
					EP 09 27 58
					EP 13 11 13
					EP 15 53 13.3
					ES 15 53 18
		EP 17 02 22.5	EP 17 02 22.5	EP 17 02 18.5	IP 17 02 19.5
			ES 17 03 12		
		EP 17 20 56.5			
			EP 17 56 55	IP 17 56 56	EP 17 56 53.3
			ES 17 57 23		
		EP 18 58 38	EP 18 58 37	EP 18 58 36	EP 18 58 36.5
		ES 18 58 55	ES 18 58 00		

Date	OBH 41	OBS 40	OBS 39	OBS 38	OBH 37

17.03.00			EP 20 44 07		
			ES 20 44 54		
	No Data			EP 21 00 19	EP 21 00 29
			EP 21 08 55		
			ES 21 09 43		
				EP 21 29 58.8	IP 21 29 57
					EP 21 40 22

18.03.00				EP 06 03 11	
		EP 06 22 14			
		ES 06 23 31			
		EP 12 43 15	EP 12 43 15		
		ES 12 44 35			
		EP 14 38 02	EP 14 38 02	EP 14 38 02	EP 14 38 01
		ES 14 38 50	ES 14 38 56		
		EP 15 44 27			
				EP 16 50 54	IP 16 50 56
		EP 22 59 41.5			
		ES 22 59 46			

19.03.00			EP 01 15 46		
		EP 02 40 35	EP 02 40 34	IP 02 40 35	EP 02 40 37
		ES 02 40 49	ES 02 40 49		
		EP 03 51 50	EP 03 51 49	IP 03 51 50.7	EP 03 51 52
		ES 03 52 20	ES 03 52 22		
			EP 08 45 06		
			ES 08 45 34		

Appendix IX

(Christian Huebscher, Eric Haase)

Parasound/ParaDigMa Bedienhilfe

Version 1.2 C. Hü. April 1997
Version 1.3 C. Hü. April 2000

Inhaltsverzeichnis

I. Vorbemerkung

Dieser Text gibt einen Überblick darüber, welche Aufgaben der Parasound Wachgänger wahrzunehmen hat. Es ist ein "dynamischer Text", der mit der Zeit wachsen und komplettiert werden soll. Anregungen werden gerne entgegengenommen. Die folgenden Ausführungen ersetzen weder eine gründliche Einführung noch das Studium der offiziellen Handbücher, sie dienen mehr als Erinnerungshilfe.
Diese überarbeitet Fassung trägt der Tatsache Rechnung, daß die Daten nicht mehr auf 9-Spur Bändern gesichert werden, sondern auf Wechselplatten gesichert werden.

I.1 Kontakte

Bitte schicken Sie Änderungsvorschläge an folgende Adresse

Dr. Christian Hübscher
Institut für Geophysik
Universität Hamburg
Bundesstrasse 55
20146 Hamburg
chuebscher@dkrz.de.

Die ParaDigMa-Programme wurden entwickelt von:

Prof. Volkhard Spieß
Fachbereich Geowissenschaften
Universität Bremen
Postfach 330 440

I.2 Was ist Parasound?

Das Parasound Sedimentecholot ist ein seismisches Meßsystem, mit dem die internen Strukturen der sedimentären Meeresbodenbedeckung entlang des Schiffskurses vermessen werden. Ein hochfrequentes Signal wird vom Schiff nach unten ausgesendet und dringt in den Meeresboden ein. Vereinfacht gesprochen wird überall dort, wo sich die Dichte im Sediment ändert, ein Teil des Signals zum Schiff reflektiert; also z.B. dort, wo sich die Zusammensetzung des Sediments ändert, und natürlich am Meeresboden selbst. Auf dem Schiff werden die zurückkehrenden Signale vom Parasound/ParaDigMa System empfangen, dargestellt und aufgezeichnet.

I.3 Systemkomponenten

Der Parasound Wachgänger muß sich mit den wesentlichen Eigenschaften von 3 Komponenten des Parasound/ParaDigMa Systems vertraut machen. Diese sind Parasound-Konsole, DESO und ParaDigMa-System.
Die Parasound-Konsole befindet sich in den Schaltschränken und besteht aus einem Bildschirm mit 2 Handgriffen sowie darunter angebrachten Bedienelementen. Auf METEOR gibt es zwei solcher Bildschirme, der relevante ist der rechte davon. In den Lotzentralen von SONNE und POLARSTERN ist nur ein System vorhanden.
Über der Parasound-Konsole befindet sich das DESO - ein Zweikanalecholot - mit Papierschreiber und zwei Schalterleisten.
Hauptkomponenten des ParaDigMa-Systems sind Data Acquisition Unit (DAU), PC mit Bildschirm, ein oder zwei Drucker .
Sowohl auf SONNE als auch auf METEOR befinden sich in der Lotzentrale Überwachungssysteme für das Fächerecholot Hydrosweep. Auf die nähere Vorstellung dieses für Kartierungszwecke entwickelten Systems wird hier verzichtet, wenn auch der Parasound Wachgänger einige wenige Funktionen dieses Systems zu überwachen hat. Der jeweilige Systemoperator wird hier gerne weitere Auskunft geben.

II. Grundwissen

Auf der Unterseite des Schiffes befinden sich Sender, die Signale mit 2 unterschiedlichen Frequenzen erzeugen. Eine Frequenz ist immer 18 kHz. Mit diesem Signal wird auch die Tiefenlotung für die Brücke durchgeführt. Das zweite Signal hat eine Frequenz zwischen 20,5 und 23,5 kHz (in 0,5 kHz Schritten einstellbar). Durch den sog. parametrischen Effekt, der aus der Nichtlinearität der Bewegungsgleichung von akustischen Wellen in einem flüssigen Medium resultiert, wird u.a. ein weiteres Signal in der Wassersäule generiert, dessen Hauptfrequenz der Differenz der beiden Frequenzen entspricht. Meistens hat das zweite ausgesendete Signal eine Frequenz von 22 kHz, so daß das parametrische Signal eine Frequenz von 4 kHz hat. Dieses Signal wird für die Sedimentecholot Messungen verwendet. Der große Vorteil des parametrischen Signals besteht darin, daß das Signal nur innerhalb eines Kegels von 4° Öffnungswinkel abgestrahlt wird. Am Meeresboden wird nur ein Gebiet erfaßt, deren Durchmesser ca. 7% der Wassertiefe entspricht. Dadurch wird eine hohe laterale Auflösung erzielt. Der Nachteil ist, daß bei Schichtneigungen von mehr als 2° keine Signale mehr zum Schiff reflektiert werden können; sie gehen am Schiff vorbei.
Das ParaDigMa-System dient der Digitalisierung und Aufzeichnung der empfangenen Signale. Die von den Empfängern registrierten Signale werden 40,000 mal pro Sekunde digitalisiert. Um die zu bearbeitende Datenmenge zu begrenzen, wird nur in dem Zeitbereich registriert, in dem auch Daten vom Meeresboden zu erwarten sind. Dieser Zeitbereich hängt von der Wassertiefe ab und muß geeignet eingestellt und nachgeführt werden. Um die Frage vorweg zunehmen: Nein, dieser Prozeß läßt sich nicht automatisieren! Die manuelle Nachführung des Registrierzeitfensters, ausgedrückt durch das Tiefenintervall, in dem sich die zu vermessenden Sedimente befinden, ist eine der wichtigsten Aufgaben des Parasound Wachgängers. Die Datensicherung geschieht mit Hilfe von Wechselfestplatten.

III. Aufgaben des Parasound Wachgängers

III.1 Antritt der Wache

Folgende Punkte sind **bei Antritt der Wache** zu prüfen:

- **Ist Name, Raum- und Telephonnummer der für den Fahrtabschnitt verantwortlichen Person bekannt?** Daß diese Frage zuerst aufgelistet wird, soll verdeutlichen, daß bei kritischen Fragen der Verantwortliche zu jeder Tages- und Nachtzeit angesprochen werden kann. **Gute Daten haben oberste Priorität!**

- **Ist Parasound/ParaDigMa und DESO aktiv?**

- **Ist genug Papier für die Online-Schriebe und das DESO vorhanden?**

- **Sind genug Protokollblätter vorrätig?**

- **Ist unten auf dem Hydrosweep Bildschirm ein rotes Quadrat neben den Buchstaben R-R zu erkennen?** Daran ist zu erkennen, daß Daten aufgezeichnet werden. Ist der Bildschirm dunkel, kann es mit der Maus aktiviert werden. Nach einigen Sekunden wird der Bildschirm hell. **(Nur auf METEOR)**

- **Ist auf dem Hydrosweep Bildschirm im Menü FAHRTKOMMANDO Start gedrückt? (Nur auf SONNE)**

III.2 Während der Wache

An der Parasound-Konsole:

- **Fenster nachführen.** Das Tiefenfenster, in dem die Daten registriert werden, muß entsprechend der Wassertiefe kontrolliert und ggf. manuell nachgeführt werden. Zwei grüne Zahlen benennen das aktuelle Tiefenfenster. Zur Nachführung dient ein kleiner Kipphebel auf der Parasound-Konsole (Aufschrift 'Phasing', rechter Hebel), mit dem das Tiefenfensters verstellt wird. **Der Meeresbodenreflektor ist in der oberen Bildschirmhälfte zu halten, damit insbesonders bei großer Eindringung auch tiefer liegende Reflektoren noch registriert werden können!** Das Umschalten soll schnell geschehen. Bitte überlegt Euch VOR dem Betätigen des Schalters eine Wunschtiefe. Da es bei jedem Umschalten zu Datenverlusten kommt, soll er immer dann, aber auch nur dann betätigt werden, wenn es nötig ist. Habt Ihr Euch um 10m vertan, sollte nur korrigiert werden, wenn der Meeresboden aus der oberen Bildschirmhälfte herausgelaufen ist.

Ist kein Signal auf dem Bildschirm zu erkennen, s. Was ist zu tun, wenn .. (s.u.)

- **Range verstellen.** Am DESO befindet sich ein Drehschalter mit der Beschriftung RANGE, der auf Werte zwischen 5 und 10000 (m) eingestellt werden kann. Über den Range wird die Länge eines Registrierzyklus, bestehend aus Senden und Empfangen einer Pulsfolge, eingestellt. Dabei gibt die Unterkante des Tiefenfensters den Zeitpunkt vor, an dem eine Umschaltung spätestens erfolgen sollte. Gleichzeitig damit muß evtl. an der Parasound-Konsole der Schalter 'Channel Select' in Stellung PAR oder PAR/NBS gebracht werden. Die Schalterstellung gibt an, ob die Wassertiefe aus dem eigentlichen 4 kHz-Nutzsignal (PAR) oder aus einem vorausgeschickten 18 kHz-Signal (PAR/NBS) bestimmt wird. Die Tabelle zeigt die zu verwendenden Schalterstellungen:

Wassertiefe	Range	Channel Select	Paperspeed
0-90 m	100	PAR	1:20000
90-400 m	500	PAR	1:20000
400-900 m	1000	PAR/NBS	1:20000
900-1900 m	2000	PAR/NBS	1:20000
1900-**4600** m	5000	PAR/NBS	1:20000
4600-9900 m	10000	PAR/NBS	1:10000

Der Papiervorschub wird am DESO mit dem Schalter PAPERSPEED verändert, wenn der Range 10000 eingestellt wird, um wegen der geringen Zahl von Lotungen einen ähnlichen Maßstab zu erzielen.

- **DESO-Rolle überwachen.** Die vom Parasound-System gelieferten analogen Daten werden von dem DESO-Schreiber auf der Papierrolle gedruckt. Wenn sich die Papierrolle dem Ende zuneigt, erscheint am oberen Rand ein roter Streifen, der dann diagonal über das Papier zum unteren Rand wandert. Bei Erscheinen des roten Streifens ist noch für etwa eine Stunde Papier vorhanden. Das Auswechseln der Papierrolle erfordert ein wenig Geschick. Das Procedere schriftlich zu beschreiben überfordert leider die schriftstellerischen Fähigkeiten des Autors. Notfalls hilft ein Systemoperator.

- **Ist die Datenqualität zufriedenstellend**? Wenn oberhalb der Meeresbodenreflektion auf dem Bildschirm der Parasound-Konsole ein starkes Rauschen auftritt, kann der THRESHOLD Schalter ganz langsam nach rechts gedreht werden, um dir "rauschenden" Farben auszublenden.

Am PC:

Hier müssen normalerweise keine Parameter verstellt, sondern nur die korrekte Funktion des Systems überwacht werden.

- **Funktioniert die DVS-Datenübertragung ?** Die DVS liefert die Navigationsdaten, die in jedem Echogrammheader und einem wichtigen Datenfile abgespeichert werden (Position, Kurs, Geschwindigkeit, etc.). Wenn sich das Schiff bewegt, sollten sich daher auch diese Daten beständig ändern. Die Navigationsdaten werden im rechten Bildschirm angezeigt (Infobox 'Large Letters').

- **Stimmen die Tiefen von Parasound und Hydrosweep in etwa überein ?** Bei Seegang und ungünstigem Kurs kann es besonders bei METEOR bei Hydrosweep zu Ausfällen kommen. Meist regelt sich das Problem nach einiger Zeit von selbst. Das Programm weist durch Tonfolgen auf das Problem hin. Notfalls lässt sich die Tonfolge im BASIC Menü abstellen.

- **Arbeiten die Drucker einwandfrei ?** Bei den Druckern kann alles schiefgehen, was bei Druckern üblicherweise schiefgeht, d.h. falscher oder schiefer Papiereinzug, Papierende, Tintenpatrone verbraucht, falscher Seitenanfang. Siehe Was ist zu tun, wenn ...

- **Schließlich bleibt noch der beliebteste Punkt: Protokoll schreiben.** In vorgegebenen Abständen werden die wesentlichen Systemparameter in den dafür vorgesehenen Formblättern protokolliert. Ein wichtiger Zweck des Protokolls ist die regelmäßige Systemkontrolle. Besondere Vorkommnisse bitte in der Spalte 'Bemerkungen' eintragen (diese Spalte ist wirklich wichtig !!!). Alle Uhrzeiten werden in UTC (Universal Time Coordinate) angegeben.

Am DVS:

- **Ist das DVS online?** Auf dem DVS-Bildschirm muß rechts unten der "Grüne Punkt" zu erkennen sein, daneben muß ONLINE stehen.

IV. Kurze Einführung in das ParaDigMa-System

Der Bildschirm gliedert sich in vier Bereiche. Den größten Ausschnitt nimmt die Darstellung der registrierten Echogramme in Anspruch. Hier werden die Daten nach Anwendung aller gewünschten Filterungen und Verstärkungen dargestellt. Gespeichert werden nur die Rohdaten. Die Filter haben daher keinen Einfluß auf die tatsächlich gesicherten Daten.
Am rechten Bildschirmrand können verschiedene Infoboxen angezeigt werden.
Der obere Bildschirmrand zeigt wahlweise eine von drei verschiedenen Menüleisten, zwischen denen mit der ESCAPE-Taste hin- und hergewechselt werden kann. Es gibt ein 'Basic Operation'-Menü (orangefarbener Hintergrund), mit dem die wichtigsten für die normale Benutzung notwendigen Funktionen schnell erreicht werden können, ein 'Main'-Menü (grauer Hintergrund), das sämtliche Funktionen über Untermenüs (blauer Hintergrund) schnell erreichbar macht, und eine allgemeine Titelleiste (blauer Hintergrund), die nur optischen Zwecken dient.
Die einzelnen Menüpunkte können durch Drücken ihrer hervorgehobenen Anfangsbuchstaben aufgerufen werden. Dabei werden dann entweder Untermenüs (blauer Hintergrund) geöffnet, oder in der rechten oberen Ecke des Bildschirms Eingabefenster angezeigt. Nach gleichzeitigem Drücken von Strg-H (wie Hilfe) werden Fenster mit Informationen über die jeweilige Funktion geöffnet. Alle Untermenüs oder Eingabefenster können mit der ESCAPE-Taste ohne Übernahme der (möglicherweise fehlerhaft oder unabsichtlich) eingegebenen Parameter wieder verlassen werden.
Eine Aufstellung aller Funktionen ist im Anhang wiedergegeben.
Bei der Eingabe von Zeichen können die im Anhang III aufgeführten Editor-Funktionen verwendet werden. Leerzeichen müssen daher auch als Leerzeichen eingegeben werden.

Tonfolgen:
Eine langsam aufsteigende Tonfolge ertönt in festen Abständen und erinnert an das Protokoll. Sollte die Musik nicht von alleine enden, hilft nach frühestens 5 Sekunden ein kurzer Druck auf die Leertaste.
Eine kurze und schnell auf- oder absteigende Tonfolge ertönt, wenn sich die Parasound-Wassertiefe dem oberen oder unteren Tiefenfensterrand nähert. Evtl. muß das Fenster verstellt werden.
Bei Verlust der Parasound-Wassertiefe, bzw. wenn Parasound und Hydrosweep Tiefe um mehr als 80 m voneinander abweichen, können Warntöne (hoch-tief im Wechsel) auftreten! In diesem Falle stellt das Tiefenfenster so ein, daß die Hydrosweep-Tiefe in der Mitte des Fensters liegt. Wenn kein Meeresboden zu erkennen ist, müßt Ihr das Tiefenfenster blind fahren, orientieren könnt Ihr Euch dann nur anhand der Hydrosweep-Tiefe (s.u.).
Wenn die Parasound Tiefe unzuverlässig ist, läßt sich das Parasound-Hydrosweep Signal auch abstellen (PS/HS SIGNAL im BASIC-Menü).

V. Was ist zu tun, wenn...

- **das Meeresbodenecho abhanden gekommen ist.** Ist das Echo aus dem Aufzeichnungsfenster herausgelaufen, kann das Fenster anhand der angegebenen Parasound- oder Hydrosweep Tiefe eingestellt werden. Wenn die Hangneigung zu groß ist, wird zu wenig Energie reflektiert, so daß keine Signale mehr sichtbar sind. Falls Parasound noch eine halbwegs plausible Wassertiefe liefert, das Tiefenfenster anhand dieser Tiefe neu positionieren und warten. Wenn nicht, hält man sich an die Hydrosweep-Tiefe. In topographisch schwierigem Gelände wie z.B. mittelozeanischen Spreizungsrücken kann sich das über Stunden hinziehen!

- **das Programm abgestürzt ist.** Bei fast allen Abstürzen bleibt das Programm stehen, so daß keinerlei Aktivität auf dem Bildschirm zu erkennen ist. Der Buchstabe auf weißem Grund oben rechts in der Ecke gibt an, welches die letzte Prozedur war. **In jedem Fall den Buchstaben im Protokoll vermerken.** In vielen Fällen liegt das Problem bei dem Online-Drucker. Wenn also das Programm stehengeblieben ist und die gelbe LED am Online-Drucker blinkt, ist das Problem erkannt. Meist ist dann entweder Papier oder der Toner zu Ende. Drückt also zuerst die Taste am Drucker unterhalb der gelben LED. Stellt nun sofort den Online-Drucker mit Strg-P aus. Nun kann Papier nachgelegt werden oder die Toner-Kartusche gewechselt werden. Nach erneutem Strg-P beginnt der Drucker erneut. Meist läuft das Programm dann problemlos weiter. Zum Tageswechsel um 00:00 Uhr kann es Schwierigkeiten mit den Navigationsdaten geben, die zum Abstürzen führen. Parasound-PC neu hochfahren (Mit Strg-Alt-Del). Mit TIME die Uhrzeit kontrollieren, sie muß auf mindestens 5 Minuten mit der UTC-Zeit übereinstimmen. PSS [Enter] drücken. Auf dem Bildschirm erscheint der Programm-Code für die DAU. Auf dem ParaDigMa-Bildschirm erscheint nach einigen Sekunden das Registrierprogramm. Zuerst den Tabellen-Plot mit Strg-T starten, damit weitere Aktivitäten dort protokolliert werden können. Strg-P startet den Online-Plot. Erscheinen Daten auf dem Bildschirm, kann die Datensicherung mit Strg-S aktiviert werden.

- **die Parasound-Tiefe falsch ist.** Ist die digitale Parasound Tiefe zu klein, reflektiert eventuell eine Sprungschicht im Wasser genug Energie, um den Meeresboden vorzugaukeln. In diesem Fall kann das Dig. Depth Gate (am DESO) heruntergesetzt werden. Das Parasound akzeptiert erst Reflexionen unterhalb des Digital Depth Gate.
  Bei zu großer Verstärkung an der Parasound-Konsole (POWER/GAIN) können ebenfalls falsche Parasound-Tiefen berechnet werden, die sowohl zu groß oder zu klein sein können. In diesem Fall hilft oft, die Verstärkung herunter zusetzen.
  Ist die Parasound-Tiefe ständig um viele 100m zu groß, am DESO Chan 1 ON setzen, GAIN auf AUTO und GAIN CHAN 1 auf Null.

- **blaue Leerspuren auf dem Bildschirm erscheinen.** In diesem Fall ist die Wassertiefe um ±300m oder ein ganzzahliges Vielfaches davon falsch eingestellt. Ist die erste bzw. letzte Spur einer Lotfolge blau, muß die Wassertiefe um diesen Wert nach unten bzw. oben gestellt werden.

- **Hydrosweep nur noch fehlerhafte Tiefen liefert.** Systemoperator rufen (in der Nacht bitte über die Brücke), er wird eventuell im SURVEY, DATA ACQUISITION, MULTIBEAM CONTROLL das System neu starten.

- **die DESO-Papierrolle zu Ende geht.** Vorschub mit dem roten Knopf am DESO ausstellen. Tagsüber Systemoperator oder Parasound-Betreuer rufen, wenn abgesprochen.

- **keine Navigationsdaten übertragen werden.** Meisten empfängt auch die Brücke in solch einem Fall keine Navigationsdaten. Dort nach der Ursache fragen. Der Fehler wird meistens schnell behoben.

- **das Signal/Rauschverhältnis zu schlecht wird?** Spielt mit der G(ain) im orangen Menü des ParaDigMa Systems. Erhöht die Gain zuerst um ca. 30%. Auf METEOR sollten die Werte zwischen 20 und 50 liegen.

- **die Hydrosweep-Daten nicht gesichert werden ?** Systemoperator (über Brücke) rufen. (METEOR)

- **Drucker-Papier gewechselt werden muß oder Drucker-Probleme auftreten?** Zunächst den Ausdruck im Programm abschalten. Mit Strg -T ("T" für Tabelle) wird der Protokolldrucker, mit Strg-P ("P" für Plot) der Online-Plot ausgeschaltet. Jetzt kann das Papier gewechselt werden. Eine neue Seite des Endlospapiers muß an der Oberkante des schwarzen Rechtecks am rechten Rand der Papierführung der Drucker stehen. Am Drucker Set TOF (Top Of Form) drücken. Nachfolgend muß im Untermenü BASIC (s.o.) der Punkt 'NewPage' aufgerufen, der einen Seitenvorschub am Drucker auslöst. Jetzt wird durch erneutes drücken der Strg-Taste mit "T" oder "P" der entsprechende Drucker wieder angeschaltet. Wenn sich die Tintenpatronen ihrem Ende nähern (meist geht am Online-Plot die gelbe Farbe aus, der Plot wird dann kräftig lilafarben), befinden sich neue Patronen in dem Regal über dem Bildschirm. Am Drucker muß dann die rechte vordere Klappe geöffnet werden. Die Verriegelung der betroffenen Patrone lösen, Patrone herausziehen, neue einlegen und Riegel wieder einrasten lassen (alles auch bei abgeschaltetem Ausdruck).

- **eine Station gefahren wird?** Solange auf Station kein Frequenztest gefahren wird, wird die Menge der registrierten Daten reduziert. In dem "rosa" ParaDigMa Menü (ctrl-d | B(asic)) findet sich der Menüpunkt WAITTIME. Gebt 60.0 (Sekunden) ein. Nun wird nur einmal pro Minute ein Seismogramm abgespeichert. Bei Ende der Station muß die WAITTIME wieder heruntergesetzt werden. Das Heruntersetzen erfolgt in 20s Schritten mit jeweils Pausen von einer Minute.

- **die Schwärzung auf dem DESO-Schrieb zu groß oder zu klein ist?** Vorsichtig mit GAIN CH2 am DESO justieren. Dazu muß aber die GAIN am Drehschalter der Parasound-Konsole bereits optimiert sein.

- **die ERROR LED am DESO leuchtet?** Total egal, tut sie immer.

Parasound/ParaDigMa Help Guide

Version 1.2 C. Hübscher April 1997
Version 1.3 C. Hübscher March 2000
Translation 1.3.1 E. Haase March 2000

TABLE OF CONTENTS

I. INTRODUCTION

This text gives an overview of the essential duties of the Parasound watchstander. It is a dynamic text that will expand and become more comprehensive over time. Any suggestions or comments are gladly accepted. The following guide neither replaces a thorough introduction nor study of the official handbook.

I. 1 ADRESSES

Please send comments or suggestions regarding this manual to:

Dr. Christian Hübscher
Institut für Geophysik
Universität Hamburg
Bundesstrasse 55
20146 Hamburg
chuebscher@dkrz.de.

The ParaDigMa-software is maintained by:

Prof. Volkhard Spieß
Fachbereich Geowissenschaften
Universität Bremen
Postfach 330 440
28334 Bremen
a13g@uni-bremen.de

I.2 WHAT IS PARASOUND

The Parasound sub-bottom profiler is a seismic system which measures the internal structures of the sedimentary cover along the ship's track. From underneath the ship, a high frequency signal is emitted that penetrates the sea floor. Simply said, when changes in density of the sediments are encountered, a portion of the signals are reflected back to the ship. An example

of this might be compositional changes in the sediment, and naturally the sea floor itself. On the ship the returned signals from the Parasound/ParaDigMa system are received, displayed and plotted.

I.3 SYSTEM COMPONENTS

The Parasound watchstander must watchover the functions of three components of the Parasound/ ParaDigMa system. These are the Parasound console, DESO and ParaDigMa system. The Parasound console is mounted in the component rack and consists of a monitor with 2 handgrips, with knobs and a control board underneath.

On the METEOR there are 2 such monitors, the relevant one is on the right. In the Hydroacoustic centers of the SONNE and POLARSTERN there is only one system onhand. Above the Parasound console is the DESO – a two channel profiler with plotter and two switchboards. The main components of the ParaDigMa system are the Data Acquisition Unit (DAU), PC with monitor, and one or two printers. Both the SONNE and the METEOR have a master control unit for Hydrosweep in their acoustic laboratories.

A more thorough introduction of this cartographically developed system will be given here. The current system administrator would like to provide further information, for when the watchstander has little to do.

II. FUNDAMENTALS

On the bottom of the ship is a transmitter that produces signals of two different frequencies. One frequency will always be 18 kHz. This signal is also used for depth sounding for the bridge. The second signal has a frequency between 20.5 kHz and 23.5 kHz, set in increments of 0.5 kHz. Through the so called parametric effect, which results from the non-linearity of the motion equation of acoustic waves in a fluid medium, another signal in the water column is generated whose primary frequency value is equal to the difference between the two main frequencies. Most of the time the second transmitted signal will have a frequency of 22 kHz, so the resulting parametric signal will have a frequency of 4 kHz. This is the signal used for the sub-bottom profiling. The big advantage of parametric signals is that they are emitted within a cone which has a 4° opening angle. On the sea floor an area is detected whose diameter will be about 7% of the total water depth, which achieves a high lateral resolution. The disadvantage is that signals returned from layers dipping more than 2° will not be received, as the ship will go by them.

The ParaDigMa system serves to plot and digitize the received signals at a rate of 40,000 samples per second. To limit the amount of data to process, only a certain time frame of signals are recorded that fall into a window expected for the sea floor returns. This time frame is dependent upon the water depth and must be appropriately set and monitored. To answer the next question: no, this process cannot be automated. Therefore, monitoring of the registration window, expressed through the depth interval in which the sediments to be measured are found, is the most important duty of the Parasound watchstander.

The data is secured with help from changing hard drives.

III. DUTIES OF THE PARASOUND WATCHSTANDERS

III.1 Taking over the watch

The following points are to be observed upon taking over the watch

- Is the name, room and telephone number of the responsible person for this part of the cruise known? Listing this question first affirms that, with critical questions, those responsible can be approached at any time day or night. Good data takes highest priority!

- Are Parasound/ParaDigMa and DESO active?

- Is enough paper for the online-printer available?

- Are enough Protocol Forms in stock?

- Is there a red square on the Hydrosweep monitor next to the letters R-R noticeable? This is to show that data will be recorded. If the screen is dark, it can be activated with the mouse. After a few seconds the monitor will become bright. (Only on METEOR)

- Is START in the FAHRTKOMMANDO menu on the Hydrosweep monitor pressed? (Only on SONNE)

- Is the starting water depth value of the DESO smaller than the actual water depth (ca. 70%)? To test it, one of the little white buttons of the DIG. DEPTH GATE on DESO should be pressed. With this button the DEPTH GATE will also be set. (Optional)

III.2 DURING THE WATCH

On the Parasound Console:

- **Adjusting the Window**. The depth-window, where the data becomes registered, must be manually adjusted to correspond with the water depth. Two green numbers define the actual depth-window. To adjust, there is a small toggle switch on the Parasound console (labeled 'Phasing', right switch), by which the depth-window may be set. **The ocean floor reflection should be kept in the top-half of the screen, to allow for the registration of the deeper reflectors when there is stronger penetration!** The adjustments should be done quickly. Please decide upon a desired depth to be set BEFORE pressing the switch. While with every adjustment data will be lost, so it should only be done when it is necessary. If there is an error, corrections of 10 meters should only done when the sea floor goes off the top of the screen.

If there is no signal on the screen, please refer to section: What to do when ...

- **Range Setting**. On DESO there is a knob labeled RANGE which can be adjusted between the values of 5 and 1,000 meters. Above the range, the length of a registration cycle can be set, which effects the transmission and reception of a pulse sequence. On the lower edge of the depth-window the point of time is given, that at the latest, adjustment should follow. At the same time as that, the Parasound console switch 'Channel Select' in the position PAR or PAR/NBS must eventually be needed.

The switch position shows, if the water depth actually comes from the 4 kHz signal (PAR) or the earlier sent 18 kHz signal (PAR/NBS). The table shows the use of the switch positions:

Water Depth	Range	Channel Select	Paperspeed
0 – 90 m	100	PAR	1:20,000
90 – 400 m	500	PAR	1:20,000
400 – 900 m	1000	PAR/NBS	1:20,000
900 – 1900 m	2000	PAR/NBS	1:20,000
1900 – 4600 m	5000	PAR/NBS	1:20,000
4600 – 9900 m	10,000	PAR/NBS	1:10,000

The paper advance on DESO is changed with the PAPERSPEED switch. The range 10,000 is selected to achieve a similar scale when there are few depth soundings.

Supervising the DESO Paper Spooler. The analog data is delivered from the Parasound system and is printed by the DESO plotter. When the paper roll approaches the end, a red stripe becomes visible on the top of the paper and will drift to the bottom side of the paper. The appearance of the red stripe indicates that about one hour still remains of the paper roll. The actual changing of the paper roll requires a little explaining. And the procedure is beyond the capabilities of the authors to put into writing. In an emergency, contact a system administrator.

Is the Data Quality Satisfactory? When the top half of the ocean bottom reflection displays strong static on the screen, one can turn the THRESHOLD knob slowly to the right to blend out noisy colors.

ON THE PC:

Normally, no parameters will need adjusting, only supervision to ensure proper functioning of the systems.

- **Is the DVS Data Transfer functioning ?** The DVS supplies the navigation data which appears in every Echo-gram header and at the end, an important data file will be saved (Position, Course, Speed, etc.). When the ship moves, the data should constantly change. The navigation data is shown on the right-hand screen (infobox 'Large Letters').

- **Are the depth measurements of Parasound and Hydrosweep somewhat in agreement?** While voyaging, especially on the METEOR, the Hydrosweep may experience difficulties. Most of the time the problem will fix itself. The program will call attention to the problem by tone sequences. In urgent situations, turn off the tone sequences in the BASIC menu.

- **Is the Printer working well ?** With the printers everything can go wrong, some common examples are: incorrect paper advancement, out of paper, starting with the wrong side, or a new ink cartridge is needed. Please refer to section WHAT TO DO, WHEN:

- **Finally, there remains the favorite point: writing Protocol.** In foresight, essential system parameters will be listed on a form letter. One important purpose of the Protocol is regular system control. Please write down any unusual events in the column named 'BEMERKUNG' (this column is very important !!!). All times should be given in UTC (Universal Coordinated Time).

IV. Short Introduction to the ParaDigMa System

The monitor screen is divided into 4 parts, and the registered Echo-gram claims the largest part of the display. Here the data will be displayed after all the filters and amplifications are applied. But only the raw data will be saved. The filters have no effect upon the recorded data. On the right hand side of the screen are shown the different Infoboxes.
On the top part of the screen is shown one of three selectable menu bars, which may be toggled through using the ESCAPE key. One of the menus has an orange colored background and is titled 'BASIC OPERATION', this is the most important menu for normal use and to quickly find necessary functions. There is a 'MAIN MENU' (gray background) by which all functions through sub-menus (blue background) can be found. And a general title bar (blue background) which serves only visual purposes.
The menu buttons can be activated and one can also open sub-menus (blue background) using the high-lighted first letters, or through the data entry screen in the top right-hand corner of the display. The simultaneous pressing of <control> H (for help) will prompt a screen to appear

with information about the selected function. All sub-menus and data entry windows can be exited using the ESCAPE key without accepting the (possibly wrong or unintentional) entered parameters. A list of all functions is given again in the Appendices.
Appendix III provides a guide for the entry of characters using the Editor-Functions. Blank spaces must be entered as blank spaces.

Tone Sequence:
A slow tone sequence with increasing pitch occurs at set intervals and serves as a reminder to make entries in the Protocol. Should the music not quit on it's own, press on the Space bar after 5 seconds.
A short then fast, or increasing pitch tone sounds when the Parasound water depth approaches the top or bottom of the depth window. Eventually the depth window must be re-set.
If the Parasound water depth is lost, or when the depth measurements from Parasound and Hydrosweep deviate more than 80 meters from one another, a warning tone (changing high-low) may sound. In this case set the depth window so that the Hydrosweep-measured-depth falls in the middle range of the depth window. When no ocean floor is recognized, one must fly blindly, and orientate oneself only with the depth given by the Hydrosweep.
When the Parasound depth is unreliable, turn off the Parasound-Hydrosweep signal (PS/HS SIGNAL in the BASIC menu).

V. What to do, when ...

- **The Ocean Floor reflection is lost.** If the echo on the display window runs off the screen, can the window be set to the depth measured by Parasound or Hydrosweep. When the slope is too steep, too little energy is reflected and the signal will no longer be visible. If the Parasound delivers a half-plausible water depth, position the depth window to this depth and wait. If no luck, try setting to the depth measured by Hydrosweep. In areas with dramatic topography, ex. middle oceanic spreading ridges, this can last for hours!

- **The Program Crashes.** With almost every crash, the program will freeze so that no activity can be seen on the screen. In the top right corner there is a letter on a white background that tells what the last procedure was. **In every case, make note of the letter in the protocol.**
In most of the cases there will be an '**O**', which represents the online plotting. Have a look at the online printer, does the yellow LED blink (assuming a DeskJet 870)? If ink or paper has finished than change cartridge or load paper. Press the button beneath the yellow LED in any case. Now immediately switch plotting off <control> P. If the letter is a **T** the Navigation plotter must be turned off and then turned on again. Often the program will then continue.
The day changeover at 00:00 am can be problematic for the navigation data, and may cause a crash. Re-boot the Parasound PC (with Control-Alt-Del). Initialize the clock with TIME, and set the clock to UTC time with an accuracy of at least 5 minutes. Press PSS and then <enter>. On the screen should be the program code for the DAU. Then after a few seconds the Registration Program should appear on Parasound.
First, start the Navigation Plotter with <control> T. So that further activity can be protocolled. <control> P will start the online plotter. Data that appears on the screen can be recorded by activating with <control> S.

- **Parasound depth reading is false.** If the digital Parasound depth is too small, eventually a water layer will reflect enough energy to simulate the ocean floor. In this case the Dig. Depth Gate (on DESO) can be lowered. Parasound accepts the first reflection under the Digital Depth Gate. With large amplifications on the Parasound console (POWER/GAIN) can cause false Parasound depth measurements to be calculated, as well as too small. What often helps in this case is to lower the amplification. If the Parasound measured depth remains several hundreds of meters too large, set channel 1 on DESO to ON, set GAIN to AUTO and GAIN CHAN 1 to zero.

- **Blue empty traces appear on the screen.** In this case, the water depth is falsely offset about ±300 meters, or a larger multiple of this. Is the first or last sounding sequence shown as a blue trace? Then the water depth must be set either lower or higher, respectively.

- **Hydrosweep delivers only erroneous depths.** Call the system operator (via the bridge during the night). He will eventually start the system again in SURVEY, DATA ACQUISITION, MULTIBEAM CONTROL.

- **The DESO Paper Roll is nearly finished.** Advance the paper with the red button on the DESO controls. During the day call the system operator or Parasound administrator.

- **No Navigation data is being received.** In most cases the bridge would also receive no navigation data. Therefore, inquire with the bridge as to the cause. The problem will usually be rapidly fixed.

- **The Signal to Noise ratio is bad.** Play with the G(ain) in the orange menu of the ParaDigMa system. Raise the gain first about 30%. On the METEOR the gain value should be between 20 and 50, on SONNE between 200 and 400 mV.

- **Hydrosweep data is not being saved.** Call the system operator, via the bridge. (METEOR)

- **Printer paper must be changed or other Printer problems occurring?** First, cancel the print-job. With <control> T ('T' is for Table) turns off the Navigation printer, and <control> P turns of the online plotter ('P' is for Plot). Now the paper can be changed. A new roll of paper must be on the top ledge of the black rectangles, on the right hand side of the paper-guide of the printer. On the printer, press TOF (Top Of Form). Afterwards go to the BASIC sub-menu, and press the button 'New Page', and a page will be advanced through the printer. To resume printing, turn on the appropriate printer by pressing <control> and either 'T' or 'P'. When the ink cartridge is getting low (most of the time the yellow color runs out, and the plot will become strongly lilac colored). Find a new cartridge in the cabinet above the monitor. The right front door of the printer must be opened. Take off the bar of the selected cartridge, pull the cartridge out, place the new one in, and return the bar . (All with the printer turned off)

- **The entire System freezes?** First, have a look at the single ASCII symbol in the very small white window in the upper right-hand corner of the screen. This symbol represents the last process. Make a note. In most of the cases there will be an 'O', which represents the online plotting. Have a look at the online printer, is the yellow LED blinking (assuming a DeskJet 870)? If the ink or paper has run out, then change the cartridge or load more paper. In any case, press the button beneath the yellow LED.

- **While on Station.** While on station, so long as there are no frequency tests, the amount of registered data will be reduced. In the pink ParaDigMa menu (<control> D | B(asic)) the menu button WAITTIME can be found. Input 60.0 (seconds). Now only one seismogram per minute will be saved. At the end of the station the WAITTIME must be reduced again. The reduction proceeds in 20 second increments with pauses of 1 minute between each level.

- **The printing level of the DESO plotter is too heavy or too light.** Carefully adjust the GAIN CH2 on the DESO. The GAIN must be optimized using the knob on the Parasound console.

ANHANG

A-I Hochfahren des Systems

Das Hochfahren sollte vom System-Operator oder zumindest von einem erfahrenen Wachgänger erfolgen.

- Alle Geräte einschalten. Auf METEOR ist über der ParaDigMa-Anlage knapp unter der Decke ein Stecker mit Kippschalter, über den alle ParaDigMa-Komponenten versorgt werden.
- Nach Start der Parasound-Anlage das Tiefenfenster so einstellen, daß der Meeresboden in der Mitte des Fensters liegt.
- An der Parasound-Konsole und DESO alle Einstellungen gemäß Anhang II vornehmen.
- Papier in Drucker einlegen.
- Parasound-PC hochfahren. Mit DATE [Enter] und TIME [Enter] diese Werte kontrollieren. Die Uhrzeit darf nur um weniger als 5 Minuten von UTC abweichen. PSS [Enter] drücken. Auf dem Bildschirm erscheint der Programm-Code für die DAU. Nach Aufforderung die orangefarbenen Tasten Clr und Rst auf der linken Forderseite der DAU drücken.
- Auf dem ParaDigMa-Bildschirm erscheint nach einigen Sekunden das Registrierprogramm.
- Strg-T für den Druck der Navigationsdaten und Laufwerksinformationen drücken.
- Mit Strg-S wird die Datensicherung aktiviert.
- Sind die ersten Daten auf dem Monitor zu erkennen, den Online-Plot mit Strg-P starten.

A-II Schalterstellungen Parasound-Konsole und DESO

DESO obere Schalterleiste (v. li. n. re.)

Dip Schalter 1500 0000 -00 (METEOR)
Dip Schalter 1500 0650 +00 (SONNE)
GAIN: MAN
DIG: INDICATION CH1
CHANNEL 1: OFF
CHANNEL 2: ON
GEN RECORD: OFF
INTENSITY: ganz rechts
DIST MARKS: 100 (500)
Kippschalter darüber: oben

DESO untere Schalterleiste (v. li. n. re.)

MODES: INT SPEED
PAPERSPEED: 1:20.000
GAIN CH1: Versucht es mit einem Startwert von. 5 (METEOR) bzw. 0,35 (SONNE)
GAIN CH2: Wert hängt von der Gain an der Parasound Konsole ab. Versucht einen Startwert von 3.
DEPTH RANGE: s. Text

DEPTH SCALE: 200

Kippschalter ganz rechts: I (schaltet DESO Ein/Aus)

SBP Gain Controll: DEEP/OFF

Parasound Konsole:

PARAMETRIC:

FREQUENCY: 4
PULSE: 2 (METEOR), 1 (SONNE)
BOTTOM TVC: OFF
GAIN: ca. 9

THRESHOLD: zw. 3 und 7 (METEOR), zw. 0 und 2 (SONNE)

CHANNEL SELECT: PAR BZW: PAR/NBS (s. Text)

NBS:

GAIN: 7,5
POWER/GAIN: Je nach Wassertiefe zw. 10 und A
BEAMWIDTH: 4°

SHIFT: ganz rechts
Lampensymbol: je nach Stimmung
SCALE EXPANDER: 1
PHASING: FAST
RANGE: 4
MODE: 4